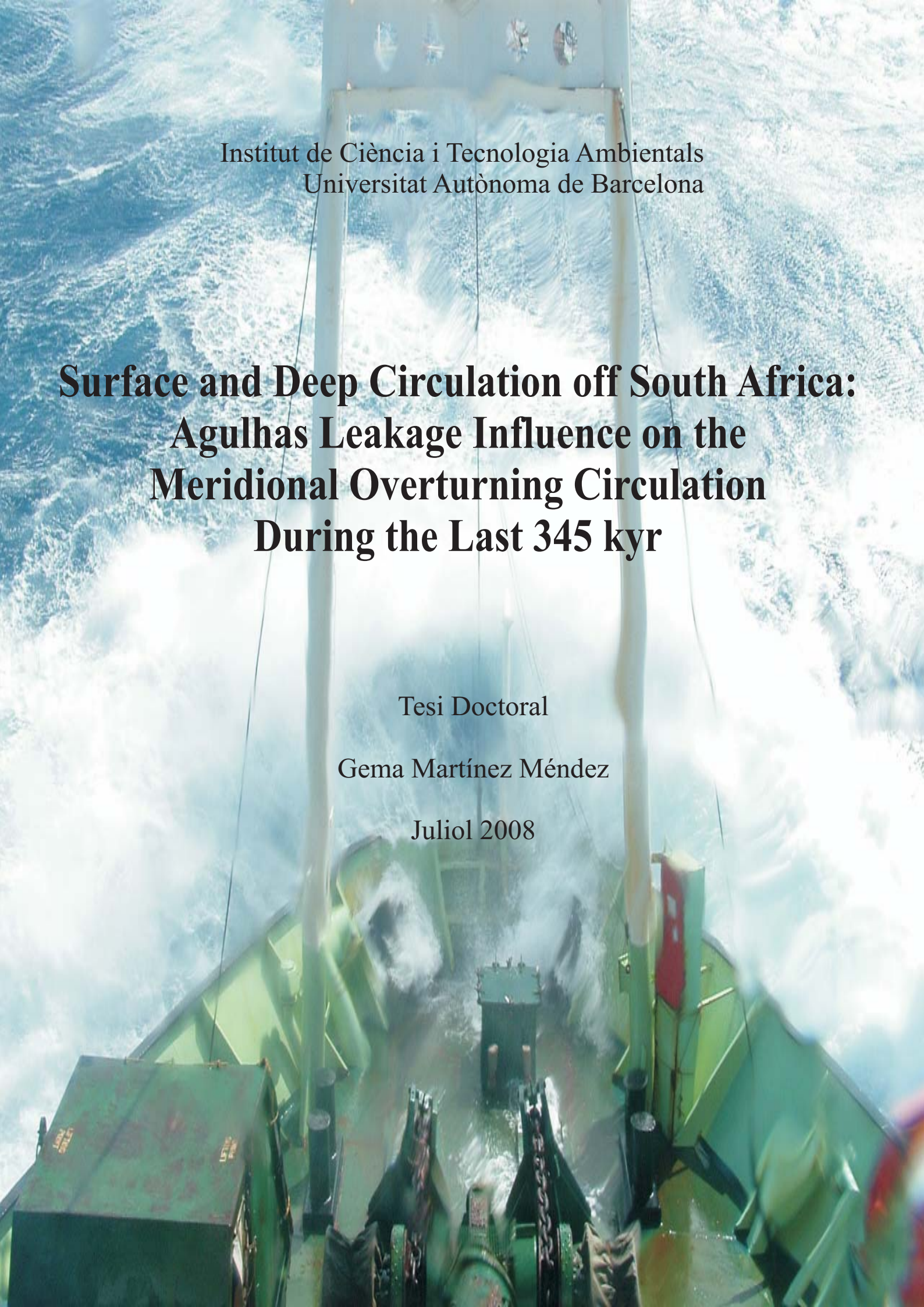

Institut de Ciència i Tecnologia Ambientals
Universitat Autònoma de Barcelona

Surface and Deep Circulation off South Africa: Agulhas Leakage Influence on the Meridional Overturning Circulation During the Last 345 kyr

Tesi Doctoral

Gema Martínez Méndez

Juliol 2008

Surface and Deep Circulation off South Africa: Agulhas Leakage Influence on the Meridional Overturning Circulation During the Last 345 kyr

Realitzada per:

Gema Martínez Méndez

sota la direcció del **Prof. Rainer Zahn**, al Institut de Ciència i Tecnologia Ambientals de la Universitat Autònoma de Barcelona dins del programa de doctorat en "Ciències Ambientals", bienni 2003-2005, per a optar al grau de Doctora

Barcelona, Juliol de 2008

La Doctoranda
Gema Martínez Méndez

El Director de Tesi
Rainer Zahn

Table of Contents

Table of Contents…….. **i**
List of Figures and Tables…… **iii**
List of Abbreviations…… **vii**
Agradecimientos…… **xi**
Abstract…….. **xv**
Resumen…… **xvii**
Resum…… **xix**

1. Introduction…….. **1**
1.1. El Papel de la Circulación Oceánica Global en el Clima…….. 3
1.2. Asincronía entre los Hemisferios: *Bipolar Seesaw*…….. 5
1.3. La "Ruta Cálida" (*Warm Water Route*) de Compensación de NADW…… 8
1.4. Motivación y Objetivos…… 11
Referencias…….. 12
2. Conceptual and Analytical Approach…… **15**
2.1. Paleoceanographic Proxies Used in this Study…… 15
2.1.1 $\delta^{18}O$ of Benthic Foraminifera……. 15
2.1.2. $\delta^{13}C$ of Benthic Foraminifera…… 21
2.1.3. Cd/Ca in Benthic Foraminifera: Paleonutrient Proxy……... 27
2.1.4. Mg/Ca in Planktonic Foraminifera: Sea Surface Paleotemperature Proxy……... 31
2.1.5. Sortable Silt Mean Size ($\overline{SS}$)…… 34
References……... 36
3. Site Location and Hydrographical Conditions…….. **41**
3.1. Agulhas Current and Agulhas Retroflection Current……... 42
3.2. Agulhas Leakage: Agulhas Rings and Agulhas Filaments…….. 47
3.3. Oceanic Fronts Between Africa and Antarctica……... 48
3.4. Intermediate Waters Below the Agulhas Current……. 51
3.5. Deep Waters in the Agulhas Region…… 53
3.6. Nutrient Content of Intermediate and Deep Waters …… 55
References……... 59
4. Methology……. **63**
4.1. Sample Preparation and Analyses…… 63
4.2. Sortable Silt Mean Size ($\overline{SS}$)…… 64
4.3. Stable Isotope and Trace Element Analyses (Planktonic and Benthic Foraminifera)…….. 64
4.3.1. Foraminiferal Selection of Preferred Species ……... 64
4.3.2. Stable Isotope Analyses (Planktonic and Benthic Foraminifera)……. 67
4.3.3. Trace Element Analyses ……... 68
4.4. Past Sea Water Cadmium (Cd_{sw}) Along MD96-2080 and Derivation of the Air-Sea $\delta^{13}C_{\Sigma CO2}$ Isotopic Signature ($\delta^{13}C_{as}$)…….. 78
4.5. Mg/Ca Derived Sea Surface Temperature (SST) and Derivation of $\delta^{18}O$ of Surface Water ($\delta^{18}O_{sw}$) and Sea Surface Salinity (SSS)……. 80
References……... 85

Annex I: Construction of a Stacked Benthic $\delta^{13}C$ Record, $\delta^{13}C_{stack}$…… 88
Annex II: Time Series of Parameters *a* and *b*……. 91
5. Results and Discussion…… 95
5.1. Age Model for MD96-2080 and MD02-2594……... 99
5.1.1. Stratigraphy of MD96-2080……..……...……..……... 99
5.1.2. Stratigraphy of MD02-2594……..…...……..….. 104
5.1.3. Splicing of MD02-2594 and MD96-2080 Into a Singular Record: Agulhas Bank Spliced (ABS)……...…...……... 109
References……. ……. 113
5.2. 345,000-year-long Multi-Proxy Records off South Africa Document Variable Contributions of Northern *versus* Southern Component Water to the Deep South Atlantic……. 117
5.2.1. Introduction……... 117
5.2.2. Core material ……...……...……... 117
5.2.3. MD96-2080 deep circulation records…….……..……...…… 119
5.2.4. Discussion……..……..….. 123
5.2.5. Conclusions……..……...……..….. 131
References……...……. 132
5.3. The South Atlantic Chemocline: New Assessments From Combined Benthic Cd/Ca and $\delta^{13}C$ Data and Inferred $\delta^{13}C_{as}$ Imprints…….. 137
5.3.1. Introduction……... 137
5.3.2. Data/Results…….. 139
5.3.3. Discussion……..……...……... 151
5.3.4. Conclusions ……..……...……... 159
References……..…….. 161
Annex I……..…….. 163
Annex II……..……. 171
5.4. Influence of Agulhas Leakage on the Meridional Overturning Circulation (MOC): insights from paired planktonic and benthic foraminifera stable isotope and trace metal analyses over the last 345 kyr…..… 175
5.4.1. Introduction……... 175
5.4.2. Core Material……...……...…... 176
5.4.3. ABS Surface Circulation Records……..…… 177
5.4.4. Discussion……..…… 184
5.4.5. Data-Model Comparison……..……...…... 196
5.4.6. Conclusions……..……...…... 198
References……... 200
6. Conclusions……...……..... 203
(English)……..……..……... 203
(Castellano)……..……... 206
Annex…… 209

List of Figures and Tables

Figura 1-1 Variaciones en la concentración de CO_2 atmosférico durante los últimos 45.000 años…… 2

Figura 1-2 Variaciones en la concentración de CO_2 atmosférico durante los últimos 800.000 años…… 2

Figura 1-3 Esquema de la circulación oceánica global…… 4

Figura 1-4 Modos de circulación oceánica global…… 5

Figura 1-5 Asincronía de temperatura entre los hemisferios…… 6

Figura 1-6 *Bipolar Seesaw* y transporte de calor inter-hemisférico…… 7

Figura 1-7 Patrones climáticos entre interestadiales y estadiales…… 8

Figura 1-8 Esquema simplificado de la circulación oceánica global…… 9

Figura 1-9 Rutas "Cálida" y "Fría" de compensación de NADW…… 10

Figure 2-1 Effects of the hydrological cycle on oxygen isotopes …… 17

Figure 2-2 Relationship between $\delta^{18}O$ and salinity in the different ocean basin…… 18

Figure 2-3 LR04 stack of Lisiecki and Raymo (2005)…… 20

Figure 2-4 Mirror relation between $\delta^{13}C$ and $(PO_4)^{3-}$…… 24

Figure 2-5 "Aging" effect on $\delta^{13}C_{\Sigma CO2}$…… 25

Figure 2-6 Curry and Oppo (2005) Western Atlantic $\delta^{13}C$ transects…… 26

Figure 2-7 Linear relationships between Cd_{sw} and $(PO_4)^{3-}$…… 28

Figure 2-8 Marchitto and Broecker (2006) Atlantic Cd_{sw} and $\delta^{13}C_{as}$ transects…… 30

Figure 2-9 Exponential fit between Mg/Ca and calcification temperature…… 32

Figure 3-1 Location of cores MD96-2080 and MD02-2594 within the Agulhas Corridor…… 41

Figure 3-2 Infrared satellite image showing the Agulhas Current…… 43

Figure 3-3 Proposed Agulhas Current pattern for winter and summer…… 45

Figure 3-4 Sea Surface Salinity around southern Africa…… 46

Figure 3-5 Sea Surface Temperature around southern Africa…… 46

Figure 3-6 Location of the Agulhas Eddy Corridor off South Africa…… 47

Figure 3-7 Southern Ocean Oceanic Fronts…… 49

Figure 3-8 Intermediate Water masses at 900 m around South Africa…… 52

Figure 3-9 Schematic deep water circulation scheme around southern Africa …… 54

Figure 3-10 Bottom potential temperature in the Southern Ocean …… 55

Figure 3-11 GEOSECS $\delta^{13}C_{\Sigma CO2}$, $(PO_4)^{3-}$, $\delta^{13}C_{bio}$, $\delta^{13}C_{as}$, Western and Eastern Atlantic transects…… 56

Figure 3-12 T-S mixing triangle of Atlantic water masses and position of T-S ambient bottom water at the location of cores MD96-2080 and MD02-2594…… 58

Figure 4-1 *Cibicidoides (Fontbotia) wuellerstorfi*…… 66

Figure 4.2a *Globigerina bulloides*…… 66

Figure 4.2b *Globorotalia inflata*…… 66

Figure 4-3 Open chambers of *Globigerina bulloides*…… 70

Figure 4-4 Solid residues left after centrifugation…… 71

Figure 4-5 Benthic Cd/Ca *versus* Mn/Ca, Al/Ca and [Ca] for MD96-2080…… 73

Figure 4-6 Planktonic Mg/Ca *versus* Mn/Ca, Al/Ca and [Ca] for MD96-2080……..…..……..… 73
Figure 4-7 Planktonic Mg/Ca *versus* Mn/Ca, Al/Ca and [Ca] for MD02-2594...……...…..……. 74
Figure 4-8 Testing for calcite dissolution in MD96-2080..……...……...……. 76
Figure 4-9 Testing for calcite dissolution in MD02-2594..……....…..……. 77
Figure 4-10 Time series of parameters *a* and *b*…...…..……. 79
Figure 4-11 Comparison of Mg/Ca-derived SST using two different calibrations...…...…..…… 82
Figure 4-12 $\delta^{18}O_{sw}$ *versus* Sea Surface Salinity for tropical latitudes……..…..……. 83
Figure 4-13 Deconvolution of the temperature effect from planktonic $\delta^{18}O$…… 84
Figure 1 Annex I Benthic foraminiferal $\delta^{13}C$ records used to construct the $\delta^{13}C_{stack}$…… 89

Figure 5.1-1 Age-depth function for MD96-2080 ^{14}C AMS dates…… 101
Figure 5.1-2 Age model for MD96-2080……... 103
Figure 5.1-3 Screen shot of the tuning procedure using Analyseries software…….…..…….. 106
Figure 5.1-4 Age model for MD02-2594……... 107
Figure 5.1-5 Age-depth function for MD02-2594 ^{14}C AMS dates…… 108
Figure 5.1-6 Splicing of MD02-2594 and MD96-2080 into a singular record: Agulhas Bank Spliced (ABS) 110
Figure 5.1-7 ABS and reference core records…… 113

Figure 5.2-1 Location of MD96-2080 and reference cores…….…...….... 118
Figure 5.2-2 Stable isotopes and Cd/Ca records of *F. wuellerstorfi* and the record of $\overline{SS}$…….. 121
Figure 5.2-3 Individual benthic carbon isotope records, meridional carbon gradient and seawater Cd compared with North Atlantic IRD abundance……. 124
Figure 5.2-4 Proxy-proxy diagrams displaying Cd_{sw} and $\delta^{13}C$ data from MD96-2080 and reference cores 130
Figure 5.2 Annex I-1 Comparison of benthic foraminiferal $\delta^{18}O$ of MD96-2080, ODP 980 and RC13-229 on their published time scales……..…...……..…… 134

Figure 5.3-1 Benthic $\delta^{13}C$ chemocline……... 139
Figure 5.3-2 Map with the position of sediment cores used in Chapter 5.3…….. 140
Figure 5.3-3 Holocene Atlantic $\delta^{13}C$, Cd_{sw} and computed $\delta^{13}C_{as}$…….. 141
Figure 5.3-4 Glacial Atlantic $\delta^{13}C$, Cd_{sw} and computed $\delta^{13}C_{as}$……. 142
Figure 5.3-5 South and Central Atlantic $\delta^{13}C$ and Cd_{sw} discriminated by their latitudinal position respect to the LGM-SAF…… 144
Figure 5.3-6 Linear trends defined by the LGM benthic $\delta^{13}C$ data from South and Central Atlantic data and glacial (LGM, MIS 6 and 8) $\delta^{13}C$ means of South Atlantic cores……...……... 146
Figure 5.3-7 Down-core South Atlantic benthic $\delta^{13}C$ records from well-ventilated and poorly ventilated chemocline domains…….. 148
Figure 5.3-8 Down-core Cd_{sw} and tentative $\delta^{13}C_{as}$ records of Atlantic cores…… 150
Figure 5.3-9 THC Modes proposed by Keeling and Stephens (2001)……... 156
Figure 5.3-10 Down-core Cd_{sw} South Atlantic benthic $\delta^{13}C$ records and gradients compared to Vostok CO_2…. 159
Figure 5.3 Annex II-1 RC113-229 records, testing for a "Mackensen effect"…….. 172

Figure 5.4-1 Location of MD96-2080 and MD02-2594 cores within the Agulhas Corridor…… 177
Figure 5.4-2 Agulhas Bank surface records…….…….……..…...… 179
Figure 5.4-3 ABS *G. bulloides* weight *versus* Mg/Ca ratio ……..……..……... 180
Figure 5.4-4 Surface paleoceanographic records for ABS…….…….…….. 183
Figure 5.4-5 Tropical/subtropical SST records…….……..…...…… 186
Figure 5.4-6 Planktonic and benthic records of ABS and CBR…..……... 189
Figure 5.4-7 MIS 6 to 5 transition……..…….……..…..…...…… 191
Figure 5.4-8 MIS 2 to 1 transition……..…….……..…..…...…… 193
Figure 5.4-9 MIS 10 to 9 transition……... 194
Figure 5.4-10 MIS 8 to 7 transition……..…….……..…..…...……... 196

Table 3-1 Water masses of the southern African region……...… 42
Table 3-2 Intermediate and deep water masses influencing the hydrography of the core sites…… 58

Table 1 Annex I (Chapter 4) Sediment cores used for the construction of the benthic $\delta^{13}C_{stack}$……... 88
Table 1 Annex II (Chapter 4) Time series of parameters *a* and *b*…..…….....……. 91

Table 5.1-1 *Globorotalia inflata* ^{14}C AMS ages and calibrated calendar years ages for MD96-2080……. 100
Table 5.1-2 Tie points for establishing the age model of MD96-2080…… 102
Table 5.1-3 *Globorotalia inflata* ^{14}C AMS ages and calibrated calendar years ages for MD02-2594……. 105
Table 5.1-4 Tie points for establishing the age model of MD02-2594…… 106
Table 5.1-5 Tie points for establishing the age model of the spiced record ABS…… 111

Table 5.2-1 Core locations……...……... 119
Table 5.2-2 $\delta^{13}C_{\Sigma CO2}$ and Cd_{sw} values of modern and glacial Atlantic water mass endmembers…….. 126
Table 5.2-3a Interglacial $\delta^{13}C_{\Sigma CO2}$ and Cd_{sw} values from Atlantic sediment cores……. 127
Table 5.2-3b Glacial $\delta^{13}C_{\Sigma CO2}$ and Cd_{sw} values from Atlantic sediment cores……... 128

Table 5.3-1 Core locations……...……... 145
Table 5.3-2 Glacial $\delta^{13}C$ values for South Atlantic sediment cores……... 145
Table 5.3 Annex I-1 North Atlantic (65º to 41ºN) published Holocene and LGM benthic $\delta^{13}C$ and Cdsw. 165
Table 5.3 Annex I-2 Centra1 Atlantic (41ºN to 10ºS) published Holocene and LGM benthic $\delta^{13}C$ and $Cd_{sw.}$ 166
Table 5.3 Annex I-3 South Atlantic (south of 22ºS) published Holocene and LGM benthic $\delta^{13}C$ and Cd_{sw}… 169

Table 5.4-1 Synoptic view of stronger/weaker presence of Agulhas Water and modes of MOC…… 197

List of Abbreviations

A_{1-4}	Antarctic Warming
aAAIW	Five member mixture of AAIW
AABW	Antarctic Bottom Water
AAIW	Antarctic Intermediate Water
AASW	Antarctic Surface Water
ABS	Agulhas Bank Spliced
AC	Agulhas Current
ACC	Antarctic Circumpolar Current
ACR	Antarctic Cod Reversal
ACW	Antarctic Circumpolar Water
AF	Agulhas Front
AFR	Agulhas Fracture Ridge
AIW	Arctic Intermediate Water
AIM	Antarctic Isotope Maximum
AMS	Accelerator Mass Spectrometry
AOGCM	Atmosphere-Ocean General Circulation Model
APF	Antarctic Polar Front
APZ	Antarctic Polar Zone
ARF	Agulhas Retroflection Front
AR	Agulhas Ring
ARC	Agulhas Return Current
AVHRR	Advanced Very high Resolution Radiometer
AW	Agulhas Water
Bio	Biological
BUS	Benguela Upwelling System
α_{A-B}	Fractionation Factor between substances A and B
CBR	Cape Basin Record
CDW	Circumpolar Deep Water
Cd_C	Cadmium content of foraminiferal calcite
Cd_{sw}	Cadmium content of sea water
dAAIW	Drake Passage AAIW end-member
D_{Cd}	Partition coefficient between Cd_{sw} and Cd_c
DIC	Total Dissolved Inorganic Carbon
DO	Dansgaard-Oeschger
DW	Deep Water
$\delta^{13}C_{as}$	$\delta^{13}C$ isotopic imprint acquired during air-sea exchange
$\delta^{18}O_{sw}$	Sea Water oxygen isotopic composition
$\delta^{18}O_b$, $\delta^{13}C_b$	Benthic foraminiferal stable oxygen and carbon isotopes
$\delta^{18}O_{plk}$, $\delta^{13}C_{plk}$	Planktonic foraminiferal stable oxygen and carbon isotopes

$\delta^{18}O_{\Sigma CO2}$,$\delta^{13}C_{\Sigma CO2}$	Ambient sea water stable oxygen and carbon isotopes
DSOW	Denmark Strait Overflow Water
EDC	EPICA Dome Concordia Ice Core
EPICA	European Project for Ice Coring in Antarctica
EDML	EPICA Dronning Maud Land Antarctic Ice Core
GEOSECS	Geochemical Ocean Section Study
GHG	Greenhouse Gases
GNAIW	Glacial North Atlantic Intermediate Water
H	Heinrich Event
IAEA	International Atomic Energy Agent in Vienna
ICP-MS	Inductively Coupled Plasma Mass Spectrometry
IIW	Indonesian Intermediate Water
IMAGES	International Marine Past Global Changes Study
IPCC	Intergovernmental Panel on Climate Change
IPEV	Institut Polaire Français – Paul Emile Victor
IRD	Ice Rafted Detritus
ISOW	Iceland–Scotland Overflow Water
LCDW	Lower Circumpolar Deep Water
LGM	Last Glacial Maximum
LSCW	Low Southern Component Water
LSW	Labrador Sea Water
Ma/Myr	Million years
MIS	Marine Isotope Stage
m.o.	Mean Ocean
MOC	Meridional Overturning Circulation
NADW	North Atlantic Deep Water
NAUSICAA	Namibian Angolan Upwelling System and Indian Connection to Austral Atlantic
NCW	Northern Component Water
NERC	Natural Environment Research Council (UK)
NH	Northern Hemisphere
NGRIP	North Greenland Ice Core Project
NOSAMS	National Ocean Science Accelerator Mass Spectrometry
NPIW	North Pacific Intermediate Water
NSTF	North Subtropical front
ODP	Ocean Drilling Program
Org	Organic
OMZ	Oxygen Minimum Zone
PF	Polar Front
ppmv	Parts per million by volume
psu	Practical salinity units
σt	Density anomaly (= density - 1000 kg/m^3)
RA	Isotopic ratio of substance A

RF	Agulhas Retroflection
RSD	Relative Standard Deviation
RSIW	Red Sea Intermediate Water
R(t)	Reservoir age
SA	South Atlantic
SAACF	Southern ACC Front
SAZ	Sub-Antarctic Zone
SAF	Sub-Antarctic Front
SAMW	Sub-Antarctic Mode Water
SASW	Sub-Antarctic Surface Water
SB	Southern Boundary of the ACC
SCW	Southern Component Water
SE	South East
SH	Southern Hemisphere
siAAIW	Southern Indian AAIW end-member
S	Salinity
SB	Southern Boundary of the ACC
SPECMAP	Mapping Spectral Variability in Global Climate Project
SSTF	South Subtropical front
$\overline{SS}$	Sortable Silt Mean Grain Size
SSS	Sea Surface Salinity
SST	Sea Surface Temperature
STC	Subtropical Convergence
STC-UB	Serveis Cientificotècnics de la Universitat de Barcelona
STF	Subtropical Front
SUERC	Scottish Universities Environmental Research Centre
Sv	Sverdrup (106 m^3/s)
$\sum CO_2$	Total Dissolved Inorganic Carbon
T	Temperature
TI-IV	Glacial Terminations I-IV
THC	Thermohaline Circulation
TOC	Total Organic carbon
T-S	Temperature-Salinity
VPDB	Vienna Pee Dee Belemnite
UCDW	Upper Circumpolar Deep Water
ULSW	Upper Labrador Sea Water
USCW	Upper Southern Component Water
yr/kyr/ka BP	years/kiloyears/ kiloannum before present
WOCE	World Ocean Circulation Experiment

Agradecimientos

Ha llegado el tan deseado momento…el de escribir los agradecimientos, que a fin de cuentas significa entrar en las etapas finalísimas de la tesis…

Sicilia 1927,

Barcelona, Junio de 2003, un calor que caían los páxaros de los árboles y un montón de cajas llenas de frasquines a rebosar de foratas… Barcelona, Julio de 2008, algo menos de calor y un montón de resultados.

Son muchas las personas que han contribuido a la consecución de este trabajo, a su realización y, tan importante como lo primero, a no sucumbir en el empeño ;).

Empezaré por mi director de tesis, Rainer Zahn. Muchas gracias por enrolarme en este proyecto en una de las regiones conocidas por sus inesperadas olas gigantes. Por tus explicaciones, correcciones e ingentes dosis de entusiasmo en todo momento. También por lo ánimos en los momentos de bajón (unos "pocos" sólo…) y por enorrrrrrmes dosis de paciencia. Herzlichen Dank.

Ich danke Joachim Schönfeld vom "Leibniz-Institut für Meereswissenschaften" (IFM-Geomar) an der Universität Kiel, der mich in die Paläo-Ozeanographie einführte und mir eine Forschungsfahrt ermöglichte. Er stellte auch den Kontakt zu Rainer Zahn her und empfahl mich für ein Projekt im sonnigen Barcelona.

I greatly appreciate our collaborator Ian Hall from Cardiff University who generated the sortable silt data, for very ensuing discussions and for following all the process of my thesis.

Many thanks are to go to the Cardiff group (current and former, most now somewhere else), Helen Medley, Ian McMillan and Julia Becker (thank you so much for lab assistance), Gian Carlo Bianchi (lot of info in MAT aspects), Paula, Vicky, Lizzie, Rehanna, Katharina for the nice moments spent there, specially to those who shared the Darwin cruise. Many thanks also to all CD154 members for the lovely time onboard that besides enriched my perspectives on the subject, Steve Goldstein, Sidney Hemming, Chris Ellinson, Alex Thomas and the galley guys…

More marine thanks are to go to the MD141-EFU participants, I learnt a lot on that cruise.

Thanks again to Steve Goldstein, Sidney Hemming, Katharina Pahnke and also to Allison Franzese for patiently waited for me to go overseas and stay at Lamont for some months, shame that it did not work out at the end.

I would also like to say thanks to Ros Rickaby, Dave Harding and John Arden from Oxford University for giving me a first training in trace element analyses and show me how tricky these analyses may be. From Oxford thank you also to many young, and less young, researchers for making the stay there very pleasant.

Many thanks are to go to Frank Peeters from Vrije Universiteit, The Netherlands, for generously sharing his knowledge on the Agulhas Current and counting quite a lot of forams for producing the leakage fauna in my record. Thank you also to Dick Kroon (Grant Institute, Edinburgh) and Ralph Schneider (Christian-Albrechts Universität, Kiel) for sharing the as yet unpublished GeoB36003 $\delta^{13}C$ data.

Muchísimas gracias también a los miembros de GRCGM de la UB, donde comencé mi tesis, por los buenos tiempos pasados allí y por hacerme sentir como si nunca me hubiese ido cada vez que volvía a hacer unos u otros análisis. Respecto a los análisis, gracias a Joaquín Perona y Rosa Mª Marimón por tantos pañales que le cambiamos juntos al baby-MAT y por seguir educándolo después cuando ya caminaba. Muchísimas gracias a Isa y Leo por volcarse tanto conmigo cuando fui a terminar los análisis de elementos traza y por interesantísimas discusiones. También a Gemma por ayudarme a reubicarme en el laboratorio. A Jaime y Leo por compartir los primeros tiempos en el "picadero" y un montón de risas y lágrimas después. Ya a nivel más folklórico, muchísimas gracias a todísimos y a las partículas adyacentes por compartir calçotadas, sesiones de playa, Santas, Sant Joanes, birras, boletadas, vicarias, trapecios, conversaciones trascendentales e intranscendentales… Marga, Cuca, Sergi, Eli, Cami, Sara, Oli, Galde (merci també per llegir-te tota la meva tesi i trobar-me les errates!!), David (mercès també per el mapa tan macu del Sud d'África), Centella, Verónica, Joan, Tina, Xánxez, Caroline, Sergi, Neus, Ben…espero no olvidarme a nadie… Cons y Montse por paleo-birras, paleo-cenas y paleo-ánimos.

Fue duro dejar un grupo tan majo una vez que me había hecho con mi nicho de marmotilla, menos mal que el grupo de acogida no era menos majo. Los primeros momentos no fueron del todo fáciles, gracias a todos los ictarios por conseguir hacer risa de una situación caótica y seguir haciéndolo después en la no-entropía. Muchas gracias a los Gepocs y Físicos por interesantes seminarios y discusiones, y por ánimos, Graham, Patrizia, Toni, Pere, Jordi, Ester, Eli, Carolina, Patri, Nuria, JManel… moltes gràcies als que m'han aguantat més, es van recordar de trucar-me "gairebé sempre" per dinar, em van ajudar a revisar la tesi i han estat uns solets: Nata, (uff, no me tiene aguantaa ni na), Marina, Alfredo, Migue, Sergi, Gemma, Susanne, Bastián, Saioa, Nuri. Je, je, además para cuando leáis esto espero poder contestar ya afirmativamente a la pregunta del millón. También gracias a las últimas incorporadas, por sobrevivirme en los momentos finales de escritura y de menor sociabilidad, Laura y Alba. César entra en todos los colectivos, gracias por interesantes discusiones sobre Agulhas y por tu envidiable filosofía ante la vida. Del ICTA gracias también a l@s "secres" que siempre nos ayudan en todos los trámites y papeleos con un humor genial.

Cinco años de alquiler dan para muchos compañeros, amigos, de piso. Gracias David por tus silencios elocuentes, Carles por tus historias raras, Óscar por tu buen humor, Mercedes por tanto cariñito. Pep, primero quinto elemento de la pensión Violant d'Hongria, después inquilino, después acoplado de avd de Madrid y más tarde inquilino de avd de Madrid, te echaré de menos en mis próximos sofases. Akgün que pasó por Violant d'Hongria y me cautivó con su conversación fácil, gracias por tantas charlas. Verito, mi mamita che, que me robó de Pep para luego robármelo a él, al final todos contentos. Papa Leo que me permitió romper tantas veces el contrato de "no ciencia en casa" y que intento tantas más (con más o menos éxito) poner un poco de raciocinio en esta cabeciña. Aquí también he de mencionar a los tiets, Jesu y Cami por estar siempre alrededor. Gracias César y Ombra por darme un hogar para la etapa final de la tesis en una primavera que no hubiese sido apta para estar bajo el puente.

Gracias lejanas al colectivo Vigués por ser tan majos y por la recarga de pilas que supone cada xuntanza, Textu, Lo, Lu, Palo, Pili, Ene, Ire, Tore… y unos cuantos más. A las asturianinas por ayudar

también a cargar las pilas, Noe, Lola… Gracias también al sector Kiel, nos vemos poco pero siempre es super güay, Miguel, Sonia (ànims noia, que hi ha llum al final del tunel!!), Mariona, Aurelié. Von “Kiel” auch, ich danke Marcus und een dike knuffe aam Natasja voor de vee opbeurende mails.

Mens sana in corpore sano, gracias a los colectivos de baloncesto, mi gente INMA y BAM. Ha estat genial descarregar tesi-tensió jugant a bàsquet amb vosaltres i fent soparets i activitats lúdico-festives.

Gracias a mis papis por tantos ánimos al otro lado de la línea telefónica. A Dani por sus preguntas claves “qué, ¿acabaste ya?”, y a Olga por muchas más horas al aparato.

Esta parte es dura, tengo que dividir la comunidad, el poder de tres en dos. Pero ¡son poderosas y sobrevivirán! Gracias a Piper (Toli) y Prue (Marino) por darme habichuelas con tomate para cenar (y otros cosas más ricas también) y por cuidarme tanto.

Hacer una tesis tiene su mérito, pero ser pareja de tesinandos creo que tiene más. Muchísimas gracias Nacho, por ser el mejor. Por tirarme un flotador cuando nadaba en el mar de la duda, por los coulants de chocolate y la pasta fresca, por cada cinco minutines, y lo más importante, por darme tu cariño y tu amor siempre.

La pecunia es muy importante para llegar al final de una tesis. Agradezco la financiación por parte del Ministerio de Educación y Ciencia (beca: BES-2003-1530, proyecto: REN-2002-01958), también a NERC por apoyo al “Agulhas Leakage Project”, a la fundación Comer Abrupt Cimate Change (EEUU), al ICTA por su beca puente y a la revista Glamour por concederme una de sus becas de postgrado que me ha permitido llegar al final del trayecto y de mes.

I also acknowledge the International Marine Global Changes program (IMAGES) and the Insitut Polaire Français (IPEV), particularly Yvon Balut for making the sediment cores available for this study.

Como última seña en esta parte de agradecimientos me gustaría decir que si me he olvidado de alguien no es porque sea menos importante para mí sino que es consecuencia de las neuronas perdidas en el proceso “tesis”, mis disculpas con antelación.

Abstract

The current climatic situation, with temperatures likely rising as a consequence of human-induced increase of greenhouse gas concentrations in the atmosphere is promoting an enhanced interest in the global climate system, its characteristics, functioning and natural variability. The past provides keys on the natural variability that allow the calibration and validation of state-of-the-art Global Climate Models in which expectations are set to predict future changes. Marine sediment records provide very valuable archives of past ocean circulation and climate variability. This Thesis is embedded in the search of knowledge of past climate variability.

The Southern Hemisphere has traditionally been considered a passive player in the oceanic and climate changes while paleocenographic research and numerical model simulations increasingly are emphasizing that it plays an important role, both in global circulation changes and in defining the state of Earth's climate.

A key region for the global circulation system is found in the neighbourhood of southern Africa. Here, surface and thermocline Indian Ocean Waters are transferred to the South Atlantic by rings and filaments of the South Indian Western Boundary Current, the Agulhas Current. At depth, the water transfer occurs in the opposite direction, with North Atlantic Deep Water (NADW) leaving the Atlantic basin and entering the Indian. The input of warm, salty Agulhas Waters to the South Atlantic is thought to influence the far distant North Atlantic by way of buoyancy perturbation, hence, being crucial for the mode and stability of the Atlantic Meridional Overturning Circulation (MOC).

In this Thesis I present 345,000-year-long records of planktonic and benthic foraminifera stable isotope, benthic Cd/Ca, planktonic Mg/Ca, sortable silt ($\overline{\text{SS}}$) and foraminiferal census counts for the penultimate glacial period from a spliced record of two mid-depth (~2500 m) sediment cores from the Agulhas Bank Slope (off South Africa). The records allow deciphering the past surface and deep circulation in the area and assessing the linkage between both, the surface flux of Indian waters towards the Atlantic and the deep flux of Atlantic waters towards the Indian Ocean.

The Atlantic deep circulation is thought to have been different during the Last Glacial Maximum (LGM), with NADW being replaced by an intermediate water mass, the so called Glacial North Atlantic Intermediate Water (GNAIW) and Southern Component Waters (SCW) spreading further north and bathing the Atlantic basin to shallower depths. We find evidence that the deep circulation during periods of the previous two glacial stages, i.e. during middle Marine Isotope Stages (MIS) 6 and 8 was similar to that of the LGM with strong presence of SCW at our site.

At the same time, we find indications that SCW was a mixture of an Upper well-ventilated component (USCW) and lower poorly ventilated one (LSCW). On the contrary, during early glacial phases of both, MIS 6 and 8, the deep Atlantic circulation was plausibly not much different from today's. This, in conjunction with values of the surface records similar to present ones, indicates presence of Agulhas Water at the core sites and suggests a persistence of the modern-type linkage between Agulhas Leakage and MOC. From these similar to interglacial values at the initiation of the

glacial periods, the surface records display increasing trends reaching maximum values well before glacial Terminations and collapsing to interglacial levels as the warm periods MIS 5e, 7e and 9c are reached. This is particularly evident during MIS 6.

Previous studies (e.g. Peeters et al., 2004) and numerical models (e.g. Knorr and Lohman, 2003) show a prominent presence of Agulhas Waters in the South Atlantic during glacial Terminations and suggest that the warm and salty input could have been pivotal for the reestablishment of interglacial climate conditions. Our records support this contention as maximum presence of Agulhas Waters occurs in parallel with the recovery to interglacial levels of the deep circulation records. It is possible that the collapse of Agulhas Waters at the beginning of interglacial periods indicates the reestablishment of a modern-type mode of Agulhas Water Leakage through Rings and the release of warm saline waters stored in the Indian Ocean.

Intriguingly, during MIS 2 and mid-glacial MIS 6 and 8, the surface circulation proxies record a strong presence of Agulhas Waters while SCW was dominating the deep hydrography.
This indicates that at these times either the prominent presence of Agulhas Waters was unable to efficiently generate a buoyancy anomaly in the South Atlantic or that other factors were able to overcome the salt anomaly imposed by the Agulhas Waters in the South Atlantic, for instance North Atlantic climatology.

Resumen

La situación climática actual, con temperaturas probablemente aumentando como consecuencia de los incrementos en las concentraciones de gases de efecto invernadero de origen antrópico, está promoviendo un interés creciente por el sistema climático global, sus características, funcionamiento y variabilidad natural. El pasado ofrece claves sobre la variabilidad natural que permiten la calibración y validación de Modelos Climáticos Globales de última generación en los que hay puestas muchas expectativas para predecir cambios futuros. Los registros sedimentarios marinos ofrecen archivos muy valiosos de la circulación oceánica pasada y de las variaciones climáticas. Esta Tesis se enmarca en la búsqueda de conocimiento sobre la variabilidad climática pasada.

El Hemisferio Sur ha sido tradicionalmente considerado un actor pasivo en los cambios oceánicos y climáticos, sin embargo, investigaciones paleocenográficas y simulaciones numéricas están haciendo cada vez más patente que desempeña un papel importante, tanto en los cambios de la circulación global como en la definición del estado climático de la Tierra.

Una región clave para el sistema de circulación global se encuentra en la región alrededor de Sudáfrica. En dicha región, aguas superficiales y de termoclina del Océano Índico son transferidas al Atlántico Sur a través de anillos y de filamentos de la Corriente de Frontera Oeste de Océano Índico, la Corriente de Agulhas. En profundidad, la transferencia de agua se produce en la dirección opuesta, con Agua Profunda del Atlántico Norte (*North Atlantic Deep Water*, NADW), abandonando la cuenca atlántica y entrando en la índica. La entrada de aguas cálidas y saladas de Agulhas al Atlántico Sur se cree que puede influir en el distante Atlántico Norte a través de perturbaciones en los balances de flotabilidad, siendo por ello crucial para el modo y la estabilidad del Circulación Meridional Atlántica (*Meridional Overturning Circulation*, MOC).

En esta Tesis presento registros de 345.000 años de isótopos estables de foraminíferos planctónicos y bentónicos, Cd/Ca de bentónicos, Mg/Ca de planctónicos, granoclasificación de arcillas (*sortable silt*, $\overline{\text{SS}}$) y censos de foraminíferos del penúltimo período glacial de un registro combinado de dos testigos de sedimento de profundidades medias (~ 2500 m) recuperados en el talud del Banco de Agulhas (aguas adentro de Sudáfrica). Los registros permiten discernir la circulación superficial y profunda pasada en la zona y evaluar la conexión entre el flujo superficial de aguas índicas hacia el Atlántico y el flujo de aguas profundas del Atlántico hacia el Índico.

La circulación profunda del Atlántico se cree que fue diferente durante el Último Máximo Glacial (*Last Glacial Maximum*, LGM), con NADW siendo sustituida por una masa de agua intermedia, la llamada Agua Intermedia del Atlántico Norte (*Glacial North Atlantic Intermediate Water*, GNAIW) y con Aguas de Componente Sur (*Southern Component Water*, SCW) expandiéndose más hacia el norte e invadiendo la cuenca a menores profundidades. Hemos encontrado evidencias de que la circulación profunda durante partes de los dos períodos glaciales anteriores, es decir, durante las partes intermedias de los Estadios Isotópicos Marinos (*Marine Isotope Stages*, MIS) 6 y 8 era similar a la del LGM con una fuerte presencia de SCW en nuestro región de estudio.

Asimismo, encontramos indicios de que la SCW es una mezcla de una masa de agua superior bien ventilada (*Upper Southern Component Water,* USCW) y una inferior mal ventilada (*Lower Southern Component Water*, LSCW). Por el contrario, durante las fases iniciales de ambos períodos glaciales, i.e. MIS 6 y 8 tempranos, la circulación profunda del Atlántico probablemente no difería substancialmente de la actual. Esto, conjuntamente con valores de los registros de superficie similares a los actuales sugiere una persistencia en el modo de conexión entre la transferencia de aguas de Agulhas y la MOC similar al actual. Desde estos valores semejantes a los interglaciales en los períodos glaciales tempranos, los registros superficiales muestran tendencias crecientes, alcanzando sus niveles máximos mucho antes de las Terminaciones y colapsando a los niveles interglaciales al entrar en los períodos cálidos MIS 5e, 7e y 9c. Esto es particularmente evidente durante MIS 6.

Estudios previos (p. ej., Peeters et al., 2004) y modelos numéricos (p. ej., Knorr y Lohman, 2003) muestran una presencia considerable de aguas de Agulhas en el Atlántico Sur durante las Terminaciones glaciales y sugieren que esta entrada de aguas cálidas y saladas podría haber sido fundamental para el restablecimiento de las condiciones de clima interglacial. Nuestros registros apoyan este postulado ya que la máxima presencia de aguas de Agulhas ocurre en paralelo con la recuperación de niveles interglaciales en los registros de circulación profunda. Es posible que el colapso de aguas de Agulhas al comienzo de los periodos interglaciales indique el restablecimiento de un modo moderno de conexión entre el *leakage* de aguas de Agulhas a través de anillos y la liberación de aguas cálidas y saladas acumuladas en el Océano Índico.

Curiosamente, durante el MIS 2 y las partes intermedias de los períodos glaciales MIS 6 y 8, los indicadores de circulación superficial registran una fuerte presencia de aguas de Agulhas a la vez que la SCW dominaba la hidrografía profunda. Esto indicaría que en estos momentos, o bien la fuerte presencia de aguas de Agulhas no podría generar de modo eficiente una anomalía de flotabilidad en el Atlántico Sur o bien que otros factores, por ejemplo, la propia climatología del Atlántico Norte, podrían prevalecer sobre la anomalía de salinidad impuesta por las aguas de Agulhas en el Atlántico Sur.

Resum

L'actual situació climàtica, amb un increment de les temperatures probablement conseqüència de l'augment de les concentracions atmosfèriques de gasos d'efecte hivernacle d'origen antròpic, està promovent un creixent interès en el sistema climàtic global, les seves característiques, funcionament i variabilitat natural. El passat conté claus sobre la variabilitat natural que permeten la calibració i validació de Models Climàtics Globals d'última generació en els quals recauen moltes expectatives per a la predicció dels canvis futurs. Els registres sedimentaris marins són uns arxius molt valuosos que contenen informació sobre la circulació oceànica del passat i la variabilitat climàtica. Aquesta Tesi s'emmarca en la recerca del coneixement sobre la variabilitat climàtica passada.

Tradicionalment, a l'Hemisferi Sud se li ha assignat un rol passiu en els canvis oceànics i del clima, però actualment les investigacions paleoceanogràfiques i les simulacions amb models numèrics revelen que té un paper important tant en els canvis de la circulació global com a l'hora de definir l'estat del clima a la Terra.

Una regió clau per a la circulació global es troba al voltant del sud d'Àfrica. Aquí, les aigües superficials i de termoclina de l'Oceà Índic es transfereixen cap a l'Atlàntic Sud per mitjà d'anells i filaments del Corrent del Marge Oest de l'Índic Sud, el Corrent d'Agulhas. En profunditat, la transferència d'aigua ocorre en sentit invers, ja que l'Aigua Profunda de l'Atlàntic Nord (*North Atlantic Deep Water*, NADW) abandona la conca Atlàntica per entrar a l'Índica. Es creu que l'input d'aigües càlides i salines del Corrent d'Agulhas a l'Atlàntic Sud influeix el distant Atlàntic Nord per efecte de la perturbació de la flotabilitat, esdevenint d'aquesta manera un input clau per a l'estat i l'estabilitat de la Circulació Meridional Atlàntica (*Atlantic Meridional Overturning Circulation*, MOC).

En aquesta Tesi presento registres de 345.000 anys amb dades d'isòtops estables de foraminífers bentònics i planctònics, Cd/Ca de bentònics, Mg/Ca de planctònics, granoclassificació d'argiles (*sortable silt*, $\overline{\text{SS}}$) i censos de foraminífers per al penúltim període glacial. El registre prové de la unió de dos testimonis sedimentaris de profunditats mitjanes (~2500 m) obtinguts al talús d'Agulhas (*Agulhas Bank Slope*), prop de Sud-àfrica i permet desxifrar la circulació superficial i profunda pretèrita en aquesta àrea, així com avaluar la connexió entre el flux superficial d'aigües de l'Índic cap a l'Atlàntic i el flux profund d'aigües atlàntiques cap a l'Oceà Índic.

Es creu que la circulació profunda de l'Atlàntic tenia una configuració diferent durant l'Últim Màxim Glacial (*Last Glacial Maximum*, LGM), on les Aigües Intermitges del Nord Atlàntic Glacial (*Glacial North Atlantic Intermediate Water*, GNAIW) reemplaçaven la NADW i on les Aigües de Component Sud (*Southern Component Water*, SCW) arribaven a latituds més altes i banyaven la conca Atlàntica a menys profunditat. Hem trobat evidències que indiquen que la circulació profunda durant els dos estadis glacials previs, es a dir, en el període central dels Estadis Isotòpics Marins (*Marine Isotope Stages*, MIS) 6 i 8, era semblant a la circulació del LGM, amb una presència important de SCW al nostre lloc d'estudi.

Alhora, hem trobat indicis que la SCW era una barreja d'un component somer ben ventilat (*Upper Southern Component Water*, USCW) i un component profund poc ventilat (*Lower Southern Component Water*, LSCW). En canvi, a l'inici de les fases glacials dels MIS 6 i 8, la circulació profunda de l'Atlàntic era possiblement molt similar a l'actual. Tot això, unit als valors dels registres de superfície, els quals presenten nivells molt semblants als actuals, indica la presència d'aigües d'Agulhas en els llocs d'estudi i suggereix la persistència de la connexió entre la transferència d'aigua d'Agulhas i la MOC de manera semblant a l'actual. Partint d'aquests valors, similars als interglacials, a l'inici dels períodes glacials, els registres de superfície mostren una tendència a l'augment, arribant als màxims valors força abans de les Terminacions glacials, i posteriorment decauen a nivells interglacials quan s'assoleixen els períodes càlids corresponents als MIS 5e, 7e i 9c. Aquest patró és particularment evident durant el MIS 6.

Estudis previs (p.e. Peeters et al., 2004) i models numèrics (p.e. Knorr and Lohman, 2003) indiquen la presència de les Aigües d'Agulhas a l'Atlàntic Sud durant les Terminacions glacials i suggereixen que l'input d'aigües càlides i salines podria haver estat crucial per al restabliment de les condicions climàtiques interglacials. El nostre registre dóna suport a aquest argument, ja que la presència màxima d'Agullas es registra en paral·lel a la recuperació dels nivells de circulació profunda fins a valors típics interglacials. És possible que el col·lapse de les aigües d'Agulhas a l'inici dels períodes interglacials indiqui el restabliment del sistema de transferència d'aigua d'Agulhas mitjançant anells i la mobilització d'aigües càlides i salines provinents de l'Oceà Índic, tal com ocorre actualment.

Curiosament, durant l'estadi MIS 2 i els mig-glacials MIS 6 i MIS 8, els proxies de circulació superficial registren una presència important d'Aigües d'Agulhas, mentres que la SCW domina la hidrografia profunda. Això indica que en aquest període o bé les Aigües d'Agulhas no podien generar l'anomalia en la flotabilitat a l'Atlàntic Sud o bé que altres factors, com ara la climatologia de l'Atlàntic Nord, podien compensar l'anomalia imposada per les aigües d'Agulhas a l'Atlàntic Sud.

1. Introducción

"…whereas all experiences are of the past, all decisions are about the future…it is the great task of human knowledge to bridge this gap and find those patterns in the past which can be projected into the future as realistic images…" Kenneth Boulding (1973).

Existen cada vez más pruebas, y más irrefutables, de que las actividades humanas, y más específicamente las emisiones crecientes de gases de efecto invernadero (GHG, *Greenhouse Gases*) desde la revolución industrial, tienen un efecto sobre el sistema climático a nivel planetario. Así, en el "Intergovernmental Panel on Climate Change (IPCC) Fourth Assessment Report (AR4)" aprobado el 17 de Noviembre de 2007 en Valencia (España) se establece que:

> *El calentamiento del sistema climático es inequívoco, como evidencian ya los aumentos observados del promedio mundial de la temperatura del aire y del océano, el deshielo generalizado de nieves y hielos, y el aumento del promedio mundial del nivel del mar.*
>
> *Las emisiones mundiales de GHG por efecto de actividades humanas han aumentado, desde la era preindustrial, en un 70% entre 1970 y 2004.*
>
> *Con un grado de confianza muy alto, el efecto neto de las actividades humanas desde 1750 ha sido un aumento de la temperatura.*
>
> *Las influencias humanas:*
>
> - *Muy probablemente han contribuido al aumento del nivel del mar durante la segunda mitad del siglo XX.*
> - *Probablemente han contribuido a alterar las pautas eólicas, afectando el recorrido de las tempestades extratropicales y las pautas de temperatura.*
> - *Probablemente han elevado la temperatura de las noches extremadamente cálidas, de las noches frías y de los días fríos.*
> - *Más probable que improbable, se han intensificado el riesgo de olas de calor y han incrementado la superficie afectada por la sequía desde los años 70 y la frecuencia de las precipitaciones intensas.*

En este contexto de creciente preocupación por el clima a nivel global y por la comprensión de su sensibilidad y vulnerabilidad, la paleoclimatología juega un papel muy importante y ha ido ganando importancia en los sucesivos informes del IPCC. Esta disciplina científica ha permitido poner sobre el nivel de base natural los niveles actuales de GHG y ver que no sólo exceden los niveles típicos de eras interglaciales sino que la tasa de cambio es muy elevada (Fig. 1-1). Por ejemplo, de forma natural los mayores y más abruptos cambios en las concentraciones de CO_2 ocurren durante las Terminaciones glaciales (paso de una época glacial a una interglacial) con una tasa de cambio aproximada de 0,01 ppmv/a. El ritmo de aumento de CO_2 actual es de 1,37 ppmv/a (Keeling y Whorf, 2005).

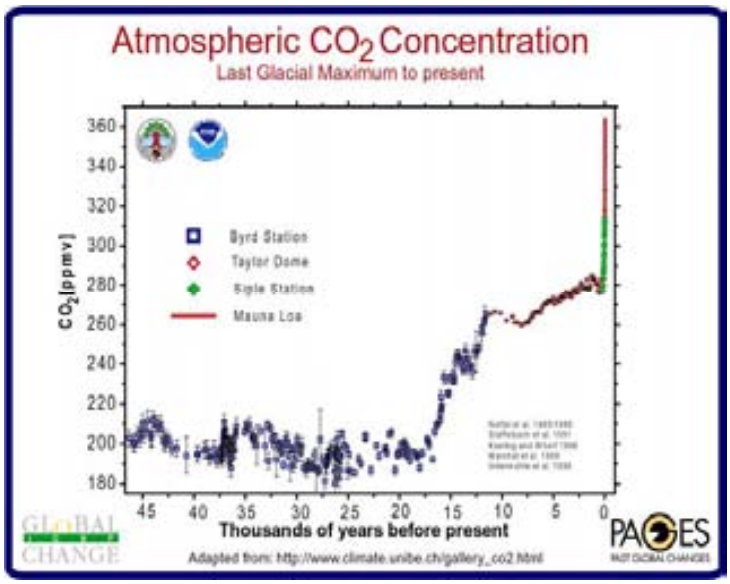

Figura 1-1 Variaciones en la concentración de CO_2 atmosférico durante los últimos 45.000 años reconstruidas a partir de medidas experimentales, registro de Mauna Loa, Hawaii, o "*Curva de Keeling*" (en rojo), medidas en testigos de hielo antárticos: Estación Siple (verde), Estación Domo Taylor (rombos rojos), Estación Byrd (azul).

Recientemente se han completado, entre otras, las mediciones de las concentraciones de CO_2 en el testigo de hielo Antártico EPICA Domo Concordia (EDC, Lüthi et al., 2008). Este registro ha permitido extender las reconstrucciones ya existentes, por ejemplo de los Testigos Domo Taylor (Indermühle et al., 1999), Vostok (Barnola et al., 1987; Petit et al., 1999), Domo Fuji (Kawamura et al., 2003); hasta los últimos 800.000 años (Lüthi et al., 2008) y demostrar que durante ese extenso período de tiempo las variaciones de CO_2 se mantenían de forma natural dentro del rango 172-300 ppmv (Fig. 1-2). Además, dichas variaciones han sido coherentes con cambios en la temperatura sobre el continente helado y por ende, a nivel general, en la Tierra lo cual sugiere que existe una conexión entre las variaciones de CO_2 y de temperatura.

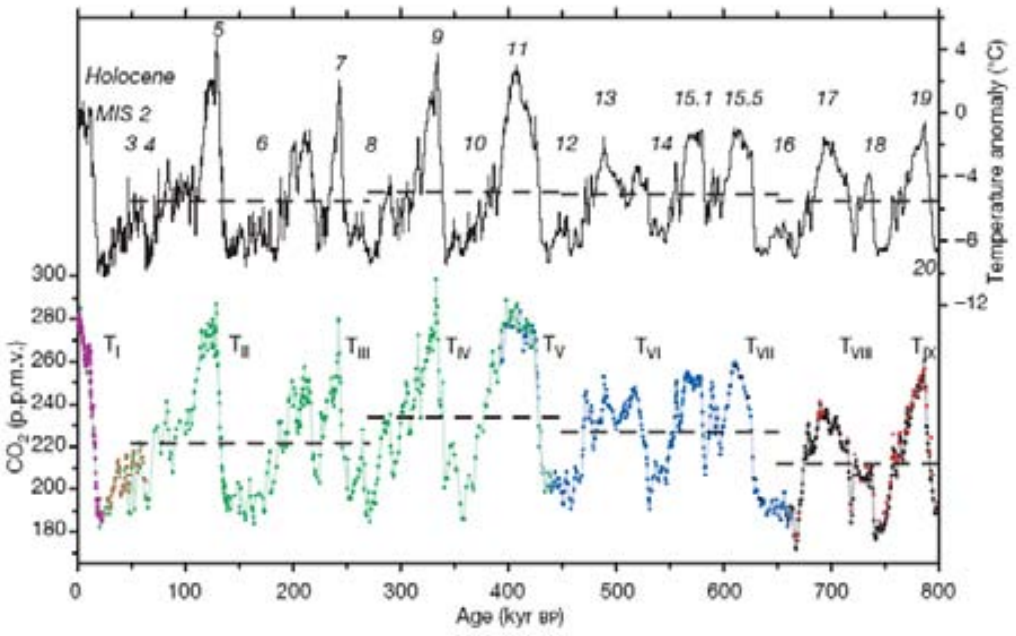

Figura 1-2 Compilación de registros de CO_2 (figura inferior) y anomalía de temperatura con respecto a la temperatura media del último milenio del testigo de hielo EPICA Domo C (figura superior) a lo largo de los últimos 800.000 años (Lüthi et al., 2008). La compilación de CO_2 se ha hecho con datos del testigo EPICA Domo C (lilas y azules, Siegenthaler et al., 2005; círculos rojos y negros, Lüthi et al., 2008), Domo Taylor (marrón, Indermühle et al., 1999) y Vostok (verde, Petit et al., 1999). Las líneas horinzotales indican valores promedio para los períodos 799–650, 650–450, 450–270 and 270–50 ka BP (miles de años antes del presente). Los estadios isotópicos marinos (*Marine Isotope Stage*, MIS) se indican en la figura superior y las Terminaciones glaciales (T) en la inferior.

1.1. El Papel de la Circulación Oceánica Global en el Clima

Los océanos juegan un papel primordial en el clima de la Tierra. Ello es debido a su capacidad para almacenar y transportar calor, agua dulce y carbono en un amplio rango de escalas espaciales y temporales. Además de su papel regulador en el clima los océanos constituyen el mayor reservorio de carbono rápidamente disponible del planeta, 40.000 GtC frente a 750 GtC de la atmósfera y 2.200 GtC terrestres, lo cual les confiere aún una mayor importancia en el esquema climático global.

A menudo se utiliza el término Circulación Termohalina (*Thermohaline Circulation*, THC) para referirse a la circulación oceánica global. Sin embargo, existen varias evidencias que sugieren que los principales mecanismos que mueven la circulación oceánica global no son las diferencias de temperatura y salinidad de las masas de agua, sino que son forzamiento por los vientos y procesos de mezcla en el interior del océano debido a mareas profundas y *eddies* (Wunsch, 2002; Wunsch y Ferrari, 2004; Kuhlbrodt et al., 2007). La convección de aguas profundas por sí sola conduciría a una especie de estanque de agua fría y estática (Munk y Wunsch, 1998). De todas maneras, las fuentes de flotabilidad superficial, sin ser los conductores de la circulación global, tienen una gran influencia en los transportes de calor y salinidad ya que determinan la densidad de las aguas que potencialmente se hundirán (Wunsch, 2002) y ambos, i.e. fuentes de flotabilidad superficial y densidad de aguas intermedias y profundas, determinan el modo en que la circulación global se encuentra en un determinado momento. De hecho, la producción de aguas profundas es muy sensible a pequeños cambios de salinidad en sus precursores superficiales. Por ejemplo, utilizando un modelo numérico de la Circulación Meridional (*Meridional Overturning Circulation*, MOC), Rahmstorf (1995) encontró que variaciones en el flujo de agua dulce hacia el Atlántico Norte de ±0,1 Sv podían detener o iniciar la convección de 14 Sv a profundidad.

El término *Meridional Overturning Circulation* es frecuentemente utilizado, si bien en sentido estricto este término es geográfico, meramente descriptivo. MOC se refiere a la circulación en un plano vertical meridional determinada por una función de corriente (Kuhlbrodt et al., 2007) y no hace ninguna alusión a sus mecanismos conductores.

Una representación de la circulación oceánica global altamente simplificado pero extensamente utilizado es el llamado "*Global Conveyor Belt*" (Broecker, 1987). Broecker (1987) acuñó este término para explicar las principales rutas de la circulación oceánica general basándose en Gordon (1986) como una gran cinta transportadora de agua, salinidad y calor. La Figura 1-3 ofrece una representación más detallada que el retrato inicial propuesto por Broecker (1987).

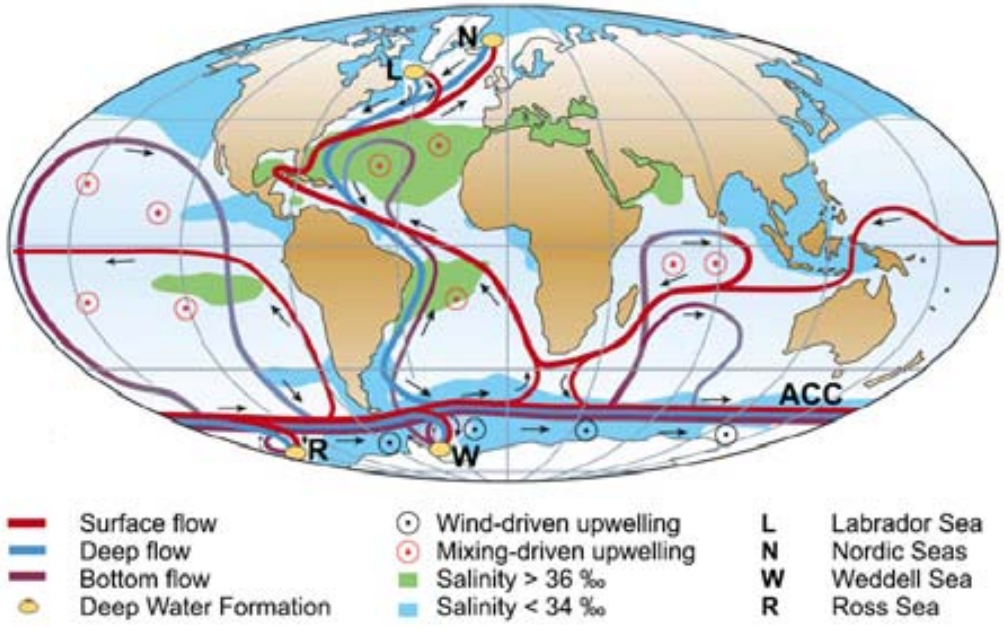

Figura 1-3 Esquema simplificado de la circulación oceánica global. L y N representan lugares de formación de aguas profundas, concretamente L se refiere a la región de formación de Agua Profunda de Labrador (*Labrador Deep Water*, LDW) y N a la formación de Agua de Fondo del Atlántico Norte (*North Atlantic Bottom Water*, NABW), cuando ambas se combinan constituyen la conocida como Agua Profunda del Atlántico Norte (*North Atlantic Deep Water*, NADW). W y R se refieren a las regiones de formación de Agua de Fondo Antártica (*Antarctic Bottom Water*, AABW) en los mares de Weddell y Ross. ACC de sus siglas en inglés (*Antarctic Circumpolar Current*) representa la Corriente Circumpolar Antártica (Kuhlbrodt et al., 2007, modificada de Rahmstorf 2002).

El ejemplo más ampliamente utilizado para ilustrar la importancia de la circulación oceánica global en el clima viene dado por registros paleoclimatológicos del último período glacial. Durante este período se observaron, primero en testigos de hielo de Groenlandia (Dansgaard et al., 1993) y después en registros sedimentarios del Atlántico (e.g. Bond, 1997; Cacho et al., 1999; Sanchez-Goñi et al., 2002) fluctuaciones del clima muy abruptas con temperaturas variando hasta 10ºC en escalas de tiempo decadales, i.e. en escala de tiempo humana. También en registros sedimentarios del Atlántico Norte se identificaron capas de material detrítico cuasi-periódicas, cada 7000 años aproximadamente, (Heinrich, 1988) que fueron más tarde relacionadas con descargas masivas de icebergs (Broecker et al., 1992). De este modo, durante el último período glacial se sucedieron una serie de períodos relativamente cálidos denominados Interestadiales (*Interstadials*) y fríos s.s., denominados Estadiales (*Stadials*), con eventos de descarga masiva de icebergs entre ellos. Hoy en día, el debate sigue abierto sobre los mecanismos exactos de descarga de "*Ice Rafted Detritus*" (IRD) y sobre su procedencia (mantos de hielo Laurentino *vs* Británico) (e.g. Hemming, 2004). Se cree que la circulación oceánica global puede haber tenido un papel fundamental en estos cambios de escala sub-orbital, bien como causante o bien como receptora y amplificadora.

Ahora, si bien todavía no está claro cual es el papel real de la MOC en estas oscilaciones climáticas rápidas, se han propuesto tres mecanismos de funcionamiento de la circulación oceánica en el Atlántico Norte para las distintas situaciones de cambio abrupto, i.e. i) eventos de Heinrich, descarga masiva de icebergs que promoverían un colapso en la convección de NADW (Fig. 1-4a), ii) Interestadial, circulación similar a la actual (Fig. 1-4c) con formación de aguas profundas en los mares Nórdicos (localizados entre Islandia, Groenlandia y Noruega) y de Labrador y con un transporte de

calor hacia el norte relativamente intenso (ver también Fig. 1-6c); iii) Estadial, en los que ocurriría una migración de los centros de convección hacia el sur y se reduciría la convección de aguas profundas y el transporte de calor hacia las altas latitudes del Atlántico Norte (Figs. 1-4b y 1-6b) (Sarnthein et al., 1994; Rahmstorf, 1996; Seidov y Maslin, 2001; Rahmstorf, 2002).

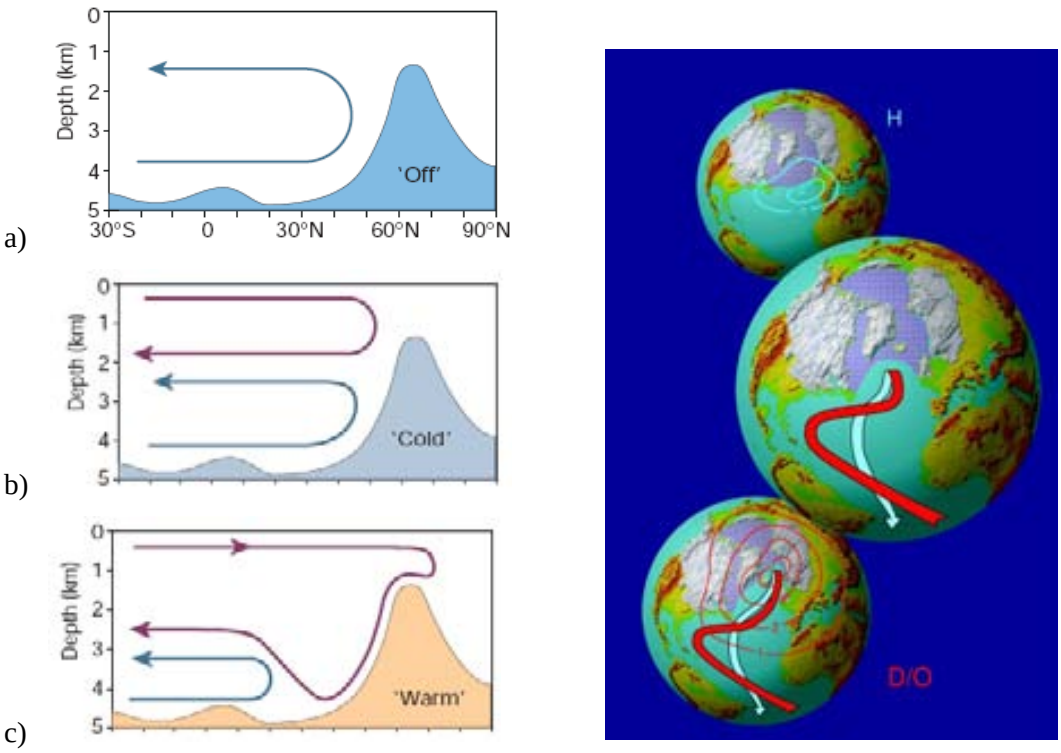

Figura 1-4 a) Evento de Heinrich, descarga masiva de icebergs, colapso en la convección de NADW; b) circulación durante Estadiales, convección menos intensa, aguas formadas no se hunden hasta el fondo del océano; c) circulación durante Interestadiales, semejante a la presente (Rahmstorf, 2002).

1.2. Asincronía entre los Hemisferios: *Bipolar Seesaw*

El reconocimiento de estos cambios abruptos en el Hemisferio Norte y su posible relación con la intensidad de formación, y eventualmente con el colapso de NADW ha dirigido la atención de la comunidad paleoclimática hacia el Atlántico Septentrional durante muchos años. Las regiones tropicales del planeta y las altas latitudes del Hemisferio Sur quedaban de lado en los estudios de variabilidad climática rápida y se las veía como receptoras pasivas de los posibles cambios acontecidos en el norte. Registros de temperatura de testigos de hielo de la Antártida mostraron que las variaciones climáticas en este continente ocurrían de forma más suave (calentamientos de unos 2ºC) y simétrica, mientras que los cambios abruptos registrados en Groenlandia son largamente asimétricos, con calentamientos muy abruptos y enfriamientos más suaves (ver Fig. 1-5). Bender et al. (1994) propusieron que las variaciones bruscas de temperatura se iniciaban en el Norte y se transmitían hacia el Sur, posiblemente a través de la MOC. Ambos factores, la menor amplitud de los calentamientos y la posibilidad de que resultasen como respuesta a cambios en el Hemisferio Norte, de nuevo parecían apuntar a un papel subyugado de las variaciones climáticas rápidas del Hemisferio Sur respecto a

aquellas del Norte. Sin embargo, a partir de análisis isotópicos de foraminíferos planctónicos y bentónicos de un testigo sedimentario del Atlántico Sur, Charles et al. (1996) postularon que las variaciones climáticas del Hemisferio Norte sucedían a las del Hemisferios Sur en unos 1,5 ka. La sincronización de los modelos de edad de testigos de hielo de Groenlandia y de la Antártida a través del CH_4 contenido en burbujas en ambos testigos (Blunier et al., 1998; Blunier y Brook, 2001) reveló que efectivamente, los calentamientos en la Antártida preceden a sus equivalentes en Groenlandia en 1-2,5 ka. Los resultados de Blunier et al. (1998) han sido recientemente corroborados con la sincronización de los testigos de hielo antárticos EPICA Droning Maud Land (EDML) y EDC (EPICA Community Members, 2006) con el testigo de hielo de Groenlandia NGRIP (North Greenland Ice Core Project Members, 2004) (Fig. 1-5).

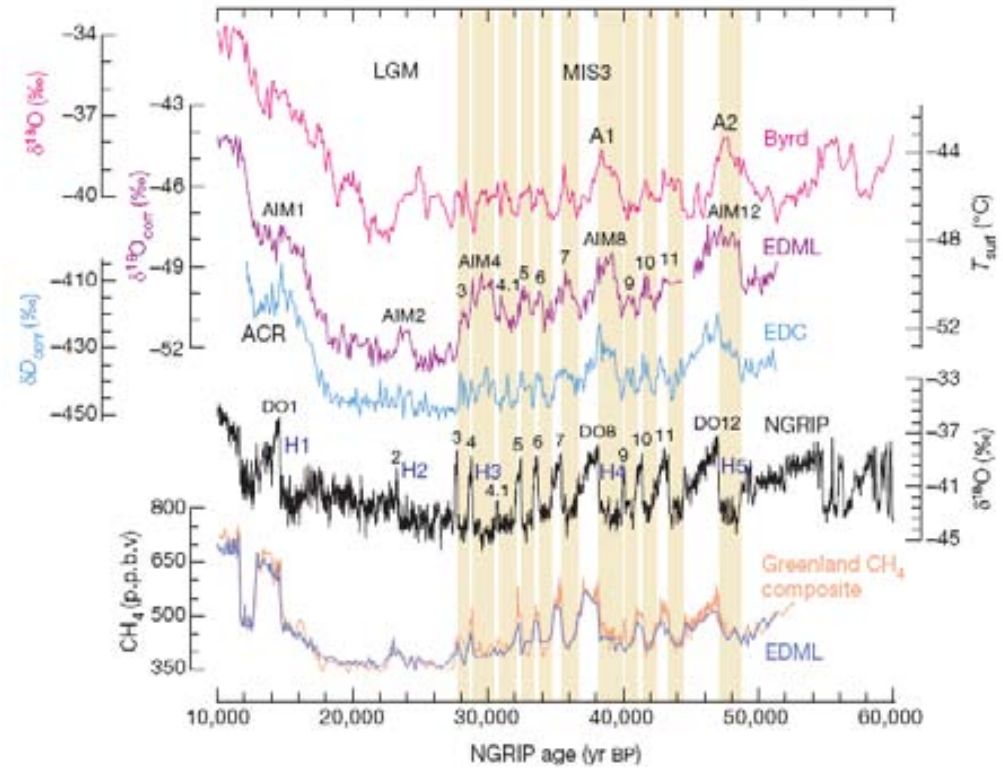

Figura 1-5 Períodos de calentamiento en la Antártida, testigos Byrd, EPICA Droning Maud Land, EPICA Domo C (EPICA Community Members, 2004, 2006), asociados con Estadiales en Groenlandia, testigo NGRIP (North Greenland Ice Core Project Members, 2004). Todos los registros están representados en sus escalas temporales sincronizadas a partir del CH_4 (EPICA Community Members, 2006). Las barras anaranjadas indican Estadiales en Groenlandia que están conectados con calentamientos en la Antártida. La ocurrencia de eventos de Heinrich en el Atlántico Norte también se indica (H) así como el LGM: *Last Glacial Maximum* (Último Máximo Glacial), MIS 3: *Marine Isotope Stage 3* (Estadio Isotópico Marino 3); DO: eventos de Dansgaard-Oeschger; ACR: *Antarctic Cold Reversal* (Inversión Antártica Fría); A: *Antarctic Warming* (Calentamiento Antártico); AIM: *Antarctic Isotope Maximum* (Máximo Isotópico Antártico).

En vista de la asincronía existente entre ambos hemisferios en lo que a variaciones climáticas abruptas se refiere, tal que cuando un hemisferio se calienta el otro se enfría, se buscaron mecanismos de conexión interhemisférica y se corroboró de forma independiente la teoría del "*Bipolar Seesaw*" (Broecker, 1998; Stocker, 1998) propuesta años antes por Crowley (1992). Este modelo conceptual para explicar la asincronía de temperatura entre ambos hemisferios se basa en la consideración de que la formación de aguas profundas en el Atlántico Norte es muy predominante respecto a otros focos de formación de aguas profundas (Broecker, 1998; Stocker, 1998). De tal modo que durante períodos de

intensa convección de aguas en el Atlántico Norte, que denominaremos de forma genérica "Aguas de Componente Norte" (*Northern Component Water*, NCW) este hemisferio "roba" calor del sur y de las zonas tropicales y calienta las latitudes altas del Atlántico Septentrional. Esta situación correspondería a un modo de la MOC similar al actual. Por otro lado, en períodos de pobre formación de aguas profundas en el Atlántico Norte la transferencia de calor desde el hemisferio sur disminuye, dicho hemisferio puede retener más calor calentándose mientras que las latitudes septentrionales entran en una fase fría. La Figura 1-6 ilustra los diferentes modos de transferencia de calor bajo distintos estados de convección de NCW (Seidov y Maslin, 2001), i.e. en diferentes estados de la MOC.

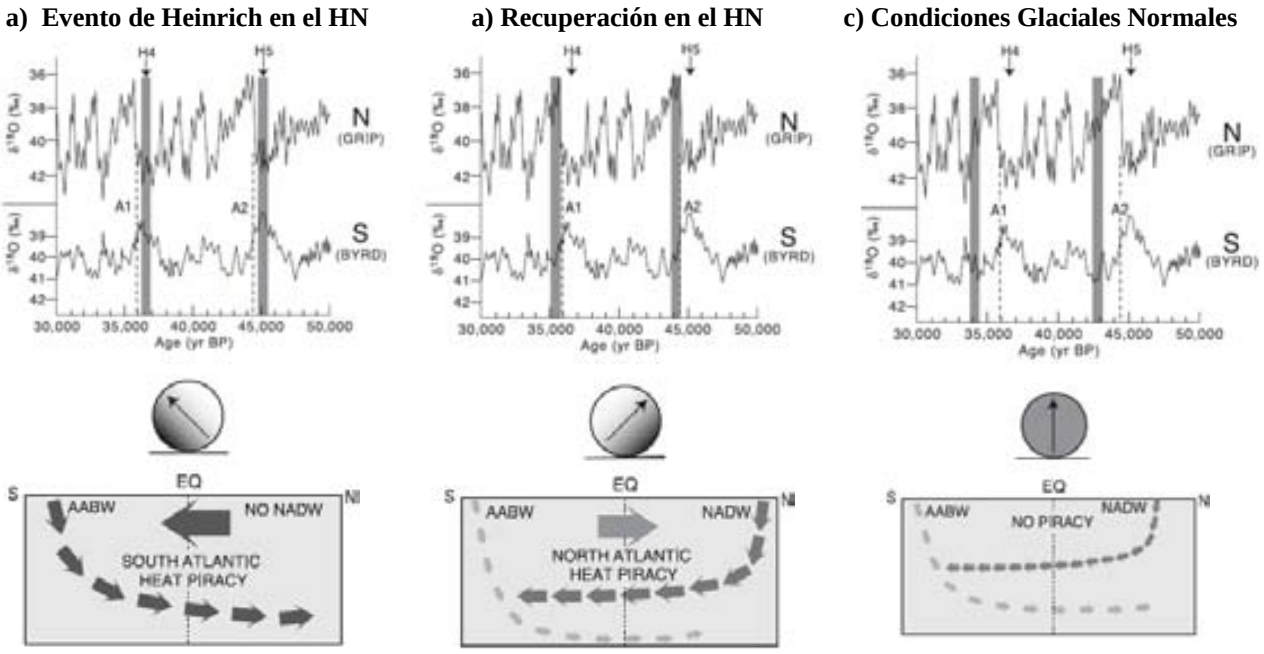

Figura 1-6 Representación del concepto de *Bipolar Seesaw* y robo de calor (Seidov and Maslin, 2001); a) modo de la MOC caracterizado por el colapso de NCW, el flujo de calor se invertiría respecto a la situación presente (ver también Fig. 1-4a); b) modo de la MOC ralentizado, con convección de NCW a menores profundidades y/o menor intensidad (ver también Fig. 1-4b); c) modo de la MOC similar al presente con intensa formación de NADW en el norte (ver también Fig. 1-4c).

Las causas y, especialmente, la dinámica de conexión asociados al concepto del *Bipolar Seesaw* no están claras. Knutti et al. (2004) proponen un reajuste del sistema por medio de ondas de Kelvin y Rossby en respuesta a eventos de descarga de agua dulce en el norte mientras que Keeling y Visbeck (2005) proponen cambios en la densidad de la ACC inducidos también por eventos de descarga de agua dulce en el norte que se transmitirían al Hemisferio Sur y que aumentarían el transporte de calor por *eddies* hacia el sur.

Para terminar de complicar la situación, distintos registros climáticos del Hemisferio Norte y Sur muestran variaciones climáticas durante el MIS 3 que son sincrónicas con uno u otro hemisferio. Völker et al. (2002) ofrecen una compilación de los mismos haciendo énfasis en el patrón de cambio que muestran (Fig. 1-7). Además, a partir de simulaciones con un Modelo de Circulación Atmosférica-Oceánica General (*Atmosphere-Ocean General Circulation*, AOGCM) Stouffer et al. (2007) encontraron distintas respuestas de la atmósfera y océano a perturbaciones por descargas de agua dulce en el norte y

sur; lo cual les hace sugerir que para llegar a interpretaciones climáticas correctas se debe tener muy en cuenta el origen de la señal que se está analizando, i.e. oceánica *vs* atmosférica o continental.

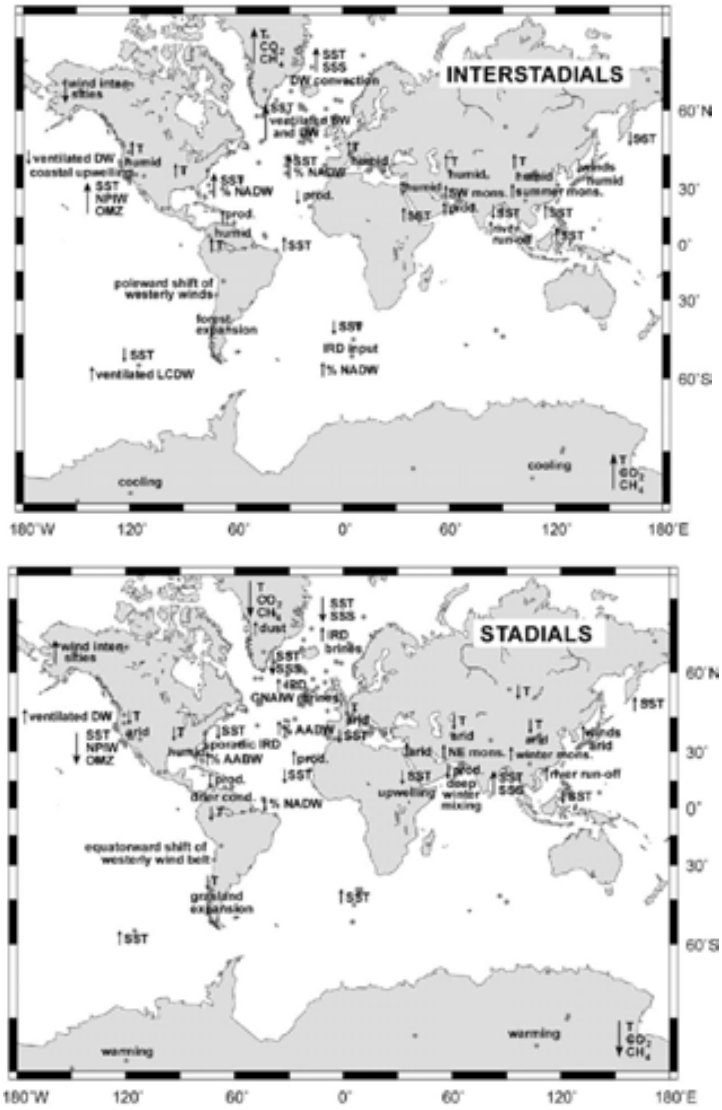

Figura 1-7 Patrones climáticos durante Interestadiales (figura superior) y Estadiales (figura inferior). La dirección y magnitud de las flechas indican las tendencias de los parámetros indicados para cada punto. T indica temperatura, SST temperatura superficial del mar (*Sea Surface Temperature*), SSS salinidad superficial del mar (*Sea Surface Salinity*), mons. Monzón (*monsoon*), prod. Productividad y cond. Condiciones, NPIW agua pacífica intermedia (*North Pacific Intermediate Water*), DW agua profunda (*Deep Water*), OMZ zona de mínimo oxígeno (*Oxygen Minimum Zone*) (Voelker, 2002).

Los fases y desfases entre registros climáticos ofrecen información sobre las relaciones de causa y efecto. El sistema climático es sensible a varios mecanismos de forzamiento y responde de forma no lineal, con mecanismos amplificadores acentuando algunos de los cambios esperados a priori. Conocer el origen y funcionamiento de las oscilaciones climáticas rápidas es importante para entender el clima de la Tierra pasado y futuro, especialmente para ser capaces de predecir cuándo, dónde y cómo pueden ocurrir cambios abruptos.

1.3. La "Ruta Cálida" (*Warm Water Route*) de Compensación de NADW

Además del concepto de *Bipolar Seesa*w, simulaciones numéricas (Weijer et al., 1999; 2001; 2002; Knorr and Lohmann, 2003, 2004) y estudios paleoclimáticos en el Hemisferio Sur (Charles et al., 1996; Flores et al., 1999; Rau et al., 2002; Pahnke et al., 2003; Peeters et al., 2004; Pahnke and Zahn, 2005; Piotrowski et al., 2005; Rau et al., 2006) están contribuyendo a demostrar que este hemisferio no es un mero actor pasivo en los cambios climáticos sino que juega un papel importante

pudiendo participar activamente en alguna de las variaciones climáticas más importantes, por ejemplo en las Terminaciones por medio del flujo de Aguas de la Corriente de Agulhas (Knorr y Lohmann, 2003; Peeters et al., 2004).

La Corriente de Agulhas ha emergido en las últimas tres décadas como una pieza clave en la circulación oceánica global (Gordon, 1986; 2003) ya que contribuye al flujo de retorno y compensación de NADW del "*Conveyor Belt*". Así, Gordon (1986) acentuaba su importante papel como parte de la rama superficial de la THC en el siguiente esquema simplificado de la misma (Fig. 1-8).

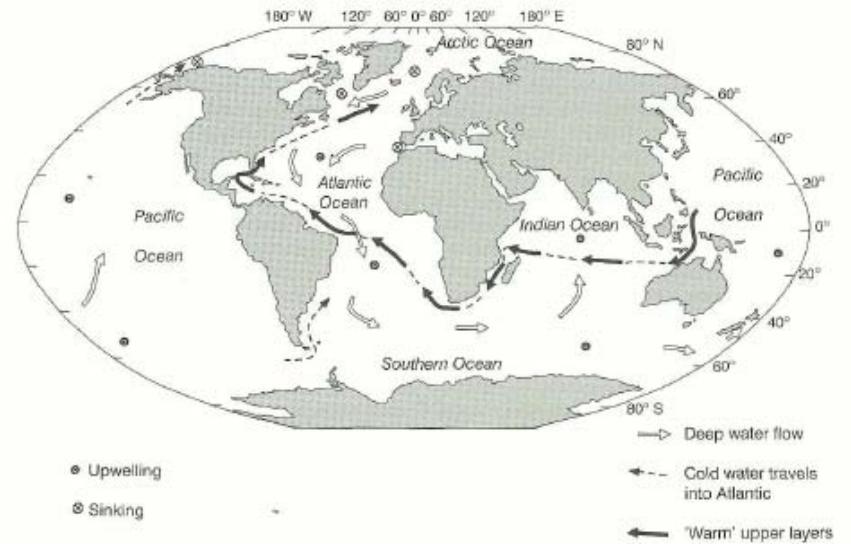

Figura 1-8 Esquema simplificado de la circulación oceánica global y el papel de la Corriente de Agulhas (Gordon, 1986).

La clave para explicar el importante papel que juega la Corriente de Agulhas se encuentra en la posición más septentrional del continente africano en comparación con América del Sur y con Oceanía (Lutjeharms, 2006 y referencias allí). Esta posición más septentrional permite que exista un flujo neto de aguas cálidas y salinas del Océano Índico al Atlántico (ver el Capítulo 3 para más detalles) que juega un papel primordial en los balances de salinidad y calor del océano receptor (e.g. Gordon, 1985; e.g. 1986; Gordon et al., 1992; Lutjeharms, 1996). El flujo no es continuo sino que ocurre por medio de Anillos y Filamentos de Agulhas (e.g. Lutjeharms, 1996) y, pese a que esta fuga (*leakage)* de aguas de Agulhas podría representar tan sólo un cuarto del flujo del retorno total del "*Conveyor Belt*" (Lutjeharms, 2006 y referencias allí), se le cree primordial para establecer el modo y estabilidad de la MOC (e.g. Weijer et al., 2001). Asumiendo la entrada de seis Anillos de Agulhas al año, van Ballegooyen et al. (1994) estima que la transferencia de calor y salinidad del Índico al Atlántico es de 0,045 PW y $78 \cdot 10^{12}$ kg de sal al año. Gordon et al. (1992) propusieron que la entrada de aguas de Agulhas podía generar una anomalía de salinidad en el Atlántico Sur de +(0,2-0,4) psu que jugaría un significativo papel en el establecimiento del modo y vigor de la formación de NADW. Más recientemente, simulaciones numéricas parecen indicar que el efecto de las aguas de Agulhas en la convección de NADW se debe a la anomalía de densidad y a los gradientes de presión a escala de cuenca atlántica y su subsiguiente desplazamiento septentrional por ondas barotrópicas y baroclínicas de Kelvin (Weijer et al., 1999; 2002).

En base a las características de las aguas transferidas alrededor del sur del continente africano, Gordon (1986) denomina a esta ruta de retorno de aguas "Ruta Cálida" (*Warm Water Route*) en contraposición a la "Ruta Fría" (*Cold Water Route*) que transfiere aguas frías y poco salinas del Pacífico al Atlántico a través del Estrecho de Drake (Fig. 1-9). Mientras que la importancia de la Ruta Cálida (Gordon, 1986; Saunders y King, 1995) respecto a la Ruta Fría (Rintoul, 1991; Schlitzer, 1996) todavía está en debate, recientemente se ha propuesto también la existencia de una "Ruta Fresca" (*Cool Water Rout*e) que trasmitiría aguas frescas y frías del Pacífico al Atlántico entre la Antártida y Tasmania pasando por el Océano Índico (Speich et al., 2001; 2002) aunque su importancia volumétrica sería menor. En última instancia es la proporción de aguas frías y frescas respecto a las cálidas y saladas lo que importa para los balances de salinidad y calor del Atlántico y para el vigor a nivel general de la circulación oceánica global (Gordon, 1997). En este aspecto, son necesarios muchos más estudios para averiguar la conexión entre variaciones en el transporte de aguas superficiales y de termoclina a través de cualquiera de las rutas y cambios en el ritmo e intensidad de convección de NADW.

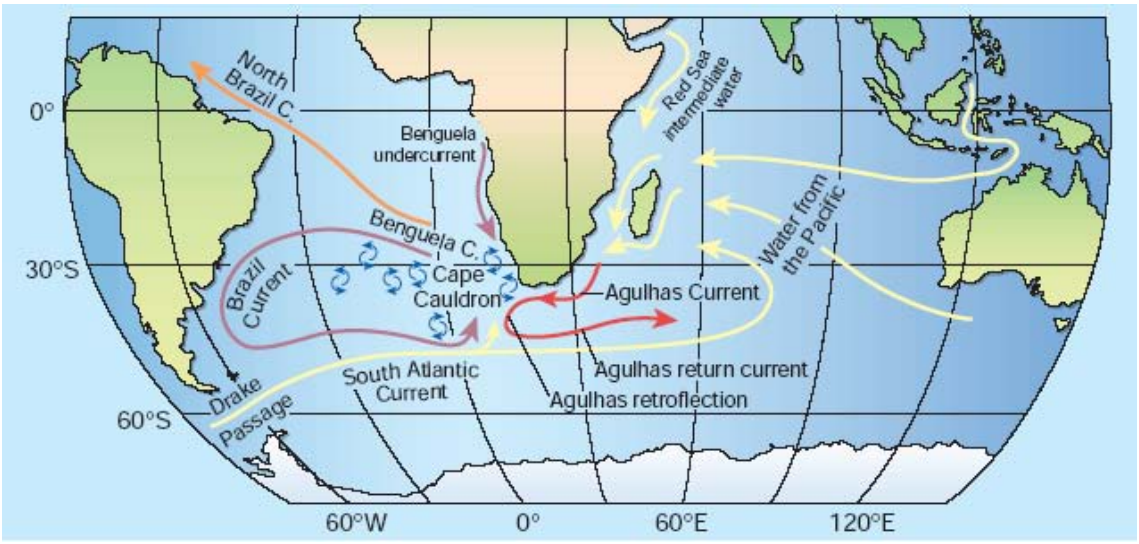

Figura 1-9 Rutas de Retorno "Tradicionales", i.e. Cálida (*Agulhas Current* y *Ring Shedding*) y Fría (a través del *Drake Passage*), de la rama superficial de la THC (Gordon, 2003).

Además de existir una transferencia de aguas entre los Océanos Índico y Atlántico en superficie, también existe una en profundidad. Ésta ocurre sin embargo en el sentido opuesto, del Atlántico hacia el Índico. El Atlántico intercambia agua profunda fría por agua cálida superficial. Gordon (1986) propuso la existencia de una relación directa entre la intensidad de ambos intercambios de tal modo que un transporte más intenso de aguas del Índico al Atlántico (en superficie) estimularía una formación de NADW más intensa la cual se traduciría en un mayor transporte de dicha agua profunda desde el Atlántico hacia el Índico y viceversa, una mayor producción de NADW requiere una compensación con aguas superficiales y de termoclina más intensa.

En los últimos 30 años el esfuerzo que se ha hecho por comprender la dinámica y variabilidad de la Corriente de Agulhas, así como su conexión con la THC, ha sido enorme como demuestran la ingente cantidad de artículos oceanográficos que se han publicado de la región (ver compilaciones por

Lutjeharms, 2006, 2007) y el creciente número de estudios paleoceanográficos (Flores et al., 1999; Rau et al., 2002; Peeters et al., 2004; Rau et al., 2006). Evidencias de la importancia de la Corriente de Agulhas en el pasado vienen dadas por simulaciones numéricas que indican un papel fundamental de la *Warm Water Route* (también de la *Cold Water Route*) en el desencadenamiento de los cambios climáticos que condujeron a la salida de los dos últimos períodos glaciales (Knorr y Lohmann, 2003). El estudio paleoceanográfico de Peeters et al. (2004) corrobora dicho importante papel de la Corriente de Agulhas en la recuperación de condiciones climáticas interglaciales durante los últimos 500.000 años. Estos autores encontraron un creciente influjo de especies de foraminíferos planctónicos típicas de los Anillos de Agulhas en un testigo del sector atlántico de África del Sur, por tanto indicando un mayor flujo de aguas de Agulhas hacia el Atlántico, con anterioridad a los momentos de máximo volumen de hielo y alcanzando los valores máximos durante las Terminaciones. Estudios anteriores habían encontrado evidencias similares (Giraudeau, 1998; Chang et al., 1999; Flores et al., 1999; Rau et al., 2002) lo cual apoya la conclusión de Peeters et al. (2004) de que el *leakage* de aguas de Agulhas puede haber sido un precursor vital para la salida de los estados glaciales.

En esta Tesis proporcionaremos evidencias adicionales de la importancia de la corriente de Agulhas para la circulación oceánica global.

1.4. Motivación y Objetivos

Esta tesis se engloba en el marco de ampliar nuestro conocimiento sobre el clima del pasado a fin de poder mejorar nuestras predicciones de cambio futuro, y más específicamente, en la búsqueda de incrementar nuestra comprensión sobre la variabilidad de la Corriente de Agulhas, su conexión con la MOC y por ende con el clima. Los principales objetivos de la investigación son:

- Generar registros de alta resolución, escala milenaria a centenal, de isótopos estables ($\delta^{18}O$ y $\delta^{13}C$) de foraminíferos bentónicos (*F. wuellerstorfi*) así como registros de escala milenaria de Cd/Ca de la misma especie a lo largo de los últimos 345.000 años, i.e. cubriendo los 3 últimos ciclos glacial-interglacial. El uso combinado de los registros facilitará la comprensión de la escena circulatoria profunda, pasada alrededor de Sudáfrica permitiendo discernir entre períodos de dominio de aguas de componente norte y sur.
- Generar registros de alta resolución, escala milenaria a centenal, de $\delta^{18}O$ y de Mg/Ca de foraminíferos planctónicos (*G. bulloides*), éste último con el fin de analizar la variabilidad de la temperatura superficial y, a través de la combinación de ambos registros, de la salinidad en la región y obtener así información sobre la mayor o menor presencia de aguas de Agulhas.
- Combinar las dos series de registros (planctónicos y bentónicos) a fin de establecer posibles conexiones entre momentos de mayor/menor presencia de aguas de Agulhas y mayor/menor intensidad de flujo en profundidad de NCW y por ende conocer el estado de la MOC.

References

Barnola, J.M., Raynaud, D., Korotkevich, Y.S. and Lorius, C., 1987. Vostok ice core provides 160,000-year record of atmospheric CO_2. Nature, 329, 408-414.

Bender, M., Sowers, T., Dickson, M.-L., Orchardo, J., Grootes, P., Mayewski, P.A. and Meese, D.A., 1994. Climate correlations between Greenland and Antarctica during the past 100,000 years. Nature, 372, 663-666.

Blunier, T. and Brook, E.J., 2001. Timing of Millennial-Scale Climate Change in Antarctica and Greenland During the Last Glacial Period. Science, 291, 109-112.

Blunier, T., Chappellaz, J., Schwander, J., Dällenbach, A., Stauffer, B., Stocker, T.F., Raynaud, D., Jouzel, J., Clausen, H.B., Hammer, C.U. and Johnsen, S.J., 1998. Asynchrony of Antarctic and Greenland climate change during the last glacial period. Nature, 394, 739-743.

Bond, G., Showers, W., Cheseby, M., Lotti, R., Almasi, P., deMenocal, P., Priore, P., Cullen, H., Hajdas, I. and Bonani, G., 1997. A pervasive millenial-scale cycle in North Atlantic Holocene and glacial climates. Science, 278, 1,257-1,266.

Broecker, W.S., 1987. The biggest chill. Natural History, 96, 74-82.

Broecker, W.S., 1998. Paleocean circulation during the last glaciation: a bipolar seesaw? Paleoceanography, 13 (2), 119-121.

Broecker, W.S., Bond, G.C., Klas, M., Clark, E. and McManus, J.F., 1992. Origin of the northern Atlantic's Heinrich events. Climate dynamics, 6, 265–273.

Cacho, I., Grimalt, J.O., Pelejero, C., Canals, M., Sierro, F.J., Flores, J.A. and Shackleton, N., 1999. Dansgaard-Oeschger and Heinrich event imprints in Alboran Sea paleotemperatures. Paleoceanography, 14 (6), 698-705.

Crowley, T.J., 1992. North Atlantic Deep Water Cools the Southern Hemisphere. Paleoceanography, 7 (4), 489-497.

Chang, Y.-P., Chang, C.-C., Wang, L.-W., Chen, M.-T., Wang, C.-H. and Yu, E.-F., 1999. Planktonic Foraminiferal Sea Surface Temperature Variations in the Southeast Atlantic Ocean: A High-Resolution Record MD96-2085 of the Past 400,000 Years from the IMAGES II - NAUSICAA Cruise. TAO, 10 (1), 185-200.

Charles, C.D., Lynch-Stieglitz, J., Ninnemann, U.S. and Fairbank, R.G., 1996. Climate connections between the hemispheres revealed by deep sea sediment core/ice core correlations. Earth and Planetary Science Letters, 142 (1-2), 19-27.

Dansgaard, W., Johnson, J.J., Clausen, B.H., Dahl-Jensen, D., Gundestrup, N.S., Hammer, C.U., Hvidberg, C.S., Steffensen, J.P., Sveinbjörndottir, A.E., Jouzel, J. and Bond, G., 1993. Evidence for a general instability of past climate from a 250 kyr ice-core record. Nature, 364, 218-220.

EPICA Community Members, 2004. Eight glacial cycles from an Antarctic ice core. Nature, 429, 623-628.

EPICA Community Members, 2006. One-to-one coupling of glacial climate variability in Greenland and Antarctica. Nature, 444, 195-198.

Flores, J.A., Gersonde, R. and Sierro, F.J., 1999. Pleistocene fluctuations in the Agulhas Current Retroflection based on the calcareous plankton record. Marine Micropaleontology, 37 (1), 1-22.

Giraudeau, J., Pierre, C. and Herve, L., 1998. A late quaternary, high -resolution record of plantonik foraminiferal species distribution in the southern Benguela region, Site 1987.

Gordon, A., 1986. Inter-Ocean exchange of thermocline water. Journal of Geophysical Research, 91 (C4), 5,037-5,046.

Gordon, A., 2003. The brawniest retroflection. Nature, 421, 904-905.

Gordon, A.L., 1985. Indian-Atlantic Transfer of Thermocline Water at the Agulhas Retroflection. Science, 227, 1,030-1,033.

Gordon, A.L., 1997. Which is it: Warm or Cold Route, or Maybe Both? International WOCE Newsletters, pp. 37-38.

Gordon, A.L., Weiss, R.F., Smethie, J.W.M. and Warner, M.J., 1992. Thermocline and intermediate water communication between the South Atlantic and Indian Oceans. Journal of Geophysical Research, 97, 7,223-7,240.

Heinrich, H., 1988. Origin and consequences of cyclic ice rafting in the northeast Atlantic Ocean during the past 130,000 years. Quaternary Research, 29, 142-152.

Hemming, S.R., 2004. Heinrich events: Massive late Pleistocene detritus layers of the North Atlantic and their global climate imprint. Reviews of Geophysics, 42, RG1005, doi:10.1029/2003RG000128.

Indermühle, A., Monnin, E., Stauffer, B., Stocker, T.F. and Wahlen, M., 1999. Atmospheric CO_2 concentration from 60 to 20 kyr BP from the Taylor Dome ice core, Antarctica. Geophysical Research Letters, 27, 735-738.

Kawamura, K., Nakazawa, T., Aoki, S., Sugawara, S., Fujii, Y. and Watanabe, O., 2003. Atmospheric CO_2 variations over the last three glacial-interglacial climatic cycles deduced from the Dome Fuji deep ice core, Antarctica using a wet extraction technique. Tellus, 55B, 126-137.

Keeling, C.D. and Whorf, T.P., 2005. Atmospheric CO_2 records from sites in the SIO air sampling network, Trends: A Compendium of Data on Global Change. Carbon Dioxide Information Analysis Center, Oak Ridge National Laboratory, U.S. Department of Energy, Oak Ridge, Tenn., U.S.A.

Keeling, R.F. and Visbeck, M., 2005. Northern ice discharges and Antarctic warming: could ocean eddies provide the link? Quaternary Science Reviews, 24 (16-17), 1809.

Knorr, G. and Lohmann, G., 2003. Southern Ocean origin for the resumption of Atlantic thermohaline circulation during deglaciation. Nature, 424, 532-536.

Knorr, G. and Lohmann, G., 2004. The Southern Ocean as a the Flywheel of the Oceanic Conveyor Belt Circulation. PAGES News, 12 (1), 11-13.

Knutti, R., Flückiger, J., Stocker, T.F. and Timmermann, A., 2004. Strong hemispheric coupling of glacial climate through freshwater discharge and ocean circulation. Nature, 430, 851-858.

Kuhlbrodt, T., Griesel, A., Montoya, M., Levermann, A., Hoffmann, M. and Rahmstorf, S., 2007. On the driving processes of the Atlantic meridional overturning circulation. Reviews of Geophysics, 45, RG2001, doi:10.1029/2004RG000166.

Lüthi, D., Le Floch, M., Bereiter, B., Blunier, T., Barnola, J.-M., Siegenthaler, U., Raynaud, D., Jouzel, J., Fischer, H., kawamura, K. and Stocker, T.F., 2008. High-resolution carbon dioxide concentration record 650,000-800,000 years before present. Nature, 453, 379-382.

Lutjeharms, J.R.E., 1996. The exchange of water between the South Indian and the South Atlantic. In: W.H.B. G. Wefer, G. Siedler and D. Webb (Editors), The South Atlantic: Present and Past Circulation. Springer-Verlag, Berlin, pp. 125-162.

Lutjeharms, J.R.E., 2006. The Agulhas Current. Springer-Verlag, Berlin, Heidelberg, 329 pp.

Lutjeharms, J.R.E., 2007. Three decades of research on the greater Agulhas Current. Ocean Science, 3 (4), 939-995.
Munk, W. and Wunsch, C., 1998. Abyssal recipes II: energetics of tidal and wind mixing. Deep Sea Research, 45 (12), 1977.
North Greenland Ice Core Project Members, 2004. High-resolution record of Northern Hemisphere climate extending into the last interglacial period. Nature, 431, 147-151.
Pahnke, K. and Zahn, R., 2005. Southern Hemisphere Water Mass Conversion Linked with North Atlantic Climate Variability. Science, 307, 1,741-1,746.
Pahnke, K., Zahn, R., Elderfield, H. and Schulz, M., 2003. 340,000-year Centennial-Scale Marine Record of Southern Hemisphere Climatic Oscillation. Science, 301, 948-952.
Peeters, F.J.C., Acheson, R., Brummer, G.-J.A., de Ruijter, W.P.M., Schneider, R., Ganssen, G., Ufkes, M.E. and Kroon, D., 2004. Vigorous exchange between the Indian and Atlantic oceans at the end of the past five glacial periods. Nature, 438, 661-665.
Petit, J.R. et al., 1999. Climate and atmospheric history of the past 420,000 years from the Vostok ice core, Antarctica. Nature, 399, 429-436.
Piotrowski, A.M., Goldstein, S.L., Hemming, S.R. and Fairbanks, R.G., 2005. Temporal Relationships of Carbon Cycling and Ocean Circulation at Glacial Boundaries. Science, 307, 1,933-1,938.
Rahmstorf, S., 1995. Bifurcations of the Atlantic thermohaline circulation in response to changes in the hydrilogical cycle. Nature, 378, 145-149.
Rahmstorf, S., 1996. On the freshwater forcing and transport of the Atlantic thermocline circulation. Climate dynamics, 12, 799-811.
Rahmstorf, S., 2002. Ocean circulation and climate during the past 120,000 years. Nature, 419, 207-214.
Rau, A.J., Rogers, J. and Chen, M.-T., 2006. Late Quaternary palaeoceanographic record in giant piston cores off South Africa, possibly including evidence of neotectonism. Quaternary International, 148 (1), 65-77.
Rau, A.J., Rogers, J., Lutjeharms, J.R.E., Giraudeau, J., Lee-Thorp, J.A., Chen, M.-T. and Waelbroeck, C., 2002. A 450-kyr record of hydrological conditions on the western Agulhas Bank Slope, south of Africa. Marine Geology, 180 (1-4), 183-201.
Rintoul, S.R., 1991. South Atlantic Interbasin Exchange. Journal of Geophysical Research, 96, 2,675-2,692.
Sanchez-Goñi, M.F., Cacho, I., Turon, J.L., Guiot, J., Sierro, F.J., Peypouquet, J.-P., Grimalt, J.O. and Shackleton, N., 2002. Synchroneity between marine and terrestrial responses to millenial sclae climatic variability during the last glacial period in the Mediterranean region. Climate dynamics, 19, 95-105.
Sarnthein, M., Winn, K., Jung, S.J.A., J.-C., D., Labeyrie, L., Erlenkeuser, H. and Ganssen, G., 1994. Changes in the east Atlantic deepwater circulation over the last 30,000 years: Eight time slice reconstructions. Paleoceanography, 9 (2), 209-267.
Saunders, P.M. and King, B.A., 1995. Oceanic Fluxes on the WOCE A11 Section. Journal of Physical Oceanography, 25 (9), 1,942-1,958.
Schlitzer, R., 1996. Mass and heat transports in the South Atlantic derived from historical hydrographic data. In: G. Wefer, W.H. Berger, G. Siedler and D.J. Webb (Editors), The South Atlantic: Present and Past Circulation. Springer-Verlag, Berlin, pp. 305-323.
Seidov, D. and Maslin, M., 2001. Atlantic ocean heat piracy and the bipolar climate see-saw during Heinrich and Dansgaard-Oeschger events. Journal of Quaternary Science, 16 (4), 321-328.
Siegenthaler, U., Stocker, T.F., Monnin, E., Luthi, D., Schwander, J., Stauffer, B., Raynaud, D., Barnola, J.-M., Fischer, H., Masson-Delmotte, V. and Jouzel, J., 2005. Stable Carbon Cycle-Climate Relationship During the Late Pleistocene. Science, 310, 1,313-1,317.
Speich, S., Blanke, B. and Madec, G., 2001. Warm and Cold Water Routes of an O.G.C.M. Thermohaline Conveyor Belt. Geophysical Research Letters, 28 (2), 311-314.
Speich, S., Blanke, B., de Vries, P., Drijfhout, S., Döös, K., Ganachaud, A. and Marsh, R., 2002. Tasman leakage: A new route in the global ocean conveyor belt. Geophysical Research Letters, 29(10), 1416, doi:10.1029/2001GL014586.
Stocker, T.F., 1998. The Seesaw Effect. Science, 282, 61-62.
Stouffer, R.J., Seidov, D. and Haupt, B.J., 2007. Climate response to external sources of freshwater: North Atlantic versus the Southern Ocean. Journal of Climate, 20 (3), 436–448.
van Ballegooyen, R.C., Grundlingh, M.L. and Lutjeharms, J.R.E., 1994. Eddy fluxes of heat and salt from the southwest Indian Ocean into the southeast Atlantic Ocean: A case study. Journal of Geophysical Research, 99, 14,053-14,070.
Voelker, A.H.L., 2002. Global distribution of centennial-scale records for Marine Isotope Stage (MIS) 3: a database. Quaternary Science Reviews, 21 (10), 1,185-1,212.
Weijer, W., De Ruijter, W.P.M. and Dijkstra, H.A., 2001. Stability of the Atlantic Overturning Circulation: Competition between Bering Strait Freshwater Flux and Agulhas Heat and Salt Sources. Journal of Physical Oceanography, 31 (8), 2,385-2,402.
Weijer, W., de Ruijter, W.P.M., Dijkstra, H.A. and van Leeuwen, P.J., 1999. Impact of Interbasin Exchange on the Atlantic Overturning Circulation. Journal of Physical Oceanography, 29, 2,266-2,284.
Weijer, W., de Ruijter, W.P.M., Sterl, A. and Driffhout, S.S., 2002. Response of the Atlantic overturning circulation to South Atlantic sources of buoyancy. Global and Planetary Change, 34, 293-311.
Wunsch, C., 2002. What Is the Thermohaline Circulation? Science, 298, 1,179-1,180.
Wunsch, C. and Ferrari, R., 2004. Vertical mixing, energy and the general circulation of the oceans. Annual review of Fluid Mechanics, 36 (1), 281-314.

2. Conceptual and Analytical Approach

In order to identify past ocean circulation modes and patterns around South Africa and to infer possible implications for the global THC, two sediment cores, MD96-2080 and MD02-2594, from the Agulhas region (see Chapter 3 for location details) have been analysed at high resolution. However, it is obvious that palaeo-data sets from a unique oceanic region will not unambiguously allow deciphering global ocean and climatic trends and therefore the new paleoceanographic records from cores MD96-2080 and MD02-2594 will be viewed and discussed in the context of similar records from nearby and more distant sediment cores that are taken from the published literature.

2.1. Paleoceanographic Proxies Used in this Study

Sediment cores are valuable archives of information on past climates and ocean circulation. The material recovered from the seafloor (as that from lakes and ice sheets) provides documentation of environmental changes in the region where the sediments have been deposited. This information has to be extracted by using "proxies" that "approximate" parameters that are related to environmental conditions at the time of sediment deposition.

A "proxy" in the paleoenvironmental reconstruction context is a measurable descriptor that is linked to "non-fossilisible" variables such as temperature, salinity, global ice volume, nutrient content, oxygen content, CO_2 concentration, wind speed, productivity, and so forth. Each proxy follows their own physical, biological and chemical rules that allow the transformation from a proxy value to the target parameter. Usually this is accomplished by using a transformation algorithm that has to be established through proxy calibration. The quality of a proxy is given by the confidence with which the calibration predicts the target (Wefer et al., 1999).

For this work the proxies used to reconstruct past deep and surface water temperature and circulation around South Africa are: stable isotopes of oxygen ($\delta^{18}O$) and carbon ($\delta^{13}C$) and trace element ratios, i.e. Mg/Ca and Cd/Ca measured on fossil planktonic and benthic foraminifera (marine micro organisms, further details are given in Chapter 4) and the Sortable Silt Index ($\overline{SS}$) (a fraction of the terrigenous component of the sediment).

2.1.1. $\delta^{18}O$ of Foraminifera

The $\delta^{18}O$ value of foraminiferal calcite is derived from that of seawater plus fractionation dependent on temperature during calcification, and additional vital effects. For details about the analytical procedure see the methods Chapter 4.

The delta notation expresses the comparison of the ratio of the heavy (^{18}O) to light (^{16}O) oxygen isotope in the sample with respect to a standard:

$$\delta^{18}O = \frac{\left(\frac{^{18}O}{^{16}O}\right)_{sample} - \left(\frac{^{18}O}{^{16}O}\right)_{std}}{\left(\frac{^{18}O}{^{16}O}\right)_{std}} \cdot 1000 \qquad \text{(in ‰)} \qquad \text{Eq. 2-1}$$

Positive values of $\delta^{18}O$ mean that the sample is enriched, while negative values mean that it is depleted with regard to the heavy ^{18}O isotope.

For marine carbonate a commonly used isotope scale is the VPDB scale (Vienna Pee Dee Belemnite, a reference calibrated to a Cretaceous belemnite limestone from the Pee Dee Formation of South Carolina). The stable oxygen and carbon isotope standard used in the laboratory to calibrate all measurement results to the VPDB scale is available from the International Atomic Energy Agency in Vienna (IAEA, http://www.iaea.or.at).

The most important fractionation processes affecting the $\delta^{18}O$ in relation to sea water are those related to the hydrological cycle.

- During evaporation, molecules composed of the light isotope evaporate in higher proportion. As a consequence the vapour formed is enriched in ^{16}O and the remaining water in ^{18}O. Fractionation during evaporation is temperature dependent in such a way that fractionation decreases with increasing temperature.

- Precipitation favours the heavy isotopes. Therefore, clouds are progressively being enriched in ^{16}O (Rayleigh distillation, Dansgaard, 1964). Temperature does not directly affect the fractionation during condensation but it indirectly influences the isotopic ratio of the cloud because the magnitude of precipitation, and therefore of loss of the heavy isotope ^{18}O from the cloud, is strongly temperature dependent. This results in a temperature *vs* precipitation isotopic composition of 0.69‰ / ºC for the range -40 to 15ºC.

These two factors work together to generate heavier oceans during glacial periods. As ^{16}O is positively discriminated during evaporation, and it remains in the clouds preferentially, the clouds that are already lighter than the parent water get enriched more and more in ^{16}O along their trajectory as the ^{18}O is returned by precipitation. The “older” the cloud, the lighter its $\delta^{18}O$. As the clouds reach the high latitudes they are depleted in $\delta^{18}O$ and transfer their isotope signal to the ice sheets; typical isotopic values for ice are -35% in Greenland (Dansgaard et al., 1993), -54% in Antarctica (Jacobs et al., 1985). The ice sheets act as long term storages for ^{16}O (time scale 10^4-10^5 years) and as a result the global ocean is left enriched in ^{18}O during glacial periods.

- Additionally, the different evaporation/precipitation behaviour of ^{16}O and ^{18}O is directly related with local effects. For example, when interpreting the data of a more humid climatic region the extra addition of ^{16}O by precipitation has to be taken into account. Similarly, in regions of intense evaporation the presence of proportionally higher ^{18}O levels needs to be considered, and when sampling nearby a river mouth the contribution of ^{16}O from continental runoff is important.

- In the case of sea ice freezing and melting, fractionation effects are very small and they are widely overlooked because it is interpreted that both cancel each other out on a yearly average.

Nonetheless it must be pointed out that the water mass that is influenced by sea ice formation is very likely not the same during the year; during winter sea ice freezing, most of the salt is rejected and remains in the sea water. The increase in salinity then causes sinking of the water and subsequently, during the next summer season the melt water from sea ice of the previous winter season with its own specific isotopic composition is added to a different i.e., new water mass (Rohling and Cooke, 1999). This fact has to be taken into account when interpreting oxygen isotope records from cores near sea ice margins.

- Another factor influencing the sea water isotopic composition is advection and mixing of water masses from different source areas. Water masses contain an isotopic composition imprinted on them by processes that operate in the formation region and is transported to other locations where other processes dominate that do not cause the same isotope fractionation. This generates a remote process of changes of isotopic composition.

These processes are compiled in Figure 2-1. Those directly affecting the oceans are shown in italics.

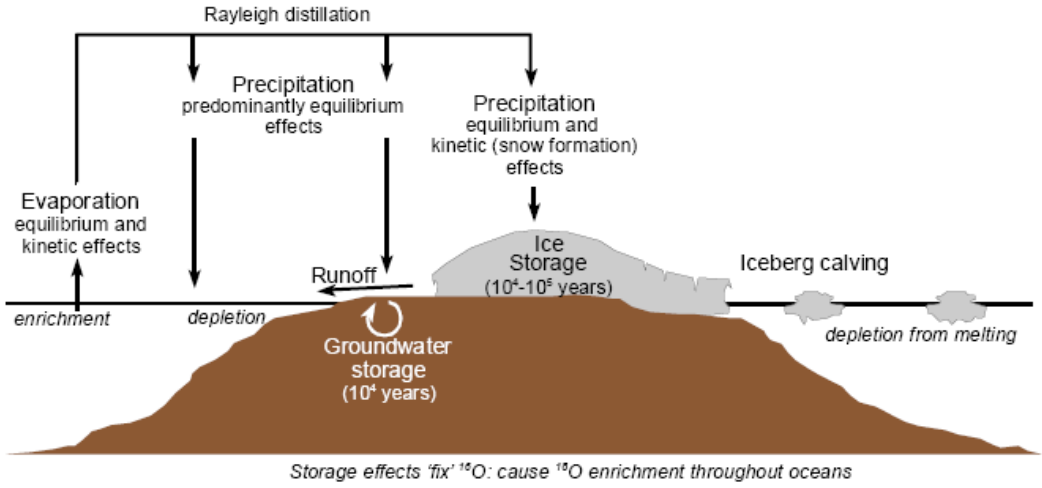

Figure 2-1 Effects of the hydrological cycle on oxygen isotopes. The direct effects on sea water are shown in italics (Rohling and Cooke, 1999).

The fractionation effects related with the water cycle results in the existence of a correspondence between $\delta^{18}O$ and salinity, the so called "salinity effect" on the $\delta^{18}O$ signature, although it would be more appropriately called the "fresh water budge effect" (Rohling and Bigg, 1998). Craig and Gordon (1965) expressed this relationship as:

$$\delta^{18}O_{sw} = a \cdot S + b \qquad \text{Eq. 2-2}$$

where b is the $\delta^{18}O$ of a freshwater end-member, S is salinity and a is the slope of the relationship.

There is not a unique relationship between $\delta^{18}O$ and salinity. They differ for different ocean regions because of varying E-P balances (in space and time, e.g. Rohling and Bigg, 1998), differences in freshwater isotopic composition (Schmidt et al., 2001) and advection and mixing with other water

masses (e.g. Bigg, 1995). Figure 2-2 illustrates (after Craig and Gordon, 1965) the relations for several water masses and oceanic regions.

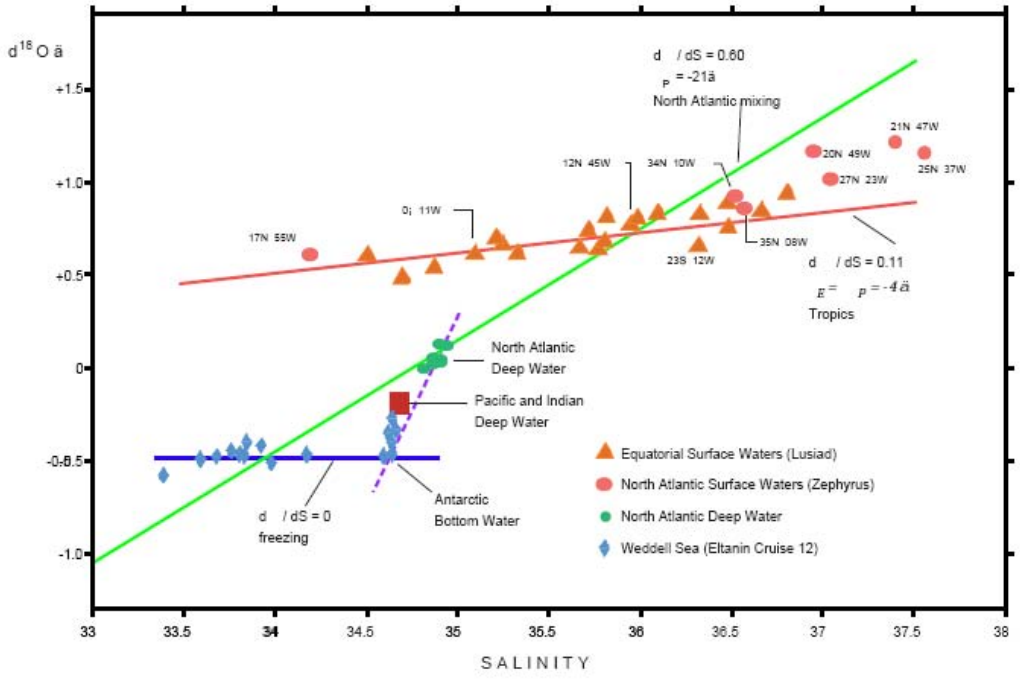

Figure 2-2 Relationships between $\delta^{18}O$ and Salinity in the different ocean basins (Craig and Gordon, 1965).

Benthic and planktonic foraminifera are marine organisms that live on the sediment surface or within the immediate surface sediments and at different depths of the water column depending on the species. They form a $CaCO_3$ shell whose oxygen isotopic composition records both, the isotopic composition of the ambient water and the temperature of the water because of the temperature dependent isotope fractionation of oxygen isotopes during calcification. As a general rule there is 0.25-0.2‰ depletion in carbonate $\delta^{18}O$ for every 1ºC temperature increase (Rohling and Cooke, 1999; Wright, 2000; Broecker, 2002).

Foraminiferal oxygen isotope values do not normally show values expected from equilibrium fractionation between calcite and sea water. For benthic foraminifera which live in an environment with stable low temperature, and in absence of photosynthesis activity, microhabitat differentiation combined with pore water and food supply may cause distinct isotope disequilibria (Grossman, 1987; Bemis et al., 1998). For planktonic foraminifera the situation is even more complicated, surface temperatures experience large station and year to year variations. Some planktonic foraminifera have symbiotic algae and it has been shown that photosynthesis may alter the micro-environment in which the isotopic fractionation to form the foraminiferal test occurs (e.g. Bijma et al., 1999). Besides, not all planktonic foraminifera live at the same depth and some of them may migrate up to hundreds of meters in the water column during their life cycle, so that it becomes complicated to precisely say to which depth corresponds the measured isotopic composition (Bijma et al., 1990; Erez et al., 1991). On the other hand, if the depth of calcification may be accurately determined, different species may be used to reconstruct the stratification of the water column (Niebler et al., 1999; Mortyn and Charles,

2003). Therefore, in order to use the oxygen isotope composition to decipher past conditions a good knowledge of the ecology, life cycle and shell calcification processes is more important when using planktonic foraminifera. Vital effects of the organism also affect their isotopic composition but they are not clearly quantified yet. Many laboratory culture studies are devoted to understanding the effects of ontogeny, symbiont photosynthesis, respiration and gametogenesis; they are mainly being performed for planktonic species (Spero and Lea, 1993; Spero and Lea, 1996; Spero et al., 1997; Bemis et al., 1998).

These factors need to be considered when interpreting stable oxygen isotope records but since regional effects on the isotopic composition of deep waters are much less important than in surface waters, benthic foraminifera may be used with high confidence as recorders of global ice volume changes and, thus of sea level variations and as deep sea paleothermometers. Their capacity for recording global changes in ice volume makes them especially useful as a stratigraphic tool, allowing correlation of isotope records from distant localities. In the case of planktonic foraminifera, it is always desirable to obtain an independent paleotemperature record based on other proxies, for instance in this work the Mg/Ca ratio of the *Globigerina bulloides* tests has been measured (see section 2.1.4.).
Imbrie et al. (1984) developed the global SPECMAP $\delta^{18}O$ record by stacking $\delta^{18}O_{plak\_calcite}$ records from various locations. The resulting $\delta^{18}O$ curve was assigned ages by tuning or adjusting the $\delta^{18}O$ patterns to match the predicted patterns based on the astronomic calculations for orbital variations. The estimated temporal precision associated with using the $\delta^{18}O$ stratigraphy is in the order of 5,000 yr (Imbrie et al., 1984). Similar attempts have been subsequently done, some examples are Martinson et al. (1987), and more recently Lisiecki and Raymo (2005). These last authors have generated a stack (the "LR04" stack) of 57 globally distributed benthic $\delta^{18}O$ records spanning the last 5.3 Myr which could make a good paleoceanographic reference for the Pliocene-Pleistocene (Fig. 2-3).

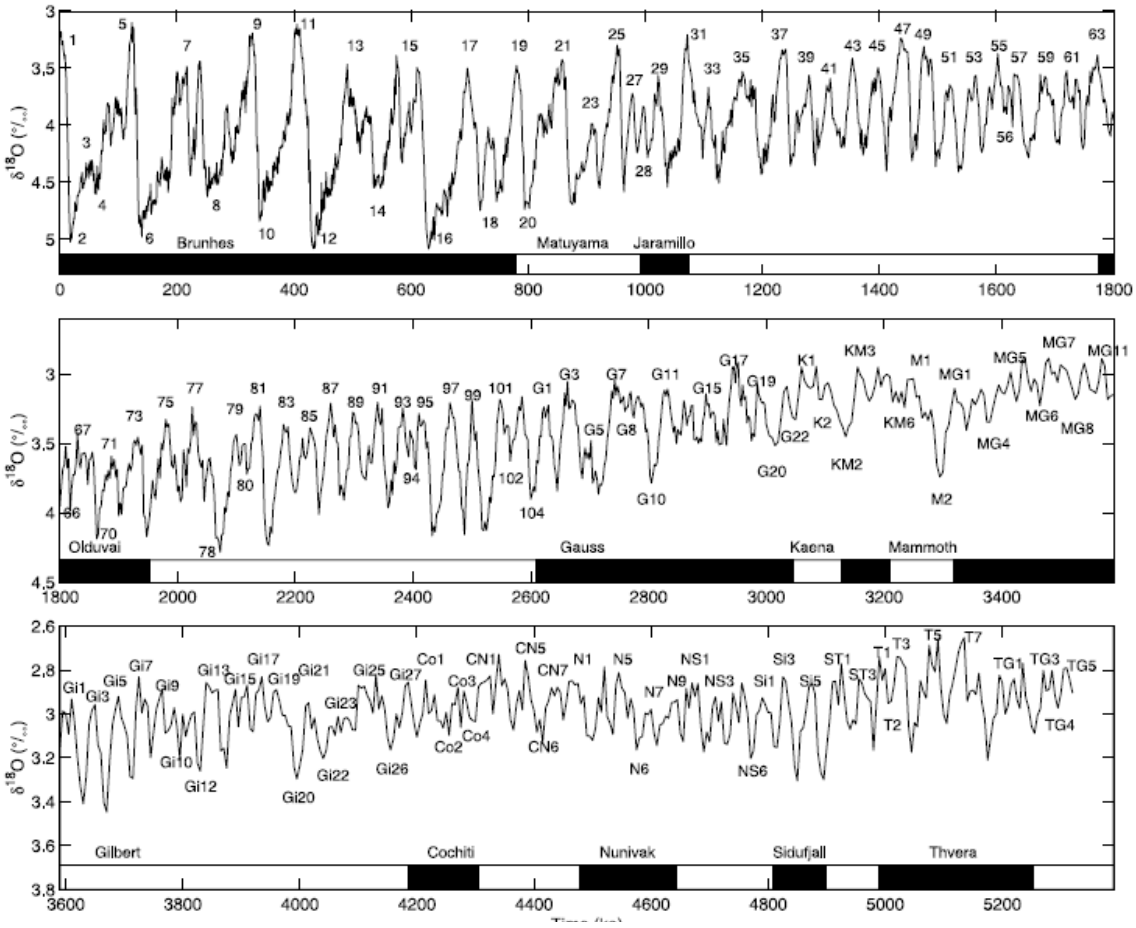

Figure 2-3 LR04 stack of Lisiecki and Raymo (2005). Labels in the figure refer to Marine Isotope Stages (MIS). Lower bar indicates magnetic polarity periods.

The linking between continental ice volume and $\delta^{18}O$ also allows inferring past sea level changes. As light ocean water is trapped on continental ice sheets during glacial progression, the global sea level is lowered. During the Last Glacial Maximum (LGM) the sea level is estimated to have been 120 m lower than today (e.g. from coral reefs, Fairbanks, 1989) and so an increase in $\delta^{18}O$ of 0.012 ± 0.001‰ per meter sea level lowering has been estimated (Labeyrie et al., 1987; Shackleton, 1987; Fairbanks, 1989). A good example of the applicability of benthic $\delta^{18}O$ to reconstruct past changes in sea level is given by Waelbroeck et al. (2002) who developed a relative sea level (RSL) curve spanning the last four glacial-interglacial cycles. This curve can be considered to represent global changes in sea level while regional differences exist due to topography, eustatic effects etc.

Despite the confounding effects of changes in oxygen isotope composition of the sea water ($\delta^{18}O_{sw}$), due to both trapping and releasing light ^{16}O in continental ice sheets and changes in the evaporation-precipitation balance ("salinity and ice-volume effect"), the "temperature effect" on calcite fractionation has also been used. Numerous paleotemperature equations have been developed, and of most interest for this work, they allow to infer past changes in the $\delta^{18}O_{sw}$ by combining $\delta^{18}O_{calcite}$ with an independent temperature proxy.

The paleotemperature equations for $\delta^{18}O$ have traditionally been expressed as quadratic expressions of the form:

$$T = a + b \cdot (\delta_c - \delta_w) + c \cdot (\delta_c - \delta_w)^2 \quad \text{Eq. 2-3}$$

where T is temperature (ºC), a is temperature when (δ_c-δ_w) (in VPDB scale) is zero, b is the slope and c is the second order term of the curvature which is not always included. Isotope fractionation increases with decreasing temperature (Urey, 1974) and therefore the slope is predicted to increase with decreasing temperature. The inverse of b represents the change in $\delta^{18}O$ (in ‰) per 1ºC change in temperature and ranges between 0.27‰ / ºC at 0ºC and 0.2‰ / ºC at 25ºC (O'Neil et al., 1969; Kim and O'Neil, 1997) (a rough estimation of 0.25‰ / ºC is commonly applied, see above). In case that the second order term is included then, the slope is not constant. Bemis et al. (1998) discuss the similar accuracy of linear and quadratic equations for the warm range of the ocean.

From the available paleotemperature equations, that derived from low-light *Orbulina universa* experiments (developed from culturing studies) of Bemis et al. (1998) seems to work well for warm temperature and can be applied to other species:

$$T = 16.5 + 4.8 \cdot (\delta_c - \delta_w) \quad \text{Eq. 2-4}$$

These authors also developed calibrations for *Globigerina bulloides* (also from culturing) with different number of chambers, and thus for different sizes; these equations may only be applied to *G. bulloides* (Bemis et al., 1998):

$$T = 12.6 + 5.07 \cdot (\delta_c - \delta_w) \quad \text{(11 chambers, approximately 301 ± 25 μm size)} \quad \text{Eq.2-5}$$

$$T = 13.2 + 4.89 \cdot (\delta_c - \delta_w) \quad \text{(12 chambers, approximately 369 ± 30 μm size)} \quad \text{Eq.2-6}$$

$$T = 13.6 + 4.77 \cdot (\delta_c - \delta_w) \quad \text{(13 chambers, approximately 414 ± 39 μm size)} \quad \text{Eq.2-7}$$

Shackleton's (1974) calibration developed from *Uvigerina spp* from core tops seems to work well for cold waters:

$$T = 16.9 + 4.38 \cdot (\delta_c - \delta_w) + 0.1 \cdot (\delta_c - \delta_w)^2 \quad \text{Eq. 2-8}$$

In Chapter 4.5 a detailed explanation about how to decouple the salinity and temperature effect of our planktonic $\delta^{18}O$ records is given.

2.1.2. $\delta^{13}C$ of Benthic Foraminifera

The $\delta^{13}C$ values recorded in benthic foraminiferal carbonate shells reflect those of the total dissolved inorganic carbon ($\sum CO_2$ or DIC) of ambient sea water, and therefore are widely used as paleonutrient and paleocirculation proxies.

As in the case of oxygen isotopes the $\delta^{13}C$ notation refers to the isotopic composition of the sample compared to that of a standard, which for marine environments again is provided on the VPDB scale.

$$\delta^{13}C = \frac{\left(\frac{^{13}C}{^{12}C}\right)_{sample} - \left(\frac{^{13}C}{^{12}C}\right)_{std}}{\left(\frac{^{13}C}{^{12}C}\right)_{std}} \cdot 1000 \quad \text{(in ‰)} \qquad \text{Eq. 2-9}$$

The main carbon reservoirs are organic matter and sedimentary carbonates. In the marine environment, the inorganic carbonate pool is governed by the carbonate reactions:

$$CO_{2(gas)} \leftrightarrow CO_{2(aq)} + H_2O \leftrightarrow H_2CO_3 \leftrightarrow (HCO_3)^- + H^+ \leftrightarrow (CO_3)^{2-} + 2H^+ \qquad \text{Eq. 2-10}$$

The carbonate system acts as a buffer in the ocean keeping sea water pH in a narrow band (7.6 - 8.8; typical value 8.2). The dominant carbon species in sea water is HCO_3^- (around 85%) and this species is used by the foraminifera to calcify their tests. The calcification process is largely temperature independent (α = (0.035 ± 0.013) ‰ / ºC at 20ºC, Emrich et al., 1970) and therefore foraminiferal and mineral carbonate are widely use to infer changes of seawater $\delta^{13}C_{\Sigma CO2}$. Differences between the $\delta^{13}C$ of benthic foraminiferal calcite and ambient sea water may arise as a result of microhabitat differentiation. Infaunal foraminifera live within the top centimetres of the sediment and their isotopic signal is influenced by that of pore waters (Zahn et al., 1986; McCorkle et al., 1990). Organisms may incorporate isotopically light CO_2 products of their own respiration, and carbonate ion concentration changes likewise play a role in the disequilibria (Wolf-Gladrow et al., 1999; Zeebe et al., 1999). Also, under high productivity regimes, a "fluffy" layer of sinking organic matter may generate an environment of light carbon isotopes as a by-product of the remineralisation of the organic material. This light $\delta^{13}C$ may alter the signal recorded by some species of benthic foraminifera (Mackensen et al., 1993; Mackensen and Licari, 2004; Diz et al., 2007). The possibility of any of these factors affecting benthic $\delta^{13}C$ at the core site studied has to be taken into account when interpreting down-core benthic $\delta^{13}C$ records.

The carbon isotopic composition of ΣCO_2 in sea water is mainly controlled by two processes, physical fractionation within the carbon system and biochemical fractionation due to formation and decay of organic matter.

The dissolution of CO_2 and subsequent transformation into carbonate species undergoes several fractionation processes. During air-sea CO_2 exchange there is a small isotopic fractionation of -1.1‰. The CO_2 hydration and dissociation step enriches $\delta^{13}C$ of the bicarbonate by 9‰, which constitutes the highest isotopic shift in the carbonate system. The isotopic change between bicarbonate and carbonate is very small, 0.5‰ (fractionation values from Mook, 1986). The main factor influencing the isotopic composition of ΣCO_2 is seawater pH as it controls the abundance of the concentration of individual carbon species. For pH > 9, the $[CO_3^{2-}]$ concentration is significantly larger and its isotopic composition influences more prominently that of ΣCO_2. For pH < 7.5, $[CO_2]_{aq}$ becomes important enough to produce variations on $\delta^{13}C_{\Sigma CO2}$. For today's pH ocean band the isotopic composition of HCO_3^- produces the major control on that of ΣCO_2.

Temperature has an influence on $\delta^{13}C_{\Sigma CO2}$ through its control during fractionation of air-sea CO_2 exchange. For this step, every 10ºC of temperature increase causes 1‰ depletion in $\delta^{13}C_{\Sigma CO2(aq)}$ (Broecker and Maier-Reimer, 1992), i.e. at equilibrium surface-ocean $\delta^{13}C_{\Sigma CO2(aq)}$ is more positive at high latitudes than at low latitudes (Kroopnick et al., 1977; Broecker and Maier-Reimer, 1992; Lynch-Stieglitz et al., 1995). This thermodynamic effect on the isotopic signature of ΣCO_2 can be enhanced due to longer air-sea contact time or high winds and due to net CO_2 efflux out of the ocean into the atmosphere (Kroopnick et al., 1977; Lynch-Stieglitz et al., 1995). The net effect of the various air-sea exchange processes spans a modern surface ocean range of 2‰ (Marchitto and Broecker, 2006 and references therein).

The $\delta^{13}C$ isotopic imprint acquired during air-sea exchange is not only of importance for surface waters but also for deep and intermediate waters which gain a distinctive isotopic signature at their formation sites that will be held constant until they enter again in contact with the atmosphere or mix with other water masses (e.g. Broecker and Maier-Reimer, 1992; Charles et al., 1993). Therefore, the air-sea isotopic signature may be regarded as a conservative tracer of water masses. Broecker and Maier-Reimer (1992) named this air-sea isotopic signature $\Delta\delta^{13}C$ and later Lynch-Stieglitz and Fairbanks (1994) renamed $\delta^{13}C_{as}$ to distinguish it from the $\delta^{13}C$ gradients commonly used in paleoceanography; we will refer to this later notation further on.

The biochemical fractionation due to formation and decay of organic matter generates the strongest isotopic variations on seawater ΣCO_2. In most cases, organisms favour molecules with lighter isotopes because they have weaker bonds which require less energy to break. Kinetic fractionation during photosynthesis causes enrichment with ^{12}C in the organic matter and leaves the ocean's surface depleted in the light isotope. Typical $\delta^{13}C$ values of marine phytoplankton range between -10 and -31‰, but most warm water plankton exhibits values between -17 and -22‰ (Degens et al., 1968; Degens, 1969). Aside from ^{12}C, photosynthesis removes nutrients. Respiration, on the other hand, returns light carbon isotopes and nutrients to the water column. This explains the observed anticorrelation between increasing $(NO_3)^{2-}/(PO_4)^{3-}$ and decreasing $\delta^{13}C$ in sea water (Fig. 2-4). Plotting $\delta^{13}C$ versus $(PO_4)^{3-}$ the values fall close to a straight line with a slope close to (-0.93‰) – (-1.1‰) $\delta^{13}C$ change per μm/kg $(PO_4)^{3-}$ change so that if the only processes acting on $\delta^{13}C$ were biological a modern oceanic range of 3‰ would be possible (Broecker and Peng, 1982; Broecker and Maier-Reimer, 1992) (Fig. 2-4b).

More precisely, Broecker and Maier-Reimer (1992) develop the following relationship between $\delta^{13}C$ and $(PO_4)^{3-}$:

$$\delta^{13}C_{bio} - \delta^{13}C_{m.o.} = \frac{\Delta photo}{\Sigma CO_2} \cdot \left(\frac{C}{P}\right)_{org} \cdot \left((PO_4)^{3-} - (PO_4)^{3-}{}_{m.o.}\right) \qquad \text{Eq. 2-11}$$

where the subscript *bio* is used to stress that this $\delta^{13}C$ refers to its purely biological component, *m.o.* stands for mean ocean, $\Delta photo$ is the carbon isotope separation during marine photosynthesis and $(C/P)_{org}$ is the carbon to phosphorus ratio in marine organic matter. For present conditions, taking

Δphoto = -19‰, (C/P)org = 128, $\Sigma CO_{2m.o.}$ = 2200 µmol/kg, $(PO_4)^{3-}_{m.o.}$ = 2.2 µmol/kg and $\delta^{13}C_{m.o.}$ = 0.3‰, the equation becomes (Broecker and Maier-Reimer, 1992):

$$\delta^{13}C_{bio} = 2.7 - 1.1 \cdot (PO_4)^{3-} \qquad \text{Eq. 2-12}$$

Decoupling of $\delta^{13}C$ from nutrient concentration specially occurs in surface waters at low temperatures when isotopic fraction between $CO_{2(g)}$ and $CO_{2(aq)}$ becomes important (e.g. Broecker and Maier-Reimer, 1992; Mackensen and Bickert, 1999).

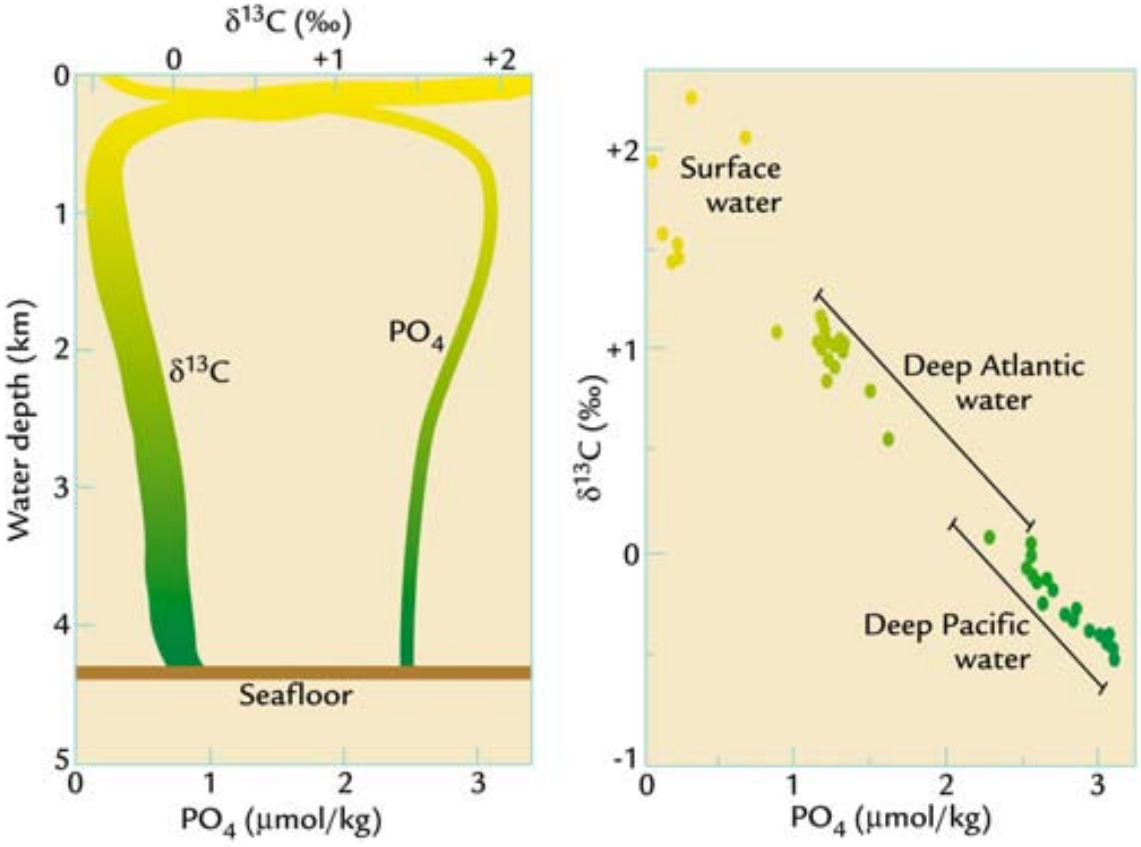

Figure 2-4 Relationship between $\delta^{13}C$ and $(PO_4)^{3-}$ in the ocean; a) Anticorrelation between $\delta^{13}C$ and $(PO_4)^{3-}$ plotted against depth. $\delta^{13}C$ at the surface is very high because of $\delta^{13}C$ enrichment during $CO_{2(g)}$ transformation in bicarbonate and removal of light isotopes during photosynthesis. Phosphate is low here because of its uptake during photosynthesis. Maximum nutrients/minimum $\delta^{13}C$ occur at the thermocline, further below respiration processes are reduced; b) $\delta^{13}C$ *vs* $(PO_4)^{3-}$. In the deep Pacific and Indian Oceans (Indian Ocean is not shown in the graph) the slope of the correlation falls along the Redfield ratio (i.e. 1.1‰). Values in the North Atlantic are separated from the Redfield ratio due to physical effects on the fractionation (from Ruddiman, 2001).

The return of light carbon to the water column by means of organic respiration raises an important application of $\delta^{13}C$ as an indicator of the deep water chemical "age". Recently formed deep waters, that have "just" been removed from direct contact with the atmosphere and the ocean layer suitable for photosynthesis display high $\delta^{13}C$ values, while "old" waters show very light $\delta^{13}C$ values (see Fig. 2-5). For example, North Atlantic Deep Water (NADW) displays $\delta^{13}C$ = 1.2‰ VPDB at its formation site, as it contributes to CDW and finally reaches the North Pacific its $\delta^{13}C$ is depleted to values of -1‰ VPDB due to chemical "aging" and mixing with other water masses (Kroopnick, 1985). In this context "age" indirectly refers to organic matter remineralisation sustained by the continued flux of marine organic matter from the surface to the deep water, rather than to a physical age because

remineralisation depends for most parts on export productivity and rapidity of organic matter decay (Rohling and Cooke, 1999).

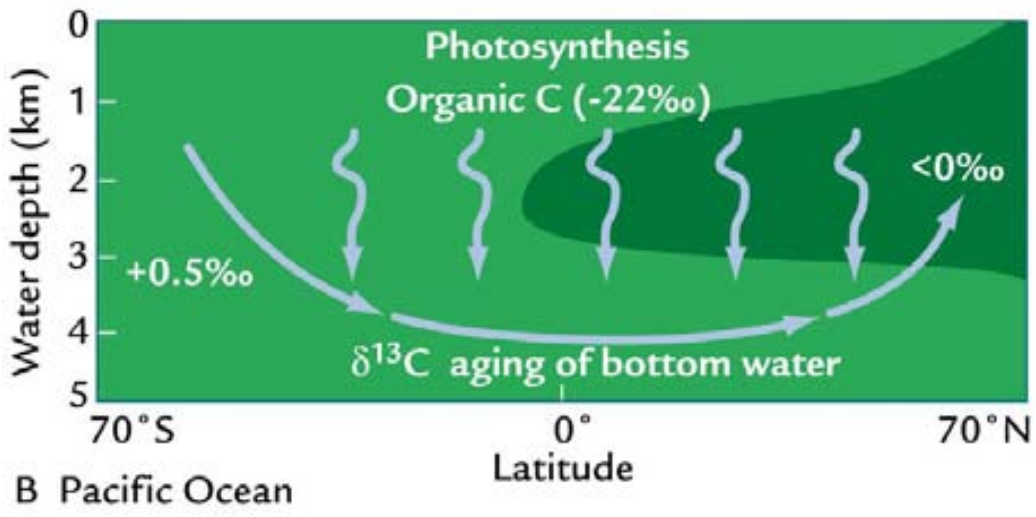

Figure 2-5 The Pacific Ocean contains the "oldest" waters of the world's oceans. Located at the end of the deep branch of the "conveyor belt" waters arriving there have been fed by nutrients settling from the surface and consequently $\delta^{13}C$ is low (from Ruddiman, 2001).

The chemical ageing of deep waters provides a powerful tool for reconstructing ocean circulation because it allows identifying deep water flow paths from their source areas. As for the North Atlantic, the differences between surface water $\delta^{13}C$ (+1.6‰ VPDB, Kroopnick et al., 1972) and deep water (+1.2‰ VPDB, Kroopnick, 1985) identify the basin as one that experiences active deep convection. In the case of the Pacific, surface values of +1.5 to +2‰ VPDB (Broecker and Peng, 1982) compare to deep values from +0.2 to -1‰ VPDB identify the deep waters as derived from remote source-regions (Rohling and Cooke, 1999 and references therein).

Figure 2-6 shows the present and past (LGM) reconstruction of the water masses distribution in the Western Atlantic based on the differences in $\delta^{13}C$ of the different water masses (Curry and Oppo, 2005). While the flow path of NADW (yellow) may be traced by its high $\delta^{13}C$ derived from its formation region, the signal is being diluted by mixing with water masses from below and above and by supply of light respiratory CO_2. Antarctic Bottom Water (AABW, dark green) has lower $\delta^{13}C$ because it is fed by aged NADW and by the oldest component of CDW. Carbon isotope reconstructions for the LGM based on benthic foraminifera suggest that the glacial NADW did not sink as deep (therefore, it is known as Glacial North Atlantic Intermediate Water, GNAIW) and reach as far south as today. Overall $\delta^{13}C$ values are lighter for the last glacial ocean, by some 0.32‰ VPDB, likely due to the entering into the ocean of light terrestrial carbon (Shackleton, 1977). In contrast, the presence in the deep ocean of southern source waters (AABW/CDW) was presumably enhanced with their $\delta^{13}C$ significantly depleted over their modern values (see also results and discussion, Chapter 5).

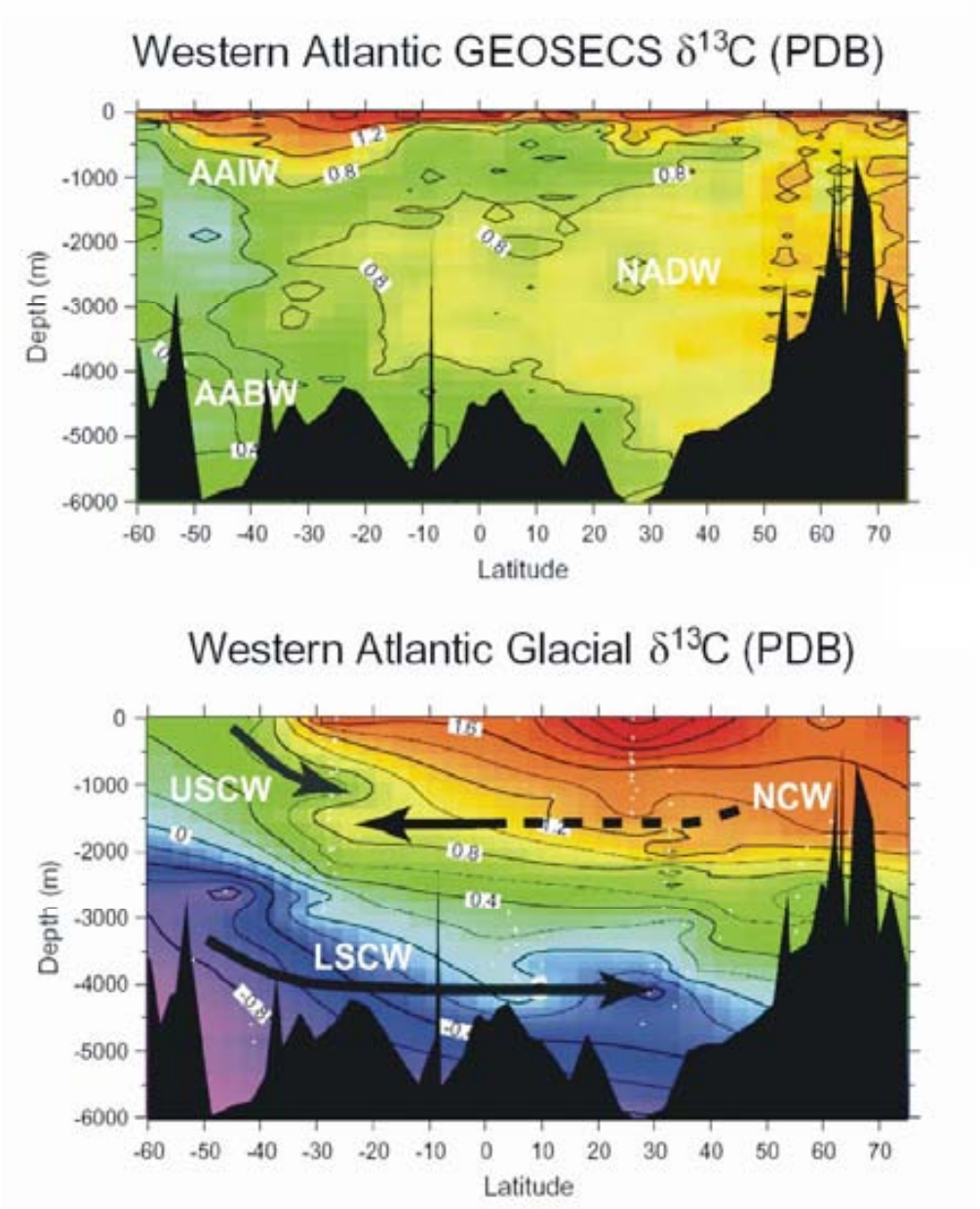

Figure 2-6 Curry and Oppo (2005) Western Atlantic $\delta^{13}C$ transects; a) Water mass carbon isotope distribution in the modern Western Atlantic Ocean based on GEOSECS measurements (Kroopnick, 1980). NADW displays high $\delta^{13}C$ values derived from its formation site in the high latitude North Atlantic. AABW on the other hand displays low $\delta^{13}C$ despite its recent formation as it is fed by NADW that has become depleted in $\delta^{13}C$ along its path to the Southern Ocean and by CDW which is very old due to its long residence time flowing around Antarctica; b) Carbon isotope reconstruction for the Atlantic LGM based on benthic foraminifera $\delta^{13}C$. The pattern suggests reduced NADW (i.e. NCW) formation and a more northward reaching AABW/CDW (i.e. SCW) (Curry and Oppo, 2005).

A possible means of discriminating the biological component and the thermodynamic component of $\delta^{13}C$ in the present ocean is normalizing to constant phosphate (Broecker and Maier-Reimer, 1992; Charles et al., 1993). That is, removing the biological component from $\delta^{13}C$. For instance using Eq. 2-12 Broecker and Maier-Reimer (1992) proposed:

$$\delta^{13}C_{as} = \delta^{13}C - \delta^{13}C_{bio} = \delta^{13}C + 1.1 \cdot (PO_4)^{3-} - 2.7 \qquad \text{Eq. 2-13}$$

Even though the slope of the $\delta^{13}C$ *vs* $(PO_4)^{3-}$ is not globally uniform and neither Δphoto and $(C/P)_{org}$ strictly follow "Redfield" stoichiometry in all regions of the ocean, the above equation provides a good approximation to establish the relative importance of gas exchange for $\delta^{13}C_{\Sigma CO2}$ in the

present ocean (Charles et al., 1993) (see Chapters 3 and 4). For paleoceanographic purposes, Oppo and Fairbanks (1989) and Lynch-Stieglitz and Fairbanks (1994) combined the above equation with the use of an independent proxy for $(PO_4)^{3-}$ (i.e. benthic Cd/Ca, see next section) and gained some insights on the past $\delta^{13}C_{as}$ signature of the water masses. The combined influence of physical and biological fractionation allows one to identify current and past sources of deep water convection and to follow their flow paths through the deep ocean (see Chapter 4.4 for further details).

2.1.3. Cd/Ca in Benthic Foraminifera: Paleonutrient Proxy

Foraminiferal shells are mainly composed of pure calcite, typically 99% by weight $CaCO_3$. The remaining 1% is comprised by trace element enriched-calcite (TE-CO_3): Mg, Ba, Sr, Cd, Zn, U etc; which foraminifera incorporate from sea water during shell calcification (e.g. Lea et al., 1999). As a result the shell composition reflects the sea water characteristics as well as physical and biological conditions during precipitation.

Cadmium is removed from sea water by foraminifera and it is expected to exhibit a systematic behaviour upon shell incorporation. The biological function of Cd is not yet clear as it is poisonous at high concentrations (Boyle, 1988), but it seems that some organism may incorporate Cd instead of Zn for playing a role in carbon anhydrase enzyme (Löscher et al., 1998 and references therein). The importance of determining past Cd concentrations in sea water (Cd_{sw}) arises from the observation that the Cd_{sw} distribution resembles that of $(PO_4)^{3-}$ (a major nutrient) (Boyle et al., 1976; Boyle, 1988), so that depleted values are found in warm surface waters while the most enriched levels are found in the deep Pacific (Boyle et al., 1976). Cd_{sw} displays an almost linear relationship with $(PO_4)^{3-}$ with a lower slope at lower phosphorus values (Fig. 2-7). There is a recognized "kink" in the Cd_{sw} *vs* $(PO_4)^{3-}$ relation at around 1.3 μmol/kg $(PO_4)^{3-}$ (approximately corresponding to a Cd_{sw} value of 0.28 nmol/kg) so that Boyle (1988) defined this relation by two linear equations:

$$Cd_{sw} = 0.21 \cdot (PO_4)^{3-} \qquad For \quad (PO_4)^{3-} < 1.3 \ \mu mol/kg \qquad \text{Eq. 2-14}$$

$$Cd_{sw} = 0.4 \cdot (PO_4)^{3-} - 0.25 \qquad For \quad (PO_4)^{3-} > 1.3 \ \mu mol/kg \qquad \text{Eq. 2-15}$$

The data leading to the "low nutrient" slope (below the "kink") mainly comes from the North Atlantic while Indian, Pacific and Southern Ocean data lead to the "high nutrient" slope (above the "kink") (Boyle, 1988; Löscher et al., 1998; Cullen, 2006).

Recently Elderfield and Rickaby (2000) have proposed that this "kink" in the relation is an artifact and that the global surface water data can be explained by preferential extraction of Cd_{sw} respect to $(PO_4)^{3-}$ from surface waters, with a constant fractionation factor ($\alpha_{Cd/P}$):

$$Cd_{sw} = \frac{1.2}{(\alpha_{Cd/P}) \cdot (3.3 / PO_4^{3-} - 1) + 1} \qquad \text{Eq. 2-16}$$

Even so, the two linear equations of Boyle (1988) are widely used in paleoceanographic studies and facilitate comparison among different data sets.

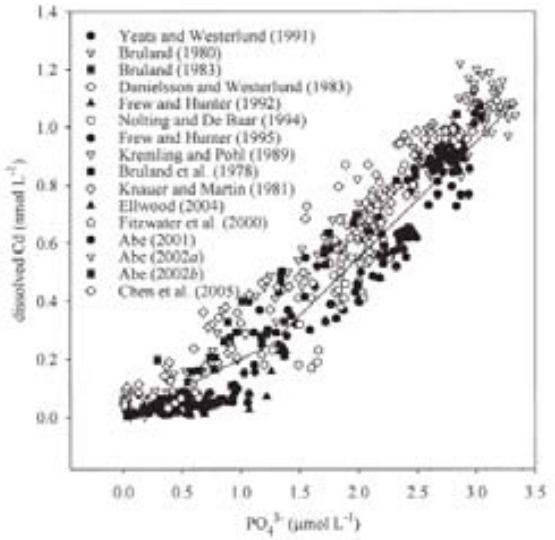

Figure 2-7 Dissolved Cd_{sw} *vs* $(PO_4)^{3-}$ compiled from the global database (Cullen, 2006). Lines represent the two distinct relationships as defined by Boyle (1988) for $(PO_4)^{3-} < 1.3$ µmol/kg, primarily Atlantic waters, and for $PO_4^{3-} > 1.3$ µmol/kg, primarily Indian–Southern–Pacific Ocean waters.

Foraminifera incorporate Cd into their shell according to a partition coefficient (D_{Cd}) which is depth dependent (Boyle, 1992):

$$D_{Cd} = \frac{\left(\frac{Cd}{Ca}\right)_{foram}}{\left(\frac{Cd}{Ca}\right)_{sw}} \Rightarrow \; Cd_{sw} = \frac{Ca_{sw}}{D_{Cd}} \cdot \left(\frac{Cd}{Ca}\right)_{foram} \qquad \text{Eq. 2-17}$$

where $(Cd/Ca)_{foram}$ in µmol/mol is the benthic foraminiferal Cd/Ca ratio and $(Cd/Ca)_{sw}$ in nmol/kg is the ratio in sea water. Ca_{sw} is the concentration of Ca in sea water and it is assumed to be constant, a value of 10 nmol/kg is typically used (e.g. Lear et al., 2002).

The reasons for the depth-dependency of D_{Cd} are not well known but it seems clear that it is not temperature related (e.g. Marchitto, 2004). Comparing benthic Cd/Ca core-top values with in situ measurements Boyle (1992) found that D_{Cd} varied between 1.3 and 2.9 and proposed to correct for the depth effect by interpolating between these values. Subsequently, he proposed the following partition coefficients for different water depths:

$$D_{Cd} = 1.3 \qquad \text{For depths < 1150 m} \qquad \text{Eq. 2-18}$$

$$D_{Cd} = 1.3 + (depth - 1150) \cdot (1.6/1850) \qquad \text{For depths (1150 – 3000) m} \qquad \text{Eq. 2-19}$$

$$D_{Cd} = 2.9 \qquad \text{For depths > 3000 m} \qquad \text{Eq. 2-20}$$

Later studies have found different partition coefficients in several oceanic regions (e.g. Tachikawa and Elderfield, 1996; Willamowski and Zahn, 2000) but for comparison reasons Boyle's (1992) are usually reported. Nevertheless, these differences point to the necessity to further investigate the variability of D_{Cd}. Infaunal species (e.g. *Uvigerina spp*) probably have lower partition coefficients despite elevated pore water Cd concentrations (Tachikawa and Elderfield, 1996, 2002), therefore they record similar Cd/Ca values as epibenthic species (observed by Boyle, 1988, 1992). Because of this last observation *Cibicidoides* and *Uvigerina* have been used interchangeably in paleoceanographic studies and success in doing so seems to have been fortuitous (Marchitto and Broecker, 2006).

Difficulties with the use of this proxy arise from the small concentrations present in foraminiferal calcite. Benthic Cd/Ca values range from 0.04 μmol/mol in the domain of NADW to 0.25 μmol/mol in the deep Pacific. Such low Cd content makes the foraminiferal shell susceptible to contamination and rigorous cleaning protocols have to be performed (see Chapter 4.3.3) (e.g. from Mn-oxides, Boyle, 1983; from CdS, Rosenthal et al., 1995). Furthermore, the saturation state of sea water can alter the original or expected Cd/Ca ratio of benthic foraminifera, either through post-depositional dissolution (e.g. McCorkle et al., 1995) or during calcite precipitation (e.g. Marchitto et al., 2002).

Ultimately Cd/Ca in benthic foraminifera is correlated with the phosphate content of the ambient waters and this ratio is used as a proxy to reconstruct past changes in the nutrient content of water masses (Hester and Boyle, 1982; Boyle and Keigwin, 1985/86; Rosenthal et al., 1997) and to eliminate the "water mass aging" effect from $\delta^{13}C$ (see above) (Lynch-Stieglitz and Fairbanks, 1994; Lynch-Stieglitz et al., 1996). Notable works on this line are those of Boyle and Keigwin (1985/86) who found higher nutrient levels in the deep North Atlantic during the LGM supporting the existent contention only based on $\delta^{13}C$ data of more intense spreading of Lower Southern Component Waters (LSCW) (e.g. Duplessy et al., 1988). Lynch-Stieglitz and Fairbanks (1994) were able to identify a positive $\delta^{13}C_{as}$ signature for the glacial equivalent of NADW (i.e. Glacial North Atlantic Intermediate Water, GNAIW) (highly in contrast to its present negative value), as well as a glacial deep water with a very depleted $\delta^{13}C_{as}$ signature of, maybe, Pacific origin. Of importance for this Thesis is the comprehensive compilation performed by Marchitto and Broecker (2006) of the available Atlantic Holocene and LGM paired benthic $\delta^{13}C$ and Cd/Ca and estimates of the derived $\delta^{13}C_{as}$. These authors presented a meridional transect of Cd_{sw} (as derived from benthic Cd/Ca) and $\delta^{13}C_{as}$, similar to those presented by Curry and Oppo (2005) on benthic $\delta^{13}C$ (Fig. 2-8).

LGM circulation patterns using both paleonutrient proxies (i.e. benthic $\delta^{13}C$ and Cd/Ca) show large discrepancies in the Atlantic sector of the Southern Ocean. This so called Southern Ocean Cd-$\delta^{13}C$ conundrum (see Boyle and Rosenthal, 1996 for a review) arises from the observation of extremely depleted glacial $\delta^{13}C$ (of up to -1 to -1.5‰, implying very high nutrient content) in deep sediment cores while Cd/Ca showed barely any glacial-interglacial variation (implying no change in nutrients). Contamination or dissolution effects alone do not seem capable to produce such a different data pattern (Boyle and Rosenthal, 1996) and the "Mackensen or Phytodetritus effect" likewise does not seem to play a prominent role (Ninnemann and Charles, 2002). It remains an active open field of investigation and, in view of the MD96-2080 and MD02-2594 benthic $\delta^{13}C$ and MD96-2080 benthic Cd/Ca records, some of its implications for the water column structure of the South Atlantic will be discussed in the present Thesis (see Chapter 5.3).

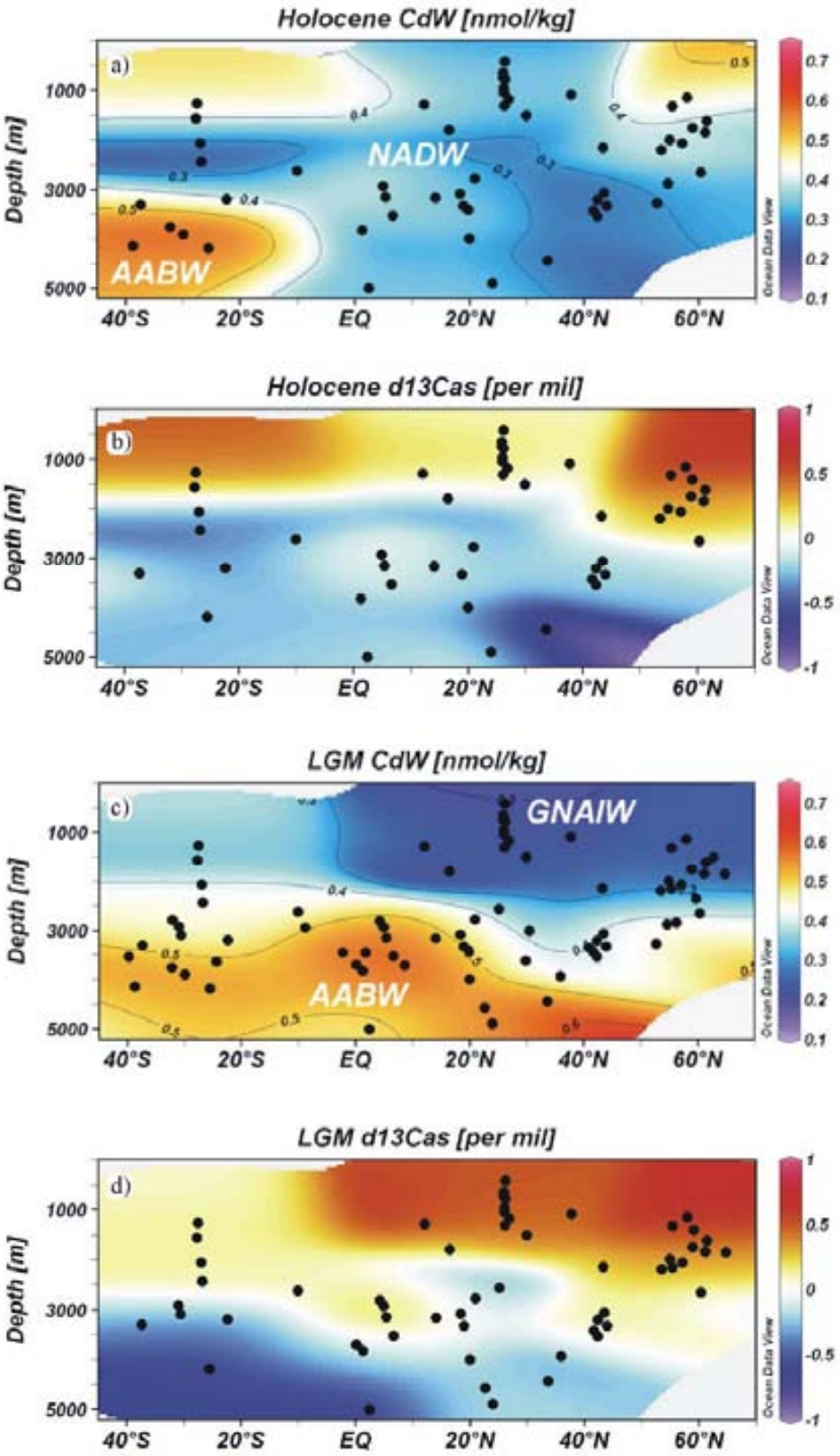

Figure 2-8 Atlantic Cd_{sw} and $\delta^{13}C_{as}$ transects from Marchitto and Broecker (2006); a) Holocene Cd_{sw} (nmol/kg); b) Holocene $\delta^{13}C_{as}$ (‰) VPDB, low-Cd_{sw} negative-$\delta^{13}C_{as}$ NADW prevail in the present Atlantic Ocean. Marchitto and Broecker (2006) noted the existence of some anomalous high Cd_{sw} values in the North Atlantic, driven the $\delta^{13}C_{as}$ towards positive values, unexpected in this region (see Chapters 3 and 5.3); c) LGM Cd_{sw} (nmol/kg); d) LGM $\delta^{13}C_{as}$ (‰) VPDB, during this period Southern Component Waters expanded while NADW vanished.

2.1.4. Mg/Ca in Planktonic Foraminifera: Sea Surface Paleotemperature Proxy (SST)

Mg, as Sr, B, V, U, Li, F, is a conservative element in the ocean so that its ratio to Ca is nearly fixed in the ocean on geological time scales (Dickson, 2002). Hence, variations in the ratio of foraminiferal calcite should reflect physical or vital effects during calcification. It was already early in the 20th century when it was observed that the Mg content of inorganic calcite, as that of foraminiferal shells, was higher when precipitation occurred at warmer temperatures (Chave, 1954). These similarities between inorganic and organic calcite provided the indication that physical, and more specifically temperature, more than biological effects should be altering the ratio. Nonetheless, initial studies failed to clearly define this temperature dependency (e.g. Lorens et al., 1977) and it was not until the early nineties when its true potential was recognized. Main studies that convinced the paleoceanographic community were those of Nürnberg (1995) and Nürnberg et al. (1996a; 1996b) using cultured, core-top and downcore planktonic foraminifera. Nürnberg's and further studies (e.g. Lea et al., 1999; Mashiotta et al., 1999) showed that the correlation of Mg/Ca and T is better explained by an exponential fit of the form:

$$\frac{Mg}{Ca} = A \cdot e^{B \cdot T} \qquad \text{Eq. 2–21}$$

where A is the pre-exponential constant, which determines the absolute temperature; e is the natural logarithm; B is the exponential constant, which indicates the change in Mg/Ca per ºC; and T is the temperature. Calibration results for ten species of planktonic foraminifera yielded exponential constants between 0.085 and 0.102, equivalent to 8.5% to 10.2% increase in Mg/Ca per ºC (Nürnberg et al., 1996a; 1996b; Lea et al., 1999; Anand et al., 2003). The values of the exponential constants depend on the calibration data set used, thus on the foraminiferal species and on the range of water temperatures. There are calibration curves that are mono-specific (Mashiotta et al., 1999; Rosenthal et al., 2000), and also those that are more generic (e.g. Fig. 2-9, Anand et al., 2003). Culturing and core top studies (e.g. Lea, 1999; Sadekov et al., 2005) have shown that there are differences in the Mg/Ca uptake by different species of foraminifera with as much as a factor of 2. Hence, it is desirable, when possible, to use mono-specific calibrations.

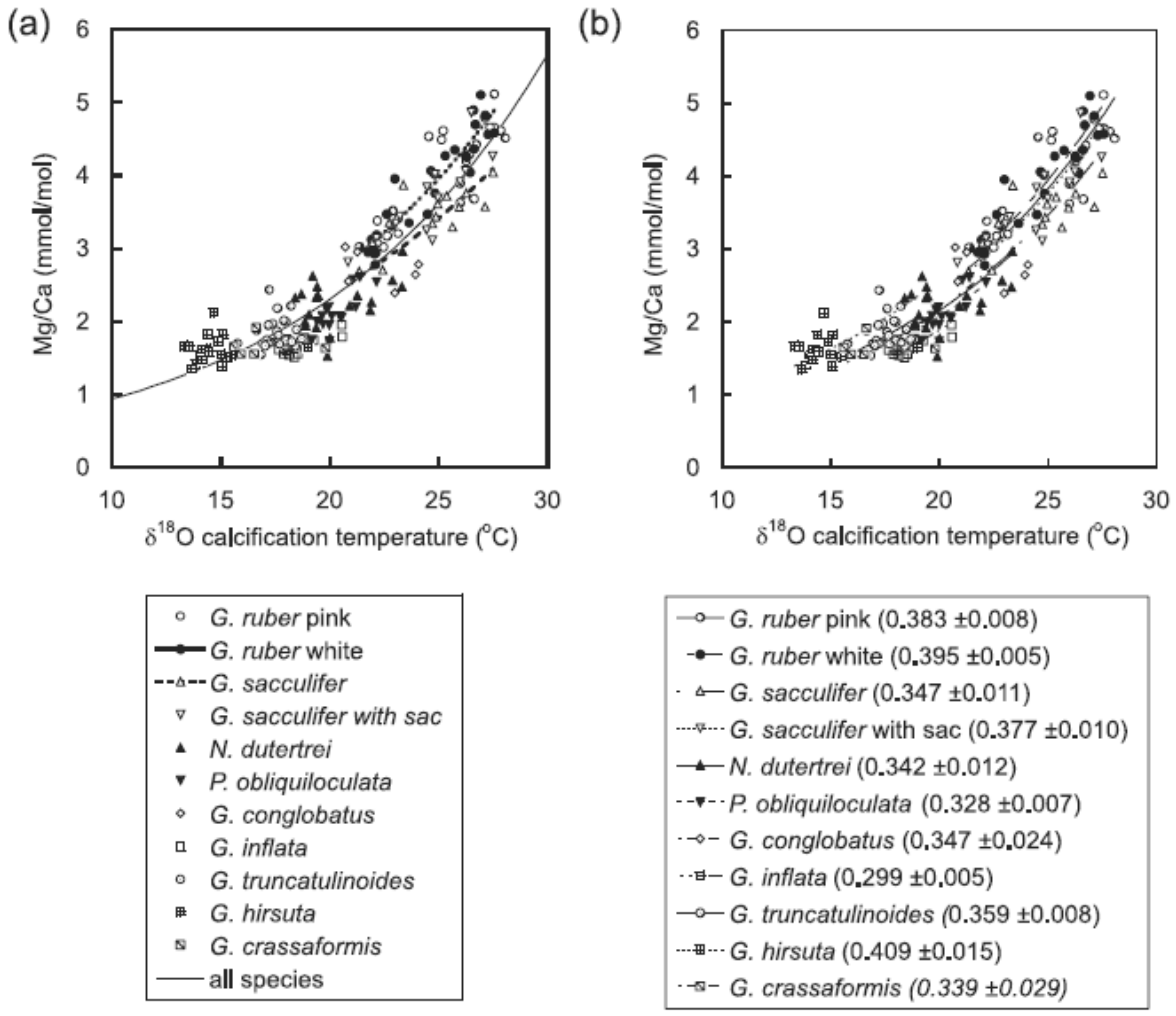

Figure 2-9 Mg/Ca versus $\delta^{18}O$ calcification temperature showing exponential fit (Anand et al., 2003); a) All species listed in the box; b) Mg/Ca versus $\delta^{18}O$ calcification temperature showing individual species calibrations assuming a constant exponential ($A = 0.09 \pm 0.03$), values of B are shown in the box.

The influence of other environmental factors, such as pH and salinity, on planktonic Mg/Ca has also been investigated (Nürnberg et al., 1996a; 1996b; Lea et al., 1999). Regarding a possible salinity influence, Nürnberg et al. (1996a) keeping a constant temperature (26.5ºC) only observed higher Mg/Ca ratios when salinity was increased drastically (between 22-45%). Under natural conditions (33-36%) temperature was demonstrated to be the main controlling factor on Mg/Ca. The work of Lea et al. (1999) corroborated the major control of temperature showing a slight relationship between salinity and Mg/Ca of 4% increase in Mg/Ca per psu at 22ºC (based on cultured *Orbulina universa*). A potential 1‰ increase in salinity in the glacial ocean would only have had a small effect on foraminiferal Mg/Ca equivalent to 0.5ºC (Lea et al., 1999). Recently, however, two independent studies, Harding (2007) and Ferguson et al. (2008), have found evidence of higher control of the salinity on the Mg/Ca ratio of *Neobloquadrina pachyderma (sinistral)* on sediment samples from the high latitude North Atlantic (Harding, 2007), and on several species from the Mediterranean Sea (Ferguson et al., 2008). These investigations anticipate the need of further studies in regard the controls of salinity on planktonic Mg/Ca.

Concerning pH, experiments with *Globigerina bulloides* at 22ºC with varying pH from 7.6 to 8.5 reveal that shell Mg/Ca decreases by 6 ± 2% per 0.1 pH unit increase (Lea et al., 1999). This change is approximately equivalent to the Mg/Ca decrease predicted for a 0.6°C decrease in temperature.

The error on the temperature estimations typically range between ±0.6ºC and 1.1ºC (e.g. Mashiotta et al., 1999; e.g. Elderfield and Ganssen, 2000), thus changes in Mg/Ca due to variations in both, salinity and pH, are within this error and, for most environments, where both, salinity and pH do not change so drastically, they can be neglected.

Investigations have also shown that there are some caveats on the use of Mg/Ca as a paleotemperature recorder:

- Post-depositional dissolution may alter the ratio by removing preferentially Mg from the biogenic carbonate (e.g. Rosenthal et al., 2000; e.g. Regenberg et al., 2006).

- Contamination by clays or metal phases (e.g. Mn and Fe oxides) may increase the Mg/Ca ratio (Barker et al., 2003; Pena et al., 2005).

- The formation of gametogenic calcite (outer calcite crust) in many foraminifera species has lower Mg/Ca composition than ontogenic calcite (inner layers) (by a factor of up to 3, Sadekov et al., 2005 and references therein). In contrast, Nürnberg et al. (1996a) found from culturing *Globigerinoides sacculifer* that the final gametogenic chambers are enriched in Mg.

These caveats highlight the necessity of investigating possible sources of contamination in our study area, in order to perform more rigorous cleaning procedures if necessary. The likelihood of dissolution on the foraminifera we intend to use for analysis should likewise be investigated. It also needs to be acknowledged when using Mg/Ca on planktonic foraminifera that their abundances are not constant throughout the year. For instance, maximum abundances of *Globigerinoides ruber* and *Neogobloquadrina pachyderma* are normally observed during the summer months, hence, it is during summer when larger amounts of shells reach the deep ocean so that the temperature recorded by these species may mainly reflect a summer temperature (Wang et al., 1995; King and Howard, 2005). On the other hand, maximum abundances of *G. bulloides* have been found in spring (Ganssen and Kroon, 2000; King and Howard, 2005; Tedesco et al., 2007) and so this species will yield lower temperatures than *G. ruber* and *N. pachyderma.*

The main advantage of the Mg/Ca ratio of foraminiferal shells in recording past SST with respect to other paleotemperature proxies (foraminiferal transfer functions, Imbrie and Kipp, 1971; UK'-37 unsaturation index, Rosell-Melé et al., 1995) is that it can be measured on the same phase as $\delta^{18}O$. For this reason, there is no spatial or temporal ambiguity in the incorporation of Mg and ^{18}O, as they both record calcification conditions. This allows discriminating between changes in foraminiferal $\delta^{18}O$ due to changing $\delta^{18}O_{sw}$ or to temperature effects (see 2.1.1.) by incorporation of Mg/Ca derived SST into the paleotemperature equations (see Chapter 4.5 for computation).

2.1.5. Sortable Silt Mean Size ($\overline{SS}$)

The Sortable Silt Mean Size ($\overline{SS}$) is defined as the mean grain size of the 10-63 μm terrigenous fraction, with biogenic carbonate and opal removed (McCave et al., 1995a).
This sedimentological parameter has been proposed as a paleocurrent strength recorder (McCave et al., 1995a; 1995b; Bianchi et al., 1999) and has been used in several oceanographic studies (Bianchi et al., 2001; Hall et al., 2001; Evans et al., 2007).

The principle is based on the observation that the silt coarser than 10 μm displays noncohesive behaviour because of the breakage of aggregates, thus responding more like single particles to hydrodynamic forces on erosion and deposition, and being size-sorted according to shear stress (McCave et al., 1995a). Silt finer than 10 μm, on the other hand, behaves in a cohesive manner because aggregates in this size class are not easily disaggregated. Additionally, other current related sediment parameters show good relationships with the $\overline{SS}$. McCave (1985) demonstrated a tight correlation between modal size and peak height of the 10-63 μm population. $\overline{SS}$ is preferred because it is experimentally more robust. The ratio of the 10-63 μm material to the total fine fraction (<63 μm) provides an additional index of the percentage-based enrichment factor. This ratio is expected to increase with increasing current speed because, on average, finer particles are found in aggregates of lower settling velocity that are transported away (McCave et al., 1995a and references therein). Another additional current index is derived from the recognition that only near-bottom currents can produce similar sorting effects in both lithogenic and biogenic fractions > 10 μm (Wang and McCave, 1990). Robinson and McCave (1994) proposed a percentage based index for combined terrigenous and carbonate material that allows eliminating competing influences on sediment texture, i.e. recording the common variance of the size of the terrigenous and biogenic fractions.

So far two main difficulties have been suggested for the use of $\overline{SS}$ as paleocirculation proxy. These are contamination of the signal by Ice Rafted Detritus (IRD, terrigenous material carried by icebergs) in the high latitudes (Hass, 2002) and the incapability of the proxy, on a purely sedimentary basis, to distinguish whether a change in the silt size is caused by a change in the mean current speed or in the variability of the peak current speed (McCave et al., 1995a).

The distorting influence of IRD in interpreting $\overline{SS}$ records has been addressed by Hass (2002; 2004). Based on sediments from the North Atlantic he proposed a method that sets ice-rafted sand in relation to the silt of both, current and ice-transported origin. Deviations from the resulting regression function are used to determine the behaviour of the silt mean grain size as a function of current speed independently from IRD bias.

Because of the difficulty of the $\overline{SS}$ to distinguish between sorting due to a “small mean-large variability” and “large mean-small variability” current regime, McCave et al. (1995a) recommend to avoid regions of high kinetic current energy. These are typically areas of high eddy activity, i.e. North American Basin (undergoes the action of the Gulf Stream), Kuroshio Current area, most of the domain beneath the flow path of Antarctic Circumpolar Current, Argentine Basin and the Agulhas Retroflection Area.

In this context it is worth noting the high degree of confidence in the available $\overline{SS}$ data from MD96-2080 and MD02-2594 as a paleocurrent recorder. The core site lies outside of the main Agulhas Retroflection Area (see Fig. 3-1a) and the $\overline{SS}$ record displays clear orbital modulation paralleling the stable isotope records (e.g. Fig. 5.1-6). This provides clear indication that climate induced changes of current strength determine the $\overline{SS}$ signal. Additional sedimentological data from core MD96-2080, such as weight % < 63 μm and % $CaCO_3$, confirm that current activity is the main factor influencing the record (I. Hall pers. comm., 2006) (see Chapter 5 for further details on the record).

References

Anand, P., Elderfield, H. and Conte, M.H., 2003. Calibration of Mg/Ca thermometry in planktonic foraminifera from a sediment trap time series. Paleoceanography, 18 (2), 1,050-1,065.

Barker, S., Greaves, M. and Elderfield, H., 2003. A study of cleaning procedures used for foraminiferal Mg/Ca paleothermometry. Geochemistry, Geophysics, Geosystems, 4 (9), 8407, doi:10.1029/2003GC000559.

Bemis, B.E., Spero, H., Bijma, J. and Lea, D.W., 1998. Reevaluation of the oxygen isotopic composition of planktonic foraminifera: experimental results and revised paleotemperature equations. Paleoceanography, 13, 150-160.

Bianchi, G.G., Vautravers, M. and Shackleton, N.J., 2001. Deep flow variability under apparently stable North Atlantic Deep Water production during the last interglacial of the subtropical NW Atlantic. Paleoceanography, 16 (3), 306-316.

Bianchi, G.G., Hall, I.R., McCave, I.N. and Joseph, L., 1999. Measurements of the sortable silt current speed proxy using the Sedigraph 5100 and Coulter Multisizer IIe: precission and accuracy. Sedimentology, 46, 1,001-1,014.

Bigg, G.R., 1995. Aridity of the Mediterranean Sea at the Last Glacial Maximum: A Reinterpretation of the $\delta^{18}O$ Record. Paleoceanography, 10 (2), 283-290.

Bijma, J., Faber, W.W. and Hemleben, C., 1990. Temperature and salinity limits for growth and survival of some planktic foraminifers in laboratory cultures. Journal of Foraminiferal Research, 20, 95-116.

Bijma, J., Spero, H.J., Lea, D.W. and Bemis, B.E., 1999. Reassessing foraminiferal stable isotope geochemistry: Impact of the oceanic carbonate system (experimental results). In: G. Fischer and W. G. (Editors), Use of proxies in paleoceanography. Examples from the South Atlantic. Springer-Verlag, Berlin, Heidelberg, pp. 489-512.

Boyle, E.A., 1983. Manganese Carbonate overgrowths on foraminifera tests. Geochimica et Cosmochimica Acta, 47 (10), 1,815-1,819.

Boyle, E.A., 1988. Cadmium: Chemical Tracer of Deep-water Paleoceanography. Paleoceanography, 3, 431-489.

Boyle, E.A., 1992. Cadmium and $\delta^{13}C$ paleochemical ocean distributions during the stage 2 glacial maximum. Annual Review of Earth and Planetary Sciences, 20, 245-287.

Boyle, E.A. and Keigwin, L.D., 1985/86. Comparison of Atlantic and Pacific paleochemical records for the last 215,000 years: changes in deep ocean circulation and chemical inventories. Earth and Planetary Science Letters, 76 (1-2), 135-150.

Boyle, E.A. and Rosenthal, Y., 1996. Chemical Hydrography of the South Atlantic during the Last Glacial Maximum: Cd *vs* $\delta^{13}C$. In: G. Wefer, W.H. Berger, G. Siedler and D. Webb (Editors), The South Atlantic: Present, Past and Future. Springer-Verlag Berlin Heidelberg New York, pp. 423-443.

Boyle, E.A., Sclater, F. and Edmond, J.M., 1976. On the marine geochemistry of Cadmium. Nature, 263, 42-44.

Broecker, W.S., 2002. The Glacial World according to Wally. Eldigio Press. Lamont-Doherty Earth Observatory of Columbia University, Lamont, 312 pp.

Broecker, W.S. and Peng, T.-H., 1982. Tracers in the Sea. Eldigio Press, Palisades, New York, 690 pp.

Broecker, W.S. and Maier-Reimer, E., 1992. The influence of air and sea exchange on the carbon isotope distribution in the sea. Global and Biogeochemical Cycles, 6 (3), 315-320.

Craig, H. and Gordon, L.I., 1965. Deuterium and oxygen 18 variations in the ocean and the marine atmosphere. In: E. Tongiorgi (Editor), Stable Isotopes in Oceanographic Studies and Paleotemperatures. Laboratorio di Geologia Nucleare, Pisa, Italy, pp. 9-130.

Cullen, J.T., 2006. On the nonlinear relationship between dissolved cadmium and phosphate in the modern global ocean: Could chronic iron limitation of phytoplankton growth cause the kink? Limnology and oceanography, 51 (3), 1,369-1,380.

Curry, W.B. and Oppo, D.W., 2005. Glacial water mass geometry and the distribution of $\delta^{13}C$ of ΣCO_2 in the western Atlantic Ocean. Paleoceanography, 20, PA1017, doi:10.1029/2004PA001021.

Charles, C.D., Wright, J.D. and Fairbanks, R.G., 1993. Thermodynamic influences on the marine carbon isotope record. Paleoceanography, 8 (6), 691-698.

Chave, K.E., 1954. Aspects of biogeochemistry of magnesium: 1. Calcareous marine organisms. Journal of Geology, 62, 266–283.

Dansgaard, W., 1964. Stable isotopes in precipitation. Tellus, 16, 436-468.

Dansgaard, W., Johnson, J.J., Clausen, B.H., Dahl-Jensen, D., Gundestrup, N.S., Hammer, C.U., Hvidberg, C.S., Steffensen, J.P., Sveinbjörndottir, A.E., Jouzel, J. and Bond, G., 1993. Evidence for a general instability of past climate from a 250 kyr ice-core record. Nature, 364, 218-220.

Degens, E.T., 1969. Biogeochemistry of stable carbon isotopes. In: M.T.J. Eglinton G. and Murphy (Editors), Organic Geochemistry. Springer-Verlag, New York, Heidelberg, Berlin, pp. 304-329.

Degens, E.T., Behrendt, M., Gotthardt, B. and Reppmann, E., 1968. Metabolic fractionation of carbon isotopes in marine plankton, II. Data on samples collected off the coasts of Peru and Ecuador. Deep Sea Research, 15, 11-20.

Dickson, J.A.D., 2002. Fossil Echinoderms As Monitor of the Mg/Ca Ratio of Phanerozoic Oceans. Science, 298, 1,222-1,224.

Diz, P., Hall, I.R., Zahn, R. and Molyneux, E.G., 2007. Paleoceanography of the southern Agulhas Plateau during the last 150 ka: Inferences from benthic foraminiferal assemblages and multispecies epifaunal carbon isotopes. Paleoceanography, 22, PA4218, doi:10.1029/2007PA001511.

Duplessy, J.C., Shackleton, N.J., Fairbanks, R.G., Labeyrie, L., Oppo, D. and Kallel, K., 1988. Deep water source variations during the last climatic cycle and their impact on the global deep water circulation. Paleoceanography, 3 (3), 343-360.

Elderfield, H. and Ganssen, G., 2000. Past temperature and $\delta^{18}O$ of surface ocean waters inferred from foraminiferal Mg/Ca ratios. Nature, 405, 442-445.

Elderfield, H. and Rickaby, R.E.M., 2000. Oceanic Cd/P ratio and nutrient utilization in the glacial Southern Ocean. Nature, 405, 305-310.

Emrich, K., Ehhalt, D.H. and Vogel, J.C., 1970. Carbon isotope fractionation during the precipitation of calcium carbonate. Earth and Planetary Science Letters, 8, 363-371.

Erez, J., Almogi, A. and Abraham, S., 1991. On the life history of planktonic foraminifera: Lunar reproduction cycle in *Globigerinoides sacculifer* (Brady). Paleoceanography, 6 (3), 295-306.

Evans, H.K., Hall, I.R., Bianchi, G.G. and Oppo, D.W., 2007. Intermediate Water links to Deep Western Boundary Current variability in the subtropical NW Atlantic during Marine Isotope Stages 5 and 4. Paleoceanography, 22, PA3209, doi:10.1029/2006PA001409.

Fairbanks, R.G., 1989. A 17,000 year glacio-esutatic sea-level record: Influence of glacial melting rates on the Younger Dryas Event and deep-ocean circulation. Nature, 342, 637-642.

Ferguson, J.E., Henderson, G.M., Kucera, M. and Rickaby, R.E.M., 2008. Systematic change of foraminiferal Mg/Ca ratios across a strong salinity gradient. Earth and Planetary Science Letters, 265 (1-2), 153.

Ganssen, G. and Kroon, D., 2000. The isotopic signature of planktonic foraminifera from NE Atlantic surface sediments: implications for the reconstruction of past oceanic conditions. Journal of the Geological Society London, 157, 693-699.

Grossman, E.L., 1987. Stable isotopes in modern benthic foraminifera: A study of vital effect. Journal of Foraminiferal Research, 17, 48-61.

Hall, I.R., McCave, N., Shackleton, N.J., Weedon, G.P. and Harris, S.E., 2001. Intensified deep Pacific inflow and ventilation in Pleistocene glacial times. Nature, 412, 809-813.

Harding, D., 2007. Quick Corruption of Conveyor Circulation; a Geochemical Approach, Oxford University, Oxford, 303 pp.

Hass, H.C., 2002. A method to reduce the influence of ice-rafted debris on a grain size record from northern Fram Strait, Artic Ocean. Polar Research, 2, 299-306.

Hass, H.C., 2004. Grain-size-based paleocurrent-speed reconstruction of IRD-contaminated sediments from the Artic Ocean, Int. Workshop HWK Delmenhorst 15-18 April 2004. From Particle Size to Sediment Dynamics.

Hester, K. and Boyle, E.A., 1982. Water chemistry control of the Cd content of benthic foraminiferal. Nature, 298, 260-261.

Imbrie, J. and Kipp, N.G., 1971. A new micropaleontological methos for quantitative paleoclimatology: Aplication to a Late Pleistocene Caribbean core. In: K. Turekian (Editor), The Late Cenozoic Glacial Ages. Yale Univ. Press., New Haven, pp. 71-181.

Imbrie, J., Hays, J.D., Martinson, D.G., McIntyre, A., Mix, A.C., Morley, J.J., Pisias, N.G., Prell, W.L. and Shackleton, N.J., 1984. The Orbital Theory of Pleistocene Climate: support from a revised chronology of the Marine $\delta^{18}O$ record. In: J.I. A. L. Berger, J. Hays, G. Kukla, B. Saltzman (Editors), Milankovitch and Climate. Series C: Mathematical and Physical Sciences. D. Reidel Publishing Company, pp. 269-305.

Jacobs, S.S., Fairbanks, R.G. and Horibe, Y., 1985. Origin and evolution of water masses near the Antarctic continental margin. In: S.S. Jacobs (Editor), Oceanology of the Antarctic Continental Shelf, Antarctic Research Series, pp. 59-85.

Kim, S.T. and O'Neil, J.R., 1997. Equilibrium and nonequilibrium oxygen isotope effects in synthetic calcites. Geochimica et Cosmochimica Acta, 61, 3,461-3,475.

King, A.L. and Howard, W.R., 2005. $\delta^{18}O$ seasonality of planktonic foraminifera from Southern Ocean sediment traps: Latitudinal gradients and implications for paleoclimate reconstructions. Marine Micropaleontology, 56 (1-2), 1-24.

Kroopnick, P., 1980. The distribution of $\delta^{13}C$ of CO_2 in the Atlantic ocean. Earth and Planetary Science Letters, 49, 469-484.

Kroopnick, P., Weiss, R.F. and Craig, H., 1972. Total CO_2, $\delta^{13}C$, dissolved oxygen - $\delta^{18}O$ at GEOSECS II in the North Atlantic. Earth and Planetary Science Letters, 16, 103-110.

Kroopnick, P.M., 1985. The distribution of $\delta^{13}C$ of CO_2 in the world oceans. Deep Sea Research, 32(1), 57-84.

Kroopnick, P.M., Margolis, S.V. and Wong, C.S., 1977. $\delta^{13}C$ variations in marine carbonate sediment as indicators of the CO_2 balance between the atmosphere and oceans. In: Andersen, N.R. and Malahoff, A. (Editors), The Fate of Fossil Fuel CO_2 in the Oceans. Plenum, New York.

Labeyrie, L.D., Duplessy, J.-C. and Blanc, P.L., 1987. Variations in mode of formation and temperature of oceanic deep waters over the past 125,000 years. Nature, 327, 477-482.

Lea, D.L., Mashiotta, Y.A. and Spero, H.P., 1999. Controls on magnesium and strontium uptake in planktonic foraminifera determined by live culturing. Geochimica et Cosmochimica Acta, 63 (16), 2,369-2,379.

Lea, D.W., 1999. Trace elements in foraminiferal calcite. In: B.K. Sen Gupta (Editor), Modern Foraminifera. Kluwer, Dordrect, pp. 259-277.

Lear, C.H., Rosenthal, Y. and Slowey, N., 2002. Benthic foraminiferal Mg/Ca-paleothermometry: a revised core-top calibration. Geochimica et Cosmochimica Acta, 66 (19), 3,375–3,387.

Lisiecki, L.E. and Raymo, M.E., 2005. A Pliocene-Pleistocene stack of 57 globally distributed benthic $\delta^{18}O$ records. Paleoceanography, 20, PA1003, doi:10.1029/2004PA001071.

Lorens, R.B., Williams, D.F. and Bender, M.L., 1977. The early nonstructural chemical diagenesis of foraminiferal calcite. Journal of Sedimentary Petrology, 47, 1,602-1,609.

Löscher, B.M., de Jong, J.T.M. and de Baar, H.J.W., 1998. The distribution and preferential biological uptake of cadmium at 6ºW in the Southern Ocean. Marine Chemistry, 62 (3-4), 259-286.

Lynch-Stieglitz, J. and Fairbanks, R.G., 1994. A conservative tracer for glacial ocean circulation from carbon isotope and paleonutrient measurements in benthic foraminifera. Nature, 369, 308-310.

Lynch-Stieglitz, J., van Geen, A. and Fairbanks, R.G., 1996. Interocean exchange of Glacial North Atlantic Intermediate Water: evidence from the subantarctic Cd/Ca and carbon isotope measurements. Paleoceanography, 11 (2), 191-201.

Lynch-Stieglitz, J., Stocker, T.F., Broecker, W.S. and Fairbanks, R.G., 1995. The influence of air-sea exchange on $\delta^{13}C$ of ΣCO_2 in the surface ocean: Observations and Modeling. Global and Biogeochemical Cycles, 9, 653-665.

Mackensen, A. and Bickert, T., 1999. Stable Carbon Isotopes in Benthic Foraminifera: Proxies for Deep and Bottom Water Circulation and New Production. In: G. Fischer and G. Wefer (Editors), Use of Proxies in Paleoceanography: Examples from the South Atlantic. Springer-Verlag Berlin Heidelberg, pp. 229-254.

Mackensen, A. and Licari, L., 2004. Carbon isotopes of live benthic foraminifera from the South Atlantic Ocean: sensitivity to bottom water carbonate saturation state and organic matter rain rates. In: G. Wefer, S. Mulitza and V. Rathmeyer

(Editors), The South Atlantic in the Late Quaternary: Reconstruction of Material Budget and Current Systems. Springer-Verlag, Berlin, pp. 623–644.

Mackensen, A., Hubberten, H.-W., Bickert, T., Fischer, G. and Fütterer, D.K., 1993. The $\delta^{13}C$ in benthic foraminiferal tests on *Fontbotia wuellerstorfi* (Schwager) relative to the $\delta^{13}C$ of dissolved inorganic carbon in southern ocean deep water: implications for glacial ocean circulation models. Paleoceanography, 8 (5), 587-610.

Marchitto, T.M., 2004. Lack of a significant temperature influence on the incorporation of Cd into benthic foraminiferal tests. Geochemistry, Geophysics, Geosystems, 5 (10), Q10D11, doi: 10.1029/2004GC000753.

Marchitto, T.M. and Broecker, W.S., 2006. Deep water mass geometry in the glacial Atlantic Ocean: A review of constraints from the paleonutrient proxy Cd/Ca. Geochemistry, Geophysics, Geosystems, 7, Q12003, doi:10.1029/2006GC001323.

Marchitto, T.M., Oppo, D.W. and Curry, W.B., 2002. Paired benthic foraminiferal Cd/Ca and Zn/Ca evidence fro a greatly increased presence of Southern Ocean water in the glacial North Atlantic. Paleoceanography, 17 (3), 1038, doi: 10.1029/2000PA000598.

Martinson, D.G., Pisias, N.G., Hays, J.D., Imbrie, J., Moore, T.C. and Shackleton, N.J., 1987. Age Dating and the Orbital Theory of the Ice Ages: Developemtn of a High-Resolution 0 to 300,000-year Chronostratigraphy. Quaternary Research, 27, 1-29.

Mashiotta, T.A., Lea, D.W. and Spero, H.J., 1999. Glacial-interglacial changes in Sub-Antarctic sea surface temperature and [delta]18O-water using foraminiferal Mg. Earth and Planetary Science Letters, 170 (4), 417-432.

McCave, I.N., 1985. Sedimentology and stratigraphy of box cores from the HEBBLE site on the Nova Scotian Continental Rise. Marine Geology, 66 (1-4), 59-89.

McCave, I.N., Manighett, B. and Robinson, S.G., 1995a. Sortable silt and fine sediment size/composition slicing: parameters for palaeocurrent speed and palaeoceanography. Paleoceanography, 10, 593-610.

McCave, I.N., Manighetti, B. and Beveridge, N.A.S., 1995b. Circulation in the glacial North Atlantic inferred from grain-size measurements. Nature, 374, 149-152.

McCorkle, D., Keigwin, L., Corliss, B. and Emerson, S., 1990. Correction to The influence of microhabitats on the carbon isotopic composition of deep-sea benthic foraminifera. Paleoceanography, 5 (3), 161-185.

McCorkle, D.C., Martin, P.A., Lea, D.W. and Klinkhammer, G.P., 1995. Evidence of a dissolution effect on benthic foraminiferal shell chemistry: $\delta^{13}C$, Cd/Ca, Ba/Ca, and Sr/Ca results from the Ontong Java Plateau. Paleoceanography, 10 (4), 699-714.

Mook, W.G., 1986. ^{13}C in atmospheric CO_2. Netherlands Journal of Sea Research, 20 (2/3), 211-223.

Mortyn, P.G. and Charles, C.D., 2003. Planktonic foraminiferal depth habitat and $\delta^{18}O$ calibrations: Plankton tow results from the Atlantic sector of the Southern Ocean. Paleoceanography, 18 (2), 1037, doi:10.1029/2001PA000637.

Niebler, H.S., Hubberten, H.W. and Gersonde, R., 1999. Oxygen Isotope Values of Planktonic Foraminifera: A Tool for the Reconstruction of Surface Water Stratification. In: G. Fischer and G. Wefer (Editors), Use of Proxies in Paleoceanography: Examples from the South Atlantic. Springer-Verlag, Berlin, Heidelberg, pp. 165-189.

Ninnemann, U.S. and Charles, C.D., 2002. Changes in the mode of Southern Ocean circulation over the last glacial cycle revealed by foraminiferal stable isotopic variability. Earth and Planetary Science Letters, 201 (2), 383-396.

Nürnberg, D., 1995. Magnesium in tests of *Neogloboquadrina pachyderma* (sinistral) from high northern and southern latitudes. Journal of Foraminifereral Research, 25, 350-368.

Nürnberg, D., Bijma, J. and Hemleben, C., 1996a. Assessing the reliability of magnesium in foraminiferal calcite as a proxy for water mass temperatures. Geochimica et Cosmochimica Acta, 60 (5), 803-814.

Nürnberg, D., Bijma, J. and Hemleben, C., 1996b. Erratum: Assessing the reliability of magnesium in foraminiferal calcite as a proxy for water mass temperatures. Geochimica et Cosmochimica Acta, 60 (13), 2,483-2,484.

O'Neil, J.R., Clayton, R.N. and Mayeda, T.K., 1969. Oxygen isotope fractionation on divalent metal carbonates. Journal of Chemical Physics, 51, 5,547-5,558.

Oppo, D.W. and Fairbanks, R.G., 1989. Carbon isotope composition of tropical surface water during the past 22,000 years. Paleoceanography, 4, 333–351.

Pena, L., Calvo, E., Cacho, I., Eggins, S. and Pelejero, C., 2005. Identification and removal of Mn-Mg-rich contaminant phases on framiniferal tests: Implications for Mg/Ca past temperature reconstructions. Geochemistry, Geophysics, Geosystems, 6, Q09P02, doi: 10.1029/2005GC000930.

Regenberg, M., Nürnberg, D., Steph, S., Groeneveld, J., Garbe-Schönberg, D., Tiedemann, R. and Dullo, W.-C., 2006. Assessing the effect of dissolution on planktonic foraminiferal Mg/Ca ratios: Evidence from Caribbean core tops. Geochemistry, Geophysics, Geosystems, 7, Q07P15, doi: 10.1029/2005GC001019.

Robinson, S.G. and McCave, I.N., 1994. Orbital forcing of bottom-current enhanced sedimentation on Feni Drift NE Atlantic during the mid-Plesitocene. Paleoceanography, 9, 943-972.

Rohling, E.J. and Bigg, G.R., 1998. Paleosalinity and $\delta^{18}O$: A critical assesment. Journal of Geophysical Research, 103 (C1), 1,307-1,318.

Rohling, E.J. and Cooke, S., 1999. Stable oxygen and carbon isotopes in foraminiferal shells. In: B.K.S. Grupta (Editor), Moder Foraminifera. Kluwer Academic Publishers.printed in Great Britain, pp. 239-279.

Rosell-Melé, A., Eglinton, G., Pflaumann, U. and Sarnthein, M., 1995. Atlantic core-top calibration of the UK-37 index as a sea-surface palaeotemperature indicator. Geochimica et Cosmochimica Acta, 59, 3,099–3,107.

Rosenthal, Y., Boyle, E.A. and Labeyrie, L., 1997. Last glacial maximum paleochemistry and deepwater circulation in the Southern Ocean: Evidence from foraminiferal cadmium. Paleoceanography, 12 (6), 787-796.

Rosenthal, Y., Lam, P., Boyle, E.A. and Thomson, J., 1995. Authigenic cadmium enrichments in suboxic sediments: Precipitation and postdepositional mobility. Earth and Planetary Science Letters, 132 (1-4), 99.

Rosenthal, Y., Lohman, G.P., Lohman, K.C. and Sherrell, R.M., 2000. Incorporation and preservation of Mg in *Globigerinoides sacculifer*: Implications for reconstructing the temperature and $^{18}O/^{16}O$ of seawater. Paleoceanography, 15 (1), 135-145.

Ruddiman, W.F., 2001. Earth's Climate: Past and Future. W.H. Freeman and Co Ltd, New York, 465 pp.

Sadekov, A.Y., Eggins, S.M. and De Deckker, P., 2005. Characterization of Mg/Ca distributions in planktonic foraminifera species by electron microprobe mapping. Geochemistry, Geophysics, Geosystems, 6 Q12P06, doi: 10.1029/2005GC000973.

Schmidt, G.A., Hoffmann, G. and Thresher, D., 2001. Isotopic Tracers in Coupled Models: A New Paleo-Tool. PAGES News, 9 (1), 10-11.

Shackleton, N.J., 1974. Attainment of isotopic equilibrium between ocean water and the benthonic foraminifera genus *Uvigerina*: Isotopic changes in the ocean during the last glacial. Colloques Internationaux du Centre National de la Recherche Scientifique, 219, 203-209.

Shackleton, N.J., 1977. Carbon 13 in *Uvigerina*: Tropical rainforest history and the equatorial Pacific carbonate dissolution cycles. In: N. R. Andersen and A. Malahoff (Editor), The Fate of Fossil Fuel CO_2 in the Oceans. Plenum, New York, pp. 401–428.

Shackleton, N.J., 1987. Oxygen Isotopes, Ice Volume and Sea Level. Quaternary Science Reviews, 6, 183-190.

Spero, H.J. and Lea, D.W., 1993. Intraspecific stable isotope variability in the planktic foraminifera *Globigerinoides sacculifer*: results from laboratory experiments. Marine Micropaleontology, 22, 221-234.

Spero, H.J. and Lea, D.W., 1996. Experimental determination of stable isotope variability in *Globigerina bulloides*: implications for paleoceanographic reconstructions. Marine Micropaleontology, 28, 231-246.

Spero, H.J., Bijma, J., Lea, D.W. and Bemis, B.E., 1997. Effect of seawater carbonate concentration on foraminiferal carbon and oxygen isotopes. Nature, 390, 497-500.

Tachikawa, K. and Elderfield, H., 1996. Chemistry of benthic Foraminiferal Shells for Recording Ocean Environments: Cd/Ca, $\delta^{13}C$ and Mg/Ca. In: M.e.a. Shiyomi (Editor), Global Environmental Change in the Ocean and on Land, pp. 249-263.

Tachikawa, K. and Elderfield, H., 2002. Microhabitat effects on Cd/Ca and $\delta^{13}C$ of benthic foraminifera. Earth and Planetary Science Letters, 202 (3-4), 607-624.

Tedesco, T., Thunell, R., Astor, Y. and Karger, F.M., 2007. The oxygen isotope composition of planktonic foraminifera from the Cariaco Basin, Venezuela: Seasonal and interannual variations. Marine Micropaleontology, 62, 180-193.

Urey, H.C., 1974. The thermodynamic properties of isotopic substances. Journal of the Chemical Society, 562-581.

Waelbroeck, C., Labeyrie, L., Michel, E., Duplessy, J.-C., McManus, J.F., Lambeck, K., Balbon, E. and Labracherie, M., 2002. Sea-level deep water temperature changes derived from benthic foraminifera isotopic records. Quaternary Science Reviews, 21, 295-305.

Wang, H. and McCave, I.N., 1990. Distinguishing climatic and current effects in mid-pleistocene sediments of Hatton and Gardar Drifts, NE Atlantic. Journal of the Geological Society London, 147, 373-383.

Wang, L., Sarnthein, M., Duplessy, J.-C., Erlenkeuser, H., Jung, S. and Pflaumann, U., 1995. Paleo sea surface salinities in the low-latitude Atlantic: The $\delta^{18}O$ record of *Globigerinoides ruber* (white). Paleoceanography, 10 (4), 749–762.

Wefer, G., Berger, W.H., Bijma, J. and Fischer, G., 1999. Clues to Ocean History: a Brief Overview of Proxies. In: G. Fischer and W. G. (Editors), Use of the Proxies in Paleoceanography. Examples of the South Atlantic. Springer-Verlag, Berlin, Heidelberg, New York, pp. 1-68.

Willamowski, C. and Zahn, R., 2000. Upper ocean circulation in the glacial North Atlantic from benthic foraminiferal isotope and trace element fingerprinting. Paleoceanography, 15 (5), 515-527.

Wolf-Gladrow, D.A., Riebesell, U., Burkhardt, S. and Bijma, J., 1999. Direct effects of CO_2 concentration on growth and isotopic composition of marine plankton. Tellus, 51B, 461-476.

Wright, J.D., 2000. Global Climate Change in Marine Stable Isotope Records. Quaternary Geochronology: Methods and Applications, 7 pp.

Zahn, R., Winn, K. and Sarnthein, M., 1986. Benthic foraminiferal $\delta^{13}C$ and accumulation of organic carbon: *Uvigerina perigerina* and *Cibicidoides wuellerstorfi*. Paleoceanography, 1 (1), 27-42.

Zeebe, R.Z., Bijma, J. and Wolf-Gladrow, D.A., 1999. A diffusion-reaction model of carbon isotope fractionation in foraminifera. Marine Chemistry, 64, 181-198.

3. Site Location and Hydrographical Conditions

Cores MD96-2080 and MD02-2594 were retrieved during the cruises NAUSICAA-MD105 (Namibia Angola Upwelling System and Indian Connection Austral Atlantic Campaign; IMAGES, International Marine Global Changes program) (Bertrand et al., 1997) and SWAF-MD128 (South West Africa Campaign) (Giraudeau et al., 2003). Both cores were recovered from close settings in the slope of the Agulhas Bank off South Africa at 2488 and 2440 m respectively. They coordinates are: 36º19.2'S; 19º28.2'E and 34º42.6'S; 17º20.3'E (Fig. 3-1a). The sediment cores are located within the corridor of Agulhas water leakage into the Atlantic and at depth they are influenced by the southern extension of North Atlantic Deep Water (NADW) (Fig. 3-1b).

The most prominent features of surface circulation in the region are the Agulhas Current and Agulhas Rings and Filaments that constitute the mean surface and thermocline water exchange between the Indian and Atlantic Ocean (Fig. 3-1a). At depth the exchange happens in the other sense, from the Atlantic to the Indian (Figs. 3-1a, b).

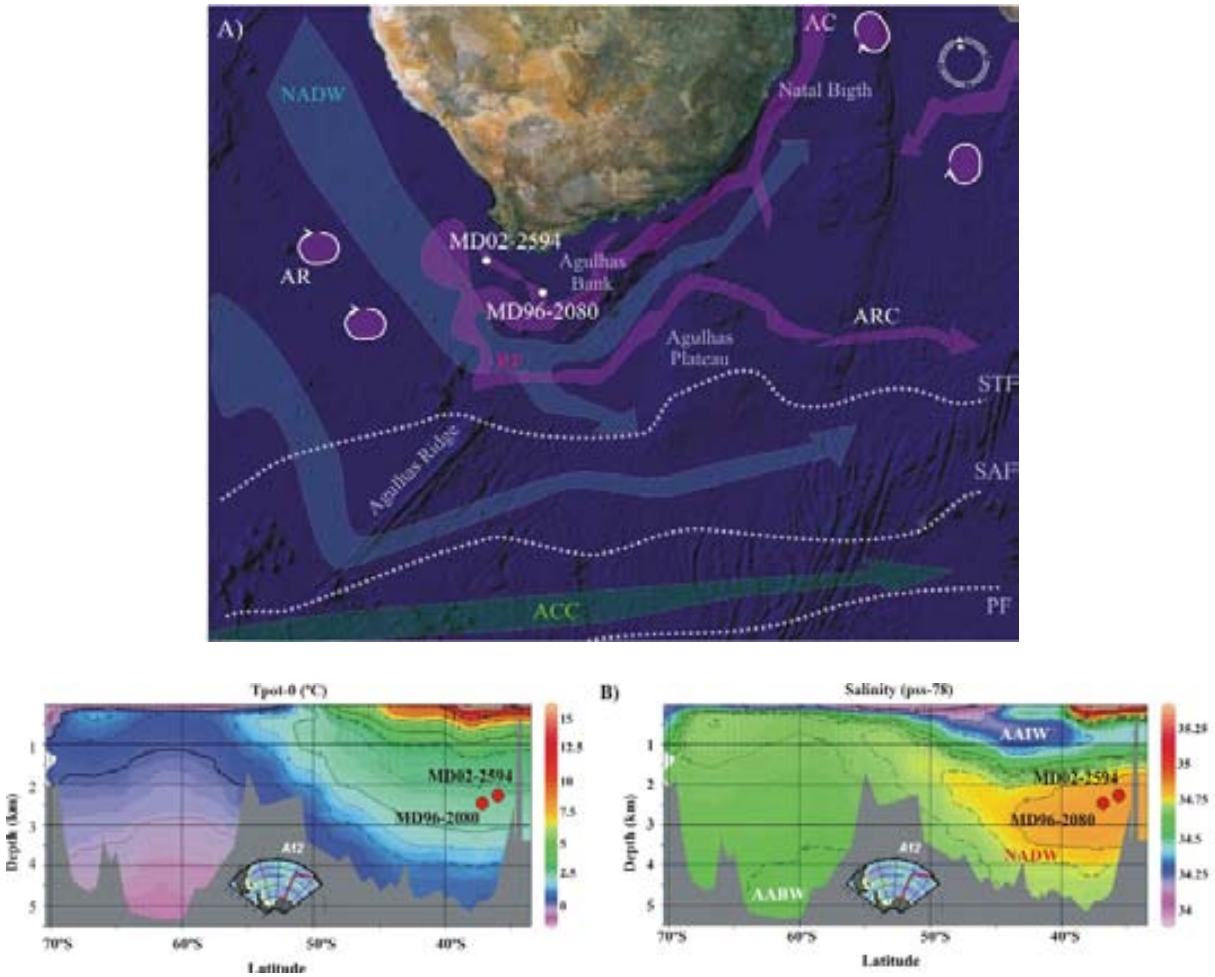

Figure 3-1 Location of Calypso cores MD96-2080 and MD02-2594 A) Within the Agulhas Leakage Corridor off South Africa (base map elaborated with the software GoogleEarth, http://earth.google.es/). Surface current patterns are displayed in red and are associated with the Agulhas Current (AC), Retroflection (RF), Agulhas Retroflection Current (ARC) and Agulhas Rings (AR). Blue arrows indicate the main path of North Atlantic Deep Water (NADW) at depth. Green arrow indicates the Antarctic Circumpolar Current (ACC). The light blue lines mark the approximate position of the Subtropical Front (STF), Sub-Antarctic Front (SAF) and Polar Front (PF). B) Meridional T-S transects across the Atlantic sector of the Southern Ocean and onwards to South Africa (modified from WOCE section SO2/A12; WOCE, 2002; http:// www.ewoce.org). Location of cores MD96-2080 and MD02-2594 is shown, displaying their position within the southern branch of NADW.

Because of the ensuing interocean water exchange (see Chapter 1), the region around southern Africa is hydrographically important for the global ocean Thermohaline Circulation (THC). The Agulhas Current is the main supplier of warm and salty thermocline waters that compose the return flow in the upper branch of the so called "Conveyor Belt" circulation (Gordon, 1986; Broecker, 1991; Gordon et al., 2003). Valentine et al. (1993) composed an overview of the various water masses present around South Africa, including temperature and salinity (T-S) characteristics and the water volume they carry (Table 3-1).

Table 3-1 Water masses of the southern African region (modified after Valentine et al., 1993).

Water mass or type	T (ºC)	S (psu)	Volume ($x10^3$ Km^3)	Percentage of total
Surface Agulhas Water	16-26	>35.5	82.1	3
Central			310.9	13
SE Atlantic	6-16	34.5-35.5		
SW Indian	8-15	34.6-35.5		
AAIW type	2.2	33.87	548.8	23
SE Atlantic	2.0-6.0	33.8-34.8		
SW Indian	2.0-10.0	33.8-34.8		
Deep Water			954.1	40
NADW (SE Atlantic)	1.5-4	34.8-35		
CDW (SW Indian)	0.1-2	34.63-34.73		
AABW	-0.9-1.7	34.64-34.72	457.9	19
Others			39.7	2

3.1. Agulhas Current and Retroflection

The Agulhas Current is the western boundary current of the South Indian Subtropical Gyre circulation. It carries some 70-78 Sv (1 Sv = 106 m^3/s) (Donohue et al., 2000; Bryden and Beal, 2001) of Indian subtropical waters with smaller and discontinuous contributions of waters from the Mozambique Channel (Sætre and Jorge da Silva, 1984; Feron et al., 1992) and from the East Madagascar Current (Lutjeharms et al., 1981; Feron et al., 1992).

The Agulhas Current is considered to be fully developed at 28ºS (Lutjeharms and de Ruijter, 1996). From this latitude on southwards the narrow current of salty and warm Agulhas Water is continuously present downstream and remains clearly visible in satellite imagery as a salient temperature anomaly (Fig. 3-2). Indeed, the satellite images indicate that the Agulhas Current can be considered to consist of a northern Agulhas Current and a southern Agulhas Current with different trajectorial behaviours (Harris et al., 1978; Lutjeharms et al., 1981). The limit between northern and southern Agulhas Current occurs approximately at the latitude of Port Elizabeth (~34ºS, South Africa, Fig. 3-2) where the continental shelf widens forming the expansion of the Agulhas Bank of southern Africa (Lutjeharms, 2007 and references therein).

The northern Agulhas Current closely follows the edge of the continental shelf with a nearly invariant flow path. Such rather stable mean trajectory contrasts with other western boundary currents such as the Gulf Stream and Kuroshio Current that display strong meandering undergoing seasonal

variability (Lutjeharms and de Ruijter, 1996 and references therein). This is probably due to the fact that the continental shelf east of South Africa is very narrow, near-uniform and with a steep slope providing optimum guidance to the current. From Cape St Lucia to East London the core of the current is located 52 km offshore with a standard deviation of its position of 14 km (Lutjeharms and de Ruijter, 1996). The only exception to this stable trajectory occurs at the Natal Bight. This is a wider part of the continental shelf north of Durban that can trigger instabilities in the Agulhas Current (see below). At Cape Seal (approximately 200 km upstream from where the current separates from the continental shelf) the mean trajectory position is identified some 130 km offshore with a standard deviation of 30 km (Goschen and Schumann, 1990). The southern Agulhas Current do develops meanders (Harris et al., 1978) which grow downstream forming also cyclonic eddies and warm plumes (Lutjeharms et al., 1989), hence, it shows a much variable flow path.

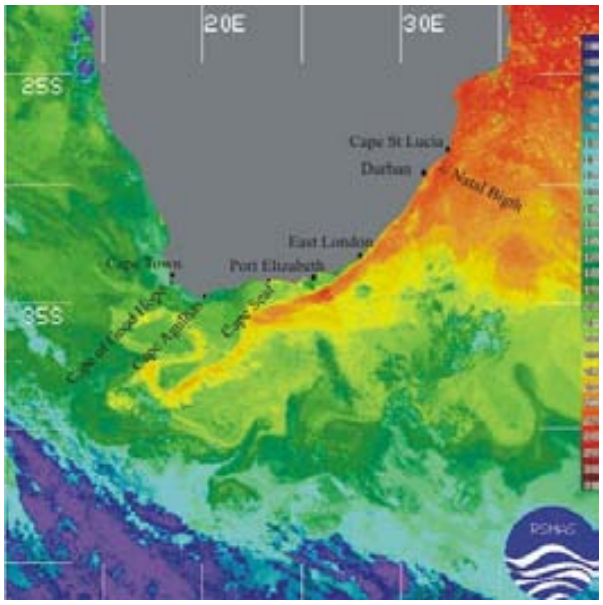

Figure 3-2 Infrared satellite image, taken on 23 March 2000. A cooled Agulhas eddy (green) surrounded by a warm filament of the Agulhas Return Current (yellow) can be observed. Modified from the image made available by the Rosenstiel School of Marine and Atmospheric Sciences (RSMAS), Miami, USA (http://www.rsmas.miami.edu/environment/imagery/) for publication in Peeters et al. (2004).

Characteristic temperature and salinity (T-S) values of surface waters carried in the Agulhas Current (Agulhas Water, AW) are 23-26ºC and 35.4 psu (Gordon et al., 1987). The hydrographical characteristics of the current do not change significantly within the upper 500 m of the water column. Nonetheless, an Agulhas Undercurrent has been discovered (Beal and Bryden, 1997). Containing mainly modified Red Sea Water (RSW) this Agulhas Undercurrent may carry some 4.2 Sv of water equatorwards (Lutjeharms, 2007). While the majority of the RSW flow is polewards within the Agulhas Current suggesting that the undercurrent is a peripheral circulation (Donohue et al., 2000). Further down in the water column temperature and salinity are influenced by northward flowing Antarctic Intermediate Water (AAIW) from the south. Yet, Agulhas Water characteristics are identifiable on occasion to water depths of 2000 m (Lutjeharms, 1996). Donohue et al (2000) measured a depth of penetration of the Agulhas Current of 2300 m in June 1995 but also to the ocean bottom in March 1995. Important for the salinity at deep levels are the Mozambique eddies that are observed in the southern part of the Mozambique channel (de Ruijter et al., 2002; Schouten et al., 2003) and contain a large amount of Red Sea/Persian Gulf outflow waters. As a result they form a high-salinity anomaly since they carry waters of salinity around 34.9 psu (de Ruijter et al., 2002).

In the region south of the Cape of Good Hope, between 15ºE and 20ºE the current turns anticlockwise and is retroflected back into the Indian Ocean as the Agulhas Return Current (ARC) (Feron et al., 1992). Several factors drive the retroflection of the Agulhas Current: the geographic position of the South African continental margin, wind patterns, inertia and planetary vorticity. The southern coast of Africa is located 5º latitude closer to the equator than the westerly wind maximum, latitude at which the western boundary currents in the subtropics are expected to separate from the continent to turn into their ocean's interior. The northerly position of Africa with respect to this wind maximum causes an early separation of the Agulhas Current from the continental margin which, together with local topography and regional to large scale wind circulation, results in the characteristic retroflection of the Agulhas Current (Gordon, 2003). After the separation from the coast, the almost 180º anticyclonic turn can be theoretically explained by the conservation of potential vorticity and advection of planetary vorticity (β effect) (de Ruijter and Boudra, 1985; Ou and de Ruijter, 1986).

Western boundary currents typically present strong seasonality (e.g. the Gulf Stream, Kelly, 1991; e.g. the Gulf Stream, Hogg and Johns, 1995) and some seasonal pattern has also been found for the Agulhas Current mainly alluding to the position of the retroflection (Quartly and Srokosz, 1993; Matano et al., 1998). Matano et al. (1998) propose that such changes occur as a result of shifts in the main path of the Agulhas Current due to the inflow of Agulhas Water. During the winter months, and likely during most of the year, the current retroflects at around 15ºE while during summer months an early retroflection (at around 25ºE) or bifurcation has been inferred form sea surface height (SSH) data. The proposed pattern is shown in Figure 3-3. Less income of Agulhas Water during winter would allow a far eastwards penetration of the current, on the other hand, during summer, local winds might cause an increase in the intensity of the inertial recirculation cell forcing an earlier retroflection due to reduce advection and planetary vorticity. Ffield et al. (1997) proposed that maximum transport of Agulhas Water occurs at the end of the summer and minimum during winter.

Studies analyzing the relation between the seasonal variability of the Agulhas Current and the leakage of Agulhas Water to the Atlantic Ocean are scarce. Garzoli and Gordon (1996) reported maximum presence of Agulhas Water in the Benguela system during autumn and minimum during summer.

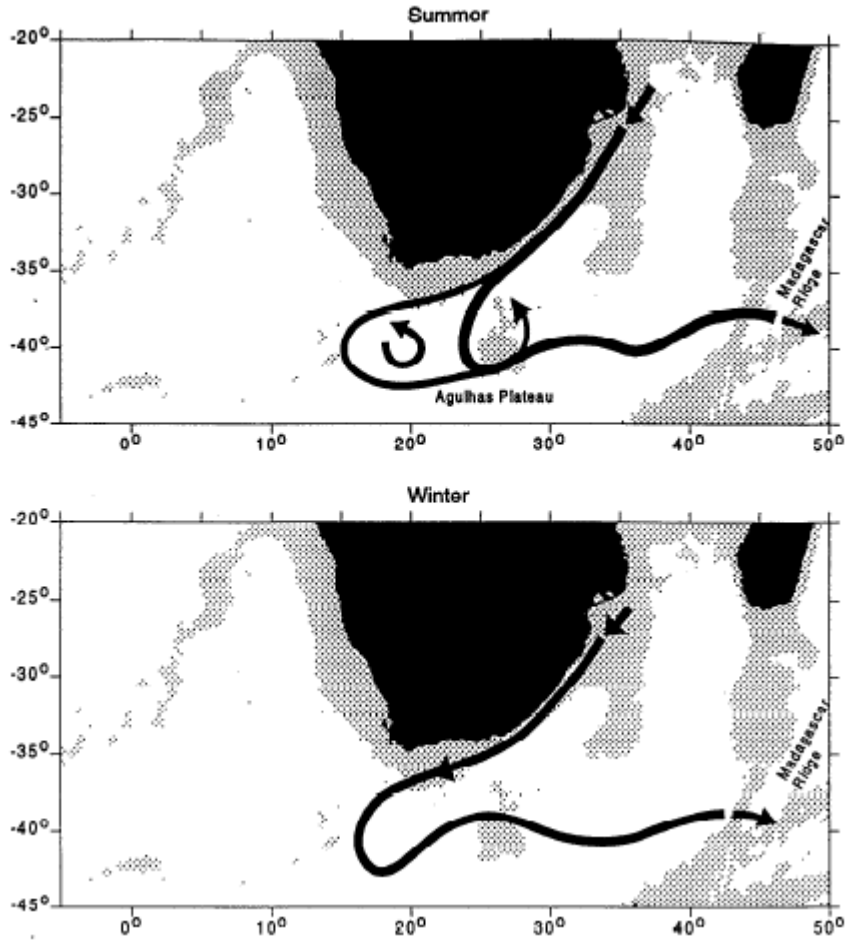

Figure 3-3 Proposed Agulhas Current pattern for winter and summer (Matano et al., 1998).

Figures 3-4 to 3-5 exemplify the changes that occur in the surface conditions around South Africa between the seasons. Towards the Southern Ocean, abrupt changes in sea surface salinity (SSS) and sea surface temperature (SST) are related to the position of the circum-Antarctic fronts (see section 3.3).

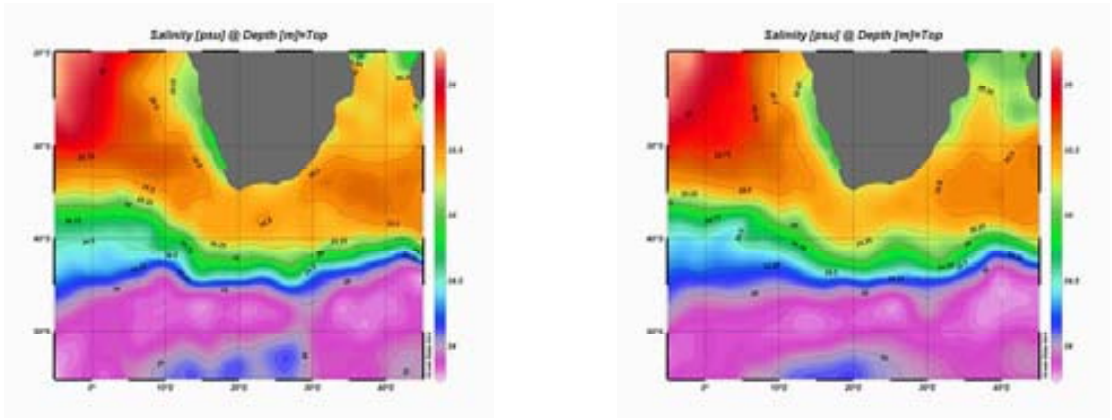

January-March (Austral Summer) *April-June (Austral Autumn)*

July-September (Austral Winter) *October-December (Austral Spring)*

Figure 3-4 SSS for Austral summer to spring around southern Africa. Plots compiled with the program Ocean Data View software (Schlitzer, 2007).

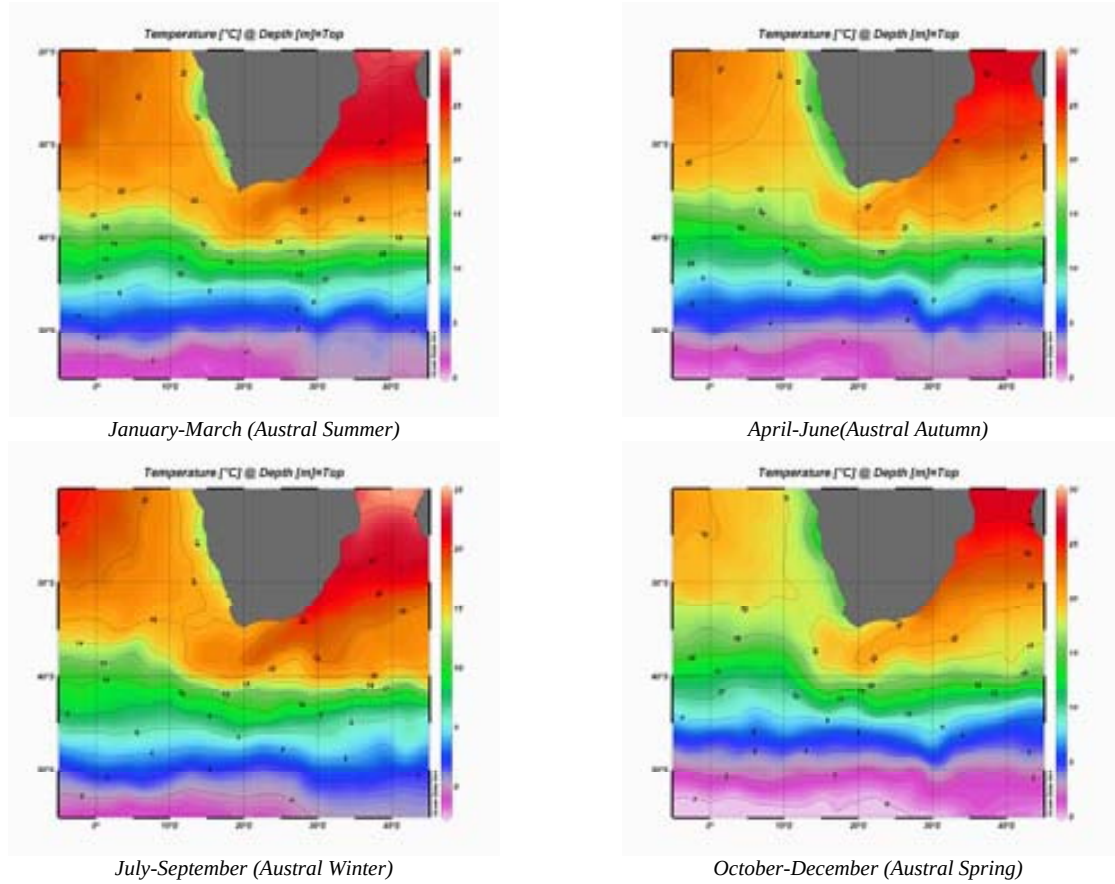

January-March (Austral Summer) *April-June(Austral Autumn)*

July-September (Austral Winter) *October-December (Austral Spring)*

Figure 3-5 SST for Summer to Spring around southern Africa. Plots compiled with the program Ocean Data View software (Schlitzer, 2007).

3.2. Agulhas Leakage: Agulhas Rings and Agulhas Filaments

The leakage of Indian Ocean water into the South Atlantic does not happen as a continuous flow but rather by means of intermittent ring shedding and filament extension. Agulhas Rings are generated at the Agulhas Retroflection, when a meander within the retroflection is pinched off and released as an eddy (Olson and Evans, 1986). The causes and mechanisms of ring formation are not entirely understood, but they seem to be closely related with the occurrence of a Natal Pulse upstream (de Ruijter et al., 1999).

Figure 3-6 shows the main path through which the Agulhas Rings are released; Garzoli and Gordon (1996) named this path the "Agulhas Eddy Corridor". In the Figure the trajectory of one Agulhas Filament measured during the surveys of Garzoli and Gordon (1996) is shown, this is passing right over the site of the cores here studied showing their ideal location to record past variations of the "Warm Water Route".

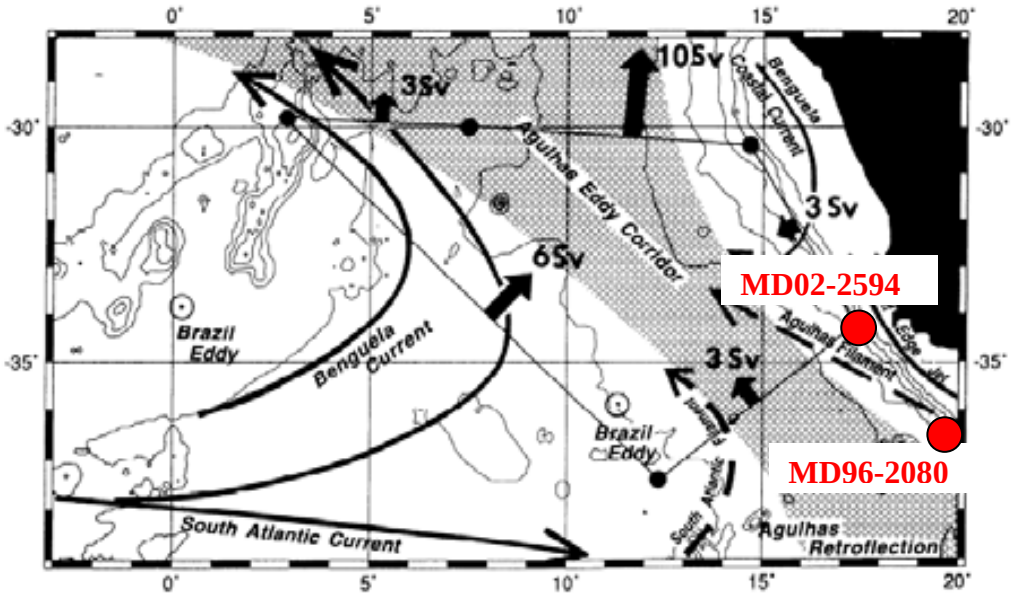

Figure 3-6 Location of the Agulhas Eddy Corridor off South Africa. Transport estimates are given for the South Atlantic and Benguela Currents. Also shown are the locations of cores MD96-2080 and MD02-2594 (modified after Garzoli and Gordon, 1996).

Natal Pulses are single meanders of the current initiated, with few exceptions, at Natal Bight (approximately 26°S) that propagate as solitons and are thought to be involved in the shedding of Agulhas Rings (Lutjeharms and de Ruijter, 1996). The triggers of Natal Pulses remain unknown; a likely producer is the absorption of deep-sea eddies onto the seaward border of the Agulhas Current (Lutjeharms and Roberts, 1988). On the other hand, Pichevin et al. (1999) did not find a relation between the Natal Pulses and the shedding of Agulhas Rings and related the ring-shedding mainly to the retroflection of the Agulhas Current itself. Recent studies have shown the existence of eddies also in the Mozambique Channel and the region south of Madagascar (de Ruijter et al., 2002; Schouten et al., 2003; de Ruijter et al., 2004). Mozambique eddies appear to be related to incoming Rossby Waves that cross the Indian Ocean and reach the Agulhas Current System with a frequency of 4-5 times per year (Schouten et al., 2003). These eddies may have an impact on the movement of the retroflection and may control the timing of Agulhas Ring shedding by generating a Natal Pulse (van Leeuwen et al.,

2000; Schouten et al., 2002). Nonetheless, during periods of absence of Natal Pulses the shedding of Agulhas Rings would persist at a reduced frequency (Penven et al., 2006).

On average some six Agulhas Rings are being formed each year transporting between 0.5 and 1.5 Sv of Indian Ocean water per ring (de Ruijter et al., 1999). Based on the analyses of 17 Agulhas Rings in the Cape Basin Duncombe Rae (1991) estimated the average diameter from maximum radial velocity to be 250 ± 40 km, with an average extension in depth of the 10ºC isotherm at the ring centre of 650 ± 130 m. Nonetheless, according to the trapped and translational capacity of particles and the deeper presence of Indian Ocean type water masses within the rings, Agulhas Rings may reach as deep as 1100 m (Duncombe Rae, 1991). Moreover, during the MARE cruise (Mixing in Agulhas Rings Experiments; Lutjeharms et al., 2000) a young ring was shown to extend to the sea bed at 4500 m depth (van Aken et al., 2002).

Based on altimetry data and on potential energy of random hydrographic measurements Byrne et al. (1995) estimated that the surface amplitude of the rings decreases by 85% over a travel distance of 5000 km. They drift away from the retroflection at a rate of 5-8 km/day (Olson and Evans, 1986) and their residence time in the South Atlantic was calculated to be 3-4 years (Byrne et al., 1995). Heat and salt transports to the South Atlantic associated with the invasion of Agulhas Rings was estimated to be around 0.045 PW/yr and $78 \cdot 10^{12}$ kg/yr respectively (van Ballegooyen et al., 1994). A minor transport of Agulhas Water occurs by means of filaments that reach some 50 m deep and are 50 km wide. While the heat carried in the Agulhas Filaments is rapidly lost to the atmosphere, as well as that of the Rings, their salt content behaves more conservatively and provides a non negligible contribution to the South Atlantic's salt budget of $29 \cdot 10^{12}$ kg/yr (Lutjeharms, 1996).

3.3. Oceanic Fronts Between Africa and Antarctica

In the region south of the African continent the characteristics of the water masses change dramatically over short distances, which allows defining a number of oceanic fronts. These are the Subtropical Front (STF), the Subantarctic Front (SAF), the Antarctic Polar Front (APF), the Southern Antarctic Circumpolar Front (SAACF) and Southern Boundary of the ACC (SB) (Fig. 3-7). These fronts delimit the flow regime of the ACC and may be traced throughout the Southern Ocean. The so-called Agulhas Front (AF) and Agulhas Retroflection Front (ARF) play additional roles in the area immediately south of Africa (Belkin and Gordon, 1996; Holliday and Read, 1998; Ansorge et al., 2005).

The oceanic fronts are mobile and have changed their position through glacial-interglacial times. Some authors have suggested changes of less than 5º latitude of northward shift of the STF during glacial periods and little variations in the southern boundary of the central gyres (Flores et al., 1999 and references therein). On the other hand, Gersonde et al. (2003) estimated a northward shift of the SAF of 5º latitude while they estimated almost no movement of the STF. As a consequence of these likely northwards migrations of some of the fronts, the thermal contrast between the sub-Antarctic and the subtropics would have increased, hence, leading to stronger winds in the area. Model simulations support the existence of increased wind speeds and northward displacement of the circum-Antarctic westerly wind belt during glacial periods (Ribbe, 2001).

Some authors (Wefer et al., 1996) suggest that a northward migration of the fronts during glacial periods may have produced the closure of the Agulhas Cape Valve. There are, however, several paleoceanographic studies that suggest a continued advection, over at least the last 850 kyr, of foraminiferal and coccolitophoral species around South Africa that are typical of the tropical-subtropical Indian Ocean (Flores et al., 1999; Chang et al., 1999; Rau et al., 2002; Peeters et al., 2004; Rau et al., 2006) suggesting that a complete closure did not occur.

Figure 3-7 displays the position as well as spatial variability of oceanic fronts around Antarctica (Belkin and Gordon, 1996). A remarkable feature in the graph is the observation that some fronts converge and diverge at different longitudes. For example, the AF merges with the STFs, SAF and PF at the Crozet Plateau (Indian Ocean) forming a singular "Crozet front" (Belkin and Gordon, 1996). Thus, the definition of the Southern Ocean Fronts, particularly referring to their surface properties, is to be viewed as long-term means. The high spatial and temporal variability of the region results in criteria defining any particular front in one location at one time may not hold several degrees to the east or west, or on a year-to-year basis (Holliday and Read, 1998). Observations made during the GoodHope I transect (Ansorge et al., 2005) are provided in the following for delimitation of the fronts but do not depict their mean position and long-term dynamics.

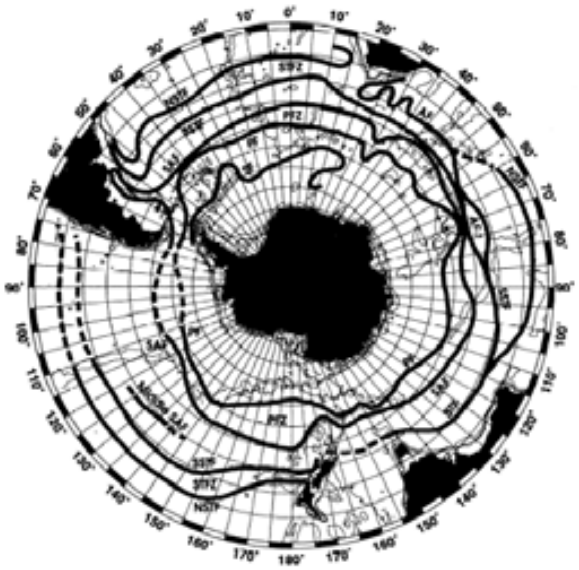

Figure 3-7 Oceanic fronts around the Southern Ocean (Belkin and Gordon, 1996). Notice the mergence and separation of some of the fronts at some locations pointing to their spatial and temporal variability.

- **Agulhas Front (AF) and Agulhas Retroflection Front (ARF)**

Although some authors do not distinguish between AF and ARF (e.g. Belkin and Gordon, 1996), Holliday and Read (1998) discuss both as separate fronts on the basis of the presence of cooler and fresher waters north of 36ºS that delimit the AF at this latitude.

The ARF is defined by the retroflection of the Agulhas Current i.e., by the re-entry of Agulhas Water into the Indian Ocean after the current retroflection causes the South Subtropical Front (SSTF, see below) to shift from 38º to 42-43ºS (Read and Pollard, 1993; Belkin and Gordon, 1996). The latitudinal variability of ARF and of the SSTF at the Indian Ocean is caused by the meandering of the Agulhas Return Current (Holliday and Read, 1998). The ARF can then be reliable traced from 15ºE up to 52ºE, on occasion up to 75ºE (Park and Gamberoni, 1991; Park et al., 1993; Belkin and Gordon,

1996). Further east in the Indian Ocean the ARF merge with the Australian SSTF (Belkin and Gordon, 1996). Read and Pollard (1993) reported a surface temperature shift of 19º to 17ºC at 40ºS, some 1700 km east of the Agulhas Retroflection (RRS Discovery 164 cruise, December 1986 - January 1987) identifying here the ARF.

- **Subtropical Front (STF)**

The Subtropical Front (STF) marks the boundary between warm, salty Subtropical Surface Water and cooler, fresher Subantarctic Surface Water to the south. It is the most northerly front associated with the ACC and the most prominent surface thermal front (Ansorge et al., 2005). Deacon (1937) estimated a SST decrease by as much as 4º-5°C over a distance of 200 km across the STF.

Thermosalinograph data collected during GoodHope I revealed two distinct surface frontal features between 39º49'S - 40º06'S and between 40º20'S - 41º15'S where surface temperatures and salinity first dropped from 18.83º - 15.16ºC and 35.49 - 34.02 psu, and then from 16.13º - 11.13ºC and 34.67 – 34.05 psu (Ansorge et al., 2005). This apparently supports the contention that in the SE Atlantic the STF may exist, as already suggested by Belkin and Gordon (1996), in two separate bands i.e., a North Subtropical Front (NSTF) and South Subtropical Front (SSTF) (Belkin and Gordon, 1996; Ansorge et al., 2005). The surface expression of the STF during GoodHope I was found between 39º39'- 40º54'S and the subsurface core, identified by the 10ºC-isotherm at 200 m, at 40º42'S (Ansorge et al., 2005).

- **Subantarctic Front (SAF)**

The Subantarctic Front (SAF) marks the northern boundary of the transitional zone between Subantarctic Surface Water (SASW) and Antarctic Surface Water (AASW), the Polar Frontal Zone (PFZ). The SAF is, in contrast to the STF, not very clear in its surface expression, extending from 4º - 8ºC (Lutjeharms, 1985). The weak nature of the front therefore makes it difficult to define the exact boundaries of the PFZ (Ansorge et al., 2005). This front is predominantly a subsurface front and can be defined by the most vertically orientated isotherm within a temperature gradient between 3º- 5ºC (Lutjeharms, 1985).

Along the GoodHope I transect, and according to the criteria described by Belkin and Gordon (1996) i.e., subsurface T and S range of 4.8º - 8.4°C and 34.11 - 34.47 psu at 200 m, with axial values 6°C, 34.3 psu; the subsurface axis of the SAF was observed at 44º07'S (Ansorge et al., 2005). Thermosalinograph data place the surface expression of the front between 44º05'S - 49º16'S (8.51 - 4.24ºC, 34.031 - 33.618 psu). A similar broad band of the SAF is often found in the South Atlantic (Smythe-Wright et al., 1998). Holliday and Read (1998) identify T-S inversions in this band that may be related to wind-induced upwelling or poleward shedding of eddies.

- **Antarctic Polar Front (APF)**

The subsurface expression of the APF is historically identified as the northern limit of the 2ºC temperature minimum at a depth of 200 m (Whitworth, 1980; Belkin and Gordon, 1996). Its surface expression can be identified by the maximum temperature gradient between 6º - 2ºC (Ansorge et al., 2005). During GoodHope I the subsurface expression of the APF was found to lie at 50º22'S. The

surface expression (4.7 - 1.46ºC, 33.796-33.894 psu) identified from the thermosalinograph was found between 50º14'S – 52º51'S. This front marks the northern limit of the Antarctic Zone; here water masses are characterized by T-S values between (-1.8)ºC - (+6ºC) and 33.4 - 34.2 psu (Ansorge et al., 2005).

- **Southern Antarctic Circumpolar Front (SAACF)**

South of the APZ Orsi et al. (1995) identified an additional front, the Southern ACC Front (SAACF) that was described as a circumpolar, deep reaching front. It corresponds to the position where the easterly and westerly wind belts separate (65ºS), but it does not separate distinct surface water masses. Rather, it is defined by the temperature and salinity characteristics of the Upper Circumpolar Deep Water (UCDW) (potential temperature 1.9-1.6ºC, salinity 34.6-34.7 psu, Smith et al., 1999) where this water mass upwells at depths around 200 m. According to this definition during GoodHope I SAACF was found between 53ºS and 55º44'S (Ansorge et al., 2005).

- **Southern Boundary of the ACC (SB)**

This boundary is described by Orsi et al. (1995) as the transition from ACC to Subpolar Waters. It is delimited by the poleward limit of the UCDW as it is entrained upwards into the mixed layer. These authors stated that there is none surface expression of the SB and it often lies very close to SAACF. However, Holliday and Read (1998) identified some surface expression for SB from thermosalinograph data based on surface features described by Sparrow et al. (1996) of T-S 0.6 - 1.5ºC / 33.84 - 33.76 psu at 65.2ºS and 0.9 - (-0.7)ºC / 33.78 - 33.09 psu at 63.4ºS.

3.4. Intermediate Waters Below the Agulhas Current

Below Agulhas Waters a melange of different sources of intermediate waters is found off South Africa that also impinge on the hydrography of ambient bottom waters at the location of cores MD96-2080 and MD02-2594. You et al. (2003) identified five remote sources of intermediate waters that influence the intermediate depth water mass patterns around South Africa. One major component is Antarctic Intermediate Water that forms in the southeast South Pacific and enters the South Atlantic through Drake Passage being subsequently modified in the Falkland Current Loop (dAAIW). dAAIW is found in the range of neutral density surfaces from σ_n = 27.25 to σ_n = 27.55. For reference and comparison with the other intermediate waters found in the area the potential temperature and salinity characteristics on σ_n = 27.40 will be used; then, for dAAIW the potential temperature (θ) is 3.52, and salinity (S) 34.22 psu (McCartney, 1977; Piola and Gordon, 1989; You, 2002; You et al., 2003). A second component is derived from AAIW while through modification in the southern Indian Ocean this component gains its own water-mass characteristics (siAAIW; σ_n = 27.25 - 27.55; on σ_n = 27.40, θ = 4.46°C, S = 34.36 psu). Intermediate water from the Indonesian Seas (IIW, ranging from σ_n = 27.25 to 27.55; on σ_n = 27.40, θ = 6.13°C, S = 34.66 psu), forming in the deep basins of the Indonesian Archipelago (You et al., 2003) are also identified in the region. Red Sea Water (RSIW, found from σ_n = 27.25 to 27.55; on σ_n = 27.40, θ = 10.26°C, S = 35.51 psu), with minor contribution of warm salty

Persian Gulf Water is the only intermediate water source found in the North Indian Ocean. This particular intermediate water component displays elevated T-S values (see above) while its oxygen contents are depleted (18.05 μmol/kg) being therefore more likely found at intermediate depths than at the thermocline or deeper waters (You et al., 2003). The fifth intermediate source is a mixing product of the four types (aAAIW). It is characterised by minima in salinity and oxygen concentration, and maximum nutrient concentrations (on σ_n = 27.40, θ = 5.40°C, S = 34.53 psu; oxygen and nutrient content on σ_n = 27.55, [O_2] = 119.88 μmol/kg; NO between 410.83 and 457.17 μmol/kg) (You et al., 2003).

These intermediate waters spread at depths between 700 - 1200 m, with varying contributions of the different sources described above. AAIW entering through Drake Passage is continuously present around South Africa while the other four water masses display a more patchy distribution: siAAIW is mostly found southeast of Madagascar; IIW enters the region through the Mozambique Channel and also along a pathway east of Madagascar; RSIW enters mainly through the Mozambique Channel below the IIW depth layer; the mixing product, aAAIW, primarily circulates in the north-western domain, equatorwards of the Subtropical Gyre, while south of Africa it is diluted by siAAIW and IIW. In conclusion, dAAIW is the dominant source (You et al., 2003) of Indian intermediate waters to the South Atlantic. Along the whole depth range at which the five intermediate water masses are found (700 - 1200 m) dAAIW contributes 60-70% of the total intermediate water with a core layer at 900 m (Fig. 3-8).

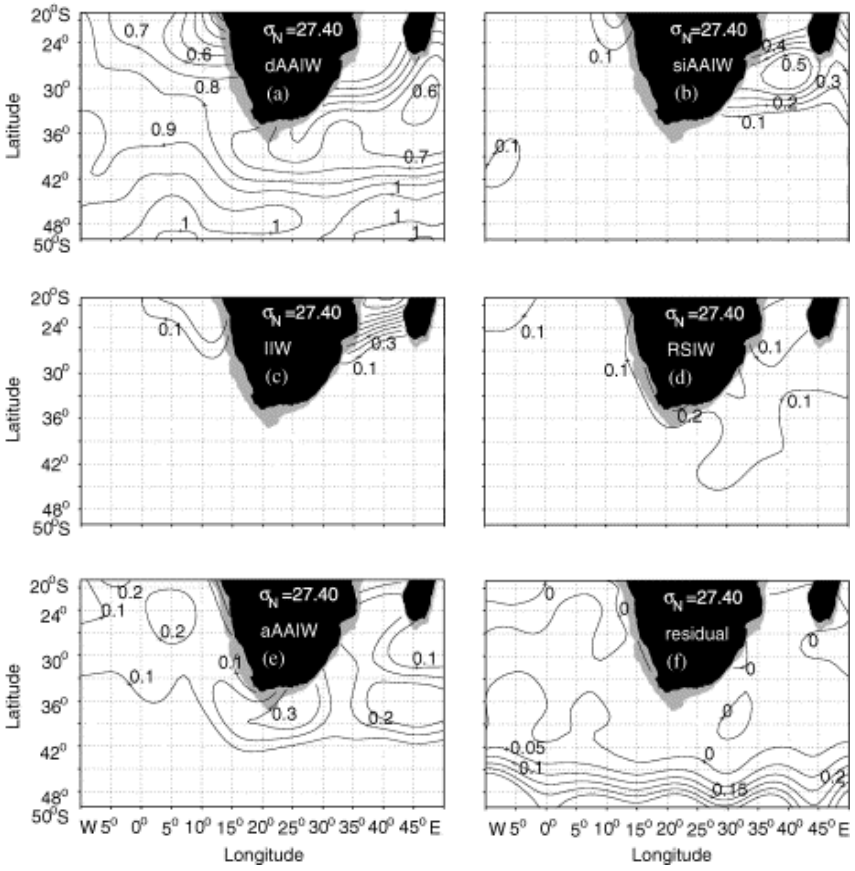

Figure 3-8 Source water-mass mixing fraction on the neutral surface σ_n = 27.40 (approximately 900 m water depth, along the core of AAIW) (You et al., 2003).

Most of the AAIW is formed in the Southeast Pacific (off Chile) (Talley, 1996 and references therein) and in the Falkland Current loop (Stramma and England, 1999 and references therein). The primary precursor of AAIW is Subantarctic Mode Water (SAMW) (McCartney, 1977; Hanawa and Talley, 2001) that subducts northward as it gains density through advective mixing with subtropical waters that decrease in temperature as they flow southwards in the Pacific Subtropical Gyre (England et al., 1993; Talley, 1999; Tomczak, 1999; Sloyan and Rintoul, 2001; Rintoul and England, 2002). The process also involves convection and surface mixing (Tomczak, 1999). The AAIW formed in the Southwest Atlantic is fresher and colder (Sloyan and Rintoul, 2001). To explain this fact Talley (1996) proposed the existence of two cool pools of winter mixed water in the West Atlantic, south of the SAF and inshore of the Malvinas Current. Recent model studies suggest that wind-driven cross frontal Ekman northward transport of cold and fresh Antarctic surface waters (Ribbe, 2001; Rintoul and England, 2002) and sea ice motion are important for the preconditioning of SAMW and final low-salinity SAMW (Saenko and Weaver, 2001; Saenko et al., 2002).

3.5. Deep Waters in the Agulhas Region

Deep waters at the core location consist of the southern extension of NADW bounded by Upper and Lower Circumpolar Deep Water (UCDW, LCDW) (Fig. 3-1b).

NADW in the South Atlantic spreads at water depths between 2000 and 3500 m (Arhan et al., 2003; van Aken et al., 2004). This water mass forms in the high latitude North Atlantic and it is a complex mixture of several water masses (Smethie and Fine, 2000 and references therein), i.e. Iceland–Scotland Overflow Water (ISOW), Denmark Strait Overflow Water (DSOW) and Labrador Sea Water (LSW). Additionally, water masses of southern hemisphere origin and from the Mediterranean Sea contribute to the lower and upper portion of NADW respectively.

The upper part of NADW is formed by LSW which forms by open ocean convection during winter in the Labrador Sea. The densest part of NADW (lower part) is formed by ISOW and DSOW with contributions of southern origin waters. ISOW and DSOW form from Atlantic waters that have been transported into the Greenland/Iceland/Norwegian seas and from Arctic Intermediate Water (AIW). These waters are modified by mixing and winter convection. After modification and sinking, ISOW enters the eastern North Atlantic across the Iceland/Scotland Ridge and is further advected towards the western North Atlantic while DSOW enters the western North Atlantic across the Greenland/Iceland Ridge.

All of the components of NADW either form in the subpolar western North Atlantic (LSW) or are advected to this region (ISOW, DSOW). As the components partially mixed and are influenced by Southern Ocean and Mediterranean waters, they end up in typical type T-S characteristics of 2.1ºC - 34.93 psu that add to a potential density at 4000 m (σ_4) of 45.93 (Broecker and Peng, 1982 and references therein; Gordon, 1986; Tomczak and Godfrey, 2003). The salinity maximum lies at 1600 m depth near the equator and at 2500 m at 25ºS (Stramma and England, 1999). At the latitudes of MD96-2080 and MD02-2594 NADW the T-S characteristics are partially altered through the admixture of

CDW but despite this mixing NADW remains readily identifiable through its salient salinity maximum (see Fig. 3-1b).

NADW leaves the Atlantic in the South directly contributing to the deep-water inflow entering the Indian Ocean through the SW Indian Ocean Gateway around South Africa, and also being entrained into the Antarctic Circumpolar Current (ACC). Circumpolar Deep Water (CDW) is colder and fresher than NADW but both have very similar densities; CDW T-S are 0.62ºC, 34.708 psu, σ_4 = 46.03, (Broecker and Peng, 1982 and references therein; Tomczak and Godfrey, 2003). The southward advection of NADW splits the CDW flow into an Upper and a Lower CDW (UCDW, LCDW) and reduces its influence in the South Atlantic (Tomczak and Godfrey, 2003). It appears feasible that the CDW would invade further north the deep South Atlantic during glacial periods when the rate of formation and southward advection of NADW was reduced.

The salinity maximum associated with NADW spreads along the eastern margin of the African continent as far north as 20ºS (see Fig. 3-9), well into the Mozambique Channel (van Aken et al., 2004). To the south, NADW leaves the South African continental slope and enters the ACC where salinity at the deep water level decreases from 34.86 at 12ºE to 34.76 at 68ºE (van Aken et al., 2004) approximating LCDW salinity values (LCDW T-S characteristics observed in the West Antarctica Peninsula are θ = 1.6-1.3ºC; S = 34.729 psu; Smith et al., 1999). LCDW flows mainly eastward along the latitude of 45ºS (below the STF) and enters the Indian and Pacific Oceans (van Aken et al., 2004). The Upper Circumpolar Deep Water (UCDW) is not as well characterized by its T-S properties but rather by a distinctive oxygen minimum (180 – 183 μmol/l) and nutrient maximum $NO_3 + NO_2 > 34$ μmol/kg, $PO_4 > 2.4$ μmol/kg) at the density surface of 27.72 (Smith et al., 1999; García et al., 2002).

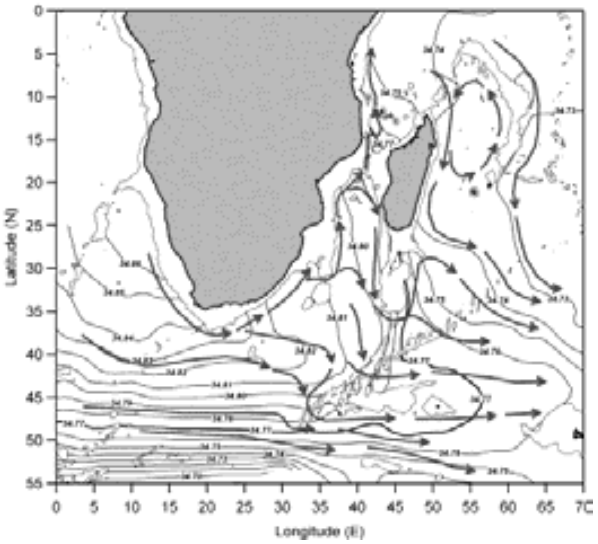

Fig. 3-9 Schematic deep water circulation scheme for the deep water (2000–3500 m) according to van Aken et al. (2004). In the background, the lateral salinity distribution in the $\sigma_{2.5}$=39.25 kg/m^3 isopycnal surface is drawn, bound by the 2500 m isobath (thin line). The 34.77 isohaline (thick line) shows the approximate boundary between the high salinity NADW and the lower salinity Antarctic Bottom Water (AABW) and North Indian Deep Water (NIDW).

Antarctic Bottom Water (AABW) forms the third major deep water mass in the area. AABW displays temperatures close to the freezing point, type T-S values are -0.6ºC to -0.8ºC and 34.66 psu (Solomon, 1983; Reid, 1996), similar to the estimations for Weddell Sea Water of -0.89ºC, 34.647 psu at σ_4 = 46.234 (Broecker, 1982 and references therein). The primary process involved with AABW

formation is brine rejection and heat loss in polynyas during sea ice formation (e.g. Martinson et al., 1981; Maqueda et al., 2004) and subsurface mixing with ACW as convection occurs on the continental shelf (Tomczak and Godfrey, 2003). Primary sites of formation are the Weddell Sea, Ross Sea, and probably also along the Adélie Coast and Enderby Land, being the Weddell Sea the most prominent site of AABW formation (Orsi et al., 1999; Tomczak and Godfrey, 2003). AABW spreads from the ACC into the three ocean basins, and can be traced readily by its low potential temperature even though its T-S values change through mixing with ACW to typical values of 0.3ºC and 34.7 psu when entering the other basins (Tomczak and Godfrey, 2003). The spreading of this very dense water mass at depth is directly influenced by topography, with topographic features rising to water depths shallower than 3500 m constituting an obstacle that alters the advection flow path of AABW. Near South Africa AABW is traced flowing north along the Agulhas and Mozambique Basins (see Fig. 3-10).

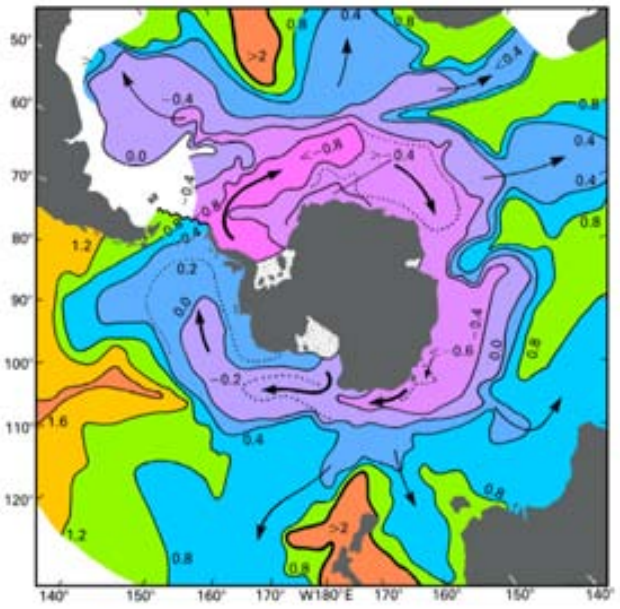

Figure 3-10 Bottom potential temperature in the Southern Ocean. Spreading of AABW to Atlantic, Indian and Pacific Basins is shown by arrows (Tomczak and Godfrey, 2003).

3.6. Nutrient Content of Intermediate and Deep Waters

Deep water masses are usually described by their T-S characteristics as these are conservative parameters that only change by mixing with other water masses. However, there are other parameters that, although being non conservative, distinguish the various water masses. Of particular interest for this study are the $\delta^{13}C_{\Sigma CO2}$ signature and the phosphate concentration ($[PO_4^{3-}]$), being this last related to the Cadmium concentration in the water column (Cd_{sw}, see Chapter 2). Both can be combined to derive the $\delta^{13}C_{as}$ signature of the water mass that constitutes a conservative tracer that, like water mass T-S signatures, will be altered in the deep ocean only by mixing (Broecker and Maier-Reimer, 1992; Zahn and Keir, 1992; Charles et al., 1993; Lynch-Stieglitz and Fairbanks, 1994; Lynch-Stieglitz et al., 1995). Figure 3-11 shows sections of $\delta^{13}C_{\Sigma CO2}$, $(PO_4)^{3-}$, the $\delta^{13}C_{bio}$ corresponding to the phosphate concentration computed using the relationship given in Broecker and Maier-Reimer (1992) (see Chapter 2, Eq. 2-12) along the western and eastern sides of the Atlantic Ocean from GEOSCES data (Kroopnick, 1980). The derived $\delta^{13}C_{as}$ obtained by removing the biological component from the actual $\delta^{13}C_{\Sigma CO2}$ (see Chapter 2, Eq. 2-13) is also shown.

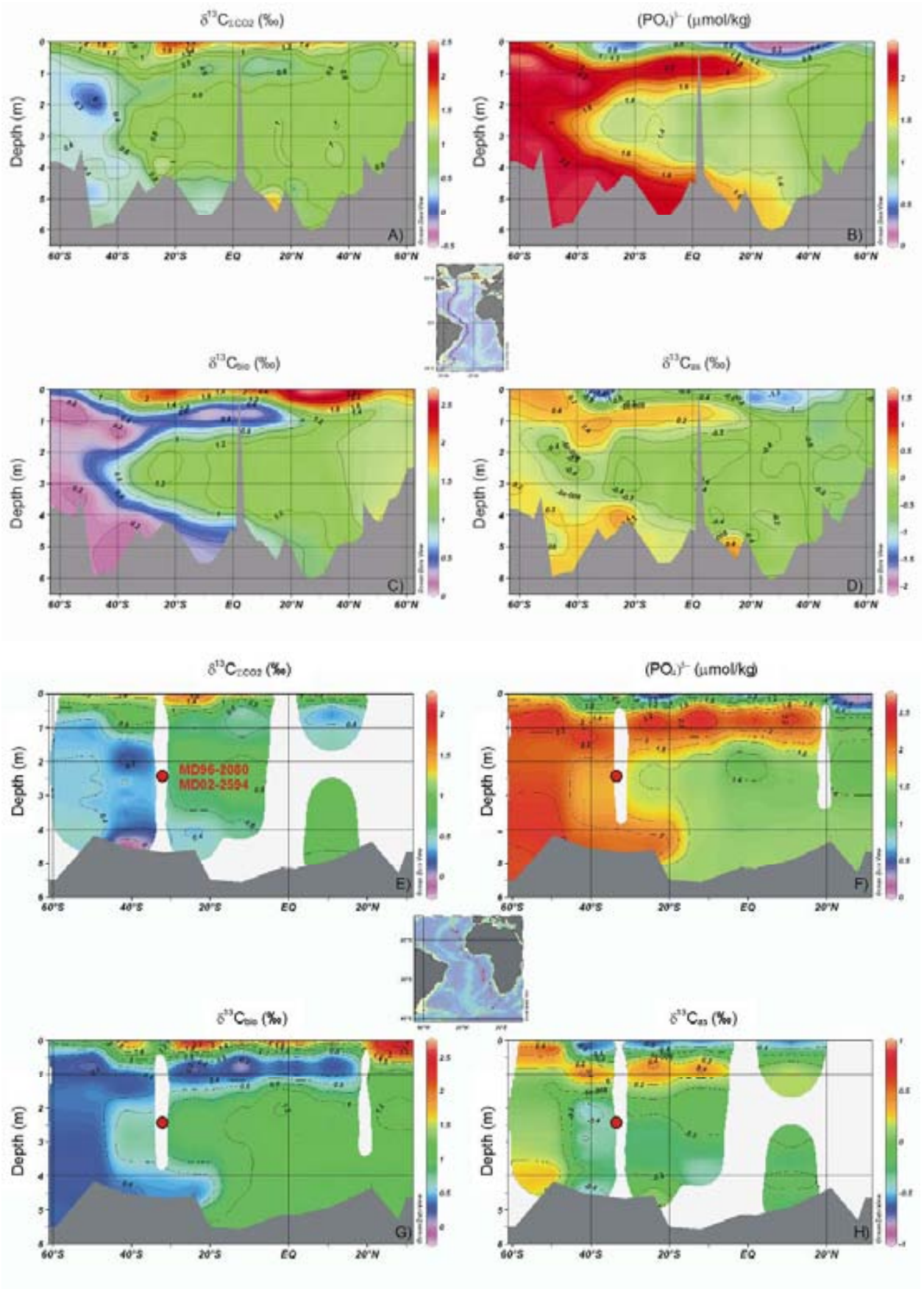

Figure 3-11 A) GEOSECS $\delta^{13}C_{\Sigma CO2}$ (‰) along the Western Atlantic (section shown in central map) (Kroopnick, 1980). B) $(PO_4)^{3-}$ (µmol/kg) along the same section. C) $\delta^{13}C_{bio}$ (‰) computed from $(PO_4)^{3-}$using the relationship of Broecker and Maier-Reimer (1992). D) $\delta^{13}C_{as}$ (‰) obtained by subtracting $\delta^{13}C_{\Sigma CO2}$ - $\delta^{13}C_{bio}$ (Eq. 2-13). Illustrations E) to H) are the same than A) to D) for the Eastern side of the Atlantic (see insert map). The red dot marks the approximate equivalent position of MD96-2080 and MD02-2594 cores in the water column. Plots compiled with the program Ocean Data View software (Schlitzer, 2007). A krigging interpolation of 70 points has been applied to represent the data as a continuous.

The main water masses present in the Atlantic Ocean can be identified in these sections. NADW is represented by positive $\delta^{13}C_{\Sigma CO2}$ values of around 1‰ (Kroopnick, 1980) and low $(PO_4)^{3-}$ of around 1.4 μmol/kg. The southward spreading of this water mass is directly traced by the positive $\delta^{13}C$ and low $(PO_4)^{3-}$ levels. NADW $\delta^{13}C_{as}$ signature is around -0.4‰ (Charles et al., 1993; Lynch-Stieglitz and Fairbanks, 1994) (see Fig. 3-11D). This negative value is related to the short residence time of surface waters in the high latitude North Atlantic during cooling and prior to sinking and to the source waters themselves. Warm surface subtropical waters transported by the Gulf Stream are depleted in $\delta^{13}C_{as}$ because air-sea fractionation at warm temperatures favors the light isotope. Also, organisms preferentially utilize the light carbon isotope during photosynthesis leaving surface waters enriched in the heavy isotope and depleted in nutrients.

NADW is bounded by nutrient enriched water masses of southern origin. These are AAIW at intermediate depths and CDW and AABW at greater depths. The $\delta^{13}C_{\Sigma CO2}$ signature of these water masses is not as accurately represented as that of NADW in Figure 3-11 due to poor data coverage. AAIW displays $\delta^{13}C_{\Sigma CO2}$ positive levels, similar to those of NADW while at the same time it carries elevated nutrient contents, $[(PO_4)^{3-}] \sim 2.2$ μmol/kg. This combination is indicative of a strong air-sea gas fractionation imprint on the $\delta^{13}C_{\Sigma CO2}$. The AAIW $\delta^{13}C_{as}$ signature is positive due to this air-sea gas equilibration at cold temperatures likely aided by strong wind intensity in the sub-Antarctic. AABW is fed by aged NADW and CDW and its $\delta^{13}C_{\Sigma CO2}$ is around 0.5‰ (Kroopnick, 1985). Yet its nutrient content is high, $[(PO_4)^{3-}] \sim 2.5$ μmol/kg. This indicates that upon formation AABW experiences some partial equilibration with the atmosphere while due to the limited efficiency of the marine biota nutrient levels remain high. Therefore AABW also presents a positive $\delta^{13}C_{as}$ signature of around 0.2‰.

The approximate position of sediment cores MD96-2080 and MD02-2594 is displayed in the Eastern sections to reiterate their location today within the southern branch of NADW and to illustrate the surrounding intermediate and deep waters in the region. The closest GEOSECS Stations to the core sites are Stations 93 (41º46'S, 18º27'E) and 103 (24º00'S, 8º30'E), which both record $\delta^{13}C_{\Sigma CO2}$ values of 0.6‰ VPDB at this water depth (Kroopnick, 1980) in agreement with the core top value of 0.7‰ VPDB of MD02-2594 (see Chapter 5).

Table 3-2 summarizes the main characteristics of the water masses influencing the deep circulation in the study area. The values are obtained from averaging data from different GEOSECS stations in the neighbourhood of the formation areas of the different water masses. The inferred values for the two stations close to the study area are also shown. The ambient water mass at the location of cores MD96-2080 and MD02-2594 is composed of approximately 70:15:15 NADW:AABW:AAIW (see mixing triangle, Fig. 3-12).

Table 3-2 Intermediate and deep water masses influencing the hydrography of the core sites.

Water mass	T (ºC)	S (psu)	$(PO_4)^{3-}$ (μmol/kg)	Cd_{sw} (mnmol/kg)	$\delta^{13}C_{\Sigma CO2}$ (‰)	Data Coverage
AAIW	3.18±0.83	34.42±0.13	2.19±0.13, 30	0.62±0.05	0.73±0.29, 10	33-55ºS; 21-55ºW; 0.75-1.1 km
NADW	2.98±0.54	34.95±0.03	1.06±0.5, 117	0.22±0.01	0.95±0.14, 42	45-60ºS; 11ºE-66ºW; 6.5-4 km
AABW	0.13±0.50	34.67±0.02	2.22±0.06, 97	0.64±0.02	0.54±0.16, 16	60-50ºN; 19ºE-43ºW; 1.5-3 km
MD96-2080 MD02-2594	2.67±0.26	34.84±0.04	1.67±0.12, 8	0.42±0.05	0.67±0.09, 3	18.5ºE,42ºS 8.5ºE, 23ºS 2-2.7 km

Note: Values are means of the data available in the sectors described in the last column, the number of data points used for T, S and $(PO_4)^{3-}$ is the same while for the $\delta^{13}C_{\Sigma CO2}$ data is scarcer.

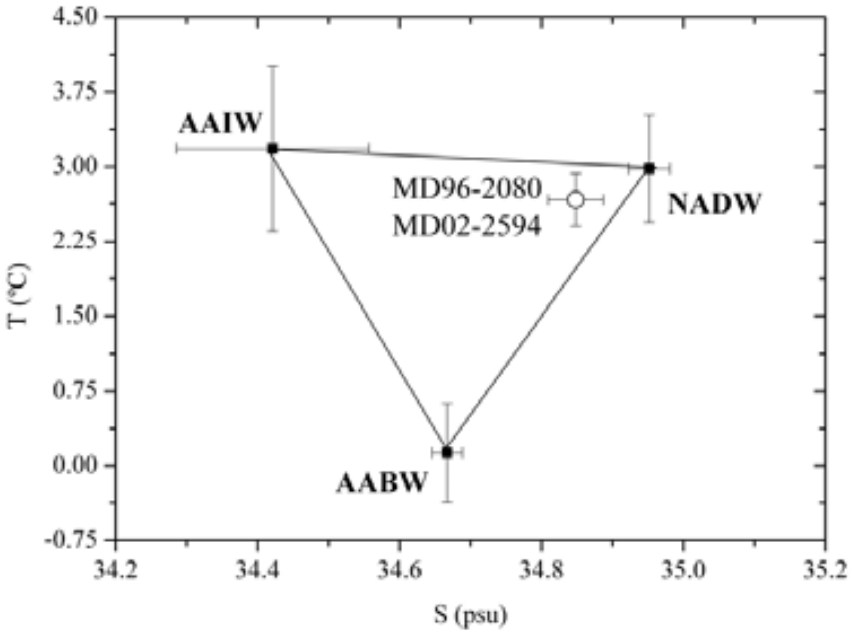

Figure 3-12 Mixing triangle of Atlantic water masses and approximate T-S value of ambient bottom water at the location of cores MD96-2080 and MD02-2594 (GEOSECS Sta. 93, 103; Ostlund et al., 1987).

References

Ansorge, I.J., Speich, S., Lutjeharms, J.R.E., Gõni, G.J., Rautenbach, C.J.d.W., Froneman, P.W., Rouault, M. and Garzoli, S., 2005. Monitoring the oceanic flow between Africa and Antarctica: Report of the first GoodHope cruise. South African Journal of Science, 101 (1-2), 29-35.

Arhan, M., Mercier, H. and Park, Y.-H., 2003. On the deep water circulation of the eastern South Atlantic Ocean. Deep Sea Research, 50, 889-916.

Beal, L.M. and Bryden, H.L., 1997. Observations of an Agulhas Undercurrent. Deep Sea Research, 44 (9-10), 1,715-1,724.

Belkin, I.M. and Gordon, A.L., 1996. Southern Ocean fronts from the Greenwich meridian to Tasmania. Journal of Geophysical Research, 101 (C2), 3,675-3,696.

Bertrand, P. et al., 1997. Les rapport de campagne à la mer à bord du Marion Dufresne - Campagne Nausicaa - IMAGES II - MD105 du 20/10/96 au 25/11/96. Institut Francais pour la Recherche et la technologie Polaires.

Broecker, W.S., 1991. The Great Ocean conveyor. Oceanography, 4, 79-89.

Broecker, W.S., 1982. Ocean Chemistry during Glacial Times. Geochimica et Cosmochimica Acta, 46, 1,689-1,705.

Broecker, W.S. and Peng, F.H., 1982. Tracers in the sea. Eldigio Press, 679 pp.

Broecker, W.S. and Maier-Reimer, E., 1992. The influence of air and sea exchange on the carbon isotope distribution in the sea. Global and Biogeochemical Cycles, 6 (3), 315-320.

Bryden, H.L. and Beal, L.M., 2001. Role of the Agulhas Current in Indian Ocean circulation and associated heat and freshwater fluxes. Deep Sea Research, 48 (8), 1,821-1,845.

Byrne, D.A., Gordon, A.L. and Haxby, W.F., 1995. Journal of Physical Oceanography. Agulhas Eddies: a synoptic view using Geosat ERM data, 25 (5), 902-917.

Chang, Y.-P., Chang, Ch.-Ch., Wang, L.-W., Cheng, M.-T., Wang, Ch.-H. and Yu, E.-F., 1999. Planktonic Foraminiferal Sea Surface Temperature Variations in the Southeast Atlantic Ocean: A High-Resolution Record MD96-2085 of the Past 400,000 Years from the IMAGES II - NAUSICAA Cruise. TAO, 10 (1), 185-200.

Charles, C.D., Wright, J.D. and Fairbanks, R.G., 1993. Thermodynamic influences on the marine carbon isotope record. Paleoceanography, 8 (6), 691-698.

de Ruijter, W.P.M. and Boudra, D.B., 1985. The wind-driven circulation in the South Atlantic-Indian Ocean - I. Numerical experiments in a one-layer model. Deep-Sea Research, 32 (5), 557-574.

de Ruijter, W.P.M., van Leeuwen, P.J. and Lutjeharms, J.R.E., 1999. Generation and evolution of Natal Pulses: solitary meanders in the Agulhas Current. Journal of Physical Oceanography, 29 (12), 3,043-3,055.

de Ruijter, W.P.M., Ridderinkhof, H., Lutjeharms, J.R.E., Schouten, M.W. and Veth, C., 2002. Observations of the flow in the Mozambique Channel. Geophysical Research Letters, 29 (10), 1502, doi:10.1029/2001GL013714.

de Ruijter, W.P.M., van Aken, H.M., Beier, E.J., Lutjeharms, J.R.E., Matano, R.P. and Schouten, M.W., 2004. Eddies and dipoles around South Madagascar: formation, pathways and large-scale impact. Deep Sea Research, 51 (3), 383-400.

de Ruijter, W.P.M., Biastoch, A., Drijfhout, S.S., Lutjeharms, J.R.E., Matano, R.P., Pichevin, T., van Leeuwen, P.J. and Weijer, W., 1999. Indian-Atlantic interocean exchange: Dynamics, estimations and impact. Journal of Geophysical Research, 104 (C9), 20,885-20,910.

Deacon, G.E.R., 1937. Hydrology of the Southern Ocean. Discovery Reports, 15, 1-123.

Donohue, K.A., Firing, E. and Beal, L., 2000. Comparison of three velocity sections of the Agulhas Current and Agulhas Undercurrent. Journal of Geophysical Research, 105 (C12), 28,585-28,594.

Duncombe Rae, C.M., 1991. Agulhas retroflection rings in the South Atlantic Ocean; an overview. South African Journal of Marine Science, 11, 327-344.

England, M.H., Godfrey, J.S., Hirst, A.C. and Tomczak, M., 1993. The mechanism for Antarctic Intermediate Water renewal in a world ocean model. Journal of Physical Oceanography, 23, 1,553-1,560.

Feron, R.C.V., de Ruijter, W.P.M. and Oskan, D., 1992. Ring Shedding in the Agulhas Current System. Journal of Geophysical Research, 97 (C6), 9,467-9,477.

Ffield, A., Toole, J. and Wilson, D., 1997. Seasonal circulation in the South Indian Ocean. Geophysical Research Letters, 24 (22), 2,773-2,776.

Flores, J.A., Gersonde, R. and Sierro, F.J., 1999. Pleistocene fluctuations in the Agulhas Current Retroflection based on the calcareous plankton record. Marine Micropaleontology, 37 (1), 1-22.

García, M.A., Blade, I., Cruzado, A., Velásquez, S., García, H., Puigdefâbregas, J. and Sospeedra, J., 2002. Observed variability of water properties and transports on the World Ocean Circulation Experiment SR1b section across the Antarctic Circumpolar Current, Geophysical Research Letters. 107 (C10), 3162, doi:10.1029/2000JC000277.

Garzoli, S.L. and Gordon, A.L., 1996. Origins and variability of the Benguela Current. Journal of Geophysical Research, 101 (1), 897-906.

Gersonde, R., Abelmann, A., Brathauer, U., Becquey, S., Bianchi, C., Cortese, G., Grobe, H., Kuhn, G., Niebler, H.-S., Segl, M., Siegr, R., Zielinski, U. and Fütterer, D.K., 2003. Last Glacial sea surface temperatures and sea-ice extent in the Southern Ocean (Atlantic-Indian sector): A multiproxy approach. Paleoceanography, 18 (3), 1061, doi: 10.1029/2002PA000809.

Giraudeau, J., Balut, Y., Hall, I.R., Mazaud, A. and Zahn, R., 2003. SWAF-MD128 Scientific Report. Institut Polaire Francias report OCE/2003/01, 108 pp.

Gordon, A.L., 1986. Inter-Ocean exchange of thermocline water. Journal of Geophysical Research, 91 (C4), 5,037-5,046.

Gordon, A.L., 2003. The brawniest retroflection. Nature, 421, 904-905.

Gordon, A.L., Lutjeharms, J.R.E. and Gründlingh, M.L., 1987. Select hydrographic sections from the Agulhas research cruises of the research vessels Knorr and Meiring Naude 0 1983. Lamont-Doherty Geological Observatory of Columbia University, Technical Report LDGO-87 - 1.

Gordon, A.L., Giulivi, C.F. and Ilahude, A.G., 2003. Deep topographic barriers within the Indonesian Seas. Deep Sea Research, 50, 2,205-2,228.

Goschen, W.S. and Schumann, E.H., 1990. Agulhas Current variability and inshore structures off the Cape Province, South Africa. Journal of Geophysical Research, 95 (1), 667-678.
Hanawa, K. and Talley, L.D., 2001. Mode Waters in Ocean circulation and climate. Academic Press, London, 715 pp.
Harris, T.F.W., Legeckis, R. and van Forest, D., 1978. Satellite infra-red images in the Agulhas Current system. Deep Sea Research, 25 (6), 543-548.
Hogg, N.G. and Johns, W.E., 1995. Western boundary currents. U.S. National Report to International Union of Geodesy and Geophysics 1991-1994, Reviews of Geophysics, 33, 1,311-1,334.
Holliday, N.P. and Read, J.F., 1998. Surface oceanic fronts between Africa and Antarctica. Deep Sea Research, 45 (2-3), 217-238.
Kelly, K.A., 1991. The meandering Gulf Stream as seen by the Geosat altimeter: surface transport, position and velocity variance from 73° to 46°W. Journal of Geophysical Research, 96, 16,721-16,738.
Kroopnick, P., 1980. The distribution of $\delta^{13}C$ of CO_2 in the Atlantic ocean. Earth and Planetary Science Letters, 49, 469-484.
Kroopnick, P.M., 1985. The distribution of $\delta^{13}C$ of CO_2 in the world oceans. Deep Sea Research, 32 (1), 57-84.
Lutjeharms, J.R.E., 1985. Location of frontal systems between Africa and Antarctica: some preliminary results. Deep-Sea Research, 32, 1,499-1,509.
Lutjeharms, J.R.E., 1996. The exchange of water between the South Indian and the South Atlantic. In: W.H.B. G. Wefer, G. Siedler and D. Webb (Editors), The South Atlantic: Present and Past Circulation. Springer-Verlag, Berlin, pp. 125-162.
Lutjeharms, J.R.E., 2007. Three decades of research on the greater Agulhas Current. Ocean Science, 3 (4), 939-995.
Lutjeharms, J.R.E. and Roberts, H.R., 1988. The Natal Pulse: An Extreme Transient on the Agulhas Current. Journal of Geophysical Research, 93 (C1), 631-645.
Lutjeharms, J.R.E. and de Ruijter, W.P.M., 1996. The influence of the Agulhas Current on the adjacent coastal ocean: possible impacts of climate change. Journal of Marine Systems, 7 (2-4), 321-336.
Lutjeharms, J.R.E., Bang, N.D. and Duncan, C.P., 1981. Characteristics of the currents east and south of Madagascar. Deep Sea Research, 28 (9), 879-899.
Lutjeharms, J.R.E., Catzel, R. and Valentine, H.R., 1989. Eddies and other border phenomena of the Agulhas Current. Continental Shelf Research, 9 (7), 597-616.
Lutjeharms, J.R.E., de Ruijter, W.P.M., Ridderinkhof, H., van Aken, H., Veth, C., van Leeuwen, P.J., Drijfhout, S.S., Jansen, J.H.F. and Brummer, G.-J.A., 2000. MARE and ACSEX: new research programmes on the Agulhas Current system. South African Journal of Marine Science, 96, 105-110.
Lynch-Stieglitz, J. and Fairbanks, R.G., 1994. A conservative tracer for glacial ocean circulation from carbon isotope and paleonutrient measurements in benthic foraminifera. Nature, 369, 308-310.
Lynch-Stieglitz, J., Stocker, T.F., Broecker, W.S. and Fairbanks, R.G., 1995. The influence of air-sea exchange on $\delta^{13}C$ of ΣCO_2 in the surface ocean: Observations and Modeling. Global and Biogeochemical Cycles, 9, 653-665.
Maqueda, M., Willmott, A. and Biggs, N., 2004. Polynya dynamics: A review of observations and modeling. Reviews of Geophysics, 42, RG1004, doi:10.1029/2002RG000116.
Martinson, D.G., Killworth, P.D. and Gordon, A.L., 1981. A convective model for the Weddell polynya. Journal of Physical Oceanography, 11, 466-488.
Matano, R.P., Simionato, C.G., de Ruijter, W.P., van Leeuween, P.J., Strub, P.T., Chelton, D.B. and Schlax, M., 1998. Seasonal variability in the Agulhas retroflection region. Geophysical Research Letters, 25 (23), 4,361-4,364.
McCartney, M., 1977. Subantarctic Mode Water. In: M. Angel (Editor), A Voyage of Discovery. Pergamon Press, London, pp. 103-119.
Olson, D.B. and Evans, R.H., 1986. Rings of the Agulhas Current. Deep Sea Research, 33 (1), 27-42.
Orsi, A.H., Whitworth, T.I. and Nowlin, J.W.D., 1995. On the meridional extent and fronts of the Antarctic Circumpolar Current. Deep Sea Research, 42, 641-673.
Orsi, A.H., Johnson, G.C. and Bullister, J.L., 1999. Circulation, mixing, and production of Antarctic Bottom Water. Progress in Oceanography, 43 (1), 55-109.
Ostlund, H.G., Craig, H., Broecker, W.S. and Spencer, D., 1987. Geosecs Atlantic, Pacific, and Indian Ocean Expeditions. Shorebased data and Graphics. National Science Foundation, 7.
Ou, H.W. and de Ruijter, W.P.M., 1986. Separation of an inertial boundary current from a curved coastline. Journal of Physical Oceanography, 16 (2), 280-289.
Park, Y.-H. and Gamberoni, L., 1991. Frontal structure and transport of the Antarctic Circumpolar Current in the south Indian Ocean sector, 40-80ºE. Marine Chemistry, 35, 45-62.
Park, Y.-H., Gambérini, L. and Charriaud, E., 1993. Frontal structure, water masses and circulation in the Crozet Basin. Journal of Geophysical Research, 98, 12,361-12,385.
Peeters, F.J.C., Acheson, R., Brummer, G.-J.A., de Ruijter, W.P.M., Schneider, R., Ganssen, G., Ufkes, M.E. and Kroon, D., 2004. Vigorous exchange between the Indian and Atlantic oceans at the end of the past five glacial periods. Nature, 438, 661-665.
Penven, P., Lutjeharms, J.R.E. and Florenchie, P., 2006. Madagascar: a pacemaker for the Agulhas Current system? Geophysical Research Letters, 33, L17609, doi:10.1029/2006GL 026854.
Pichevin, T., Nof, D. and Lutjeharms, J.R.E., 1999. Why are There Agulhas Rings? Journal of Physical Oceanography, 29 (4), 693-707.
Piola, A.R. and Gordon, A., 1989. Intermediate Waters in the Southwest South-Atlantic. Deep Sea Research, 36 (1), 1-16.
Quartly, G.D. and Srokosz, M.A., 1993. Seasonal variations in the region of the Agulhas Retroflection: Studies with Geosat and FRAM. Journal of Physical Oceanography, 23, 2,107-2,124.
Rau, A.J., Rogers, J. and Chen, M.-T., 2006. Late Quaternary palaeoceanographic record in giant piston cores off South Africa, possibly including evidence of neotectonism. Quaternary International, 148 (1), 65-77.
Rau, A.J., Rogers, J., Lutjeharms, J.R.E., Giraudeau, J., Lee-Thorp, J.A., Chen, M.-T. and Waelbroeck, C., 2002. A 450-kyr record of hydrological conditions on the western Agulhas Bank Slope, south of Africa. Marine Geology, 180 (1-4), 183-201.

Read, J.F. and Pollard, R.T., 1993. Structure and Transport of the Antarctic Circumpolar Current and Agulhas Return Current at 40ºE. Journal of Geophysical Research, 98 (C7), 12,281-12,295.

Reid, J.L., 1996. On the circulation of the South Atlantic. In: G. Wefer, W.A. Berger, G. Siedler and D. Webb (Editors), The South Atlantic: Present and Past Circulation. Springer-Verlag, Berlin, Heidelberg, pp. 13-44.

Ribbe, J., 2001. Intermediate Water Mass Production Controlled by Southern Hemisphere Winds. Geophysical Research Letters, 28, 535-538.

Rintoul, S.R. and England, M.H., 2002. Ekman Transport Dominates Local Air-Sea Fluxes in Driving Variability of Subantarctic Mode Water. Journal of Physical Oceanography, 32 (5), 1,308-1,321.

Saenko, O., Schmittner, A. and Weaver, A.J., 2002. On the role of wind-driven sea ice motion on ocean ventilation. Journal of Physical Oceanography, 32, 3,376-3,395.

Saenko, O.A. and Weaver, A.J., 2001. Importance of wind-driven sea ice motion for the formation of Antarctic Intermediate Water in a global climate model. Geophysical Research Letters, 28, 4,147-4,150.

Sætre, R. and Jorge da Silva, A., 1984. The circulation of the Mozambique Channel. Deep Sea Research, 31 (5), 485-508.

Schlitzer, R., 2007. Ocean Data View. In: http://odv.awi.de.

Schouten, M.A., de Ruijter, W.P.M., van Leeuwen, P.J. and Dijkstra, H.J., 2002. An oceanic teleconnection between the equatorial and southern Indian Ocean. Geophysical Research Letters, 9 (16), 1812, doi: 10.1029/2001GL014542.

Schouten, M.A., de Ruijter, W.P.M., van Leeuwen, P.J. and Ridderinkhof, H., 2003. Eddies and variability in the Mozambique Channel. Deep Sea Research, 50 (12-13), 1,987-2,003.

Sloyan, B.M. and Rintoul, S.R., 2001. Circulation, Renewal, and Modification of Antarctic Mode and Intermediate Water. Journal of Physical Oceanography, 31, 1,005-1,030.

Smethie, W.M. and Fine, R.A., 2000. Rates of North Atlantic Deep Water formation calculated from chlorofluorocarbon inventories. Deep Sea Research, 48 (1), 189-215.

Smith, D.A., Hofmann, E.E., Klinck, J.M. and Lascara, C.M., 1999. Hydrography and circulation of the West Antarctic Peninsula Continental Shelf. Deep Sea Research, 46, 925-949.

Smythe-Wright, D., Chapman, P., Duncombe Rae, C., Shannon, L.V. and Boswell, S.M., 1998. Characteristics of the South Atlantic subtropical frontal zone between 15°W and 5°E. Deep Sea Research, 45, 167-192.

Solomon, H., 1983. Vertical Mixed Layer Convection in the Weddell Sea. Atmosphere-Oceans, 21 (2), 187-206.

Sparrow, M.D., Heywood, K.J., Brown, J. and Stevens, D.P., 1996. Current structure of the south Indian Ocean. Journal of Geophysical Research, 101 (C3), 6,377-6,392.

Stramma, L. and England, M., 1999. On the water masses and mean circulation of the South Atlantic Ocean. Journal of Geophysical Research, 104, 20,863-20,883.

Talley, L.D., 1996. Antarctic Intermediate Water in the South Atlantic. In: W.H.B. G. Wefer, G. Siedler and D. Webb (Editors), The South Atlantic: Present and Past Circulation. Springer-Verelag, Berlin, pp. 219-238.

Talley, L.D., 1999. Some aspects of ocean heat transport by the shallow, intermediate and deep overturning circulation. Mechanisms of Global Climate at Millennial Time Scales. Geophysical Monograph, 112, American Geophysical Union, 1-22.

Tomczak, M., 1999. Some historical, theoretical and applied aspects of quantitative water mass analysis. Journal of Marine Research, 57, 275-303.

Tomczak, M. and Godfrey, S.J., 2003. Regional Oceanography: an Introduction. Pergamon, 390 pp.

Valentine, H.R., Lutjeharms, J.R.E. and Brundrit, G.B., 1993. The water masses and volumetry of the southern Agulhas Current region. Deep Sea Research, 40 (6), 1,285-1,305.

van Aken, H.M., Ridderinkhof, H. and de Ruijter, W.P.M., 2004. North Atlantic Deep Water in the south-western Indian Ocean. Deep Sea Research, 51, 755-776.

van Aken, H.M., van Veldhoven, A.K., Veth, C., de Ruijter, W.P.M., van Leeuwen, P.J., Drijfhout, S.S., Whittle, C.P. and Rouault, M., 2002. Observations of a young Agulhas ring, Astrid, during MARE in March 2000. Deep Sea Research, 50, 167-195.

van Ballegooyen, R.C., Grundlingh, M.L. and Lutjeharms, J.R.E., 1994. Eddy fluxes of heat and salt from the southwest Indian Ocean into the southeast Atlantic Ocean: A case study. Journal of Geophysical Research, 99, 14,053-14,070.

van Leeuwen, P.J., de Ruijter, W.P.M. and Lutjeharms, J.R.E., 2000. Natal Pulses and the formation of Agulhas rings. Journal of Geophysical Research, 105 (C3), 6,425-6,436.

Wefer, G., Berger, W.H., Bickert, T., Donner, B., Fischer, G., Kemle-von Mücke, S., Meinecke, G., Müller, P.J., Mulitza, S., Niebler, H.-S., Pätzold, J., Schmidt, H., Schneider, R.R. and Segl, M., 1996. Late Quaternary Surface Circulation in the South Atlantic: the Stable Isotope Record and Implications for Heat Transport and Productivity. In: G. Wefer, W.H. Berger, G. Siedler and D. Webb (Editors), The South Atlantic: Present and Past Circulations. Springer, Berlin, pp. 461-502.

Whitworth, T.I., 1980. Zonation and geostrophic flow of the Antarctic Circumpolar Current at the Drake Passage. Deep Sea Research, 27, 497-507.

You, Y., 2002. Quantitative estimate of Antarctic Intermediate Water contributions from the Drake Passage and the southwest Indian Ocean to the South Atlantic. Journal of Geophysical Research, 107 (C4), doi: 10.1029/2001JC000880.

You, Y., Lutjeharms, J.R.E., Boebel, O. and de Ruijter, W.P.M., 2003. Quantification of the interocean exchange of intermediate water masses around southern Africa. Deep Sea Research, 50 (1), 197-228.

Zahn, R. and Keir, R., 1992. Tracer-Nutrient correlations in the upper ocean: observational and box model constrains on the use of benthic foraminiferal $\delta^{13}C$ and Cd/Ca as paleo-proxies for the intermediate-depth ocean. In: R. Zahn, T.F. Pedersen, M.A. Kaminski and L. Labeyrie (Editors), Carbon Cycling in the Glacial Ocean: Constrains on the Ocean's Role in Global Change. Springer, Berlin, pp. 195-221.

4. Methodology

4.1. Sample Preparation and Analyses

The total length of the sediment cores used for this Thesis is 22.23 m for MD96-2080 and 39.15 m for MD02-2594. For the purposes of this study the primary interest is on the last three glacial-interglacial cycles, from Marine Isotope Stage 1 (MIS 1) to MIS 9, i.e. the past 345 kyr. Low resolution stable isotope and faunal abundance records have been previously reported along the whole length of core MD96-2080 and hint at orbital scale variations in Agulhas Current water transports and deep water conditions over the past 850 kyr (Rau et al., 2002; 2006). This low resolution isotope stratigraphy (10 cm sampling interval) for MD96-2080 core depicts full glacial MIS 10 at 8 m core depth. Thus, the upper 8 m of core MD96-2080 have been resampled at 1 cm intervals at the University of Bordeaux back to full interglacial MIS 9, including glacial Termination IV. From our detailed age modelling we have found evidence that MIS 3 and 4 are missing from MD96-2080 (see Chapter 5.1). This time period is provided by the sediment core MD02-2594. Preliminary 10 cm step stable isotope measurements along this core showed that the upper 7.5 m cover the last 80 kyr.

Along MD96-2080 stable isotope analyses were performed at 1 cm intervals or 1-2 cm on occasion because of foraminifera scarcity, resulting in a centennial time resolution of the records in sections of high sedimentation rates and multi-centennial in sections of low sedimentation rates (see Chapter 5.1.). Trace element analyses where performed every 1-14 cm for *Fontbotia wuellerstorfi* (3-4 cm step along the majority of the record) and every 3-5 cm for *Globigerina bulloides* on average. Sample step was increased in sections of interest, i.e. MIS 5, which had showed little benthic $\delta^{13}C$ variability (see Chapters 5.2 and 5.3) and glacial Terminations. The resulting time step for the trace element records is millenial. Sortable silt analyses on MD96-2080 were performed at Cardiff University at 1 cm step all throughout the 8 m analysed.

Sedimentation rates are significantly higher at MD02-2594 than at MD96-2080, and, in order to obtain similar to finer time resolution, samples have been analysed every 5 cm for Termination I and every 2 cm for the entire last glacial period for planktonic foraminifera stable isotopes (*Globigerina bulloides* and *Globorotalia inflata*). For planktonic foraminifera Mg/Ca analyses the sample step has been slightly larger, every 10 cm for Termination I and every 2-4 cm for the last glacial period. Regarding bottom water conditions, only low resolution benthic stable isotopes and $\overline{SS}$ analyses at 10 cm sample step have been performed for this Thesis.

All samples taken during the sampling parties were freeze-dried to facilitate disaggregating and to minimize mechanical wear on microfossils during wet sieving. The samples were then washed through a 63 μm sieve. The fine fraction was collected during washing for determination of grain size population in the silt fraction, the sortable silt mean size ($\overline{SS}$). The fraction > 63 μm has been used for

micropaleontological analyses and selecting foraminiferal samples for stable isotope and trace element analyses.

Those records generated for both cores, i.e. *G. bulloides* and *F. wuellerstorfi* stable isotopes, *G. bulloides* Mg/Ca and $\overline{SS}$, have been spliced into singular records. Details about the splicing are given in Chapter 5.1. We have named the spliced record Agulhas Bank Spliced (ABS).

4.2. Sortable Silt Mean Size ($\overline{SS}$)

Grain size distributions of the terrigenous fraction were determined by Dr Ian Hall and Ms Helen Medley, MSc, in the sediment laboratory of the Department of Earth Sciences at Cardiff University using a Coulter Multisensor III. The data have been produced and provided as a complementary study to gain a comprehensive view of the past physical and chemical ventilation in deep waters off South Africa.

Subsequent to the collection of the washed fraction < 63 μm after wet sieving, the analytical procedure to compute the mean size of the sortable silt comprise carbonate removal by dissolution in 1 M acetic acid solution (48 h) at room temperature, and biogenic opal by digestion in 2 M sodium carbonate solution (85ºC for 5 h). The samples cleaned from these components, that otherwise would add non desirable sources of variability to the size distribution of the silt population, are introduced in the Coulter Multisensor III. The Coulter Counters is a resistance pulse counter, which operates on the principle that a particle passing through an electric field maintained in an electrolyte will cause a voltage change proportional to its volume. The pulses are related to spherical particle volume by calibration experiments (Bianchi et al., 1999 and references therein). Volume percentage and mean are calculated as the percentage of the 10 - 63 μm fraction out of the total fines and the mean grain size of that fraction (McCave et al., 1995). The analytical precision was 1-4%.

4.3. Stable Isotope and Trace Element Analyses (Planktonic and Benthic Foraminifera)

4.3.1. Foraminiferal Selection of Preferred Species

The epibenthic foraminiferal species *Fontbotia wuellerstorfi* (Schwager, 1866) (also referred in the literature as *Planulina, Cibicides, Cibicidoides* genus) (Fig. 4-1) was chosen for benthic stable isotope and trace element analyses because it lives on the sediment surface and therefore it is expected to directly record ambient bottom water chemical and isotope composition. It is one of the preferred species of benthic foraminifera in paleoceanography because its shell $\delta^{13}C$ composition closely mirrors the $\delta^{13}C$ signal of total CO_2 dissolved in ambient bottom water ($\delta^{13}C_{\Sigma CO2}$). Only under high surface productivity regimes, this species appears to not reliably record ambient $\delta^{13}C_{\Sigma CO2}$ because the high

amounts of organic material that reach the ocean floor generate a microenvironment of low $\delta^{13}C$ that is then recorded by *F. wuellerstorfi* (Mackensen et al., 1993; Mackensen and Bickert, 1999; Diz et al., 2007). This is assumed to be particularly the case at core sites in the Southern Ocean where Holocene to LGM $\delta^{13}C$ depletions are higher than 1‰ (e.g. Schmiedl and Mackensen, 1997; Mackensen et al., 2001; e.g. Hodell et al., 2003). On the other hand, the $\delta^{18}O$ composition of its shell calcite shows an offset of -0.64‰ with respect to calcite that is precipitated in $\delta^{18}O$ equilibrium with ambient sea water $\delta^{18}O$ and temperature. The offset from equilibrium is considered constant which allows correcting the $\delta^{18}O$ values by adding 0.64‰ (Shackleton, 1977).

F. wuellerstorfi is also commonly used for Cd/Ca analyses. The interest of using this species arise from the fact that it is a reliable recorder of both Cd content in sea water (Cd_{sw}) and $\delta^{13}C_{\Sigma CO2}$, and therefore allows separating the nutrient-driven signal from benthic $\delta^{13}C$ from the isotopic signature obtained during air-sea gas interchange at the source of deep water formation (see Chapter 2 and section 4.4.). Caveats on the use of benthic Cd/Ca occur in environments were the foraminiferal shells may have experienced some post-mortem dissolution. McCorkle et al. (1995) working with cores from the Ontong-Java Plateau found a preferential loss of Cd (and other trace elements) at sites deeper than 2.5 km, therefore, leading to lower Cd/Ca ratios which could be interpreted as lower nutrient content. Marchitto et al. (2000) showed that changes in the sea water CO_3^{2-} saturation state ($\Delta(CO_3)^{2-}$) may affect the Cd/Ca not only by dissolution but also during the foraminiferal uptake of Cd by altering the distribution coefficient between $Cd_{calcite}$ and Cd_{sw} (D_{Cd}). However, the limit upon which Cd/Ca may be influenced by $\Delta(CO_3)^{2-}$ (roughly beyond 5 μmol/kg) prevent the use of Cd/Ca as paleoproxy for Cd_{sw} in most parts of the Atlantic ocean and large portions of the Pacific (above 3 km water depth) (Marchitto et al., 2000).

The abundance of this species along cores MD96-2080 and MD02-2594 is sufficient to establish mono-specific benthic stable isotope and trace element records.

Figure 4-1 *Cibicidoides (Fontbotia) wuellerstorfi* (Schwager, 1866). Test forms a compressed, discoidal, very low trochospire; planoconvex in cross-section, with a flattened, evolute spiral side, a slightly convex, partially evolute, umbilical side and a truncate, keeled periphery. The (approximately) 10 narrow, curved, slightly inflated chambers in the final whorl increase rapidly in size and are separated by thickened, strongly curved sutures, slightly-depressed in final chambers on the spiral side, and sinuoid or hooked in final chambers on the umbilical side. Chamber walls are calcareous and coarsely perforate on the spiral side, finely perforate on the umbilical side. The primary aperture is an equatorial slit with a narrow lip extending beneath the umbilical folium (Holbourn and Henderson, 2002).

The planktonic foraminifera *Globigerina bulloides* (d'Orbigny, 1826) (Fig. 4-2a) is a non-symbiotic species that lives within the mixed layer in transitional to polar waters. This foraminiferal species has a shallow apparent calcification depth (<50 m or 0-100 m, depending on authors, Mashiotta et al., 1999; Niebler et al., 1999) and a wide geographic distribution that makes it one of the preferred species for reconstruction of sea surface temperatures. It is abundant in a wide range of thermal environments (at least 5-20ºC) and its quantity commonly increases during periods of upwelling or bloom conditions (Mortyn and Charles, 2003 and references therein). *G. bulloides* has been found to calcify mainly in spring in the North Atlantic, the Cariaco Basin and the Southern Ocean (Ganssen and Kroon, 2000; King and Howard, 2005; Tedesco et al., 2007).

This species was continuously present along MD96-2080 and MD02-2594 in sufficient abundances for stable isotope and trace element analyses. Besides, there exist mono-specific calibration functions to convert *G. bulloides* Mg/Ca ratios into sea surface temperature (SST) developed from culture and core tops from the Southern Ocean (Mashiotta et al., 1999) and from North Atlantic core tops (Elderfield and Ganssen, 2000) (see Chapter 4.5).

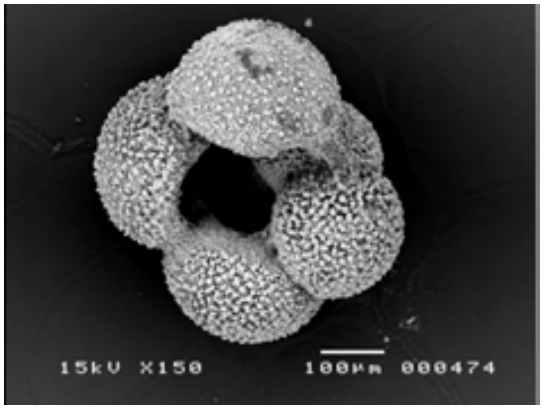

Figure 4-2a *Globigerina bulloides* (d'Orbigny, 1826) (http://www.soton.ac.uk/~bam2/col-index/fossi-lindex/Forams/Eelco/med-levantine/images/).

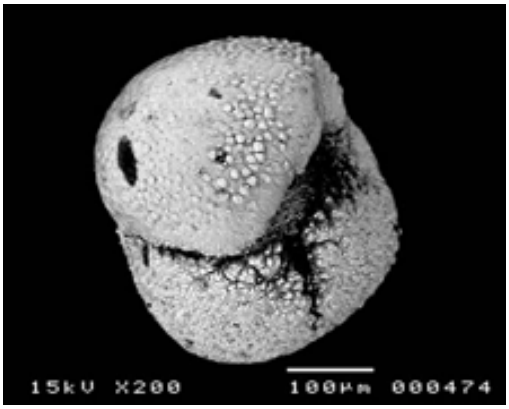

Figure 4-2b *Globorotalia inflata* (d'Orbigny, 1826). (http://www.soton.ac.uk/~bam2/col-index/fossi-lindex/Forams/Eelco/med-levantine/images/).

The planktonic foraminifera *Globorotalia inflata* (d'Orbigny, 1826) (Fig. 4-2b) is a non-symbiotic deep-dwelling species most common in transitional waters between subpolar and subtropical regions (Bé and Hutson, 1977; Hemleben et al., 1989). It can apparently live in a wide range of temperatures, but it is less frequent in high-salinity conditions (Manighetti and Northcote, 2000). Plankton tow studies in the Atlantic sector of the Southern Ocean show that this species is most abundant at subsurface depths between 50 and 300 m (Mortyn and Charles, 2003), plankton tows in the Cape Basin showed maximum abundances around 20-80 m and presence up to 500 m water depth (Wilke et al., 2006). Ganssen and Kroon (2000) found that this species reflects temperatures at around 100 to 400 m water depth in the North Atlantic while Loncaric et al. (2006) using stratified plankton tows at the central Walvis Ridge found that *G. inflata* record the temperature between 150 and 350 m, depending on the season and the shell size. In contrast with these findings, King and Howard (2001) reported that *G. inflata* exhibited in the Pacific sector of the Southern Ocean $\delta^{18}O$ values which are equivalent to predicted $\delta^{18}O_{calcite}$ values at around 50 m water depth. It seems that this species experiences large migrations along its life cycle in the water column (Molina, 2002) and likely accommodates for a preferred living temperature moving in the water column according to such temperature. As a consequence of this fact, this species does not seem a reliable recorder for past changes in sub-surface water temperatures (I. Cacho, pers.comm. 2006).

4.3.2. Stable Isotope Analyses (Planktonic and Benthic Foraminifera)

For stable isotope and micropalaeontological work the > 63 μm size fraction was dried at < 50ºC and 3 to 7 individuals of the epibenthic foraminifera *F. wuellerstorfi* were picked from the size fraction 250-315 μm, or >250 μm in sections where abundance of *F. wuellerstorfi* was low. In the case of planktonic foraminifera, 17 individuals of *G. bulloides* were picked from the size fraction 250-315 μm, abundance of *G. bulloides* was always sufficient to maintain this size range. In samples where paired trace element and stable isotope measurements were performed, between 10 and 25 individuals of *F. wuellerstorfi* and between 50 and 80 individuals of *G. bulloides* respectively were crushed together under clean glass plates, the crushed fragments were then homogenized and a small fraction (equivalent to around 4 benthic and 17 planktonic individuals) was separated for stable isotopes analyses. The larger fraction was used for trace element analyses (see below). In addition to these two species, 5 to 9 individuals of the planktonic foraminifera *G. inflata* were analysed along MD02-2594. Analyzing also this species in MD02-2594 core has been of utility as a support for establishing the age model of this core by comparison with the *G. inflata* record of MD96-2081 (F. Peeters, unpublished data) (see Chapter 5.1.).

Prior to analysis all samples were cleaned involving mechanical crushing under methanol to release possible sediment fillings. Crushed fragments in methanol were sonicated for 10-20 s to remove sediment coatings, and dried in a gravity convection oven at < 40ºC. Stable isotopes were then measured with a ThermoFinnigan MAT 252 isotope ratio gas mass spectrometer that was linked online to a CARBO Kiel individual sample reaction carbonate preparation line at the Serveis

Cientificotècnics of the Universitat de Barcelona (STC-UB). The initial low resolution stable isotope measurements along MD02-2594 performed to find out the time coverage of this record were carried out at the School of Earth and Planetary Science of the Cardiff University, using also a MAT 252 isotope ratio gas mass spectrometer online linked to a CARBO Kiel device. Subsequent high resolution analyses (on planktonic foraminifera) along this core were accomplished at the STC-UB. External reproducibility was monitored through routine repeat measurements of an internal laboratory standard (Solenhofen Limestone, SHK) and was 0.021 for $\delta^{13}C$ and 0.040 for $\delta^{18}O$. During the period in which the MD96-2080 measurements were performed external reproducibility transiently dropped to 0.035 for $\delta^{13}C$ and 0.082 for $\delta^{18}O$. This affected measurements within the core section corresponding to MIS 5. Data integrity was confirmed by remeasuring 25 samples of planktonic foraminifera and 4 samples of benthic foraminifera in that section. All isotope values are referred to the Vienna Peedee Belemnite scale (VPDB) through calibration to the VNBS19 marble carbonate standard.

4.3.3. Trace Element Analyses

- **Trace Element Analyses in Planktonic Foraminifera**

For trace element analyses between 50 and 80 planktonic foraminifera from the species *G. bulloides* were picked from the size fraction 250-315 μm. A first introduction and early training on this technique was received at the Earth Science Department of the Oxford University in collaboration with Drs R. Rickaby, D. Harding and J. Arden. Some experiments were carried out there to test for the efficiency of the cleaning methods on MD96-2080 samples. Subsequent to the stay in Oxford, the analyses which comprise the final records *s.s.* were performed in collaboration with scientists from the Universitat de Barcelona (Drs Isabel Cacho and Leopoldo Pena, and Gemma Herrera). The cleaning protocol employed for the planktonic samples is the so called “oxidative cleaning” or “Mg-cleaning protocol” (Martin and Lea, 2002; Barker et al., 2003) *vs* the so called “reductive cleaning” or “Cd-cleaning protocol” (Boyle and Keigwin, 1985/86; Rosenthal et al., 1997) which was employed for the benthic samples (see next section). Details about the implementation of the cleaning protocols at the Universitat de Barcelona are given in Pena et al. (2005). A brief description about them is provided here.

The “oxidative cleaning” encompasses three main steps: clay removal, oxidative cleaning and weak acid leach. Each of the steps aims to eliminate specific contaminants from the foraminiferal test.

First, foraminifera are gently crushed between two clean glass plates, only sufficiently enough to open the chambers to the cleaning. It is important not to crush the foraminifera in excess as this increases sample loss and dissolution during cleaning (physical and chemical sample lost). In the case that trace element and stable isotope analyses were to be performed in the same sample (ideally), the crushed fragments were homogenized with a brush and around 1/3 of the sample was separated for stable isotope analyses and 2/3 for trace element analyses (or an approximately equivalent to 4 *F. wuellerstrofi* and 17 *G. bulloides*, see above). The sample was then transferred to acid leach cleaned Eppendorf vials. In order to clean the vials, these were completely filled with 10% HNO_3 so that no air

bubbles remain, and then left in the acid between 12 and 24 hours. After this time the vials were rinsed 6 times with MilliQ water.

The cleaning protocol *s.s.* was undertaken in a clean lab and most of the steps were carried out within a laminar flow to ensure that none external particle fall into the samples.

- "*Clay removal*", this step has been specifically design to remove detritic impurities that may fill the foraminiferal shells or be attached to their surfaces. Initially 20-30 μl of MilliQ water are added to each vial, the vials are ultrasonicated for 15-20 seconds in order to bring the clays into suspension. After ultrasonication more MilliQ water is added to each vial (around 300 μl) so that clays, but also foraminiferal fragments are brought into suspension. Foraminiferal fragments settled much faster than clays, they are allowed to settle (for some 30 seconds) and suspended clays are removed cautiously to avoid siphoning foraminiferal fragments. This step is repeated at least three times. Two additional methanol rinses are performed afterwards, also including ultrasonic treatment, the lower viscosity of methanol allows resistant clays to get into solution and be removed. A final MilliQ water rinse is performed to eliminate any methanol residue. In especially dirty samples (identified under the microscope during the crushing or in which the third water rinse is still "milkish") one or two additional water rinses were performed.

- The "*oxidative step*" aims for the elimination of remains of organic matter. An alkali buffered (NaOH) hydrogen peroxide (H_2O_2) 1% solution is used. Vials filled with 250 μl of oxidative agent were placed in a bath with boiling water for 10 minutes. After 2.5, 5, 7.5 and 10 minutes the rack of samples was slapped against the bench to remove possible air bubbles that could trapped foraminifera fragments and impede its reaction with the oxidative agent. After 5 and 10 minutes, besides slapping against the bench, the samples were briefly ultra-sonicated (10-15 seconds) with the same purpose and also to promote reaction. Subsequently the samples were rinsed 3 times with ultra-pure MilliQ water to eliminate any remain of reagent; also the lids of the vials were rinsed. Foraminifera fragments tend to attach to the vial walls at this step and special caution should be applied when rinsing the water. Sample lost may be critical at this point.

- "*Weak acid leach*", the objective of this step is to remove any remaining contaminant phase or particle that could be still attached to the foraminiferal shells. The acid employed is HNO_3 0.001M. After adding 250 μl the samples are ultra-sonicated during 30 s and subsequently the acid is removed by three MiliQ water rinses.

Sample dissolution prior to ICP-MS analyses was done the day before measuring with ultra pure HNO_3 (1%) and centrifuged during 5 minutes at 6000 rpm. The solution was transferred into clean vials. A small residue of solution was always left in the Eppendorf vial to prevent any solid impurity to be measured.

An internal standard of known Mg/Ca ratio was measured within each run of ICP-MS so that foraminiferal results could be corrected for any possible drift during the measurements. Long term internal reproducibility based on the measurements of this internal standard along the period of measurements was 2.474±0.102% (RSD).

The photographs and side-graphs (Figs. 4-3 and 4-4) show fragments of *G. bulloides* prior to cleaning taken during the stay at Oxford University to illustrate some of the impurities found attached to the tests.

a)

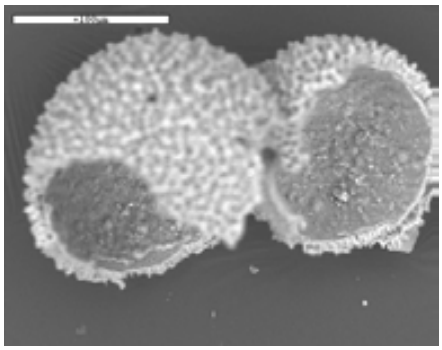

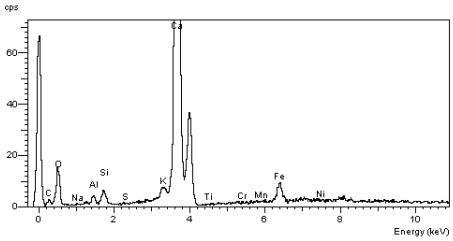

b)

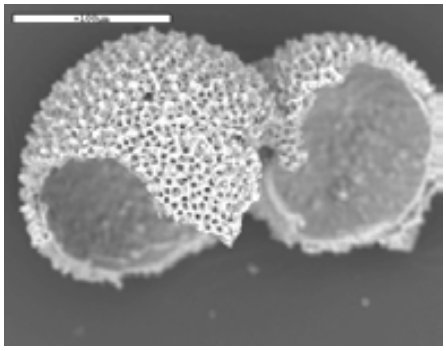

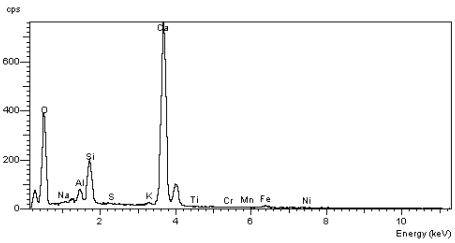

c)

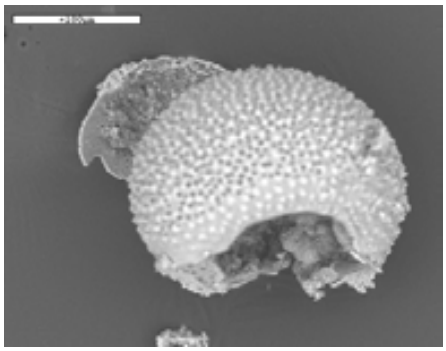

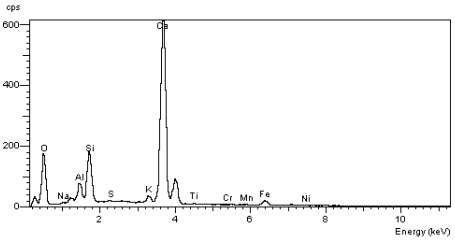

d)

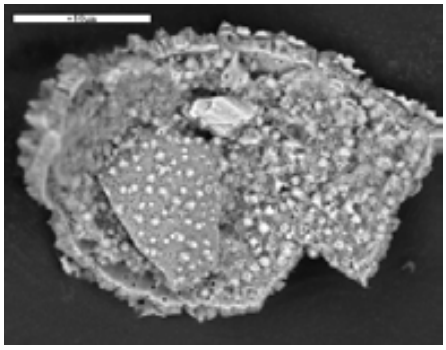

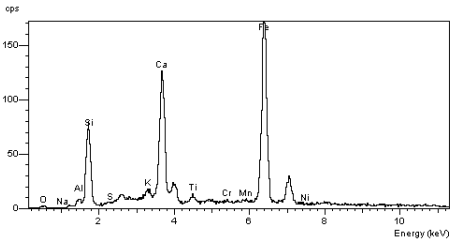

Figure 4-3 Open chambers of *Globigerina bulloides* and spectrum showing the main chemical elements present in the tests. In the inner chambers we see tracers of O, Si, Al and Fe, that could indicate the presence of clays and Fe-Oxides. On the outer shell we do not observed the Fe peak (spectrums a) an b) respectively) indicating that clays are the main source of contamination in the exterior. In photograph c) we observed very clearly the presence of clays. In photograph d) a grain is very apparent and its composition reflects a big amount of Fe (SEM images taken at the Department of Earth Sciences, Oxford University).

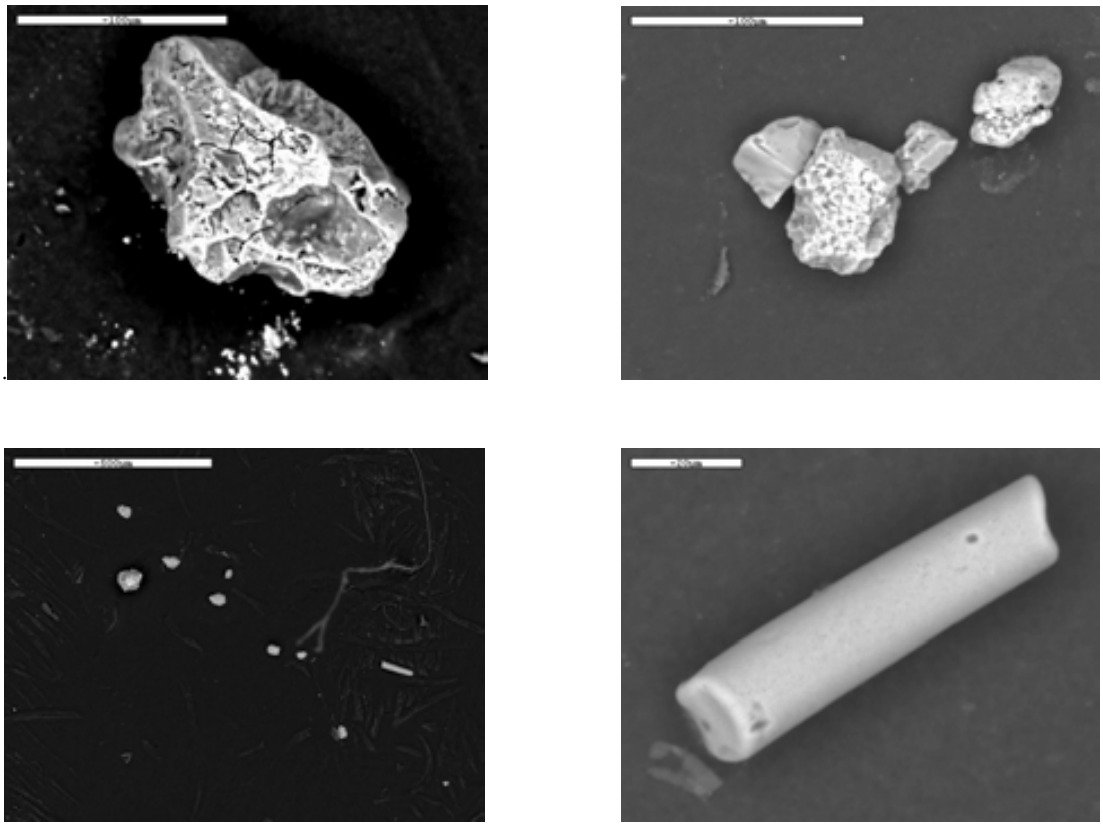

Figure 4-4 These photographs illustrate the importance of centrifuging the samples prior to analyzing in the ICP-MS. The images show impurities that were left in the vial after the analyses (some 10 μl of sample solution are always left in the vial when transferring the sample to the measuring vials, any possible impurity is brought to the bottom during the centrifugation and left there) (SEM images taken at the Earth Sciences Department, Oxford University).

- **Trace Element Analyses in Benthic Foraminifera**

For trace element analyses in benthic foraminifera at least 20 individuals of *F. wuellerstorfi* were selected from the 250-315 μm size fraction, when not enough foraminifera were found on this size fraction, the > 63 μm fraction was revised. The cleaning protocol used is extensively described in Pena et al. (2005) and it is based on that of Boyle and Keigwin (1985/86). Basically it comprises the five steps explained for the oxidative cleaning but with an additional "*reductive step*" between the clay removal and the oxidative cleaning. This step was designed to eliminate metal phases, e.g. Mn and Fe Oxides. The reductive reagent used was a mixture of hydrazine hydroxide, citric acid and ammonia hydroxide. The reagent was added to each vial and the rack is placed inside a hot (around 100ºC) ultrasonic bath during 30 minutes. Every two minutes the samples were briefly ultrasonicated to promote reaction. This is the most corrosive step, dissolution may occur along the sequence and therefore it is very important to clean the samples immediately after the reaction time to avoid further reaction and dissolution. The reagent was cleaned by three rinses of ultra-pure MilliQ water (also the lids of the vials were cleaned), then, two more rinses with hot water (approximately 80ºC) with a waiting time of five minutes between each rinse were performed. A final rinse with cold water was made.

The sequence of the steps is important, i.e. the reductive step must be performed before the oxidative step. Rosenthal et al. (1995; 1997) suggest that in samples from the Cape Basin that were deposited under certain oceanographic regimes, i.e. sub-oxic to anoxic conditions, a Cadmium Sulfide (CdS) may precipitate. These authors observed that samples cleaned with the "full" protocol but with the oxidative cleaning performed before the reductive cleaning yielded high Cd values. From this they concluded that the oxidative cleaning was strengthening the bonds of the CdS that may be in the foraminiferal shell impeding its elimination by the reductive step. When the reductive step was performed before the oxidative one, the Cd levels were much lower and the reproducibility of the analyses much better. This was observed in samples from the Cape Basin but it may likely happen in samples from other locations under similar conditions as well.

The error associated with the Cd/Ca measurements was ±2.4% (RSD) based on replicate analyses of an internal standard run during a three month period. Nonetheless, it needs to be noted that the error associated to each benthic foraminiferal measurement is larger than this. For the MD96-2080 the average error of all individual measurements in total is ±15% (RSD).

- **Efficiency of the Cleaning Methods and Dissolution Effects**

The efficiency of the cleaning for both, oxidative and reductive methods was assessed by monitoring Mn and Al concentrations. Mn/Ca ratios above 100-150 μmol/mol are assumed to represent potential contamination by Mn-carbonate overgrowths (e.g. Boyle, 1983; Boyle and Rosenthal, 1996). All trace element sample solutions, both planktonic and benthic, along MD96-2080 yielded Mn/Ca ratios below 80 μmol/mol (Figs. 4-5 to 4-7). In the case of MD02-2594 some Mn/Ca ratios ranged between 110-90 μmol/mol (Fig. 4-8). This may reflect sediment phases with higher concentrations of Mn while the planktonic Mg/Ca ratios do not seem contaminated. The concentration of Al/Ca ratio was monitored in order to detect potential contamination by clays. While a threshold value of Al/Ca is not commonly used the values in the majority of sample solutions were negligible and below the detection limit of the ICP-MS. For benthic MD96-2080 samples only seven out of 198 analyses yielded Al/Ca > 220 μmol/mol. Of these, only a single sample solution yielded a significantly higher Cd/Ca ratio than the surrounding data points and was neglected. Similarly, only ten planktonic MD96-2080 samples yielded Al/Ca > 220 μmol/mol, we reject one of them because it departs from the general trend of Mg/Ca. For MD02-2594, only two out of 212 analyses yielded Al/Ca > 100 μmol/mol, one of them was discarded because of having a significantly high Al/Ca (800 μmol/mol). One sample with Al/Ca around 77 μmol/mol was also discarded because of being associated with relatively high Mn/Ca levels (106 μmol/mol). Additionally, in order to ensure clean conditions during the sample preparation, procedure blanks were generated and measured for each sample batch. The blanks yielded in all cases low values, at the detection limit of the ICP-MS. In the following ratio-ratio plots are presented to strengthen the lack of correlation between Mn/Ca, Al/Ca and [Ca] with Mg/Ca and Cd/Ca respectively, thus ensuring the quality of the data set.

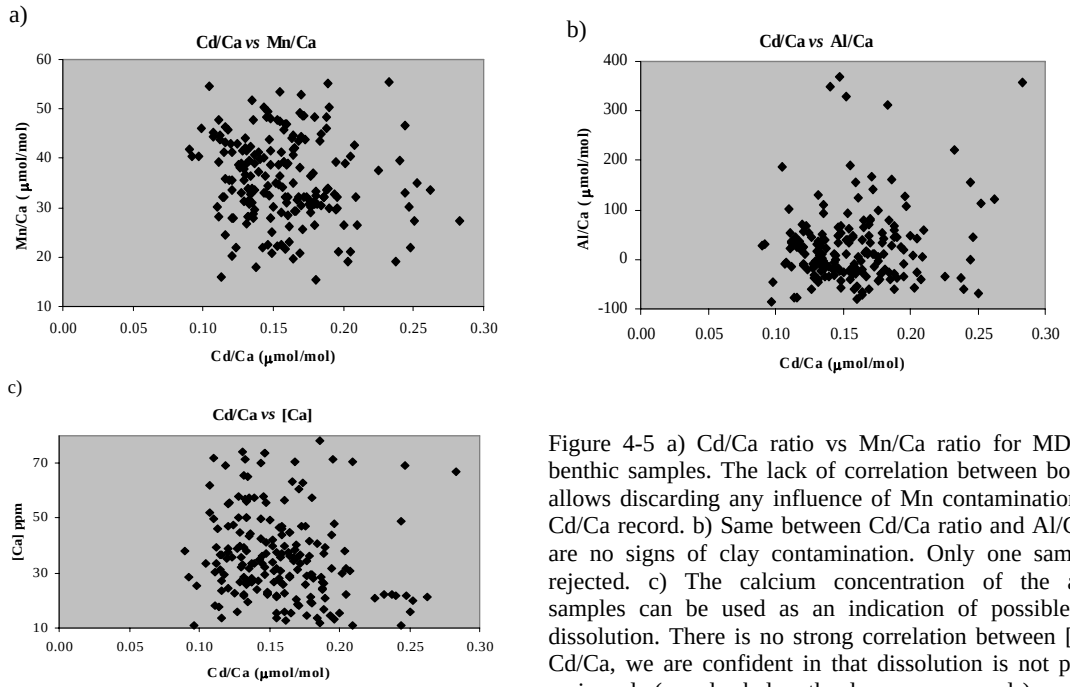

Figure 4-5 a) Cd/Ca ratio vs Mn/Ca ratio for MD96-2080 benthic samples. The lack of correlation between both ratios allows discarding any influence of Mn contamination on the Cd/Ca record. b) Same between Cd/Ca ratio and Al/Ca, there are no signs of clay contamination. Only one sample was rejected. c) The calcium concentration of the analysed samples can be used as an indication of possible sample dissolution. There is no strong correlation between [Ca] and Cd/Ca, we are confident in that dissolution is not playing a major role (see also below the down-core records).

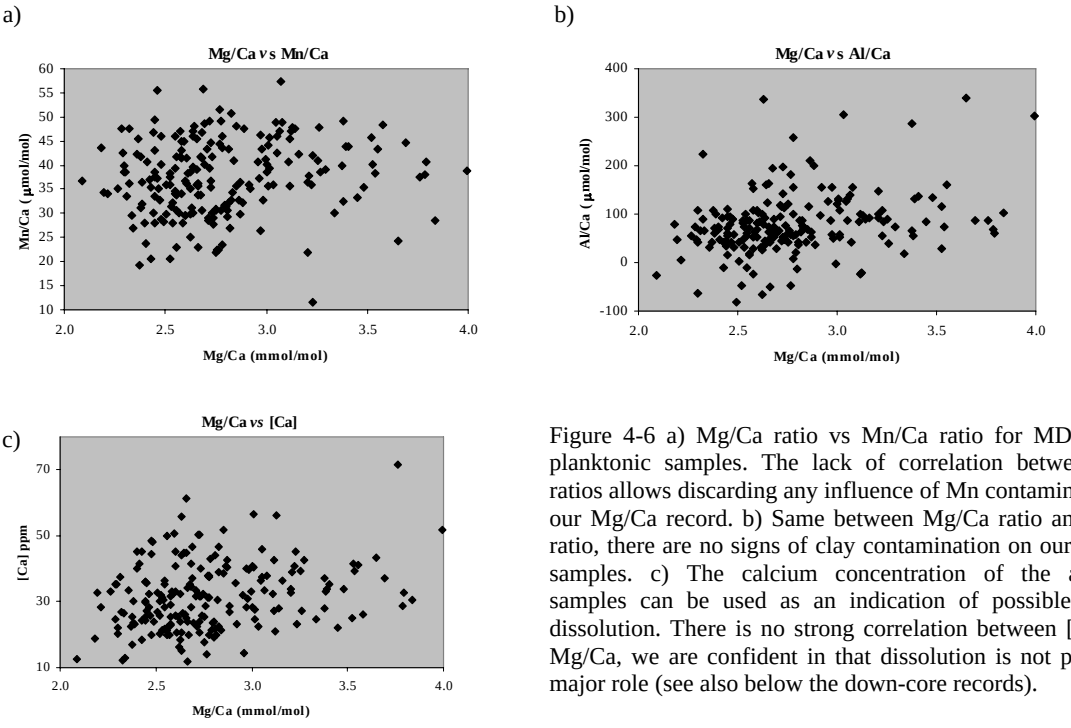

Figure 4-6 a) Mg/Ca ratio vs Mn/Ca ratio for MD96-2080 planktonic samples. The lack of correlation between both ratios allows discarding any influence of Mn contamination on our Mg/Ca record. b) Same between Mg/Ca ratio and Al/Ca ratio, there are no signs of clay contamination on our cleaned samples. c) The calcium concentration of the analysed samples can be used as an indication of possible sample dissolution. There is no strong correlation between [Ca] and Mg/Ca, we are confident in that dissolution is not playing a major role (see also below the down-core records).

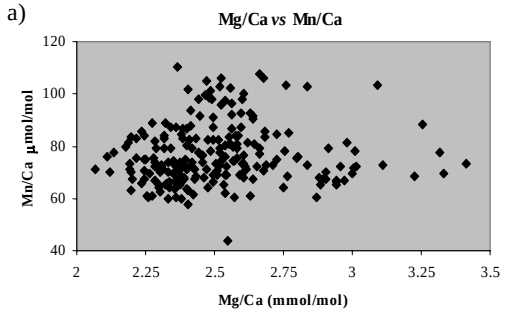

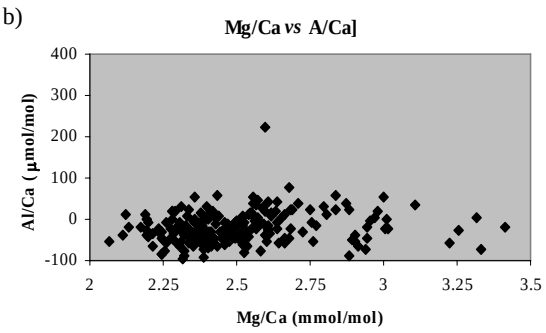

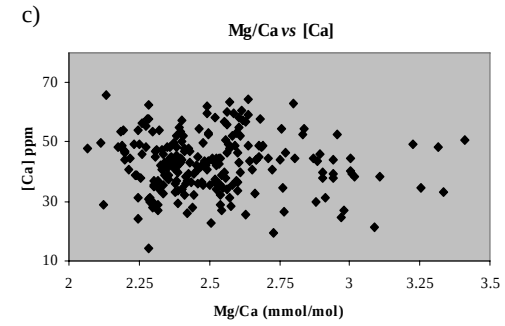

Figure 4-7 a) Mg/Ca ratio vs Mn/Ca ratio for planktonic MD02-2594 samples. The lack of correlation between both ratios allows discarding any influence of Mn contamination on our Mg/Ca record. b) Same between Mg/Ca ratio and Al/Ca ratio, there are no signs of clay contamination on our cleaned samples. c) The calcium concentration of the analysed samples can be used as an indication of possible sample dissolution. There is no strong correlation between [Ca] and Mg/Ca, we are confident in that dissolution is not playing a major role (see also below the down-core records).

Post-mortem dissolution is known to alter the final trace element to Ca ratios (McCorkle et al., 1995; Brown and Elderfield, 1996; Deckens et al., 2002; Regenberg et al., 2006). Calcite in which Ca has been substituted for other trace elements is more prone to dissolution and therefore samples affected by dissolution would yield lower Mg/Ca and Cd/Ca ratios.

Both sediment cores studied in this Thesis lie at around 2500 m water depth. Volbers and Henrich (2002) placed the sedimentary calcite lysocline (depth at which significant calcite dissolution is observed) in the Cape Basin at the present NADW/AABW boundary (at around 4000 m) in contrast to the "hydrographical lysocline" ($[CO_3^{2-}]$ critical or undersaturation depth), which is around 4400 m in the Cape Basin. MD96-2080 and MD02-2594 cores are well above the present day Atlantic lysocline, and probably this has also been the case during previous interglacials. The lysocline is known to have shoaled during glacial times. Volbers and Henrich (2004) placed the depth of the lysocline in the Cape Basin during the LGM at around 3500 m. This value may be indicative of the shoaling the lysocline may experience during glacial conditions and suggest that our cores were also likely above the lysocline during glacial intervals and dissolution should not play a major role in our trace element ratios.

We had four means to test for dissolution effects on our Me/Ca ratios.

One was the calcium concentration of the sample solutions analyzed (Figs. 4-5 to 4-7). There was no correlation between the [Ca] and neither Cd/Ca nor Mg/Ca in the benthic or planktonic samples of both MD96-2080 and MD02-2594. Nonetheless, this [Ca] may only be used as indicative since not only post-mortem foraminiferal dissolution, but also chemical dissolution and physical sample lost during the cleaning protocol are affecting the measured concentration.

Low and moderate resolution records of *G. bulloides* weight for MD96-2080 and MD02-2594 respectively were generated. Shell weight of planktonic foraminifera has traditionally been interpreted as an index of dissolution at the sea floor and thus as an indicator of the saturation state of the bottom waters. Nevertheless, studies by Barker and Elderfield (2002) have showed that the shell weight may vary at the surface, during calcification, as a function of ambient [CO_3^{2-}]. In order to distinguish between a [CO_3^{2-}]-calcification or a dissolution control on weight records of planktonic foraminiferal it is desirable to have several nearby sediment cores at different water depths (Barker et al., 2004) or some other independent control on foraminiferal dissolution. Therefore, the comparison of this record with the Mg/Ca record was done in the context of the other available means to test for dissolution (Fig. 4-8) (see next).

A common tool for deciphering about foraminiferal dissolution is the Fragmentation Index (FI). This is a measure of the fragments of foraminifera with respect to the whole foraminifera present in the sample; more fragments mean that the sample has undergone more dissolution (e.g. Le and Shackleton, 1992).

The $CaCO_3$ content of the sediment also provides some insight on the state of saturation of the ambient water although other factors affect this measurement such as calcite flux, fluxes of other sedimentary components or organic rain ratio (e.g. Emerson and Archer, 1990). Low resolution records of fragmentation index as well as content of $CaCO_3$ (in percent) were available for MD96-2080 from Rau et al. (2002) (Fig. 4-8).

In Figure 4-8 the Mg/Ca record of MD96-2080 is represented together with the profile of weight of *G. bulloides* and the available FI, $CaCO_3$ and percent of weight of the sand fraction (> 63 μm) and sedimentation rates (see Chapter 5.1 for details about the computation of the sedimentation rates).

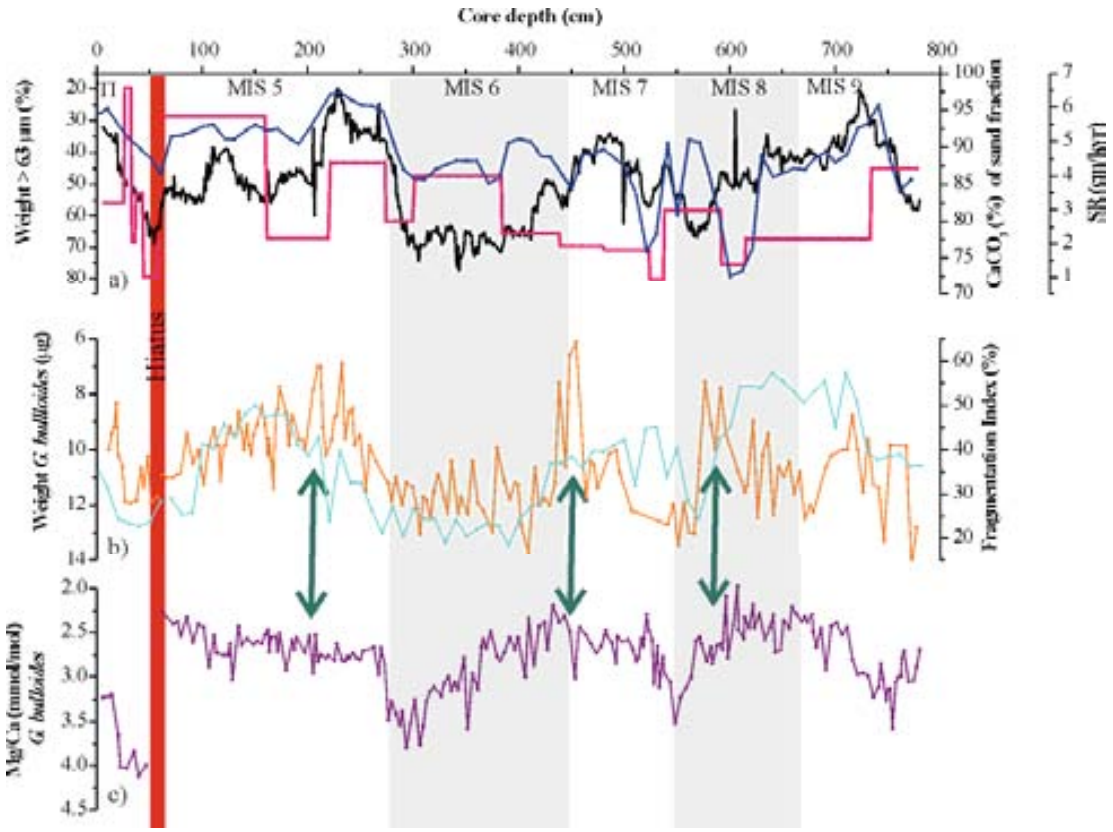

Figure 4-8 a) Weight > 63 µm (in percent) (black), it provides a good reference for the stratigraphic control on this figure as it resembles the foraminiferal $\delta^{18}O$ records (see Chapter 5); sedimentation rates (in cm/kyr) (pink); percent of $CaCO_3$ in the sand fraction of the sediment (Rau et al., 2002) (blue); b) Weight of *G. bulloides* (µg), (orange); Fragmentation Index (%) (Rau et al., 2002) (cyan); c) *G. bulloides* Mg/Ca (mmol/mol). The red bar marks a hiatus in the sediment core (see Chapter 5.1 for details). Green arrows show the moments where we could have some shell dissolution. TI: Termination one; MIS: Marine Isotope Stages. Vertical shading highlights glacial periods MIS 6 and 8 (see Chapter 5.1 for details on the age model construction).

FI and weight of *G. bulloides* show signs of better preservation during glacials (heavier foraminifera and lower FI). On the other hand, the $CaCO_3$ content of the sand fraction is higher during interglacials, which a priori would be indicative of enhanced preservation in these periods. Visual inspection of the foraminifera during hand picking indeed indicates better preservation during glacial stages. This contrasts with our knowledge of the depth of the lysocline in the Cape Basin which is deeper during interglacials. Other factors should then be involved in this pattern of variability, such as carbonate production and $[CO_3^{2-}]$ effect on shell weight.

In general the Mg/Ca record does not follow the weight of *G. bulloides* and FI records. If dissolution were to play a role in shaping the Mg/Ca record it would act to lower the ratios during the interglacials (where preservation is apparently poorer). However, the pattern of variability of the records during interglacials is not parallel to those of FI and *G. bulloides* weight and furthermore $CaCO_3$ is increased in the warm periods. If at all, we could expect some dissolution-lowered Mg/Ca in the parts of the interglacial periods indicated by green arrows (see Fig. 4-8). This would mean that some of the shifts in our Mg/Ca could be less pronounced but they would not disappear. Nevertheless the drop in temperature from 276.5 to 273.5 cm (entering MIS 5e, see Chapter 5) seems difficult to explain by a rather sudden increase in carbonate undersaturation of ambient bottom waters at the core

location. We are confident that our Mg/Ca record is not significantly affected by dissolution and that we can therefore use it to record past sea surface temperatures (SST) in the Agulhas area.

Similarly to MD96-2080 the *G. bulloides* weight is heavier along the glacial section of MD02-2594 (Fig. 4-9), which could be interpreted as an indication of better preservation of samples of glacial age. Nonetheless, we need to keep in mind the observations of Barker and Elderfield (2002) about a possible [CO_3^{2-}] influence on planktonic shell calcification that could modulate the record without existing a dissolution related effect. Low Mg/Ca during MIS 3 and 4 correlates with heavier foraminifera. Thus, if dissolution lowered the Mg/Ca during the Holocene and MIS 5a, then the glacial-interglacial shift could have been larger but the general pattern of the Mg/Ca record would not change. Furthermore, foraminiferal preservation seems very good in this core upon visual inspection.

As a last note on our confidence on our *G. bulloides* Mg/Ca recording past SST is provided by the recent study of Mekik et al. (2007). These authors have found evidence that the Mg/Ca in surface-dwelling foraminifera, and more specifically in *G. bulloides*, is controlled by calcification temperature and is largely unaffected by carbonate dissolution (as estimated from *Menardii* Fragmentation Indexes, MFI) (see also Mekik and François, 2006). In contrast, these authors found that Mg/Ca in deeper dwelling *G. menardii* is nearly insensitive to temperature and its Mg/Ca mostly reflects dissolution. Other species showed effects of both, temperature and dissolution.

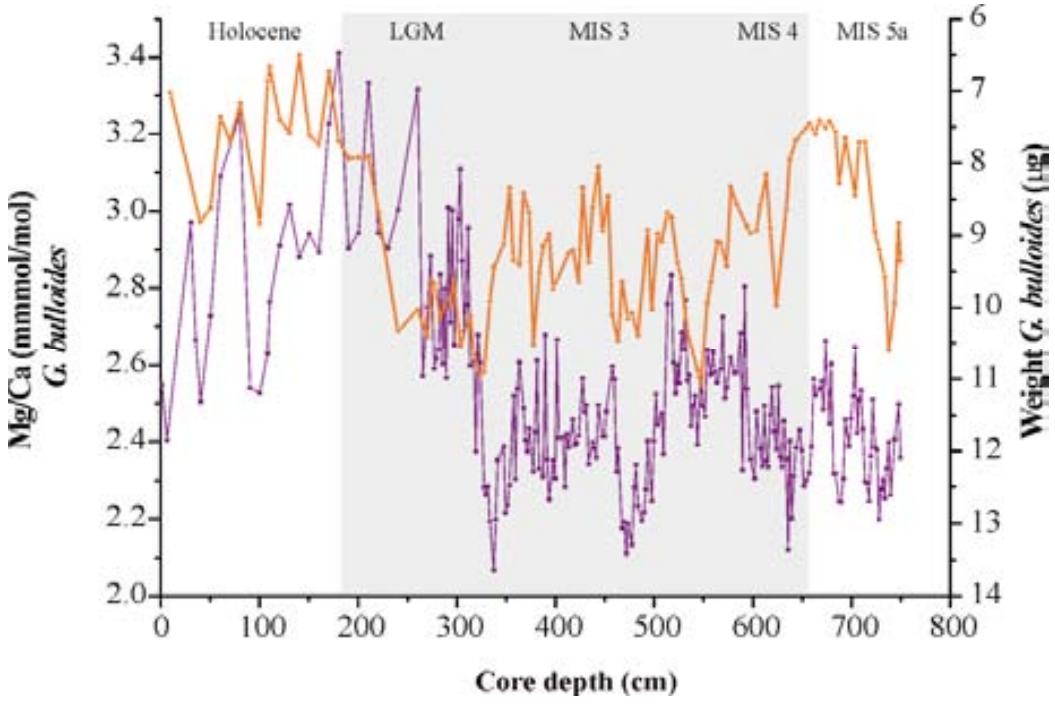

Figure 4-9 MD02-2594 weight of *G. bulloides* (µg) (orange) and *G. bulloides* Mg/Ca (mmol/mol) (purple). Note reversed scale of Mg/Ca respect to Figure 4-9. Vertical shading highlights the last glacial period (from the LGM to MIS 4) (see Chapter 5.1).

A record of shell weight of benthic foraminifera has not been generated. Benthic species are typically more robust than planktonic ones; therefore, if we do not see clear evidence of foraminiferal dissolution in planktonic foraminifera we can be rather confident that this is not affecting the benthic samples.

4.4. Past Sea Water Cadmium (Cd_{sw}) Along MD96-2080 and Derivation of the Air-Sea $\delta^{13}C_{\Sigma CO2}$ Isotopic Signature ($\delta^{13}C_{as}$)

Water column $\delta^{13}C_{\Sigma CO2}$ is influenced by a series of factors (see Chapter 2), including air-sea gas exchange and associated carbon isotope fractionation, variations of the marine carbon reservoir, biological nutrient cycling and water mass "aging", and mixing between water masses that carry their own individual end-member $\delta^{13}C_{\Sigma CO2}$ signature (Kroopnick, 1985; Broecker and Maier-Reimer, 1992; Lynch-Stieglitz and Fairbanks, 1994; Lynch-Stieglitz et al., 1995). Benthic foraminiferal Cd/Ca as proxy for Cadmium content in sea water (Cd_{sw}, see Chapter 2) is likewise linked with biological nutrient cycling and water mass "aging" but is not influenced by the other secular factors modulating foraminiferal $\delta^{13}C$ (see Chapter 2) and therefore may be considered a more conservative nutrient tracer (Boyle, 1981; Hester and Boyle, 1982; Boyle and Keigwin, 1985/86; Boyle, 1988). Benthic Cd/Ca has been previously used to separate the signals of nutrient cycling from other secular signals contained in benthic $\delta^{13}C$ records and to derive the water mass carbon isotope air-sea exchange signature ($\delta^{13}C_{as}$ as named by Lynch-Stieglitz and Fairbanks, 1994) which is a conservative, though not unique, water mass tracer (e.g. Lynch-Stieglitz and Fairbanks, 1994; Lynch-Stieglitz et al., 1996; Marchitto and Broecker, 2006).

Lynch-Stieglitz and Fairbanks (1994) and Lynch-Stieglitz et al. (1996) combined the Broecker and Maier-Reimer (1992) relation between $\delta^{13}C$ and $(PO_4)^{3-}$ (Eq. 2-12) with Boyle's (1988) Cd_{sw}-$(PO_4)^{3-}$ relationships (Eqs. 2-14, 2-15) in order to estimate $\delta^{13}C_{as}$ using benthic Cd/Ca and $\delta^{13}C$ and propose the following equations:

$$\delta^{13}C_{as} = \delta^{13}C - \delta^{13}C_{bio} = \delta^{13}C + 2.75 \cdot Cd_{sw} - 2 \qquad For \quad Cd_{sw} > 0.28 \ nmol/kg \qquad \text{Eq. 4-1}$$

$$\delta^{13}C_{as} = \delta^{13}C - \delta^{13}C_{bio} = \delta^{13}C + 5.29 \cdot Cd_{sw} - 2.7 \qquad For \quad Cd_{sw} < 0.28 \ nmol/kg \qquad \text{Eq. 4-2}$$

For the LGM Lynch-Stieglitz et al. (1996) modified equations 4-1 and 4-2 to account for a 2‰ increase in $\delta^{13}C$ of the organic matter (Rau et al., 1991), 0.3‰ decrease in mean ocean $\delta^{13}C$ (Curry et al., 1988; Duplessy et al., 1988), an increase of total inorganic carbon of 4% and assuming no change in the Cd_{sw} and $(PO_4)^{3-}$ inventories and in the relationship between both. The resulting equations are:

$$\delta^{13}C_{as} = \delta^{13}C - \delta^{13}C_{bio} = \delta^{13}C + 2.375 \cdot Cd_{sw} - 1.46 \qquad For \quad Cd_{sw} > 0.28 \ nmol/kg \qquad \text{Eq. 4-3}$$

$$\delta^{13}C_{as} = \delta^{13}C - \delta^{13}C_{bio} = \delta^{13}C + 4.57 \cdot Cd_{sw} - 2.05 \qquad For \quad Cd_{sw} < 0.28 \ nmol/kg \qquad \text{Eq. 4-3}$$

Equations 4-1 to 4 can be written in a general form as:

$$\delta^{13}C_{as} = \delta^{13}C - \delta^{13}C_{bio} = \delta^{13}C + a \cdot Cd_{sw} - b \qquad \text{Eq. 4-5}$$

The solutions of this equation can be plotted in a Cd_{sw} *vs* $\delta^{13}C$ diagram as isolines of constant $\delta^{13}C_{as}$. Displacement of $\delta^{13}C/Cd_{sw}$ coordinates along isolines of constant $\delta^{13}C_{as}$ are related only to water mass "aging" while displacements across isolines represent water mass mixing.

The objectives of this study extend beyond LGM and Holocene reconstructions. In Chapter 5.2 Cd_{sw} *vs* $\delta^{13}C$ diagrams are used in order to investigate past changes, from MIS 5 to 9, in the dominant water masses around South Africa. Furthermore, we have attempted to construct a continuous record of $\delta^{13}C_{as}$ back to 345 kyr for MD96-2080 and for other sediment cores that are then used for comparison (see Chapter 5.3). Most likely the above Holocene and LGM parameterizations do not apply to the same extent to previous interglacial and glacial periods. We have no independent estimate of past changes of marine $\delta^{13}C_{org}$ or the size of the ocean's carbon and nutrient inventories for pre-LGM times. For this reason and in order to obtain time series of parameters *a* and *b* we have fixed their Holocene and LGM values to the structure of a benthic $\delta^{13}C$ stack ($\delta^{13}C_{stack}$) and assumed that this stack represents global changes in benthic $\delta^{13}C$ and that shifts in $\delta^{13}C$ of the organic matter, increase of total inorganic carbon and carbon pool variations are linearly related. We use the benthic $\delta^{13}C$ stack of Stüber (1999) that was also used by Zahn and Stüber (2002) to correct for mean ocean changes in benthic $\delta^{13}C$ in time windows different from the LGM (see Annex I for a detailed explanation of the construction of this stack). The $\delta^{13}C_{stack}$ was rescaled to fit with the Holocene and LGM parameterization of equation 4-5 so that time series for *a* and *b* could be derived (see Fig. 4-10, time series are provided in Annex II). This procedure, while a simplification of the processes involved in defining the temporal evolution of equation 4-5 eliminates influences of whole ocean $\delta^{13}C_{\Sigma CO2}$ on the estimate of $\delta^{13}C_{as}$.

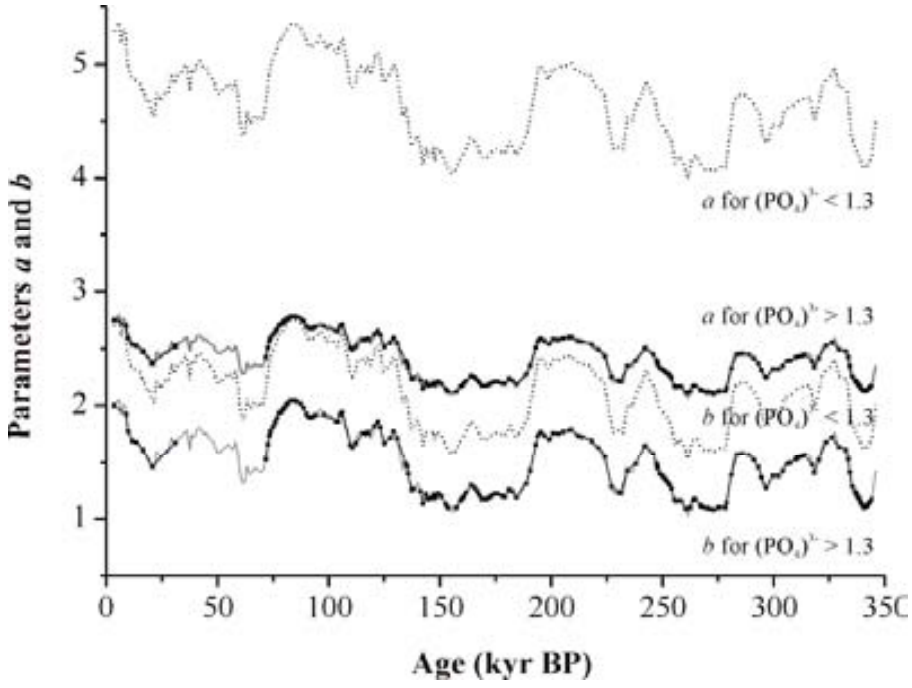

Figure 4-10 Time series of parameters *a* and *b* in Eq. 4-5 derived from the benthic $\delta^{13}C$ stack of Stüber (1999) and Zahn and Stüber (2002). Grey dashed line for Cd_{sw} < 0.28 nmol/kg; grey line for Cd_{sw} > 0.28 nmol/kg; black dotted lines show the time series for Cd_{sw} > 0.28 nmol/ kg rescaled to the Cd/Ca resolution of MD96-2080 as these will be the points used to develop its $\delta^{13}C_{as}$ record back to 345 kyr.

Core MD96-2080 lies at 2488 m water depth, consequently a partition coefficient of 2.46 was used in order to convert benthic Cd/Ca into Cd_{sw} (Eq. 2-19, Boyle, 1988). Derived Cd_{sw} values for this core are consistently higher than 0.28 nmol/kg falling in the "upper kink" South Atlantic, Indian, Southern, Pacific oceans domain (see Chapter 2), hence only the derived records of a and b for Cd_{sw} > 0.28 nmol/kg are used to generate the $\delta^{13}C_{as}$ record of MD96-2080.

The temporal resolution of the Cd/Ca record along MD96-2080 is slightly lower than that of the benthic $\delta^{13}C_{stack}$ so that the obtained series of parameters a and b have been resampled to match this resolution using the software package Analyseries (Paillard et al., 1996). In order to subtract the Cd_{sw}-derived $\delta^{13}C_{bio}$ from the measured benthic $\delta^{13}C$, the latter was also resampled to the Cd/Ca sample step. The final benthic $\delta^{13}C_{as}$ record has the same resolution as the Cd/Ca record, which is multi-centennial to millennial (see Chapter 5.1 for details on time resolution of the records).

4.5. Mg/Ca Derived Sea Surface Temperature (SST) and Derivation of $\delta^{18}O$ of Surface Water ($\delta^{18}O_{sw}$) and Sea Surface Salinity (SSS)

Sea surface temperatures derived from planktonic Mg/Ca are a useful input into oxygen isotope palaeotemperature equations in an attempt to eliminate the temperature influence on planktonic $\delta^{18}O$. This then allows to estimate sea water $\delta^{18}O$ ($\delta^{18}O_{sw}$) and ultimately to obtain estimations of past changes in sea surface salinity (see Chapter 2).

For the derivation of the Agulhas Bank Spliced (ABS) $\delta^{18}O_{sw}$ record the eleven chambers *G. bulloides* paleotemperature equation of Bemis et al. (1998) (Eq. 2-5) seems appropriate. This equation was developed from culture studies for the same species we analysed in our cores and eleven chambers correspond approximately to the size range selected (250-315 μm). Besides, this calibration works well for warm surface waters. The inferred interglacial estimates of sea surface salinity (SSS) are closer to present observations on the study area than those obtained using the palaeotemperature equation of Shackleton (1974).

$$T = 12.6 + 5.07 \cdot (\delta_c - \delta_w) \qquad \text{11 chambers, approximately 301 ± 25 μm size} \qquad \text{Eq. 2-5}$$

Temperature is obtained from planktonic Mg/Ca through empirical calibration equations (see Chapter 2). Mashiotta et al. (1999) and Elderfield and Ganssen (2000) propose mono-specific calibrations for *G. bulloides* that appear suitable for our records.

Mashiotta's et al. (1999) calibration (Eq. 4-6) was developed from culturing and core tops from the Subantarctic Indian core RC11-120 and from the Subantarctic Pacific core E11-2.

$$\frac{Mg}{Ca} = 0.474 \cdot e^{0.107 \cdot T} \qquad \text{Eq. 4-6}$$

The calibration of Elderfield and Ganssen (2000) (Eq. 4-7) was developed with core tops from a latitudinal transect in the North Atlantic from 30º to 60ºN at about 25ºW, corresponding to a range of annual SST of about 8 to 22ºC.

$$\frac{Mg}{Ca} = 0.56 \cdot e^{0.10 \cdot T} \qquad \text{Eq. 4-7}$$

Recent studies have put forward the possibility that different cryptic species (same morphotype but different genotypes) may respond differently to the uptake of trace elements and to the isotopic fractionation (e.g. Darling et al., 2004). For that reason it is better, whenever possible, to choose not only a mono-specific calibration, but also from a nearby region. Although studies in order to decipher whether indeed different genotypes calcify differently are in progress, it is clear that individual genotypes prefer specific habitats (Darling et al., 2007). In the case of the South Atlantic, Darling et al. (2007) found at least two different genotypes of *G. bulloides*, the one living preferably at waters below 10ºC and the other living in waters above 10ºC. It is very likely that the calibration by Mashiotta et al. (1999) is based mostly on the "cold genotype" since the core tops they used belong to high latitude Southern Hemisphere locations, hence this calibration could underestimate SST at our site where SSTs are above 10ºC year round. On the other hand, the data set used by Elderfield and Ganssen (2000), due to its wide latitudinal coverage, plausibly contains a range of genotypes of *G. bulloides* (more than 2). The temperatures estimated for ABS using this last calibration are consistently around 0.5ºC lower than using Maschiotta et al. (1999) (Fig. 4-11). A factor contributing to the lower values obtained using the Elderfield and Ganssen (2000) calibration is that these authors calibrated *G. bulloides* Mg/Ca against δ^{18}O-derived calcification temperatures. *G. bulloides* lives in the sub-surface (<50 m or 0-100 m, depending on authors, Mashiotta et al., 1999; Niebler et al., 1999) and as a consequence this calibration yields ambient temperatures, likely slightly lower than surface temperatures s.s. Although the difference in temperature using these two calibrations is within the error of the Mg/Ca-derived SST estimates (which are around 1ºC), we choose the Maschiotta et al. (1999) calibration which gives warmer temperatures, in better agreement with today's ambient temperature at the core site and probably develop with one single genotype. Besides, choosing the Maschiotta et al (1999) calibration also ensures that we reconstruct true sea surface temperatures that can then be compared with actual present data. The standard error of Eq. 4-6 is ±0.09 units of Ln(Mg/Ca), which corresponds to ±0.8ºC. The 95% confidence interval varies along the regression from ±0.3º at 16ºC to ±0.6º at 25ºC (Mashiotta et al., 1999).

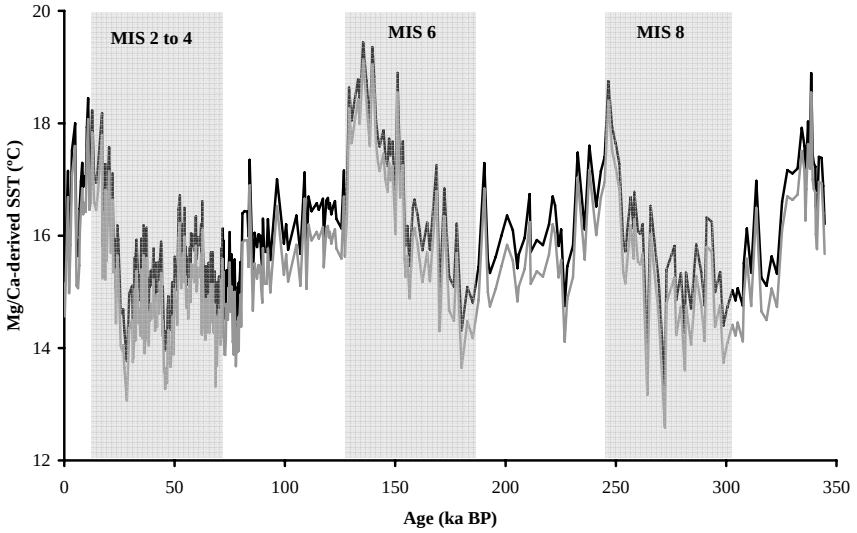

Figure 4-11 Comparison of the SST temperature records for the Agulhas Bank Spliced (ABS) using the calibrations of Mashiotta et al. (1999) (in black) and of Elderfield and Ganssen (2000) (in grey). Vertical shading highlights glacial periods (see Chapter 5.1 for details about the splicing of both cores and about the development of the age model).

Planktonic $\delta^{18}O$ (as well as benthic $\delta^{18}O$) is affected by global changes in $\delta^{18}O_{sw}$ that occur as a consequence of the storage of light ^{16}O in the ice sheets during glacial stages. This effect is directly related to changes in sea level. In order to remove the ice-volume/sea-level effect from our planktonic $\delta^{18}O$ records we subtract available mean ocean $\delta^{18}O_{sw}$ records.

Waelbroeck et al. (2002) developed a sea level-$\delta^{18}O_{sw}$ equivalent curve from benthic $\delta^{18}O$ records which goes back to the MIS 11-12 boundary. The planktonic $\delta^{18}O$ part corresponding to MD02-2594, from present to 80 ka, shows fine structure which is not detailed in the Waelbroeck's et al. (2002) record. Siddall et al. (2003) offer a finer detailed record of sea level change along MIS 3, from 26 to 72 ka with an average time step of 207 ± 107 years. We have converted this sea level curve into $\delta^{18}O_{sw}$ assuming a $\delta^{18}O_{sw}$: sea level slope of 0.008‰ / m (Schrag et al., 2002) and implemented it within the Waelbroeck's et al. (2002) curve to obtain a combined, more detailed curve (Fig. 4-13a). After synchronizing the records in their chronologies to minimise artefacts arising from temporal offsets, we have subtracted the combined global $\delta^{18}O_{sw}$ curve from our planktonic $\delta^{18}O$ ABS record. The resulting record ($\delta^{18}O_c = \delta^{18}O_{plk}$ – mean ocean $\delta^{18}O_{sw}$, Fig. 4-13a) encloses local $\delta^{18}O_{sw}$ variations and temperature effect. We obtain $\delta^{18}O_c$ in the VPDB scaled, in order to convert it to the SMOW scale a value of 0.27 is added to $\delta^{18}O_c$ (Hut, 1987).

$\delta^{18}O_{plk}$ and hence, $\delta^{18}O_c$, have higher resolution than the Mg/Ca-derived SST record. We have resampled the $\delta^{18}O_c$ record to the time step of SST and used both as input into the paleotemperature equation of Bemis et al. (1998) (Eq. 2-5). Ultimately we obtained the local $\delta^{18}O_{sw}$ record (Fig. 4-13c). Local $\delta^{18}O_{sw}$ is linearly related with sea surface salinity (SSS) although the relation varies regionally (Craig and Gordon, 1965) ($\delta^{18}O_{sw} = a \cdot S + b$, Eq. 2-2, Chapter 2). At mid-latitudes, the freshwater endmember (the term b in Eq. 2-2) is typical of local precipitation and the slope of the $\delta^{18}O_{sw}$ *vs* SSS relationship is high (~0.5‰ / psu) (LeGrande and Schmidt, 2006). In the tropics, most of the water

exchanged between the ocean and atmosphere through evaporation-precipitation remains in the same area so the freshwater endmember is close to the initial evaporate and the slope of the $\delta^{18}O_{sw}$ *vs* SSS relationship is smoother (~0.1 to 0.3‰ / psu) (LeGrande and Schmidt, 2006).

Agulhas waters are tropical sourced; they originate from tropical and subtropical Indian Waters. Therefore, rather than calculating the $\delta^{18}O_{sw}$ *vs* SSS relationship with data from the latitude of our cores, we have computed the relationship between $\delta^{18}O_{sw}$ and SSS of the available surface tropical data (shallower than 300 m) from the latitudinal band Equator-20ºS (n = 256, Fig. 4-12) (Schmidt, 1999; Schmidt et al., 1999; Bigg and Rohling, 2000). From this compilation we have removed data with salinities below 30 psu, which are likely close to river mouths.

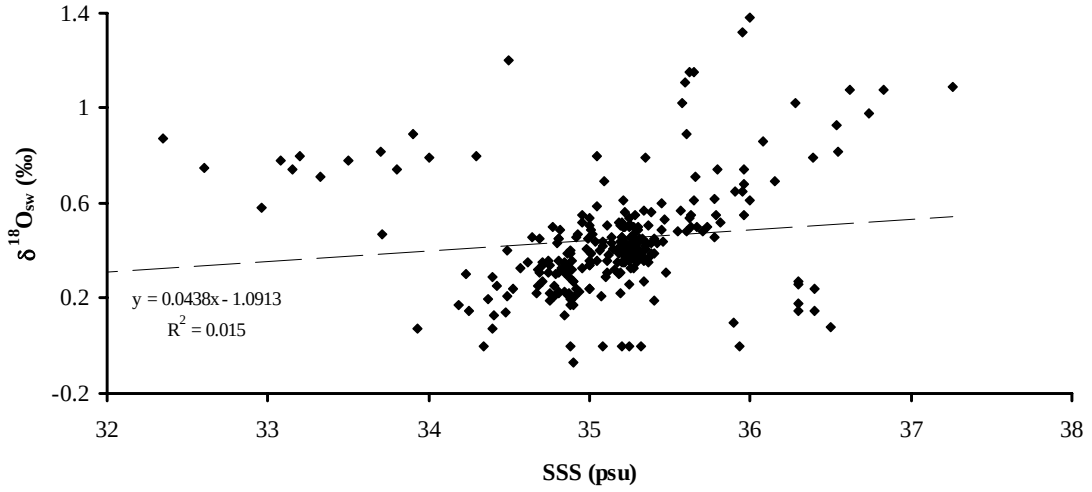

Figure 4-12 $\delta^{18}O_{sw}$ *vs* SSS relationship for modern tropical latitudes. Data from the latitudinal band Equator to 20ºS for depth > 300 m and salinity > 30 psu (data from Schmidt, 1999; Schmidt et al., 1999; data from Bigg and Rohling, 2000).

The regression between $\delta^{18}O_{sw}$ *vs* SSS yielded the equations:

$$SSS = 0.342 \cdot \delta^{18}O_{sw} + 34.959 \quad \text{(psu)} \quad R^2 = 0.015 \quad \text{Eq. 4-8}$$

$$\delta^{18}O_{sw} = 0.0439 \cdot SSS - 1.091 \quad \text{(SMOW)} \quad R^2 = 0.015 \quad \text{Eq. 4-9}$$

The storage of freshwater in the ice caps during glacial periods, besides affecting $\delta^{18}O_{sw}$ globally, has a concentration effect in the salinity of the global ocean. Adkins and Schrag (2001) estimated that the ocean salinity during the LGM was about 2.5 ± 0.1% higher than today (around 0.9 psu). In order to estimate the concentration effect for previous glacial periods, we use the combined sea level curve of Sidall et al. (2003) and Waelbroeck et al. (2002) and scale it to the Holocene-LGM change of 0.9 psu. We then incorporate these global mean salinity changes into our computed local sea surface salinity.

The obtained interglacial salinities estimates are in agreement with present observed SSS in the area. Nonetheless, the estimation of paleosalinities incorporate many uncertainties, notably, the propagated error of the various measurements and relationships used, and applying a modern tropical $\Delta\delta^{18}O_{sw}$ *vs* SSS relationship which most likely has not remained constant through time. This last

uncertainty is related to the changes exerted in the hydrological cycle, and thus in the water isotopes, by climate reorganizations on orbital and shorter time scales. Moreover, the amount of water exchanged between ocean basins and exported from one region to another varied further altering the relationships between water isotopes and climate through time (e.g. Le Grande and Schmidt, 2007). For that reason, in addition to the estimations of $\delta^{18}O_{sw}$ and SSS, we present the $\delta^{18}O_{sw}$ and SSS anomalies ($\Delta\delta^{18}O_{sw}$ and ΔSSS) relative to present levels which have been calculated by averaging Holocene data from 0 to 5 ka.

Figure 4-13 shows the various records used for the computation of local $\delta^{18}O_{sw}$ and SSS, i.e. *G. bulloides* $\delta^{18}O$ and Mg/Ca-derived SST, global $\delta^{18}O_{sw}$ sea level-equivalent and global ΔS record (Waelbroeck et al., 2002; Siddall et al., 2003) and $\delta^{18}O_{plk}$ - global $\delta^{18}O_{sw}$ ($\delta^{18}O_c$).

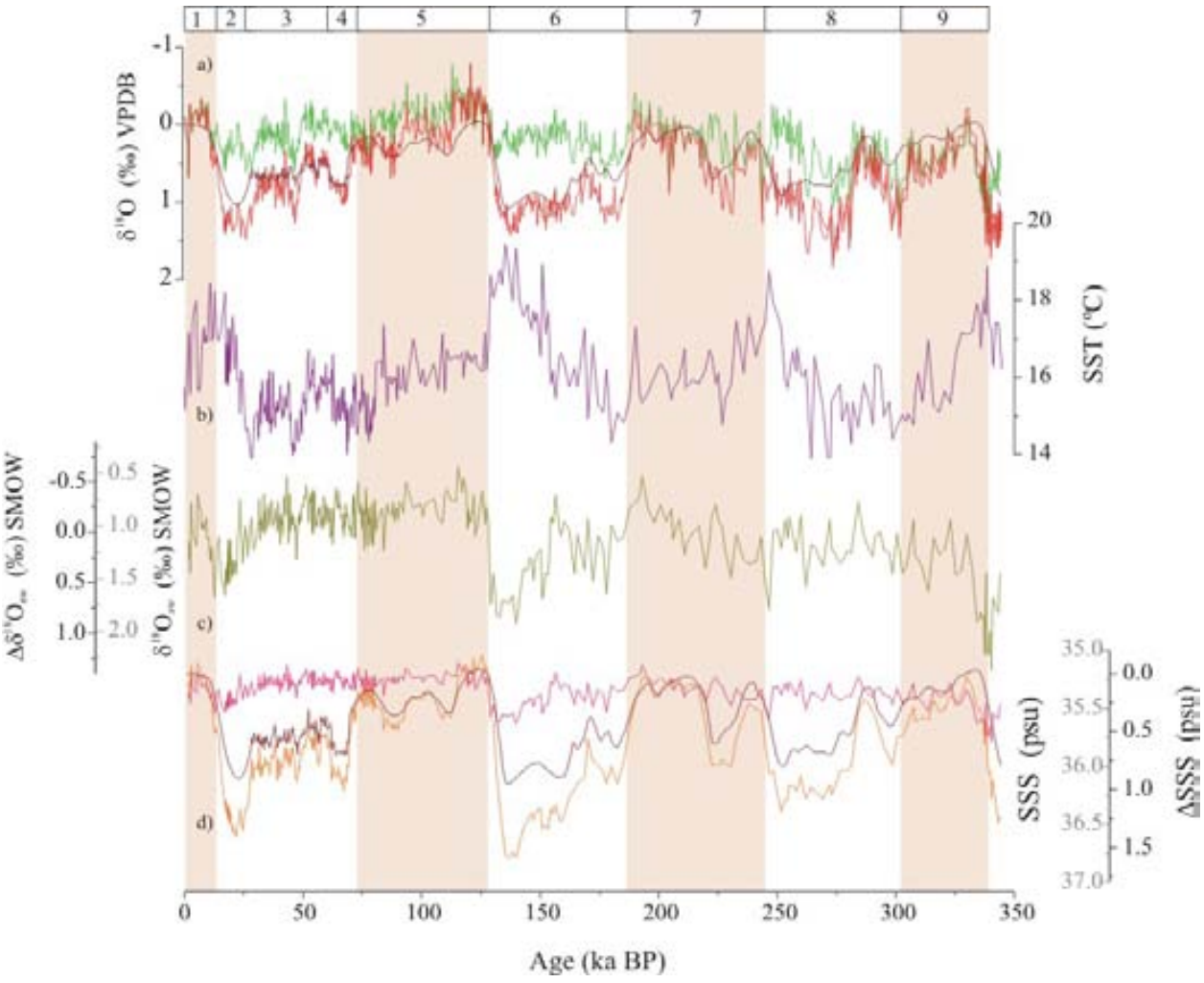

Figure 4-13 Deconvolution of the temperature effect from planktonic $\delta^{18}O$; a) ABS *G. bulloides* $\delta^{18}O$ (red); global $\delta^{18}O_{sw}$ sea level-equivalent combining the sea level curves of Siddall et al. (2002) and Waelbroeck et al. (2003) (brown); *G. bulloides* $\delta^{18}O$ minus global $\delta^{18}O_{sw}$ sea level-equivalent ($\delta^{18}O_c$); b) ABS *G. bulloides* Mg/Ca-derived SST; c) ABS $\Delta\delta^{18}O_{sw}$ (outer scale) and estimated $\delta^{18}O_{sw}$ (inner scale); d) ABS ΔSSS (outer scale) and estimated SSS (inner scale); pink curve shows the local SSS variations without including mean salinity changes; orange curve include this changes. Brown curve displays global salinity variations related to the concentration effect as a consequence of storage of fresh water in ice sheets during glacial periods.

References

Adkins, J.F. and Schrag, D.P., 2001. Pore Fluid Constraints on Deep Ocean Temperature and Salinity During the Last Glacial Maximum. Geophysical Research Letters, 28 (5), 771-774.

Barker, S. and Elderfield, H., 2002. Foraminiferal Calcification Response to Glacial-Interglacial Changes in Atmospheric CO_2. Science, 297, 833-836.

Barker, S., Greaves, M. and Elderfield, H., 2003. A study of cleaning procedures used for foraminiferal Mg/Ca paleothermometry. Geochemistry, Geophysics, Geosystems, 4 (9), 8407, doi: 10.1029/2003GC000559.

Barker, S., Kiefer, T. and Elderfield, H., 2004. Temporal changes in North Atlantic circulation constrained by planktonic foraminiferal shell weights. Paleoceanography, 19, PA3008, doi: 10.1029/2004PA001004.

Bé, A.W.H. and Hutson, W.H., 1977. Ecology of planktonic foraminifera and biogeographic patterns of life and fossil assemblages in the Indian Ocean. Micropaleontology, 23, 369–414.

Bemis, B.E., Spero, H., Bijma, J. and Lea, D.W., 1998. Reevaluation of the oxygen isotopic composition of planktonic foraminifera: experimental results and revised paleotemperature equations. Paleoceanography, 13, 150-160.

Bianchi, G.G., Hall, I.R., McCave, I.N. and Joseph, L., 1999. Measurements of the sortable silt current speed proxy using the Sedigraph 5100 and Coulter Multisizer IIe: precission and accuracy. Sedimentology, 46, 1,001-1,014.

Bigg, G.R. and Rohling, E.J., 2000. An oxygen isotope data set for marine waters. Journal of Geophysical Research, 105 (C4), 8,527-8,535.

Boyle, E.A., 1981. Cadmium, zinc, copper, and barium in foraminifera tests. Earth and Planetary Science Letters, 53 (1), 11-35.

Boyle, E.A., 1983. Manganese Carbonate overgrowths on foraminifera tests. Geochimica et Cosmochimica Acta, 47 (10), 1,815-1,819.

Boyle, E.A., 1988. Cadmium: Chemical Tracer of Deep-water Paleoceanography. Paleoceanography, 3, 431-489.

Boyle, E.A. and Keigwin, L.D., 1985/86. Comparison of Atlantic and Pacific paleochemical records for the last 215,000 years: changes in deep ocean circulation and chemical inventories. Earth and Planetary Science Letters, 76 (1-2), 135-150.

Boyle, E.A. and Rosenthal, Y., 1996. Chemical Hydrography of the South Atlantic during the Last Glacial Maximum: Cd *vs* $\delta^{13}C$. In: G. Wefer, W.H. Berger, G. Siedler and D. Webb (Editors), The South Atlantic: Present, Past and Future. Springer-Verlag Berlin Heidelberg New York, pp. 423-443.

Broecker, W.S. and Maier-Reimer, E., 1992. The influence of air and sea exchange on the carbon isotope distribution in the sea. Global and Biogeochemical Cycles, 6 (3), 315-320.

Brown, S.J. and Elderfield, H., 1996. Variations in Mg/Ca and Sr/Ca ratios of planktonic foraminiferal caused by postdepositional dissolution: Evidence of shallow Mg-dependent dissolution. Paleoceanography, 11 (5), 543-551.

Craig, H. and Gordon, L.I., 1965. Deuterium and oxygen 18 variations in the ocean and the marine atmosphere. In: E. Tongiorgi (Editor), Stable Isotopes in Oceanographic Studies and Paleotemperatures. Laboratorio di Geologia Nucleare, Pisa, Italy, pp. 9-130.

Curry, W.B., Duplessy, J.C., Labeyrie, L.D. and Shackleton, N.J., 1988. Changes in the distribution of $\delta^{13}C$ of deep water ΣCO_2 between the last glaciation and the Holocene. Paleoceanography, 3 (3), 317-341.

d'Orbigny, A., 1826. Tableau Méthodique de la classe des Céphalopodes, 3-me ordre, Foraminiféres. Annals of Science Natural, 7, 245-314.

Darling, K., Kucera, M. and Wade, C., 2007. Genetic Diversity of *Globigerina bulloides* and genotype seasonality in the North Atlantic, 9th International Conference on Paleoceanography, Shanghai, China.

Darling, K.F., Kucera, M., Pudsey, C.J. and Wade, C.M., 2004. Molecular evidence links cryptic diversification in polar planktonic protists to Quaternary climate dynamics. PNAS, 101 (20), 7,657-7,662.

Deckens, P.S., Lea, D.W., Pak, D.K. and Spero, H.J., 2002. Core top calibration of Mg/Ca in tropical foraminifera: Refining paleotemperature estimation. Geochemistry, Geophysics, Geosystems, 3 (4), 10.1029/2001GC000200.

Diz, P., Hall, I.R., Zahn, R. and Molyneux, E.G., 2007. Paleoceanography of the southern Agulhas Plateau during the last 150 ka: Inferences from benthic foraminiferal assemblages and multispecies epifaunal carbon isotopes. Paleoceanography, 22, PA4218, doi: 10.1029/2007PA001511.

Duplessy, J.-C., Shackleton, N.J., Fairbanks, R.G., Labeyrie, L., Oppo, D.W. and Kallel, N., 1988. Deepwater source variations during the last climatic cycle and their impact on the global deepwater circulation. Paleoceanography, 3, (3), 343-360.

Elderfield, H. and Ganssen, G., 2000. Past temperature and $\delta^{18}O$ of surface ocean waters inferred from foraminiferal Mg/Ca ratios. Nature, 405, 442-445.

Emerson, S.R. and Archer, D., 1990. Calcium carbonate preservation in the ocean. Philosophical Transactions of the Royal Society of London, Series A 331 (1616), 29-40.

Ganssen, G. and Kroon, D., 2000. The isotopic signature of planktonic foraminifera from NE Atlantic surface sediments: implications for the reconstruction of past oceanic conditions. Journal of the Geological Society London, 157, 693-699.

Hemleben, C., Spindler, M. and Anderson, O.R., 1989. Modern planktic foraminifera. Springer Verlag, Clarenton Press, 363 pp.

Hester, K. and Boyle, E.A., 1982. Water chemistry control of the Cd content of benthic foraminiferal. Nature, 298, 260-261.

Hodell, D.A., Venz, K., Charles, C.D. and Ninnemann, U.S., 2003. Pleistocene vertical carbon isotope and carbonate gradients in the South Atlantic sector of the Southern Ocean. Geochemistry, Geophysics, Geosystems, 4 (1), 1004, doi:10.1029/2002GC000367.

Holbourn, A.E. and Henderson, A.S., 2002. Re-Illustratin and Revised Taxonomy for Selected Deep-Sea Benthic Foraminifers. Palaeontologia Electronica, 4 (2), pp. 34.

Hut, G., 1987. Consultants' group meeting on stable isotope reference samples for geochemical and hydrological investigations. Vienna, 1-42.

King, A.L. and Howard, W.R., 2001. Seasonality of foraminiferal flux in sediment traps at Chatham Rise, SW Pacific: implications for paleotemperature estimates. Deep Sea Research Part, 48 (7), 1,687-1,708.

King, A.L. and Howard, W.R., 2005. $\delta^{18}O$ seasonality of planktonic foraminifera from Southern Ocean sediment traps: Latitudinal gradients and implications for paleoclimate reconstructions. Marine Micropaleontology, 56 (1-2), 1-24.

Kroopnick, P.M., 1985. The distribution of $\delta^{13}C$ of CO_2 in the world oceans. Deep Sea Research, 32 (1), 57-84.

Le Grande, A.N. and Schmidt, G., 2007. Orbital influences on paleosalinity indicators, American Geophysical Union Fall Meeting, San Francisco.

Le, J. and Shackleton, N.J., 1992. Carbonate dissolution fluctuation in the western equatorial Pacific during the late Quaternary. Paleoceanography, 7 (1), 21-42.

LeGrande, A.N. and Schmidt, G.A., 2006. Global gridded data set of the oxygen isotopic composition in seawater. Geophysical Research Letters, 33, L12604, doi: 10.1029/2006GL026011.

Loncaric, N., Peeters, F.J.C., Kroon, D. and Brummer, G.-J.A., 2006. Oxygen isotope ecology of recent planktic foraminifera at the central Walvis Ridge (SE Atlantic). Paleoceanography, 21, PA3009, doi: 10.1029/2005PA001207.

Lynch-Stieglitz, J. and Fairbanks, R.G., 1994. A conservative tracer for glacial ocean circulation from carbon isotope and paleonutrient measurements in benthic foraminifera. Nature, 369, 308-310.

Lynch-Stieglitz, J., van Geen, A. and Fairbanks, R.G., 1996. Interocean exchange of Glacial North Atlantic Intermediate Water: evidence from the subantarctic Cd/Ca and carbon isotope measurements. Paleoceanography, 11 (2), 191-201.

Lynch-Stieglitz, J., Stocker, T.F., Broecker, W.S. and Fairbanks, R.G., 1995. The influence of air-sea exchange on $\delta^{13}C$ of ΣCO_2 in the surface ocean: Observations and Modeling. Global and Biogeochemical Cycles, 9, 653-665.

Mackensen, A. and Bickert, T., 1999. Stable Carbon Isotopes in Benthic Foraminifera: Proxies for Deep and Bottom Water Circulation and New Production. In: G. Fischer and G. Wefer (Editors), Use of Proxies in Paleoceanography: Examples from the South Atlantic. Springer-Verlag Berlin Heidelberg, pp. 229-254.

Mackensen, A., Rudolph, M. and Kuhn, G., 2001. Late Pleistocene deep-water circulation in the subantarctic eastern Atlantic. Global and Planetary Change, 30 (3-4), 197.

Mackensen, A., Futterer, D.K., Grobe, H. and Schmiedl, G., 1993. Benthic foraminiferal assemblages from the eastern South Atlantic Polar Front region between 35º and 57ºS: Distribution, ecology and fossilization potential. Marine Micropaleontology, 22 (1-2), 33-69.

Manighetti, B. and Northcote, L., 2000. Fabulous Foraminifera: examining past climates using microscopic marine organisms. Water and Atmosphere, 8 (3), 24-26.

Marchitto, T.M. and Broecker, W.S., 2006. Deep water mass geometry in the glacial Atlantic Ocean: A review of constraints from the paleonutrient proxy Cd/Ca. Geochemistry, Geophysics, Geosystems, 7, Q12003, doi:10.1029/2006GC001323.

Marchitto, T.M., Curry, W.B. and Oppo, D.W., 2000. Zn concentrations in benthic foraminifera reflect seawater chemistry. Paleoceanography, 15 (3), 299-306.

Martin, P.A. and Lea, D.W., 2002. A simple evaluation of cleaning procedures on fossil benthic foraminiferal Mg/Ca. Geochemistry, Geophysics, Geosystems, 3 (10), 8401, doi: 10.1029/2001GC000280.

Mashiotta, T.A., Lea, D.W. and Spero, H.J., 1999. Glacial-interglacial changes in Subantarctic sea surface temperature and [delta]18O-water using foraminiferal Mg. Earth and Planetary Science Letters, 170 (4), 417-432.

McCave, I.N., Manighett, B. and Robinson, S.G., 1995. Sortable silt and fine sediment size/composition slicing: parameters for palaeocurrent speed and palaeoceanography. Paleoceanography, 10, 593-610.

McCorkle, D.C., Martin, P.A., Lea, D.W. and Klinkhammer, G.P., 1995. Evidence of a dissolution effect on benthic foraminiferal shell chemistry: $\delta^{13}C$, Cd/Ca, Ba/Ca, and Sr/Ca results from the Ontong Java Plateau. Paleoceanography, 10 (4), 699-714.

Mekik, F. and François, R., 2006. Tracing deep-sea calcite dissolution: Agreement between the Globorotalia menardii fragmentation index and elemental ratios (Mg/Ca and Mg/Sr) in planktonic foraminifers. Paleoceanography, 21, PA4219, doi: 10.1029/2006PA001296.

Mekik, F., François, R. and Soon, M., 2007. A novel approach to dissolution correction of Mg/Ca–based paleothermometry in the tropical Pacific. Paleoceanography, 22, PA3217, doi: 10.1029/2007PA001504.

Molina, E., 2002. Micropaleontología. Colección de textos docentes, 93. Prensas Universitarias, Zaragoza, 634 pp.

Mortyn, P.G. and Charles, C.D., 2003. Planktonic foraminiferal depth habitat and $\delta^{18}O$ calibrations: Plankton tow results from the Atlantic sector of the Southern Ocean. Paleoceanography, 18 (2), 1037, doi: 10.1029/2001PA000637.

Niebler, H.S., Hubberten, H.W. and Gersonde, R., 1999. Oxygen Isotope Values of Planktonic Foraminifera: A Tool for the Reconstruction of Surface Water Stratification. In: G. Fischer and G. Wefer (Editors), Use of Proxies in Paleoceanography: Examples from the South Atlantic. Springer-Verlag, Berlin, Heidelberg, pp. 165-189.

Paillard, D., Labeyrie, L. and Yiou, P., 1996. Macintosh program performs time-series analysis. EOS, AGU, 77, 379.

Pena, L., Calvo, E., Cacho, I., Eggins, S. and Pelejero, C., 2005. Identification and removal of Mn-Mg-rich contaminant phases on framiniferal tests: Implications for Mg/Ca past temperature reconstructions. Geochemistry, Geophysics, Geosystems, 6, Q09P02, doi: 10.1029/2005GC000930.

Rau, A.J., Rogers, J. and Chen, M.-T., 2006. Late Quaternary palaeoceanographic record in giant piston cores off South Africa, possibly including evidence of neotectonism. Quaternary International, 148 (1), 65-77.

Rau, A.J., Rogers, J., Lutjeharms, J.R.E., Giraudeau, J., Lee-Thorp, J.A., Chen, M.-T. and Waelbroeck, C., 2002. A 450-kyr record of hydrological conditions on the western Agulhas Bank Slope, south of Africa. Marine Geology, 180 (1-4), 183-201.

Rau, G.H., Froelich, T., Takahashi, T. and Des Marais, D.J., 1991. Does sedimentary organic $\delta^{13}C$ record variations in Quaternary ocean $[CO_{2(aq)}]$? Paleoceanography, 6, 335-347.

Regenberg, M., Nürnberg, D., Steph, S., Groeneveld, J., Garbe-Schönberg, D., Tiedemann, R. and Dullo, W.-C., 2006. Assessing the effect of dissolution on planktonic foraminiferal Mg/Ca ratios: Evidence from Caribbean core tops. Geochemistry, Geophysics, Geosystems, 7, Q07P15, doi: 10.1029/2005GC001019.

Rosenthal, Y., Boyle, E.A. and Labeyrie, L., 1997. Last glacial maximum paleocemistry and deepwater circulation in the Southern Ocean: Evidence from foraminiferal cadmium. Paleoceanography, 12 (6), 787-796.

Rosenthal, Y., Boyle, E.A., Labeyrie, L. and Oppo, D., 1995. Glacial enrichements of authigenic Cd and U in Subantarctic sediments: A climatic control on the elements' oceanic budget? Paleoceanography, 10 (3), 395-413.

Schmidt, G.A., 1999. Forward modeling of carbonate proxy data from planktonic foraminifera using oxygen isotope tracers in a global ocean model. Paleoceanography, 14 (4), 482-497.

Schmidt, G.A., Bigg, G.R.B. and Rohling, E.J., 1999. Global Seawater Oxygen-18 Database. http://data.giss.nasa.gov/o18data/.

Schmiedl, G. and Mackensen, A., 1997. Late Quaternary paleoproductivity and deep water circulation in the eastern South Atlantic Ocean: Evidence from benthic foraminifera. Palaeogeography, Palaeoclimatology, Palaeoecology, 130 (1-4), 43-80.

Schrag, D.P., Adkins, J.F., McIntyre, K., Alexander, J.L., Hodell, D.A., Charles, C.D. and McManus, J.F., 2002. The oxygen isotopic composition of seawater during the Last Glacial Maximum. Quaternary Science Reviews, 21 (1-3), 331-342.

Schwager, C., 1866. Fossile Foraminiferen von Kar Nikobar, Reise der Oesterreichischen Fregatte Novara um Erde in den Jahren 1857, 1858, 1859 unten den Befehlen des Commodore B. Von Wuellerstorf-Urbair. Geologischer Theil, Geologische Beobachtung no. 2, Palaeontologische Mittheilung, 2 (1), 187-268.

Shackleton, N.J., 1974. Attainment of isotopic equilibrium between ocean water and the benthonic foraminifera genus *Uvigerina*: Isotopic changes in the ocean during the last glacial. Colloques Internationaux du Centre National de la Recherche Scientifique, 219, 203-209.

Shackleton, N.J., 1977. Carbon 13 in Uvigerina: Tropical rainforest history and the equatorial Pacific carbonate dissolution cycles. In: N. R. Andersen and A. Malahoff (Editors), The Fate of Fossil Fuel CO_2 in the Oceans. Plenum, New York, pp. 401–428.

Siddall, M., Rohling, E.J., Almogi-Labin, A., Hemleben, C., Meischner, D., Schmelzer, I. and Smeed, D.A., 2003. Sea-level fluctuations during the last glacial cycle. Nature, 423, 853-859.

Stüber, A., 1999. Spätpleistocene Variabilität der Zwischenwasserzirkulation im subtropischen Westatlantik auf glazial-interglazialen und suborbitalen Zeitskalen: Rekonstruktion anhand stabiler Kohlenstoffisotope und Spurenmetallverhältnissen in kalkschaligen Benthosforaminiferen, Christian-Albrechts Universität, Kiel, 118 pp.

Tedesco, T., Thunell, R., Astor, Y. and Karger, F.M., 2007. The oxygen isotope composition of planktonic foraminifera from the Cariaco Basin, Venezuela: Seasonal and interannual variations. Marine Micropaleontology, 62, 180-193.

Volbers, A.N.A. and Henrich, R., 2002. Present water mass calcium carbonate corrosiveness in the eastern South Atlantic inferred from ultrastructural breakdown of *Globigerina bulloides* in surface sediments. Marine Geology, 186 (3-4), 471-486.

Volbers, A.N.A. and Henrich, R., 2004. Calcium carbonate corrosiveness in the South Atlantic during the Last Glacial Maximum as inferred from changes in the preservation of *Globigerina bulloides*: A proxy to determine deep-water circulation patterns? Marine Geology, 204 (1-2), 43-57.

Waelbroeck, C., Labeyrie, L., Michel, E., Duplessy, J.-C., McMAnus, J.F., Lambeck, K., Balbon, E. and Labracherie, M., 2002. Sea-level deep water temperature changes derived from benthic foraminifera isotopic records. Quaternary Science Reviews, 21, 295-305.

Wilke, I., Bickert, T. and Peeters, F.J.C., 2006. The influence of seawater carbonate ion concentration [CO_3^{2-}] on the stable carbon isotope composition of the planktic foraminifera species *Globorotalia inflata*. Marine Micropaleontology, 58 (4), 243-258.

Zahn, R. and Stüber, A., 2002. Suborbital intermediate water variability inferred from paired benthic foraminiferal Cd/Ca and $\delta^{13}C$ in the tropical West Atlantic and linking with North Atlantic climates. Earth and Planetary Science Letters, 200, 191-205.

Annex I: Construction of a Stacked Benthic $\delta^{13}C$, $\delta^{13}C_{stack}$

A benthic $\delta^{13}O_{stack}$ was used by Stüber (1999) and Zahn and Stüber (2002) to aid the correction of individual benthic $\delta^{13}C$ records used in their studies for longer term ocean carbon pool variations and it has been used here with the same purpose. This section provides a fuller account about how the $\delta^{13}C_{stack}$ record was constructed; such account was not provided with the initial publication in 2002. The stack is based on benthic $\delta^{13}C$ records of 8 sediment cores from the Atlantic, one record from the Indian and two records from the Pacific. Core sites are listed in Table 1 Annex I; individual benthic $\delta^{13}C$ records are displayed in Figure 1 Annex I.

From 0 to 146 ka, $\delta^{13}C$ profiles from Atlantic cores M16004, M15669, M15612, Pacific cores V19-27; RC 13-110 and Indian core 14807 were sampled at 1 kyr steps using a Gaussian filter with 3 kyr window width. From 146 to 388 ka, long $\delta^{13}C$ profiles from Atlantic Sites 502, 552, 607, 659 and Pacific core RC13-110 were used. The temporal resolution of these profiles is lower and therefore, they were resampled at 2 kyr steps. Next, the resampled $\delta^{13}C$ data profiles were combined and averaged into a mean-ocean $\delta^{13}C$ profile that was normalized to the Holocene $\delta^{13}C$ level and the Holocene-to-LGM amplitude was set to 0.32‰ (Duplessy et al., 1988). The suite of sediment cores combined in the stack obviously does not provide for a full representation of the ocean carbon pool. The cores constitute an only small subset of the global data base used by (Duplessy et al., 1988) to determine the mean-ocean $\delta^{13}C$ signal for the LGM. Therefore the stacked benthic $\delta^{13}C$ record is not to be considered a full representation of the marine carbon reservoir while the structure of the $\delta^{13}C_{stack}$ record is used here only as an indication of changes through time in mean-ocean $\delta^{13}C$. Beyond the expected glacial-interglacial changes the record also displays a longer-term i.e., 350 kyr-long trend towards more positive values that likely represents modulation of the carbon pool by the 400 kyr orbital eccentricity cycle.

Table 1 Annex I. Sediment cores used for the construction of the benthic $\delta^{13}C_{stack}$

Core name	Latitude	Longitude	Water depth (m)	$\delta^{13}C$ Reference
Atlantic:				
M16004	30ºN	11ºW	1512	(Zahn-Knoll, 1986)
Site 502	11ºN	80ºW	1800 [a]	(DeMenocal et al., 1992)
M15669	35ºN	8ºW	2022	(Zahn-Knoll, 1986)
Site 552	56ºN	23ºW	2301	(Shackleton and Hall, 1984)
M13519	6ºN	20ºW	2862	(Sarnthein et al., 1984)
M15612	45ºN	26º30'W	3050	(Zahn-Knoll, 1986)
Site 659	18ºN	21ºW	3070	(Tiedemann, 1991)
Site 607	42ºN	33º W	3427	(Raymo et al., 1989; Ruddiman et al., 1989)
Indic:				
14807	17ºS	119ºE	1186	(Sarnthein et al., 1982)
Pacific:				
V19-27	0.5ºS	82ºW	1373	(Mix et al., 1991)
RC13-110	0.1ºN	96ºW	3231	(Mix et al., 1991)

[a] The actual water depth is 3051 m. The water depth considered here is the Caribbean sill depth defining the inflow of mid-depth waters from the Atlantic.

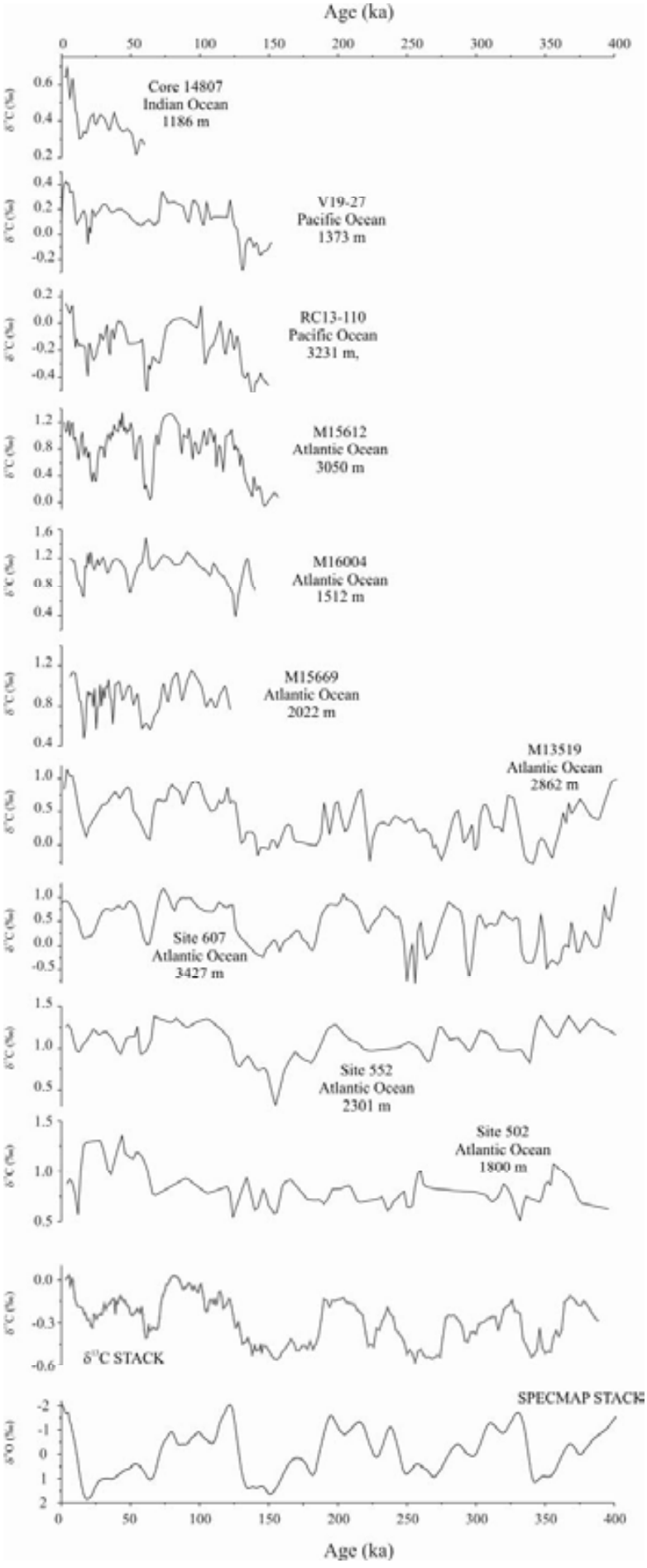

Figure 1 Annex I The benthic foraminiferal $\delta^{13}C$ records used in the construction of the stack. The records shown have been sampled at 1 kyr time step. The final $\delta^{13}C$ stack record is shown at the bottom together with the SPECMAP stack (Imbrie et al., 1984) for stratigraphic and temporal resolution reference.

References

DeMenocal, P.B., Oppo, D.W., Fairbanks, R.G. and Prell, W.L., 1992. Pleistocene $\delta^{13}C$ variability of North Atlantic Intermediate Water. Paleoceanography, 7, 229-250.

Duplessy, J.-C., Shackleton, N.J., Fairbanks, R.G., Labeyrie, L., Oppo, D.W. and Kallel, N., 1988. Deepwater source variations during the last climatic cycle and their impact on the global deepwater circulation. Paleoceanography, 3 (3), 343-360.

Imbrie, J., McIntyre, A. and Mix, A.C., 1984. Oceanic Response to Orbital Forcing in the Late Quaternary: Observational and Experimental Strategies. In: A. Berger, S.H. Schneider and J.-C. Duplessy (Editors), Climate and Geosciences, A Challenge for Science and Society in the 21st Century. D. Reidel Publishing Company.

Mix, A.C., Pisias, N.G., Zahn, R., Rugh, W., López, C. and Nelson, K., 1991. Carbon 13 in Pacific deep and intermediate waters, 0-370 ka: Implications for ocean circulation and Pleistocene CO_2. Paleoceanography, 6 (2), 205–226.

Raymo, M.E., Ruddiman, W.F., Backman, J., Clement, B.M. and Martinson, D.G., 1989. Late Pliocene variation in Northern Hemisphere ice sheets and North Atlantic deep water circulation. Paleoceanography, 4 (4), 413-446.

Ruddiman, W.F., Raymo, M.E., Martinson, D.G., Clement, B.M. and Backman, J., 1989. Mid-Pleistocene evolution of Northern Hemisphere climate. Paleoceanography, 4, 353-412.

Sarnthein, M., Erlenkeuser, H., von Grafenstein, R. and Schroeder, C., 1984. Stable-isotope stratigraphy for the last 750,000 years: “Meteor” core 13519 from the eastern equatorial Atlantic. Meteor Forshung Ergebnisse, C38, 9-24.

Sarnthein, M., Erlenkeuser, H. and Zahn, R., 1982. Termination I: The continental climate in the subtropics as recorded in deep-sea sediments. Bull. Inst. Geol. Bassin d'Aquitaine, Bordeaux, 31, 393-407.

Shackleton, N.J. and Hall, M.A., 1984. Oxygen and carbon isotope stratigraphy of Deep Sea Drilling Project Hole 552A: Plio-Pleistocene glacial history. In: D.G. Roberts, D. Schnitker and e. al. (Editors), Initial Reports. DSDP, 81: Washington: (U.S. Govt. Printing Office), pp. 599-609.

Stüber, A., 1999. Spätpleistocene Variabilität der Zwischenwasserzirkulation im subtropischen Westatlantik auf glazial-interglazialen und suborbitalen Zeitskalen: Rekonstruktion anhand stabiler Kohlenstoffisotope und Spurenmetallverhältnissen in kalkschaligen Benthosforaminiferen, Christian-Albrechts Universität, Kiel, 118 pp.

Tidemann, 1991. Acht Millionen Jahre Klimageschichte von Nordwest Afrika und Paläo-Ozeanographie des angrenzenden Atlantiks. Ber. Rep. Geol.- Paläontol. Inst. und Mus., Christian-Albrechts-Univ., 46, 190.

Zahn-Knoll, R., 1986. Spätquartäre Entwicklung von Küstenauftrieb und Tiefenwasserzirkulation im Nordost-Atlantik. Rekonstruktion anhand stabiler Isotope kalkschaliger Foraminiferen, Christian-Albrechts-Universität, Kiel, 111 pp.

Zah n, R. and Stüber, A., 2002. Suborbital intermediate water variability inferred from paired benthic foraminiferal Cd/Ca and $\delta^{13}C$ in the tropical West Atlantic and linking with North Atlantic climates. Earth Planetary Sciences Letters, 200, 191-205.

Annex II: Time Series of Parameters *a* and *b*.

In Table 2 we provide the time series of parameters a and b back to 350 ka obtained by rescaling the $\delta^{13}C_{stack}$ to fit with the Holocene and LGM parameterization of equation:

$$\delta^{13}C_{as} = \delta^{13}C - \delta^{13}C_{bio} = \delta^{13}C + a \cdot Cd_{sw} - b \qquad \text{Eq. 4-5}$$

Column Age refers to the original age model of the benthic $\delta^{13}C_{stack}$ (Stüber, 1999, Zahn and Stüber, 2002).

Table 1 Annex II. Time series of parameters a and b.

Age (ka)	$\delta^{13}C$ mean ocean	a for P> 1.3	b for P> 1.3	a for P> 1.3	b for P> 1.3
0	0	2.75	2	5.29	2.7
3.20	0.005	2.755	2.008	5.300	2.709
4.44	0.016	2.769	2.027	5.326	2.733
5.50	0.033	2.789	2.056	5.364	2.767
6.55	-0.048	2.694	1.920	5.183	2.604
7.59	0.009	2.760	2.014	5.309	2.717
8.65	-0.015	2.733	1.975	5.257	2.670
9.74	-0.129	2.599	1.782	5.000	2.438
11.60	-0.183	2.536	1.692	4.879	2.329
13.59	-0.190	2.527	1.680	4.863	2.314
15.58	-0.203	2.512	1.657	4.832	2.287
16.60	-0.238	2.471	1.598	4.754	2.216
17.18	-0.229	2.482	1.614	4.775	2.235
17.79	-0.253	2.454	1.573	4.721	2.186
18.79	-0.279	2.423	1.530	4.663	2.134
19.96	-0.274	2.429	1.538	4.674	2.144
21.24	-0.320	2.376	1.461	4.571	2.051
22.56	-0.332	2.361	1.440	4.543	2.026
23.38	-0.244	2.464	1.589	4.742	2.205
24.08	-0.243	2.466	1.591	4.744	2.207
25.36	-0.273	2.430	1.539	4.675	2.145
26.75	-0.250	2.457	1.578	4.728	2.193
28.21	-0.237	2.472	1.600	4.756	2.218
28.89	-0.245	2.463	1.587	4.739	2.202
29.51	-0.238	2.471	1.599	4.755	2.217
30.15	-0.205	2.509	1.653	4.828	2.283
31.03	-0.166	2.555	1.720	4.916	2.363
32.30	-0.207	2.508	1.651	4.825	2.280
33.86	-0.172	2.549	1.711	4.904	2.352
35.40	-0.163	2.559	1.725	4.923	2.369
36.94	-0.136	2.590	1.770	4.983	2.423
37.85	-0.132	2.596	1.778	4.994	2.433
38.57	-0.193	2.524	1.674	4.856	2.308
39.08	-0.234	2.475	1.605	4.763	2.224
39.65	-0.149	2.575	1.748	4.954	2.397
40.26	-0.165	2.557	1.722	4.919	2.365
40.87	-0.164	2.558	1.724	4.922	2.368
41.48	-0.144	2.581	1.757	4.966	2.408
42.10	-0.123	2.606	1.792	5.013	2.450
42.71	-0.117	2.613	1.803	5.027	2.463
43.32	-0.119	2.611	1.800	5.023	2.459
43.93	-0.132	2.595	1.777	4.993	2.432
44.55	-0.142	2.583	1.760	4.970	2.411
45.15	-0.152	2.572	1.744	4.948	2.391
46	-0.144	2.581	1.757	4.966	2.407
47	-0.169	2.552	1.715	4.910	2.357
48	-0.181	2.538	1.695	4.884	2.333
49	-0.196	2.521	1.670	4.850	2.302
50	-0.237	2.473	1.601	4.758	2.220
51	-0.247	2.460	1.583	4.733	2.197
52	-0.244	2.465	1.589	4.742	2.205
53	-0.228	2.483	1.616	4.778	2.237
54	-0.221	2.491	1.627	4.793	2.251
55	-0.202	2.513	1.659	4.835	2.289
56	-0.216	2.497	1.636	4.804	2.261
57	-0.232	2.478	1.608	4.767	2.228
58	-0.191	2.527	1.678	4.861	2.313
59	-0.242	2.467	1.592	4.746	2.209
60	-0.354	2.335	1.403	4.494	1.981
61	-0.406	2.274	1.315	4.376	1.875
62	-0.400	2.281	1.325	4.390	1.888
63	-0.317	2.379	1.465	4.577	2.056
64	-0.357	2.332	1.398	4.487	1.975
65	-0.351	2.338	1.407	4.500	1.987
66	-0.329	2.365	1.445	4.551	2.033
67	-0.337	2.356	1.432	4.533	2.016
68	-0.341	2.350	1.424	4.523	2.007
69	-0.348	2.342	1.413	4.507	1.994
70	-0.329	2.364	1.444	4.549	2.031
71	-0.262	2.443	1.558	4.701	2.168
72	-0.168	2.553	1.717	4.912	2.359
73	-0.117	2.613	1.802	5.026	2.462
74	-0.101	2.632	1.830	5.063	2.495
75	-0.073	2.664	1.877	5.126	2.552
76	-0.033	2.711	1.944	5.216	2.633
77	-0.031	2.713	1.947	5.220	2.637
78	-0.010	2.738	1.983	5.267	2.679
79	0.005	2.756	2.009	5.302	2.711

Age (ka)	$\delta^{13}C$ mean ocean	*a* for P> 1.3	*b* for P> 1.3	*a* for P> 1.3	*b* for P> 1.3
80	0.021	2.775	2.035	5.337	2.743
81	0.028	2.782	2.046	5.352	2.756
82	0.027	2.782	2.045	5.351	2.755
83	0.022	2.776	2.037	5.340	2.745
84	0.017	2.770	2.029	5.329	2.735
85	0.003	2.754	2.006	5.298	2.707
86	-0.015	2.733	1.975	5.257	2.670
87	-0.048	2.694	1.919	5.182	2.603
88	-0.065	2.674	1.891	5.144	2.569
89	-0.061	2.679	1.897	5.153	2.577
90	-0.051	2.691	1.914	5.176	2.597
91	-0.045	2.698	1.924	5.189	2.609
92	-0.021	2.726	1.965	5.243	2.658
93	-0.031	2.714	1.948	5.220	2.637
94	-0.049	2.693	1.917	5.180	2.600
95	-0.070	2.668	1.882	5.132	2.557
96	-0.045	2.697	1.924	5.189	2.609
97	-0.061	2.679	1.897	5.153	2.576
98	-0.077	2.660	1.870	5.116	2.543
99	-0.090	2.645	1.848	5.088	2.517
100	-0.048	2.694	1.919	5.182	2.603
101	-0.029	2.716	1.951	5.225	2.641
102	-0.082	2.654	1.862	5.106	2.534
103	-0.134	2.594	1.775	4.990	2.429
104	-0.204	2.511	1.656	4.831	2.286
105	-0.221	2.491	1.627	4.793	2.251
106	-0.207	2.507	1.651	4.824	2.279
107	-0.152	2.572	1.743	4.947	2.391
108	-0.139	2.588	1.766	4.978	2.419
109	-0.146	2.579	1.754	4.962	2.404
110	-0.165	2.557	1.722	4.920	2.366
111	-0.133	2.594	1.776	4.991	2.430
112	-0.172	2.549	1.710	4.904	2.351
113	-0.149	2.576	1.749	4.956	2.398
114	-0.091	2.643	1.846	5.085	2.515
115	-0.083	2.652	1.859	5.102	2.531
116	-0.115	2.615	1.806	5.031	2.466
117	-0.199	2.516	1.664	4.841	2.295
118	-0.194	2.523	1.673	4.854	2.307
119	-0.172	2.548	1.709	4.903	2.350
120	-0.167	2.554	1.718	4.914	2.361
121	-0.135	2.592	1.772	4.986	2.426
122	-0.138	2.588	1.766	4.979	2.419
123	-0.183	2.536	1.692	4.879	2.329
124	-0.239	2.469	1.596	4.751	2.214
125	-0.286	2.415	1.518	4.647	2.119
126	-0.331	2.362	1.441	4.545	2.027
127	-0.322	2.372	1.456	4.565	2.046
128	-0.295	2.404	1.502	4.625	2.100
129	-0.340	2.351	1.426	4.524	2.009
130	-0.393	2.290	1.337	4.406	1.902
131	-0.448	2.225	1.244	4.282	1.790

Age (ka)	$\delta^{13}C$ mean ocean	*a* for P> 1.3	*b* for P> 1.3	*a* for P> 1.3	*b* for P> 1.3
132	-0.437	2.237	1.262	4.306	1.812
133	-0.433	2.242	1.269	4.315	1.820
134	-0.421	2.257	1.290	4.344	1.846
135	-0.406	2.275	1.315	4.377	1.876
136	-0.437	2.237	1.262	4.306	1.812
137	-0.459	2.213	1.226	4.258	1.768
138	-0.520	2.141	1.123	4.120	1.644
139	-0.485	2.182	1.182	4.200	1.716
140	-0.456	2.215	1.230	4.264	1.773
141	-0.492	2.174	1.171	4.184	1.702
142	-0.487	2.179	1.178	4.193	1.710
143	-0.483	2.184	1.184	4.203	1.718
144	-0.454	2.218	1.234	4.269	1.778
145	-0.508	2.155	1.143	4.147	1.668
146	-0.460	2.211	1.223	4.254	1.765
148	-0.464	2.206	1.217	4.246	1.758
150	-0.491	2.175	1.172	4.186	1.703
152	-0.525	2.135	1.114	4.108	1.633
154	-0.550	2.106	1.072	4.053	1.583
156	-0.556	2.099	1.063	4.040	1.572
158	-0.535	2.123	1.098	4.087	1.614
160	-0.499	2.166	1.158	4.168	1.687
162	-0.478	2.190	1.193	4.214	1.729
164	-0.451	2.222	1.239	4.276	1.785
166	-0.414	2.265	1.301	4.359	1.859
168	-0.436	2.239	1.264	4.308	1.814
170	-0.491	2.175	1.171	4.185	1.703
172	-0.491	2.175	1.171	4.185	1.703
174	-0.463	2.208	1.219	4.249	1.760
176	-0.461	2.210	1.222	4.253	1.764
178	-0.481	2.187	1.189	4.208	1.723
180	-0.428	2.248	1.277	4.326	1.830
182	-0.483	2.184	1.185	4.203	1.719
184	-0.449	2.223	1.242	4.279	1.787
186	-0.396	2.286	1.332	4.399	1.896
188	-0.276	2.427	1.535	4.670	2.140
190	-0.135	2.592	1.773	4.987	2.427
192	-0.146	2.579	1.753	4.961	2.403
194	-0.189	2.528	1.681	4.864	2.316
196	-0.145	2.580	1.756	4.964	2.406
198	-0.149	2.576	1.749	4.956	2.398
200	-0.138	2.589	1.768	4.981	2.421
202	-0.134	2.593	1.773	4.988	2.427
204	-0.125	2.603	1.789	5.009	2.446
206	-0.155	2.569	1.739	4.942	2.386
208	-0.161	2.562	1.729	4.929	2.374
210	-0.167	2.554	1.718	4.914	2.361
212	-0.172	2.548	1.709	4.903	2.350
214	-0.211	2.502	1.643	4.815	2.271
216	-0.225	2.487	1.621	4.784	2.243
218	-0.247	2.461	1.584	4.735	2.199
220	-0.366	2.321	1.382	4.466	1.956

Age (ka)	$\delta^{13}C$ mean ocean	*a* for P> 1.3	*b* for P> 1.3	*a* for P> 1.3	*b* for P> 1.3
222	-0.462	2.208	1.220	4.250	1.761
224	-0.451	2.222	1.239	4.276	1.784
226	-0.466	2.204	1.214	4.242	1.754
228	-0.337	2.355	1.431	4.532	2.016
230	-0.351	2.339	1.408	4.501	1.988
232	-0.289	2.411	1.512	4.640	2.113
234	-0.250	2.457	1.578	4.727	2.192
236	-0.192	2.525	1.676	4.858	2.310
238	-0.238	2.471	1.598	4.754	2.216
240	-0.262	2.443	1.557	4.700	2.167
242	-0.351	2.339	1.408	4.500	1.987
244	-0.371	2.316	1.375	4.456	1.947
246	-0.395	2.287	1.334	4.401	1.898
248	-0.432	2.244	1.271	4.318	1.823
250	-0.517	2.144	1.128	4.127	1.650
252	-0.488	2.178	1.177	4.193	1.709
254	-0.516	2.145	1.129	4.128	1.651
256	-0.576	2.075	1.028	3.994	1.530
258	-0.499	2.165	1.158	4.167	1.686
260	-0.484	2.183	1.184	4.201	1.717
262	-0.523	2.138	1.118	4.114	1.638
264	-0.541	2.116	1.088	4.073	1.602
266	-0.536	2.122	1.095	4.084	1.611
268	-0.548	2.108	1.075	4.057	1.587
270	-0.540	2.118	1.089	4.076	1.604
272	-0.527	2.132	1.110	4.103	1.629
274	-0.536	2.122	1.095	4.083	1.611
276	-0.402	2.278	1.321	4.385	1.883
278	-0.272	2.432	1.542	4.679	2.149
280	-0.248	2.460	1.582	4.732	2.197
282	-0.252	2.454	1.574	4.722	2.188
284	-0.247	2.460	1.583	4.733	2.197
286	-0.267	2.437	1.549	4.689	2.157
288	-0.291	2.409	1.508	4.635	2.108
290	-0.328	2.366	1.447	4.552	2.034
292	-0.423	2.254	1.286	4.338	1.841
294	-0.432	2.243	1.270	4.317	1.822
296	-0.368	2.319	1.379	4.462	1.952
298	-0.362	2.326	1.390	4.476	1.966
300	-0.375	2.310	1.367	4.446	1.938
302	-0.311	2.386	1.475	4.590	2.068
304	-0.301	2.398	1.493	4.614	2.090
306	-0.293	2.407	1.505	4.631	2.105
308	-0.274	2.429	1.538	4.674	2.144
310	-0.267	2.437	1.549	4.689	2.157
312	-0.256	2.450	1.568	4.714	2.180
314	-0.260	2.445	1.561	4.704	2.171
316	-0.350	2.340	1.410	4.503	1.989
318	-0.291	2.409	1.509	4.636	2.110
320	-0.210	2.504	1.646	4.818	2.273
322	-0.188	2.529	1.682	4.866	2.317
324	-0.175	2.545	1.704	4.896	2.344
326	-0.142	2.584	1.761	4.971	2.412
328	-0.219	2.494	1.631	4.798	2.256
330	-0.221	2.491	1.627	4.793	2.251
332	-0.237	2.472	1.600	4.756	2.218
334	-0.411	2.268	1.306	4.365	1.865
336	-0.454	2.218	1.235	4.269	1.779
338	-0.493	2.173	1.169	4.181	1.699
340	-0.537	2.121	1.094	4.082	1.609
342	-0.522	2.138	1.119	4.115	1.639
344	-0.490	2.175	1.173	4.187	1.704
346	-0.341	2.351	1.425	4.524	2.008
348	-0.468	2.201	1.210	4.237	1.749
350	-0.512	2.150	1.135	4.137	1.659

5. Results and Discussion

This Chapter is devoted to the description of the records generated in this Thesis for MD96-2080 and MD02-2594 and to their interpretation in the context of past changes of circulation in the Agulhas Gateway, at depth and in the surface during the last three glacial-interglacial cycles, from MIS 1 to the boundary of MIS 9 and 10. The Chapter is divided in four Sub-chapters:

5.1. Age Model for MD96-2080 and MD02-2594

In this first Sub-chapter, a description of the generation of the age models for the two cores studied here is given as well as about the splicing of both cores into a singular record, that we named Agulhas Bank Spliced (ABS).

5.2. 345,000-year-long Multi-Proxy Records off South Africa Document Variable Contributions of Northern *versus* Southern Component Water to the Deep South Atlantic

This Sub-chapter describes benthic stable isotopes, benthic Cd/Ca and $\overline{SS}$ records of MD96-2080 in order to infer past modes of deep circulation around South Africa and assert the varying predominance of deep water masses from the North and South.

5.3. The South Atlantic Chemocline: New Assessments From Combined Benthic Cd/Ca and $\delta^{13}C$ Data and Inferred $\delta^{13}C_{as}$ Imprints

Here, a review of the available Holocene *vs* LGM benthic $\delta^{13}C$ and Cd/Ca data with the addition of data of our sediment cores from the Agulhas region is done in the context of the postulated existence of a chemical divide in the glacial South Atlantic between upper well ventilated waters and deep poorly ventilated waters. Furthermore, the benthic $\delta^{13}C$ down-core record of ABS and benthic Cd/Ca of MD96-2080 are also set in this context.

5.4. Influence of Agulhas Leakage on the Meridional Overturning Circulation (MOC): Insights From Paired Planktonic and Benthic Foraminifera Stable Isotope and Trace Metal Analyses Over the Last 345 kyr

The Agulhas Leakage has been postulated to be pivotal for the modulation and stability of the Meridional Overturning Circulation (MOC). In this Sub-chapter, planktonic and benthic records from ABS are analysed and inferences drawn about the relation between surface (Agulhas Water) and Deep circulation (vigour of NCW).

Chapter 5.1

Age Model for MD96-2080 and MD02-2594

5.1. Age Model for MD96-2080 and MD02-2594

5.1.1. Stratigraphy of MD96-2080

The age model for core MD96-2080 was derived from a combination of radiocarbon dating (Accelerator Mass Spectrometry, AMS) and graphical correlation of the benthic $\delta^{18}O$ record with core MD97-2120 from Chatham Rise in the southwest Pacific (45º32′S, 174º57′E, Pahnke et al., 2003; 45º32′S, 174º57′E, Pahnke and Zahn, 2005). MD97-2120 has been selected for correlation because it spans the last three glacial-interglacial cycles at high resolution and has a robust age model that is based on 15 radiocarbon dates, the Kawakawa tephra event (26.17 ka, Wilson et al., 1988; 26.17 ka, Carter et al., 2000), tuning through the benthic $\delta^{18}O$ isotope records to MD95-2042 (Shackleton et al., 2000) and through the foraminiferal Mg/Ca derived Sea Surface Temperature record to the Vostok ice core deuterium (δD) record (Petit et al., 1999).

Radiocarbon analyses were performed on 14 mono-specific planktonic foraminiferal samples (*Globorotalia inflata*) containing at least 10 mg of carbon (Table 5.1-1). The ^{14}C analyses were carried out at the NERC Radiocarbon Laboratory in East Kilbride, Scotland. All samples were subsequently calibrated to the calendar year scale following Fairbanks et al. (2007), which allowed for calibration back to 55 ka. We applied a marine reservoir age R(t) of 615 ± 52 years estimated from pre-bomb mollusc shells in the immediate neighbourhood of our core site (34º50′S, 18º60′E, Cape of Good Hope; Southon et al., 2002).

Table 5.1-1 details sample depths, conventional radiocarbon age (years before present, yr BP being present 1,950 by convention), sample carbon content, $\delta^{13}C$ (used to correct for carbon isotope fractionation) and calibrated dates using Fairbanks' et al. (2007) calibration.

Table 5.1-1 *Globorotalia inflata* ^{14}C AMS ages and calibrated calendar year ages for core MD96-2080.

Publication Code	Simple Identifier MD96-2080 (cm) *G.. inflata*	^{14}C Enrichment (% Modern ± 1σ)	Conventional Radiocarbon Age (years BP ± 1σ)	Carbon Content (% by wt.)	$\delta^{13}C_{PDB}$ (‰ ± 0.1)	Calibrated ^{14}C (calendar years ± σ)	Calibration Tool
SUERC-4646	MD96-2080 15-16	30.28 ± 0.12	9,598 ± 31	10.6	0.4	10,166 ± 75	(Fairbanks et al., 2007)
SUERC-4647	MD96-2080 26-27	21.68 ± 0.14	12,281 ± 50	10.6	0.3	13,530 ± 81	(Fairbanks et al., 2007)
SUERC-4648	MD96-2080 33-34	19.54 ± 0.11	13,117 ± 45	10.7	0.3	14,484 ± 160	(Fairbanks et al., 2007)
SUERC-4649	MD96-2080 37-38	16.57 ± 0.11	14,442 ± 52	10.6	0.4	16,102 ± 143	(Fairbanks et al., 2007)
SUERC-4650	MD96-2080 44-45	13.77 ± 0.11	15, 927 ± 62	10.8	0.4	18,556 ± 93	(Fairbanks et al., 2007)
SUERC-4653	MD96-2080 58-59	3.15 ± 0.10	27,773 ± 2,58	10.5	0.5	32,474 ± 321	(Fairbanks et al., 2007)
SUERC-4654	MD96-2080 65-66	0.27 ± 0.10	47,432 ± 2,951	10.5	0.6	-	
SUERC-4655	MD96-2080 74-75	0.38 ± 0.10	44,721 ± 2,113	10.7	0.6	-	
SUERC-4657	MD96-2080 84-85	0.24 ± 0.10	48,473 ± 3,360	10.6	0.6	-	
SUERC-4658	MD96-2080 95-96	-	> 46,400	10.7	0.6	-	
SUERC-4659	MD96-2080 105-106	0.22 ± 0.10	49,176 ± 3,667	10.6	0.6	-	
SUERC-4660	MD96-2080 116-117	0.23 ± 0.10	48,958 ± 3,570	10.7	0.6	-	
SUERC-4663	MD96-2080 125-126	-	> 46,400	10.5	0.4	-	
SUERC-4664	MD96-2080 145-146	0.29 ± 0.10	46,916 ± 2,768	10.5	0.6	-	
SUERC-4665	MD96-2080 279-280 BGRD	0.40 ± 0.01	44,274 ± 201	10.5	0.0	-	
SUERC-4666	MD96-2080 329-330 BGRD	0.38 ± 0.01	44,787± 209	10.9	0.2	-	

Notes: 1) Sample codes containing BGRD were analysed as background ^{14}C material and are reported as measured, i.e. with no background corrections made. 2) The results from the deep foraminifera (BGRD codes) were greater than those for iceland spar calcite, routinely run to quantify ^{14}C background for carbonate samples. The mean of the deep foraminifera results was used to correct all sample results. 3) Non-finite ages or results indistinguishable from background are reported as defined in Stuiver and Polach (1977).

Of the fourteen ^{14}C dates only the upper six display a continuous increase in age with core depth (see Fig. 5.1-1). Between 58.5 and 65.5 cm core depth ages abruptly increase from 27.8 ^{14}C ka to 47.4 ^{14}C ka BP. Below this depth all ^{14}C ages remain virtually unchanged within their error bars and cluster around an age of 45 ^{14}C ka. A similar age has been obtained for the two samples at 279.5 cm and 329.5 cm that were taken from MIS 6 to monitor background ^{14}C levels in the accelerator mass spectrometer. From the nearly constant age of the samples below 65.5 cm core depth and their similarity in age with the MIS 6 background ^{14}C test samples we infer that these samples are beyond the laboratory ^{14}C dating limit i.e., significantly older than ~40 ka. The discontinuity of the age-depth function suggests loss of sediment i.e., presence of a hiatus in core MD96-2080. The length of the hiatus was estimated by graphical correlation of the benthic and planktonic foraminiferal stable isotope records ($\delta^{18}O$, $\delta^{13}C$) with published available records e.g. the SPECMAP global $\delta^{18}O$ stack (Imbrie et al., 1984), the Antarctic Vostok ice core deuterium record (Petit et al., 1999; Shackleton et al., 2000), and fine-scale planktonic and benthic isotope records of core MD97-2120 (Pahnke et al., 2003; Pahnke and Zahn, 2005). From this correlation we inferred that the "warm" (light $\delta^{18}O$) values for planktonic $\delta^{18}O$ at 65.5 cm and positive benthic $\delta^{13}C$ reflect that this section of the core corresponds to MIS 5a. Graphic correlation of the benthic $\delta^{18}O$ record with the spliced benthic $\delta^{18}O$ record from nearby cores GeoB3603-2 (35º08'S, 17º33'E, 2840 m) and MD96-2081(35º35'S, 17º4º'E, 3164 m) (Cape Basin Record, CBR) of Peeters et al. (2004) supports the interpretation that the hiatus spans the interval between 33 to 70 ka i.e., MIS 3 and 4 are missing from the record (Figs. 5.1-2b-c) (Martínez-Méndez, 2005; Martínez-Méndez et al., 2008). Nonetheless, new data from MD02-2594 sediment core, while supporting the absence of most of the sediments of MIS 3-4 age, opens the possibility of having multiple hiatuses, with some of the sediments ascribed to MIS 5a belonging indeed to MIS 3 (see below and 5.1-3 for explanation). The hiatus has not been previously identified and our stratigraphy thus differs from that published by Rau et al. (2002; 2006).

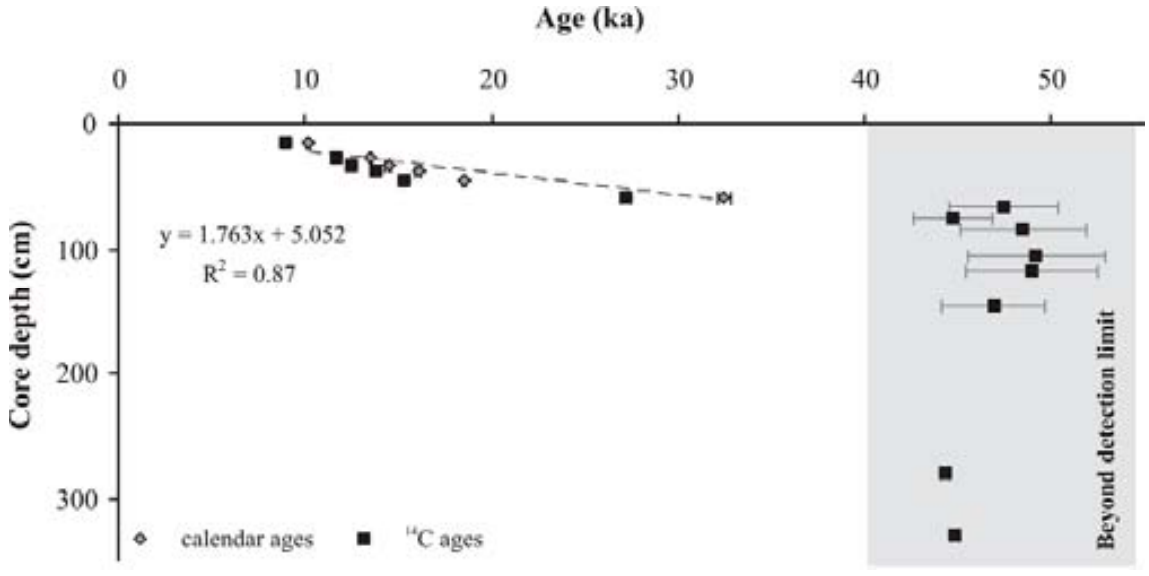

Figure 5.1-1 Age-depth function for MD96-2080 ^{14}C AMS dates. Conventional (black) and calibrated (grey).

We have also modified the published MD96-2080 chronology (Rau et al., 2002; 2006) in the lower section here studied. A void interval (749-769 cm) described on board (Bertrand et al., 1997), was left as a data gap in the initial stratigraphy. However, considering the good data match (stable isotopes and $\overline{SS}$) between the gap extremes we decided to eliminate it, leaving a continuous sedimentary sequence, a result which is further supported by the consistency in the resulting sedimentation rates.

The stratigraphy below 59.5 cm core depth was obtained by graphically correlating the benthic $\delta^{18}O$ record with that of core MD97-2120 (Pahnke and Zahn, 2005) using the Analyseries software (Paillard et al., 1996) (Figs. 5.1-2b-c). The correlation was further corroborated by the resulting fit of the benthic $\delta^{13}C$ and planktonic $\delta^{18}O$ records between MD96-2080 and MD97-2120 (Pahnke et al., 2003; Martínez-Méndez, 2005; Martínez-Méndez et al., 2008). Age correlation tie points for the MD96-2080 age model are listed in Table 5.1-2.

Table 5.1-2 Tie points for establishing the age model of MD96-2080.

Core depth (cm)	Age (yr BP)	Age control point	^{14}C calibration and references
15.5	10,166	^{14}C AMS	(Fairbanks et al., 2007)
26.5	13,530	^{14}C AMS	(Fairbanks et al., 2007)
33.5	14,484	^{14}C AMS	(Fairbanks et al., 2007)
37.5	16,102	^{14}C AMS	(Fairbanks et al., 2007)
44.5	18,556	^{14}C AMS	(Fairbanks et al., 2007)
58.5	32,474	^{14}C AMS	(Fairbanks et al., 2007)
61.5	33,530	$\delta^{18}O_{benthic}$ tuned to $\delta^{18}O_{benthic}$ of MD97-2120	(Pahnke et al., 2003; Pahnke and Zahn, 2005)
62.5	71,284	$\delta^{18}O_{benthic}$ tuned to $\delta^{18}O_{benthic}$ of MD97-2120	(Pahnke et al., 2003; Pahnke and Zahn, 2005)
161.5	88,548	$\delta^{18}O_{benthic}$ tuned to $\delta^{18}O_{benthic}$ of MD97-2120	(Pahnke et al., 2003; Pahnke and Zahn, 2005)
221.5	116,292	$\delta^{18}O_{benthic}$ tuned to $\delta^{18}O_{benthic}$ of MD97-2120	(Pahnke et al., 2003; Pahnke and Zahn, 2005)
274.5	128,349	$\delta^{18}O_{benthic}$ tuned to $\delta^{18}O_{benthic}$ of MD97-2120	(Pahnke et al., 2003; Pahnke and Zahn, 2005)
301.5	138,466	$\delta^{18}O_{benthic}$ tuned to $\delta^{18}O_{benthic}$ of MD97-2120	(Pahnke et al., 2003; Pahnke and Zahn, 2005)
384.5	159,241	$\delta^{18}O_{benthic}$ tuned to $\delta^{18}O_{benthic}$ of MD97-2120	(Pahnke et al., 2003; Pahnke and Zahn, 2005)
439.5	183,118	$\delta^{18}O_{benthic}$ tuned to $\delta^{18}O_{benthic}$ of MD97-2120	(Pahnke et al., 2003; Pahnke and Zahn, 2005)
481.5	204,869	$\delta^{18}O_{benthic}$ tuned to $\delta^{18}O_{benthic}$ of MD97-2120	(Pahnke et al., 2003; Pahnke and Zahn, 2005)
524.5	228,503	$\delta^{18}O_{benthic}$ tuned to $\delta^{18}O_{benthic}$ of MD97-2120	(Pahnke et al., 2003; Pahnke and Zahn, 2005)
538.5	243,242	$\delta^{18}O_{benthic}$ tuned to $\delta^{18}O_{benthic}$ of MD97-2120	(Pahnke et al., 2003; Pahnke and Zahn, 2005)
592.5	261,388	$\delta^{18}O_{benthic}$ tuned to $\delta^{18}O_{benthic}$ of MD97-2120	(Pahnke et al., 2003; Pahnke and Zahn, 2005)
615.5	278,033	$\delta^{18}O_{benthic}$ tuned to $\delta^{18}O_{benthic}$ of MD97-2120	(Pahnke et al., 2003; Pahnke and Zahn, 2005)
734.5	333,763	$\delta^{18}O_{benthic}$ tuned to $\delta^{18}O_{benthic}$ of MD97-2120	(Pahnke et al., 2003; Pahnke and Zahn, 2005)
773.5	343,000	$\delta^{18}O_{benthic}$ tuned to $\delta^{18}O_{benthic}$ of MD97-2120	(Pahnke et al., 2003; Pahnke and Zahn, 2005)

According to our age model, the upper 800 cm of core MD96-2080 span the past 345 kyr. Sedimentation rates vary between 1-7 cm/kyr with mean rates of 3 cm/kyr (Fig. 5.1-2b). Sedimentation rates are higher, 3-4 cm/kyr, across glacial Terminations III and IV with values dropping to 1-2 cm/kyr early in the subsequent interglacial intervals. During Termination II the pattern

is different in that sedimentation rates are lower, 2.5 cm/kyr, and increase during MIS 5e to 4 cm/kyr (Fig. 5.1-2b). Higher sedimentation rates of 6 cm/kyr are suggested for the section around the lower boundary of the hiatus, at 70 ka.

Time steps along both the stable isotope and sortable silt records vary between 0.2 and 1.5 kyr while those along the benthic Cd/Ca record increase to >4 kyr in some sections.

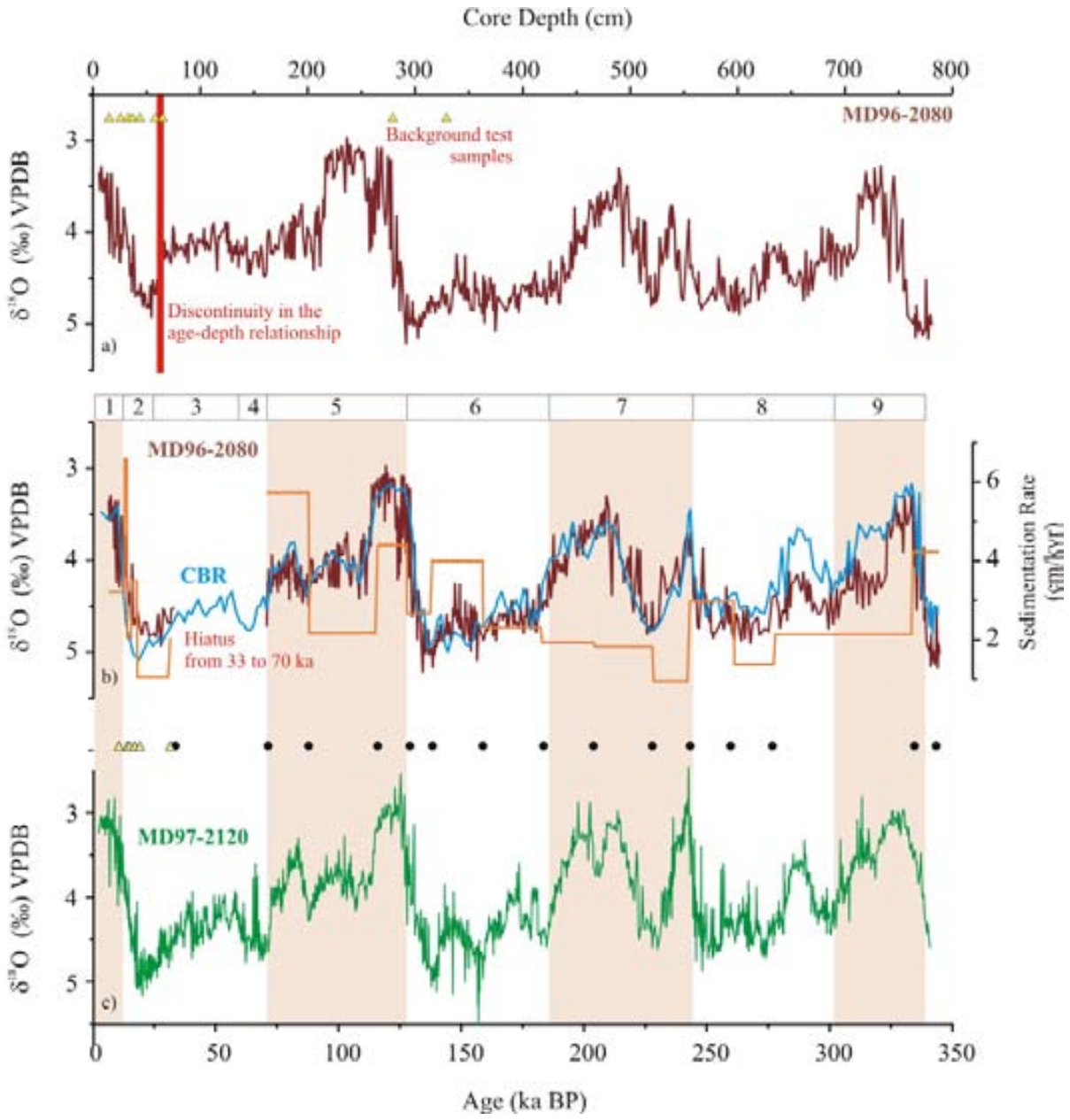

Figure 5.1-2 Age model for MD96-2080. a) Benthic $\delta^{18}O$ (brown) on depth-in-core scale. Yellow triangles indicate position of ^{14}C-AMS dates used for age modeling. Red bar indicates incursion of age-depth discontinuity (see Fig. 5.1-1); b) benthic $\delta^{18}O$ (brown) and spliced Cape Basin Record (CBR, blue) from Peeters et al. (2004) retuned to the age model of MD96-2080. Sedimentation rate profile (cm/kyr) for MD96-2080 is shown in orange. Top bar gives Marine Isotope Stages; c) MD97-2120 benthic $\delta^{18}O$ (Pahnke and Zahn, 2005). Yellow triangles as in panel a). Black circles denote tie points for graphical correlation of the MD96-2080 profile with that of MD97-2120 shown in c). Vertical shading highlights interglacials.

5.1.2. Stratigraphy of MD02-2594

Preliminary 10 cm step stable isotope measurements along MD02-2594 indicated that the upper 750 cm cover the last 80 kyr. The current age model for this sediment core has been developed on the basis of radiocarbon dating and tuning to the $\delta^{18}O$ record of EPICA Dronning Maud Land Antarctic ice core (EDML, EPICA Community Members, 2006) which is a proxy for atmospheric surface temperature. EDML is in the Atlantic sector of Antarctica and for that reason we consider that the atmospheric temperature variations over this site and off South Africa are more likely to be similar than with any of the other available records from Antarctica (e.g. Byrd, Blunier et al., 1998; Vostok, Petit et al., 1999; Dome Fuji, Watanabe et al., 2003; EPICA Dome C, EPICA Community Members, 2004). We choose for the tuning the planktonic $\delta^{18}O$ record over correlating the benthic $\delta^{18}O$ record to other benthic records (by example that of MD97-2120, Pahnke and Zahn, 2005), despite being benthic records more commonly used as stratigraphic tool and having correlated MD96-2080 benthic $\delta^{18}O$ to MD97-2120 benthic $\delta^{18}O$ because the planktonic $\delta^{18}O$ record provides much higher resolution. Planktonic sample step for stable isotopes is 5 cm for Termination I and 2 cm for the entire last glacial period yielding time steps of around 300 yr (see below) while the benthic records are produced at only 10 cm steps resulting in time steps of around 1000 yr. The low resolution MD02-2594 benthic $\delta^{18}O$ does not offer detail enough for the correlation. Also, we reject a comparison of the planktonic Mg/Ca-derived SST record of MD02-2594 with $\delta^{18}O$ of EDML even though being Mg/Ca a better indicator of sea surface temperature than planktonic $\delta^{18}O$ because the Mg/Ca record shows certain particularities, such as warm SST during MIS 2 (see Fig. 5.1-4), which makes it different from type paleoclimatic temperature variations and indicates that factors in addition to global climate are affecting the sea surface temperatures in the Agulhas region (see discussion).

The ^{14}C analyses for this core were carried out at the National Ocean Science Accelerator Mass Spectrometry facility (NOSAMS) at Woods Hole Oceanographic Institution, Massachusetts (WHOI). Radiocarbon analyses were performed on eleven mono-specific planktonic foraminiferal samples (*Globorotalia inflata*) containing more than 3 mg of carbon which is the minimum amount required by the NOSAMS facility. We applied the same marine reservoir age R(t) of 615 ± 52 years (Southon et al., 2002) as for MD96-2080. All samples were subsequently calibrated to the calendar year scale following Fairbanks et al. (2007). See Table 5.1-3 for details about the samples.

Table 5.1-3 *Globorotalia inflata* ^{14}C AMS ages and calibrated calendar year ages for core MD02-2594.

Publication Code NOSAMS	Sample Identifier MD02-2594 (cm) *G. inflata*	Fraction Modern (Fm ± 1σ)	Conventional Radiocarbon Age (years BP ± 1σ)	Sample weight (mg)	$\delta^{13}C_{PDB}$ (‰ ± 0.1)	Calibrated ^{14}C (calendar years ± σ)	Calibration Tool
OS-65271	MD02-2594 50-51	0.6598 ± 0.0026	3,340 ± 30	5.54	0.82	2,815 ± 57	(Fairbanks et al., 2007)
OS-65110	MD02-2594 110-111	0.4316 ± 0.0022	6,750 ± 40	3.81	0.75	7,014 ± 97	(Fairbanks et al., 2007)
OS-64823	MD02-2594 155-156	0.3243 ± 0.0015	9,050 ± 35	3.97	0.69	9,460 ± 49	(Fairbanks et al., 2007)
OS-64964	MD02-2594 165-166	0.3073 ± 0.0029	9,480 ± 75	3.32	0.64	9,966 ± 185	(Fairbanks et al., 2007)
OS-65269	MD02-2594 210-211	0.2442 ± 0.0019	11, 300 ± 65	4.80	0.62	12,626 ± 75	(Fairbanks et al., 2007)
OS-65111	MD02-2594 245-246	0.1711 ± 0.0018	14,200 ± 85	4.09	0.39	15,813 ± 157	(Fairbanks et al., 2007)
OS-64824	MD02-2594 255-256	0.1541 ± 0.001	15,000 ± 50	4.11	0.62	16935 ± 154	(Fairbanks et al., 2007)
OS-65113	MD02-2594 295-296	0.1324 ± 0.0001	16,250 ± 60	4.22	0.64	18,833 ± 93	(Fairbanks et al., 2007)
OS-65274	MD02-2594 345-346	0.0393 ± 0.0007	26,000 ± 140	5.40	0.68	30,559 ± 203	(Fairbanks et al., 2007)
OS-64965	MD02-2594 405-406	0.0162 ± 0.0004	33,100 ± 190	3.65	0.70	37,881 ± 249	(Fairbanks et al., 2007)
OS-65112	MD02-2594 465-466	0.0062 ± 0.0003	40,800± 370	4.16	0.71	44,887 ± 382	(Fairbanks et al., 2007)

Notes: 1) Fraction Modern (Fm) is a measurement of the deviation of the $^{14}C/C$ ratio of a sample from "modern." Modern is defined as 95% of the radiocarbon concentration (in AD 1950) of NBS Oxalic Acid I normalized to $\delta^{13}C_{VPDB}$ = -19 ‰ (Olsson, 1970). AMS results are calculated using the internationally accepted modern value of 1.176 ±0.010 x 10-12 (Karlen et al., 1968) and a final $^{13}C_{correction}$ is made to normalize the sample Fm to a δ13CVPDB value of -25 ‰. 2) Reporting of ages and/or activities follows the convention outlined by Stuiver and Polach (1977) and Stuiver (1980). Radiocarbon ages are calculated using 5,568 (yrs) as the half-life of radiocarbon and are reported without reservoir corrections or calibration to calendar years. A $\Delta^{14}C$ activity normalized to 1950 is also reported according to these conventions. The activity, or $\Delta^{14}C$ of the sample is further corrected to account for the decay between collection (or death) and the time of 10/6/2005 measurement if a collection date is specified on the submittal form, otherwise $\Delta^{14}C$ is reported assuming that collection and measurement date are the same.

Figure 5.3-1 shows the tie points, i.e. the calendar ages plus additional correlation tie points used for developing the age model of MD02-2594 (see also Table 5.1-4). For tuning the lower part of the record, we have used the assistance of the spliced record of MD02-2594 and MD96-2080 (Agulhas Bank Spliced, ABS) (see section 5.1.3). The structural fit of ABS planktonic $\delta^{18}O$ with EDML in MIS 5a has enabled placing the last pointer between MD02-2594 and EDML at 79,984 yr.

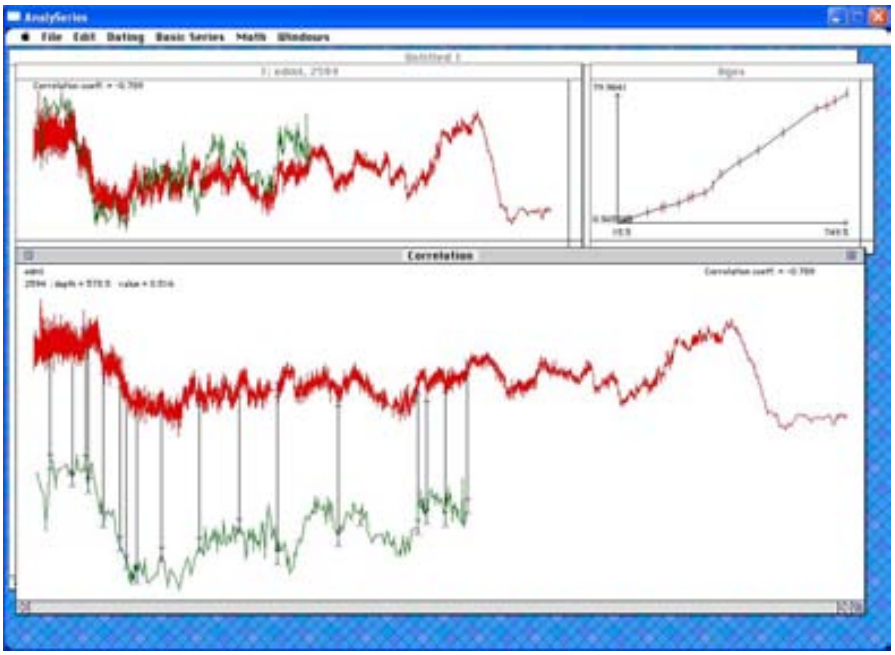

Figure 5.1-3 Screen shot of the tuning procedure using AnalySeries software (Paillard et al., 1996). MD02-2594 planktonic $\delta^{18}O$ record (green) and EDML $\delta^{18}O$ record (red) (EPICA Community Members, 2006). Lines indicate the tie points between both records.

Table 5.1-4 Tie points for establishing the age model of MD02-2594.

Core depth (cm)	Age (yr BP)	Age control point	^{14}C calibration and references
50.5	2,815	^{14}C AMS	(Fairbanks et al., 2007)
110.5	7,014	^{14}C AMS	(Fairbanks et al., 2007)
155.5	9,460	^{14}C AMS	(Fairbanks et al., 2007)
165.5	9,966	^{14}C AMS	(Fairbanks et al., 2007)
210.5	12,626	^{14}C AMS	(Fairbanks et al., 2007)
245.5	15,813	^{14}C AMS	(Fairbanks et al., 2007)
255.5	16,935	^{14}C AMS	(Fairbanks et al., 2007)
295.5	18,833	^{14}C AMS	(Fairbanks et al., 2007)
319.5	23,444	$\delta^{18}O_{planktonic}$ tuned to EDML $\delta^{18}O$	(EPICA Community Members, 2006)
345.5	30,559	^{14}C AMS	(Fairbanks et al., 2007)
405.5	37,881	^{14}C AMS	(Fairbanks et al., 2007)
465.5	44,887	^{14}C AMS	(Fairbanks et al., 2007)
543.5	56,162	$\delta^{18}O_{planktonic}$ tuned to EDML $\delta^{18}O$	(EPICA Community Members, 2006)
651.5	70,761	$\delta^{18}O_{planktonic}$ tuned to EDML $\delta^{18}O$	(EPICA Community Members, 2006)
685.5	72,380	$\delta^{18}O_{planktonic}$ tuned to EDML $\delta^{18}O$	(EPICA Community Members, 2006)
709.5	75,892	$\delta^{18}O_{planktonic}$ tuned to EDML $\delta^{18}O$	(EPICA Community Members, 2006)
749.5	79,984	$\delta^{18}O_{planktonic}$ tuned to EDML $\delta^{18}O$	(EPICA Community Members, 2006)

For further details on the correlation, Figure 5.1-4 shows the MD02-2594 planktonic $\delta^{18}O$ record in depth-in-core scale with the ^{14}C ages and tie points imposed for the tuning (panel a) and the resulting age model of planktonic $\delta^{18}O$ record and SST (panels b and c) compared to the EDML $\delta^{18}O$ record (EPICA Community Members, 2006) (panel d).

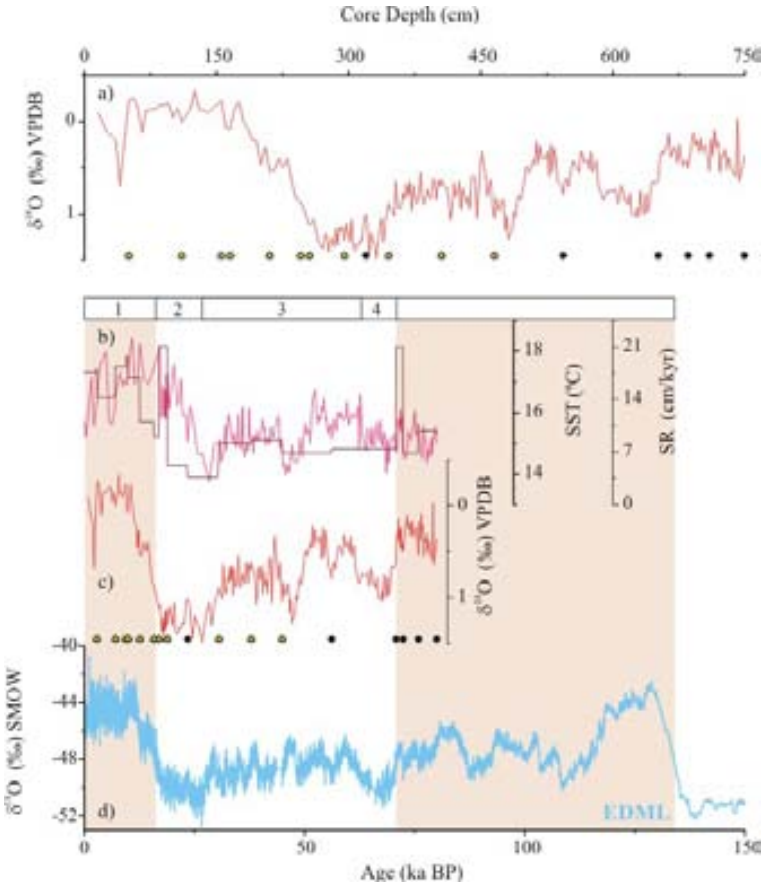

Figure 5.1-4 Age model for MD02-2594; a) planktonic $\delta^{18}O$ (red) on depth-in-core scale. Yellow triangles indicate position of ^{14}C-AMS dates used for age modeling. Black dots indicate tie points used for the tuning to EDML (EPICA Community Members, 2006); b) Mg/Ca-derived SST (ºC) (pink) and sedimentation rate profile (cm/kyr) (brown) for MD02-2594. Top bar gives Marine Isotope Stages; c) planktonic $\delta^{18}O$ (red) on age scale. Yellow triangles and black circles as in panel a); d) EDML $\delta^{18}O$ (EPICA Community Members, 2006). Vertical shading highlights interglacials.

The structural fit between MD02-2594 and EDML is good in general with one prominent exception between 43-48 cal ka. Here, a peak of high $\delta^{18}O$ in EDML, indicating warmer atmospheric temperatures, is associated with high $\delta^{18}O_{plk}$ in MD02-2594, which indicates low sea surface temperatures (see Figs. 5.1-3 and 4). The tie point associated to a radiocarbon date at 44.9 cal ka (40.8 ka ^{14}C age) falls within this event. The NOSAMS facility allows for calibration back to 52 ka and there is not sign of contamination in this sample and the ^{14}C date is reported as robust (K. Elder, pers. comm. 2008). On the other hand, 40.8 ka is close to the time of occurrence of the Laschamp Event around 40.3–41.7 ka cal BP (Roperch et al., 1988; Laj et al., 2000; Voelker et al., 2000). The Laschamp Event is characterized by a minimum in the Earth's geomagnetic field strength which allowed for an increased in atmospheric ^{14}C (Laj et al., 2000), thus the difference between ^{14}C ages and calendar ages may increase by up to 7,500 years in this interval. One might shift the minimum $\delta^{18}O_{plk}$ value in MD02-2594 at around 43 cal ka such that it matches with the maximum in $\delta^{18}O$ in EDML at around 47 cal ka. In order to test whether the inferred age of 44.9 cal ka may be indeed underestimated, we have evaluated the age differences between the densely ^{14}C dated marine core PS2644 and GISP2 ice core computed by Völker et al. (2000) in the neighbourhood of 40.8 ^{14}C ka.

This comparison shows that the age differences between ^{14}C ages in PS2644 and calendar ages in GISP2 vary between 1,500 and 3,000 years in this interval, hence, moving the ^{14}C age from 40.8 ka to near 48 ka seems implausible. Likely, regional climatic signals recorded in both, MD02-2594 and EDML, are the cause of this discrepancy. As higher resolution benthic stable isotope records for MD02-2594 become available, the age model of this core could be refined, if needed, in this section.

For the youngest part of the record, sediment samples above 50.5 cm (our first radiocarbon age), we have assigned ages by extrapolation. To do so, we have assumed an age of 0 for the sample at 1 cm core depth (sample interval 0-2 cm) and computed the equation of the straight line between that present age and our first ^{14}C calendar age at 2,815 yr (50.5 cm sample depth, Fig. 5.1-5). We have used this equation to compute all ages younger than 2,815 yr.

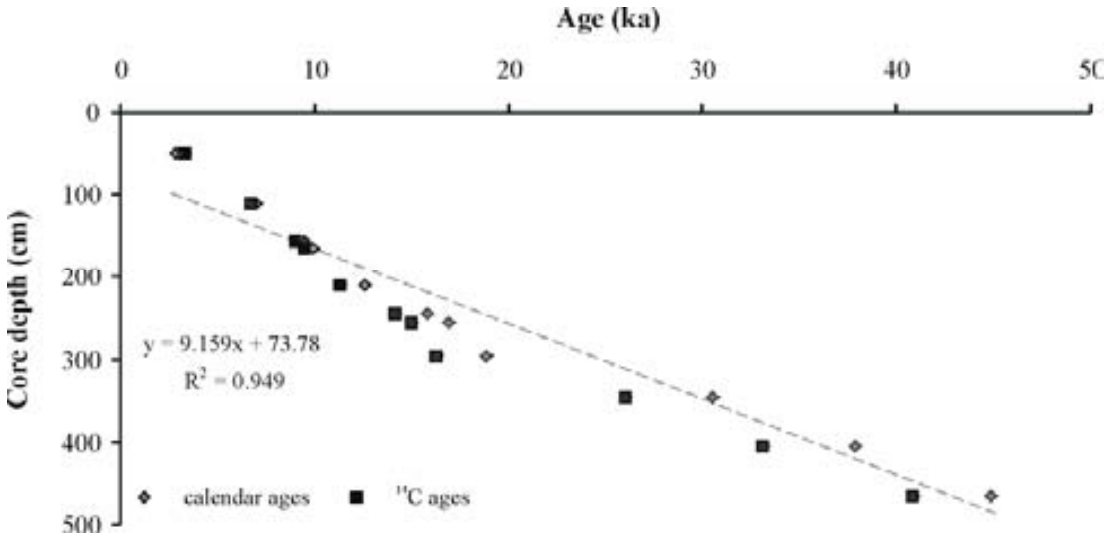

Figure 5.1-5 Age-depth function for MD02-2594 ^{14}C AMS dates. Conventional (black) and calibrated (grey).

The resulting age model yields sedimentation rates that vary between 21 and 4 cm/kyr. Maximum rates are recorded around Termination I and for the Holocene while minima occur during MIS 2 (see Fig. 5.1-4).

The records with higher resolution that we have generated, i.e. planktonic stable isotopes, resolve climate variability at a time step of 296 ± 136 years. The time step of the Mg/Ca record is slightly lower, 357 ± 237 years and the bottom records, i.e. benthic stable isotopes and $\overline{SS}$ are only resolved at a millennial time resolution, time step of 1,045 ± 503 years.

5.1.3. Splicing of MD02-2594 and MD96-2080 Into a Singular Record: Agulhas Bank Spliced (ABS)

The MD02-2594 records fill in the data gap from MIS 3 to 4 in MD96-2080 that was left due to the presence of a hiatus in this interval. We have spliced together both records in order to obtain a continuous time series of *Globigerina bulloides* stable isotopes and Mg/Ca, and benthic stable isotopes and named it Agulhas Bank Spliced (ABS, Fig. 5.1-7).

In order to do so, first of all, we compare the MD02-2594 planktonic stable isotopes (*Globigerina bulloides* and *Globorotalia inflata*), *G. bulloides* Mg/Ca, benthic stable isotopes and $\overline{SS}$ (Hall, unpublished data) records (see Chapter 4 for details on sample steps) with those of MD96-2080 and of CBR (Peeters et al., 2004 and D. Kroon, R. Schneider umplished data) (Fig. 5.1-5). We add the sedimentation rates of MD02-2594 and MD96-2080 to the comparison.

All the records except planktonic and benthic $\delta^{13}C$ of both Agulhas Bank Slope (i.e. MD02-2594 and MD96-2080) cores show a good matching around 80 ka (Fig. 5.1-6). We are confident that MD02-2594 data are complete and intact as the core did not show any sign of a hiatus, or sediment disturbance and the foraminiferal preservation is very good along the whole 750 cm studied for this Thesis. We have less confidence in the MIS 5a section of MD96-2080 due to the presence of the hiatus and the description in the on-board report of core disturbance in the upper section of this core (Bertrand et al., 1997). The disagreement between planktonic and benthic $\delta^{13}C$ of both cores suggest the possibility that part of the sediments of MD96-2080 ascribe to MIS 5a could indeed belong to some section of MIS 3 and that multiple hiatuses existed in this core. We have no control on that and in order to stay on the secure side we give preference to the data of MD02-2594 in MIS 5a and take the first data point from MD96-2080 just after the last age of MD02-2594 at 79,984 yr. Minor fine tuning of the initial age model of MD96-2080 around MIS 5a has been necessary to improve the graphical correlation with the EDML $\delta^{18}O$ record (EPICA Community Members, 2006). For this retuning, we have initially spliced the Agulhas Bank Records along their independent age scales and set as pointers ages from these independent age scales before and after the section that needs modification, i.e. around 80-90 kyr. Seven additional tie points have been necessary to improve the correlation of ABS planktonic $\delta^{18}O$ with the EDML $\delta^{18}O$ record (Table 5.1-5).

We observe that MIS 2 data of all MD96-2080 records is closer to Holocene values than that of MD02-2594. We suspect that disturbance in the upper meter of MD96-2080 produced mixing of sediments of "Holocene" and MIS 2 age erasing the full glacial signatures. Also note that most of the Holocene is lost in MD96-2080 due to flow out during core recovering. The Mg/Ca-derived SST of both cores in the upper part disagrees in which MD96-2080 Mg/Ca-derived SST reaches 20ºC while the estimations from MD02-2594 hardly reach 18ºC. We only have data for seven samples of MD96-2080 in this upper section against 30 in MD02-2594. Although we do not have a satisfactory explanation for this discrepancy, visual inspection shows much better foraminiferal preservation in MD02-2594 than in MD96-2080 and therefore we also give preference to the data of MD02-2594 in the upper section.

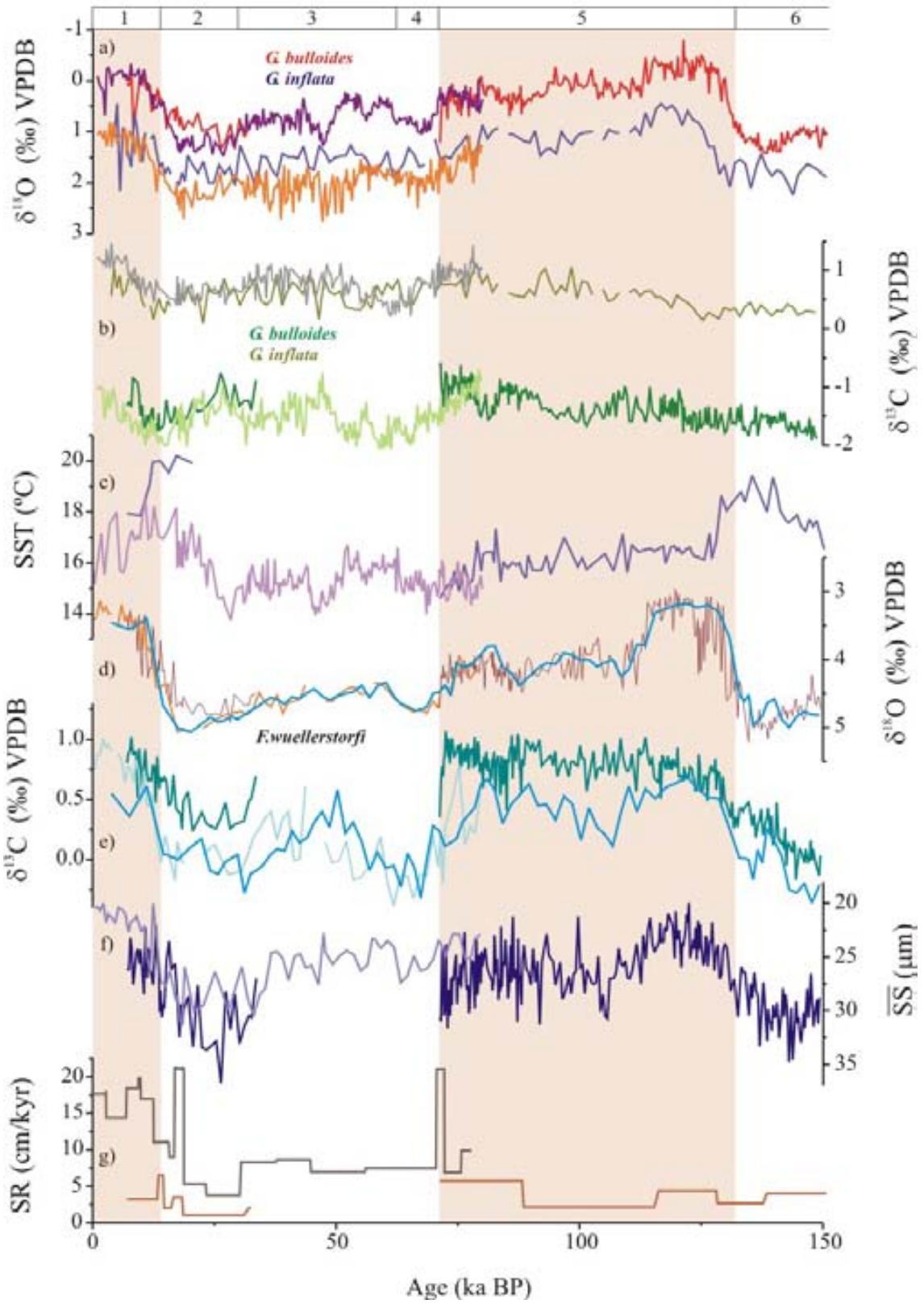

Figure 5.1-6 MD96-2080, MD02-2594 and CBR (Peeters et al., 2004; D. Kroon, R. Schneider unpublished data) records. a) Planktonic $\delta^{18}O$, MD96-2080 *G. bulloides* (red) and MD02-2594 (purple); MD96-2081 *G. inflata* (blue, F. Peeters, unpublished data) and MD02-2594 (violet). b) Planktonic $\delta^{13}C$, MD96-2080 *G. bulloides* (green) and MD02-2594 (ligth green); MD96-2081 *G. inflata* (dark yellow, F. Peeters, unpublished data) and MD02-2594 (grey). c) MD96-2080 (pink) and MD02-2594 (light violet) *G. bulloides* Mg/Ca-derived SST (ºC). d) Benthic $\delta^{18}O$ (all *F. wuellerstorfi*), MD96-2080 (brown) and MD02-2594 (orange), CBR (blue, Peeters et al., 2004). e) Benthic $\delta^{13}C$ (all *F. wuellerstorfi*), MD96-2080 (cyan), MD02-2594 (light cyan), CBR (dark blue, D. Kroon, R. Schneider unpublished data). f) MD96-2080 (navy) and MD02-2594 (light blue) $\overline{SS}$ (I. Hall, unpublished data). g) MD96-2080 (light brown) and MD02-2594 (grey) sedimentation rates (SR, cm/kyr). Top bar displays Marine Isotope Stages. Vertical shading highlights interglacials.

Table 5.1-5 Tie points for establishing the age model of the spliced record ABS.

Age (yr BP) Spliced	Age (yr BP) Fine tuned	Age control point	^{14}C calibration and references
2,815	2,815	^{14}C AMS	(Fairbanks et al., 2007)
7,014	7,014	^{14}C AMS	(Fairbanks et al., 2007)
9,460	9,460	^{14}C AMS	(Fairbanks et al., 2007)
9,966	9,966	^{14}C AMS	(Fairbanks et al., 2007)
12,626	12,626	^{14}C AMS	(Fairbanks et al., 2007)
15,813	15,813	^{14}C AMS	(Fairbanks et al., 2007)
16,935	16,935	^{14}C AMS	(Fairbanks et al., 2007)
18,833	18,833	^{14}C AMS	(Fairbanks et al., 2007)
23,444	23,444	$\delta^{18}O_{planktonic}$ tuned to EDML $\delta^{18}O$	(EPICA Community Members, 2006)
30,559	30,559	^{14}C AMS	(Fairbanks et al., 2007)
37,881	37,881	^{14}C AMS	(Fairbanks et al., 2007)
44,887	44,887	^{14}C AMS	(Fairbanks et al., 2007)
56,162	56,162	$\delta^{18}O_{planktonic}$ tuned to EDML $\delta^{18}O$	(EPICA Community Members, 2006)
70,761	70,761	$\delta^{18}O_{planktonic}$ tuned to EDML $\delta^{18}O$	(EPICA Community Members, 2006)
72,380	72,380	$\delta^{18}O_{planktonic}$ tuned to EDML $\delta^{18}O$	(EPICA Community Members, 2006)
75,892	75,892	$\delta^{18}O_{planktonic}$ tuned to EDML $\delta^{18}O$	(EPICA Community Members, 2006)
79,984	79,984	$\delta^{18}O_{planktonic}$ tuned to EDML $\delta^{18}O$	(EPICA Community Members, 2006)
85,061	87,283	$\delta^{18}O_{planktonic}$ tuned to EDML $\delta^{18}O$	(EPICA Community Members, 2006)
93,1723	92,3211	$\delta^{18}O_{planktonic}$ tuned to EDML $\delta^{18}O$	(EPICA Community Members, 2006)
100,108	100,108	Original Age Scale MD96-2080	(Martínez-Méndez et al., 2008)
105,195	105,195	Original Age Scale MD96-2080	(Martínez-Méndez et al., 2008)
110,743	110,743	Original Age Scale MD96-2080	(Martínez-Méndez et al., 2008)
115,367	115,367	Original Age Scale MD96-2080	(Martínez-Méndez et al., 2008)
120,842	120,842	Original Age Scale MD96-2080	(Martínez-Méndez et al., 2008)
124,709	124,709	Original Age Scale MD96-2080	(Martínez-Méndez et al., 2008)
133,220	133,220	Original Age Scale MD96-2080	(Martínez-Méndez et al., 2008)
136,218	136,218	Original Age Scale MD96-2080	(Martínez-Méndez et al., 2008)
141,470	141,470	Original Age Scale MD96-2080	(Martínez-Méndez et al., 2008)
143,472	143,472	Original Age Scale MD96-2080	(Martínez-Méndez et al., 2008)
150,230	150,230	Original Age Scale MD96-2080	(Martínez-Méndez et al., 2008)

The resulting spliced records that will be used and discussed in the next chapters of this Thesis are presented in Figure 5.1-7.

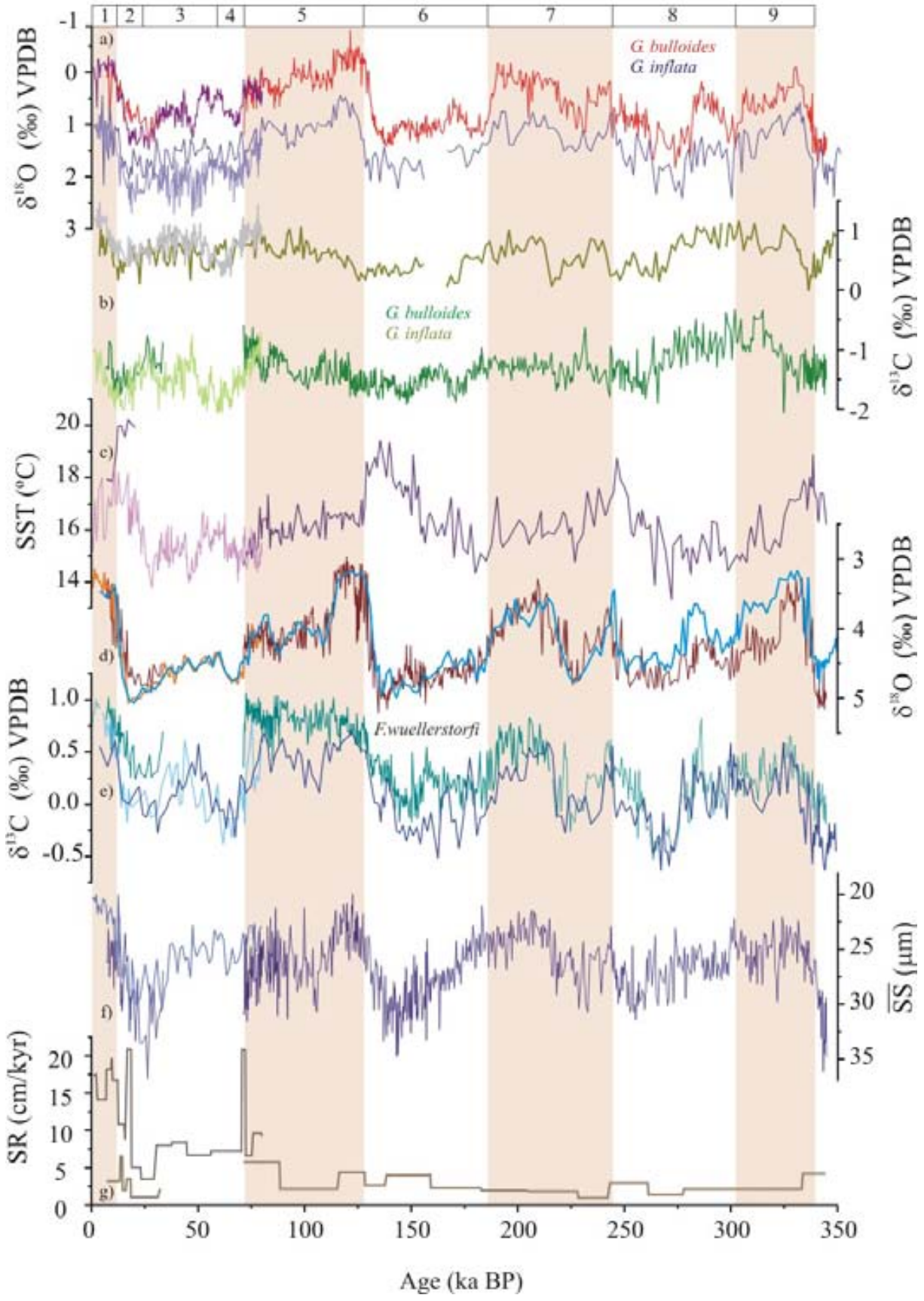

Figure 5.1-7 Same as 5.1-6 down to 350 kyr.

References

Bertrand, P. et al., 1997. Les rapport de campagne à la mer à bord du Marion Dufresne - Campagne Nausicaa - IMAGES II - MD105 du 20/10/96 au 25/11/96. Institut Francais pour la Recherche et la technologie Polaires.

Blunier, T., Chappellaz, J., Schwander, J., Dällenbach, A., Stauffer, B., Stocker, T.F., Raynaud, D., Jouzel, J., Clausen, H.B., Hammer, C.U. and Johnsen, S.J., 1998. Asynchrony of Antarctic and Greenland climate change during the last glacial period. Nature, 394, 739-743.

Carter, L., Neil, H.L. and McCave, I.N., 2000. Glacial to interglacial changes in non-carbonate and carbonate accumulation in the SW Pacific Ocean, New Zealand. Palaeogeography, Palaeoclimatology, Palaeoecology, 162, 333-356.

EPICA Community Members, 2004. Eight glacial cycles from an Antarctic ice core. Nature, 429, 623-628.

EPICA Community Members, 2006. One-to-one coupling of glacial climate variability in Greenland and Antarctica. Nature, 444, 195-198.

Fairbanks, R.G., Mortlock, R.A., Chiu, T.-C., Cao, L., Kaplan, A., Guilderson, T.P., Fairbanks, T.W., Bloom, A.L., Grootes, P.M. and Nadeau, M.-J., 2007. Radiocarbon age to calendar age conversion. http://radiocarbon.ldeo.columbia.edu/research/radcarbcal.htm.

Imbrie, J., Hays, J.D., Martinson, D.G., McIntyre, A., Mix, A.C., Morley, J.J., Pisias, N.G., Prell, W.L. and Shackleton, N.J., 1984. The Orbital Theory of Pleistocene Climate: support from a revised chronology of the Marine $\delta^{18}O$ record. In: Berger, A.L., Hays, J., Kukla, G. and Saltzman, B. (Editors), Milankovitch and Climate. Series C: Mathematical and Physical Sciences. D. Reidel Publishing Company, pp. 269-305.

Karlen, I., Olsson, I.U., Kallburg, P. and Kilici, S., 1968. Absolute determination of the activity of two ^{14}C dating standards. Arkiv Geofysik, 4, 465-471.

Laj, C., Kissel, C., Mazaud, A., Channell, J.E.T. and Beer, J., 2000. North Atlantic paleointensity stack since 75 ka (NAPIS-75) and the duration of the Laschamp event. Philosophical Transactions of the Royal Society A: Mathematical, Physical and Engineering Sciences, 358, 1,009-1,025.

Martínez-Méndez, G., 2005. Deep circulation around South Africa: Northern *vs* Southern Sources. M.S. Thesis, Universitat Autònoma de Barcelona, Cerdanyola, 100 pp.

Martínez-Méndez, G., Zahn, R., Hall, I.R., Pena, L.D. and Cacho, I., 2008. 345,000-year-long multi-proxy records off South Africa document variable contributions of Northern versus Southern Component Water to the Deep South Atlantic. Earth and Planetary Science Letters, 267 (1-2), 309-321.

Olsson, I.U., 1970. The use of Oxalic acid as a Standard. In: Olsson, I.U. (Editor), Radiocarbon Variations and Absolute Chronology, Nobel Symposium, 12th Proc. John Wiley & Sons, New York, pp. 17.

Pahnke, K. and Zahn, R., 2005. Southern Hemisphere Water Mass Conversion Linked with North Atlantic Climate Variability. Science, 307, 1,741-1,746.

Pahnke, K., Zahn, R., Elderfield, H. and Schulz, M., 2003. 340,000-year Centennial-Scale Marine Record of Southern Hemisphere Climatic Oscillation. Science, 301, 948-952.

Paillard, D., Labeyrie, L. and Yiou, P., 1996. Macintosh program performs time-series analysis. EOS, AGU, 77, 379.

Peeters, F.J.C., Acheson, R., Brummer, G.-J.A., de Ruijter, W.P.M., Schneider, R., Ganssen, G., Ufkes, M.E. and Kroon, D., 2004. Vigorous exchange between the Indian and Atlantic oceans at the end of the past five glacial periods. Nature, 438, 661-665.

Petit, J.R. et al., 1999. Climate and atmospheric history of the past 420,000 years from the Vostok ice core, Antarctica. Nature, 399, 429-436.

Rau, A.J., Rogers, J. and Chen, M.-T., 2006. Late Quaternary palaeoceanographic record in giant piston cores off South Africa, possibly including evidence of neotectonism. Quaternary International, 148 (1), 65-77.

Rau, A.J., Rogers, J., Lutjeharms, J.R.E., Giraudeau, J., Lee-Thorp, J.A., Chen, M.-T. and Waelbroeck, C., 2002. A 450-kyr record of hydrological conditions on the western Agulhas Bank Slope, south of Africa. Marine Geology, 180 (1-4), 183-201.

Roperch, P., Bonhommet, N. and Levi, S., 1988. Paleointensity of the earth's magnetic field during the Laschamp excursion and its geomagentic implications. Earth and Planetary Science Letters, 88, 209–219.

Shackleton, N.J., Hall, A. and Vincent, E., 2000. Phase relationships between millenial-scale events 64.000-24.000 years ago. Paleoceanography, 15 (6), 565-569.

Southon, J., Kashgarian, M., Fontugne, M., Metivier, B. and Yim, W.W.-S., 2002. Marine reservoir corrections for the Indian Ocean and Southeast Asia. Radiocarbon, 44 (1), 167-180.

Stuiver, M., 1980. Workshop on ^{14}C data reporting. Radiocarbon, 22, 964-966.

Stuiver, M. and Polach, H.A., 1977. Discussion reporting of 14C data. Radiocarbon, 19 (3), 355-365.

Voelker, A.H.L., Grootes, P.M., Nadeau, M.-J. and Sarnthein, M., 2000. Radiocarbon levels in the Iceland Sea from 25-53 ky and their link to the Earth´s magnetic Field intensity. Radiocarbon, 42 (3), 437-452.

Watanabe, O., Jouzel, J., Johnsen, S., Parrenin, F., Shoji, H. and Yoshida, N., 2003. Homogeneous climate variability across East Antarctica over the past three glacial cycles. Nature, 422, 509-512.

Wilson, C.J.N., Switsur, V.R. and Ward., A.P., 1988. A new ^{14}C age for the Oruanui (Wairakei) eruption, New Zealand. Geological Magazine, 125, 297-300.

Chapter 5.2

345,000-year-long Multi-Proxy Records off South Africa Document Variable Contributions of Northern *versus* Southern Component Water to the Deep South Atlantic

Abstract

Millennial to multi-centennial benthic foraminiferal stable isotope, sortable silt mean grain size ($\overline{SS}$) and benthic foraminiferal Cd/Ca records are presented for core MD96-2080 from 2488 m water depth at the western Agulhas Bank Slope off South Africa. The data demonstrate the interplay between northern and southern component waters as the Atlantic Meridional Overturning Circulation (MOC) shifted between glacial and interglacial modes. During early phases of Marine Isotope Stages (MIS) 6 and 8, the Atlantic MOC was little different from its interglacial mode. Benthic foraminiferal $\delta^{13}C$ modulation during these stages can be explained by mean ocean $\delta^{13}C$ changes, while, only subtle benthic foraminiferal Cd/Ca increases indicate a continued influence of Northern Component Waters (NCW). Later glacial stages are characterized by a progressive incursion of nutrient-enriched waters presumably a mixture of upper and lower Southern Component Water (SCW). Maximum $\overline{SS}$ values during middle glacial ventilation minima suggest increased near-bottom flow speeds. The combined ventilation and flow-speed pattern indicates an enhanced influence of SCW, most likely linked with a northward migration of the Antarctic Circumpolar Current (ACC) which progressively decreased the influence of NCW at site MD96-2080. Peak maximum seawater Cd concentrations (Cd_{sw}, derived from benthic foraminiferal Cd/Ca) overlap in time with increased deposition of ice-rafted debris (IRD) in the North Atlantic and plot outside the $\delta^{13}C/Cd_{sw}$ field in the South Atlantic. The anomalies conceivably are the South Atlantic equivalents of peak Cd_{sw} maxima associated with Heinrich-type events in the North Atlantic and reflect a substantially reduced Atlantic MOC.

5.2. 345,000-year-long Multi-Proxy Records off South Africa Document Variable Contributions of Northern *versus* Southern Component Water to the Deep South Atlantic

5.2.1. Introduction

The inter-ocean water exchange around the southern tip of Africa constitutes a key component of the global ocean thermohaline circulation (Gordon, 1986; Gordon et al., 1992; Weijer et al., 1999). Interest in the surface-ocean paleoceanography in this region has increased in recent years (e.g. Knorr and Lohmann, 2003; Peeters et al., 2004) but the evolution of the deep water circulation around South Africa has attracted less attention. Traditionally deep-water paleoceanographic records from the South Atlantic have been used to infer an interplay between North Atlantic Deep Water (NADW) and southern hemisphere water masses as a function of mode shifts in Atlantic Meridional Overturning Circulation (MOC) (e.g. Charles et al., 1996; Piotrowski et al., 2005). Many of these core sites are positioned within the advection pathway of lower deep water to bottom water levels containing a prominent contribution of Antarctic Bottom Water (AABW). We present a multi-proxy reconstruction that documents deep water variability in the southern South Atlantic at a water depth that is more prominently influenced by NADW than the records published previously from greater water depth. Our new records provide further insight into the variability of the Atlantic MOC from a region underrepresented in the global paleoceanographic data base.

5.2.2. Core Material

For this study we concentrate in the records generated for MD96-2080 which allow for inferences on past deep circulation schemes, i.e. benthic foraminiferal stable isotopes and Cd/Ca and the $\overline{SS}$ paleocurrent record. These records are shown in Figure 5.2-2. In this Figure, we also present a benthic $\delta^{13}C$ stack ($\delta^{13}C_{stack}$ panel B). This stack was used by Stüber (1999) and Zahn and Stüber (2002) to correct for changes in the marine carbon pool in time windows different to the LGM. Details about the development of the stack are given in the Annex I of Chapter 4. In the present study, the benthic $\delta^{13}C_{stack}$ has been used to correct for shifts in the mean ocean $\delta^{13}C$ signature along the past 345 kyr (see Sections 5.2.3 and 5.2.4).

The deep circulation records of MD96-2080 are compared to records from published data bases (Table 5.2-1) which are suitable to reconstruct past variations of Northern and Southern Component Waters (NCW, SCW). Figure 5.2-1 shows the geographical location of these records in the Atlantic Ocean; in the inset latitudinal sections the position of these cores in the water column are displayed for present and for Last Glacial Maximum (LGM) conditions.

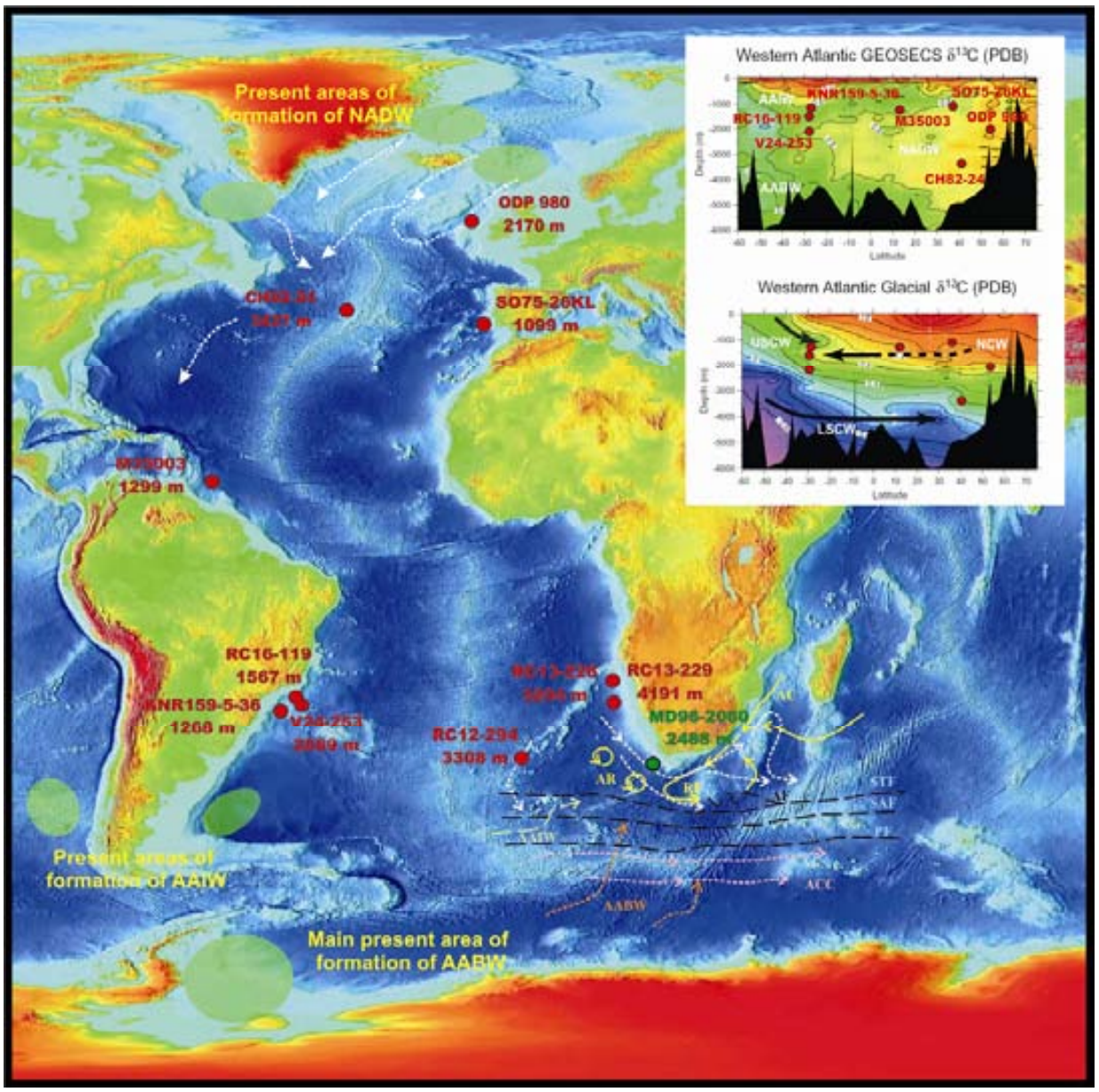

Figure 5.2-1 Location of MD96-2080 and reference cores (see Table 5.2-1). The main hydrographical features around South Africa are drawn in the Figure. Labels are Agulhas Current (AC), Agulhas Retroflection (RF), Agulhas Rings (AR), Antarctic Circumpolar Current (ACC), North Atlantic Deep Water (NADW), Antarctic Bottom Water (AABW), Antarctic Intermediate Water (AAIW), Subtropical Front (STF), Subantarctic Front (SAF), Agulhas Front (AF), and Polar Front (PF). The inset latitudinal sections display the location of the reference cores of the western side of the Atlantic in modern and LGM Labels are Antarctic Intermediate Water (AAIW), Antarctic Bottom Water (AABW), North Atlantic Deep Water (NADW), Upper and Lower Southern Component Water are indicated (USCW, LSCW), Northern Component Water (NCW). The main areas of formation of NADW, AAIW and AABW are shown by the green shading. Base map from National Geophysical Data Center and National Oceanic and Atmospheric Administration, http://www.ngdc.noaa.gov/).

North Atlantic cores ODP 980 (McManus et al., 1999), SO75-26KL (Willamowski and Zahn, 2000), CH82-24 (Boyle and Keigwin, 1985/86) have been used to investigate past changes in the depth of penetration of NCW and of northward extension of SCW during glacial times. Core M35003 (Zahn and Stüber, 2002) at intermediate depths, as well as intermediate depth cores from the Brazil Margin are at present under a strong influence of AAIW and allow inferences above shifts in the hydrographical characteristics of the upper water column. Cores V24-253 (Oppo and Horowitz, 2000), MD96-2080 (this study), RC13-228 and RC12-294 (Boyle, 1992; Rosenthal et al., 1997) are presently under a strong

influence of NADW while the deeper core RC13-229 (Oppo and Rosenthal, 1994) has been under a measurably contribution of SCW during glacial periods over the past 730 kyr (Oppo and Rosenthal, 1994).

Table 5.2-1 Core locations

Sediment core	Water depth (m)	Core location	Reference
ODP 980	2170	55°N, 14°W; North Atlantic	McManus et al. (1999)
SO75-26KL	1099	38ºN, 9.5ºW; Iberian Margin	Willamowski and Zahn (2000)
M35003	1299	12.5ºN, 61ºW; Tobago Basin	Zahn and Stüber (2002)
KNR159-5-36	1268	27.5ºS, 46.5ºW; Brazilian Margin	Oppo and Horowitz (2000); Came et al. (2003)
RC16-119	1567	28ºS, 46.5ºW; Brazilian Margin	Oppo and Horowitz (2000)
V24-253	2069	27°S, 45°W; Brazilian Margin	Oppo and Horowitz (2000)
MD96-2080	2488	36ºS, 19ºE; Agulhas Bank Slope	This study
RC13-228	3204	22ºS, 11ºE; Cape Basin	Boyle (1992); Rosenthal et al. (1997)
RC12-294	3308	37ºS, 10ºW; Central South Atlantic	Boyle (1992); Rosenthal et al. (1997)
CH82-24	3427	43ºN, 33ºW; Central North Atlantic	Boyle and Keigwin (1985/86)
RC13-229	4191	25.5ºS, 11ºE; Cape Basin	Oppo et al. (1990) Oppo and Rosenthal (1994)

5.2.3. MD96-2080 Deep Circulation Records

- **Benthic Foraminiferal Oxygen Isotopes**

The benthic foraminiferal $\delta^{18}O$ profile displays distinctive orbital modulation with additional sub-orbital variability (Fig. 5.2-2a). Due to disturbance of the uppermost core section the Holocene is not well developed in the record and thus, Termination I is not considered representative of the full glacial/interglacial isotopic amplitude. Benthic foraminiferal $\delta^{18}O$ shifts for the previous glacial Terminations are 1.96‰ (TII), 1.08‰ (TIII) and 1.66‰ (TIV). These $\delta^{18}O$ amplitudes are well in excess of the mean-ocean change of 0.8-1.1‰. that went along with global changes in ice volume and sea level during these climatic transitions (Schrag et al., 2002; Waelbroeck et al., 2002). The excess isotopic change therefore documents changes in deep water properties, i.e. temperature and seawater $\delta^{18}O$ (salinity) of ambient bottom water at the core site.

Amplitudes of orbital modulation along the record are reduced within interglacial intervals with sub-stage variation being less prominent than typically seen in benthic foraminiferal $\delta^{18}O$ records (e.g. Peeters et al., 2004; e.g. Pahnke and Zahn, 2005). For instance, MIS 5a-d sub-stages are barely visible while sub-stage MIS 7b is indistinguishable and MIS 7e does not reach full interglacial values. Benthic foraminiferal $\delta^{18}O$ values in the section prior to MIS 7e remain more positive when compared with other sediment cores in the region, by example the CBR spliced record (Peeters et al., 2004) (Fig. 5.2-2a) and South Atlantic ODP Site 1089 and TNO57-6 (Hodell et al., 2003) cores. These sites are between 1000 and 2000 m deeper in the water column so that the apparent discrepancy in benthic foraminiferal $\delta^{18}O$ may reflect genuine differences in the properties of the waters masses invading the

sites. Also notable is the enhanced variability in MD96-2080 of benthic foraminiferal $\delta^{18}O$ during Termination II that has been reproduced with replicate analyses.

- **Benthic Foraminiferal Carbon Isotopes**

Benthic foraminiferal $\delta^{13}C$ along MD96-2080 displays glacial-interglacial orbital modulation, with glacial levels depleted below interglacial values (Fig. 5.2-2b). Amplitude modulation is reduced in interglacial intervals, a feature noted in the MD96-2080 benthic foraminiferal $\delta^{18}O$ and also seen in other southern records (Hall et al., 2001; Holbourn et al., 2005; McCave et al., 2005; Pahnke and Zahn, 2005). Benthic foraminiferal $\delta^{13}C$ values along MD96-2080 remain more positive than in sediment cores from the Southern Ocean and South Atlantic sites that are within the advection pathway of AABW (Schmiedl et al., 1997; Mackensen, 2001; Hodell et al., 2003).

Since core-top sediments in MD96-2080 are not representative of modern water column $\delta^{13}C_{\Sigma CO2,}$ we compare core-top sediments of nearby core MD02-2594 (34º43′S, 17º20′E, 2440 m water depth) which are assumed to be modern in age to ambient bottom water $\delta^{13}C_{\Sigma CO2}$ from GEOSECS Stations 93 (41º46′ S, 18º27’ E) and 103 (24º00S, 8º30′E). Core-top MD02-2594 benthic foraminiferal $\delta^{13}C$ of +0.7‰ VPDB is similar to $\delta^{13}C_{\Sigma CO2}$ of +0.6‰ VPDB measured at both GEOSECS stations at this water depth (Ostlund et al., 1987). Applying a modern $\delta^{13}C_{\Sigma CO2}$ value of +0.6 to +0.7‰ VPDB it suggests glacial benthic foraminiferal $\delta^{13}C$ was depleted by 0.3 to 0.4‰ at the LGM which is close to the coeval mean-ocean $\delta^{13}C$ shift (Duplessy et al., 1988). Benthic foraminiferal $\delta^{13}C$ shifts across the MIS 6/5 and 8/7 transitions were 0.2 to 0.4‰, similar to the glacial-interglacial $\delta^{13}C$ amplitude displayed in a stacked benthic foraminiferal $\delta^{13}C$ record derived from sediment cores from the Atlantic, Indian and Pacific Oceans (Stüber, 1999; Zahn and Stüber, 2002) (Fig. 5.2-2b) (see Annex I of Chapter 4 for explanatory notes on $\delta^{13}C_{stack}$ record development). It is only during middle glacial MIS 6 and 8 (indicated by arrows on the figure) that depletions are larger than coeval shifts displayed in the $\delta^{13}C_{stack}$ record. Peak-negative $\delta^{13}C$ values reach levels 0.8‰ and 0.7‰ below benthic foraminiferal $\delta^{13}C$ of the subsequent interglacial periods and exceed the coeval $\delta^{13}C_{stack}$ amplitude by 0.5‰ and 0.3‰. A further prominent benthic foraminiferal $\delta^{13}C$ depletion event is recorded in MD96-2080 during MIS 7d, with values 0.4‰ lighter than coeval shifts in the $\delta^{13}C_{stack}$.

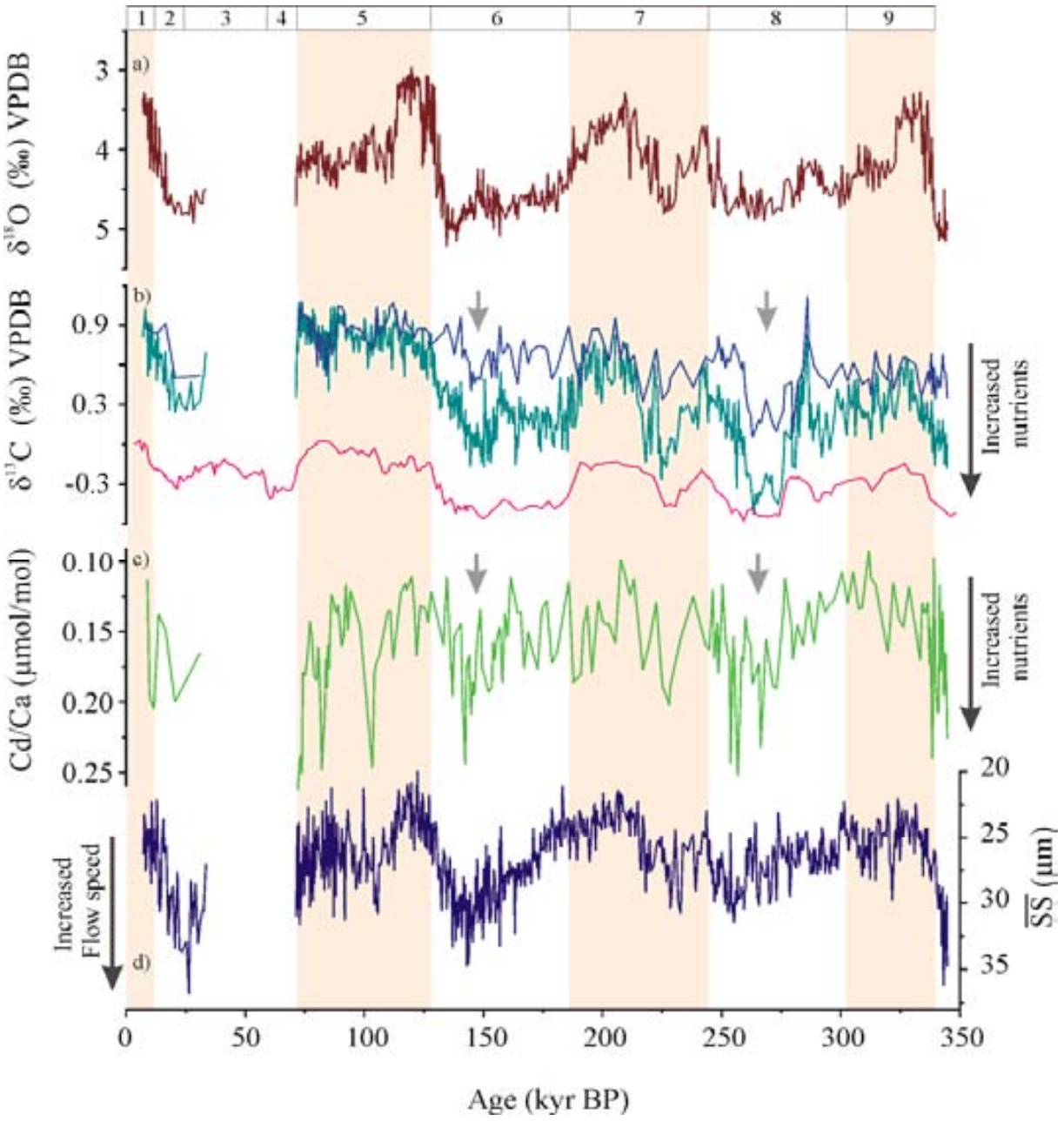

Figure 5.2-2 Stable isotope and Cd/Ca records of *F. wuellerstorfi* and the record of sortable silt. a) Benthic $\delta^{18}O$ (‰ VPDB) on the *Uvigerina* scale; b) (cyan) *F. wuellerstorfi* $\delta^{13}C$ (‰ VPDB) compared with the benthic $\delta^{13}C_{stack}$ (pink) (see Annex I of Chapter 4 for details). Blue record is the carbon-pool corrected epibenthic (*F. wuellerstorfi*) $\delta^{13}C$; c) *F. wuellerstorfi* Cd/Ca (µmol/mol) (see Fig. 5.2 Annex I-1 for same record with individual data points indicated); d) Sortable silt mean grain size (µm). Top bar displays Marine Isotope Stages. Vertical shading highlights interglacials. Grey arrows highlight strong $\delta^{13}C$ depletions and coeval Cd/Ca increases during middle glacials.

- **Benthic Foraminiferal Cd/Ca**

Benthic foraminiferal Cd/Ca displays glacial trends towards maximum values that are reached in middle stages of glacial periods, MIS 6 and 8 (Fig. 5.2-2c). During MIS 6 this trend contains recurrent excursions to minimum Cd/Ca ratios that approach interglacial levels. Applying a cadmium distribution coefficient (D_{Cd}) of 2.46 (Boyle, 1992), the down-core benthic foraminiferal Cd/Ca variation in MD96-2080 translates into equivalent seawater Cd concentrations (Cd_{sw}) of 0.37-0.81 nmol/kg (Fig. 5.2-3c) (excluding the short-lived maximum Cd/Ca excursions along the record) (see Chapter 4). This range of values remains above Cd_{sw} in modern unaltered NADW (Boyle, 1992) and

only marginally overlaps with glacial-interglacial Cd_{sw} ranges inferred at deep water core sites in the North Atlantic (Cdsw = 0.17-0.45 nmol/kg, Keigwin and Boyle, 1985; Cdsw = 0.17-0.45 nmol/kg, Boyle and Keigwin, 1985/86). Interglacial Cd_{sw} values (0.37-0.67 nmol/kg) at MD96-2080 encompass Cd_{sw} levels inferred at South Atlantic sites at >3000 m water depth (e.g. Cdsw = 0.34-0.69 nmol/kg, Boyle, 1992; Oppo and Rosenthal, 1994; Lea, 1995; Rosenthal et al., 1997) while they are elevated over Holocene values at west South Atlantic sites located around 2000-2500 m water depth (e.g. Cd_{sw} = 0.24-0.21 nmol/kg, Oppo and Horowitz, 2000). Elevated interglacial Cd_{sw} values suggest the presence at the MD96-2080 site of "aged" NADW possibly with contributions of Southern Component Water (SCW). Maximum Cd_{sw} values in excess of 1.0 nmol/kg are reached during brief excursions within MIS 5 and the middle parts of MIS 6 and 8. These maxima are single-point excursions (see Fig. 5.2 Annex I-1 to this Chapter) but we exclude possible contamination on the basis of Mn/Ca below 60 μmol/mol and Al/Ca values below 220 μmol/mol for all these samples. Similar elevated Cd/Ca values are known from other core sites in the northern and tropical Atlantic (see discussion below).

- **Sortable Silt Mean Grain Size ($\overline{SS}$)**

The $\overline{SS}$ paleocurrent record displays increased values in glacial sections (Fig. 5.2-2d). This reflects high near bottom flow speeds that fits with similar $\overline{SS}$ patterns reported from the Southwest Pacific (ODP Site 1123, 3290 m water depth; Hall et al., 2001) and the Agulhas Plateau (MD02-2589, 2660 m water depth; Molyneux et al., 2007) suggesting the pattern is representative of the circum-Antarctic region. In the lower section of the MD96-2080 record, before 250 ka, orbitally modulated amplitudes of $\overline{SS}$ change are reduced. The $\overline{SS}$ grain size range of 17 to 37 μm in core MD96-2080 is considerably larger than the range documented in the southwest Pacific (13-19 μm) by Hall et al. (2001) and at the southern Agulhas Plateau (19-24 μm) by Molyneux et al. (2007). McCave and Hall (2006) alluded to the particularly subtle way in which size distributions might be altered by sediment source-related signatures, through the fine tails of turbidity currents (see also Hall and McCave, 2000). While, in core MD96-2080, there is no visual evidence of major (i.e. turbidity current) down-slope deposition (Bertrand et al., 1997), an influence of down-slope deposition of fine material on the $\overline{SS}$ cannot entirely be disregarded. Rau et al. (2002) noted small but significant glacial increase in the lithogenic sand size fraction, suggesting either a likely source from the Antarctic ice sheet via iceberg transport, or from downslope transfer of upper slope and shelf material. Either way an associated delivery of a substantial amount of unsorted terrigenous silt could cryptically affect the $\overline{SS}$ proxy record. In several sections of core MD96-2080 we observe a correspondence between inferred high flow speed, elevated coarse fraction (>63μm, not shown but consisting of foraminiferal sand) abundance and low sedimentation rates which is consistent with our interpretation of a dominant current sorted influence. Therefore we remain confident that the MD96-2080 $\overline{SS}$ signal predominantly provides an indication of climate induced changes of near bottom current strength. The $\overline{SS}$ record suggests glacially increased

near-bottom flow is a persistent feature at high southern latitude locations, opposite to North Atlantic flow speed patterns (e.g. Hall and McCave, 2000).

5.2.4. Discussion

- **Northern *versus* Southern Component Waters**

Palaeocirculation studies draw a consistent picture that deep water convection in the last glacial North Atlantic was reduced to shallower depths (e.g. Boyle and Keigwin, 1985/86; Curry et al., 1988; Duplessy et al., 1988; Sarnthein et al., 1994) and lower rates (Rutberg et al., 2000; McManus et al., 2004; Piotrowski et al., 2005; Hall et al., 2006). Radiogenic isotopes (Yu et al., 1996) suggest southward advection of deep waters from the North Atlantic to the Southern Ocean at a rate similar to today while this contention has been challenged by numerical modelling (Marchal et al., 2000).

In the MD96-2080 benthic foraminiferal $\delta^{13}C$ record much of the depletion in early MIS 6 and 8 can be explained by mean ocean changes suggesting little change in chemical ventilation (Fig. 5.2-2b). Cd_{sw} at the same time indicates a progressive increase in nutrient concentrations (Fig. 5.2-2c). During MIS 6 (and lesser MIS 8) the trend of increasing Cd_{sw} is superimposed by suborbital variability with values sporadically dropping to full-interglacial levels suggesting episodic incursions of a more nutrient-depleted water mass, presumably NCW. Only in the middle sections of MIS 6 and 8 does benthic foraminiferal $\delta^{13}C$ drop to peak minimum values that coincide with maximum Cd_{sw} levels. This suggests the progression towards full-glacial water mass ventilation at site MD96-2080 was gradual, with additional suborbital oscillation visible in MIS 6.

To assess benthic foraminiferal $\delta^{13}C$ and Cd_{sw} data patterns in MD96-2080 in the framework of the Atlantic MOC we compare our records with similar records from other Atlantic core sites (Table 5.2-1). ODP Site 980 (McManus et al., 1999) is positioned within newly formed deep water in the North Atlantic and serves as a reference for NCW formation and ventilation. First we enhanced graphical correlation between the benthic foraminiferal $\delta^{18}O$ record of ODP Site 980 and MD96-2080 for better synchrony between them (see Fig. 5.2 Annex I-1) and then sampled both benthic foraminiferal $\delta^{13}C$ records at 2 kyr time steps to determine the north-south gradient (Figs. 5.2-3a-b). The gradient maximizes in the middle parts of MIS 6 and notably, of MIS 8 as $\delta^{13}C$ at ODP Site 980 remains positive while values at MD96-2080 drop to lower levels. Comparison of the north-south $\delta^{13}C$ gradient with Cd_{sw} at MD96-2080 (Figs. 5.2-3b-c) shows maximum gradients coincide with elevated Cd_{sw} that are indicative of enhanced nutrient concentrations in the south. Modulation of the $\delta^{13}C$ gradient from the south in conjunction with incursions of Cd_{sw} maxima at MD96-2080 either indicate reduced formation and southward advection of NCW, stronger northward advection of SCW, or some combination of both.

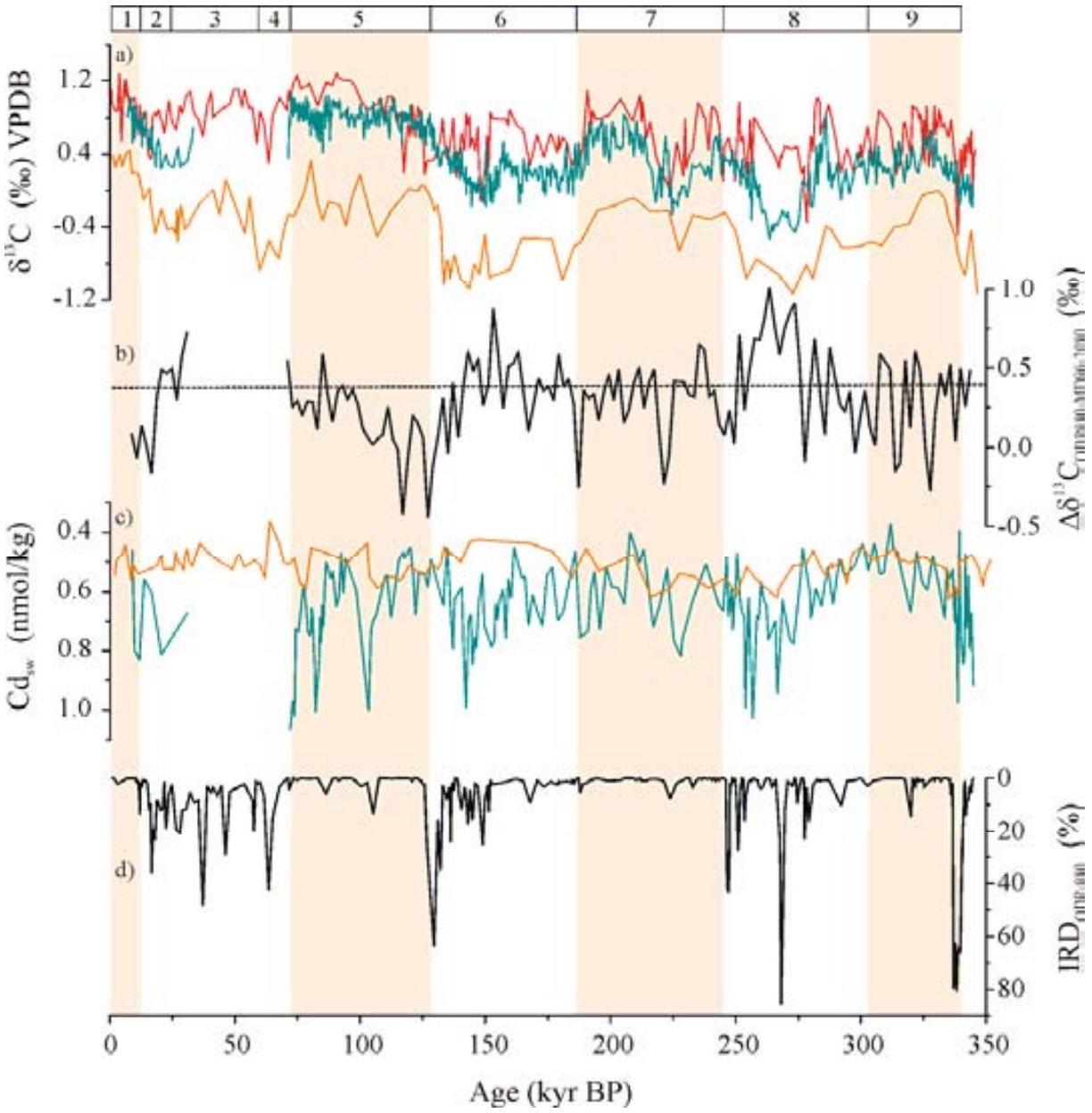

Figure 5.2-3 Individual benthic carbon isotope records, meridional carbon isotope gradient and seawater Cd compared with North Atlantic IRD abundance; a) Benthic $\delta^{13}C$ records (‰ VPDB) of MD96-2080 (cyan), North Atlantic ODP Site 980 (red, McManus et al. 1999) and Cape Basin core RC13-229 (orange, Oppo et al., 1990; Oppo and Rosenthal, 1994). Age models are synchronized with MD96-2080 (see Fig. 5.2 Annex I-1); b) $\delta^{13}C$ offset between MD96-2080 and Site 980. Dotted line denotes present $\delta^{13}C_{\Sigma CO2}$ gradient between the core sites as computed from GEOSECS Stations 93 (41º46′S, 18º27'E, 2597 m, 0.6‰ VPDB) and 23 (60º25′N, 18º37'W, 2241 m, 1.04‰ VPDB); c) Cd_{sw} records of MD96-2080 (cyan) and RC13-229 (orange) (see Fig. 5.2 Annex I-1); d) Ice-rafted debris (% IRD) record from ODP Site 980 (McManus et al., 1999).

Next we compare the MD96-2080 records with benthic $\delta^{13}C$ and Cd_{sw} records of core RC13-229 from the deep Cape Basin at 25ºS (Figs. 5.2-1, 5.2-3a and c) (Oppo and Fairbanks, 1987; Oppo et al., 1990; Oppo and Rosenthal, 1994; Lea, 1995). The Cd_{sw} record of RC13-229 was inferred from Cd/Ca applying a partition coefficient of 2.9 (Boyle, 1992). At 4191 m water depth the RC13-229 core likely remained under a variable but persistent influence of SCW. Benthic $\delta^{13}C$ values along RC13-229 are consistently 0.7-1.0‰ VPDB more negative than in MD96-2080 reflecting better ventilation of the upper water column. Cd_{sw} on the other hand are nearly identical in both cores during interglacial periods mimicking modern $(PO_4)^{3-}$ patterns (Fig. 3-11, Chapter 3). Similar

Cd_{sw} levels during early MIS 6 and 8 support our contention that deep ventilation was not substantially different at the initiation of glacial stages. Cd_{sw} values are increased at MD96-2080 over those at the deep core RC13-229 during middle glacial times (Figs. 5.2-3a and c) suggesting elevated nutrient content in the upper water column. Cd_{sw} in RC13-229 shows little glacial-interglacial variation which contrasts with high-amplitude benthic $\delta^{13}C$ shifts in the core. Taken at face value, this suggests nutrient-enriched water masses with positive $\delta^{13}C$ that prevailed at MD96-2080 did not reach the northerly and deeper site RC13-229.

An alternative explanation would be that benthic foraminiferal Cd/Ca at RC13-229 is underestimating glacial Cd_{sw} as a consequence of the invasion of bottom waters with lower carbonate ion concentration, either through dissolution of Cd bearing calcite (McCorkle et al., 1995) or through decreases of the D_{Cd} for cadmium uptake by the benthic foraminifera (e.g. Marchitto et al., 2000). While such influences cannot be ruled out, the Cd_{sw} and benthic foraminiferal $\delta^{13}C$ pattern suggests that MD96-2080 during middle glacials was prominently influenced by nutrient-laden SCW maintaining a positive $\delta^{13}C$ signature, presumably through air-sea gas exchange (Zahn and Keir, 1992; Charles et al., 1993). Increased glacial flow speeds as indicated by the $\overline{SS}$ record (Fig. 5.2-2d) are likewise consistent with a stronger influence of SCW as has been inferred from other $\overline{SS}$ records from high southern latitudes (Hall et al., 2001; Molyneux et al., 2007). If the RC13-229 data adequately reflect bottom water biogeochemistry low nutrient concentrations at this site during glacials suggest enhanced nutrient transfer to the upper cell of the Southern Ocean overturning from depths, steepening nutrient gradients between RC13-229 and MD96-2080. Topographically steered upwelling of ACC flow provides a mechanism for such deep-to-shallow nutrient transfer (Garabato et al., 2007).

A series of recurrent peak Cd_{sw} maxima is observed along MD96-2080 reaching levels of ~1 nmol/kg, about threefold higher than Holocene levels and 1.5-2 times higher than LGM values in the area (Boyle, 1992; Rosenthal et al., 1997; Oppo and Horowitz, 2000). Cd_{sw} anomalies of similar magnitude have been reported for the last glacial from equatorial and North Atlantic cores (Willamowski and Zahn, 2000; Zahn and Stüber, 2002; Rickaby and Elderfield, 2005) and coincide with Heinrich events when NCW formation experienced slowdown. Comparison with the IRD record from ODP Site 980 (McManus et al., 1999) on a synchronized time scale shows the Cd_{sw} excursions in MD96-2080 overlap with periods of elevated IRD abundance in the North Atlantic (Figs. 5.2-3c and d). This correlation holds for Cd_{sw} maxima during MIS 5a-d that coincide with modest IRD maxima at ODP 980 (McManus et al., 1999) and in SU90-03 in the North Atlantic (Chapman et al., 2000). We consider the overlap between IRD events in the North and Cd_{sw} peak maxima at MD96-2080 indicates a slowed Atlantic MOC that enabled SCW to exert influence on South Atlantic mid-depth nutrient inventories.

- **$\delta^{13}C$ - Cd_{sw} Fingerprinting**

Air-sea gas exchange in the Southern Ocean in conjunction with its thermodynamic imprint on carbon isotope fractionation decouples $\delta^{13}C$ regionally from global nutrient stoichiometry (Broecker and Maier-Reimer, 1992; Zahn and Keir, 1992). Benthic foraminiferal Cd/Ca is linked with biological nutrient cycling but is not influenced by air-sea exchanges and constitutes a more conservative nutrient proxy (Boyle, 1988). Paired benthic foraminiferal Cd/Ca and $\delta^{13}C$ therefore enables to derive the offset between measured benthic foraminiferal $\delta^{13}C$ and a $\delta^{13}C$ signal predicted from biological nutrient cycling ($\delta^{13}C_{bio}$) that can be estimated from Cd/Ca (or Cd_{sw}) using nutrient stoichiometry (Lynch-Stieglitz and Fairbanks, 1994; Lynch-Stieglitz et al., 1996; Marchitto and Broecker, 2006) (see Chapter 4.4. for details about the computational scheme).

We use proxy-proxy diagrams to plot sediment core $\delta^{13}C/Cd_{sw}$ coordinates together with $\delta^{13}C_{as}$ fractionation isolines and water mass end-member $\delta^{13}C/Cd_{sw}$ from published data bases (Fig. 5.2-4, Tables 5.2-1 to 3). Cd_{sw} has been derived from benthic foraminiferal Cd/Ca using Boyle's (1992) partition coefficients. $\delta^{13}C_{as}$ isolines are computed using Holocene parameterization and $\delta^{13}C$ core data are corrected for mean-ocean $\delta^{13}C$ shifts using the $\delta^{13}C_{stack}$ record (see above) i.e., glacial and interglacial data are carbon-pool corrected and normalized to Holocene levels. Water mass end-member values are given for Holocene and LGM (see Table 5.2-2 for references) but we note that these values may have been slightly different during previous glacials and interglacials (e.g. Raymo et al., 2004). This approach is compatible with LGM data distributions using non-corrected LGM $\delta^{13}C$ and $\delta^{13}C_{as}$ fractionation lines computed from glacial-maximum parameterization (Figure 6 in Marchitto and Broecker, 2006).

Table 5.2-2 $\delta^{13}C_{\Sigma CO2}$ and Cd_{sw} values of modern and glacial Atlantic water mass endmembers

Water mass	$\delta^{13}C_{\Sigma CO2} \pm 1\sigma$, n (‰ PDB)	$Cd_{sw} \pm 1\sigma$, n (nmol/kg)	Data source	Reference
Modern		**derived from $(PO_4)^{3-}$**	**Atlantic GEOSECS Stations**[2]	
NADW	0.98±0.09, 36	0.22 ± 0.01, 112	60-50ºN; 19ºE-43ºW; 1.5-3 km	1
AAIW	0.73 ± 0.29, 10	0.62 ± 0.51, 33	33-55ºS; 21-55ºW; 0.75-1.1 km	1
AABW	0.55 ± 0.16, 14	0.64 ± 0.02, 82	45-60ºS; 11ºE-66ºW; 6.5-4 km	1
Glacial [1]		**derived from benthic Cd/Ca**	**LGM benthic data**	
NCW	1.75 ± 0.2, 11	0.24 ± 0.1, 12	20º-65ºN; 1000-2000 m water depth	2-7
USCW	1.08 ± 0.31, 4	0.69 ± 0.13, 4	Off Tasmania, 800-1500 m water depth	8
LSCW	-0.48 ± 0.15, 8	0.70 ± 0.1	Southern Ocean, > 3000 m water depth, and data extrapolation [3]	7,9

[1] Glacial $\delta^{13}C_{\Sigma CO2}$ data are corrected for carbon pool changes by adding 0.32‰. No reservoir correction is applied to glacial Cd_{sw} (Boyle, 1988).
References used are (1) Ostlund et al., (1987); (2) Boyle (1992); (3) Bertram et al. (1995); (4) Willamowski and Zahn (2000); (5) Marchitto et al. (1998); (6) Rickaby et al. (2000); (7) Marchitto and Broecker (2006); (8) Lynch-Stieglitz et al. (1996); (9) Ninnemann and Charles (2002).
[2] To compute the $\delta^{13}C$ signature and the Cd_{sw} concentration of NADW, $\delta^{13}C_{\Sigma CO2}$ data below 0.7‰ was consider as not representative of this water mass and neglected. Similarly, to compute the $\delta^{13}C$ signature and the Cd_{sw} concentration of AABW, data from stations with measured potential temperature above 0.5ºC were not considered.
[3] $\delta^{13}C$ derived from benthic data; Cd_{sw} extrapolated using Atlantic $\delta^{13}C/Cd_{sw}$ relation from Figure 6 in Marchitto and Broecker (2006).

Table 5.2-3a Interglacial $\delta^{13}C_{\Sigma CO2}$ and Cd_{sw} values from Atlantic sediment cores [1,2]

Sediment core	Holocene $\delta^{13}C \pm 1\sigma$, n (‰ VPDB)	Holocene $Cd_{sw} \pm 1\sigma$, n (nmol/kg)	MIS 5e $\delta^{13}C \pm 1\sigma$, n (‰ VPDB)	MIS 5e $Cd_{sw} \pm 1\sigma$, n (nmol/kg)	MIS7a $\delta^{13}C \pm 1\sigma$, n (‰ VPDB)	MIS 7a $Cd_{sw} \pm 1\sigma$, n (nmol/kg)	MIS 9c $\delta^{13}C \pm 1\sigma$, n (‰ VPDB)	MIS 9c $Cd_{sw} \pm 1\sigma$, n (nmol/kg)
SO75-26KL	-	-	-	-	-	-	-	-
M35003	0.98 ± 0.25; 3	0.47 ± 0.1; 3	-	-	-	-	-	-
KNR159-5-36[3]	1.14	0.5	-	-	-	-	-	-
RC16-119[3]	1.1	0.41	-	-	-	-	-	-
V24-253[3]	1.1	0.24	-	-	-	-	-	-
MD96-2080	-	-	0.86 ± 0.015; 5	0.58 ± 0.06; 5	0.79 ± 0.1; 5	0.56 ± 0.04; 4	0.66 ± 0.1; 6	0.56 ± 0.06; 6
RC13-228[3]	0.5	0.34	-	-	-	-	-	-
RC12-294[3]	0.81	0.44	-	-	-	-	-	-
CH82-24	1.19 ± 0.12; 4	0.23 ± 0.02; 4	1.13 ± 0.17; 5	0.31 ± 0.04; 5	1.05 ± 0.1; 6	0.25 ± 0.03; 7	-	-
RC13-229	0.36 ± 0.07; 7	0.51 ± 0.04; 7	0.16 ± 0.1; 4	0.53 ± 0.03; 2	-0.01 ± 0.07; 3	0.50 ± 0.04; 2	0.18 ± 0.1; 4	0.50 ± 0.03; 2

Table 5.2-3b Glacial $\delta^{13}C_{\Sigma CO2}$ and Cd_{sw} values from Atlantic sediment cores [1,2]

Sediment core	LGM $\delta^{13}C \pm 1\sigma$, n (‰ VPDB)	LGM $Cd_{sw} \pm 1\sigma$, n (nmol/kg)	Middle MIS 6 $\delta^{13}C \pm 1\sigma$, n (‰ VPDB)	Middle MIS 6 $Cd_{sw} \pm 1\sigma$, n (nmol/kg)	Early MIS 6 $\delta^{13}C \pm 1\sigma$, n (‰ VPDB)	Early MIS 6 $Cd_{sw} \pm 1\sigma$, n (nmol/kg)	Middle MIS 8 $\delta^{13}C \pm 1\sigma$, n (‰ VPDB)	Middle MIS 8 $Cd_{sw} \pm 1\sigma$, n (nmol/kg)	Early MIS 8 $\delta^{13}C \pm 1\sigma$, n (‰ VPDB)	Early MIS 8 $Cd_{sw} \pm 1\sigma$, n (nmol/kg)
SO75-26KL	1.99 ± 0.03; 4	0.13 ± 0.04; 4	-	-	-	-	-	-	-	-
M35003	1.55 ± 0.1; 5	0.30 ± 0.07; 6	-	-	-	-	-	-	-	-
KNR159-5-36[3]	0.88	0.4	-	-	-	-	-	-	-	-
RC16-119[3]	1.31	0.29	-	-	-	-	-	-	-	-
V24-253[3]	0.8	0.42	-	-	-	-	-	-	-	-
MD96-2080	-	-	0.50 ± 0.1; 6	0.72 ± 0.1; 6	0.66 ± 0.1; 7	0.64 ± 0.1; 7	0.22 ± 0.1; 10	0.68 ± 0.1; 9	0.54 ± 0.1; 7	0.481 ± 0.07; 7
RC13-228[3]	0.01	0.36	-	-	-	-	-	-	-	-
RC12-294[3]	0.09	0.51	-	-	-	-	-	-	-	-
CH82-24	0.75 ± 0.08; 4	0.36 ± 0.03; 4	0.57 ± 0.2; 9	0.37 ± 0.04; 9	0.90 ± 0.2; 8	0.32 ± 0.03; 8	-	-	-	-
RC13-229	-0.075 ± 0.2; 5	0.50 ± 0.02; 5	-0.42 ± 0.1; 9	0.46 ± 0.3; 6	-0.1 ± 0.04; 2	0.45 ± 0.02; 2	-0.46 ± 0.2; 5	0.52 ± 0.05; 4	-0.26 ± 0.05; 5	0.495 ± 0.04; 4

[1] All data are carbon pool corrected.
[2] For data sources see references in Table 4.2-1.
[3] Data are compiled in Tables 1 and 3 in Marchitto and Broecker (2006) from published sources.

The Holocene $\delta^{13}C/Cd_{sw}$ coordinates of North Atlantic cores (CHN82-24, SO75-26KL) plot close to the northern endmember reflecting the influence of NADW at these sites (Fig. 5.2-4) (Boyle and Keigwin, 1985/86; Willamowski and Zahn, 2000). NADW is also recorded at South Atlantic cores V24-253 (Oppo and Horowitz, 2000) and RC13-228 (Boyle, 1992; Rosenthal et al., 1997). $\delta^{13}C/Cd_{sw}$ of mid-depth core M35003 from the western tropical Atlantic mirrors the influence of AAIW at this location (Zahn and Stüber, 2002) which is also seen in cores KNR159-5-36 (Oppo and Horowitz, 2000; Came et al., 2003) and RC16-119 (Oppo and Horowitz, 2000) from the upper Brazilian Margin.

The Holocene section of MD96-2080 is compromised by coring disturbance and is not used in this compilation. Instead we plot $\delta^{13}C/Cd_{sw}$ coordinates of interglacials MIS 5, 7 and 9. The modern *T-S* field at MD96-2080 indicates the presence of NADW and AABW that are mixing at a ratio of roughly 70:30. $\delta^{13}C/Cd_{sw}$ coordinates of MIS 5, 7, and 9 are shifted to Cd_{sw} values slightly higher than expected from mixing reflecting water mass chemical "aging". Interglacial $\delta^{13}C/Cd_{sw}$ coordinates of core RC13-229 from the deep Cape Basin likewise are shifted away from a conservative mixing line between AABW and NADW towards "aged" values.

$\delta^{13}C/Cd_{sw}$ coordinates of MIS 6 and 8 from MD96-2080 plot close to the $\delta^{13}C_{as}$ fractionation line of NCW in the north potentially indicating the presence of an aged NCW. This probably was the case during the early glacial stages when nutrient levels were only slightly increased. Middle glacial $\delta^{13}C/Cd_{sw}$ are increased in nutrients and directly plot on the mixing line between Upper and Lower Southern Component Water (USCW and LSCW) (Fig. 5.2-4b). We consider this an indication of a prominent influence of SCW at the core location during advance glacial stages with the $\delta^{13}C_{as}$ signature of MD96-2080 being a result of mixing between USCW and LSCW. This corroborates the meridional gradient in $\delta^{13}C$ across the Atlantic (see above) and supports our contention of a contribution of positive $\delta^{13}C$ to the core site from USCW. LGM data from the Brazilian Margin fit with this interpretation as they indicate NCW at approximately 1500 m and nutrient enriched SCW above and below (Oppo and Horowitz, 2000). Deep (>3000 m) South Atlantic data cluster close to the LSCW endmember confirming the invasion at depth of the basin by LSCW with a negative $\delta^{13}C_{as}$ signature, and therefore, supporting the contrasting pattern in $\delta^{13}C$ and Cd_{sw} between RC13-229 and MD96-2080.

Recurrent peak-maximum Cd_{sw} anomalies along MD96-2080 plot substantially outside the $\delta^{13}C/Cd_{sw}$ field defined by glacial end-embers and sediment core data and are shifted to elevated $\delta^{13}C_{as}$ levels of +1-1.5‰. This mimics data patterns observed for Heinrich events in the North Atlantic (Willamowski and Zahn, 2000; Zahn and Stüber, 2002; Rickaby and Elderfield, 2005) confirming the suggestion that the Cd_{sw} anomalies at MD96-2080 are the South Atlantic equivalents of peak Cd_{sw} maxima associated with H-type IRD events in the North Atlantic and a substantially reduced Atlantic MOC.

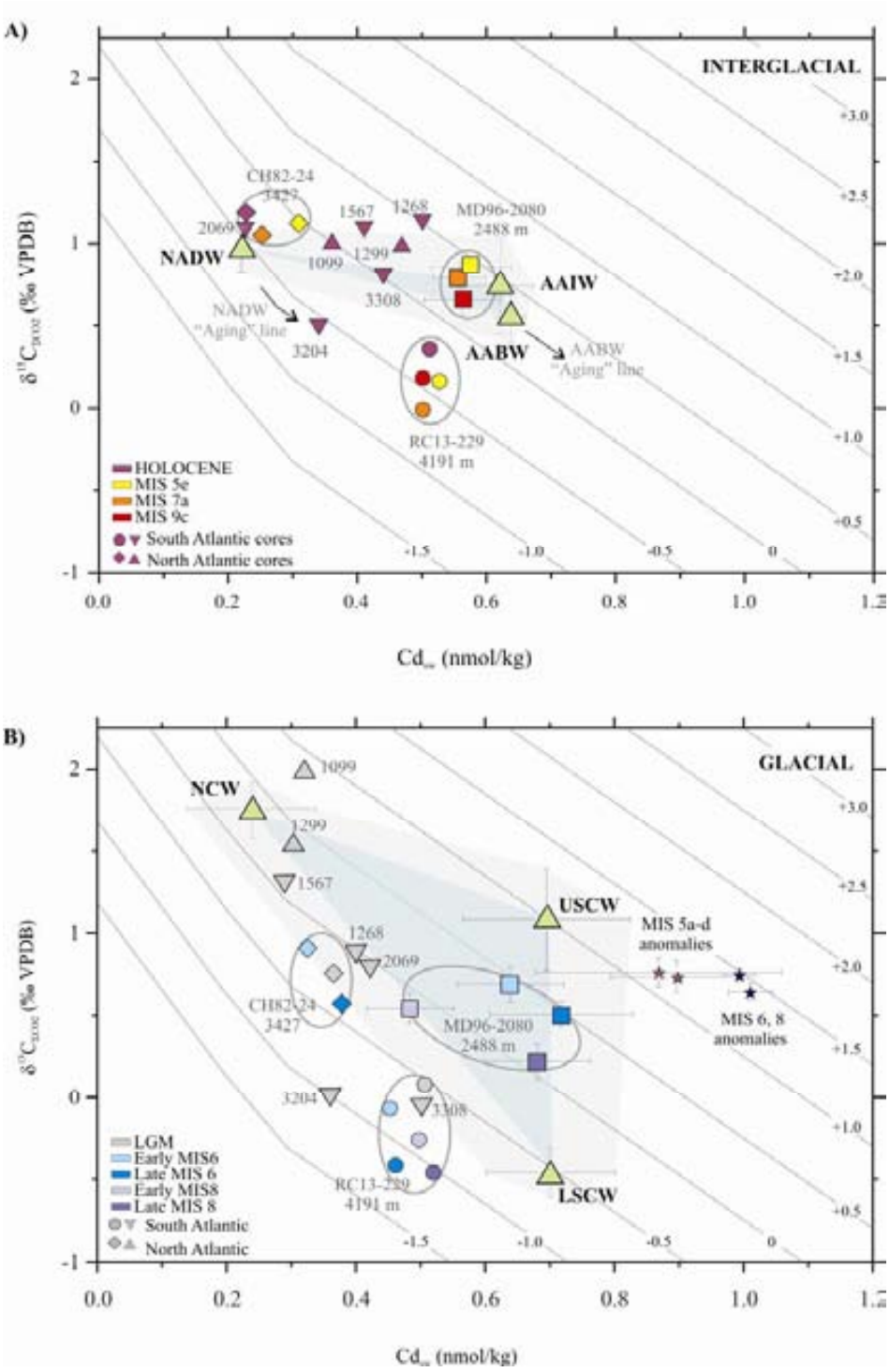

Figure 5.2-4 Proxy-proxy diagrams displaying Cd_{sw} and $\delta^{13}C$ data from core MD96-2080 and reference cores. $\delta^{13}C_{as}$ isolines are computed using modern parameterization (Lynch-Stieglitz and Fairbanks, 1994; Lynch-Stieglitz et al., 1996) (see Chapter 4 for details). Glacial and interglacial sediment core $\delta^{13}C$ data are carbon-pool corrected to account for shifts in the marine carbon reservoir isotope signature. All data hence are normalized to Holocene level. Mixing fields between endmembers are highlighted with blue shading; faint shading indicates mixing field applying standard deviations (1σ) of endmember means. A) Interglacial Cd_{sw} versus $\delta^{13}C$ means from Atlantic sediment cores CH82-24 (diamonds, Boyle and Keigwin, 1985/86), SO75-26KL, M35003 (inverted triangles, Willamoski and Zahn, 2000; Zahn and Stüber, 2002), KNR159-5-36, RC16-119, V24-253, RC12-294, RC13-228 (triangles, Boyle et al., 1992; Rosenthal et al., 1997; Oppo and Horowitz, 2000; Came et al., 2003), RC13-229 (circles, Oppo et al., 1990; Oppo and Rosenthal, 1994) and MD96-2080 (squares). Water mass endmembers (green triangles) are North Atlantic Deep Water (NADW), Antarctic Intermediate Water (AAIW), and Antarctic Bottom Water (AABW) (see also Table 5.2-2). B) Same as in A but for glacials. Endmembers are Northern Component Water (NCW), Upper and Lower Southern Component Water (USCW, LSCW) (see also Table 5.2-2). The cluster of elevated Cd_{sw} values >0.8 nmol/kg represents peak-maximum Cd_{sw} anomalies observed in MD96-2080 during MIS 5a-d (brown) and middle MIS 6 and 8 (navy). Error bars for MD96-2080 data (1σ) combine analytical reproducibility and standard deviation of means. Uncertainty (standard deviation) associated with the Cd partition coefficient (D_{Cd}) between benthic Cd/Ca and Cd/Ca in seawater of 2.9 ± 0.6 (Boyle, 1988) is not included.

5.2.5. Conclusions

High resolution benthic foraminiferal stable isotope, Cd/Ca and $\overline{SS}$ profiles from IMAGES core MD96-2080 record changes in past modes of ocean circulation in the South Atlantic. Benthic foraminiferal $\delta^{13}C$ and Cd/Ca display prominent orbital modulation with lower $\delta^{13}C$ and elevated Cd/Ca during glacial periods while the $\overline{SS}$ profile records elevated values suggesting higher near-bottom flow speeds at the same time when chemical ventilation was reduced. Transitions from interglacial to glacial modes of ventilation are gradual in the benthic $\delta^{13}C$ and Cd/Ca records with ventilation during the early phase of glacials MIS 6 and 8 similar to interglacial conditions. Substantial reduction in ventilation is then recorded during middle stages of these glacial periods when southward advection of NCW was weakened as is indicated by maximum Cd_{sw} (inferred from benthic Cd/Ca) and minimum benthic foraminiferal $\delta^{13}C$. We conclude that the high-latitude South Atlantic increasingly came under the influence of SCW during middle glacial periods likely in conjunction with northward expansion of the fast flowing ACC. Benthic foraminiferal $\delta^{13}C$ remains more positive than at core sites in the deep Cape Basin while Cd_{sw} indicates higher nutrient concentrations during middle glacials at MD96-2080. From this we infer an influence of air-sea gas exchange on $\delta^{13}C$ pointing at a contribution of upper SCW similar to modern-day AAIW.

Recurrent Cd_{sw} peak maxima in MD96-2080 overlap in time with increased deposition of IRD in the North Atlantic and plot outside the $\delta^{13}C/Cd_{sw}$ field for water mass mixing in the South Atlantic. Overlap between IRD events in the North and Cd_{sw} maxima at MD96-2080 suggests the Atlantic MOC was substantially reduced at these times, similar to the 'collapsed' state of MOC during Heinrich events of the last glacial.

References

Bertram, C.J., Elderfield, H., Shackleton, N.J. and MacDonald, J.A., 1995. Cadmium/calcium and carbon isotope reconstructions of the glacial northeast Atlantic Ocean. Paleoceanography, 10 (3), 563-578.

Bertrand, P. et al., 1997. Les rapport de campagne à la mer à bord du Marion Dufresne - Campagne Nausicaa - IMAGES II - MD105 du 20/10/96 au 25/11/96. Institut Francais pour la Recherche et la technologie Polaires.

Boyle, E.A., 1988. Cadmium: Chemical Tracer of Deep-water Paleoceanography. Paleoceanography, 3 (4), 431-489.

Boyle, E.A., 1992. Cadmium and $\delta^{13}C$ paleochemical ocean distributions during the stage 2 glacial maximum. Annual Review of Earth and Planetary Sciences, 20, 245-287.

Boyle, E.A. and Keigwin, L.D., 1985/86. Comparison of Atlantic and Pacific paleochemical records for the last 215,000 years: changes in deep ocean circulation and chemical inventories. Earth and Planetary Science Letters, 76 (1-2), 135-150.

Broecker, W.S. and Maier-Reimer, E., 1992. The influence of air and sea exchange on the carbon isotope distribution in the sea. Global and Biogeochemical Cycles, 6 (3), 315-320.

Came, R.E., Oppo, D.W. and Curry, W.B., 2003. Atlantic Ocean circulation during the Younger Dryas: Insights from a new Cd/Ca record from the western subtropical South Atlantic. Paleoceanography, 18 (4), 1086, doi: 10.1029/2003PA000888.

Curry, W.B., Duplessy, J.C., Labeyrie, L.D. and Shackleton, N.J., 1988. Changes in the distribution of $\delta^{13}C$ of deep water ΣCO_2 between the last glaciation and the Holocene. Paleoceanography, 3 (3), 317-341.

Charles, C.D., Wright, J.D. and Fairbanks, R.G., 1993. Thermodynamic influences on the marine carbon isotope record. Paleoceanography, 8 (6), 691-698.

Charles, C.D., Lynch-Stieglitz, J., Ninnemann, U.S. and Fairbank, R.G., 1996. Climate connections between the hemispheres revealed by deep sea sediment core/ice core correlations. Earth and Planetary Science Letters, 142 (1-2), 19-27.

Duplessy, J.-C., Shackleton, N.J., Fairbanks, R.G., Labeyrie, L., Oppo, D.W. and Kallel, N., 1988. Deepwater source variations during the last climatic cycle and their impact on the global deepwater circulation. Paleoceanography, 3 (3), 343-360.

Garabato, A.C.N., Stevens, D.P., Watson, A.J. and Roether, W., 2007. Short-circuiting of the overturning circulation in the Antarctic Circumpolar Current. Nature, 447, 194-197.

Gordon, A., 1986. Inter-Ocean exchange of thermocline water. Journal of Geophysical Research, 91 (C4), 5,037-5,046.

Gordon, A.L., Weiss, R.F., Smethie, J.W.M. and Warner, M.J., 1992. Thermocline and intermediate water communication between the South Atlantic and Indian Oceans. Journal of Geophysical Research, 97, 7,223-7,240.

Hall, I.R. and McCave, I.N., 2000. Palaeocurrent reconstruction, sediment and thorium focusing on the Iberian margin over the last 140 ka. Earth and Planetary Science Letters, 178 (1-2), 151-164.

Hall, I.R., McCave, N., Shackleton, N.J., Weedon, G.P. and Harris, S.E., 2001. Intensified deep Pacific inflow and ventilation in Pleistocene glacial times. Nature, 412, 809-813.

Hall, I.R., Moran, S.B., Zahn, R., Knutz, P.C., Shen, C.-C. and Edwards, R.L., 2006. Accelerated drawdown of meridional overturning in the late-glacial Atlantic triggered by transient pre-H event freshwater perturbation. Geophysical Research Letters, 33, L16616 doi: 10.1029/2006GL026239.

Hodell, D.A., Venz, K., Charles, C.D. and Ninnemann, U.S., 2003. Pleistocene vertical carbon isotope and carbonate gradients in the South Atlantic sector of the Southern Ocean. Geochemistry, Geophysics, Geosystems, 4 (1), 1004, doi:10.1029/2002GC000367.

Holbourn, A., Kuhnt, W., Kawamura, H., Jian, Z., Grotes, P., Erlenkeuser, H. and Xu, J., 2005. Orbitally paced paleoproductivity variations in the Timor Sea and Indonesian Throughflow variability during the last 460 ky. Paleoceanography, 20, PA3002, doi: 10.1029/2004PA001094.

Keigwin, L.D. and Boyle, E.A., 1985. Carbon isotopes in deep-sea benthic foraminifera: precession and low latitude changes in biomass. In: E. Sundquist and W.S. Broecker (Editors), The carbon cycle and atmospheric CO_2: Natural variations archean to present; Proceedings of the Chapman Conference on Natural Variations in Carbon Dioxide and the Carbon Cycle. Tarpon Springs, FL, Jan, pp. 319-329.

Knorr, G. and Lohmann, G., 2003. Southern Origin for the resumption of Atlantic thermohaline circulation during deglaciation. Nature, 424, 532-536.

Lea, D.W., 1995. A trace metal perspective on the evolution of Antarctic Circumpolar Deep Water Chemistry. Paleoceanography, 10 (4), 733-748.

Lynch-Stieglitz, J. and Fairbanks, R.G., 1994. A conservative tracer for glacial ocean circulation from carbon isotope and paleonutrient measurements in benthic foraminifera. Nature, 369, 308-310.

Lynch-Stieglitz, J., van Geen, A. and Fairbanks, R.G., 1996. Interocean exchange of Glacial North Atlantic Intermediate Water: evidence from the subantarctic Cd/Ca and carbon isotope measurements. Paleoceanography, 11 (2), 191-201.

Mackensen, A., 2001. Oxygen and carbon stable isotope tracers of Weddell Sea water masses: new data and some paleoceanographic implications. Deep Sea Research, 48 (6), 1401-1422.

Marchitto, T.M. and Broecker, W.S., 2006. Deep water mass geometry in the glacial Atlantic Ocean: A review of constraints from the paleonutrient proxy Cd/Ca. Geochemistry, Geophysics, Geosystems, 7, Q12003, doi:10.1029/2006GC001323.

Marchitto, T.M., Curry, W.B. and Oppo, D., 1998. Millennial-scale changes in North Atlantic circulation since the last glaciation. Nature, 393, 557-561.

Marchitto, T.M., Curry, W.B. and Oppo, D.W., 2000. Zn concentrations in benthic foraminifera reflect seawater chemistry. Paleoceanography, 15 (3), 299-306.

McCave, I.N. and Hall, I.R., 2006. Size sorting in marine muds: Processes, pitfalls, and prospects for paleoflow-speed proxies. Geochemistry, Geophysics, Geosystems, 7, Q10N05, doi: 10.1029/2006GC001284.

McCave, I.N., Kiefer, T., Thornalley, D.J.R. and Elderfield, H., 2005. Deep flow in the Madagascar-Mascarene Basin over the last 150,000 years. Philosophical Transactions of the Royal Society of London, Series A: Physical Sciences and Engineering, 363 (1826), 81-99.

McCorkle, D.C., Martin, P.A., Lea, D.W. and Klinkhammer, G.P., 1995. Evidence of a dissolution effect on benthic foraminiferal shell chemistry: $\delta^{13}C$, Cd/Ca, Ba/Ca, and Sr/Ca results from the Ontong Java Plateau. Paleoceanography, 10 (4), 699-714.

McManus, J.F., Oppo, D.W. and Cullen, J.L., 1999. A 0.5-Million-Year Record of Millennial-Scale Climate Variability in the North Atlantic. Science, 283, 971-975.

McManus, J.F., Francois, R., Gherardi, J.-M., Keigwin, L.D. and Brown-Leger, S., 2004. Collapse and rapid resumption of Atlantic meridional circulation linked to deglacial climate changes. Nature, 428, 834-837.

Molyneux, E.G., Hall, I.R., Zahn, R. and Diz, P., 2007. Deep water variability on the southern Agulhas Plateau: Interhemispheric links over the past 170 ka. Paleoceanography, 22, PA4209, doi: 10.1029/2006PA001407.

Ninnemann, U.S. and Charles, C.D., 2002. Changes in the mode of Southern Ocean circulation over the last glacial cycle revealed by foraminiferal stable isotopic variability. Earth and Planetary Science Letters, 201 (2), 383-396.

Oppo, D.W. and Fairbanks, R.G., 1987. Variability in the deep and intermediate water circulation of the Atlantic Ocean during the past 25,000 years: Northern Hemisphere modulation of the Southern Ocean. Earth and Planetary Science Letters, 86, 1-15.

Oppo, D.W. and Rosenthal, Y., 1994. Cd/Ca changes in a deep Cape Basin core over tyhe past 730,000 years: response of circumpolar deepwater variability to northern hemisphere ice sheet melting? Paleoceanography, 9 (5), 661-675.

Oppo, D.W. and Horowitz, M., 2000. Glacial deep water geometry: South Atlantic benthic foraminiferal Cd/Ca and $\delta^{13}C$ evidence. Paleoceanography, 15 (2), 147-160.

Oppo, D.W., Fairbanks, R.G., Gordon, A.L. and Shackleton, N.J., 1990. Late Pleistocene Southern Ocean $\delta^{13}C$ variability: North Atlantic Deep Water modulation of atmospheric CO_2. Paleoceanography, 5, 43-55.

Ostlund, H.G., Craig, H., Broecker, W.S. and Spencer, D., 1987. Geosecs Atlantic, Pacific, and Indian Ocean Expeditions. Shorebased data and Graphics. National Science Foundation, 7.

Pahnke, K. and Zahn, R., 2005. Southern Hemisphere Water Mass Conversion Linked with North Atlantic Climate Variability. Science, 307, 1,741-1,746.

Peeters, F.J.C., Acheson, R., Brummer, G.-J.A., de Ruijter, W.P.M., Schneider, R., Ganssen, G., Ufkes, M.E. and Kroon, D., 2004. Vigorous exchange between the Indian and Atlantic oceans at the end of the past five glacial periods. Nature, 438, 661-665.

Piotrowski, A.M., Goldstein, S.L., Hemming, S.R. and Fairbanks, R.G., 2005. Temporal Relationships of Carbon Cycling and Ocean Circulation at Glacial Boundaries. Science, 307, 1,933-1,938.

Raymo, M.E., Oppo, D.W., Flower, B.P., Hodell, D.A., McManus, J.F., Venz, K.A., Kleiven, K.F. and McIntyre, K., 2004. Stability of North Atlantic water masses in face of pronounced climate variability during the Pleistocene. Paleoceanography, 19, PA2008, doi: 10.1029/2003PA000921.

Rickaby, R.E.M. and Elderfield, H., 2005. Evidence from the high-latitude North Atlantic for variations in Antarctic Intermediate water flow during the last deglaciation. Geochemistry, Geophysics, Geosystems, 6, Q05001, doi: 10.1029/2004GC000858.

Rickaby, R.E.M., Greaves, M.J. and Elderfield, H., 2000. Cd in planktonic and benthic foraminiferal shells determined by thermal ionisation mass spectrometry. Geochimica et Cosmochimica Acta, 64 (7), 1229-1236.

Rosenthal, Y., Boyle, E.A. and Labeyrie, L., 1997. Last glacial maximum paleocemistry and deepwater circulation in the Southern Ocean: Evidence from foraminiferal cadmium. Paleoceanography, 12 (6), 787-796.

Rutberg, R.L., Hemming, S.R. and Goldstein, S.L., 2000. Reduced North Atlantic deep Water flux to the glacial Southern Ocean inferred from Neodymium isotope ratios. Nature, 405, 935-938.

Sarnthein, M., Winn, K., Jung, S.J.A., J.-C., D., Labeyrie, L., Erlenkeuser, H. and Ganssen, G., 1994. Changes in the east Atlantic deepwater circulation over the last 30,000 years: Eight time slice reconstructions. Paleoceanography, 9 (2), 209-267.

Schmiedl, G., Mackensen, A. and Muller, P.J., 1997. Recent benthic foraminifera from the eastern South Atlantic Ocean: Dependence on food supply and water masses. Marine Micropaleontology, 32 (3-4), 249-287.

Schrag, D.P., Adkins, J.F., McIntyre, K., Alexander, J.L., Hodell, D.A., Charles, C.D. and McManus, J.F., 2002. The oxygen isotopic composition of seawater during the Last Glacial Maximum. Quaternary Science Reviews, 21 (1-3), 331-342.

Stüber, A., 1999. Spätpleistocene Variabilität der Zwischenwasserzirkulation im subtropischen Westatlantik auf glazial-interglazialen und suborbitalen Zeitskalen: Rekonstruktion anhand stabiler Kohlenstoffisotope und Spurenmetallverhältnissen in kalkschaligen Benthosforaminiferen, Christian-Albrechts Universität, Kiel, 118 pp.

Waelbroeck, C., Labeyrie, L., Michel, E., Duplessy, J.-C., McMAnus, J.F., Lambeck, K., Balbon, E. and Labracherie, M., 2002. Sea-level deep water temperature changes derived from benthic foraminifera isotopic records. Quaternary Science Reviews, 21, 295-305.

Weijer, W., de Ruijter, W.P.M., Dijkstra, H.A. and van Leeuwen, P.J., 1999. Impact of Interbasin Exchange on the Atlantic Overturning Circulation. Journal of Physical Oceanography, 29, 2,266-2,284.

Willamowski, C. and Zahn, R., 2000. Upper ocean circulation in the glacial North Atlantic from benthic foraminiferal isotope and trace element fingerprinting. Paleoceanography, 15, 515-527.

Yu, E.-F., Francois, R. and Bacon, M.P., 1996. Similar rates of modern and last-glacial ocean thermohaline circulation inferred from radiochemical data. Nature, 379, 689-694.

Zahn, R. and Keir, R., 1992. Tracer-Nutrient correlations in the upper ocean: observational and box model constrains on the use of benthic foraminiferal $\delta^{13}C$ and Cd/Ca as paleo-proxies for the intermediate-depth ocean. In: R. Zahn, T.F. Pedersen, M.A. Kaminski and L. Labeyrie (Editors), Carbon Cycling in the Glacial Ocean: Constrains on the Ocean's Role in Global Change. Springer, Berlin, pp. 195-221.

Zahn, R. and Stüber, A., 2002. Suborbital intermediate water variability inferred from paired benthic foraminiferal Cd/Ca and $\delta^{13}C$ in the tropical West Atlantic and linking with North Atlantic climates. Earth and Planetary Science Letters, 200, 191-205.

Annex I

Benthic $\delta^{13}C$ of ODP 980 and benthic Cd/Ca of RC13-229 are used for reference to similar records from MD96-2080 so as to compute meridional $\delta^{13}C$ gradients and assess nutrient changes as a function of water depth. For this the stratigraphic fit was optimized between the two reference cores and age model of MD96-2080.

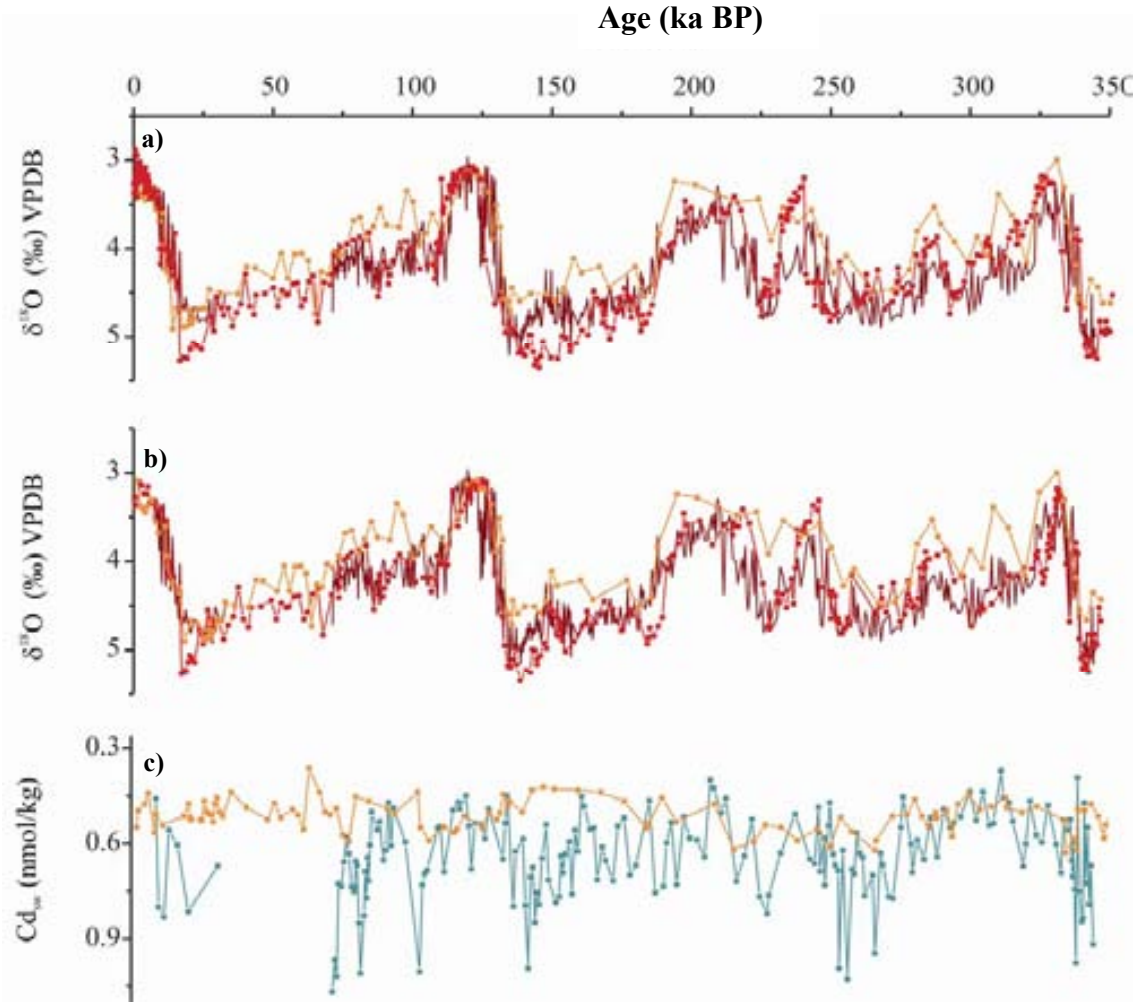

Figure 5.2 Annex I-1 a) Benthic foraminiferal $\delta^{18}O$ of MD96-2080 (brown) compared to benthic $\delta^{18}O$ of ODP Site 980 (red) and RC13-229 (orange) on their published time scales; b) same as in A but now Site 980 and RC13-229 fitted to age model of MD96-2080. c) Cd_{sw} for MD96-2080 (cyan) and RC13-229 (orange) on synchronized age model. Cd_{sw} records of RC13-229 and MD96-2080 are displayed with individual data points indicated to display sampling density of both records.

Chapter 5.3

The South Atlantic Chemocline: New Assessments From Combined Benthic Cd/Ca and $\delta^{13}C$ Data and Inferred $\delta^{13}C_{as}$ Imprints

Abstract

The glacial structure of the oceans was different than today with intermediate to mid-depth waters being significantly more $\delta^{13}C$ enriched than deep waters. This contrast was especially abrupt in the South Atlantic and led to the postulation of the development of a sharp chemical divide at around 2500 m water depth between upper and lower layers. We evaluate the existing benthic $\delta^{13}C$, Cd/Ca and derived $\delta^{13}C_{as}$ data sets for the Last Glacial Maximum (LGM) Atlantic and observe that the vertical sharp divide may be flawed by the core selection. Benthic $\delta^{13}C$ data north of the position of the Sub-Antarctic Front at the LGM (LGM-SAF) smoothly decrease with water depth, without any sign of a sharp divide at 2500 m. On the other hand, all benthic $\delta^{13}C$ data south of the LGM-SAF from 2500 m water depth to the ocean bottom show values around -0.8‰. This suggests that the chemocline was a horizontal, rather than a vertical feature. Benthic Cd/Ca does not change with water depth in the South Atlantic indicating that the chemocline, is not a nutricline, we propose to term it "carbocline". The differential vertical distribution between $\delta^{13}C$ and Cd/Ca also suggest that the source of well-ventilated upper waters in the South Atlantic was Upper Southern Component Water (USCW) with similar nutrient content to Lower Southern Component Water (LSCW) but with a positive $\delta^{13}C_{as}$ signature.

Comparing $\delta^{13}C$ downcore records from the "well-ventilated" water mass domain (MD02-2594/MD96-2080 cores, Agulhas Bank Slope, ~2500 m) with benthic records from other South Atlantic sites, we conclude that the carbocline could have developed under different modes of circulation, i.e. when Northern Component Waters were still a prominent contributor to the South Atlantic (early MIS 6 and 8) and when Southern Component Waters were dominating the regional hydrography (middle MIS 6 and 8).

5.3. The South Atlantic Chemocline: New Assessments From Combined Benthic Cd/Ca and $\delta^{13}C$ Data and Inferred $\delta^{13}C_{as}$ Imprints

5.3.1. Introduction

The chemical structure of the glacial ocean was different from the modern one. The most extensive data sets correspond to the Atlantic Ocean for the Last Glacial Maximum (LGM). According to our current understanding, during the LGM, NADW did not form as dense a water mass as today, and as a consequence it did not sink to the same depth level. It rather formed as an intermediate water mass, the so called GNAIW, while the abyssal depths were invaded by nutrient rich, $\delta^{13}C$ depleted waters of southern origin (Duplessy et al., 1988; Sarnthein et al., 1994), with the transition between both water masses occurring between 2200 and 2700 m (Curry and Oppo, 2005; Marchitto and Broecker, 2006). Benthic $\delta^{13}C$ and Cd/Ca data from the Brazil Margin show low intermediate Cd/Ca values in conjunction with positive $\delta^{13}C$ levels (associated with GNAIW) bounded above and below by higher Cd/Ca values and led Oppo and Horowitz (2000) to postulate the existence of an Upper Southern Component Water (USCW). The updated western Atlantic transect of $\delta^{13}C$ of Curry and Oppo (2005) also favours the existence of USCW. This water mass may have been similar to present SAMW/AAIW, but its characteristics and spatial extension are not well constrained yet.

The glacial structure of the ocean was relatively homogenous world-wide, i.e. intermediate to mid-depth layers were enriched in $\delta^{13}C$ relative to deep layers in the Atlantic, Pacific and Indian Oceans. However, the Atlantic sector of the Southern Ocean (we will refer to it as ASO in this Chapter) shows a particular sharp divide between deep and intermediate to mid-depth layers.

By comparing benthic $\delta^{13}C$ records from South Atlantic cores of a depth transect between 1300 – 5000 m water depths between the LGM and Holocene Ninnemann and Charles (2002) suggested the presence of a well developed chemocline in the South Atlantic at the LGM. Hodell et al. (2003) added new data from the Agulhas Basin supporting the observation of LGM substantial differences in the glacial-interglacial evolution of benthic $\delta^{13}C$ between upper ocean and deep records and enabling to better constrain the divide between upper and lower waters at around 2500 m (Fig. 5.3-1). Additionally, these authors compared long benthic $\delta^{13}C$ records from mid-depths and depth levels of the Cape Basin and suggested that the development of a mid-depth chemocline may have been a persistent feature of glacial periods back to 1.1 Ma. A possible mechanism to produce low $\delta^{13}C$ benthic data in the ASO was proposed by Mackensen et al. (1993a) through increases in rain rates of organic matter to the ocean floor (the so called "phytodetritus or Mackensen effect", see Chapter 2). However, Ninnemann and Charles (2002) and Hodell et al. (2003) discard a major influence of this effect on the cores they analysed based on the observation that large glacial-interglacial shifts are measured everywhere in the South Atlantic independently of sedimentary environment or productivity regime. These authors rather relate the chemical divide in the Southern Ocean to ocean circulation. As

possible sources for mid-depth ventilation, Hodell et al. (2003) suggest GNAIW and a glacial equivalent of Sub-Antarctic Mode Water (SAMW) from the southeast Pacific sector of the Southern Ocean that would be transported through the Drake Passage.

Another intriguing feature of the glacial hydrography of the ASO is that, despite dramatic depletions in $\delta^{13}C$ experienced by the deep waters, benthic Cd/Ca data show no glacial increase in nutrients (see Boyle and Rosenthal, 1996 for a review). Cd/Ca ratios in benthic foraminifera can be influenced by dissolution of Cd bearing-calcite (McCorkle et al., 1995) or alterations of the D_{Cd} in carbonate ion undersaturated waters (Marchitto et al., 2000). Assuming that both, $\delta^{13}C$ and Cd/Ca faithfully record past ambient conditions, differences in the vertical distribution of both proxies should be related to differences in the air-sea signature of the water masses involved. Hence, the existence of a sharp $\delta^{13}C$ divide between mid-depth and deep waters in the Southern Ocean with deep waters being significantly $\delta^{13}C$ depleted is suggestive of a role of this region as carbon sink and has implications for the atmospheric CO_2 (e.g. Marinov et al., 2006).

The glacial-interglacial CO_2 variation, with atmospheric CO_2 levels decreasing by some 80 ppmv during glacial times (e.g. Berner et al., 1980; e.g. Barnola et al., 1987; Petit et al., 1999) is one of the most puzzling questions of climate change. The ocean is one of the largest sinks of CO_2 as it is involved in the "biological and physical pumps". Boyle (1988) was the first to seek a linking between the glacial ocean $\delta^{13}C$ distribution and atmospheric CO_2. He proposed that there was a transfer of nutrients from the intermediate to the deep layers in glacial periods. This transferral potentially influences ocean alkalinity thereby increasing the oceans capacity to hold CO_2. More recent models (Keeling and Stephens, 2001; Toggweiler et al., 2006) proposed physical mechanisms, i.e. sea-ice shielding (Keeling and Stephens, 2001), density contrasts and changing wind patterns (Toggweiler et al., 2006), in conjunction with increase ocean stratification (e.g. Francois et al., 1997; Sigman and Boyle, 2000) to impede fresh ventilation of the deep ocean so as to trap CO_2 in the deep layers, with implications for the vertical distribution of $\delta^{13}C$ (see discussion).

In this chapter first we evaluate the available Holocene-LGM shifts of $\delta^{13}C$ and Cd/Ca in the Atlantic and of computed $\delta^{13}C_{as}$ in the context of the chemocline with two additional cores from the Agulhas area, i.e. MD02-2594 (34º43'S, 17º20'E, 2440 m water depth), MD02-2589 (41º26'S, 25º15'E, 2660 m, Molyneux, 2007; Molyneux et al., 2007). Next we assess the position of the Agulhas Bank Spliced, spliced record of MD02-2594 and MD96-2080 cores (ABS, see Chapter 5.1.3 for details) in regard to the chemocline back to MIS 9. The contents of this chapter are the subject of a joined manuscript that is currently in preparation with colleagues from Cardiff University, Drs Elizabeth Molyneux and Ian Hall. Some of the interpretations and part of the discussion have therefore been elaborated within this collaboration.

Figure 5.3-1 represents the chemocline as proposed by Hodell et al. (2003) on the basis of $\delta^{13}C$ data alone from the South Atlantic Sector of the Southern Ocean.

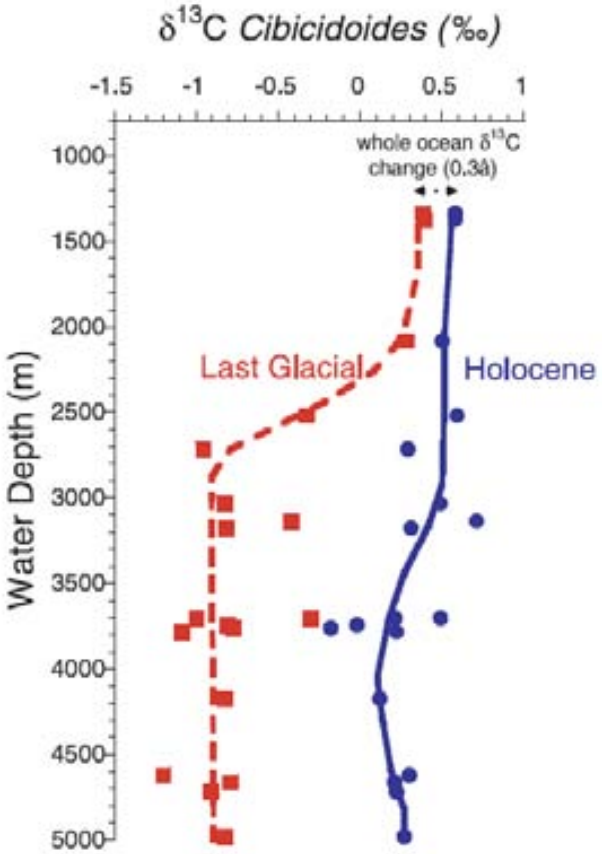

Figure 5.3-1 Benthic $\delta^{13}C$ chemocline (Hodell et al., 2003).

5.3.2. Data/Results

- **Holocene-LGM**

We plot the available Atlantic $\delta^{13}C$ and Cd/Ca data bases (Zahn et al., 1987, see Annex I to this Chapter; Table 2, Hodell et al., 2003; Tables 1 and 2, Curry and Oppo, 2005; Tables 1 to 3, Marchitto and Broecker, 2006) and data from MD02-2594 (this Thesis) and MD02-2589 (Molyneux, 2007; Molyneux et al., 2007) together with derived $\delta^{13}C_{as}$ (see Chapter 4 for details on the derivation of $\delta^{13}C_{as}$) as depth profiles (Figs. 5.3-3 to 6). In these representations the data are clustered as: North Atlantic (from 41ºN to 65ºN); Central Atlantic (from 41ºN to 10ºS) and South Atlantic (south of 22ºS). We restrict the North Atlantic data to latitudes north of 41ºN in order to evaluate the variations of NADW/GNAIW with the less possible mixing with southern sources. On the other hand, our northward latitudinal limit for the South Atlantic reaches 22ºS because data coverage in the South Atlantic is much poorer and we need to extend our cluster in order to get enough information to compare with the North Atlantic pattern. Besides, the modern vertical architecture of the whole South Atlantic is rather homogenous with AAIW overlaying NADW and AABW at the bottom. We enclose all the data in between as Central Atlantic. Figure 5.3-2 shows a map with the data sets used, for further details in these data sets we refer to the Annex I of this chapter.

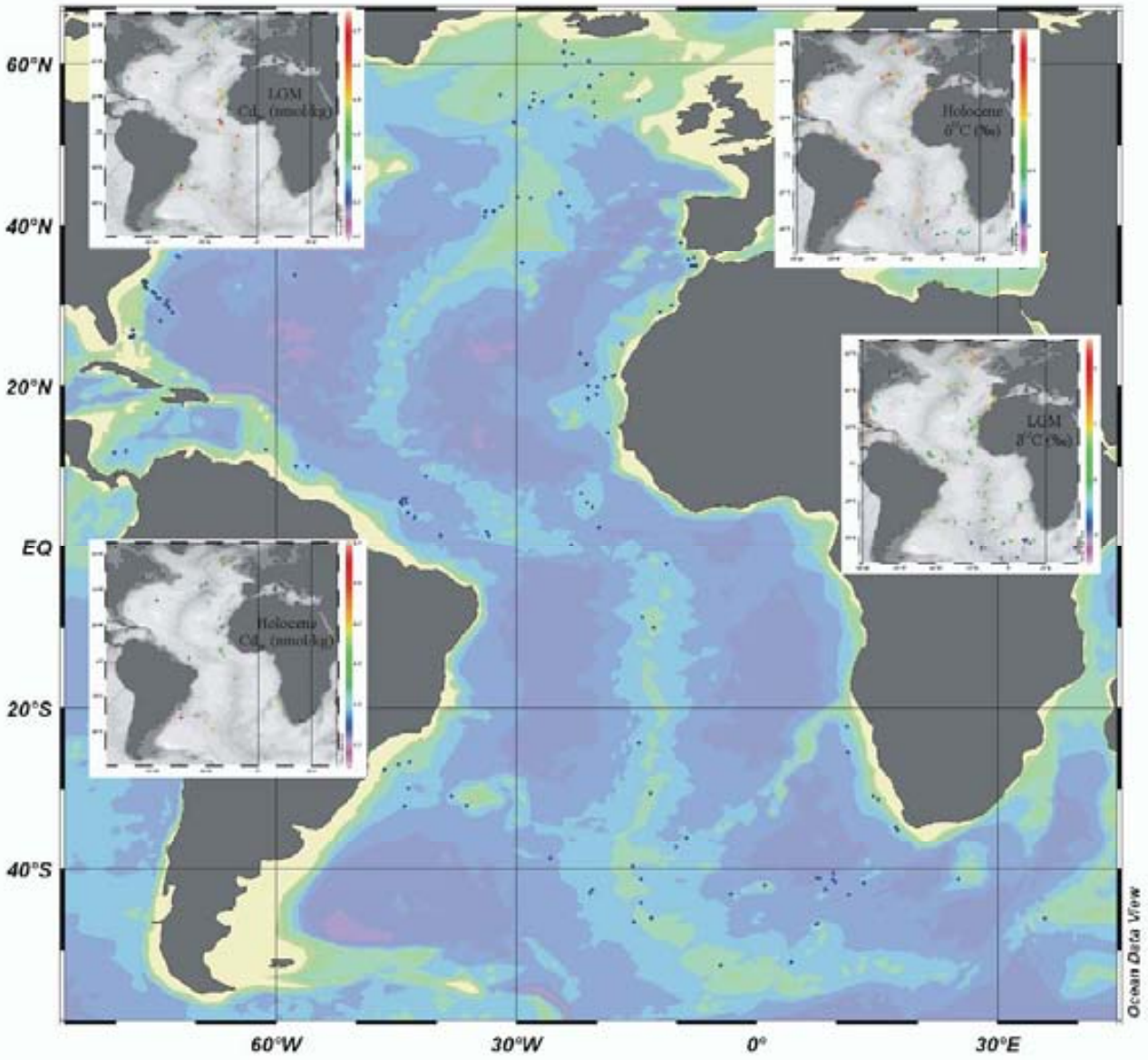

Figure 5.3-2 Map with the position of the sediment cores used in this chapter (see Annex I for details about the coordinates, water depths and references). Note that there do not exits paired benthic $\delta^{13}C$ and Cd/Ca (Cd_{sw}) for Holocene and LGM for all these cores. The insert maps displayed the cores for which each of the measurements is available. Maps elaborated with the software Ocean Data View (Schlitzer, 2007).

The Holocene $\delta^{13}C$ and Cd_{sw} (Fig. 5.3-3) depth profiles provide a good reflection of the present circulation (see Curry and Oppo, 2005 for a detailed discussion on $\delta^{13}C$ latitudinal transects; Marchitto and Broecker, 2006 on Cd_{sw} latitudinal transects). North Atlantic $\delta^{13}C$ and Cd/Ca data cover depths between 1500-3500 m and cluster around values of 1.2‰ and 0.3 nmol/kg respectively. This indicates that deep water isopycnals are ventilated by NADW. This water mass extends southwards and as a result the Central Atlantic data set also cluster close to $\delta^{13}C$ values of ~ 1‰ and Cd_{sw} close to 0.35 nmol/kg from 1000 m down the water column. Slightly depleted $\delta^{13}C$ and enriched Cd_{sw} values in Central Atlantic waters are the result of "ageing" of NADW en route to the South Atlantic. Cd_{sw} concentrations in the southerly Central Atlantic domain are slightly higher at intermediate water

depths (around 0.38 nmol/kg) indicating mixing with $\delta^{13}C$ positive but nutrient-rich AAIW. This is confirmed by Cd_{sw} values of 0.5-0.4 nmol/kg at around 1000 m water depth in the South Atlantic at positive $\delta^{13}C$ levels. The abyssal South Atlantic show values of $\delta^{13}C$ of around 0.3‰ combined with high Cd_{sw} values (around 0.5-0.7 nmol/kg) indicating the presence of nutrient rich AABW. Between these two southern origin water masses, i.e. AAIW and AABW, aged and partially altered by mixing with the southern endmembers NADW ventilates the South Atlantic. $\delta^{13}C$ values of the aged NADW (between 1500-3500 m water depth) in the South Atlantic range between around 1.1 and 0.5‰. The Cd_{sw} values at mid-depth to deep levels when compare with in situ $(PO_4)^{3-}$ values seem to underestimate the expected nutrient content (see Oppo and Horowitz, 2000 for a more detailed discussion).

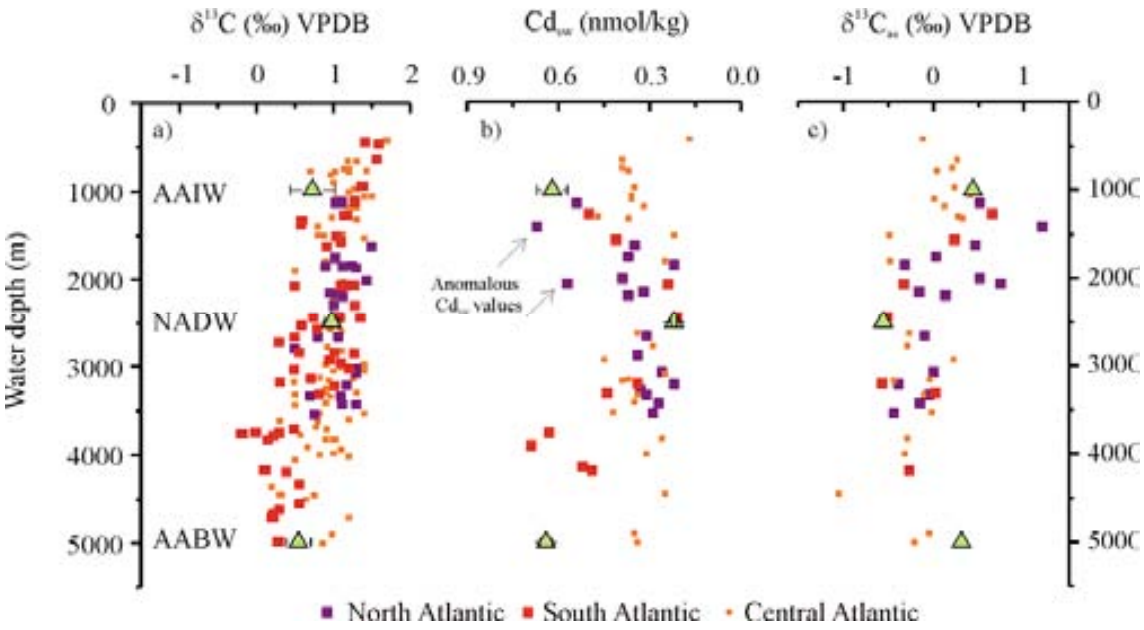

Figure 5.3-3 Holocene Atlantic $\delta^{13}C$, Cd_{sw} and computed $\delta^{13}C_{as}$; a) benthic $\delta^{13}C$ (‰) VPDB; b) Cd_{sw} (nmol/kg) (derived from Cd/Ca using Boyle's (1992) partition coefficients, D_{Cd}); c) computed $\delta^{13}C_{as}$ (‰) VPDB (see Chapter 4 for details on the computation). Triangles indicate signatures of the endmembers AAIW, NADW and AABW (see Table 5.2-2, Chapter 5.2).

Holocene negative $\delta^{13}C_{as}$ at depths between 1500 and 5000 m demonstrates the predominance of NADW (NADW $\delta^{13}C_{as}$ ~ -0.4‰, Lynch-Stieglitz and Fairbanks, 1994) in the Atlantic hydrography. Values close to zero at intermediate depths in the Central Atlantic are likely caused by mixing between positive AAIW (e.g. Charles et al., 1993) and negative NADW. Marchitto and Broecker (2006) noticed the existence of some anomalously positive $\delta^{13}C_{as}$ values (around 0.5-1‰) in the North and Central Atlantic at intermediate water depths caused by anomalously high Cd_{sw} levels (pointed by arrows in Figure 5.3-3b). Bertram et al. (1995) and Willamoski and Zahn (2000) proposed using local partition coefficients to transform benthic Cd/Ca into Cd_{sw} which set the $\delta^{13}C_{as}$ to values close to 0‰ which appear more coherent with present observations (Marchitto and Broecker, 2006). These sites are close to continental margins at intermediate depths, a possible explanation for the departure of Boyle's (1992) depth dependence partition coefficients could be the presence of extra Cd washed out from the continental shelves. We opt to neglect two of those cores (which show very high Cd_{sw} ~ 0.55 to 0.7

nmol/kg, indicated by arrows in Figure 5.3-3b) for the LGM representation and use Boyle's (1992) partition coefficients for the rest of the cores for consistency with the remaining data used. Because of these anomalous intermediate values, Marchitto and Broecker (2006) pointed out that the Holocene representation of $\delta^{13}C_{as}$ does not perfectly reproduce the present distribution of water masses in the Atlantic and therefore, glacial $\delta^{13}C_{as}$ data should be looked at carefully.

The LGM profiles are radically different (Fig. 5.3-4). The most recent and comprehensive glacial $\delta^{13}C$ distribution has been compiled by Curry and Oppo (2005). These authors remarked that the glacial ocean had a much larger range of $\delta^{13}C$ than the modern one. Positive $\delta^{13}C$ at upper North and Central Atlantic depths represent the glacial equivalent of NADW, i.e. GNAIW. On the other hand, the more depleted and nutrient enriched deep layers are traditionally interpreted as being ventilated by the glacial equivalent of AABW, i.e. Low Southern Component Water (LSCW). Curry and Oppo (2005) and Oppo and Horowitz (2000) inferred a third water mass to explain the glacial $\delta^{13}C$ and Cd_{sw} distribution at the Brazilian Margin. They proposed the existence of an USCW, maybe similar to present AAIW, with $\delta^{13}C$ around 0.3-0.5‰ (Curry and Oppo, 2005) and Cd_{sw} of around 0.4 nmol/kg (Oppo and Horowitz, 2000). Lynch-Stieglitz and Fairbanks (1994) and Lychn-Stieglitz et al. (1996) found evidence of the existence of a $\delta^{13}C_{as}$ rich water mass in cores off Tasmania. We have used these cores to compute the characteristics of the USCW endmember (see Table 5.2-2, Chapter 5.2) because we consider that they may more faithfully record USCW. They are close to the proposed formation region of such a water mass, i.e. the South Antarctic Front (SAF) and they are far away from the influence of NCW so that they may show a purer USCW signature.

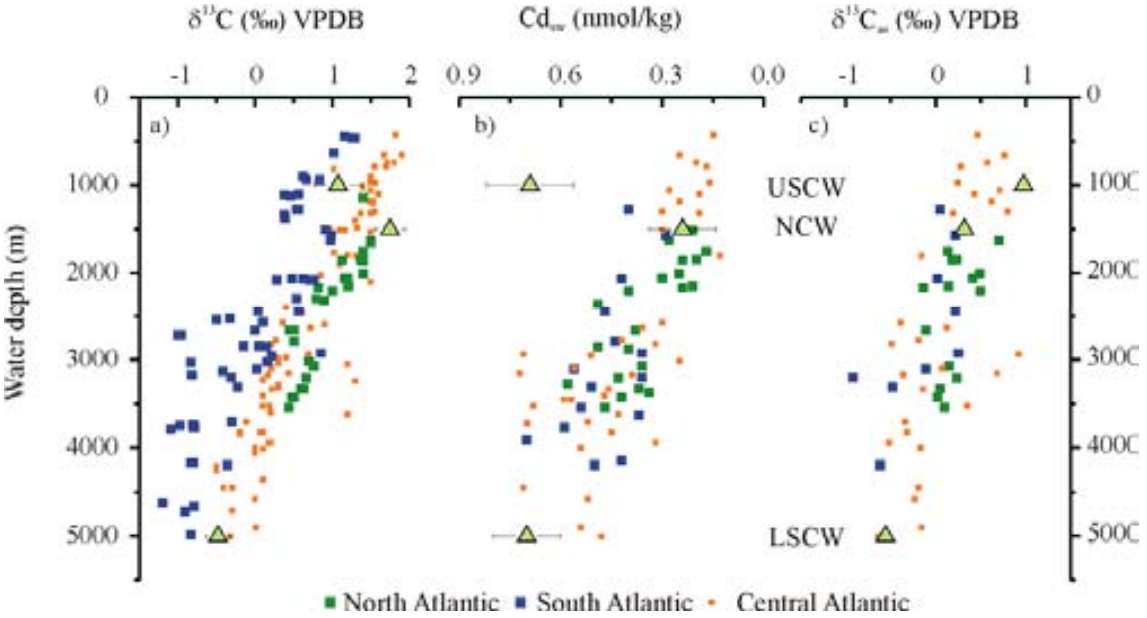

Figure 5.3-4 Glacial Atlantic $\delta^{13}C$, Cd_{sw} and computed $\delta^{13}C_{as}$; a) benthic $\delta^{13}C$ (‰) VPDB; b) Cd_{sw} (nmol/kg) (derived from Cd/Ca using Boyle's (1992) partition coefficients, D_{Cd}); c) computed $\delta^{13}C_{as}$ (‰) VPDB (see Chapter 4 for details on the computation). Triangles indicate signatures of the endmembers USCW, NCW and LSCW (see Table 5.2-2, Chapter 5.2).

Despite the non-coherent picture drawn from the Holocene $\delta^{13}C_{as}$ depth profiles, the LGM representation fits our current understanding of the last glacial peak circulation. Intermediate data in the Central Atlantic reflects the presence of positive $\delta^{13}C$, low Cd_{sw} GNAIW which likely had a positive $\delta^{13}C_{as}$ signature (maybe as high as +0.8‰, Lynch-Stieglitz and Fairbanks, 1994; Lynch-Stieglitz et al., 1996) owning to stronger gas exchange in response to higher wind stirring in the formation area, colder temperatures and likely longer residence time. In the South, LSCW was extremely negative in $\delta^{13}C$ (Ninnemann and Charles, 2002) and may have had a Cd_{sw} value around 0.7 nmol/kg (Marchitto and Broecker, 2006). Marchitto and Broecker (2006) predicted a $\delta^{13}C_{as}$ for this water mass between –0.5 to -1‰. Most of the Central and North Atlantic LGM $\delta^{13}C_{as}$ distribution can, in principle, be explained by mixing between these two endmembers, i.e. GNAIW and LSCW.

North and Central Atlantic glacial $\delta^{13}C$ and Cd_{sw} data show linear trends of increasing nutrients with water depth. The South Atlantic data distribution does apparently not show any linear trend in $\delta^{13}C$ and Cd_{sw}. Rather, a "chemocline" in $\delta^{13}C$ is observed, defined by Hodell et al. (2003). On closer inspection the $\delta^{13}C$ chemocline seems largely determined by cores located to the South of the presumed position of the SAF at the LGM (Fig. 5.3-5) (Molyneux, 2007; Martínez-Méndez and Molyneux et al. in prep.). Considering a latitude around 42ºS for the position of the SAF at the LGM (Howard and Prell, 1992; Brathauer and Abelmann, 1999; Gersonde et al., 2005), Molyneux (2007). observed that sites north of the SAF exhibit a LGM-Holocene benthic $\delta^{13}C$ depletion of 0.2 at shallow to 0.6‰ at mid-depth water sites, only slightly greater than the 0.32-0.46‰ global carbon shift (Curry et al., 1988; Duplessy et al., 1988). At the deep water sites $\delta^{13}C_{Hol\text{-}LGM}$ shows large depletions of 1.1 – 1.5‰. Sites to the south of the SAF display consistently higher Holocene-LGM depletions of around 1.2‰ from mid-depth to deep waters (Fig 5.3-5). Besides, we observe that the South Atlantic $\delta^{13}C$ data to the north of 42ºS, similarly to Central and North Atlantic data, show a linear trend of decreasing $\delta^{13}C$ with water depth. Data to the South of the LGM-SAF deviate from this linear trend and, below 2500 m, abruptly shifts to $\delta^{13}C$ values of around –1‰. All the South Atlantic Cd_{sw} data available are from cores located north of 42ºS. These data do not show a linear trend of increasing Cd_{sw} with water depth and rather seems to cluster around a value of 0.4 nmol/kg.

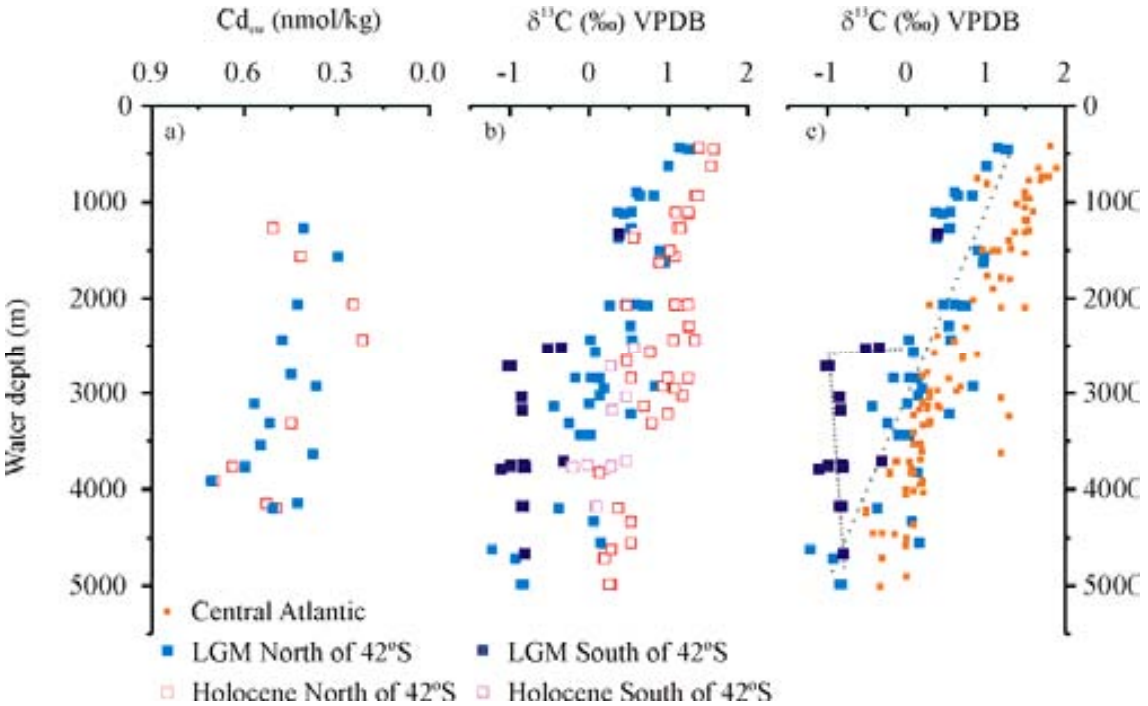

Figure 5.3-5 South and Central Atlantic $\delta^{13}C$ and Cd_{sw} data discriminated by their latitudinal position respect to the postulated location of the Sub-Antarctic Front (SAF) at the LGM at around 42ºS (Howard and Prell, 1992; Brathauer and Abelmann, 1999; Gersonde et al., 2005); a) Cd_{sw} (nmol/kg), all data belongs to the north-SAF domain; b) South Atlantic $\delta^{13}C$ for the Holocene and LGM, north and south of 42ºS; c) LGM South (north and south of 42ºS) and Central Atlantic $\delta^{13}C$.

- **Chemocline in MIS 6 and 8**

Hodell et al. (2003) proposed, by comparing downcore $\delta^{13}C$ records of ODP sites 1088 and 1090 that the chemical divide between upper and lower layers in the South Atlantic is a persistent feature of the last 1.1 Ma. Note that ODP site 1090 is a relocation of TNO57-6 and that this core composes the upper record used by Hodell et al. (2003), we use only data from TNO57-6 because it encompasses the time period here analysed.

The latitudinal discrimination of South Atlantic cores, north and south of the SAF observed by Molyneux (2007) (Figs. 5.3-5b and c) for the LGM data set puts forward the possibility that the inferences about the chemocline are biased by the core selection. As a result we performed a detailed comparison between our ABS benthic $\delta^{13}C$ record with those of TNO57-6 (Agulhas Ridge, south of the LGM-SAF, 3751 m, Hodell et al., 2003), ODP Site 1088 and 1089 (Agulhas Ridge, at the LGM-SAF at 2100 and 4621 m, Hodell et al., 2003); core R13-229 (Cape Basin, north of the LGM-SAF, deep site, 4191 m water depth, Oppo and Rosenthal, 1994) (see Table 5.3-1). The age models of the cores used for comparison have been retuned slightly through their $\delta^{18}O$ records to our age model to enhance compatibility for the comparisons (Fig. 5.3-7). We will also compare our Cd_{sw} record and derived $\delta^{13}C_{as}$ with those of four sediment cores from different water depths assumed to represent NCW and SCW variability (Fig. 5.3-8) in order to elaborate on the origin of the well ventilated upper chemocline waters.

Table 5.3-1 Core locations

Sediment core	Water depth (m)	Core location	Reference
ODP 1088	2082	42ºS, 13ºE; Agulhas Ridge	(Hodell et al., 2003)
ODP 1089	4621	41ºS, 9º5'E; Agulhas Ridge	(Hodell et al., 2003)
TNO57-6	3751	42.5ºS, 9ºE; Agulhas Ridge	(Hodell et al., 2003)
MD02-2589	2660	41.26ºS, 25.15ºE; Agulhas Basin	(Molyneux, 2007; Molyneux et al., 2007)
MD02-2594 (ABS 0-80 kyr)	2440	34ºS, 17ºE; Agulhas Bank Slope	This study
MD96-2080 (ABS 80-345 kyr)	2488	36ºS, 19ºE; Agulhas Bank Slope	This study
RC13-229	4191	25.5ºS, 11ºE; Cape Basin	Oppo et al. (1990) Oppo and Rosenthal (1994)

In Figure 5.3-6 we represent the linear trends observed from the data patterns in the South Atlantic (Fig. 5.3-5c) together with the $\delta^{13}C$ vertical position of the above mentioned cores (Table 5.3-1). ODP sites 1088, 1089 and TNO57-6, on which Hodell et al. (2003) based their conclusion about the recurrence of a glacial chemocline, are represented in yellow to emphasize their vertical position compared to the other cores. The LGM distribution of all the cores lies on the linear trend of South Atlantic data north of 42ºS. So that we do not need to call into a sharp vertical divide between upper and lower layers to explain the vertical distribution of these cores. The vertical distribution of $\delta^{13}C$ could equally be explained by mixing of bottom $\delta^{13}C$ negative waters and upper $\delta^{13}C$ positive waters. The linear trends defined by the LGM data clusters were very probably different in previous glacial periods. We maintain them in Figure 5.3-6b as indicative and plot here the vertical distribution of the South Atlantic cores for early and middle MIS 6 and 8. Similarly to the LGM representation, the data pattern could be explained by mixing of upper well ventilated waters with bottom poorly ventilated waters without the need to call for a chemocline. It is possible that the chemocline was not a vertical structure but rather a horizontal feature and that the true sharp-divide in $\delta^{13}C$ occurs latitudinal at the glacial position of the SAF. In order to test this hypothesis $\delta^{13}C$ data, not yet available, from cores south of the SAF at mid to intermediate depths are needed.

Table 5.3-2 Glacial $\delta^{13}C$ values for South Atlantic sediment cores

Sediment core	LGM $\delta^{13}C \pm 1\sigma$, n (‰ VPDB)	Middle MIS 6 $\delta^{13}C \pm 1\sigma$, n (‰ VPDB)	Early MIS 6 $\delta^{13}C \pm 1\sigma$, n (‰ VPDB)	Late MIS 8 $\delta^{13}C \pm 1\sigma$, n (‰ VPDB)	Early MIS 8 $\delta^{13}C \pm 1\sigma$, n (‰ VPDB)
ODP 1088	0.28 ± 0; 2	-0.08 ± 0.02; 3	0.19 ± 0.01; 3	-0.02 ± 0.01; 2	0.22 ± 0.04; 2
ODP 1089	-1.2 ± 0.1; 4	-1.1 ± 0.1; 27	-0.92 ± 0.15; 30	-1.1 ± 0.3; 40	-0.5 ± 0.3; 27
TNO57-6	-0.27 ± 0.2; 5	-0.46 ± 0.1; 3	-0.85 ± 0.1; 4	-1.24 ± 0.2; 5	-0.39 ± 0.1; 2
RC13-229	-0.36 ± 0.2; 5	-0.89 ± 0.1; 9	-0.53 ± 0.01; 2	-0.91 ± 0.1; 5	-0.6 ± 0.02; 5
MD02-2589	0	-	-	-	-
ABS	0.04 ± 0.08; 4	-0.01 ± 0.05; 6	0.22 ± 0.1; 7	-0.31 ± 0.1; 10	0.24 ± 0.1; 7

[1]Error values in the table refer to the standard deviation of means; n is the number of data points used to compute the means.

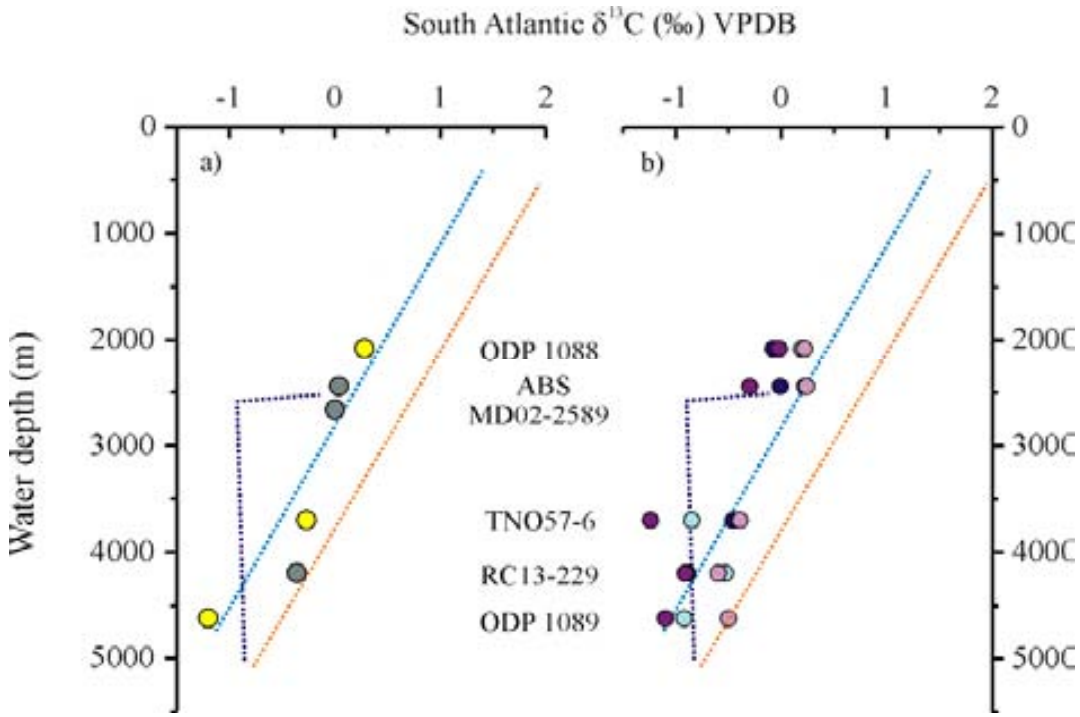

Figure 5.3-6 Linear trends defined by the LGM benthic $\delta^{13}C$ data of Central and South Atlantic data and glacial (LGM, MIS 6 and 8) $\delta^{13}C$ means of South Atlantic cores, a) LGM linear trends and LGM benthic $\delta^{13}C$, yellow dots represent the LGM value of ODP site 1088, TNO57-6 and 1089 which are at or south of 42ºS; grey dots represent the LGM value of cores ABS, MD02-2589 and RC13-229 which are north of 42ºS (Table 5.3-2); b) LGM linear trends and MIS 6 and 8 benthic $\delta^{13}C$, dots represent benthic $\delta^{13}C$ for different glacial periods (Table 5.3-2): early MIS 6 (light blue), middle MIS 6 (dark blue), early MIS 8 (light pink) and middle MIS 8 (dark pink). Note that the linear trends for previous glacial times have likely been different than for the LGM.

ABS $\delta^{13}C$ are more positive than those of the deeper cores and only slightly more enriched that those of ODP 1088 for all glacial periods. We extend the comparison to the whole records and observed that this characteristic holds for the last 345 kyr (Figure 5.3-7).

Holocene to LGM $\delta^{13}C$ depletions of the mid-depth cores ABS and ODP 1088 are comparable to the global marine shift of 0.32-0.46‰ (Curry et al., 1988; Duplessy et al., 1988) (see above). Global marine carbon pool variations are not well constrained for pre-LGM glacial times. As a reference we use the benthic $\delta^{13}C$ stack of Zahn and Stüber (2002) (see Annex I of Chapter 5.2.) and infer that the maximum benthic $\delta^{13}C$ shift between MIS 6 and 5, and between MIS 8 and 7 are 0.47‰ and 0.36‰ respectively. Thus, the large benthic $\delta^{13}C$ depletions (1-1.5‰) observed in RC13-229, ODP 1089 and TNO57-6 are well in excess of these mean ocean variations. Maximum benthic $\delta^{13}C$ depletions at ABS occur during the LGM, MIS 4 and middle MIS 6 and 8. In the case of MIS 6 and 8 these maxima depletions occur well before the onset of the glacial termination, and are also larger than mean ocean shifts (see Chapter 5.2.3). We have inferred that during mid MIS 6 and 8 MD96-2080 (lower part of ABS) is under a strong influence of SCW (see Chapter 5.2), but nevertheless the core remained at more positive levels than RC13-229, ODP 1089 and TNO57-6, in a well-ventilated chemocline domain.

Glacial depletions along MIS 6 and 8 at TNO57-6 are of larger amplitude than at ODP Site 1089 such that benthic $\delta^{13}C$ from both cores converge (Fig. 5.3-7). This convergence at more negative

$\delta^{13}C$ levels during glacial periods south of the SAF initially indicates strongly diminished presence of glacial Northern Component Water (NCW) at TNO57-6 depth levels, and a more prominent influence of $\delta^{13}C$-depleted deep southern source waters (i.e. LSCW). Core R13-229 benthic $\delta^{13}C$ levels match those of TNO57-06 and ODP Site 1089 in middle MIS 6 and MIS 8, while during early MIS 6 remained slightly more positive (Fig. 5.3-7), likely indicating the presence at this core site of Lower Southern Component Water (LSCW) with an admixture of well ventilated NCW from above (see Chapter 5.2). Benthic $\delta^{13}C$ of the deep cores converge before MIS 8. During MIS 2 to 4, benthic $\delta^{13}C$ of RC13-229 and TNO57-6 remained between those of ABS and ODP 1089 but closer to those of ABS, plausibly indicating the presence of USCW in the South Atlantic during this period.

We have computed the $\delta^{13}C$ gradient between ABS and the deeper cores. In order to do so, first we resampled the records at 4 kyr steps to keep only the long-term variability and to avoid possible artefacts in our computed gradients related to different time resolutions. The benthic $\delta^{13}C$ gradients ($\Delta\delta^{13}C$) between ABS and the three deep records are offset in the Holocene, MIS 5 and MIS 7e as benthic $\delta^{13}C$ of these records are gradually more negative in the sites under a stronger influence of AABW (i.e. $\delta^{13}C_{TNO57\text{-}6} > \delta^{13}C_{RC13\text{-}229} > \delta^{13}C_{ODP1089}$). Similarities in the benthic $\delta^{13}C$ of TNO57-6, RC13-229 and ODP 1089 from MIS 8 to 9 drive the $\Delta\delta^{13}C$ between ABS and these three records to vary in coherence. $\Delta\delta^{13}C$ between ABS and TNO57-6 and ODP 1089 is larger in early MIS 6 and MIS 8 due to the stronger benthic $\delta^{13}C$ depletions showed by these cores. In middle MIS 6 and 8, the $\Delta\delta^{13}C$ between ABS and RC13-229 reaches the levels of the $\Delta\delta^{13}C$ between ABS and the most southerly records, i.e. TNO57-6 and ODP 1089. This large $\Delta\delta^{13}C$ seems coherent with maxima in the North-South $\Delta\delta^{13}C$ between ABS and ODP 980 (Fig. 5.3-7e, see also Chapter 5.2) further supporting our earlier contention that the N-S gradient is modulated from the south (Chapter 5.2). Furthermore, coherence enlarged South Atlantic mid-depth to deep and North to South Atlantic $\Delta\delta^{13}C$ are coeval with northwards migrations of the South Tropical Front (STF) (Fig. 5.3-7) as indicated by a foraminiferal association of the split record CBR (Peeters et al., 2004). The maxima development of the chemocline seems to occur when surface and deep Southern Source waters extend northwards. During MIS 2 to 4, the benthic $\Delta\delta^{13}C_{ABS\text{-}1089}$ is large and coincides with an increase in the N-S gradient.

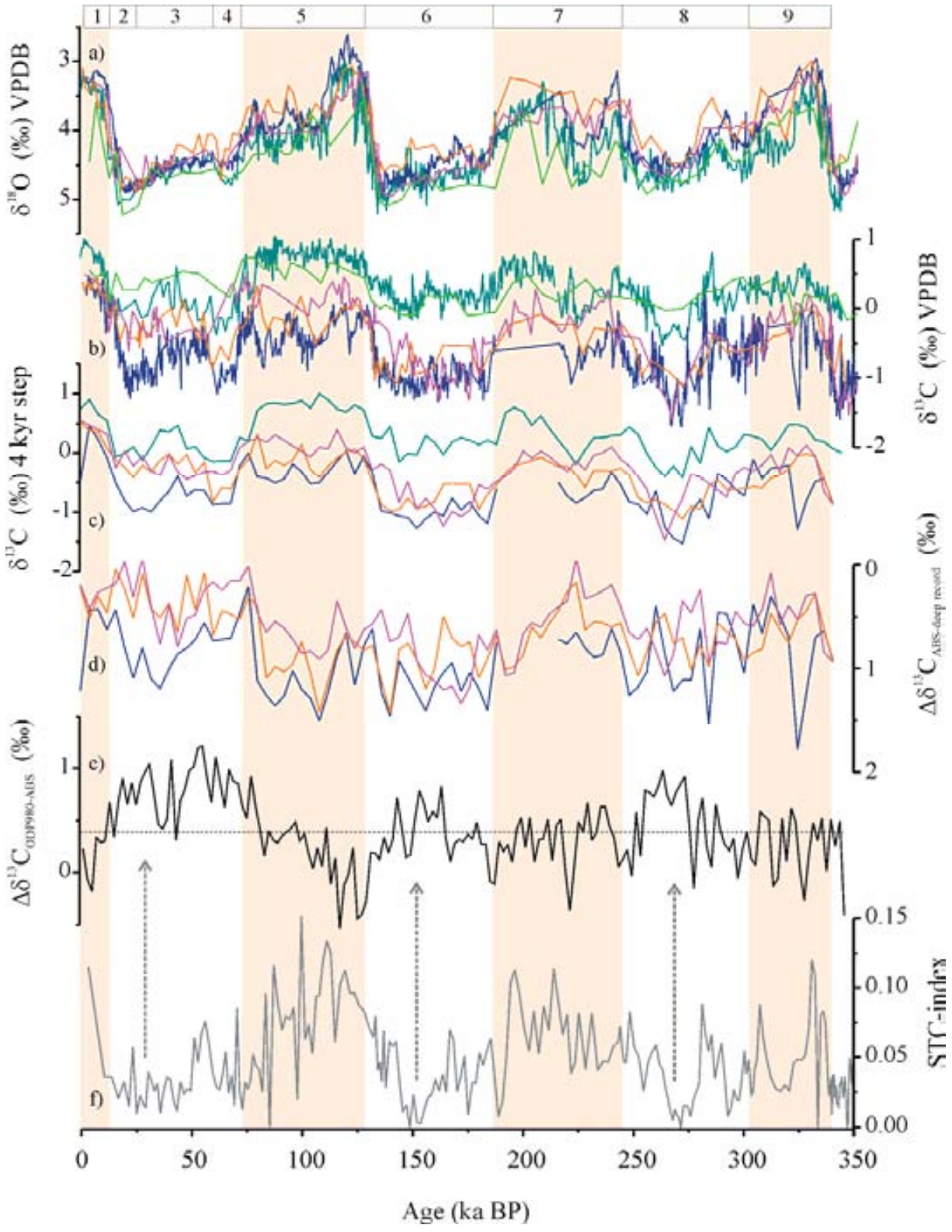

Figure 5.3-7 Down-core South Atlantic benthic $\delta^{13}C$ records from well-ventilated and poorly-ventilated chemocline domains; a) benthic $\delta^{18}O$ of ABS (cyan); ODP 1088 (green), TNO57-6 (pink), ODP 1089 (blue) (Hodell et al., 2003) and RC13-229 (orange) (Oppo et al., 1990; Oppo and Rosenthal, 1994) to show the stratigraphic fit between the records. The age models of TNO57-6, RC13-229, ODP 1088 and ODP 1089 have been retuned to that of ABS; b) benthic $\delta^{13}C$ of ABS (cyan), ODP 1088 (green), TNO57-6 (pink), ODP 1089 (blue) and RC13-229 (orange); c) same benthic $\delta^{13}C$ records resampled at 4 kyr time steps; d) benthic $\delta^{13}C$ gradients computed between ABS and the deeper records, i.e. $\Delta\delta^{13}C_{ABS\text{-}TNO57\text{-}6}$ (pink), $\Delta\delta^{13}C_{ABS\text{-}RC13\text{-}229}$ (orange), $\Delta\delta^{13}C_{ABS\text{-}ODP1089}$ (blue); e) benthic $\delta^{13}C$ North-South gradient computed between ABS and ODP980; f) South Tropical Convergence Index (STC-index) of Peeters et al. (2004).

Our benthic $\delta^{13}C$ records at around 2500 m water depth allow extension of the domain of the relatively positive $\delta^{13}C$ glacial upper waters from 2100 m (i.e. site 1088, Hodell et al., 2003) to at least 2500 m water depth. The latitudinal $\delta^{13}C$ pattern between these four cores further suggests that well ventilated waters were bathing the mid-depth South Atlantic during MIS 6 and 8 and that benthic $\delta^{13}C$ depleted deep southern source waters (namely LSCW) were spreading as far north as 25ºS in the abyssal depths. Based on benthic $\delta^{13}C$ and Cd/Ca for different cores and time windows, we have concluded that MD96-2080 is bathed in early glacial times by NCW and in late glacial times by an admixture of Upper and Lower Southern Component Water (i.e. $SCW_{s.l.}$) (Chapter 5.2.). An outcome of this observation is that there is not a unique hydrographical regime that can produce a chemocline in the South Atlantic (see discussion).

In order to extend on the analyse of the characteristics of upper and lower chemocline waters we use the $\delta^{13}C$, Cd/Ca and derived $\delta^{13}C_{as}$ downcore records (see Chapter 4 for details on the computation of $\delta^{13}C_{as}$ downcore) from four sediment cores from different water depths assumed to represent NCW and SCW variability (Fig. 5.3-8) (see also Chapter 5.2). Core MD96-2080 from the Agulhas Bank represents the mid-depth cores north of the SAF in the well-ventilated, upper chemocline domain. Core RC13-229 (25.5ºS, 11ºE, 4191 m) from the deep Cape Basin is a good candidate to represent the variability of LSCW. Core SO75-26KL from the upper Iberian Margin (37º49′N, 09º30′W, 1099 m water depth) is a good candidate to record Upper NCW (UNCW) variability and has been used previously to document thermohaline overturn in the North Atlantic (Willamowski and Zahn, 2000), whilst core CH82-24 (43º30'N, 29º52'W, 3070 m) provides constrains about the interplay of Lower NCW (LNCW) and LSCW in the deep North Atlantic back to MIS 7 (Boyle and Keigwin, 1985/86).

Cd_{sw} values in CH82-24 increase in glacial periods indicating the influence at this deep North Atlantic site of SCW. Nonetheless, the increases are only moderate and the levels never reached those of the South Atlantic cores indicating that nutrient-poor NCW was still influencing this core site. The contrasting pattern between RC13-229 and MD96-2080 Cd_{sw} has been used in Chapter 5.2 to eliminate LSCW as the sole influence of the large benthic $\delta^{13}C$ depletions and coeval Cd_{sw} increases in middle MIS 6 and 8 in MD96-2080. Rather, an extra water mass seems indicated, USCW, with a more positive $\delta^{13}C$ signature and higher nutrient concentrations, thus with positive values of the conservative tracer $\delta^{13}C_{as}$.

The $\delta^{13}C_{as}$ values at the mid-depth Iberian margin site are around -0.4‰ during the Holocene and +0.5‰ for the LGM (Figs. 5.3-3 and 4), in line with values documented at other North Atlantic sites (Marchitto and Broecker, 2006). Deep North Atlantic core CH82-24 $\delta^{13}C_{as}$ values fall within the range -0.3 to +0.3‰, with no clearly defined glacial-interglacial pattern (Fig. 5.3-8). From the LGM values of SO75-26KL and RC13-229, the LGM values at CH82-24 seem better explained by the admixture of NCW and LSCW while the same interglacial $\delta^{13}C_{as}$ levels most likely represent true endmember NADW. Despite being $\delta^{13}C_{as}$ a conservative water mass tracer, a similar value may be achieved by the presence of a single water mass or by admixture of various water masses. $\delta^{13}C_{as}$

values should be evaluated on view of their $\delta^{13}C$ and Cd_{sw}. Along the deep Cape Basin core, $\delta^{13}C_{as}$ is consistently negative (between -0.2 and -1‰), especially during the glacials. Benthic $\delta^{13}C$ along this core which was raised in the neighbourhood of the Namibia upwelling system could be altered by the "Mackensen effect" i.e., F. wuellerstorfi may have recorded lowered $\delta^{13}C$ values than those of true ambient bottom waters due to the development of a "fluffy layer" of low $\delta^{13}C$ resultant from organic matter degradation. We test the influence of a possible "Mackensen effect" on the $\delta^{13}C_{as}$ of this record. In order to do so, we use the available Total Organic Content (TOC) record (Oppo and Rosenthal, 1994) of this core and assume that the maximum TOC is capable to produce a maximum $\delta^{13}C$ depletion of 0.4‰ (see Annex II for details). We observed that if this effect is considered the $\delta^{13}C_{as}$ values are only slightly less negative (light brown dashed line Fig. 5.3-8) so that a possible artefact in the $\delta^{13}C$ data of RC13-229 cannot explain the negative $\delta^{13}C_{as}$ values. The $\delta^{13}C_{as}$ record of MD96-2080 remains offset from that of RC13-229 and shifted to higher values throughout (between 0 and +0.5‰), reflecting the more positive benthic $\delta^{13}C$ at MD96-2080 at similar Cd_{sw} levels. Positive $\delta^{13}C_{as}$ values are found today at both, intermediate and deep isopycnal levels in the Southern Ocean and involve upwelling of nutrient-laden deep waters to the upper layer and subsequent air-sea gas exchange that causes $\delta^{13}C_{\Sigma CO2}$ to increase. Positive $\delta^{13}C_{as}$ has also been reported for GNAIW (maybe as high as +0.8‰, Lynch-Stieglitz and Fairbanks, 1994). The positive glacial $\delta^{13}C_{as}$ values along MD96-2080 indicates the need for positive $\delta^{13}C_{as}$ sources in the South Atlantic, these were likely NCW during early and USCW during middle glacial phases (see Chapter 5.2).

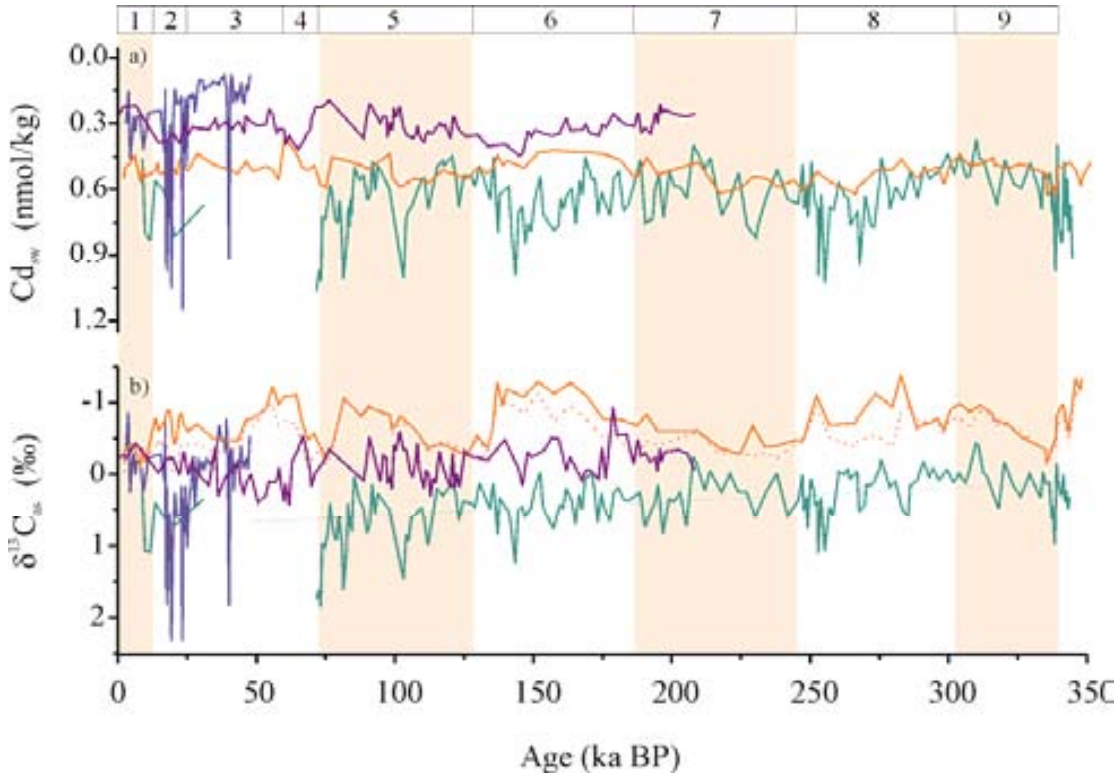

Figure 5.3-8 Down-core Cd_{sw} and tentative $\delta^{13}C_{as}$ records of Atlantic cores; a) Cd_{sw} for SO75-26KL (navy), CH82-24 (purple), RC13-229 (orange) and MD96-2080 (cyan, lower part of ABS), Boyle's (1992) partition coefficients have been used to compute Cd_{sw} for all the cores; b) tentative $\delta^{13}C_{as}$ records for these cores (see Chapter 4 for computation scheme), same colour coding. Dotted light brown line represents $\delta^{13}C_{as}$ for RC13-229 if a productivity overprint on benthic $\delta^{13}C$ is considered (see Annex II for details on the estimation of a productivity effect on the benthic $\delta^{13}C$ of RC13-229).

5.3.3. Discussion

The existence of a glacial chemocline divide in the distribution of $\delta^{13}C$ in the ASO suggests a potential role of this region in trapping and releasing atmospheric CO_2 on glacial-interglacial time scales. There are several hypotheses aiming to explain atmospheric reductions of CO_2 during glacial times by way of changes in the ventilation conditions of the Southern Ocean. In this chapter we are going to focus on those of Keeling and Stephens (2001) and Toggweiler et al. (2006) that relate the trapping of CO_2 in the deep layers of the Southern Ocean with physical barriers to ventilation.

- Keeling and Stephens (2001) base their model on changes in the rates of air-sea CO_2 exchange. Year-round Antarctic sea-ice coverage, or wintertime coverage combined with ice-induce stratification during summer, reduces deep-water ventilation and helps trapping CO_2 in the deep ocean.

- Toggweiler et al. (2006) likewise argue for decreases in ventilation in the Southern Ocean to explain the lowering of CO_2. They allude to decreases in the vertical exchange between deep and intermediate waters; likely due to reduced upwelling of deep waters as a consequence of the northwards displacement of the westerly wind belt during glacial times (see also Toggweiler and Russell, 2008). Under this scenario, $\delta^{13}C$ of the deep layers becomes much depleted without involving any significant change in the nutrient inventories.

The existing data sets for the LGM and longer time periods could be explained by these models.

- **Holocene-LGM Chemocline**

The LGM water mass distribution in the Atlantic has traditionally been interpreted as caused by mixing of the glacial equivalent of NADW, i.e. GNAIW and the glacial equivalent of AABW, i.e. LSCW. Oppo and Horowitz (2000) and Curry and Oppo (2005) postulate an influence of an intermediate water mass of southern origin to explain the $\delta^{13}C$ and Cd_{sw} data patterns in the South Atlantic. We have also shown evidence for the existence of an intermediate to mid-depth water mass of southern origin with a positive $\delta^{13}C_{as}$ signature in late phases of MIS 6 and 8 at site MD96-2080 and will show here further indications of the existence of such water mass at the LGM.

North Atlantic $\delta^{13}C$ data between 2.5-3.5 km cluster around 0.6‰. If we consider an endmember $\delta^{13}C$ value of 1.43‰ for GNAIW and an endmember value of -0.8‰ for LSCW (Table 5.3-2, Chapter 5.2), then the deep NA would be filled by around 60% GNAIW and 40% LSCW. If we use Cd_{sw} instead, taking a GNAIW endmember value of 0.24 nmol/kg and 0.7 nmol/kg for LSCW (Table 5.3-2, Chapter 5.2) we obtained mixing rates of 45:55%. $\delta^{13}C$ and Cd_{sw} are not conservative water mass tracers; LSCW at the high latitudes of the North Atlantic is far away from its formation site and therefore should have undergone significant "ageing" along its northward travel. $\delta^{13}C$ of LSCW should be substantially more negative and Cd_{sw} should be higher when reaching the high latitude North Atlantic than in the source region; hence, these mixing ratios are to be considered lower estimates of LSCW reaching the North Atlantic. $\delta^{13}C_{as}$ is considered a conservative water mass tracer which does not change once a water mass has sunk to depth and loss contact with the atmosphere. GNAIW has a positive $\delta^{13}C_{as}$, around +0.5‰, (maybe as high as +0.8‰, Lynch-Stieglitz and

Fairbanks, 1994) while LSCW is thought to have a negative $\delta^{13}C_{as}$ signature, around -0.5, perhaps even as low as -1‰ (Marchitto and Broecker, 2006). $\delta^{13}C_{as}$ values in the deep NA are around 0‰, depending on the endmember value considered for GNAIW and LSCW the mixing ratio varies between 77:33 and 50:50. These estimates make a strong case that LSCW spread to the high latitude north Atlantic at the LGM, but did not upwell there i.e., a reverse overturning circulation pattern plausibly did not occur in the North Atlantic. It has often been claimed that GNAIW was not dense enough to sink to depth. However, our estimations of mixing ratios show that this water mass had a significant influence down to at least 3500 m water depth in the North and Central Atlantic. It could be possible that GNAIW was dense enough to convect to deeper levels but denser LSCW impeded the further sinking to even greater depths.

Alternatively, LSCW could not be the only endmember to mix with GNAIW. Molyneux (2007) latitudinal discrimination of the chemocline data set adds some clues regarding this alternative hypothesis. $\delta^{13}C$ data from South Atlantic cores to the north of the SAF at the LGM define a linear trend of increasing $\delta^{13}C$ with water depth, thus reproducing the mixing pattern in the Central and North Atlantic between GNAIW and LSCW. On the other hand, cores to the south of the glacial-maximum SAF are vertically uniform at a $\delta^{13}C$ of around -0.8‰, alluding to water column homogeneity south of the front (at least from 2500 m water depth to the bottom, Fig. 5.3-5). The contrasting pattern north and south of the SAF could be related to the "Mackensen effect" lowering the $\delta^{13}C$ of the most southerly cores. Ninnemann and Charles (2002), and Hodell et al. (2003) elaborated on this possibility and conclude that such effect could not be the major driver of the $\delta^{13}C$ variability in the cores they studied because they observed strong glacial $\delta^{13}C$ depletions in various cores regardless of sedimentological and productivity regimes. Without calling on artefacts in the $\delta^{13}C$ or Cd_{sw} data (dissolution, McCorkle et al., 1995; e.g. alterations of the Dcd, Marchitto et al., 2000) the existent pattern can be explained by a different circulation regime during the LGM.

The linear trend in the South Atlantic cores north of the SAF suggests mixing of LSCW with overlying $\delta^{13}C$ positive waters. Taking a mean value of $\delta^{13}C_{as}$ of 0‰ for the upper layers of South Atlantic data (1000-3000 m, Fig. 5.3-4) we obtain the same mixing ratio between LSCW and GNAIW as for North Atlantic waters between 2500-3500 m water depth (see above). This makes it difficult to accept that LSCW could penetrate so far in the Atlantic to be an active mixer with GNAIW and at the same time have undergone active mixing with GNAIW just when moving from south to north of the SAF. Furthermore, GNAIW should have experienced significant ageing when reaching the South Atlantic, and as a consequence its $\delta^{13}C$ would not be positive and Cd_{sw} not low enough to substantially change the characteristics of LSCW, which is close to its source region in the Southern Ocean. On the other hand, the available Cd_{sw} data in the South Atlantic do not show a linear trend of increasing values with water depth but rather suggest that the water column was homogenously distributed in this element. This rejects the possibility that the water column structure in the South Atlantic was similar to that in the North Atlantic. GNAIW cannot be the sole $\delta^{13}C$ positive water mass that alters the

negative $\delta^{13}C$ of LSCW in the South Atlantic. We lean towards those studies that propose the existence of an "extra" water mass of southern origin to explain the data distribution of the South Atlantic, e.g. Oppo and Horowitz (2000) and Curry and Oppo (2005). In the view of LSCW being very negative in $\delta^{13}C$, this "extra" water mass is expected to be $\delta^{13}C$ positive. Furthermore, it should have a similar Cd_{sw} content to that of LSCW so that it does not change the Cd_{sw} signal of LSCW when this crosses the SAF, hence, explaining why a linear trend in the vertical Cd_{sw} distribution is not observed to the north of the SAF. Paleoceanographic evidence and modeling studies suggest the existence of glacial intermediate to mid-depth waters forming in the subantarctic region, i.e. Upper Southern Component Water (USCW) (Oppo and Horowitz, 2000; Keeling and Stephens, 2001; Saenko et al., 2003; Curry and Oppo, 2005; Pahnke and Zahn, 2005). However, the chemical characteristics of USCW are not well defined yet. The deep Atlantic Ocean seems more likely filled in with an admixture of USCW and LSCW ($SCW_{s.l.}$). This also explains why deep waters in the Central and North Atlantic, despite being significantly more negative than GNAIW, are considerably more positive than the extremely depleted LSCW. A consequence of these postulations is that LSCW can not serve as an endmember for mixing with GNAIW. It is not possible at this time to deduce the characteristics of the SCW and notably, of USCW that spreads through the South Atlantic, because the data available to date from mid-depths in the South Atlantic is scarce and thus more reliable mixing ratios between SCW and GNAIW cannot be determined.

Another outcome from the contrasting pattern between the vertical Cd_{sw} and the $\delta^{13}C$ distribution is that the chemocline is not nutrient related, i.e. it is not a nutricline. We opt for re-refreshing the term "chemocline" and name the divide in $\delta^{13}C$ between, apparently, upper and lower layers in the ASO as "carbocline". Moreover, the existence of a linear trend in the $\delta^{13}C$ data north of 42ºS with depth raises the question whether a vertical carbocline truly existed in the South Atlantic or whether it is an artefact of combining sediment cores from different oceanographic settings.

- **Chemocline in Previous Glacial Periods**

Hodell et al. (2003) proposed that the chemocline (carbocline) existed in previous glacial times back to 1.1 Ma. $\delta^{13}C$ data of ABS allow us to extend the domain of well ventilated waters from 2100 m (ODP 1088) to 2500 m. However, the $\delta^{13}C$ comparison of ABS, ODP 1088, 1089, TNO57-6 and RC13-229 does not necessary imply that a vertical carbocline existed in the South Atlantic and rather this could be a horizontal feature developed at the glacial SAF. The water column from at least 2500 m to the bottom south of the SAF was likely filled by $\delta^{13}C$ depleted LSCW which flowed out of the Southern Ocean only at depth. North of the SAF, LSCW bathed the abyssal depths while either NCW during early MIS 6 and 8 or $SCW_{s.l.}$ at the LGM, MIS 4 and middle MIS 6 and 8 ventilated the mid-depth South Atlantic layers (see also Chapter 5.2).

It is noticeable that the $\delta^{13}C_{as}$ levels at MD96-2080 (lower part of ABS) are more positive than in any of the records chosen to represent NCW and LSCW (except for the LGM $\delta^{13}C_{as}$ values of SO75-26KL, Fig. 5.3-8). This confirms that USCW was $\delta^{13}C$ enriched, which is further supported by the

$\delta^{13}C_{as}$ excursions during middle MIS 6 and 8 and during MIS 5 a-d (see Chapter 5.2). During early glacial periods we have concluded (see Chapter 5.2), based on benthic $\delta^{13}C$ and Cd/Ca data, that there is a strong contribution of NCW with some admixture of USCW at MD96-2080. A NCW similar in nature to LGM GNAIW (positive in $\delta^{13}C_{as}$) altered by mixing could provide for the $\delta^{13}C_{as}$ signatures in early MIS 6 ad 8 while USCW+LSCW will produce the same signature during middle MIS 6 and 8.

An outcome from the varying evolution of the circulation at site MD96-2080, Northern *versus* Southern sources, is that there is not a single water mass, and thus, a unique hydrographical regime that can explain the existence of a carbocline in the South Atlantic. During early MIS 8 benthic $\delta^{13}C$ depletions in MD96-2080 and the deeper records are of similar amplitude (Fig. 5.3-7), this supports our contention that NCW was actively ventilating the South Atlantic. The carbocline apparently did not develop as is also indicated by only subdued variations in the $\Delta\delta^{13}C_{ABS\text{-}deeper}$. In late MIS 8, on the other hand, $\delta^{13}C$ depletions are larger at the deep records, driving the $\Delta\delta^{13}C_{ABS\text{-}deeper}$ to increase, leading to the observation of a carbocline. Likely, the deep records became under a strong influence of LSCW while a mixture of USCW and LSCW reached core MD96-2080. In the case of the penultimate glacial period, in early phases NCW is present at MD96-2080 and maybe affected the $\delta^{13}C$ signature of RC13-229 while the deeper and southerly cores seem under a prominent influence of LSCW from the onset of MIS 6. The carbocline developed between upper layers ventilated by NCW and lower layers by Southern Sources. During middle MIS 6, the circulation was similar to that in middle MIS 8, with USCW+LSCW ventilating the site of MD96-2080. In any case, the upper ocean remains significantly more positive that the deep ocean, the carbocline existed when NCW was still a prominent water mass in the South Atlantic (early MIS 6) and also when this was replaced by USCW+LSCW (middle MIS 6).

The gradient between MD96-2080 and the deeper South Atlantic cores (Fig. 5.3-7) is larger in those periods where the circum-Antarctic fronts migrate northwards and there is a dominance of southern source waters at MD96-2080. This increase in the gradient is also coherent with maxima gradients between the North and South Atlantic (i.e. between ODP site 980 and MD96-2080, see Chapter 5.2). Maximum North-South gradients occur in conjunction with increase levels of IRD in the North Atlantic and are likely linked with periods of MOC slowdown (see Chapter 5.2). The carbocline seems more pronounced during times of more intense northwards spreading of SCW and probably is a reflection of a stronger influence of the Southern Ocean on the THC.

It seems plausible to consider that middle MIS 6 and 8 with a prominent influence of SCW at site MD96-2080 are analogs of the LGM, when we also observed strong northwards penetration of SCW. On the other hand, the circulation during early MIS 6 and 8 could be more similar to that proposed during MIS 3, i.e. a weak mode of the present circulation with NCW sinking to intermediate rather than to deep levels but still being able to upwell in the Southern Ocean (e.g. Keeling and Stephens, 2001; Rahmstorf, 2002). Formation of SCW in this early-interglacial mode of circulation would be more vigorous than at present.

- **Data-Model Comparison**

Extensive sea ice cover around Antarctica during glacial periods make it difficult to explain the formation of a water mass with very positive $\delta^{13}C$ as sea-ice cover would impeded air-sea $\delta^{13}C$ equilibration and hence shift $\delta^{13}C$ towards more negative levels and $\delta^{13}C_{as}$ to lower values. Therefore, such water mass must have formed outside the region of sea-ice cover, presumably in the immediate sub-Antarctic ice-free region, as Michel et al. (1995); Keeling and Stephens (2001) and Saenko et al. (2003) propose.

Keeling and Stephens (2001) suggest that expanded sea ice covered during glacial times would have shielded waters forming around Antarctica from contact with the atmosphere allowing forming deep waters with a very negative $\delta^{13}C$ signature. In their conceptual vision, the glacial counterpart of AAIW would have formed at the edge of the sea-ice limits and possibly convected to deeper levels because of higher salinity (Fig. 5.3-9). They envision different modes of circulation in the south in connection with the three MOC regimes for the Atlantic: Interglacial "on", Glacial "on" and Glacial "off" modes. Glacial "on" and "off" modes are similar to the glacial "warm" and "cold" modes proposed to exist in the last glacial (MIS 2-4) based on palecoeanographic data (Sarnthein et al., 1994; Alley and Clark, 1999) and numerical models (Rahmstorf, 2002).

- Interglacial "on" (Fig. 5.3-9a) corresponds to the present mode of circulation with strong convection in the North Atlantic.

- Glacial "on" (Fig. 5.3-9b) corresponds to a colder climate in which deep waters formed in the North Atlantic are close to the freezing point. The exposure of these cold waters to the surface in the Southern Ocean leads to extensive sea-ice formation which shields deep waters from contact with the atmosphere. Some conversion of NADW into a glacial equivalent of AAIW would occur in a narrow convective band within ACC. In this glacial mode of circulation, NADW would be fresher (but colder) rather than saltier than "glacial AAIW" but still dense enough to sink below so that the overturning could be destabilized through feedbacks involving salinity (see also Saenko et al., 2003). This mode of circulation would apply for "interstadial events" (warm periods within the glacials) of the late Pleistocene.

This mode of circulation could fit with the existence of a carbocline in the South Atlantic during early MIS 6 when a persistence presence of NCW at MD96-2080 was inferred. LSCW (i.e. AABW in Fig. 5.3-9) could become $\delta^{13}C$ depleted due to impeded air-sea contact by sea-ice shielding while $\delta^{13}C$ positive NCW would be bathing the mid-depth layers. The glacial equivalent of AAIW could not have sunk deep enough to reach the ABS location.

- Glacial "off" mode (Fig. 5.3-9c) corresponds to a collapsed conveyor. The wind-driven upwelling around Antarctica is broken because deep convection in the north produces waters not dense enough (i.e. GNAIW) to sink under AAIW. In this mode AAIW immediately overlies AABW and therefore a significant portion of the deep ocean is filled with waters formed around Antarctica (i.e. SCW). Besides, AAIW convection occurs at the sea ice limit allowing for air-sea interchange to generate a positive $\delta^{13}C_{as}$ signature of this water mass. Keeling and Stephens (2001) suggest that this

glacial mode of circulation would represent "stadial events" (cold periods within the glacials) of the late Pleistocene, including the last glacial maximum.

This glacial mode could explain the vertical distribution of $\delta^{13}C$ and Cd_{sw} in the South Atlantic with AABW and AAIW (LSCW and USCW) having very different $\delta^{13}C$ signature but similar Cd_{sw} content. It fits with our hypothesis from $\delta^{13}C$, Cd_{sw} and derived $\delta^{13}C_{as}$ (see discussion above and Chapter 5.2) of LSCW mixing with USCW before spreading in the Atlantic during the LGM and middle MIS 6 and 8.

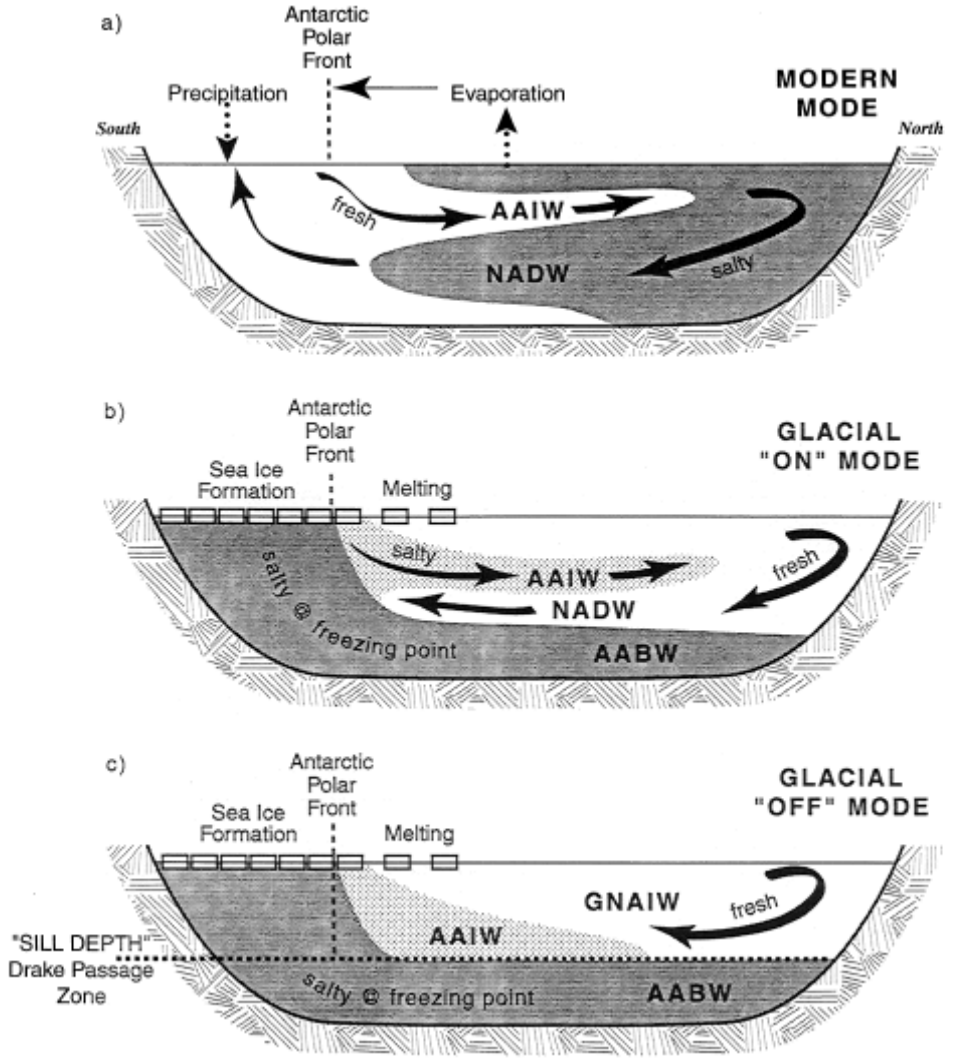

Figure 5.3-9 THC Modes proposed by Keeling and Stephens (2001) a) Modern b) Glacial "on", during interstadials c) Glacial "off", during stadials.

The conceptual model of Keeling and Stephens (2001) are largely based on buoyancy changes between the different modes of circulation. Recently, Toggweiler et al. (2006) and Toggweiler and Russell (2008) have proposed a more prominent role of the wind forcing in conditioning the state of the global THC circulation (also consistent with Wunsch and Ferrari, 2004).

Toggweiler et al. (2006) propose an alternative physical mechanism that would explain the existence of the chemical divide in the Atlantic portion of the Southern Ocean based on changes in the wind pattern around Antarctica. Glacial atmospheric cooling causes the westerly wind belt to migrate

northward which in turn reduces Ekman upwelling of Circumpolar Deep Water. The reduced upwelling decreases the CO_2 out-gassing of deep waters and allows for the accumulation of respired CO_2 at depth, thus making the deep ocean layer depleted in $\delta^{13}C_{\Sigma CO2}$ while leaving the upper layer enriched. Evidence for a northward shift and intensification of the westerly wind belt during the LGM comes from paleohydrographic records (Gasse, 2000); paleovegetation recors (Moreno et al., 1999) and grain size and clay mineralogy studies (Lamy et al., 1999). Additionally, a higher density contrast between intermediate and bottom water would restrict respired CO_2 transfer from the lower to the upper layer due to more stable water mass stratification that would act to reduce upward mixing (Toggweiler, 1999). These changes occur without substantial variations in the $(PO_4)^{3-}$ content of both ocean layers, hence potentially also explaining the lack of glacial-interglacial variability in the Cd_{sw} records of the Deep South Atlantic sites (RC12-267, RC12-294, RC16-86, RC16-85, RC13-228, RC13-229; Boyle, 1992; Oppo and Rosenthal, 1994; Lea, 1995; Rosenthal et al., 1997; Oppo and Horowitz, 2000). Toggweiler (1999) proposed that upper layer waters are of northern origin (e.g. Yu et al., 1996). In any case, these mid-depth waters in the Southern Ocean may become $\delta^{13}C_{\Sigma CO2}$ enriched with no substantial change in nutrients and would show positive estimated $\delta^{13}C_{as}$ levels. Although Toggweiler et al. (2006) consider the shift of the westerly wind belt the major driving force in changing the glacial circulation, they also allude to increased stratification in the Southern Ocean (e.g. Francois et al., 1997; Sigman and Boyle, 2000) and sea-ice shielding (Keeling and Stephens, 2001) in their conceptual model to retain CO_2 at depth.

This conceptual model claims to be capable of explaining on the one hand the, *a priori*, vertical $\delta^{13}C$ structure of the South Atlantic and on the other hand the apparent absence of glacial-interglacial variability in Cd_{sw} in deep records from the South Atlantic (see above). However, we doubt that a vertical carbocline really existed in the South Atlantic north of the SAF and we lack mid-depth cores shallower than 2500 m water depth southwards of 42ºS so that we cannot ensure that the upper layers in the Southern Ocean were well-ventilated. If well-ventilated USCW formed at the SAF, then we would expect that the water column to the south would be homogenously $\delta^{13}C$ depleted (Figs. 5.3-9b and c can serve as illustration). With the available data sets, we cannot asses the existence of a vertical carbocline in the South Atlantic. Nevertheless, the latitudinal variation of $\delta^{13}C$ suggests that the carbocline was horizontally developed at the SAF.

In regard to the different hydrographies we postulate to have existed in the South Atlantic during early and middle MIS 6 and 8, this model does not initially allow distinguishing between both modes. A plausible mechanism to explain this restructuring could be the degree of equatorwards displacement of the westerly wind belt. Only minor migrations at the initiation of MIS 6 and 8 would reduce the upwelling of deep waters in the Antarctic zone but still permit upwelling of intermediate-depth waters (namely NCW) in the Sub-Antarctic zone; while maxima northward migrations could be related to the periods of dominance of SCW, i.e. LGM and middle MIS 6 and 8.

A possible positive feedback in both the Keeling and Stephens (2001) or Toggweiler et al. (2006) mechanisms relates to the intensification of the fast flowing ACC. Several studies have reported

evidence for increased bottom flow speed at sites close to areas under the influence of ACC, notably coming from $\overline{SS}$ profiles (Pudsey and Howe, 1998; Hall et al., 2001; Molyneux et al., 2007). Similar evidence is provided by the $\overline{SS}$ record from MD96-2080 (see Chapter 5.2) that shows increased near-bottom flow velocities in glacial periods with maximum flow speeds coinciding with the presence of SCW at the core site. A northward expanded and faster flowing ACC plausibly acted to impede the southward penetration of NCW into the Southern Ocean by forming an efficient physical barrier to latitudinal mixing between SCW and NCW.

- **Implications for Atmospheric CO_2**

Hodell et al. (2003) noted a parallelism between the benthic $\Delta\delta^{13}C$ between ODP sites 1088 and 1090 and the Vostok atmospheric CO_2 record. We also observed this parallelism with the $\delta^{13}C$ gradients computed between ABS and the deep South Atlantic records at or south of 42ºS (ODP sites 1089, TNO57-6) (Fig. 5.3-10) but not with the $\delta^{13}C$ gradient between ABS and RC13-229. This reinforces the hypothesis that the carbocline was a horizontal feature and its existence in the South Atlantic suggests a role of this part of the ocean for the glacial sinking of atmospheric CO_2. Along MIS 8, the mid-depth to deep gradient maximizes in the middle of the glacial period, and coincides with minimum atmospheric CO_2 concentrations. For the penultimate glaciation, apparently the carbocline develop at its onset. In this glacial period we observed that atmospheric CO_2 concentrations also decrease at the beginning of the cold phase. During MIS 2 to 4, the gradient increases more substantially between ABS and ODP 1089 than between ABS and TNO57-6. During this interval there are depletions and increases in the Vostok atmospheric CO_2 record, whose link with the benthic gradients likely responds to changes in deep ocean circulation.

A glacial "on" mode of circulation *sensu* Keeling and Stephens (2001) could correspond only to subdued northwards migrations of the westerly wind belt *sensu* Toggweiler et al. (2006), which may have displaced the upwelling region from the Antarctic to the sub-Antarctic. The MOC would continue to work in a similar manner to the interglacial "on" mode but in contrast to this mode, where AABW and NADW densities are not very different, a higher density contrast between LSCW and NCW would restrict diapycnal transferences of respired CO_2, initiating in this way the glacial depletions of this greenhouse gas. If the equatorward shift continued, then the upwelling could be suppressed and the circulation could become the "off" mode of Keeling and Stephens (2001), in the case of middle MIS 8 this mode seems more efficient in trapping CO_2.

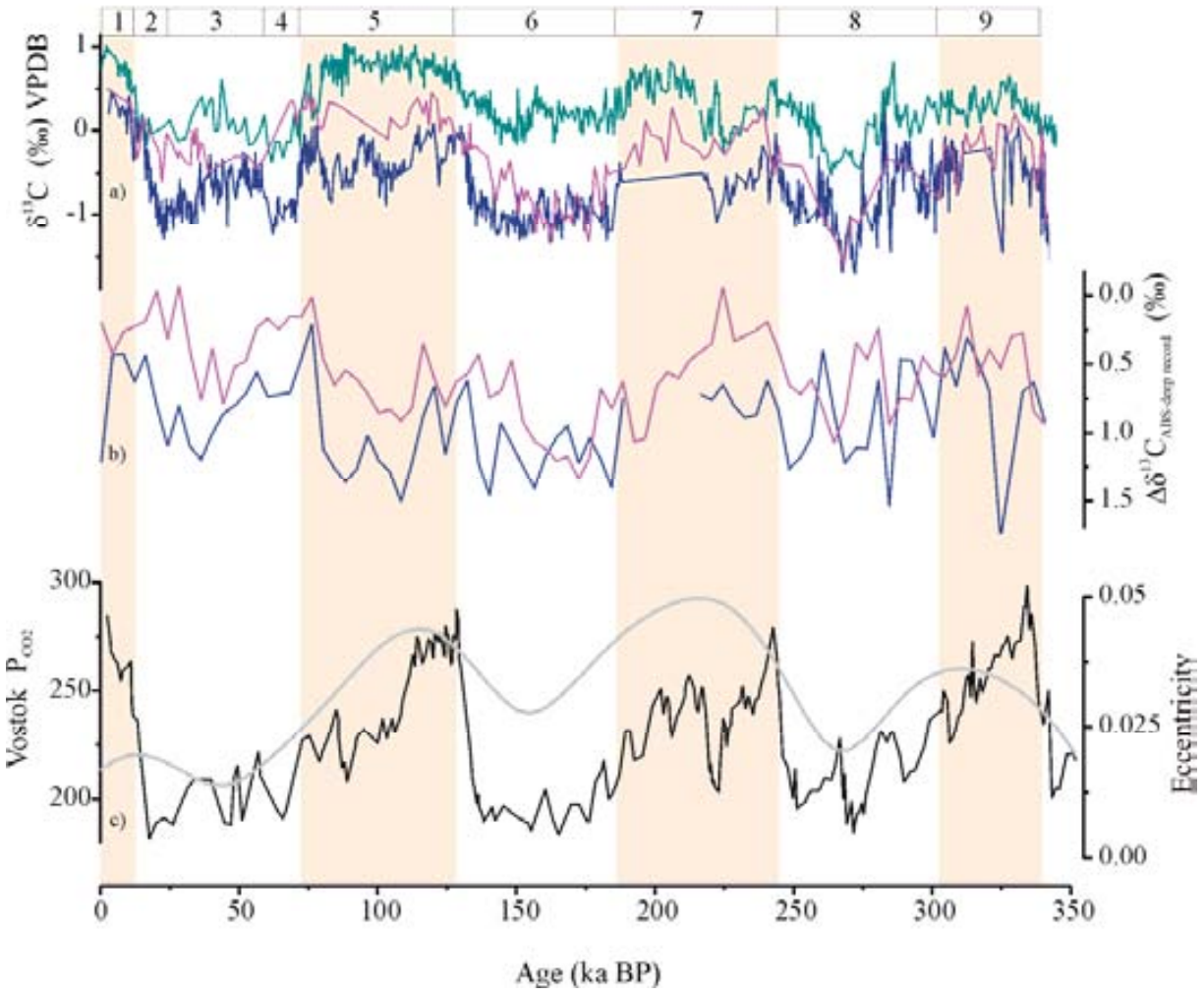

Figure 5.3-10 Down-core South Atlantic benthic $\delta^{13}C$ records and gradients compared to Vostok CO_2; a) benthic $\delta^{13}C$ of ABS (cyan), TNO57-6 (pink), ODP 1089 (blue); b) benthic $\delta^{13}C$ gradients computed between ABS and the deeper records located at and south of 42ºS (LGM position of the SAF), i.e. $\Delta\delta^{13}C_{ABS\text{-}TNO57\text{-}6}$ (pink) and $\Delta\delta^{13}C_{ABS\text{-}ODP1089}$ (blue); c) Vostok CO_2 record (black) (Barnola et al., 1987; Petit et al., 1999), also shown the eccentricity curve as reference (Laskar, 1990).

5.3.4. Conclusions

We evaluate the existing benthic $\delta^{13}C$, Cd_{sw} and derived $\delta^{13}C_{as}$ data sets for the LGM Atlantic and we conclude that their distribution is better explained by a northwards spreading of a mixture of Upper and Lower Southern Component waters at depth and Northern Component Water at intermediate levels.

USCW could have formed at the glacial SAF, outside the Antarctic sea-ice area, and thus have a positive $\delta^{13}C_{as}$ signature. LSCW likely formed in the Southern Ocean where sea-ice capping would have impeded air-sea transferences of CO_2 leading to very negative $\delta^{13}C_{as}$ signatures. LSCW could have left the Southern Ocean domain only at depth and mix with USCW when crossing the SAF.

The existence of a sharp vertical divide in the $\delta^{13}C$ distribution of the South Atlantic may be flawed by the core selection. Only cores southwards of the glacial SAF display much depleted $\delta^{13}C$ values from 2500 m down the water column. If at all, a carbocline during the LGM developed horizontally rather than vertically.

Comparison with $\delta^{13}C$ records of ABS allowed an extension of the domain of well-ventilated waters from 2100 m (i.e. ODP 1088) to at least 2500 m. The source of significantly better ventilated mid-depth than abyssal waters shifted with the progression of MIS 6 and 8. During early MIS 6 and 8 the circulation was likely similar to that of today (glacial "on") being NCW the source of well-ventilated waters. As glaciation progressed, SCW became the primarily contributors to the hydrography (glacial "off"). Positive USCW mixed with negative LSCW and generated the relatively well-ventilated water mass that we record at 2500 m in the Agulhas Bank area. This mode of circulation suggests that middle MIS 6 and 8 were analogs of the LGM, so that also in previous glaciations the sharp contrast in $\delta^{13}C$ occurred horizontally at the SAF. This observation reinforces older hypotheses that the Southern Ocean became isolated during extreme glacial times.

Regardless of its nature, horizontal or vertical, the match between Vostok atmospheric CO_2 and the benthic $\delta^{13}C$ gradients, suggest an active role of the Southern Ocean in trapping atmospheric CO_2 during glacial times.

References

Alley, R.B. and Clark, P.U., 1999. The deglaciation of the Northern Hemisphere: a global perspective. Annual Review of Earth and Planetary Sciences, 27, 149-182.

Barnola, J.M., Raynaud, D., Korotkevich, Y.S. and Lorius, C., 1987. Vostok ice core provides 160,000-year record of atmospheric CO_2. Nature, 329, 408-414.

Berner, W.H., Oescgger, H. and Stauffer, B., 1980. Information on the carbon dioxide cycle from ice-core studies. Radiocarbon, 22, 227-235.

Bertram, C.J., Elderfield, H., Shackleton, N.J. and MacDonald, J.A., 1995. Cadmium/calcium and carbon isotope reconstructions of the glacial northeast Atlantic Ocean. Paleoceanography, 10 (3), 563-578.

Bickert, T. and Mackensen, A., 2003. Last Glacial to Holocene changes in South Atlantic deep water circulation. In: G. Wefer, S. Mulitza and V. Rathmeyer (Editors), The South Atlantic during the Late Quaternary. Spirnger, Berlin, pp. 671-695.

Boyle, E.A., 1992. Cadmium and $\delta^{13}C$ paleochemical ocean distributions during the stage 2 glacial maximum. Annual Review of Earth and Planetary Sciences, 20, 245-287.

Boyle, E.A. and Keigwin, L.D., 1985/86. Comparison of Atlantic and Pacific paleochemical records for the last 215,000 years: changes in deep ocean circulation and chemical inventories. Earth and Planetary Science Letters, 76 (1-2), 135-150.

Boyle, E.A. and Rosenthal, Y., 1996. Chemical Hydrography of the South Atlantic during the Last Glacial Maximum: Cd *vs* $\delta^{13}C$. In: G. Wefer, W.H. Berger, G. Siedler and D. Webb (Editors), The South Atlantic: Present, Past and Future. Springer-Verlag Berlin Heidelberg New York, pp. 423-443.

Brathauer, U. and Abelmann, A., 1999. Late Quaternary variations in sea surface temperatures and their relationship to orbital forcing recorded in the Southern Ocean (Atlantic sector). Paleoceanography, 14 (2), 135-148.

Curry, W.B. and Oppo, D.W., 2005. Glacial water mass geometry and the distribution of $\delta^{13}C$ of ΣCO_2 in the western Atlantic Ocean. Paleoceanography, 20, PA1017, doi: 10.1029/2004PA001021.

Curry, W.B., Duplessy, J.C., Labeyrie, L.D. and Shackleton, N.J., 1988. Changes in the distribution of $\delta^{13}C$ of deep water ΣCO_2 between the last glaciation and the Holocene. Paleoceanography, 3 (3), 317-341.

Charles, C.D., Wright, J.D. and Fairbanks, R.G., 1993. Thermodynamic influences on the marine carbon isotope record. Paleoceanography, 8 (6), 691-698.

Duplessy, J.C., Shackleton, N.J., Fairbanks, R.G., Labeyrie, L., Oppo, D. and Kallel, K., 1988. Deep water source variations during the last climatic cycle and their impact on the global deep water circulation. Paleoceanography, 3 (3), 343-360.

Francois, R., Altabet, M.A., Yu, E.-F., Sigman, D.M., Bacon, M.P., Frank, M., Bohrmann, G., Bareille, G. and Labeyrie, L.D., 1997. Contribution of Southern Ocean surface-water stratification to low atmospheric CO2 concentrations during the last glacial period. Nature, 389, 929-935.

Gasse, F., 2000. Hydrological changes in the African tropics since the Last Glacial Maximum. Quaternary Science Reviews, 19 (1-5), 189-211.

Gersonde, R., Crosta, X., Abelmann, A. and Armand, L., 2005. Sea-surface temperature and sea ice distribution of the Southern Ocean at the EPILOG Last Glacial Maximum-a circum-Antarctic view based on siliceous microfossil records. Quaternary Science Reviews, 24 (7-9), 869-896.

Hall, I.R., McCave, N., Shackleton, N.J., Weedon, G.P. and Harris, S.E., 2001. Intensified deep Pacific inflow and ventilation in Pleistocene glacial times. Nature, 412, 809-813.

Hodell, D.A., Venz, K., Charles, C.D. and Ninnemann, U.S., 2003. Pleistocene vertical carbon isotope and carbonate gradients in the South Atlantic sector of the Southern Ocean. Geochemistry, Geophysics, Geosystems, 4 (1), 1004, doi: 10.1029/2002GC000367.

Howard, W.R. and Prell, W.L., 1992. Late Quaternary Surface Circulation of the Southern Indian Ocean and its Relationship to Orbital Variations. Paleoceanography, 7 (1), 79-117.

Keeling, R.F. and Stephens, B.B., 2001. Antarctic sea ice and the control of plesitocene climate instability. Paleoceanography, 16 (1), 112-131.

Lamy, F., Hebbeln, D. and Wefer, G., 1999. High-Resolution Marine Record of Climatic Change in Mid-latitude Chile during the Last 28,000 Years Based on Terrigenous Sediment Parameters. Quaternary Research, 51 (1), 83-93.

Laskar, J., 1990. The chaotic motion of the solar system - A numerical estimate of the size of the chaotic zones. Icarus, 88, 266-291.

Lea, D.W., 1995. A trace metal perspective on the evolution of Antarctic Circumpolar Deep Water Chemistry. Paleoceanography, 10 (4), 733-748.

Lynch-Stieglitz, J. and Fairbanks, R.G., 1994. A conservative tracer for glacial ocean circulation from carbon isotope and paleonutrient measurements in benthic foraminifera. Nature, 369, 308-310.

Lynch-Stieglitz, J., van Geen, A. and Fairbanks, R.G., 1996. Interocean exchange of Glacial North Atlantic Intermediate Water: evidence from the subantarctic Cd/Ca and carbon isotope measurements. Paleoceanography, 11 (2), 191-201.

Mackensen, A., Futterer, D.K., Grobe, H. and Schmiedl, G., 1993a. Benthic foraminiferal assemblages from the eastern South Atlantic Polar Front region between 35º and 57ºS: Distribution, ecology and fossilization potential. Marine Micropaleontology, 22 (1-2), 33-69.

Mackensen, A., Hubberten, H.-W., Bickert, T., Fischer, G. and Fütterer, D.K., 1993b. The $\delta^{13}C$ in benthic foraminiferal tests on *Fontbotia wuellerstorfi* (Schwager) relative to the $\delta^{13}C$ of dissolved inorganic carbon in southern ocean deep water: implications for glacial ocean circulation models. Paleoceanography, 8, 587-610.

Marchitto, T.M. and Broecker, W.S., 2006. Deep water mass geometry in the glacial Atlantic Ocean: A review of constraints from the paleonutrient proxy Cd/Ca. Geochemistry, Geophysics, Geosystems, 7, Q12003, doi: 10.1029/2006GC001323.

Marchitto, T.M., Curry, W.B. and Oppo, D.W., 2000. Zn concentrations in benthic foraminifera reflect seawater chemistry. Paleoceanography, 15 (3), 299-306.
Marinov, I., Gnanadesikan, A., Toggeweiler, J.R. and Sarmiento, J.L., 2006. The Southern Ocean biogeochemical divide. Nature, 441, 964-967.
McCorkle, D.C., Martin, P.A., Lea, D.W. and Klinkhammer, G.P., 1995. Evidence of a dissolution effect on benthic foraminiferal shell chemistry: $\delta^{13}C$, Cd/Ca, Ba/Ca, and Sr/Ca results from the Ontong Java Plateau. Paleoceanography, 10 (4), 699-714.
Michel, E., Labeyrie, L.D., Duplessy, J.-C., Gorfti, N., Labracherie, M. and Turon, J.-L., 1995. Could Deep Subantarctic Convection Feed the World Deep Basins during the Last Glacial Maximum? Paleoceanography, 10 (5), 927–941.
Molyneux, E.G., 2007. Surface and deep water variability on the Agulhas Plateau over the past 170 ka, Cardiff University, Cardiff, PhD Thesis, 332 pp.
Molyneux, E.G., Hall, I.R., Zahn, R. and Diz, P., 2007. Deep water variability on the southern Agulhas Plateau: Interhemispheric links over the past 170 ka. Paleoceanography, 22, PA4209, doi: 10.1029/2006PA001407.
Moreno, P.I., Lowell, T.V., Jacobson Jr, G.L. and Denton, G.H., 1999. Abrupt Vegetation and Climate Changes During the Last Glacial Maximumand Last Termination in The Chilean Lake District: A Case Study from Canal De La Puntilla (41ºS). Geografiska Annaler, Series A: Physical Geography, 81 (2), 285-311.
Ninnemann, U.S. and Charles, C.D., 2002. Changes in the mode of Southern Ocean circulation over the last glacial cycle revealed by foraminiferal stable isotopic variability. Earth and Planetary Science Letters, 201 (2), 383-396.
Oppo, D.W. and Rosenthal, Y., 1994. Cd/Ca changes in a deep Cape Basin core over tyhe past 730,000 years: response of circumpolar deepwater variability to northern hemisphere ice sheet melting? Paleoceanography, 9 (5), 661-675.
Oppo, D.W. and Horowitz, M., 2000. Glacial deep water geometry: South Atlantic benthic foraminiferal Cd/Ca and $\delta^{13}C$ evidence. Paleoceanography, 15 (2), 147-160.
Oppo, D.W., Fairbanks, R.G., Gordon, A.L. and Shackleton, N.J., 1990. Late Pleistocene southern ocean $\delta^{13}C$ variability. Paleoceanography, 5 (1), 43-54.
Pahnke, K. and Zahn, R., 2005. Southern Hemisphere Water Mass Conversion Linked with North Atlantic Climate Variability. Science, 307, 1,741-1,746.
Peeters, F.J.C., Acheson, R., Brummer, G.-J.A., de Ruijter, W.P.M., Schneider, R., Ganssen, G., Ufkes, M.E. and Kroon, D., 2004. Vigorous exchange between the Indian and Atlantic oceans at the end of the past five glacial periods. Nature, 438, 661-665.
Petit, J.R. et al., 1999. Climate and atmospheric history of the past 420,000 years from the Vostok ice core, Antarctica. Nature, 399, 429-436.
Pudsey, C.J. and Howe, J.A., 1998. Quaternary history of the Antarctic Circumpolar Current: evidence from the Scotia Sea. Marine Geology, 148, 83-112.
Rahmstorf, S., 2002. Ocean circulation and climate during the past 120,000 years. Nature, 419, 207-214.
Rosenthal, Y., Boyle, E.A. and Labeyrie, L., 1997. Last glacial maximum paleochemistry and deepwater circulation in the Southern Ocean: Evidence from foraminiferal cadmium. Paleoceanography, 12 (6), 787-796.
Saenko, O.A., Weaver, A.J. and Gregory, J.M., 2003. On the Link between the Two Modes of the Ocean Thermohaline Circulation and the Formation of Global-Scale Water Masses. Journal of Climate, 16 (17), 2,797-2,801.
Sarnthein, M., Winn, K., Jung, S.J.A., J.-C., D., Labeyrie, L., Erlenkeuser, H. and Ganssen, G., 1994. Changes in the east Atlantic deepwater circulation over the last 30,000 years: Eight time slice reconstructions. Paleoceanography, 9 (2), 209-267.
Schlitzer, R., 2007. Ocean Data View. In: http://odv.awi.de.
Sigman, D.M. and Boyle, E.A., 2000. Glacial/interglacial variations in atmospheric carbon dioxide. Nature, 407, 859-869.
Toggweiler, J.R., 1999. Variation of atmospheric CO_2 by ventilation of the ocean´s deepest water. Paleoceanography, 14 (5), 571-588.
Toggweiler, J.R. and Russell, J., 2008. Ocean circulation in a warming climate. Nature, 451, 286-288.
Toggweiler, J.R., Russell, J.L. and Carson, S.R., 2006. Midlatitude westerlies, atmospheric CO_2, and climate change during the ice ages. Paleoceanography, 21 PA2005, doi: 10.1029/2005PA001154.
Willamowski, C. and Zahn, R., 2000. Upper ocean circulation in the glacial North Atlantic from benthic foraminiferal isotope and trace element fingerprinting. Paleoceanography, 15 (5), 515-527.
Wunsch, C. and Ferrari, R., 2004. Vertical mixing, energy and the general circulation of the oceans. Annual review of Fluid Mechanics, 36 (1), 281-314.
Yu, E.-F., Francois, R. and Bacon, M.P., 1996. Similar rates of modern and last-glacial ocean thermohaline circulation inferred from radiochemical data. Nature, 379, 689-694.
Zahn, R. and Stüber, A., 2002. Suborbital intermediate water variability inferred from paired benthic foraminiferal Cd/Ca and $\delta^{13}C$ in the tropical West Atlantic and linking with North Atlantic climates. Earth and Planetary Science Letters, 200, 191-205.
Zahn, R., Sarnthein, M. and Erlenkeuser, H., 1987. Benthic isotope evidence for changes of the Mediterranean Outflow during the late Quaternary. Paleoceanography, 2 (6), 543-559.

Annex I

Available Holocene and LGM Atlantic benthic $\delta^{13}C$ and Cd/Ca data bases (Zahn et al., 1987; Bickert and Mackensen, 2003; Table 2, Hodell et al., 2003; Tables 1 and 2, Curry and Oppo, 2005; Tables 1 to 3, Marchitto and Broecker, 2006) and data from MD02-2594 (this Thesis) and MD02-2589 (Molyneux et al., 2007). Benthic Cd/Ca has been converted into Cd_{sw} using Boyle's (1992) partition coefficients.

The original references are detailed in the following tables and are:

(1) Bertram, C.J., Elderfield, H., Shackleton, N.J. and MacDonald, J.A., 1995. Cadmium/calcium and carbon isotope reconstructions of the glacial northeast Atlantic Ocean. Paleoceanography, 10 (3), 563-578.

(2) Beveridge, N.A.S., Elderfield, H. and Shackleton, N.J., 1995. Deep thermohaline circulation in the low-latitude Atlantic during the last glacial. Paleoceanography, 10 (3), 643-660.

(3) Bickert, T., Curry, W.B.C. and Wefer, G., 1997. Late Pliocene to Holocene (2.6-0 Ma) western equatorial Atlantic deep-water circulation: Inferences from stable isotopes. Proceedings of the Ocean Drilling Program Scientific Results, 154, 239– 253.

(4) Bickert, T. and Mackensen, A., 2003. Last Glacial to Holocene changes in South Atlantic deep water circulation. In: G. Wefer, S. Mulitza and V. Rathmeyer (Editors), The South Atlantic during the Late Quaternary. Spirnger, Berlin, pp. 671-695.

(5) Boyle, E.A., 1992. Cadmium and $\delta^{13}C$ paleochemical ocean distributions during the stage 2 glacial maximum. Annual Review of Earth and Planetary Sciences, 20, 245-287.

(6) Boyle, E.A. and Keigwin, L., 1987. North Atlantic thermohaline circulation during the past 20,000 years linked to high-latitude surface temperature. Nature, 330, 35-40.

(7) Came, R.E., Oppo, D.W. and Curry, W.B., 2003. Atlantic Ocean circulation during the Younger Dryas: Insights from a new Cd/Ca record from the western subtropical South Atlantic. Paleoceanography, 18 (4), 1086, doi:10.1029/2003PA000888.

(8) Curry, W.B., 1996. Late Quaternary deep circulation in the western equatorial Atlantic, in The South Atlantic: Present and past circulation. In: G. Wefer, W.H. Berger, G. Siedler and D. Webb (Editors), The South Atlantic: Present and past circulation. Springer, New York, pp. 577–598.

(9) Curry, W.B., Duplessy, J.C., Labeyrie, L.D. and Shackleton, N.J., 1988. Changes in the distribution of $\delta^{13}C$ of deep water ΣCO_2 between the last glaciation and the Holocene. Paleoceanography, 3 (3), 317-341.

(10) Curry, W.B. and Oppo, D.W., 2005. Glacial water mass geometry and the distribution of $\delta^{13}C$ of ΣCO_2 in the western Atlantic Ocean. Paleoceanography, 20, PA1017, doi: 10.1029/2004PA001021.

(11) Charles, C.D., Lynch-Stieglitz, J., Ninnemann, U.S. and Fairbank, R.G., 1996. Climate connections between the hemispheres revealed by deep sea sediment core/ice core correlations. Earth Planetary Sciences Letters, 142 (1-2), 19-27.

(12) Hodell, D.A., Venz, K., Charles, C.D. and Ninnemann, U.S., 2003. Pleistocene vertical carbon isotope and carbonate gradients in the South Atlantic sector of the Southern Ocean. Geochemistry, Geophysics, Geosystems, 4 (1), 1004, doi: 10.1029/2002GC000367.

(13) Keigwin, L.D., 2004. Radiocarbon and stable isotope constraints on Last Glacial Maximum and Younger Dryas ventilation in the western North Atlantic. Paleoceanography, 19, PA4012, doi: 10.1029/2004PA001029.

(14) Keigwin, L.D. and Schlegel, M.A., 2002. Ocean ventilation and sedimentation since the glacial maximum at 3 km in the western North Atlantic. Geochemistry, Geophysics, Geosystems, 3 (6), 1034, doi: 10.1029/2001GC000283.

(15) Lea, D.W., 1995. A trace metal perspective on the evolution of Antarctic Circumpolar Deep Water Chemistry. Paleoceanography, 10 (4), 733-748.

(16) Mackensen, A., Rudolph, M. and Kuhn, G., 2001. Late Pleistocene deep-water circulation in the subantarctic eastern Atlantic. Global and Planetary Change, 30 (3-4), 197-229.

(17) Marchitto, T.M. and Broecker, W.S., 2006. Deep water mass geometry in the glacial Atlantic Ocean: A review of constraints from the paleonutrient proxy Cd/Ca. Geochemistry, Geophysics, Geosystems, 7, Q12003, doi: 10.1029/2006GC001323.

(18) Marchitto, T.M., Curry, W.B. and Oppo, D., 1998. Millennial-scale changes in North Atlantic circulation since the last glaciation. Nature, 393, 557-561.

(19) Marchitto, T.M., Oppo, D.W. and Curry, W.B., 2002. Paired benthic foraminiferal Cd/Ca and Zn/Ca evidence fro a greatly increased presence of Southern Ocean water in the glacial North Atlantic. Paleoceanography, 17 (3), 1038, doi: 10.1029/2000PA000598.

(20) Martin, P.A. and Lea, D.W., 1998. Comparison of water mass changes in the deep tropical Atlantic derived from Cd/Ca and carbon isotope records: Implications for changing Ba composition of deep Atlantic water masses. Paleoceanography, 13 (6), 572-585.

(21) Molyneux, E.G., Hall, I.R., Zahn, R. and Diz, P., 2007. Deep water variability on the southern Agulhas Plateau: Interhemispheric links over the past 170 ka. Paleoceanography, 22, PA4209, doi: 10.1029/2006PA001407.

(22) Ninnemann, U.S. and Charles, C.D., 2002. Changes in the mode of Southern Ocean circulation over the last glacial cycle revealed by foraminiferal stable isotopic variability. Earth Planetary Sciences Letters, 201 (2), 383-396.

(23) Oppo, D.W. and Fairbanks, R.G., 1987. Variability in the deep and intermediate water circulation of the Atlantic Ocean during the past 25,000 years: Northern Hemisphere modulation of the Southern Ocean. Earth Planetary Sciences Letters, 86, 1-15.

(24) Oppo, D.W. and Horowitz, M., 2000. Glacial deep water geometry: South Atlantic benthic foraminiferal Cd/Ca and $\delta^{13}C$ evidence. Paleoceanography, 15 (2), 147-160.

(25) Oppo, D.W., Horowitz, M. and Lehman, S.J., 1997. Marine core evidence for reduced deep water production during Termination II followed by a relative stable substage 5e (Eemian). Paleoceanography, 12 (1), 51-63.

(26) Oppo, D.W. and Lehman, S.J., 1993. Middepth circulation of the subpolar North Atlantic during the Last Glacial Maximum. Science, 259, 1,148– 1,152.

(27) Oppo, D.W. and Rosenthal, Y., 1994. Cd/Ca changes in a deep Cape Basin core over tyhe past 730,000 years: response of circumpolar deepwater variability to northern hemisphere ice sheet melting? Paleoceanography, 9 (5), 661-675.

(28) Pierre, C., Saliege, J.F., Urrutiaguer, M.J. and Giraudeau, J., 2001. Stable isotope record of the last 500 k.y. at Site 1087 (Southern Cape Basin). In: G. Wefer, W.H.B. Berger and C. Richter (Editors), Proc. of Ocean Drill. Program, Sci. Results. Ocean Drill. Program, College Station, Tex., pp (Available at http://www-odp.tamu.edu/publications/175_SR/chap_12/chap_12.htm).

(29) Rickaby, R.E.M., Greaves, M.J. and Elderfield, H., 2000. Cd in planktonic and benthic foraminiferal shells determined by thermal ionisation mass spectrometry. Geochimica Cosmochimica Acta, 64 (7), 1229 -1236.

(30) Rosenthal, Y., Boyle, E.A. and Labeyrie, L., 1997. Last glacial maximum paleochemistry and deepwater circulation in the Southern Ocean: Evidence from foraminiferal cadmium. Paleoceanography, 12 (6), 787-796.

(31) Sarnthein, M., Winn, K., Jung, S.J.A., J.-C., D., Labeyrie, L., Erlenkeuser, H. and Ganssen, G., 1994. Changes in the east Atlantic deepwater circulation over the last 30.000 years: Eight time slice reconstructions. Paleoceanography, 9 (2), 209-267.

(32) Slowey, N.C. and Curry, W.B.C., 1995. Glacial-Interglacial differences in circulation and carbon cycling within the upper western Atlantic. Paleoceanography, 10 (4), 715– 732.

(33) Willamowski, C. and Zahn, R., 2000. Upper ocean circulation in the glacial North Atlantic from benthic foraminiferal isotope and trace element fingerprinting. Paleoceanography, 15 (5), 515-527.

(34) Zahn, R., Sarnthein, M. and Erlenkeuser, H., 1987. Benthic isotope evidence for changes of the Mediterranean Outflow during the late Quaternary. Paleoceanography, 2 (6), 543-559.

(35) Zahn, R. and Stüber, A., 2002. Suborbital intermediate water variability inferred from paired benthic foraminiferal Cd/Ca and $\delta^{13}C$ in the tropical West Atlantic and linking with North Atlantic climates. Earth Planetary Sciences Letters, 200, 191-205.

Table 5.3 Annex I-1 North Atlantic (from 65ºN to 41ºN) published Holocene and LGM benthic $\delta^{13}C$ (‰) and Cd_{sw} (nmol/kg) (from benthic Cd/Ca). $\Delta\delta^{13}C$ represents the different between Holocene and LGM benthic $\delta^{13}C$

Core	Long. (º)	Lat. (º)	Depth (m)	Hol. $\delta^{13}C$ (‰)	LGM $\delta^{13}C$ (‰)	$\Delta\delta^{13}C$ (‰)	Hol. Cd_{sw} (nmol/kg)	LGM Cd_{sw} (nmol/kg)	Ref.
V28-14	-29.57	64.78	1855	1.12	1.13	-0.01		0.24	5
NEAP-3K	-23.95	62.83	1510					0.21	29
NEAP-4K	-24.17	61.48	1627	1.5	1.5	0	0.35	0.28	29, 5
EW9302-14JPC	-24.11	61.42	1653		1.5	-1.5			25
V29-204	-23.02	61.18	1849	1.24	1.37	-0.13	0.22	0.2	19
V29-202	-20.97	60.38	2658	1.06	0.45	0.61	0.31	0.38	19
NEAP-8K	-23.90	59.78	2360					0.49	29
V29-198	-15.57	58.73	1139	1.1	1.4	-0.3			26
BOFS14K	-19.44	58.62	1756	1.02	1.4	-0.38	0.37	0.17	1
V28-73	-20.87	57.18	2063	1.17	1.16	0.01	0.57	0.3	19
NEAP-15K	-27.80	56.35	2848					0.49	29
M17051	-31.99	56.16	2295	1	0.8	0.2			31
DSDP 552	-23.23	56.05	2311		0.9	-0.9			31
ODP 980	-14.70	55.48	2168	1.04	0.82	0.22		0.24	19
M17050	-27.89	55.47	2795	0.5	0.5	0			31
M17049	-26.73	55.26	3331	0.7	0.6	0.1			31
BOFS11K	-20.35	55.19	2004	1.43	1.4	0.03	0.39	0.25	1
NEAP-17K/18B	-28.35	54.68	2880				0.34	0.4	29
M23414	-20.29	53.54	2196	1.12	1	0.12	0.37	0.4	33
NEAP-18K/19B	-30.33	52.75	3275				0.33	0.58	29
V29-179	-24.53	44.00	3331	1.1	0.63	0.47	0.31	0.37	5
CHN82-20	-29.87	43.50	3070	1.3	0.76	0.54	0.26	0.36	5, 19
CHN82-15	-28.23	43.37	2151	1.1	1.2	-0.1			6

Table 5.3 Annex I-2 Central Atlantic (from 41ºN to10ºS) published Holocene and LGM benthic $\delta^{13}C$ (‰) and Cd_{sw} (nmol/kg) (from benthic Cd/Ca). $\Delta\delta^{13}C$ represents the different between Holocene and LGM benthic $\delta^{13}C$

Core	Long. (º)	Lat. (º)	Depth (m)	Hol. $\delta^{13}C$ (‰)	LGM $\delta^{13}C$ (‰)	$\Delta\delta^{13}C$ (‰)	Hol. Cd_{sw} (nmol/kg)	LGM Cd_{sw} (nmol/kg)	Ref.
SO75-26KL	-9.50	37.82	1099	1.02	1.6	-0.58	0.36	0.19	33
V26-176	-72.00	36.00	3942		0.18			0.32	5
LY-II-13A	-7.81	35.97	1201	1.205	1.523	-0.32			34
M11944	-8.5	35.65	1765		1.028				34
CH74-227	-29.25	35.27	3225		0.1	-0.1			34
M15670	-7.58	34.9	1482	1.123	1.323	-0.2			34
M15669	-7.82	34.88	2022	1.122	0.852	0.27			34
M15672	-8.2	34.85	2455	1.115	0.61	0.51			34
EN120-GGC1	-57.62	33.67	4450	0.33	-0.41	0.74	0.25	0.71	6
KNR140-61GGC	-76.36	33	1005	1.2					13
KNR140-63JPC	-76.41	32.99	900	1	1.5	-0.5			13
KNR140-59GGC	-76.32	32.9	1205	1.2					13
KNR140-68GGC	-76.55	32.94	775	0.7					13
KNR140-56GGC	-76.3	32.94	1400	0.8	1.3	-0.5			13
KNR140-54GGC	-76.28	32.93	1495	0.8					13
KNR140-53GGC	-76.25	32.93	1605	1.1					13
KNR140-51GGC	-76.12	32.78	1790	0.9	1.2	-0.3			13
KNR140-50GGC	-76.24	32.75	1903	0.5	1.1	-0.6			13
KNR140-64GGC	-76.13	32.74	2101		1.2	-1.2			13
KNR140-67JPC	-76.13	32.74	2102		1.5	-1.5			13
KNR140-66GGC	-76.29	32.50	2155	1					13
KNR140-1JPC	-76.38	32.38	2243	1					13
KNR140-2JPC	-76.29	32.23	2394		0.4	-0.4			13
KNR140-43GGC	-76.07	32.02	2590	1.1	0.9	0.2			13
KNR140-37JPC	-75.43	31.69	2972	0.9	0.4	0.5			14
KNR140-39GGC	-75.42	31.67	2975	1.4	0.3	1.1			14
KNR140-36JPC	-75.06	31.36	3007	1.1					13
KNR140-32GGC	-74.8	30.80	3615	0.3					13
KNR140-30GGC	-74.47	30.73	3433	0.5					13
V24-1	-73.50	30.50	3012					0.25	5
KNR140-28GGC	-73.84	30.1	4211	0.4	-0.5	0.9			13
KNR140-29GGC	-73.60	30.02	3978	1					13
M16004	-10.65	29.98	1512	1.03	1.1	-0.07	0.22	0.3	33
V26-17	-45.08	29.93	3623					0.43	5
KNR140-26GGC	-73.40	29.7	3845		-0.2	0.2			13
M15627	-12.08	29.17	1021		1.395				34
KNR140-12JPC	-72.9	29.08	4250		-0.5	0.5			13
KNR140-22JPC	-74.41	28.03	4712	1.2	-0.3	1.5			13
OC205-2-97JPC	-77.85	26.94	1183	1.23	1.53	-0.3	0.32	0.25	17
OC205-2-149JPC	-77.67	26.26	423	1.68	1.82	-0.14	0.17	0.15	18
OCE205-33GGC	-77.671	26.22	783	1.2	1.7	-0.5			32
OC205-2-33GGC	-77.69	26.22	783	1.02	1.55	-0.53	0.37	0.17	18
OC205-2-7JPC	-77.74	26.14	1320	1.3	1.37	-0.07	0.37	0.19	18
OCE205-7JPC	-77.74	26.14	1320	1.3	1.5	-0.2			32
OCE205-103GGC	-78.07	26.07	965	1.3	1.5	-0.2			32
OC205-2-103GGC	-78.06	26.07	965	1.27	1.56	-0.29	0.35	0.16	18
OCE205-100GGC	-78.03	26.06	1057	1.5	1.5	0			32

Core	Long. (°)	Lat. (°)	Depth (m)	Hol. $\delta^{13}C$ (‰)	LGM $\delta^{13}C$ (‰)	$\Delta\delta^{13}C$ (‰)	Hol. Cd_{sw} (nmol/kg)	LGM Cd_{sw} (nmol/kg)	Ref.
OC205-2-100GGC	-78.03	26.06	1057	1.4	1.5	-0.1	0.36	0.28	27
OCE205-117JPC	-77.878	26.04	1535	1.4	1.5	-0.1			32
OCE205-108GGC	-78.18	25.98	743	1.2	1.8	-0.6			32
OC205-2-106GGC	-78.18	25.98	654	1.19	1.67	-0.48	0.39	0.25	18
OC205-2-108GGC	-78.18	25.98	743	1.14	1.71	-0.57	0.39	0.2	18
OCE205-106GGC	-78.181	25.98	654	1.3	1.9	-0.6			32
M12392	-16.83	25.17	2573	0.96	0.36	0.6		0.3	5
BOFS28K	-22.00	24.00	4900	0.98	0.01	0.97	0.35	0.54	2
V23-100	-21.30	22.68	4579		0			0.52	5
M16017	-17.8	21.25	812	0.967	1.021	-0.054			34
M16030	-18.05	21.23	1500	0.882	0.97	-0.088			34
M12328	-19.00	21.00	2778	0.92	0.27	0.65	0.29	0.42	2
BOFS29K	-21.00	20.00	4000	0.82	0	0.82	0.31	0.54	2
V30-51	-19.92	19.87	3409				0.35	0.47	5
BOFS31K	-20.00	19.00	3330	0.96	0.22	0.74	0.34	0.46	2
V30-49	-21.08	18.43	3093		0.21		0.25	0.56	5, 20
KNR64-5	-74.80	16.52	1800	0.89	1.31	-0.42	0.25	0.13	24
V22-197	-18.58	14.17	3167	0.49	0.17	0.32	0.39	0.39	5
M35003	-61.25	12.08	1299	0.98	1.55	-0.57	0.47	0.3	34
V28-122	-78.68	11.93	3623	0.8	1.2	-0.4			23
V28-127	-80.13	11.65	3237	0.9	1.3	-0.4			23
CH75-03	-57.53	10.05	3410	0.9	0.1	0.8			10
CH75-04	-56.01	10.01	3820	0.9	-0.2	1.1			10
V22-26	-41.25	8.72	3720					0.7	17
EN66-10	-21.90	6.65	3527	0.82	0.19	0.63	0.42	0.68	5
GeoB4403-1	-43.44	6.13	4503	0.64	0.01	0.63			4
ODP929	-43.74	5.98	4358	0.2	0.1	0.1			3
EW9209-1JPC	-44.2	5.91	4056	0.5	0	0.5			8
EW9209-2JPC	-44.47	5.64	3528	1.4	0.1	1.3			8
EN66-16	-21.13	5.47	3152	0.94	0.43	0.51	0.37	0.72	5
ODP927	-44.48	5.46	3315	0.5	0.3	0.2			10
ODP928	-43.75	5.46	4012	1.2	0.1	1.1			10
GeoB1508-4	-34.03	5.33	3682	0.77	0.19	0.58			4
EW9209-3JPC	-44.26	5.31	3288	0.9	0.3	0.6			8
EN66-38	-20.50	4.92	2931	0.98	0.69	0.29	0.45	0.71	5
GeoB1520-1	-41.93	4.59	3911	0.66	0.21	0.45			4
KNR110-82	-43.49	4.34	2816	1.11	0.21	0.9		0.32	5
GeoB1515-1	-43.67	4.24	3129	1.26	0.4	0.86			4
ODP925	-43.49	4.21	3041	1.4	0.3	1.1			3
GeoB1523-1	-41.62	3.83	3291	1.3	0.31	0.99			4
ODP926	-42.71	3.72	3598	1.2	0.2	1			3
EN66-32	-19.73	2.47	5003	0.86	-0.32	1.18	0.34	0.48	5
GeoB1503-1	-30.65	2.31	2306		0.76	-0.76			4
GeoB1505-1	-33.01	2.27	3705	0.91	-0.13	1.04			4
RC13-188	-33.68	1.82	3451					0.57	17
V25-59	-33.48	1.37	3824	1	0.1	0.9			10
V25-59	-39.48	1.37	3824	1.03	0.07	0.96	0.26	0.45	5, 30
V30-40	-23.13	0.20	3706		-0.11			0.52	5
GeoB2215-10	-23.5	0.01	3711		0.05	-0.05			4

Core	Long. (°)	Lat. (°)	Depth (m)	Hol. $\delta^{13}C$ (‰)	LGM $\delta^{13}C$ (‰)	$\Delta\delta^{13}C$ (‰)	Hol. Cd_{sw} (nmol/kg)	LGM Cd_{sw} (nmol/kg)	Ref.
RC24-10	-11.25	-2.18	3451					0.59	17
GeoB3104-1	-37.72	-3.67	767	1.43	0.9	0.53			4
GeoB1112-4	-10.75	-5.78	3125	0.82	0.28	0.54			4
GeoB2204-2	-34.02	-8.53	2072	1.26	0.3	0.96			4
GeoB1903-3	-11.85	-8.68	3161		0.27	-0.27			4
V22-175	-14.28	-8.77	2950					0.51	17
V22-174	-12.82	-10.07	2630	0.8	0.72	0.08	0.34	0.36	5
GeoB1417-1	-12.71	-15.54	2845		0.54	-0.54			4
GeoB1419-2	-17.07	-15.54	4024		0.22	-0.22			4
GeoB1905-1	-13.99	-17.14	2974		0.64	-0.64			4
GeoB1035-4	5.03	-21.59	4456	0.75	-0.14	0.89			4
GeoB1034-3	5.42	-21.74	3772	0.57	0.07	0.5			4

Table 5.3 Annex I-3 South Atlantic (south fo 22ºS) published Holocene and LGM benthic $\delta^{13}C$ (‰) and Cd_{sw} (nmol/kg) (from benthic Cd/Ca). $\Delta\delta^{13}C$ represents the different between Holocene and LGM benthic $\delta^{13}C$

Core	Long. (º)	Lat. (º)	Depth (m)	Hol. $\delta^{13}C$ (‰)	LGM $\delta^{13}C$ (‰)	$\Delta\delta^{13}C$ (‰)	Hol. Cd_{sw} (nmol/kg)	LGM Cd_{sw} (nmol/kg)	Ref.
RC13-228	11.20	-22.33	3204	0.5	-0.31	0.81	0.34	0.36	5, 30
GeoB1032-3	6.04	-22.92	2505	0.9	0.03	0.87			4
GeoB1220-1	5.31	-24.03	2265		0.37	-0.37			4
GeoB5115-2	-14.04	-24.14	3291	1.03	0.59	0.44			4
GeoB5121	-12.36	-24.17	3486	0.98	0.55	0.43			4
RC8-19	-14.70	-24.29	3636					0.37	17
RC13-229	11.33	-25.50	4191	0.39	-0.36	0.75	0.49	0.5	5, 30
KNR159-153JPC	-45.69	-26.39	898		0.62				10
KNR159-10GGC	-45.93	-26.48	630	1.56	1.02	0.54			10
KNR159-14GGC	-46.5	-26.68	441	1.41	1.16	0.25			10
KNR159-136GGC	-46.34	-26.69	462	1.59	1.26	0.33			10
KNR159-137JPC	-46.34	-26.69	462		1.29				10
RC16-84	-43.33	-26.70	2438	1.08	0.56	0.52	0.21	0.47	24
RC16-83	-43.33	-26.7	2438	1.35	0.57	0.78			10
V24-253	-44.68	-26.95	2069	1.1	0.48	0.62	0.24	0.42	24
V29-253	-44.68	-26.95	2069	1.27	0.62	0.65			10
KNR159-37GGC	-46.63	-27.25	938	1.39	0.84	0.55			10
KNR159-36GGC	-46.47	-27.27	1268	1.18	0.54	0.64			10
KNR159-38JPC	-46.63	-27.27	936	1.36	0.66	0.7			10
KNR159-105JPC	-46.63	-27.35	1108	1.11	0.38	0.73			10
KNR159-90GGC	-46.63	-27.35	1105	1.27	0.56	0.71			10
KNR159-5-36	-46.47	-27.51	1268	1.14	0.56	0.58	0.5	0.4	7
KNR159-33GGC	-46.19	-27.56	2082	1.11	0.76	0.35			10
KNR159-34JPC	-46.19	-27.56	2082	1.16	0.71	0.45			10
RC16-119	-46.52	-27.70	1567	1.1	0.99	0.11	0.41	0.29	7
RC16-119	-46.47	-27.7	1507	1.04	0.91	0.13			10
KNR159-17JPC	-46.49	-27.7	1627	0.91	0.98	-0.07			10
KNR159-42JPC	-46.63	-27.76	2296	1.28	0.54	0.74			10
KNR159-73GGC	-46.04	-27.89	1128	1.28	0.46	0.82			10
KNR159-20JPC	-45.54	-28.64	2951	1.1	0.21	0.89			10
KNR159-115GGC	-45.53	-28.74	3021	1.2	0.16	1.04			10
KNR159-112GGC	-45.7	-28.87	2843	1.27	0.15	1.12			10
KNR159-113JPC	-45.68	-28.87	2837	1.01	-0.15	1.16			10
GeoB3801-6	-8.31	-29.51	4546	0.55	0.17	0.38			4
RC16-85	-43.42	-29.92	3909				0.69	0.7	24
V19-240	-13.28	-30.58	3103		0.02			0.56	5
GeoB3808-6	-14.71	-30.81	3213	1.01	0.55	0.46			4
GeoB2819-1	-38.34	-30.85	3435		0.04	-0.04			4
GeoB2004 2	14.54	-30.87	2569	0.79	0.1	0.69			4
AII107-131	-38.05	-30.88	2925	0.95	0.85	0.1		0.36	5
ODP 1087	15.18	-31.27	1372	0.58	0.39	0.19			28
GeoB1312-2	-29.65	-31.66	3436		-0.09	0.09			4
AII107-65	-36.19	-32.03	2795					0.44	5
RC16-86	-43.93	-32.17	3759				0.63	0.59	24
GeoB3813-3	-21.97	-32.27	4331	0.55	0.08	0.47			4
MD02-2594	17.33	-34.73	2440	0.739	0.041	0.698			This study

Core	Lat. (°)	Long. (°)	Depth (m)	Hol. $\delta^{13}C$ (‰)	LGM $\delta^{13}C$ (‰)	$\Delta\delta^{13}C$ (‰)	Hol. Cd_{sw} (nmol/kg)	LGM Cd_{sw} (nmol/kg)	Ref.
GeoB3603-2	17.54	-35.13	2840	0.55	0.05	0.5			28
GeoB2019 1	-8.78	-36.06	3825	0.15					28
GeoB2019-1	-8.78	-36.06	3825		0.15	-0.15			4
RC12-294	-10.10	-37.27	3308	0.81	-0.23	1.04	0.44	0.51	5, 30
RC12-267	-25.78	-38.68	4144				0.52	0.42	5
RC12-292	-15.48	-39.68	3541					0.54	17
ODP 1089	9.53	-40.56	4621	0.3	-1.2	1.5			12
TN057-21	7.49	-41.08	4981	0.27	-0.83	1.1			22
MD02-2589	25.15	-41.26	2660	0.5		0.5			21
PS2495-3	-14.49	-41.28	3134	0.71	-0.42	1.13			16
RC11-83	9.8	-41.6	4718	0.2	-0.9	1.1			11
ODP 1088	13.33	-41.8	2082	0.5	0.28	0.22			12
TN057-20	1	-42	1335	0.6	0.4	0.2			22
ODP 1090	8.53	-42.5	3702	0.49	-0.3	0.79			12
TN057-06	8.58	-42.54	3751	0.3	-0.97	1.27			22
RC15-94	-20.85	-42.98	3762	-0.2	-0.8	0.6			22
V22-108	-3.15	-43.11	4171	0.12	-0.83	0.95			22
PS2082-1	11.45	-43.13	4661	0.21	-0.79	1			16
V22-108	-3.25	-43.18	4171	0.1	-0.8	0.9			22
PS2498-1	-14.49	-44.15	3783	0.22	-1.09	1.31			16
RC15-93	-13.13	-46.06	2714	0.29	-0.96	1.25			22
PS2564-3	35.9	-46.14	3034	0.49	-0.83	1.32			16
PS2499-5	-15.33	-46.51	3175	0.31	-0.82	1.13			16
PS1754-1	7.61	-46.77	2519	0.59	-0.33	0.92			16
ODP 704	7.42	-46.88	2532	0.58	-0.5	1.08			4
TN057-15	4.31	-51.54	3744	-0.02	-0.81	0.79			22

Annex II

RC13-229 is located close to the Namibian upwelling system, and therefore, a possible imprint of a "phytodetritus" effect (Mackensen et al., 1993b) on benthic $\delta^{13}C$ cannot be discarded. Lowering of the true benthic $\delta^{13}C$ by this effect could then affect the estimated $\delta^{13}C_{as}$.

In order to test for such an effect, we use the available Total Organic Carbon record (TOC in %) of RC13-229 (Oppo and Rosenthal, 1994) and we assume that at present there is none "phytodetritus" effect while at the LGM we assume that this effect could have lower benthic $\delta^{13}C$ by 0.5‰ (Mackensen et al., 1993b consider the maximum of this effect between 0.4-0.6 ‰). Then we relate the TOC increase between the Holocene and LGM of 0.88 % to a decrease of the benthic $\delta^{13}C$ of 0.5‰ and scale the downcore benthic $\delta^{13}C$ RC13-229 record to this amplitude of change. The resulting benthic $\delta^{13}C$ corrected record is then implemented in the computation of $\delta^{13}C_{as}$.

It needs to be mentioned that the benthic $\delta^{13}C$, benthic Cd/Ca and TOC records of RC13-229 are not measured on the same samples, therefore we have needed to rescaled the benthic $\delta^{13}C$ to the TOC scale and then the corrected record to the Cd/Ca scale to compute the $\delta^{13}C_{as}$. This may add some uncertainty in the final $\delta^{13}C_{as}$ corrected record but for our purposes of observing the magnitude of change in the $\delta^{13}C_{as}$ related to the "phytodetritus" is not decisive.

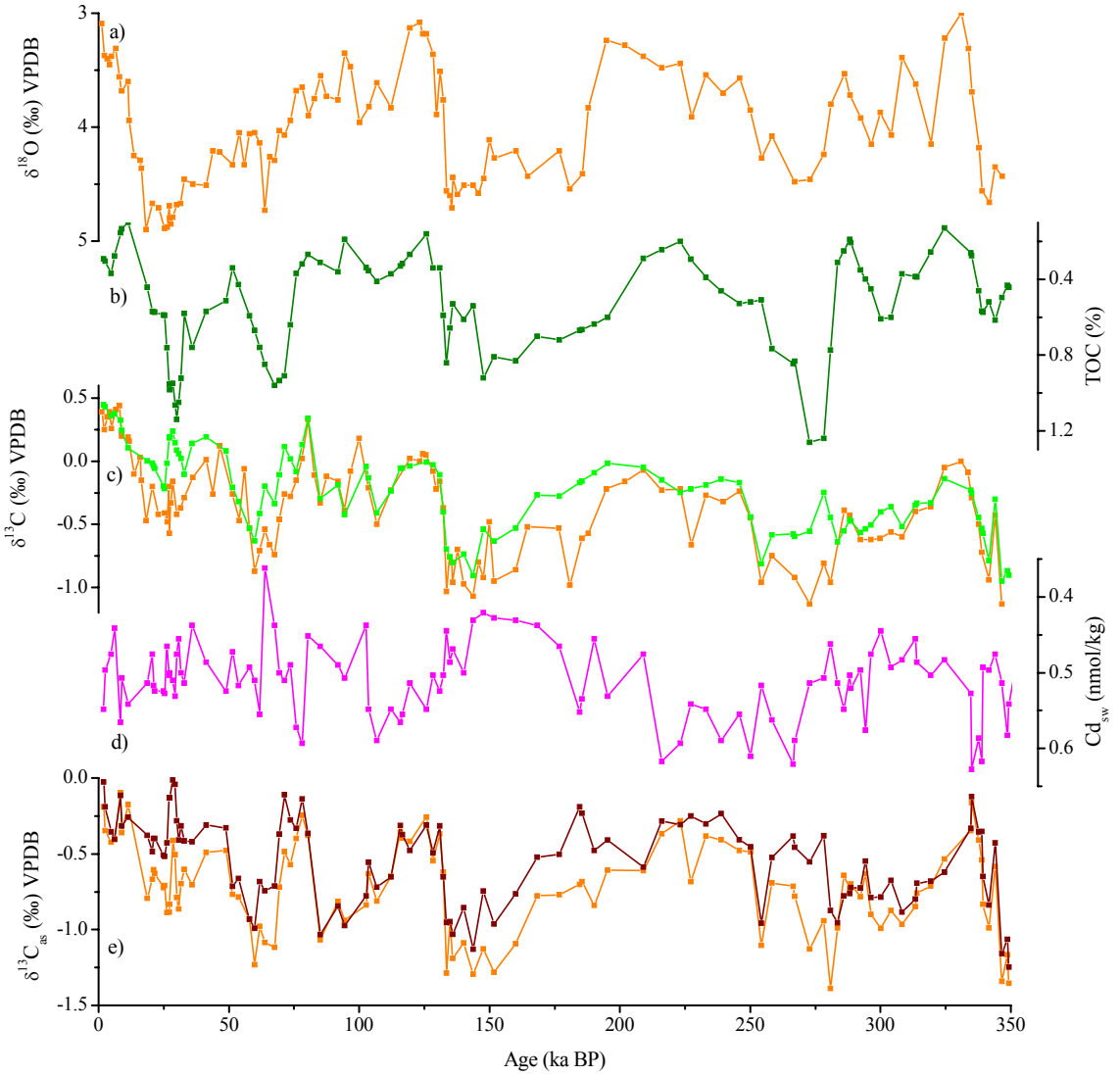

Figure 5.3 Annex II-1 RC13-229 records; a) benthic $\delta^{18}O$ (‰) VPDB; b) TOC (%); c) $\delta^{13}C$ (‰) VPDB (uncorrected, orange, and corrected for a possible "phytodetritus" effect, green on the Cd_{sw} sample resolution); d) Cd_{sw} (nmol/kg); e) $\delta^{13}C_{as}$ (uncorrected , orange, and corrected for a possible "phytodetritus" effect, brown). Note the different sample depths for which each of the measurements were performed.

References

Mackensen, A., Hubberten, H.-W., Bickert, T., Fischer, G. and Fütterer, D.K., 1993. The $\delta^{13}C$ in benthic foraminiferal tests on *Fontbotia wuellerstorfi* (Schwager) relative to the $\delta^{13}C$ of dissolved inorganic carbon in southern ocean deep water: implications for glacial ocean circulation models. Paleoceanography, 8 (5), 587-610.

Oppo, D.W. and Rosenthal, Y., 1994. Cd/Ca changes in a deep Cape Basin core over tyhe past 730,000 years: response of circumpolar deepwater variability to northern hemisphere ice sheet melting? Paleoceanography, 9 (5), 661-675.

Chapter 5.4

Influence of Agulhas Leakage on the Meridional Overturning Circulation (MOC): Insights From Paired Planktonic and Benthic Foraminifera Stable Isotope and Trace Metal Analyses Over the Last 345 kyr

Abstract

The Agulhas Current off South Africa plays a key role in the Atlantic Meridional Overturning Circulation (MOC) as salty and warm Indian waters are transported to the Atlantic Ocean and influence its buoyancy budget. Its importance is also highlighted in paleoceanographic data profiles and numerical models that suggest that increased water transports from the Indian to Atlantic prior to and during glacial Terminations may contribute to the onset of interglacial conditions. We have generated 345 kyr long records of planktonic $\delta^{18}O$ and Mg/Ca-derived SST from the Agulhas Bank Slope off South Africa; and abundance of Agulhas Leakage Fauna for the MIS 6 section of sediment core MD96-2080. These surface records demonstrate that during glacial periods the presence of Agulhas Waters evolved at this location from interglacial levels at the glacial onset to reach maximum values well before the subsequent glacial Termination. This is particularly evident during MIS 6. The analyses of benthic $\delta^{13}C$ and Cd/Ca from co-registered samples and the comparison with similar records from the area permit assessments of the relationship between the intensity of the Agulhas Water presence at the sites and changes in the mode of the MOC. During early glacial phases benthic $\delta^{13}C$ and Cd/Ca ratios document a continuous influence of Northern Component Water (NCW) at depth at the same time when our surface records indicate the presence of Agulhas Water similar to interglacials, suggesting a persistence of the modern-type linkage between Agulhas Leakage and MOC. Maximum presence of Agulhas Waters during late glacial phases coincides with the onset of benthic $\delta^{13}C$ and Cd/Ca resumption to interglacial levels. This supports the hypothesis that Agulhas Leakage may play a key role in the resumption of an interglacial mode of MOC. Conversely, during MIS 2 and mid-MIS 6 and 8 high values of our Agulhas indicators are coeval with maximum presence of SCW at depth. This indicates that at these times either the prominent presence of Agulhas Waters was unable to efficiently generate a buoyancy anomaly in the South Atlantic or that other factors were able to overcome the salt anomaly imposed by the Agulhas Waters in the South Atlantic, for instance North Atlantic climatology.

5.4. Influence of Agulhas Leakage on the Meridional Overturning Circulation (MOC): Insights From Paired Planktonic and Benthic Foraminifera Stable Isotope and Trace Metal Analyses Over the Last 345 kyr

5.4.1. Introduction

The transfer of Agulhas Waters (AW) from the Indian to the Atlantic Ocean forms the so-called "warm water route" for North Atlantic Deep Water (NADW) compensation *versus* the "cold water route" which is formed by the entering of surface and thermocline waters from the Pacific to the Atlantic through the Drake Passage (Gordon, 2003). Warm, saline waters from the tropical and subtropical Indian Ocean are transferred to the Atlantic by virtue of Agulhas Rings and Filaments. Gordon et al. (1992) suggested that this water transfer causes a salinity anomaly of +(0.2-0.4) psu in the South Atlantic thermocline that is of significance for the mode and vigour of NADW formation in the North Atlantic. Hence this Indian-Atlantic connection may play a role in global climate (Gordon, 1985). Numerical models (Weijer et al., 1999; 2001; 2002) support this concept albeit through different mechanisms. Weijer et al. (2002) observed responses in the strength of the MOC to the application of buoyancy sources in the South Atlantic by modifications of the basin wide density and pressure gradients.

Furthermore, around the southern end of Africa, there is water transfer at depth from the Atlantic to the Indian basin. The Atlantic trades cold deep waters for warm upper waters. Gordon (1986) proposed that there is a direct linking between the intensity of both the interchange at the surface and at depth in such a way that a more vigorous salt-warm input to the Atlantic (at the surface) will stimulate a stronger convection in the high latitude North Atlantic that then causes a more intense formation of NADW and its subsequent export to the Indian Ocean.

Peeters et al. (2004) showed that maximum Agulhas Leakage (AL) as reflected in foraminiferal assemblages directly linked with Agulhas Current waters, the so called "Agulhas Leakage Fauna" (ALF), occurs in the middle of glacial Terminations, pointing to a direct link between AL and the resumption of interglacial conditions. Analogous evidence of maximum AL during glacial Terminations was previously found in sediment cores of the area on the basis of foraminiferal and nannofossil assemblages (Chang et al., 1999; Flores et al., 1999; Rau et al., 2002) while not directly linked with the MOC. Also, Knorr and Lohman (2003) based on 3D ocean circulation model simulations found a linkage between a gradual warming of the Southern Ocean and the abrupt resumption of an interglacial mode of circulation triggered by increased mass transports of the warm and cold water route into the Atlantic.

We have generated high resolution paired benthic and planktonic stable isotope and moderate resolution trace element records from two sediment cores in the Agulhas Corridor to further assess the potential influence of AL on the MOC. The novelty of our study consists in the combined

interpretation of planktonic and benthic data from the same core, therefore, avoiding ambiguities regarding timing differences between deep and surface variations. To our knowledge, in the Agulhas region such approach has so far only been employed by (Cortese et al., 2007) for ODP Site 1089, near the Agulhas Ridge. However, at the surface that core rather reflects climatic variations linked to the movement of the Subtropical Front (STF) with some influence from the Agulhas Retroflection and at depth it is strongly influence by Low Southern Component Water (LSCW) properties. Our records on the Agulhas Bank Slope at mid-depths more likely reflect direct variations in Agulhas Leakage and concomitant changes in the intensity of NADW formation.

5.4.2. Core Material

For this chapter we use the Agulhas Bank Spliced record (ABS) which combines cores MD02-2594 (34º43'S, 17º20'E, 2440 m) spanning the last glacial cycle, from present to 80 ka and MD96-2080 (36º19'S, 19º28'E, 2488 m) spanning the previous two glacial-interglacial cycles, from MIS 5 to MIS 9. Details of the age models of both cores and about the splicing into a singular record are given in Chapter 5.1.

Our surface proxy records, i.e. *G. bulloides* $\delta^{18}O$, Mg/Ca-derived SST and Agulhas Leakage Fauna abundance (ALF) enable to develop scenarios of past surface circulation off South Africa with implications for the Agulhas Current (AC) variability and ensuing Agulhas Leakage (AL). The surface results are then linked with the deep circulation drawn on the basis of benthic $\delta^{13}C$, Cd/Ca-derived Cd_{sw} and $\overline{SS}$ (Chapters 5.2. and 5.3). Furthermore, we extend the comparison to planktonic records of the nearby Cape Basin Record (CBR) that combines cores GeoB3603-2 (35º08'S, 17º33'E, 2840 m) and MD96-2081 (35º35'S, 17º4º'E, 3164 m) (Peeters et al., 2004) (Fig. 5.4-5). GeoB3603-2 benthic $\delta^{13}C$ is likewise available (personal communication with Prof. Dirk Kroon, Institute of Earth Science, Edinburgh*;* Prof. Ralph Schneider, Institut für Geowissenschaft, Christian Albrechts Universität zu Kiel) and is used here as reference for comparison with the ABS benthic $\delta^{13}C$ record, in the following we will refer to it as CBR benthic $\delta^{13}C$.

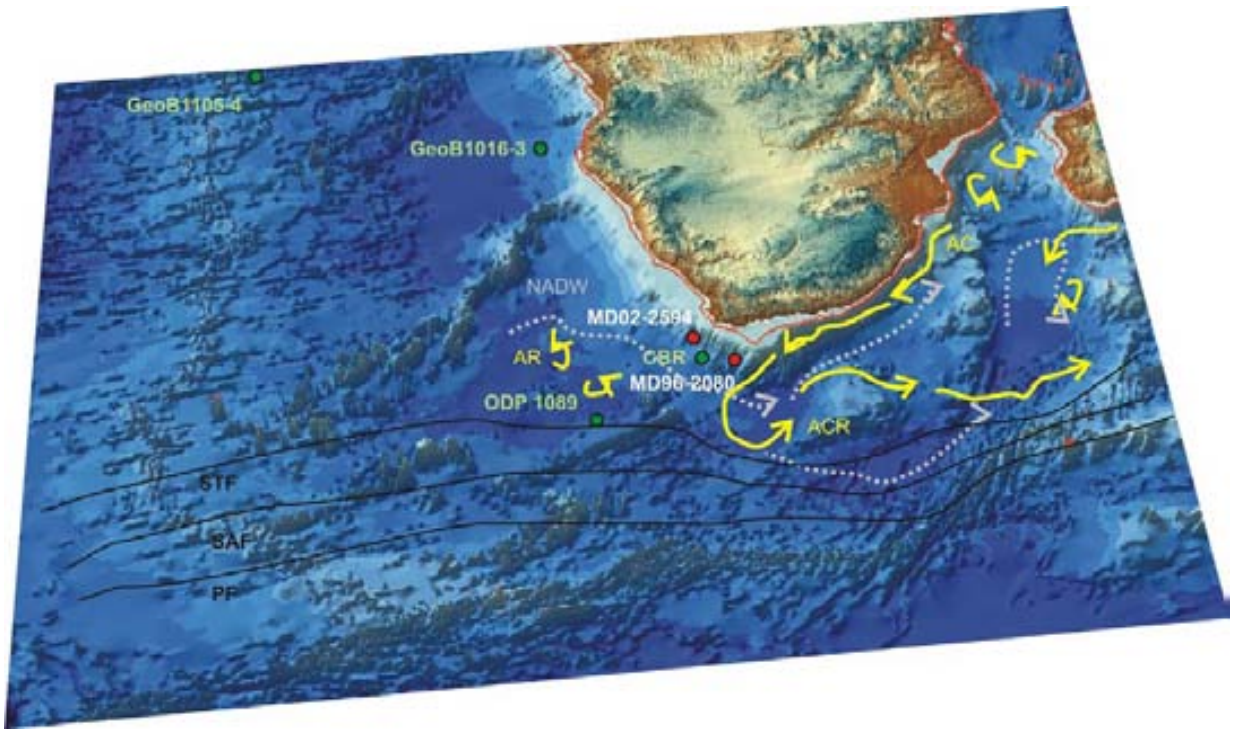

Figure 5.4-1 Location of MD96-2080 and MD02-2594 cores (red dots) within the Agulhas Corridor. Green dots indicate the position of cores CBR, ODP 1089, GeoB1016-3 and GeoB1105-4 that are used in this Chapter for comparison. Main surface and deep circulation patterns are displayed by arrows; they are: Agulhas Current (AC), Retroflection (ACR) and Rings (AR) (yellow) and the path of NADW. Black lines denote the approximate position of the Subtropical, Sub-Antarctic and Polar Fronts (STF, SAF, PF). Red line indicates the 120 m isobath (see discussion). Based map provided by D. Amblàs (GRCGM-Universitat de Barcelona).

5.4.3. ABS Surface Circulation Records

- **Planktonic Foraminiferal Oxygen Isotopes**

Planktonic $\delta^{18}O$ shows pronounced orbital modulation. Glacial-interglacial shifts during Terminations I, II, III and IV are 1.60, 1.89, 0.85 and 1.59‰, except for Termination III (Fig. 5.4-2a), exceeding $\delta^{18}O$ variations related to sea level changes (e.g. Waelbroeck et al., 2002). Therefore, in addition to global changes due to ice volume accumulation in ice caps during cold periods, the data indicate variations in local sea surface temperatures and sea surface $\delta^{18}O$ ($\delta^{18}O_{sw}$) related to alterations in the evaporation-precipitation balance of the source waters. When compared with the planktonic $\delta^{18}O$ record of MD97-2120 (Pahnke et al., 2003) from Chatham Rise in the Southwest Pacific, the glacial-interglacial amplitude of change along ABS seems up to 50% smaller (Fig. 5.4-5). Temperature and salinity associated with variable influence of Agulhas Water affect $\delta^{18}O$ in an opposite direction, i.e. warmer temperatures diminish isotope fractionation leading to lighter $\delta^{18}O$ signatures while saltier waters carry heavier $\delta^{18}O$ signals. Hence, at this specific locality the variations in $\delta^{18}O_{sw}$ likely reflect shifts in the predominant water masses, i.e. South Atlantic Surface Water (SASW), Agulhas Water (AW) and Sub-Antarctic Surface Water (SAASW).

Variations of planktonic $\delta^{18}O$ from present to MIS 5a (MD02-2594 data) correlate well with atmospheric proxy records, i.e. $\delta^{18}O$ and δD, in Antarctic ice cores Byrd (Blunier and Brook, 2001), EPICA Dronning Maud Land (EDML) (EPICA Community Members, 2006), Vostok (Petit et al.,

1999) (Fig. 5.4-2). For instance, there are signs of an Antarctic Cold Reversal-like event in ABS and Antartcic warmings A3 and A4 (Blunier and Brook, 2001) are reproduced in ABS $\delta^{18}O$. This has also been observed between Antarctic temperature records and planktonic $\delta^{18}O$ from sediment cores in the east equatorial Indian Ocean (Ferrer Carrillo, 2007) and in the southwest Pacific (Pahnke et al., 2003) suggesting that Antarctic climate exerts a large influence on the atmospheric conditions of the wider Southern Hemisphere. However, for the period prior to MIS 5 (MD96-2080 data) the coherence between planktonic $\delta^{18}O$ and Antarctic temperature is not so clear. Peak interglacials MIS 5e, and specially 7e and 9c are not well developed in ABS planktonic $\delta^{18}O$. MIS 5e and 9c are only slightly more $\delta^{18}O$ depleted than the rest of the interglacial period, i.e. MIS 5a-d and 9a-b respectively, by around 0.8-0.4‰; while MIS 7e is heavier than MIS 7a by around 0.4‰ and than c by around 0.1‰. We observe sub-orbital variability during MIS 6 but when compared with other $\delta^{18}O$ planktonic records (e.g. Pahnke et al., 2003) or with the Vostok Deuterium record (Petit et al., 1999), this variability appears subdued (Fig. 5.4-2).

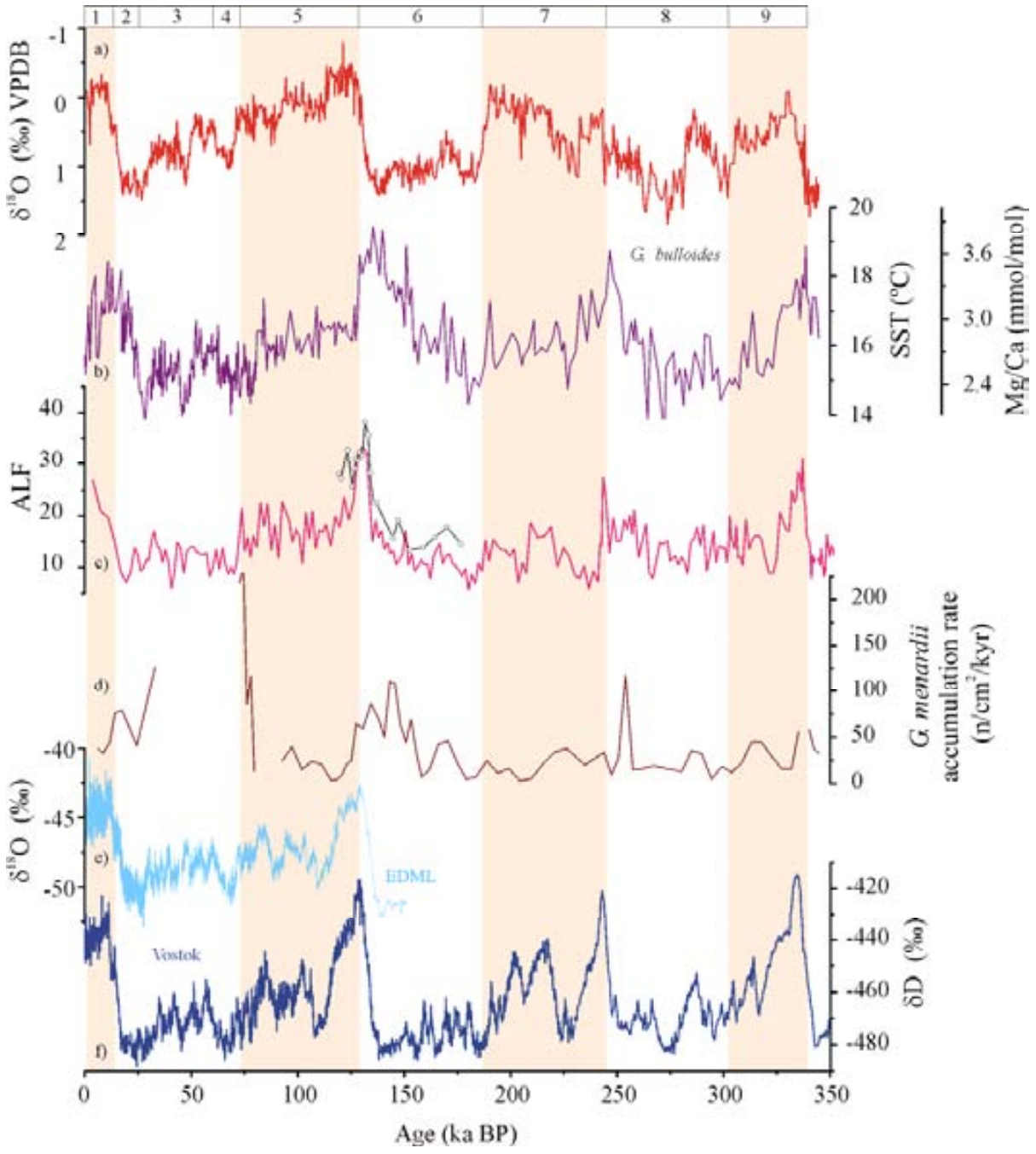

Figure 5.4-2 Agulhas Bank surface records, a) ABS *G. bulloides* $\delta^{18}O$; b) ABS Mg/Ca-derived SST (ºC), outer scale indicates Mg/Ca ratios; c) relative abundance of Agulhas Leakage Fauna (ALF, Peeters et al., 2004) of CBR (pink) and ABS (black-dotted); d) *G. menardii* accumulation rate in MD96-2080 (n/cm^2/kyr) (Rau et al., 2002). Antarctic records for stratigraphic reference; f) EDML $\delta^{18}O$ (EPICA Community Members, 2006); e) Vostok δD (Petit et al., 1999). Vertical shading highlights interglacials.

- **Planktonic Foraminiferal Sea Surface Temperature (SST)**

The *G. bulloides* Mg/Ca record and derived SST differ considerably from the $\delta^{18}O_{plk}$ record (Fig. 5.4-2b). The most outstanding differences occur during full-glacials MIS 2 and MIS 6 when sustained warming develops across these glacial stages with no measurable signal seen in $\delta^{18}O_{plk}$.

The discrepancy between the Mg/Ca and $\delta^{18}O_{plk}$ could be interpreted as being indicative of alterations in any of the proxies but planktonic $\delta^{18}O_{plk}$ follows the general glacial-interglacial structure widely observed in paleoceanographic records. Mg/Ca, in contrast, displays atypical structure in that

the data show trends of increasing Mg/Ca ratios from early phases of glacial periods reaching maximum levels prior to glacial Terminations and collapsing when entering the interglacial period. Hence the question arises whether the anomalous Mg/Ca pattern reflects an original while anomalous SST signal or if other secondary overprints have distorted the trace element record; for instance, post-depositional contamination by clays (Barker et al., 2003), secondary carbonate overgrowth (Pena et al., 2005), or carbonate dissolution (Rosenthal et al., 2000). One way to test for such secondary effects is to measure Al/Ca and Mn/Ca ratios that are indicative of contamination by clays or Mn-oxides. Based on such measurements sample contamination has been discarded because Al/Ca and Mn/Ca ratios remain low (see Chapter 4). Regarding possible dissolution effects, we have compared the Mg/Ca records of both, MD02-2594 and MD96-2080 with the records of weight of *G. bulloides* (see Fig. 5.4-3 for representation of weight of *G. bulloides vs* Mg/Ca ratio of ABS). For MD96-2080 we have also used the foraminiferal fragmentation index and percent $CaCO_3$ of the sediment sand fraction (available from Rau et al., 2002) to test for possible dissolution in the record (see Chapter 4 for details). From these comparisons we conclude that if dissolution affected the planktonic Mg/Ca record, this would have occurred only in MIS 5e, 7a and 8e, so that the temperatures of these periods would be underestimated. Nonetheless, this would not alter the pattern of early warming observed across the glacials and into the Terminations.

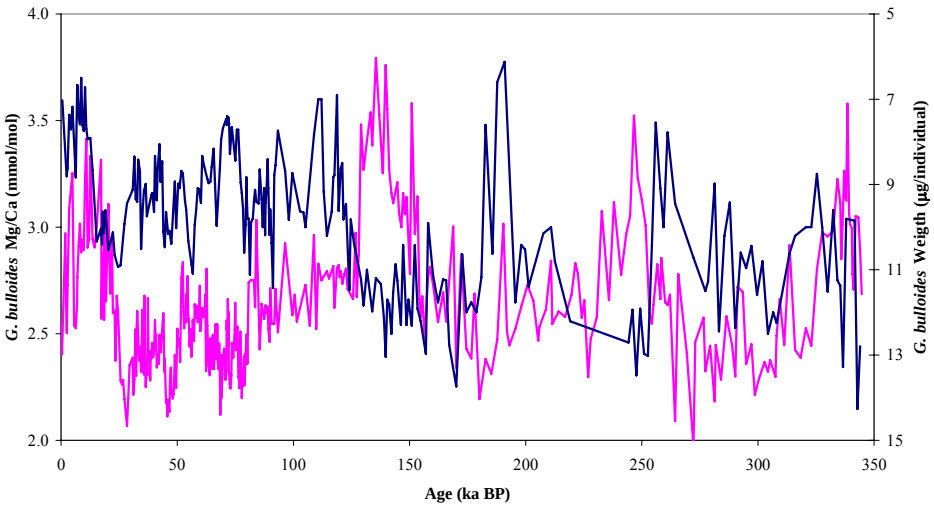

Figure 5.4-3 ABS *G. bulloides* weight (µg/individual) (blue) *versus* Mg/Ca ratio (pink).

The majority of the Mg/Ca-derived SST record, and more specifically its interglacial sections, lies within 16.5 and 14.5ºC which falls inside the range of observed temperatures at the core site during austral winter today (see Fig. 3-6, Chapter 3). During glacial periods we observe trends of increasing temperatures reaching their maxima when ice volume is largest in MIS 2 and 6 and during mid-Terminations III and IV. The absolute maximum of the warming trends occurs at the end of MIS 6 when it reaches 18-20ºC at 139 kyr BP staying high until 129 kyr B.P.

We hypothesize that the warming trend observed during MIS 6 and 2 is related to a progressively stronger influence of warm Agulhas Waters at the core site (see discussion).

- **Planktonic Foraminiferal Census Counts: Agulhas Leakage Fauna Index (ALF)**

Foraminiferal census counts from 21 samples across the warming trend in MIS 6 were performed (F. Peeters, Vrije Universiteit, Amsterdam, personal communication) and used to compute the Agulhas Leakage Fauna Index (ALF). Peeters et al. (2004) observed this specific assemblage of foraminifera to exist within the Agulhas Rings and used its abundance variation along the CBR record to assess the amount of Agulhas Water transferred to the Atlantic in the past.

We present ALF data from ABS in Figure 5.4-2c together with the ALF record generated for the spliced core CBR (Peeters et al., 2004) for reference and comparison. We also present the MD96-2080 record of mass accumulation rate of *G. menardii* of Rau et al. (2002) (Fig. 5.4-2d). *G. menardii* is a tropical planktonic species abundant in warm water. Rau et al. (2002) and Rau et al. (2006) found this species along the full length of MD96-2080 suggesting that the Leakage of Agulhas Water into the Atlantic never ceased during the last 850 kyr. Furthermore, Rau et al. (2002) observed that the pattern of accumulation rate of *G. menardii* is substantially different from that of tropical/subtropical species. The percentage of tropical/subtropical species is low in MIS 2, 6 and 8, while *G. menardii* accumulation rates display peaks centred before Terminations II, III and IV (Fig. 5.4-2d). The *G. menardii* peak maximum observed around 70 ka was positioned in the initial stratigraphy of Rau et al. (2002) in MIS 2 and ascribed to weakness of the age model in this upper part of the record. This anomalous peak in *G. menardii* accumulation rate is not accompanied by a peak in SST. In view of the hiatus in MD96-2080 in this section (see Chapter 5.1), we conclude that the anomalous peak at 70 ka maybe an artefact of uncertainty in the age model that then causes enhanced accumulation rates. Maxima in *G. menardii* accumulation rates at glacial Terminations are coherent with maxima SST in ABS reinforcing the hypothesis that these maxima are related to Agulhas Waters.

The ALF abundance pattern in MIS 6 of ABS resembles that of the CBR record suggesting a similar influence of water from the Agulhas Current on both core sites during this period. The SST record of CBR is also available (Schneider et al., 1999) while based on a different proxy, i.e. on the alkenone $U_{37}^{k'}$ index. Both SST records are very different; SST in CBR in a general sense follows a typical $\delta^{18}O$ structure and displays consistently higher SST than ABS, this differences may likely be relate to the seasonality of each proxy or to the different depth habitats of alkenone producing cocolitophores and foraminifera (e.g. Bard, 2001). The ALF record of CBR shows trends similar to the SST of ABS such as a progressive increase of the ALF across MIS 6 and a subsequent collapse to low values when entering MIS 5e. During Terminations I, III and IV early increases are also seen in ALF that coincide with warming trends in ABS. Closer inspection reveals differences such as the maximum in ALF being concentrated in the middle of glacial Terminations, while, very notably during MIS 6, maximum SST in MD96-2080 is reached around 8 kyr before peak ALF. This seems to indicate that Agulhas flow may cause maximum temperature while faunal components have not yet maximized.

- **Sea Water Oxygen Isotopes**

Combining planktonic $\delta^{18}O$ and SST we have derived a record of sea water oxygen isotope composition ($\delta^{18}O_{sw}$) which has been further translated into sea surface salinity estimates (SSS) (see Chapter 4 for details on the computation). These are presented in Figure 5.4-4c as $\delta^{18}O_{sw}$ and SSS anomalies ($\Delta\delta^{18}O_{sw}$ and ΔSSS) relative to present levels which have been calculated by averaging Holocene data from 0 to 5 ka. The Holocene SSS estimate of 35.23 psu is in good agreement with present values in the area, 35.3-35.4 psu. The Holocene $\delta^{18}O_{sw}$ estimate of 1.06‰ SMOW appears enriched by a factor of 2 respect to $\delta^{18}O_{sw}$ values extracted from published surface data in the neighbourhood of the Agulhas Current (Schmidt, 1999; Schmidt et al., 1999; Bigg and Rohling, 2000) while it is in the range of $\delta^{18}O_{sw}$ measurements performed on water samples collected along the pathway of the Agulhas Current during the Charles Darwin cruise CD154 in December-January 2003-2004 (Hall and Zahn, 2004) which vary between 1.9 and 1‰ SMOW. The Holocene estimate is also close to values within the South Atlantic Subtropical Gyre, which are around 0.86‰ SMOW (Schmidt, 1999; Schmidt et al., 1999; Bigg and Rohling, 2000).

Negative $\Delta\delta^{18}O_{sw}$ values are observed in MIS 1, MIS 3 to 5e, MIS 7a-b and in two excursions in MIS 6 and 8. $\Delta\delta^{18}O_{sw}$ indicates therefore the presence of isotopically lighter waters during most warm periods. Positive $\Delta\delta^{18}O_{sw}$ are displayed in MIS 2, late MIS 6 and from MIS 7d to Termination IV with maximum values in this last Termination. Around the transition from MIS 8 to 7 there are indications of a positive anomaly but this is not as clear as those of the other three transitions. Regarding the SSS reconstruction (Fig. 5.4-4d), we must be aware of the uncertainties associated with these estimations notably, the propagated error of the various measurements and relationships used, and applying a modern tropical $\Delta\delta^{18}O_{sw}$ *vs* salinity relationship (see Chapter 4) which most likely has not remained constant through time. This last uncertainty is related to the changes exerted in the hydrological cycle, and thus in the water isotopes, by climate reorganizations on orbital and shorter time scales. Besides, the amounts of waters exchanged between ocean basins and exported from one region to another varied further altering the relationships between water isotopes and climate through time (e.g. Le Grande and Schmidt, 2007). Moreover, the storage of freshwater in the ice sheets during glacial times produces a concentration effect on the salinity of the global ocean which Adkins and Schrag (2001) estimated to be about 2.5 ± 0.1% higher (around 0.9 psu). As a first order approximation we use the combined sea level curves of Waelbroeck et al. (2002) and Sidall et al. (2003) (that we have also used to correct for global $\delta^{18}O_{sw}$ changes related to sea level, see Chapter 4) to estimate past changes in global mean salinity by scaling the combined curve to the Holocene-LGM change of 0.9 psu. By incorporating these global mean salinity changes into our computed local sea surface salinity anomalies (ΔSSS) we obtain the total salinity change experience at our core site. These total ΔSSS estimations (orange curve in Fig. 5.4-4d) are largely modulated by the global shifts (brown curve in Fig. 5.4-4d). Strong differences between the salinity changes related to sea-level shifts and salinity changes at our location mainly occur in late glacial phases where local effects on salinity, as derived

from local $\delta^{18}O_{sw}$, adds to the global variability. While global shifts add to the salinity variation at any core site, in order to asses the variable contribution of Agulhas Waters to any core site, the local salinity variations are more useful. Indeed, the ABS local salinity record remains nearly constant at 35.3 ± 0.3 psu with only strong departures in MIS 2, late MIS 6 and around Termination IV. Such a departure in the salinity trend is not observed in MIS 8.

The observation that the warming trends observed during MIS 2, 6 and Termination IV coincide with salinity increases and are coeval with increases in ALF provides strong evidence of a prominent presence of Agulhas Waters at the core sites during these glacial periods. The implications of these findings will be analyzed next (see discussion).

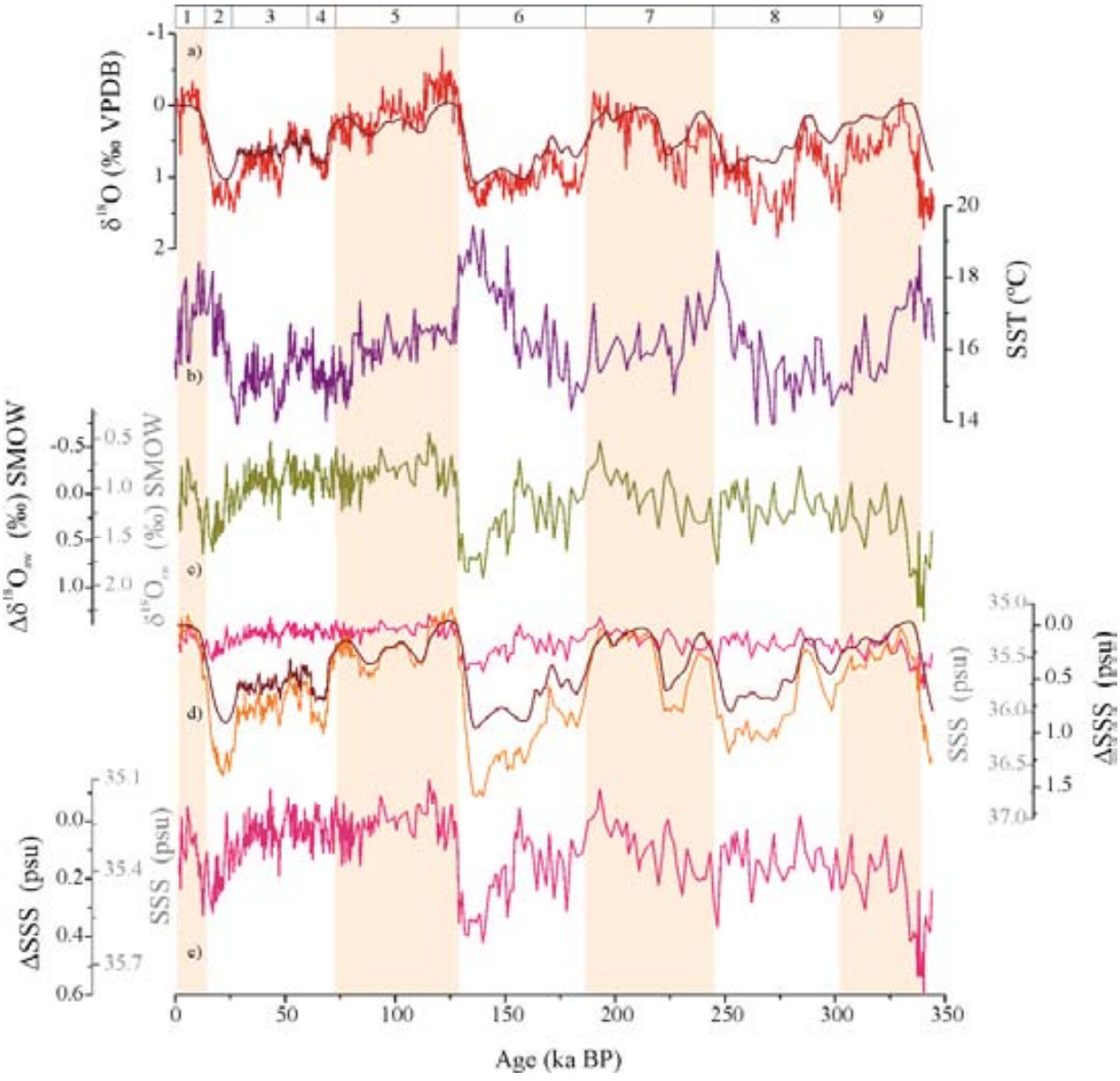

Figure 5.4-4 Surface paleoceanographic records for ABS; a) ABS *G. bulloides* $\delta^{18}O$ (red); brown curve is a combination of the $\delta^{18}O_{sw}$ records related to sea level curves of Waelbroeck et al. (2002) and Siddall et al. (2003) shown for reference; b) ABS *G. bulloides* Mg/Ca-derived SST; c) ABS $\Delta\delta^{18}O_{sw}$ (left-hand scale) and estimated $\delta^{18}O_{sw}$ (right-hand scale); d) ABS ΔSSS (outer scale) and estimated SSS (inner scale); Brown curve displays global salinity variations related to the concentration effect as a consequence of storage of fresh water in ice sheets during glacial periods. This has been computed by scaling the combined $\delta^{18}O_{sw}$ curve of Waelbroeck et al. (2002) and Siddall et al. (2003) to the salinity change of 0.9 psu between the Holocene and LGM estimated by Adkins and Schrag (2001); e) detail of local ABS ΔSSS (outer scale) and estimated local SSS (inner scale) at expanded scale.

5.4.4. Discussion

The Agulhas Current is the main component of the so-called warm water route for NADW compensation (Gordon, 2003). Conceptual (Gordon, 1986) and numerical models (Weijer et al., 1999; 2002) postulate a major role of the leakage of warm and salty Agulhas Water into the Atlantic in modulating the state of the MOC and hence of global climate. These postulations are reinforced by long-term simulations (e.g. Knorr and Lohmann, 2003) which reveal a potential role of the Agulhas system as trigger for the resumption of interglacial modes of circulation on glacial-interglacial times scales, a contention that is corroborated by some proxy records (e.g. Peeters et al., 2004).

Peeters et al. (2004) were the first in directly linking paleoceanographic evidence of increases in the amount of Agulhas Water at glacial Terminations in the South Atlantic with the resumption of interglacial conditions. Existing proxy records also showed evidence of major inflow of Agulhas Waters to the South Atlantic while not directly linked to variations in the MOC (Chang et al., 1999; Flores et al., 1999; Rau et al., 2002).

With our combine planktonic-benthic study we add further insights in the Indian-Atlantic connection not only at the surface but also at depth. This deep-surface comparison allows assessments on the influence of the Agulhas Leakage (AL) on the MOC.

- ***Globigerina bulloides* as Recorder of Agulhas Water Variability**

Before entering in the discussion about the significance of the SST, $\Delta\delta^{18}O_{sw}$ and ΔSSS patterns that we observe in our cores, it is worth mentioning the constraints for using $\delta^{18}O$ and Mg/Ca of *G. bulloides* as recorders of Agulhas Current and Leakage variability although this species is not a type warm water species. *G. bulloides* is not included in the ALF identified within the Agulhas Rings by Peeters et al. (2004) and its presence is low in sediments below the Agulhas Current (F. Peeters, pers. comm.). Agulhas Rings contain waters that are derived from the tropical and subtropical Indian Ocean and hence they are oligotrophic and warmer than ambient South Atlantic surface and thermocline waters. South Atlantic waters are more eutrophic and hence the flux of *G. bulloides* in mixed South Atlantic-Agulhas waters increases as the South Atlantic is invaded by Agulhas Rings and mesotrophic waters form as a result of the mixing (F. Peeters, pers. comm.). Whenever we have a strong presence of Agulhas Waters at ABS site, the Mg/Ca ratio of *G. bulloides* will reflect the temperature of the mixed waters. This means that it cannot record the maximum temperature associated with pure Agulhas Water but it can provide a good estimate of the amount of these waters reaching the site (F. Peeters, pers. comm.). In order to get the purer, hence higher, temperatures associated with Agulhas Waters, the Mg/Ca ratio of a species existing within the rings would be more appropriate (e.g. *Globigerinoides ruber*). As a conclusion, we may say that our Mg/Ca-derived SST does not necessarily represent, or at least not only, warming or cooling of the Agulhas Current but rather stronger or weaker input of these waters to the site.

- **Comparison of ABS SST With Other South Hemisphere Records**

Schneider et al. (1999) compiled tropical and subtropical alkenone $U_{37}^{k'}$ index derived SST records mainly from the Atlantic but also from the Pacific and Indian Oceans and observed three patterns of variability. Type 1 encompasses records which show warmer temperatures in MIS 6 than in MIS 2, 4 and 8 and with the coldest temperatures occurring 10-15 kyr before maximum ice volume in all glacial periods. Type 2 is similar to type 1 in the sense that they also show moderate temperatures in MIS 6 with maximum cooling in the mid-glacial while for MIS 2, 4 and 8 maximum cooling occurs coevally with maximum ice volume, thus, exhibiting a pattern more similar to $\delta^{18}O$ records. Type 3 includes records whose SST generally parallel $\delta^{18}O$ variations. Type 1 is reported from cores in the equatorial Indian Ocean, east-equatorial Pacific, off Oman and off West Africa. Type 2 is found in the central and west-equatorial Atlantic and type 3 in cores below the subtropical gyre circulation (Schneider et al., 1999 and references therein). It seems that type 1 and 2 are typical from low latitudes and that this tropical signal can be transmitted to mid-latitude cores through the Agulhas system. Schneider et al. (1999) observed disagreement between the alkenone $U_{37}^{k'}$ index derived SST and SST derived from foraminiferal assemblages in those cores on which they based their tropical/subtropical classification in that SST derived from foraminiferal census counts were coherent with $\delta^{18}O$ variations for all the SST types they defined (i.e. types 1 to 3). Since alkenone $U_{37}^{k'}$ index derived SST aside of the anomalous type 1 and 2 also record SST variability of type 3, these authors conclude that it is a reliable method for recording tropical SST.

The pattern of SST variability of ABS does not perfectly match any of these types (Fig. 5.4-5), it looks closer to type 1 as maximum glacial cooling is observed well before maximum in ice volume and it shows glacial warming trends starting several thousand years prior to Terminations. However, the ABS temperature pattern differs from type 1 in that temperatures during late glacials are warmer than interglacial ones. It needs to be mentioned, nonetheless, that while SST derived from alkenone $U_{37}^{k'}$ index and from foraminiferal Mg/Ca are more comparable than using other approaches, for instance foraminiferal or radiolarian assemblages, differences between SST derived by these two methods in the same cores have also been observed (e.g. Steinke et al., 2008 and references therein). The reasons of the discrepancy are under debate (e.g. Bard, 2001); they are generally ascribed to differences in the time of the signal, i.e. the season in which $U_{37}^{k'}$ producing cocolitophores and foraminifera live, and different depth habitats. Consequently, the comparison between tropical-subtropical SST records here performed should be taken only as indicative.

We propose that the anomalous ABS pattern, i.e. differing from any three type defined by Schneider et al. (1999), is due to a more prominent presence of Agulhas Waters at the site during full glacial periods. Perhaps in the form of a semi-permanent filament of Agulhas Waters existing over the Agulhas Bank and reaching our core site (see below). Under interglacial (high-stand) conditions the short-lived and migrating Agulhas Filaments and Rings would not necessary leave their imprint in the

signal recorded by *G. bulloides* at our location. This contention is supported by our inferred positive $\Delta\delta^{18}O_{sw}$ anomalies in glacial periods, coeval maximum accumulation of *G. menardii* and by the similarities between our Mg/Ca-derived temperature and the ALF records of ABS and CBR of Peeters et al. (2004). Interestingly, the alkenone $U_{37}^{k'}$ index derived SST record of GeoB3603-2 (Schneider et al., 1999) (one of the cores spliced to form the CBR record of Peeters et al., 2004) belongs to type 3 and as a consequence displays a very different pattern to that of ABS.

Despite the differences between the SST of both records, ABS Mg/Ca-derived SST show similarities with the ALF record of CBR (which also differs from its own SST record). The fact that the two proxies based on planktonic foraminifera which may provide hints on the Agulhas Leakage variability are in agreement provides additional confidence that our Mg/Ca-derived SST pattern traces Agulhas Current changes and likely alludes to a strong seasonal offset between the alkenone $U_{37}^{k'}$ index derived SST and the *G. bulloides* Mg/Ca-derived SST.

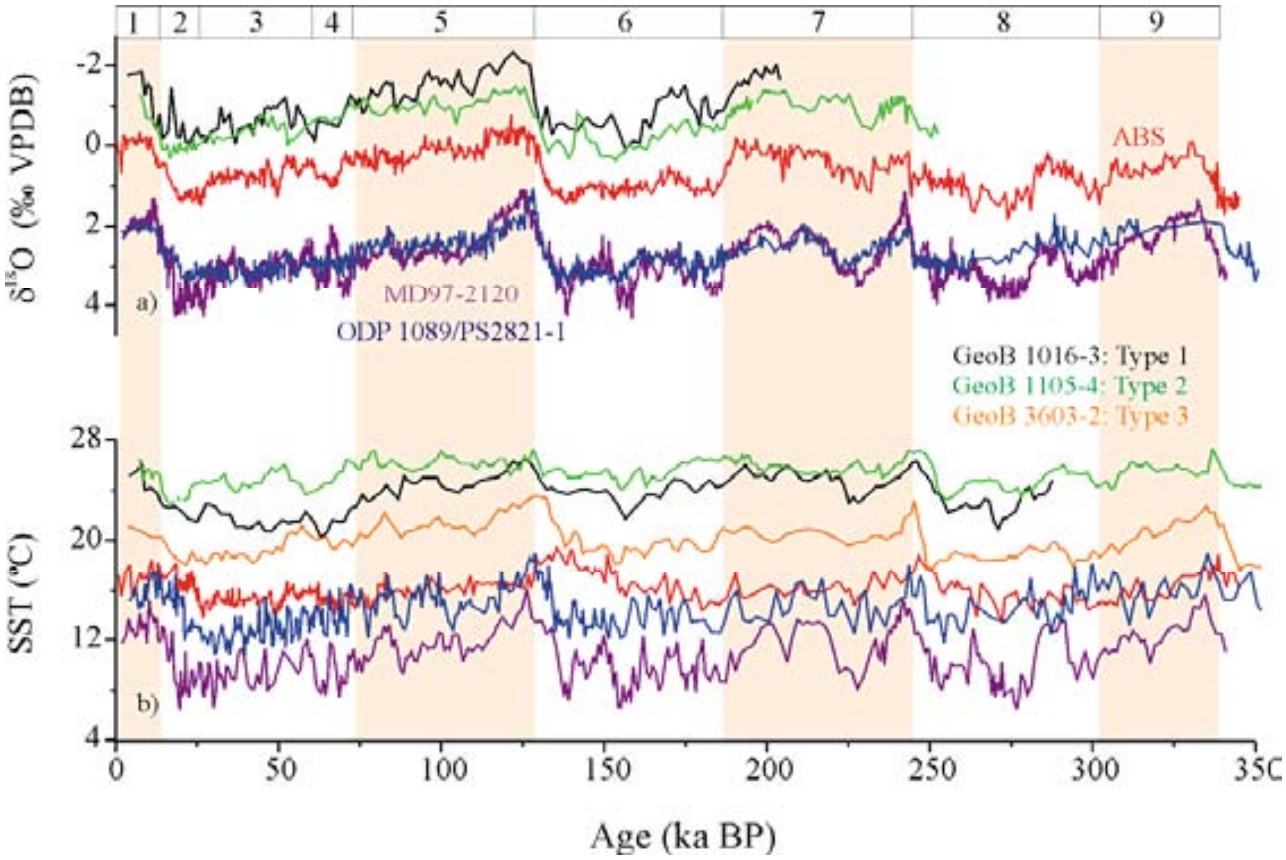

Figure 5.4-5 Tropical/subtropical SST records. a) Planktonic $\delta^{18}O$ of the different records for stratigraphic reference: *G. ruber* of GeoB1016-3 (black, Angola current, 11º46'S, 11º41'W) (Schneider et al., 1995); *G. ruber* of GeoB1105-4 (green, South Equatorial Current, 1º40'S, 12º26'W) (Schneider et al., 1996); ABS *G. bulloides* (red, this study); *G. bulloides* of the spliced ODP 1089/PS2821-1 (navy, Cortese et al., 2007); *G. bulloides* of MD97-2120 (purple, Pahnke et al., 2003); b) SST (ºC) for the same records and in orange alkenone $U_{37}^{k'}$ index derived SST for GeoB3603-2 (Schneider et al., 1999) (this record forms part of the CBR of Peeters et al., 2004). Same colour coding; GeoB1016-3 alkenone $U_{37}^{k'}$ index derived SST (Schneider et al., 1995); GeoB1105-4 alkenone $U_{37}^{k'}$ index derived SST (Schneider et al., 1996); ABS *G. bulloides* Mg/Ca-derived SST (this study); Spliced ODP 1089/PS2821-1 Radiolarian assemblages-SSST (Cortese et al., 2007); MD97-2120 *G. bulloides* Mg/Ca-derived SST. The age models of all records have been retuned to that of ABS to enhanced correlation except that of MD97-2120 which was used as reference for the generation of ABS age model from MIS 5a to MIS 9 (see Chapter 5.1).

Next we extend the comparison of our SST to core MD97-2120 (Pahnke et al., 2003) and the spliced record of ODP 1089/PS2821-1 (Cortese et al., 2007).

MD97-2120 is located on the Chatham Rise (Southwest Pacific) immediately to the south of the Subtropical Front (STF). SST in this core is also derived from Mg/Ca in *G. bulloides* and thus, the SST record is analytically compatible with ours.

ODP 1089/PS2821-1 are located just underneath the STF near the Agulhas Ridge. SST is derived from radiolarian assemblages and corresponds to summer conditions (SSST) (Cortese et al., 2007).

The SST records of these two cores are similar on orbital and sub-orbital time scales (Fig. 5.4-5). They show large glacial/interglacial fluctuations, between 6-8ºC, and prominent suborbital variability, with glacial warm events that reach half of the total glacial/interglacial amplitude. Cortese et al. (2007) proposed that the similarities between both records are likely indicating the influence of the Subtropical Front (STF) at both distant locations.

In contrast, the SST record of ABS (and of the other tropical/subtropical records, Fig. 5.4-5) displays lower glacial/interglacial amplitudes of around 3-4ºC, compared to 6-8ºC in MD97-2120 and ODP1089/PS2821-1, and only subdued intra-glacial variability. The discrepancy between our record and those under the influence of the STF on the one hand and some similarities between ABS SST and those of tropical and subtropical records on the other hand indicates that despite northward migrations of the frontal system, ABS SST were always modulated mainly by the tropics. This modulation could have been drawn, either by transmitting tropical temperatures to the South Atlantic or through variation in the wind pattern that alters the speed and intensity of the Agulhas Current and consequently variations in the Agulhas Water spillage. Nonetheless, the movement of the STF may have had an influence on the Agulhas Leakage (e.g. de Ruijter, 1982) as will be discussed in the following section.

- **Surface *versus* Deep Circulation: Role of the Agulhas Leakage in the MOC**

In order to assess a possible linking between Agulhas Leakage and the mode of the Atlantic MOC (see introduction) we compare our planktonic records and those of CBR (Peeters et al., 2004) with their corresponding benthic records (Fig. 5.4-6).

Benthic records of MD96-2080, have allowed investigating the varying contributions of Northern *versus* Southern sources to the core site (see Chapter 5.2). Benthic $\delta^{13}C$ of CBR, around 500 m deeper than ABS, on the orbital time scale is coherent with that of ABS while the CBR $\delta^{13}C$ record is depleted relative to the ABS one during MIS 5a-d, 6 and 7e, probably indicating less influence of NCW at the deeper site in those periods. Based only on benthic $\delta^{13}C$, as a general note we can say that our inferred deep circulation patterns at ABS (i.e. MD96-2080, Chapter 5.2 and 5.3) also apply for most of the deeper CBR, while the existing differences will be discussed below.

In addition to the planktonic and benthic records, in Figures 5.4-6 to 10 we also represent the Subtropical Convergence Movement Index (STC-index) of Peeters et al. (2004). This index based on

foraminiferal assemblages provides indications on the northward-southward migration of the STF in glacial-interglacial time scales. The position of the STF is though to have an influence in the Leakage of Agulhas Water (e.g. de Ruijter, 1982) and its northward migrations to have contributed to vanish the Agulhas Leakage in glacial times (e.g. Berger and Wefer, 1996), hence the interest of obtaining some hints on the latitudinal movement of the frontal system. Besides, we have used the available foraminiferal census counts of Rau et al. (2002) to compute the same index for MD96-2080. The indexes at both sites display a similar glacial-interglacial modulation with the STF lying northward during glacial periods; but the amplitude of change in the CBR STC-index record is much larger. Whereas these differences may be related to the different location of cores, with MD96-2080 one degree to the south and two degrees to the west of CBR, hence closer to a more direct influence of the Agulhas Current, it needs to be noticed that the index has not been validated yet and is considered here as being indicative only.

For this surface-deep comparison, we first concentrate on the data pattern in MIS 6 and on into MIS 5e that displays systematic shifts. Next we examine the transitions from MIS 2 to 1 and 10 to 9c that show similarities with that of MIS 6 to 5e. Last we examine the one from MIS 8 into 7e which appears different in that a prominent positive anomaly of $\Delta\delta^{18}O_{sw}$ is not observed (Figs. 5.4-7 to 10). The deep circulation patterns that we describe in the following were inferred based on the evaluation of benthic $\delta^{13}C$, Cd/Ca and $\overline{SS}$ and are extensively described in Chapters 5.2 and 5.3.

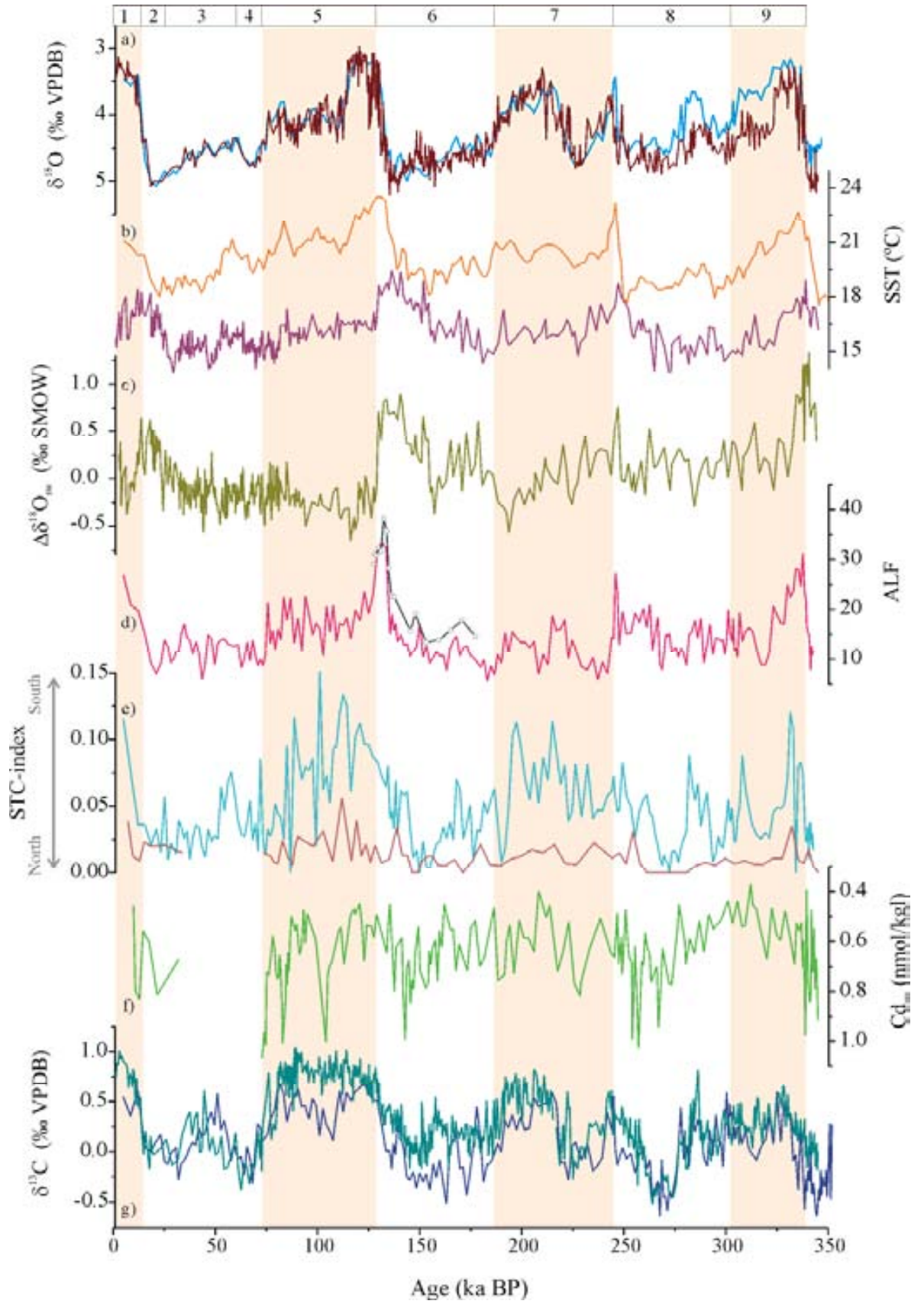

Figure 5.4-6 Planktonic and benthic records of ABS and CBR. a) *F. wuellerstorfi* $\delta^{18}O$ for the ABS spliced (brown curve); CBR *F. wuellerstorfi* $\delta^{18}O$ (blue) (Peeters et al., 2004); b) ABS *G. bulloides* Mg/Ca-derived SST (purple); CBR $U^{k'}_{37}$ derived SST (Schneider et al., 1999) (orange); c) ABS $\Delta\delta^{18}O_{sw}$ (‰) SMOW; d) Agulhas Leakage Fauna (ALF) of CBR (Peeters et al., 2004) (pink); ALF of ABS (MD96-2080 section) (black-dotted); e) Subtropical Convergence Index (STC-index) for CBR (Peeters et al., 2004) (light blue); STC-index for MD96-2080 computed using the foraminiferal census counts available from Rau et al. (2002) (light brown); f) MD96-2080 Cd_{sw} (nmol/kg) derived from benthic Cd/Ca (see Chapter 5.2); g) ABS *F. wuellerstorfi* $\delta^{13}C$ (cyan); CBR *F. wuellerstorfi* $\delta^{13}C$ (D. Kroon, R. Schneider, unpublished data) (blue).

- MIS 6 and Termination II

The data patterns displayed along the ABS profile in MIS 6 and across Termination II differ substantially from those recorded at other core sites in that SST progressively increases across the whole penultimate glacial period (Fig. 5.4-7). The SST rise starts with the onset of glacial conditions, and after 12 kyr it reaches a plateau in SST lasting around 10 kyr. In a third step SST then reaches peak maximum values, some 3°C higher than core-top SST, in late MIS 6 as global ice volume is at a maximum. Maximum SST prevails into Termination II until they abruptly collapse as full-interglacial conditions of MIS 5e are approached. This SST evolution is paralleled by a three-step ALF increase along the CBR and ABS records while the increase in ALF is more subtle in the first step, the plateau lasts for 22 kyr and in the final increase is much steeper. The $\Delta\delta^{18}O_{sw}$ record parallels the SST behaviour from middle to late MIS 6 while its first increasing step commences within MIS 7a at around 193 ka.

During the first step of increasing SST and ALF Northern Component Water (NCW) remains an active contributor to the hydrography of ABS. This is suggested by a benthic $\delta^{13}C$ depletion that remains in the range of mean ocean $\delta^{13}C$ changes and moderate Cd_{sw} levels (see Chapter 5.2). During mid-MIS 6, 153-141 kyr, prominent benthic $\delta^{13}C$ depletions are observed coinciding with elevated Cd_{sw} levels and increased $\overline{SS}$ values that indicate enhanced deep flow speed, suggesting a major influence of Southern Component Water (SCW) (see Chapter 5.2). This coincides with the third and more pronounced SST raise and with increasing $\Delta\delta^{18}O_{sw}$, both indicative of a prominent influence of Agulhas Waters (AW) at this site.

Benthic $\delta^{13}C$ commences to increase from around 148 kyr. First, $\delta^{13}C$ gradually increases by 0.35‰ until 140 ka when the increase comes to an intermittent halt and $\delta^{13}C$ remains at constant levels, from 142 to 132 ka. Next a further $\delta^{13}C$ increase begins that lasts to 127 ka when benthic $\delta^{13}C$ reaches full-interglacial values of 0.8‰. The initial $\delta^{13}C$ increase coincides with an increase in warm waters with increased $\Delta\delta^{18}O_{sw}$ and a southward displacement of the STF (Fig. 5.4-7). The second increase of benthic $\delta^{13}C$ after the plateau towards full-interglacial levels likewise coincides with maximum SST, maximum $\delta^{18}O_{sw}$ and with a southward migration of the STF. At this time a peak maximum abundance of ALF occurs. As benthic $\delta^{13}C$ reaches full-interglacial values SST, ALF and $\Delta\delta^{18}O_{sw}$ abruptly collapse to background values.

This data pattern suggests that during MIS 6 the surface-ocean climatology at our core site progressively changed toward warmer SST, plausibly indicating an increasing influence of Agulhas and/or mixed waters at the site. This trend is mimicked by a continuous increase in ALF abundance along the CBR record that ultimately mounts in an abrupt ALF maximum in the later stage of Termination II. Intriguingly, during mid-MIS 6 increased AW at our core site coincides with a prominence presence of SCW at depth. The onset of the benthic $\delta^{13}C$ increase then occurs when the STF starts moving south, an event that is embedded in an apparent AW increase already well

underway. A maximum influence of AW, as signified by peak maximum ALF presence, then occurs immediately before the final step of benthic $\delta^{13}C$ increase to full-interglacial levels.

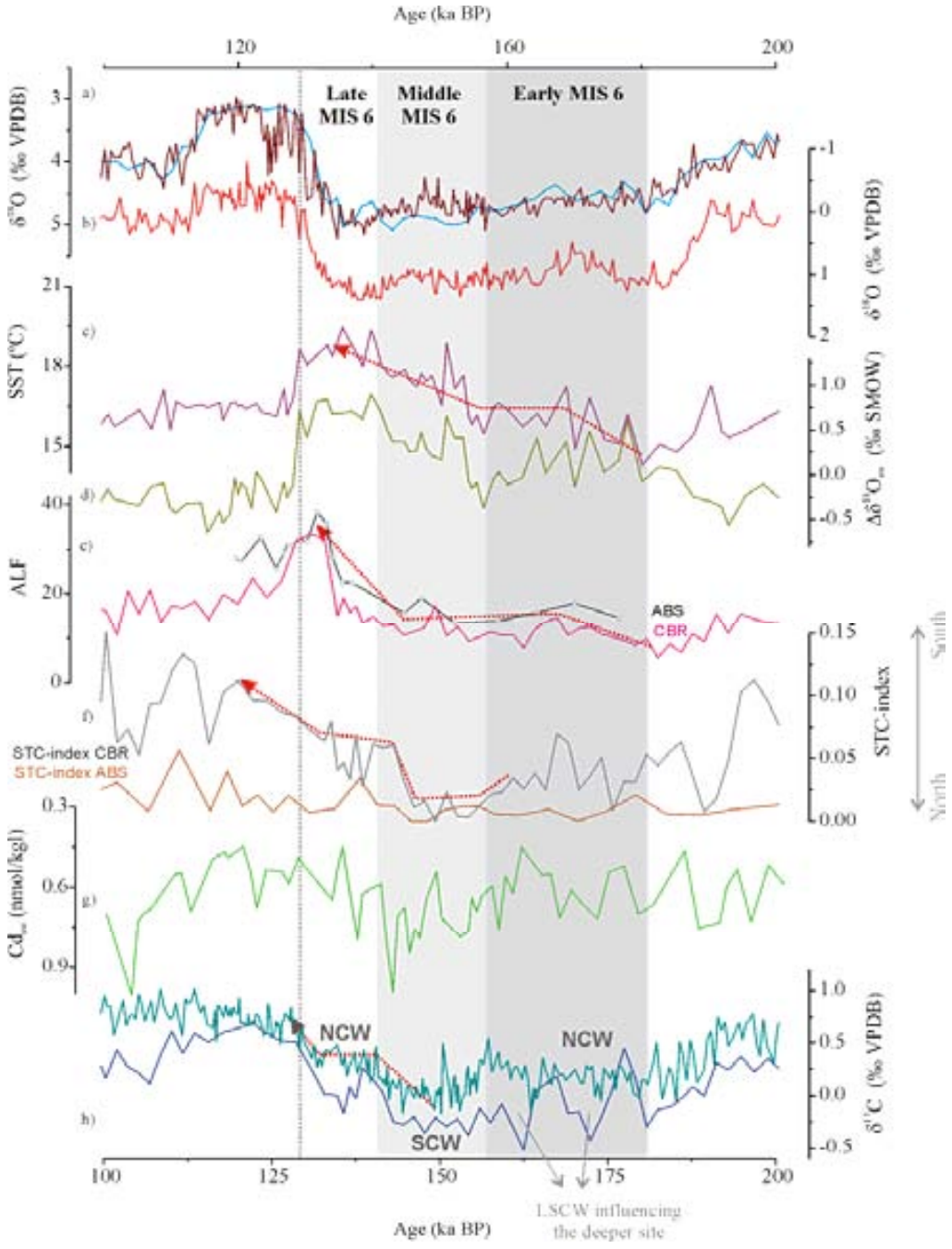

Figure 5.4-7 MIS 6 to 5 Transition, a) ABS *F. wuellerstorfi* $\delta^{18}O$ (brown), CBR *F. wuellerstorfi* $\delta^{18}O$ (blue); b) ABS *G. bulloides* $\delta^{18}O$; c) ABS *G. bulloides* Mg/Ca-derived SST; d) ABS $\Delta\delta^{18}O_{sw}$ (‰ SMOW); e) Agulhas Leakage Fauna (ALF) of CBR (Peeters et al., 2004) (pink); ALF of ABS (MD96-2080 section) (black-dotted); f) Subtropical Convergence Index (STC-index) for CBR (Peeters et al., 2004) (light blue); STC-index for MD96-2080 computed using the foraminiferal census counts of Rau et al. (2002) (light brown); g) MD96-2080 benthic Cd/Ca-derived Cd_{sw} (nmol/kg); h) ABS *F. wuellerstorfi* $\delta^{13}C$ (cyan); CBR *F. wuellerstorfi* $\delta^{13}C$ (D. Kroon, R. Schneider, unpublished data) (blue). Grey shading indicates the glacial period MIS 6.

- Transition From MIS 2 to 1

This transition shows some similarities with that from MIS 6 to 5. Warm waters and positive $\Delta\delta^{18}O_{sw}$ during MIS 2 reflect the presence of Agulhas and mixed waters at the core site during full glacial conditions. The increase in SST commences at the MIS 3/2 transition, well before the LGM (18-21 ka) and maximum SST is reached at the beginning of Termination I (Fig. 5.4-8). From this point, SST shows a decreasing trend into the Holocene. On the other hand, the build up of $\delta^{18}O_{sw}$ enriched surface waters starts even earlier, at around 36 ka. $\Delta\delta^{18}O_{sw}$ shows a depletion at around 14 ka as a result of the combination of a plateau in planktonic $\delta^{18}O$ and a slight decrease in SST. After this depletion, $\Delta\delta^{18}O_{sw}$ recovers to positive values and from 13 ka displays a decreasing trend that continues into the Holocene. The ALF of CBR (Peeters et al., 2004) initiates a rather abrupt increase from a minimum value at 20 ka. This is 3 ka prior to the initiation of the southward migration of the STF (Figs. 5.4-6 and 8).

Regarding the deep circulation, benthic $\delta^{13}C$ of around 0‰, depleted by 0.4‰ beyond the mean ocean depletion plausibly indicate the presence of SCW at the core site during MIS 2. This suggests that the deep circulation during MIS 2 was likely similar to that during middle MIS 6 and 8 (see Chapters 5.2 and 5.3). Besides, similarly to middle MIS 6, the presence of SCW at depth coincides with maximum presence of Agulhas Water at the surface. The restoration of more positive benthic $\delta^{13}C$ values starts at 17 ka. Holocene benthic $\delta^{13}C$ of 0.74‰ are reached at 10.6 kyr, and coincides with maximum SST and with a decrease in $\Delta\delta^{18}O_{sw.}$ At this time, the STC-index experiences a steep increase likely indicating a southward displacement of the STF.

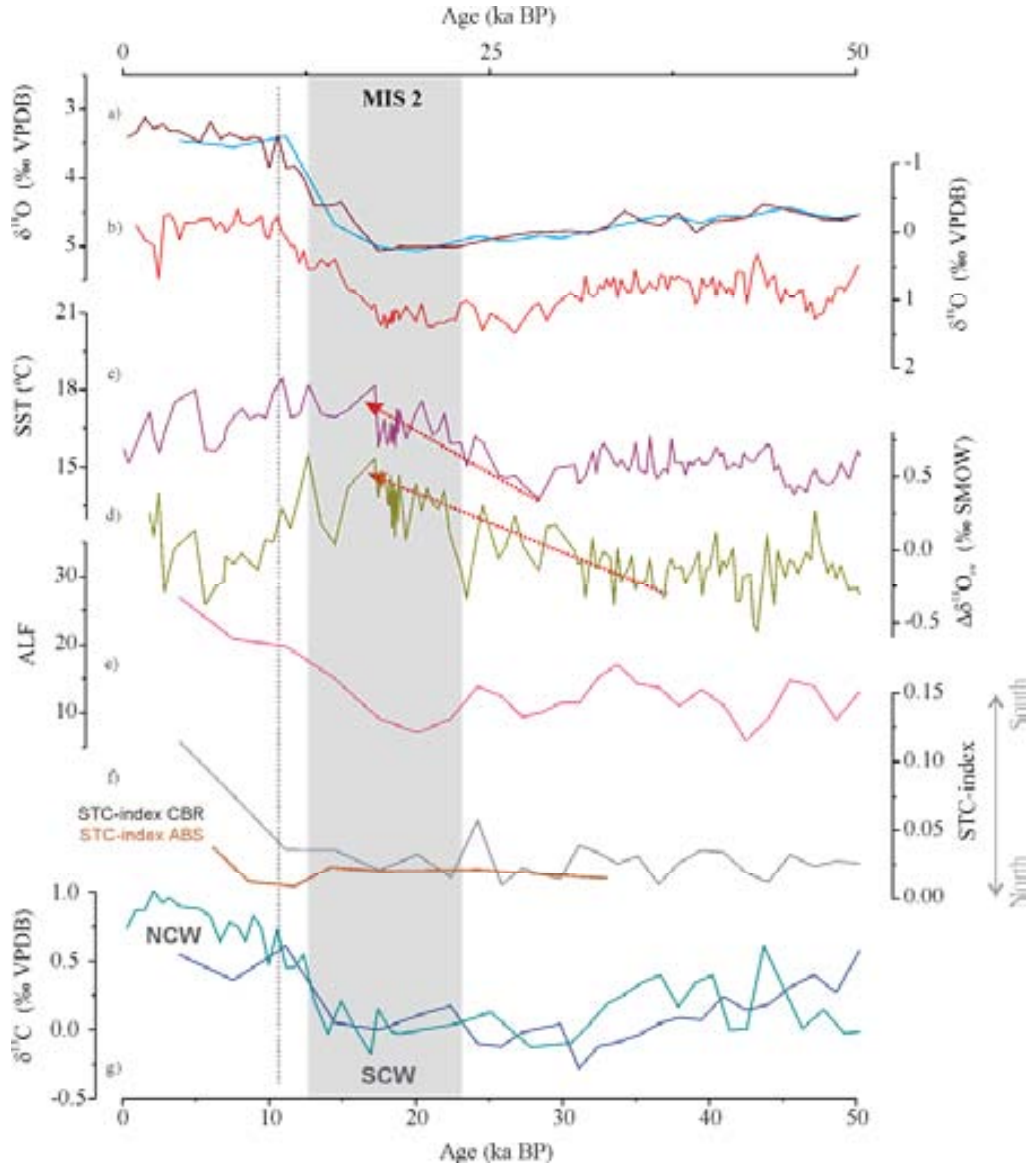

Figure 5.4-8 MIS 2 to 1 Transition, a) ABS *F. wuellerstorfi* $\delta^{18}O$ (brown), CBR *F. wuellerstorfi* $\delta^{18}O$ (blue); b) ABS *G. bulloides* $\delta^{18}O$; c) ABS *G. bulloides* Mg/Ca-derived SST; d) ABS $\Delta\delta^{18}O_{sw}$ (‰ SMOW); e) Agulhas Leakage Fauna (ALF) of CBR (Peeters et al., 2004) (pink); f) Subtropical Convergence Index (STC-index) for CBR (Peeters et al., 2004) (light blue); STC-index for MD96-2080 computed using the foraminiferal census counts of Rau et al. (2002) (light brown); g) ABS *F. wuellerstorfi* $\delta^{13}C$ (cyan); CBR *F. wuellerstorfi* $\delta^{13}C$ (D. Kroon, R. Schneider, unpublished data) (blue). Grey shading indicates the glacial period MIS 2.

- Transition From MIS 10 to 9

During Termination IV ABS records a pronounced positive $\Delta\delta^{18}O_{sw}$ anomaly, coevally with warm SST and peak ALF in CBR (Fig. 5.4-9). However, the ALF of CBR does not show an increasing trend across the whole glacial MIS 10 as is seen in MIS 6, but rather is more alike to MIS 2 with the increase in ALF starting only before Termination IV when ice volume is at its maximum. The accumulation rate of *G. menardii* of MD96-2080 (Rau et al., 2002) on the other hand, does show an early increase commencing at the onset of the glacial period, plausibly indicating an influence of Agulhas Waters at MD96-2080 site.

Negative benthic $\delta^{13}C$ of around of -0.6‰ in late MIS 10 in CBR is suggestive of a predominance of LSCW at levels deeper than 3000 m, while MD96-2080 benthic $\delta^{13}C$ of around 0‰

(Rau et al., 2002) may indicate some influence of $\delta^{13}C$ enriched NCW or USCW at mid-depths (see Chapters 5.2 and 5.3). The deep circulation could have been similar to that during early MIS 6 and 8, with strong presence of NCW or to that during middle MIS 6 and 8 with preponderance of $SCW_{s.l.}$, in absence of Cd_{sw} we cannot favour any of these two scenarios.

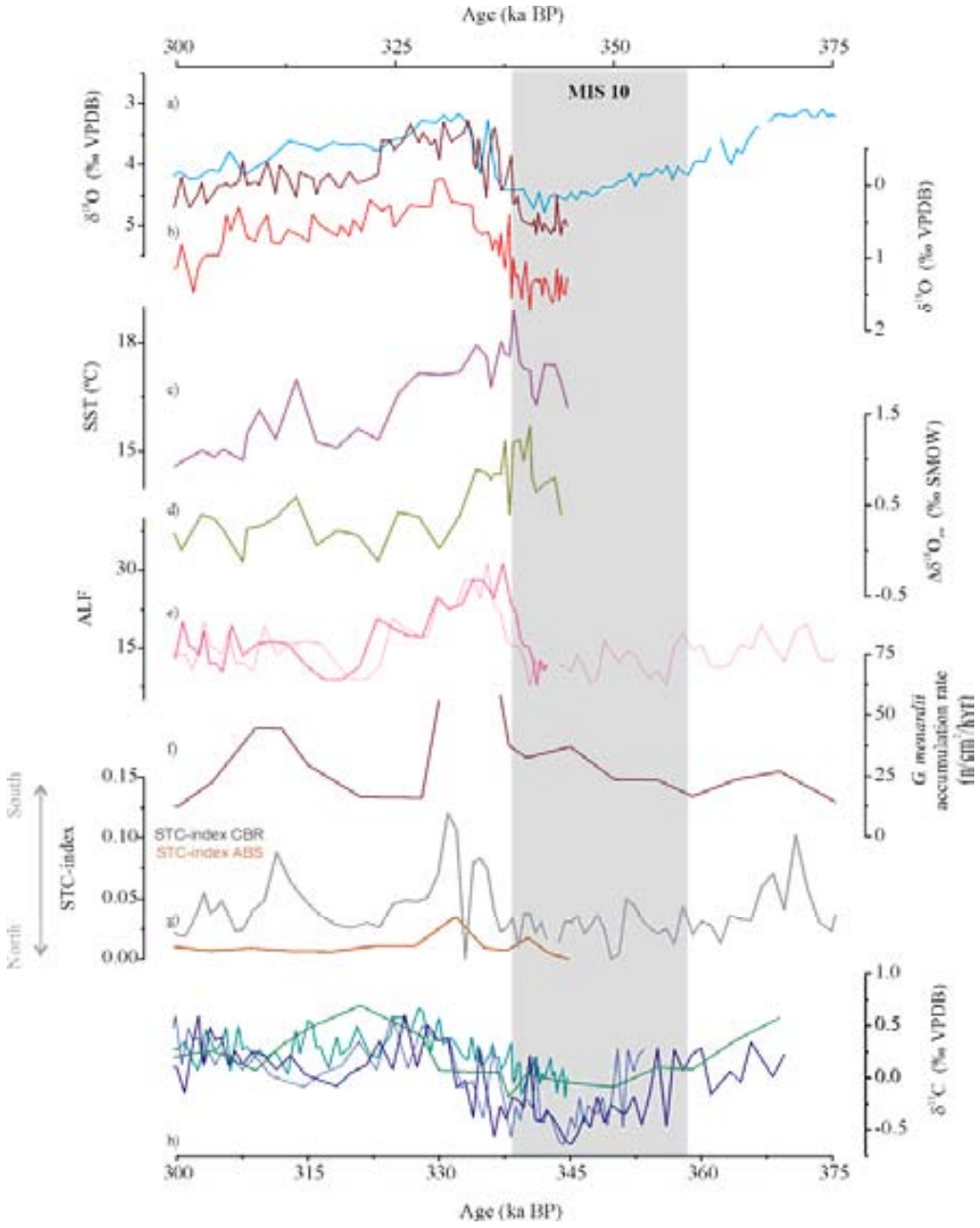

Figure 5.4-9 MIS 10 to 9 Transition, a) ABS *F. wuellestrofi* $\delta^{18}O$ (brown), CBR *F. wuellestrofi* $\delta^{18}O$ (blue); b) ABS *G. bulloides* $\delta^{18}O$; c) ABS *G. bulloides* Mg/Ca-derived SST; d) ABS $\Delta\delta^{18}O_{sw}$ (‰ SMOW); e) Agulhas Leakage Fauna (ALF) of CBR (Peeters et al., 2004) (pink); dotted line shows the record retuned to ABS while the straight line displays the original age model of Peeters et al. (2004); f) *G. menardii* accumulation rate of MD96-2080 (n/cm2/kyr) (Rau et al., 2002); g) Subtropical Convergence Index (STC-index) for CBR (Peeters et al., 2004) (light blue); dotted line as in panel; STC-index for MD96-2080 computed using the foraminiferal census counts of Rau et al. (2002) (light brown); h) ABS *F. wuellerstorfi* $\delta^{13}C$ (cyan); MD96-2080 *F. wuellerstorfi* $\delta^{13}C$ (green) (Rau et al., 2002); CBR *F. wuellerstorfi* $\delta^{13}C$ (blue, D. Kroon, R. Schneider, unpublished data); dotted and straight line as in panel e). Grey shading indicates the glacial period MIS 10.

Cortese et al. (2004) observed coeval SST and SSS anomalies during MIS 10 at ODP Site 1089 from the Agulhas Ridge (see Fig. 5.4-1 for location). The nature of the combined anomaly, i.e. SST and SSS, that is moreover accompanied by increased surface productivity in the area (Cortese et al., 2004) led these authors to conclude that it reflects a spill-over of Agulhas Waters. Apparently the ALF of CBR (Peeters et al., 2004) does not record this spill-over of Agulhas Water while the accumulation rate of *G. menardii* (Rau et al., 2002) would support the existence of AW at MD96-2080 during MIS 10. It is plausible that the changing path of the Agulhas Current and the varying position and width of the main corridor of Agulhas Rings and Filaments generate different signals in nearby core sites.

- Transition From MIS 8 to 7

In the course of the deglaciation from glacial MIS 8 into glacial MIS 7e SST in ABS starts to rise early, at around 262 ka, approximately 10 kyr before the commencement of ice sheet retreat globally (Fig. 5.4-10). The ALF of CBR also commences to increase during mid-MIS 8, at 268 ka, remaining high and achieving peak maxima during Termination III. The SST and ALF increases approximately coincide with the southward displacement of the STF (Fig. 5.4-10e). Whereas high SST and ALF are indicative of strong presence of AW, $\Delta\delta^{18}O_{sw}$, however, does not show signs of prominent positive anomalies. We observe a subdued anomaly around 262 ka and a more pronounce, though short-lived, one in Termination III with $\Delta\delta^{18}O_{sw}$ values close to zero in between. Thus, according to ABS SST and CBR ALF the presence of Agulhas Waters was also enhanced in this glacial period but the lack of a coeval positive $\Delta\delta^{18}O_{sw}$ anomaly likely indicate that the input of Agulhas Waters, while existing was not as intense as those in MIS 6 and 2.

Concerning the deep circulation, the evolution from mid-MIS 8, with a strong presence of SCW (Chapter 5.2), onwards to MIS 7e, with NCW dominance, is similar to that from middle MIS 6 into MIS 5e in that benthic $\delta^{13}C$ in ABS and CBR starts to increase to positive values around 10-12 kyr before the onset of global deglaciation. Conversely, in contrast to the MIS 6-5 transition, we do not observe a plateau along the progression to positive values in ABS while such plateau exists in the CBR benthic $\delta^{13}C$ record between 258 and 247 kyr. The initial increase in CBR benthic $\delta^{13}C$ followed by the plateau coincides with the subsidence of the small $\Delta\delta^{18}O_{sw}$ anomaly at 262 kyr. Both, ABS and CBR achieve maximum benthic $\delta^{13}C$ of 0.6‰ at around 244 kyr coeval with the collapse of ALF, SST and the transient strong $\Delta\delta^{18}O_{sw}$ anomaly to interglacial background levels.

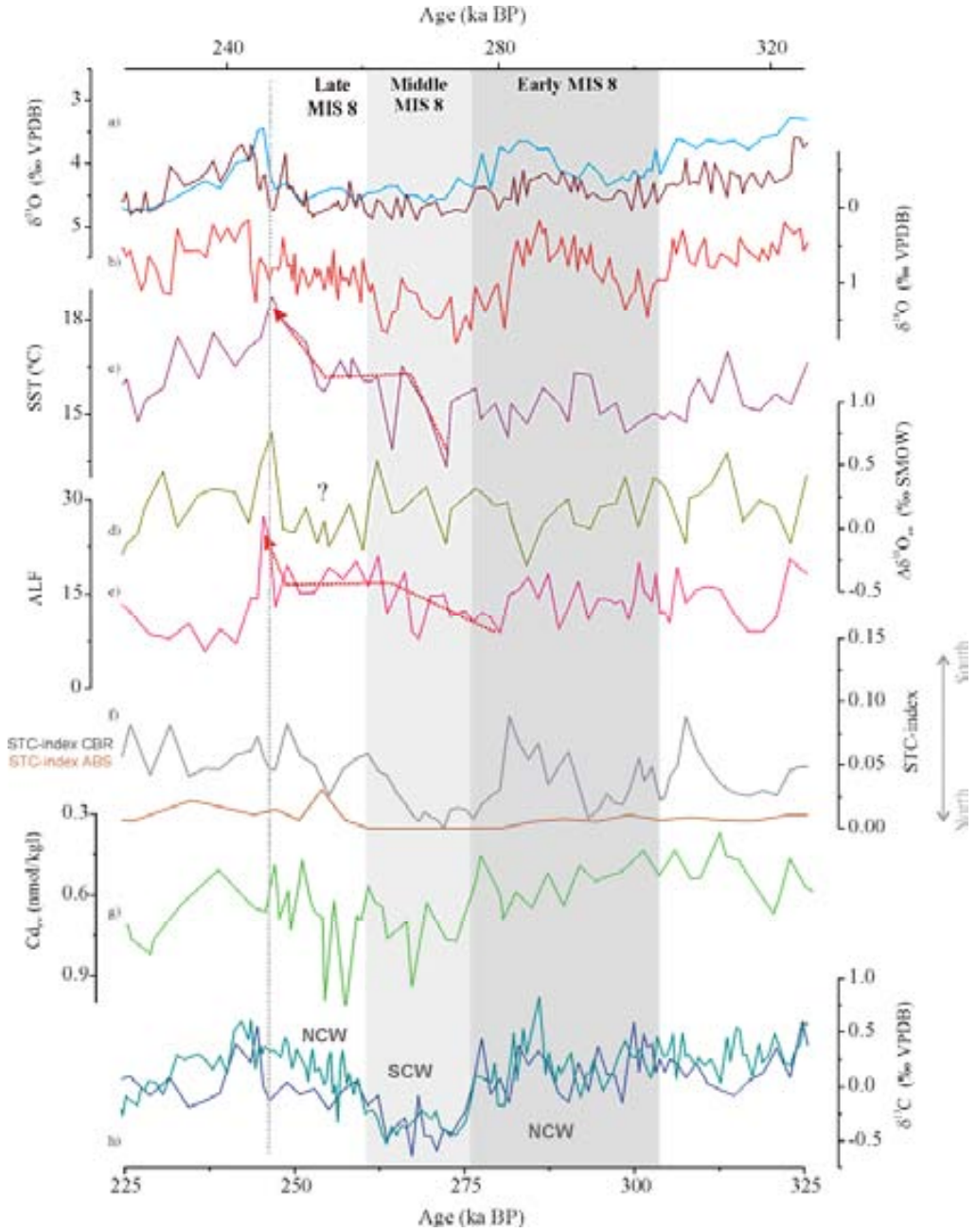

Figure 5.4-10 MIS 8 to 7 Transition, a) ABS *F. wuellerstorfi* $\delta^{18}O$ (brown), CBR *F. wuellerstorfi* $\delta^{18}O$ (blue); b) ABS *G. bulloides* $\delta^{18}O$; c) ABS *G. bulloides* Mg/Ca-derived SST; d) ABS $\Delta\delta^{18}O_{sw}$ (‰ SMOW); e) Agulhas Leakage Fauna (ALF) of CBR (Peeters et al., 2004) (pink); f) Subtropical Convergence Index (STC-index) for CBR (Peeters et al., 2004) (light blue); STC-index for MD96-2080 computed using the foraminiferal census counts of Rau et al. (2002) (light brown); g) ABS *F. wuellerstorfi* $\delta^{13}C$ (cyan); CBR *F. wuellerstorfi* $\delta^{13}C$ (D. Kroon, R. Schneider, unpublished data) (blue). Grey shading indicates the glacial period MIS 8.

5.4.5. Data Model Comparison

Numerical modelling and conceptual considerations postulate a linking between Agulhas Water transports to the South Atlantic and the strength of the Atlantic MOC by way of salt inputs to the Atlantic that impact on meridional density gradients (e.g. Gordon, 1986; Weijer et al., 2002). According to our data such feedback might have existed in intervals of the glacial periods, particularly prior to Terminations when benthic $\delta^{13}C$ increased in harmony with AW indicators (ALF, SST, $\Delta\delta^{18}O_{sw}$). However, early increases of AW in MIS 2, middle MIS 6 and middle MIS 8 coincide with

benthic $\delta^{13}C$ depleted beyond mean ocean values (see Chapter 5.2) and maximum Cd_{sw} and $\overline{SS}$ for those periods, hence indicating minimum ventilation at depth and maximum presence of SCW. These developments do not suggest an influence of AW leakage on the convection strength and depth of formation of NCW. Whether this points to the existence of a threshold input of AW to the Atlantic before the MOC shifts to a state with intense and deep formation of NCW remains open. North Atlantic climatology likely plays a role in such scenarios as freshwater input from disintegrating ice sheets will impose buoyancy anomalies in the North whose impact on the state of the MOC might not easily be overcome by AW salt water input in the South. For instance, the IRD record of ODP site 980 suggests that the northern ice sheets were unstable during these three full glacial periods (Fig. 5.2-3, Chapter 5.2). On the other hand, during early MIS 6 and 8, our AW indicators display levels close to those recorded during interglacials and would suggest a connection between Agulhas Leakage and strong NCW convection in a similar fashion to today.

Table 5.4-1 presents a synoptic view of the stronger or weaker presence of Agulhas Water, qualitatively estimated according to higher/lower SST, $\Delta\delta^{18}O_{sw}$ and ALF; presence of SCW and/or NCW at ABS (~2500 m) and CBR (~3000 m) sites and, based on the previous, state of the MOC. We interpret that the presence of NCW at both, ABS and CBR, sites indicates a vigorous formation of deep NCW, similarly to today, i.e. an interglacial mode of the MOC. Presence of NCW at ABS and varying influence of SCW and NCW at CBR would indicate that the convection of NCW was not reaching deep levels, i.e. a glacial "on" mode of the MOC (Sarnthein et al., 1994; Keeling and Stephens, 2001; Seidov and Maslin, 2001; Rahmstorf, 2002). Last, we take the presence of SCW at ABS and CBR as indication of shallow convection of NCW, maybe also weak, i.e. a glacial "off" mode of the MOC (Sarnthein et al., 1994; Keeling and Stephens, 2001; Seidov and Maslin, 2001; Rahmstorf, 2002) (see also Chapter 5.3). Note that the glacial "off" mode as proposed by Keeling and Stephens (2001 see Fig. 5.3-8) in essence is similar to that proposed by Sarnthein et al. (1994), Seidov and Maslin (2001) and Rahmstorf (2002) but does not necessarily imply a complete shut-down of the NCW overturning cell.

Table 5.4-1 Qualitative indication of stronger or weaker presence of Agulhas Water (AW) at surface, Southern and Northern Component Waters (SCW, NCW) at depth and concomitant responses of the MOC.

	MIS 2	MIS 6			MIS 8			Termination IV
		Late	Middle	Early	Late	Middle	Early	
Presence of AW	↑↑	↑↑↑	↑↑	-	↑↑	↑	-	↑↑↑
SCW at ABS	∨		∨			∨		?
SCW at CBR	∨	∨	∨	∨	∨	∨		∨
NCW at ABS		∨		∨	∨		∨	?
NCW at CBR		∨		∨			∨	
Mode of the MOC	G "off"	G "on"	G "off	G "on"	G "on"	G "off"	I	G "off"?

"↑"strong presence, "-" interglacial levels, G "on", "off": glacial "on" , "off" modes sensu Keeling and Stephens (2001), I: interglacial

The observation that an increasing AW influence is recorded at our site in MIS 2 and mid-MIS 6 and 8 while the MOC entered a state with SCW dominance would suggest either that North Atlantic climatology was not favouring the convection at depth of NCW despite the salinity input of AW, or that

other components of the upper branch of the THC, for example waters entering through the Drake Passage from the Pacific, were not contributing enough to join to the Agulhas contribution and contribute both to the NCW compensation, or that AW transfer into the South Atlantic even in the view of a strong presence of this waters recorded at our site was not being efficiently transmitted to the Atlantic.

Regarding the last option, a plausible scenario would be that the Leakage of Agulhas Waters was not preferentially occurring by Agulhas Rings as today, but rather through Filaments. Today, water transfer to the South Atlantic by way of AW Filaments involves the uppermost water layers only, probably top-50 m (Lutjeharms, 1996), and hence, they contribute far less to the South Atlantic buoyancy budget than the salt input through deep-reaching Agulhas Rings. A sort of semi-permanent Agulhas Filament located close to our core site could have imprinted this strong Agulhas signature on our surface records while the net transfer of AW to the Atlantic might have been reduced. An altered shape of the coast line in response to a lowered sea level (e.g. Waelbroeck et al., 2002, Fig. 5.4-1) possibly in conjunction with glacial ocean fronts at northerly positions might have steered the Agulhas Retroflection further to the west allowing the formation of such filaments. Such scenario would be supported by the continuous presence of subtropical planktonic foraminiferal species such as *G. menardii* that are transported to the core site with waters derived from the Agulhas Current passing over the Agulhas Bank (Rau et al., 2002). In Figure 5.4-1 the 120 m isobath is highlighted to demonstrate the altered coastline during glacial sea level low stands.

If so, then there should have been a net accumulation of Agulhas Waters in the Indian Ocean. Sicre et al. (2005) found evidence of strong advection of warm alkenones from the Agulhas Retroflection system in a sediment core close to the Kerguelan Plateau during MIS 2, which would support the hypothesis that most of the Agulhas Current was retroflected back into the Indian Ocean at this time. As a consequence of such scenario, the Indian Ocean sector off South Africa might have become a pool of saline and warm waters. Schmidt et al. (2004; 2006) propose a similar scenario of warm, salty waters accumulating in the Caribbean during glacials intervals, and particularly during stadials, whose liberation to the North Atlantic may have contributed to amplified the North Atlantic thermohaline circulation. The release of these waters accumulated in the SW Indian Ocean prior and during glacial Terminations could explain the prominent presence of AW in ABS and CBR and the subsequent collapse of the Agulhas indicators to interglacial levels as the Agulhas Leakage was set back to a Ring-shedding dominant mode once a modern state of the MOC was re-established.

5.4.6. Conclusions

Combined planktonic $\delta^{18}O$, Mg/Ca and Agulhas Leakage Fauna abundance and benthic $\delta^{13}C$ and Cd/Ca from a spliced record of mid-depth cores MD02-2594 and MD96-2080, Agulhas Bank Splice (ABS), from the Agulhas Corridor allow inferences about past deep and surface circulation in the South Atlantic with implications for the MOC.

In agreement with previous studies, our surface records suggest that the input of waters from the Agulhas Current to the South Atlantic has never stopped in the last 345 kyr. Intriguingly, however,

our records show that the presence of Agulhas Waters in the western side of the Agulhas Bank was indeed progressively increased in the course of the glacial periods, and very especially in MIS 6.

Numerical and conceptual models claim a linkage exists between the input of Agulhas Waters to the South Atlantic and the mode of the Atlantic MOC. During early MIS 6 and 8 our indicators show that both, surface and deep circulation were similar to that of interglacial periods, thus supporting the existence of a connection between the Agulhas Leakage and the vigour and depth of NCW convection. On the other hand, during full glacial MIS 2, middle MIS 6 and middle MIS 8, increased amounts of Agulhas Water at ABS coincide with a strong presence of SCW at depth as indicated by strong benthic $\delta^{13}C$ depletions, high Cd_{sw} levels and increased $\overline{SS}$. This surface *versus* deep circulation pattern does not seem to support the existence of a connection between Agulhas Leakage and a vigorous and deep NCW formation. At this time other factors might have been at work that overwhelmed the positive feedback of Agulhas Water on the MOC. For instance, North Atlantic climate variability, stability of Northern Ice sheets, reduction of other sources of surface and thermocline waters for the compensation of NCW formation, or the actual efficiency of the transfer of tropical-subtropical Indian Waters.

With regard to the last option, an altered shape of the coast line in response to a lowered sea level possibly in conjunction with northward displacement of the sub-Antarctic oceanic fronts might have steered the Agulhas Retroflection westward allowing the formation of filaments but reducing the leakage through rings. A sort of semi-permanent filament located close to our cores sites could have caused the strong presence of Agulhas Waters that we record while the net transfer of buoyancy sources to the Atlantic could have been small. An outcome of this scenario is that much of the Agulhas Current may likely have returned to the Indian Ocean and accumulated there, hence, contributing to precondition the system for a return to a strong mode of NADW convection later.

Prior to glacial Terminations, our Agulhas Water indicators show maximum presence of these waters with a collapse to background levels as full-interglacials MIS 5e, 7e and 9c are reached. It is possible that this collapse indicates the reestablishment of a modern-type mode of Agulhas Water Leakage through Rings and the release of warm saline waters stored in the Indian Ocean.

Our surface and deep records support the hypothesis of a link between the leakage of Agulhas Waters and the strength of the Atlantic MOC during early and late glacial periods. The contrasting pattern in mid-glacials, on the other hand, either indicates that our records are recording a prominent presence of Agulhas Waters which are in turn not efficiently generating a buoyancy anomaly in the South Atlantic or that other factors are overcoming the salt anomaly imposed by the Agulhas Waters in the South Atlantic.

References

Adkins, J.F. and Schrag, D.P., 2001. Pore Fluid Constraints on Deep Ocean Temperature and Salinity During the Last Glacial Maximum. Geophysical Research Letters, 28 (5), 771-774.

Bard, E., 2001. Comparison of alkenone estimates with other paleotemperatture proxies. Geochemistry, Geophysics, Geosystems, 2 (1), 1002, doi: 10.1029/2000GC000050.

Barker, S., Greaves, M. and Elderfield, H., 2003. A study of cleaning procedures used for foraminiferal Mg/Ca paleothermometry. Geochemistry, Geophysics, Geosystems, 4 (9), 8407, doi: 10.1029/2003GC000559.

Berger, W.H. and Wefer, G., 1996. Expeditions into the Past: Paleoceanographic Studies in the South Atlantic. In: G. Wefer, W.H. Berger, G. Siedler and D. Webb (Editors), The South Atlantic:Present, Past and Future. Springer-Verlag, Berlin Heidelberg, pp. 363-410.

Bigg, G.R. and Rohling, E.J., 2000. An oxygen isotope data set for marine waters. Journal of Geophysical Research, 105 (C4), 8,527-8,535.

Blunier, T. and Brook, E.J., 2001. Timing of Millennial-Scale Climate Change in Antarctica and Greenland During the Last Glacial Period. Science, 291, 109-112.

Cortese, G., Abelmann, A. and Gersonde, R., 2004. A glacial warm water anomaly in the subantarctic Atlantic Ocean, near the Agulhas Retroflection. Earth and Planetary Science Letters, 222 (3-4), 767-778.

Cortese, G., Abelmann, A. and Gersonde, R., 2007. The last five glacial-interglacial transitions: A high-resolution 450,000-year record from the subantarctic Atlantic. Paleoceanography, 22, PA4203, doi: 10.1029/2007PA001457.

Chang, Y.-P., Chang, c.-C., Wang, L.-W., Chen, M.-T., Wang, C.-H. and Yu, E.-F., 1999. Planktonic Foraminiferal Sea Surface Temperature Variations in the Southeast Atlantic Ocean: A High-Resolution Record MD962085 of the Past 400,000 Years from the IMAGES II - NAUSICAA Cruise. TAO, 10 (1), 185-200.

de Ruijter, W.P.M., 1982. Asymptotic analysis of the Agulhas and Brazil Current systems. Journal of Physical Oceanography, 12, 361-373.

EPICA Community Members, 2006. One-to-one coupling of glacial climate variability in Greenland and Antarctica. Nature, 444, 195-198.

Ferrer Carrillo, M., 2007. Estudi del canvis climàtics a l'Oceà Índic Tropical i Subantàrtic amb biomarcadors. PhD Thesis, Universitat Politècnica de Catalunya, Barcelona, 198 pp.

Flores, J.A., Gersonde, R. and Sierro, F.J., 1999. Pleistocene fluctuations in the Agulhas Current Retroflection based on the calcareous plankton record. Marine Micropaleontology, 37 (1), 1-22.

Gordon, A.L., 1985. Indian-Atlantic Transfer of Thermocline Water at the Agulhas Retroflection. Science, 227, 1,030-1,033.

Gordon, A.L., 1986. Inter-Ocean exchange of thermocline water. Journal of Geophysical Research, 91 (C4), 5,037-5,046.

Gordon, A.L., 2003. The brawniest retroflection. Nature, 421, 904-905.

Gordon, A.L., Weiss, R.F., Smethie, J.W.M. and Warner, M.J., 1992. Thermocline and intermediate water communication between the South Atlantic and Indian Oceans. Journal of Geophysical Research, 97, 7,223-7,240.

Hall, I.R. and Zahn, R., 2004. RRS Charles Darwin Cruise 154. Agulhas 'Leakage' and Abrupt Climate Change, Cardiff.

Keeling, R.F. and Stephens, B.B., 2001. Antarctic sea ice and the control of plesitocene climate instability. Paleoceanography, 16 (1), 112-131.

Knorr, G. and Lohmann, G., 2003. Southern Ocean origin for the resumption of Atlantic thermohaline circulation during deglaciation. Nature, 424, 532-536.

Le Grande, A.N. and Schmidt, G., 2007. Orbital influences on paleosalinity indicators, American Geophysical Union Fall Meeting, San Francisco.

Lutjeharms, J.R.E., 1996. The exchange of water between the South Indian and the South Atlantic. In: W.H.B. G. Wefer, G. Siedler and D. Webb (Editors), The South Atlantic: Present and Past Circulation. Springer-Verlag, Berlin, pp. 125-162.

Pahnke, K., Zahn, R., Elderfield, H. and Schulz, M., 2003. 340,000-year Centennial-Scale Marine Record of Southern Hemisphere Climatic Oscillation. Science, 301, 948-952.

Peeters, F.J.C., Acheson, R., Brummer, G.-J.A., de Ruijter, W.P.M., Schneider, R., Ganssen, G., Ufkes, M.E. and Kroon, D., 2004. Vigorous exchange between the Indian and Atlantic oceans at the end of the past five glacial periods. Nature, 438, 661-665.

Pena, L., Calvo, E., Cacho, I., Eggins, S. and Pelejero, C., 2005. Identification and removal of Mn-Mg-rich contaminant phases on framiniferal tests: Implications for Mg/Ca past temperature reconstructions. Geochemistry, Geophysics, Geosystems, 6, Q09P02, doi: 10.1029/2005GC000930.

Petit, J.R. et al., 1999. Climate and atmospheric history of the past 420,000 years from the Vostok ice core, Antarctica. Nature, 399, 429-436.

Rahmstorf, S., 2002. Ocean circulation and climate during the past 120,000 years. Nature, 419, 207-214.

Rau, A.J., Rogers, J. and Chen, M.-T., 2006. Late Quaternary palaeoceanographic record in giant piston cores off South Africa, possibly including evidence of neotectonism. Quaternary International, 148 (1), 65-77.

Rau, A.J., Rogers, J., Lutjeharms, J.R.E., Giraudeau, J., Lee-Thorp, J.A., Chen, M.-T. and Waelbroeck, C., 2002. A 450-kyr record of hydrological conditions on the western Agulhas Bank Slope, south of Africa. Marine Geology, 180 (1-4), 183-201.

Rosenthal, Y., Lohman, G.P., Lohman, K.C. and Sherrell, R.M., 2000. Incorporation and preservation of Mg in *Globigerinoides sacculifer*: Implications for reconstructing the temperature and $^{18}O/^{16}O$ of seawater. Paleoceanography, 15 (1), 135-145.

Sarnthein, M., Winn, K., Jung, S.J.A., J.-C., D., Labeyrie, L., Erlenkeuser, H. and Ganssen, G., 1994. Changes in the east Atlantic deepwater circulation over the last 30,000 years: Eight time slice reconstructions. Paleoceanography, 9 (2), 209-267.

Schmidt, G.A., 1999. Forward modeling of carbinate proxy data from planktonic foraminifera using oxygen isotope tracers in a global ocean model. Paleoceanography, 14, 482-497.

Schmidt, G.A., Bigg, G.R.B. and Rohling, E.J., 1999. Global Seawater Oxygen-18 Database. http://data.giss.nasa.gov/o18data/.

Schmidt, M.W., Spero, H.J. and Lea, D.W., 2004. Links between salinity variation in the Caribbean and North Atlantic thermohaline circulation. Nature, 428, 160-163.

Schmidt, M.W., Vautravers, M.J. and Spero, H.J., 2006. Rapid subtropical North Atlantic salinity oscillations across Dansgaard-Oeschger cycles. Nature, 443, 561-564.

Schneider, R., Müller, P.J., Ruhland, G., Meinecke, G., Schmidt, H. and Wefer, G., 1996. Late Quaternary surface temperatures and productivity in the east-equatorial South Atlantic: Response to changes in trade/monsoon wind forcing and surface water advection. In: G. Wefer, W.H. Berger, G. Siedler and D. Webb (Editors), The South Atlantic: Present and Past Circulation. Springer, Berlin, Heidelberg, pp. 527-551.

Schneider, R.R., Müller, P.J. and Ruhland, G., 1995. Late Quaternary Surface Circulation in the East Equatorial South Atlantic: Evidence from Alkenone Sea Surface Temperatures. Paleoceanography, 10 (2), 197-219.

Schneider, R.R., Müller, P.J. and Acheson, R., 1999. Atlantic Alkenone Sea-Surface Temperature Records: Low versus Mid Latitudes and Differences between Hemispheres. In: F. Abrantes and A.C. Mix (Editors), Reconstructing Ocean History: A Window into the Future. Kluwer Academic/Plenum Publisher, New York, pp. 33-55.

Seidov, D. and Maslin, M., 2001. Atlantic ocean heat piracy and the bipolar climate see-saw during Heinrich and Dansgaard-Oeschger events. Journal of Quaternary Science, 16 (4), 321-328.

Sicre, M.A., Labeyrie, L., Ezat, U., Duprat, J., Turon, J.L., Schmidt, S., Michel, E. and Mazaud, A., 2005. Mid-latitude Southern Indian Ocean response to Northern Hemisphere Heinrich events. Earth and Planetary Science Letters, 240 (3-4), 724-731.

Siddall, M., Rohling, E.J., Almogi-Labin, A., Hemleben, C., Meischner, D., Schmelzer, I. and Smeed, D.A., 2003. Sea-level fluctuations during the last glacial cycle. Nature, 423, 853-859.

Steinke, S., Kienast, M., Groeneveld, J., Lin, L.-C., Chen, M.-T. and Rendle-Bühring, R., 2008. Proxy dependence of the temporal pattern of deglacial warming in the tropical South China Sea: toward resolving seasonality. Quaternary Science Reviews, 27 (7-8), 688-700.

Waelbroeck, C., Labeyrie, L., Michel, E., Duplessy, J.-C., McMAnus, J.F., Lambeck, K., Balbon, E. and Labracherie, M., 2002. Sea-level deep water temperature changes derived from benthic foraminifera isotopic records. Quaternary Science Reviews, 21, 295-305.

Weijer, W., De Ruijter, W.P.M. and Dijkstra, H.A., 2001. Stability of the Atlantic Overturning Circulation: Competition between Bering Strait Freshwater Flux and Agulhas Heat and Salt Sources. Journal of Physical Oceanography, 31 (8), 2,385-2,402.

Weijer, W., de Ruijter, W.P.M., Dijkstra, H.A. and van Leeuwen, P.J., 1999. Impact of Interbasin Exchange on the Atlantic Overturning Circulation. Journal of Physical Oceanography, 29, 2,266-2,284.

Weijer, W., de Ruijter, W.P.M., Sterl, A. and Driffhout, S.S., 2002. Response of the Atlantic overturning circulation to South Atlantic sources of buoyancy. Global and Planetary Change, 34, 293-311.

6. Conclusions

(*English*)

In this Thesis multi-proxy records covering the last 345,000 years from the Agulhas Bank Slope off southern Africa have been presented. The variety of records, which comprise benthic and planktonic foraminiferal stable isotopes, benthic Cd/Ca, planktonic Mg/Ca, the sortable silt index ($\overline{SS}$), and planktonic foraminiferal census counts for Marine Isotope Stage (MIS) 6 have allowed deciphering changes in the deep and surface circulation in a key region for the global oceanic circulation, and hence for Earth's climate.

Shifts in the mode of the deep circulation have been inferred from *F. wuellerstorfi* $\delta^{13}C$ and Cd/Ca, and from the $\overline{SS}$. Interglacial levels of *F. wuellerstorfi* $\delta^{13}C$ and Cd_{sw} (inferred from *F. wuellerstorfi* Cd/Ca) similar to modern values in the area indicate that in previous interglacials the circulation was very similar to present. Transitions from interglacial to glacial modes of ventilation are gradual in the benthic $\delta^{13}C$ and Cd/Ca records with ventilation during the early phase of glacials MIS 6 and 8 similar to interglacial conditions. Substantial reduction in ventilation is recorded in the middle of these glacial periods and this reduction is coeval with Cd_{sw} increases. Both indicating a weakening in the southward advection of Northern Component Waters (NCW) and, conversely, a prominent presence of Southern Component Waters (SCW) at mid-depths in the mid-latitude South Atlantic. Furthermore, the reduction in ventilation and enhancement in nutrient levels coincide with the fastest bottom flow speeds as inferred by increase values of the $\overline{SS}$.

The mid-latitude South Atlantic increasingly came under the influence of SCW during middle MIS 6 and 8 likely in conjunction with northward expansion of the fast flowing Circumpolar Antarctic Current (ACC). This circulation scheme was likely analogous to that known for the LGM.

Despite the reduction in chemical ventilation, benthic foraminiferal $\delta^{13}C$ remains more positive than at core sites in the deep Cape Basin while Cd_{sw} indicates higher nutrient concentrations during mid-glacials MIS 6 and 8. From this an influence of air-sea gas exchange on $\delta^{13}C$ is inferred pointing at a contribution of upper SCW similar to modern-day AAIW. Hence, it is likely that both an Upper and a Lower Southern Component Waters (USCW, LSCW) existed during full glacial periods.

USCW could have formed at the glacial SAF, outside the Antarctic sea-ice area, and thus have a positive $\delta^{13}C_{as}$ signature. LSCW likely formed in the Southern Ocean where sea-ice capping would have impeded air-sea transfer of CO_2 leading to very negative $\delta^{13}C_{as}$ signatures. LSCW could have left the Southern Ocean domain only at the bottom and mix with USCW when crossing the SAF.

These inferences about the existence of an USCW and a LSCW different in nature led to the revisiting of the existing concept about the existence of a sharp vertical divide in the glacial $\delta^{13}C$ distribution of the South Atlantic. This divide has being termed "chemocline", however, since it is observed in benthic $\delta^{13}C$ but not in benthic Cd/Ca, the pattern of a "nutricline" can be excluded. It

appears still possible that it describes a “carbocline” if indeed carbon isotopes are directly linked with carbon content. Besides, it seems plausible that the existence of a carbocline may be an artefact based on core selection. Only cores south of the glacial SAF display much depleted $\delta^{13}C$ values from 2500 m down the water column. If at all, a carbocline during the LGM developed horizontally rather than vertically. This observation reinforces older hypotheses that the Southern Ocean became isolated during extreme glacial times with implications for the trapping of atmospheric CO_2.

Regarding the surface circulation, combined planktonic $\delta^{18}O$, Mg/Ca and Agulhas Leakage Fauna abundance suggest, in agreement with previous studies, that the input of waters from the Agulhas Current to the South Atlantic has never stopped in the last 345 kyr. Intriguingly, however, the records here presented show that the presence of Agulhas Waters on the western side of the Agulhas Bank progressively increased in the course of glacial periods, reaching maximum levels well before glacial Terminations and collapsing when entering the subsequent interglacial period. This is particularly evident during MIS 6.

Combining the deep circulation patterns derived from benthic $\delta^{13}C$, Cd/Ca and $\overline{SS}$ with the surface records, i.e. planktonic $\delta^{18}O$, Mg/Ca and Agulhas Leakage Fauna abundance, inferences about the influence of the inflow of Agulhas Waters into the South Atlantic and changes in the state of the Meridional Overturning Circulation (MOC) have been drawn.

During early glacial phases benthic $\delta^{13}C$ and Cd/Ca ratios document a continuous influence of NCW at depth at the same time when the surface records indicate a presence of Agulhas Water similar to interglacials, suggesting a persistence of a modern-type linkage between Agulhas Leakage and MOC.

On the other hand, during full glacial MIS 2, middle MIS 6 and middle MIS 8, increased presence of Agulhas Water at the site coincide with a dominace of SCW at depth as indicated by strong benthic $\delta^{13}C$ depletions, high Cd_{sw} levels and increased $\overline{SS}$. This surface *versus* deep circulation pattern does not seem to support the existence of a direct connection between Agulhas Leakage and a vigorous and deep NCW formation. At this time other factors might have been at work that overwhelmed the positive feedback between Agulhas Water and the MOC; for instance, North Atlantic climate variability, stability of Northern Ice sheets, reduction of other sources of surface and thermocline waters for the compensation of NCW formation, or the actual efficiency of the transfer of tropical-subtropical Indian Waters.

A possible means of recording strong presence of Agulhas Waters at the site studied while the MOC was in a glacial state is by an altered shape of the coast line in response to a lowered sea level possibly in conjunction with northward displacement of the sub-Antarctic oceanic fronts. This configuration might have steered the Agulhas Retroflection westward allowing the formation of filaments, which are less efficient in causing a buoyancy anomaly in the South Atlantic, but reducing the leakage through rings. A sort of semi-permanent filament located close to the site could have caused the strong presence of Agulhas Waters recorded while the net transfer of salt to the Atlantic could have been small. An outcome of this scenario is that much of the Agulhas Current may have

been retroflected to the Indian Ocean and accumulated there, hence, contributing to preconditioning the MOC for a return to a strong mode of NADW convection later.

Prior to glacial Terminations, the Agulhas Water indicators show maximum presence of these waters with a collapse to background levels as full-interglacials MIS 5e, 7e and 9c are reached. It is possible that this collapse indicates the reestablishment of a modern-type mode of Agulhas Water Leakage through Rings and the release of warm, saline waters stored in the Indian Ocean. This observation would support previous suggestions based on paleoceanographic profiles and on numerical model simulations about the Agulhas Leakage being crucial for the reestablishment of an interglacial mode of circulation (Peeters et al., 2004, Knorr and Lohman, 2003).

In summary, the surface and deep records presented in this Thesis support the hypothesis of a link between the leakage of Agulhas Waters into the Atlantic and the strength of the Atlantic MOC during early and late glacial periods. The contrasting pattern in mid-glacials, on the other hand, either indicates that the records are recording a prominent presence of Agulhas Waters which is in turn not efficiently generating a buoyancy anomaly in the South Atlantic or that other factors are overcoming the salt anomaly imposed by the Agulhas Waters in the South Atlantic.

(*Castellano*)

En esta Tesis se han presentado registros de múltiples *proxies* del talud del Banco de Agulhas, mar adentro de Sudáfrica, cubriendo los últimos 345.000 años. La variedad de registros, que comprende isótopos estables de foraminíferos bentónicos y planctónicos, Cd/Ca bentónico, Mg/Ca planctónico, índice de granoselección de arcillas (*sortable silt,* $\overline{SS}$) y censos de foraminíferos del Estadio Isotópico Marino (*Marine Isotope Stage,* MIS) 6 han permitido discernir cambios en la circulación oceánica profunda y superficial en una región clave para la circulación oceánica global, y por tanto, para el clima terrestre.

A partir de *F. wuellerstorfi* $\delta^{13}C$ y Cd/Ca, y de $\overline{SS}$ se han inferido cambios en el modo de la circulación profunda. Niveles de *F. wuellerstorfi* $\delta^{13}C$ y Cd_{sw} (derivado del Cd/Ca bentónico) similares a los actuales en la región indican que la circulación en interglaciales previos era muy similar a la presente. Las transiciones de un modo de ventilación interglacial a uno glacial ocurren de forma gradual en los registros bentónicos de $\delta^{13}C$ y Cd_{sw} siendo la ventilación en las fases glaciales tempranas de los MIS 6 y 8 similar a la de las condiciones interglaciales. Reducciones significativas en la ventilación se registran en el medio de estos períodos glaciales y dicha reducción coincide con aumentos de Cd_{sw}. Ambos factores indican un debilitamiento en la advección hacia el sur de Aguas de Componente Norte (*Northern Component Water*, NCW) e, inversamente, una presencia preponderante de Aguas de Componente Sur (*Southern Component Water*, NCW) a profundidades medias en las latitudes medias del Atlántico Sur. Además, la reducción en la ventilación y el incremento en nutrientes coinciden con las mayores velocidades de corriente, deducidas a partir de elevados valores de $\overline{SS}$.

Las latitudes medias del Atlántico Sur cayeron bajo una influencia progresiva de SCW durante las fases intermedias de MIS 6 y 8, posiblemente en combinación con un desplazamiento hacia el norte de la rápida Corriente Circumpolar Antártica (*Circumpolar Antarctic Current*, ACC). Esta escena circulatoria era probablemente análoga a la existente en el Último Máximo Glacial (*Last Glacial Maximum*, LGM).

Pese a la reducción en la ventilación química, el $\delta^{13}C$ de foraminíferos bentónicos permaneció más positivo que el de testigos de sedimentos de las zonas profundas de la Cuenca del Cabo (*Cape Basin*) mientras que el Cd_{sw} indica mayores nutrientes durante los períodos glaciales medios MIS 6 y 8. De este patrón, se deduce una influencia del intercambio aire-mar en el $\delta^{13}C$ señalando hacia una contribución de SCW superior semejante a la AAIW moderna. En consecuencia, es posible que ambas, SCW Superior e Inferior (*Upper, Lower Southern Component Water,* USCW, LSCW) existieran durante estos períodos plenamente glaciales.

La USCW se podría haber formado en la región del Frente Sub-Antártico (*Sub-Antarctic Front,* SAF) glacial, fuera de la región cubierta por hielo marino, y por ello podría tener una señal de $\delta^{13}C_{as}$ positiva. La LSCW posiblemente se formó en el Océano Antártico (*Southern Ocean*) donde la cubierta de hielo marino habría impedido el intercambio aire-mar de CO_2 conduciendo a señales de

$\delta^{13}C_{as}$ muy negativas. La LSCW podría haber abandonado el dominio del Océano Antártico sólo por el fondo oceánico y mezclarse con la USCW al cruzar el SAF.

Estas deducciones acerca de la existencia de una USCW y una LSCW de naturaleza diferente ha conllevado a la reevaluación del concepto existente de que existe una brusca división vertical en la distribución glacial de $\delta^{13}C$ en el Atlántico sur. Esta división se ha denominado "quemoclina", sin embargo, ya que se observa en el $\delta^{13}C$ bentónico pero no en el Cd/Ca bentónico, el patrón de una "nutriclina" se puede excluir. Parece más apropiado describirla como una "carboclina", si de hecho los isótopos de carbono se pueden asociar directamente con el contenido en carbono. Además, parece posible que su existencia sea un artefacto de la selección de testigos de sedimento. Sólo los testigos al sur del SAF glacial muestran valores de $\delta^{13}C$ mucho menores desde 2500 m hasta el fondo. Si es que realmente se generó una carboclina, ésta sería más bien horizontal que vertical. Esta observación refuerza antiguas hipótesis sobre que el Océano Antártico se quedó aislado durante períodos glaciales extremos con implicaciones para la captura de CO_2.

En cuanto a la circulación superficial, la combinación de registros de $\delta^{18}O$, Mg/Ca planctónico y el índice de abundancia de Fauna de Agulhas (*Agulhas Leakage Fauna*, ALF) sugieren, en concordancia con estudios previos, que el influjo de aguas de la Corriente de Agulhas al Atlántico Sur no cesó en ningún momento durante los últimos 345 ka. Curiosamente, sin embargo, los registros aquí presentados muestran que la presencia de aguas de Agulhas en la parte oeste del Banco de Agulhas aumentó progresivamente con el transcurso de los períodos glaciales, alcanzando sus niveles máximos mucho antes de las Terminaciones glaciales y colapsando al entrar en el período glacial subsiguiente. Ello es particularmente evidente durante MIS 6.

Combinando los patrones de circulación profunda derivados de $\delta^{13}C$, Cd/Ca bentónicos y de $\overline{SS}$ con los registros superficiales, i.e. $\delta^{18}O$, Mg/Ca planctónicos y *Agulhas Leakage Fauna*, se han obtenido deducciones sobre la influencia del influjo de aguas de Agulhas al Atlántico sur y cambios en el estado de la Circulación Meridional Atlántica (*Meridional Overturning Circulation*, MOC).

Durante las fases glaciales tempranas el $\delta^{13}C$ y la ratio Cd/Ca de foraminíferos bentónicos documentan una contribución continua de NCW en profundidad a la vez que los registros superficiales indican una presencia de aguas de Agulhas similar a la interglacial, sugiriendo una persistencia del tipo de conexión moderna en el modo de transferencia de aguas de Agulhas y estado de la MOC.

Por otra parte, durante los períodos plenamente glaciales MIS 2, MIS 6 y MIS 8 medios, aumentos en la presencia de aguas de Agulhas coinciden con una preponderancia de SCW en profundidad indicado por fuertes reducciones en el $\delta^{13}C$ bentónico, altos niveles de Cd_{sw} y elevado $\overline{SS}$. Este patrón circulatorio superficial *versus* profundo no parece apoyar la existencia de una conexión directa entre la transferencia de aguas de Agulhas y el vigor y profundidad de convección de NCW. En estos momentos, deben haber actuado otros factores cuyo efecto contrarrestaría los mecanismos de retroalimentación positivos que generan las aguas de Agulhas en la MOC; por ejemplo, la variabilidad climática en el Atlántico norte, la estabilidad de los casquetes de hielo del norte, la reducción de otras

fuentes de aguas superficiales y de termoclina para la compensación de la formación de NCW, o la eficiencia real de la transferencia de aguas tropicales-subtropicales del Océano Índico.

Un mecanismo posible para registrar una fuerte presencia de aguas de Agulhas en la región de estudio a la vez que la MOC se encontraba en un estado glacial es a través de una alteración de la línea de costa como respuesta a la disminución del nivel del mar, probablemente en conjunción con una migración hacia el norte de los frentes sub-Antárticos. Esta configuración podría haber dirigido la Retroflección de Agulhas hacia el oeste permitiendo la formación de filamentos, que son menos eficientes a la hora de causar una anomalía de flotabilidad en el Atlántico Sur, pero reduciendo la transferencia a través de anillos. Una especie de filamento semi-permanente situado próximo a la región de estudio podría causar la fuerte presencia de aguas de Agulhas registradas, mientras que la transferencia neta de sal hacia el Atlántico sur podría haber sido pequeña. Una consecuencia derivada de este escenario es que la mayoría de la Corriente de Agulhas podría haber sido retroflectada hacia el Océano Índico acumulando sus aguas allí, y por ello, contribuyendo a precondicionar a la MOC para su retorno más tarde a un modo de convección de NADW.

Antes de las Terminaciones glaciales, los indicadores de aguas de Agulhas muestran la máxima presencia de dichas aguas con un colapso a niveles de base cuando se alcanzan los períodos cálidos MIS 5e, 7e y 9c. Es posible que este colapso indique el restablecimiento de un modo moderno de transferencia de aguas de Agulhas a través de anillos y la liberación de aguas cálidas y saladas acumuladas en el Océano Índico. Esta observación apoyaría sugerencias previas basadas en perfiles paleoceanográficos y en modelos numéricos sobre la decisiva influencia del *leakage* de Agulhas para el restablecimiento de un modo de circulación interglacial (Peeters et al., 2004, Knorr y Lohman, 2003).

En resumen, los registros superficiales y profundos presentados en esta Tesis apoyan la hipótesis de la existencia de una conexión entre el *leakage* de aguas de Agulhas hacia el Atlántico y la intensidad de la MOC durante las fases tempranas y tardías de los períodos glaciales. Por otro lado, el patrón diferente en períodos intermedios de las épocas glaciales, o bien indica que se está registrando una presencia prominente de aguas de Agulhas que de hecho no están generando una anomalía de flotabilidad en el Atlántico Sur de forma eficiente, o bien que otros factores están contrarrestando la anomalía de salinidad impuesta por las aguas de Agulhas al Atlántico Sur.

Annex

Available online at www.sciencedirect.com
ScienceDirect
Earth and Planetary Science Letters 267 (2008) 309–321
EPSL
www.elsevier.com/locate/epsl

345,000-year-long multi-proxy records off South Africa document variable contributions of Northern versus Southern Component Water to the Deep South Atlantic

Gema Martínez-Méndez [a,*], Rainer Zahn [a,b], Ian R. Hall [c], Leopoldo D. Pena [d], Isabel Cacho [d]

[a] Universitat Autònoma de Barcelona, Institut de Ciencia i Tecnologia Ambientals, ICTA, i Departament de Geologia, Edifici Cn Campus UAB, E-08193 Bellaterra, Spain
[b] Institució Catalana de Recerca i Estudis Avançats, ICREA, Spain
[c] School of Earth, Ocean and Planetary Sciences, Cardiff University, Main Building, Park Place, Cardiff CF10 3YE, United Kingdom
[d] GRC Geociències Marines, Departament d'Estratigrafia, P. i Geociències Marines, Universitat de Barcelona, C/ Martí i Franquès, s/n, E-08028 Barcelona, Spain

Received 5 July 2007; received in revised form 21 November 2007; accepted 24 November 2007
Available online 14 December 2007
Editor: M.L. Delaney

Abstract

Millennial to multi-centennial benthic foraminiferal stable isotope, sortable silt mean grain size ($\overline{SS}$) and benthic foraminiferal Cd/Ca records are presented for core MD96-2080 from 2488 m water depth at the western Agulhas Bank Slope off South Africa. The data demonstrate the interplay between Northern and Southern Component Waters as the Atlantic Meridional Overturning Circulation (MOC) shifted between glacial and interglacial modes. During early phases of Marine Isotope Stages (MIS) 6 and 8, the Atlantic MOC was little different from its interglacial mode. Benthic foraminiferal $\delta^{13}C$ modulation during these stages can be explained by mean-ocean $\delta^{13}C$ changes, while, only subtle benthic foraminiferal Cd/Ca increases indicate a continued influence of Northern Component Waters (NCW). Later glacial stages are characterized by a progressive incursion of nutrient-enriched waters presumably a mixture of Upper and Lower Southern Component Waters (SCW). Maximum $\overline{SS}$ values during late glacial ventilation minima suggest increased near-bottom flow speeds. The combined ventilation and flow-speed pattern indicates an enhanced influence of SCW, most likely linked with a northward migration of the Antarctic Circumpolar Current (ACC) which progressively decreased the influence of NCW at site MD96-2080. Peak-maximum seawater Cd concentrations (Cd_{sw}, derived from benthic foraminiferal Cd/Ca) overlap in time with increased deposition of ice-rafted debris (IRD) in the North Atlantic and plot outside the $\delta^{13}C/Cd_{sw}$ field in the South Atlantic. The anomalies conceivably are the South Atlantic equivalents of peak Cd_{sw} maxima associated with Heinrich-type events in the North Atlantic and reflect a substantially reduced Atlantic MOC.

Keywords: Meridional Overturning Circulation; paleocurrent speed; paleocirculation; stable isotopes; trace elements; sortable silt

1. Introduction

The inter-ocean water exchange around the southern tip of Africa constitutes a key component of the global ocean thermohaline circulation (Gordon, 1986; Gordon et al., 1992; Weijer et al., 1999). Interest in the surface-ocean paleoceanography in this region has increased in recent years (e.g. Knorr and Lohmann, 2003; Peeters et al., 2004) but the evolution of the deep-water circulation around South Africa has attracted less attention. Traditionally deep-water paleoceanographic records from the South Atlantic have been used to infer an interplay between North Atlantic Deep Water (NADW) and southern hemisphere water masses as a function of mode shifts in Atlantic Meridional Overturning Circulation (MOC) (e.g. Charles et al., 1996; Piotrowski et al., 2005). Many of these core sites are positioned within the lower deep water to bottom water

* Corresponding author.
E-mail addresses: gema.martinez@uab.cat (G. Martínez-Méndez), rainer.zahn@uab.cat (R. Zahn), hall@cardiff.ac.uk (I.R. Hall).

0012-821X/$ - see front matter © 2007 Elsevier B.V. All rights reserved.
doi:10.1016/j.epsl.2007.11.050

pathway containing a prominent contribution of Antarctic Bottom Water (AABW). We present a multi-proxy reconstruction that documents deep-water variability in the southern South Atlantic at a water depth that is more prominently influenced by NADW than the records published previously from greater water depth. Our new records provide further insight into the variability of the Atlantic MOC from a region underrepresented in the global paleoceanographic data base.

2. Core material and site location

Giant "Calypso" piston core MD96-2080 was retrieved during the IMAGES (International Marine Global Change Studies) Campaign II 'NAUSICAA' cruise in 1996 from the western slope of the Agulhas Bank (36°19.2′S; 19°28.2′E), off South Africa, at a water depth of 2488 m (Fig. 1A) (Bertrand, 1997). The core site is located within the corridor of Agulhas surface water leakage into the Atlantic and at depth it is influenced by the southern extension of NADW that spreads in the South Atlantic at water depths between 2000 and 3500 m and is bounded above and below by Upper and Lower Circumpolar Deep Water (UCDW, LCDW) (Fig. 1B) (van Aken et al., 2004). One branch of NADW exits the Atlantic through the Atlantic–Indian Ocean gateway directly contributing to the deep-water inflow entering the Indian Ocean (Arhan et al., 2003; van Aken et al., 2004). Another branch enters the Antarctic Circumpolar Current (ACC) (van Aken et al., 2004) and is incorporated into LCDW that flows eastward along the latitude of 45°S (below the Subtropical Frontal Zone (STFZ)) and enters the Indian and Pacific Oceans (van Aken et al., 2004).

3. Methods

Low resolution paleoceanographic records have been reported along the whole length of core MD96-2080 (22.23 m) (Rau et al., 2002, 2006). We have produced finer-scale records covering the upper 800 cm of the core that span the last three glacial–interglacial cycles, from Marine Isotope Stage (MIS) 1

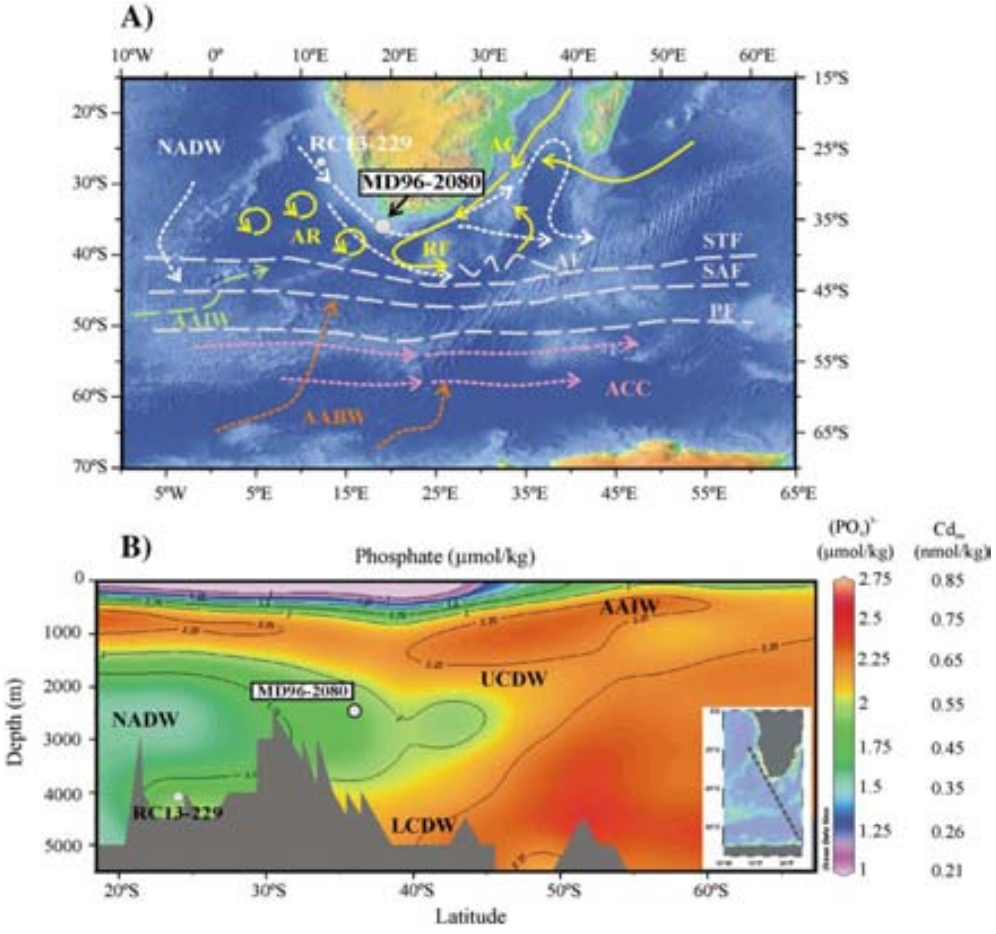

Fig. 1. Location of core MD96-2080 and regional hydrographic features. A) Agulhas "Corridor" off southern Africa. Labels are Agulhas Current (AC), Agulhas Retroflection (RF), Agulhas Rings (AR), Antarctic Circumpolar Current (ACC), North Atlantic Deep Water (NADW), Antarctic Bottom Water (AABW), Antarctic Intermediate Water (AAIW), Subtropical Front (STF), Subantarctic Front (SAF), Agulhas Front (AF), and Polar Front (PF). Base map from National Geophysical Data Center and National Oceanic and Atmospheric Administration, http://www.ngdc.noaa.gov/). B) Meridional phosphate transect from the Atlantic sector of the Southern Ocean to the southern tip of Africa (transect displayed in inset map). WOCE annual dataset using Ocean Data View (R. Schlitzer, ODV 2005; http://odv.awi-bremerhaven.de; WOCE, 2002). Isolines and labels are phosphate concentrations (µmol/kg). Right-hand scales are $(PO_4)^{3-}$ from WOCE dataset and estimated seawater Cd concentrations (Cd_{sw}, nmol/kg) as derived from Cd:$(PO_4)^{3-}$ stoichiometry (Boyle, 1988). Upper and Lower Circumpolar Deep Water are indicated (UCDW, LCDW). Core RC13-229 is used in this study as SCW reference.

to the MIS 9/10 transition, i.e. the past 345 kyr while we find evidence that MIS 3 and 4 are missing (see below). The time series offer multi-centennial resolution of benthic foraminiferal stable isotopes and Cd/Ca, along with a quantitative record of grain-size distribution. All data are available as electronic supplement to this paper.

All samples were freeze-dried to facilitate disaggregation and to minimize mechanical wear on microfossils during wet sieving. The samples were then washed over a 63-μm screen to separate the sediment coarse and fine fractions. The fine fraction (<63 μm) was oven-dried at 50 °C and weighed. For stable isotope analysis 3–7 specimens of epibenthic foraminifera *Fontbotia wuellerstorfi* (also commonly referred to as *Cibicidoides* or *Planulina*) were picked from the size fraction 250–315 μm, or >250 μm in sections of low abundance of *F. wuellerstorfi*. This species is considered to reliably record the $\delta^{13}C$ of total dissolved CO_2 ($\delta^{13}C_{\Sigma CO_2}$) in ambient bottom water (Duplessy et al., 1984; Zahn et al., 1986). Only under high productivity conditions with elevated flux of organic matter to the sea floor may the isotopic signal recorded by *F. wuellerstorfi* be offset from ambient bottom water $\delta^{13}C_{\Sigma CO_2}$ (Diz et al., 2007; Mackensen et al., 1993; Mackensen and Bickert, 1999). Stable isotope samples were cleaned prior to analysis, involving light mechanical crushing under methanol followed by ultrasonication for 10–20 s to remove sediment coatings and release possible sediment infill. Stable isotopes were measured with a ThermoFinnigan MAT 252 mass spectrometer linked online to a single acid bath CarboKiel-II carbonate preparation device. Measurements were performed at 1-cm steps throughout most of the records, while some sample intervals are 2 cm. External reproducibility was monitored through an internal laboratory standard (Solenhofen Limestone) and was 0.04‰ VPDB for $\delta^{13}C$ and 0.08‰ VPDB for $\delta^{18}O$ (1σ, $n=497$). Isotope values are calibrated to the Vienna Peedee Belemnite scale (VPDB) with the NBS-19 carbonate standard. Benthic foraminiferal $\delta^{18}O$ values have been shifted by +0.64‰ to accommodate offset of *F. wuellerstorfi* from oxygen isotope equilibrium (Shackleton, 1974).

For Cd/Ca analyses, between 10 and 25 individuals of *F. wuellerstorfi* from the sub-fraction >250 μm were cleaned following the protocol of Pena et al. (2005) which is adapted from Boyle and Rosenthal (1996). Prior to cleaning, the foraminifera were gently crushed between clean glass plates to break open individual chambers. Cleaning steps comprise removal of clays, Mn–Fe oxides and other mineral phases by a reductive cleaning step, oxidative cleaning to eliminate organic matter and weak acid leaching to remove remaining impurities from the shell surfaces. Trace element measurements were performed using a Perkin Elmer Elan 6000 Inductively Coupled Plasma Mass Spectrometer (ICP-MS). Calcium concentrations typically were in the ranges of 20–70 ppm which did not make a calcium matrix correction necessary. The error associated with the Cd/Ca measurements was ±2.4% (RSD) based on replicate analyses of an internal standard (1σ, $n=308$). Efficiency of the cleaning was assessed by monitoring Mn and Al concentrations. Mn/Ca ratios above 100–150 μmol/mol are assumed to represent potential contamination by Mn-carbonate overgrowths (e.g. Boyle, 1983; Boyle and Rosenthal, 1996). All trace element sample solutions yielded Mn/Ca ratios below 60 μmol/mol. Al/Ca was monitored to detect potential contamination by clays. The values in the majority of sample solutions were negligible, at the detection limit of the ICP-MS (4 ppb for Al). Only 7 out of 198 yielded Al/Ca ratios higher than 220 μmol/mol, one of these samples was anomalously more elevated in Cd/Ca than surrounding data points being discarded. Additionally, to ensure clean conditions during the sample preparation, procedure blanks were measured for each sample batch. Blanks yielded in all cases values at the detection limit. Average sampling interval for the Cd/Ca record is 4 cm.

To examine the variability in the deep ocean flow intensity we analyzed the grain-size distribution within the terrigenous sub-fraction 10–63 μm (i.e. with biogenic carbonate and opal removed), or "sortable silt" ($\overline{SS}$) fraction, as defined by McCave et al. (1995). $\overline{SS}$ has been shown to be a particularly sensitive index of near-bottom physical flow strength (McCave and Hall, 2006) in that $\overline{SS}$ fluctuations reflect relative changes in the intensity of the near-bottom current through selective deposition, with a higher value representing stronger physical current flow and vice versa. Prior to $\overline{SS}$ analysis carbonate was removed from the fine fraction by dissolution in 1 M acetic acid solution (48 h at room temperature); biogenic opal was removed by digestion in 2 M sodium carbonate solution (85 °C for 5 h). $\overline{SS}$ grain-size measurements were undertaken on the residual terrigenous sub-fraction using a Coulter Multisizer III as detailed in Bianchi et al. (1999). Samples analyzed for this study have a $\overline{SS}$ abundance of 8–10% enabling the determination of the $\overline{SS}$ with an error of ±2.0% (Bianchi et al., 1999).

The age model for core MD96-2080 was derived from a combination of radiocarbon dating (Accelerator Mass Spectrometry, AMS) and graphical correlation of the benthic foraminiferal $\delta^{18}O$ record with core MD97-2120 from Chatham Rise in the southwest Pacific (45°32′S, 174°57′E, Pahnke and Zahn, 2005; Pahnke et al., 2003). MD97-2120 spans the last three glacial–interglacial cycles at high resolution, has a robust age model based on radiocarbon dating and a tephrochronological marker event and it is further synchronized with isotope records from the North Atlantic and Antarctica (Pahnke and Zahn, 2005; Pahnke et al., 2003).

Radiocarbon analyses were performed on 14 mono-specific planktonic foraminiferal samples (*Globorotalia inflata*) containing at least 10 mg of carbon (Table 1 Supplementary information). All samples were calibrated to the calendar year scale following Fairbanks et al. (2005) which allows for calibration back to 50 ka. We applied a marine reservoir age $R(t)$ of 615±52 yr estimated from pre-bomb mollusk shells in the immediate neighborhood of our core site (34°50′S, 18°60′E, Cape of Good Hope; Southon et al., 2002). Only the upper six ^{14}C dates display a continuous increase in age with core depth (see Fig. S1 in Supplementary materials S1). Between 58.5 cm and 65.5 cm ages abruptly increase from 27.8 ^{14}C ka to 47.4 ^{14}C ka BP. Below this depth all ^{14}C ages cluster around an age of 45 ^{14}C ka. A similar age has been obtained for the two samples at 279.5 cm and 329.5 cm that were taken from MIS 6 to monitor background ^{14}C levels in the accelerator mass spectrometer (Fig. 2A). From the nearly constant age of the samples below

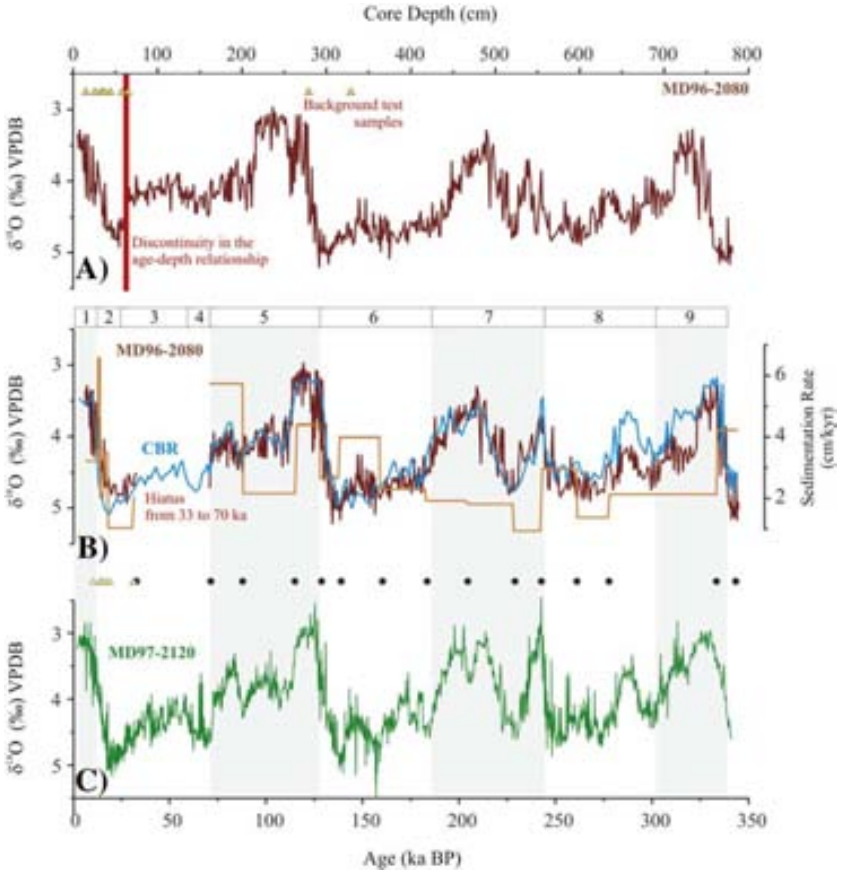

Fig. 2. Age model for MD96-2080. A) Benthic δ^{18}O profile on depth-in-core scale. Triangles indicate position of ^{14}C-AMS dates used for age modeling. Vertical bar at around 60 cm core depth indicates incursion of age–depth discontinuity (see Fig. S1 in Supplementary information S1). B) Benthic δ^{18}O (brown) and spliced Cape Basin Record(CBR, blue) from Peeters et al. (2004) retuned to the age model of MD96-2080. Orange line is sedimentation rate profile (cm/kyr) for MD96-2080. Top bar gives Marine Isotope Stages (MIS). C) MD97-2120 benthic δ^{18}O (Pahnke and Zahn, 2005). Triangles as in panel A. Black circles denote tie points used for graphical correlation of the MD96-2080 profile with that of MD97-2120 (see Supplementary information S1). Vertical shading highlights interglacials. (For interpretation of the references to colour in this figure legend, the reader is referred to the web version of this article.)

65.5 cm core depth that is close to the MIS 6 test samples we infer that all these samples are beyond the laboratory ^{14}C dating limit i.e., significantly older than ~40 ka. This suggests loss of sediment i.e., presence of a hiatus in core MD96-2080. Graphic correlation between the benthic foraminiferal δ^{18}O records of core MD96-2080 and of core MD97-2120 (Pahnke and Zahn, 2005) and the close structural fit with the spliced benthic foraminiferal δ^{18}O record from nearby cores GeoB3603-2 and MD96-2081 of Peeters et al. (2004) (Cape Basin Record, CBR) confirms that the hiatus in MD96-2080 spans the interval between 33 to 70 ka (Fig. 2B, C). The hiatus has not been previously identified and our stratigraphy thus differs from that published by Rau et al. (2002, 2006).

We have also modified the published MD96-2080 chronology of Rau et al. (2002, 2006) in the lower section of the core. A void interval (749–769 cm) described on board (Bertrand, 1997), possibly due to a break in the sediment column caused during coring, was recorded as a gap in the initial stratigraphy. The good match of data (stable isotopes and $\overline{\text{SS}}$) from above and below the gap suggests that the sedimentary sequence is continuous. Therefore we closed this gap in our depth and age scales.

The stratigraphy below 59.5 cm core depth was obtained by graphically correlating the benthic foraminiferal δ^{18}O record with that of core MD97-2120 (Pahnke and Zahn, 2005) using the Analyseries software (Paillard et al., 1996) (Fig. 2A–C; see also Table 2 of the Supplementary information S1).

According to our age model, the upper 800 cm of core MD96-2080 spans the past 345 kyr. Sedimentation rates vary between 1 and 7 cm/kyr with mean rates of 3 cm/kyr (Fig. 2B). Elevated sedimentation rates of 6 cm/kyr are estimated for the section around the lower boundary of the hiatus, at 70 ka. We do not consider this an artifact of positioning the hiatus but rather infer the sediments immediately underlying the hiatus are of MIS 5 age due to the close fit with benthic foraminiferal δ^{18}O values in the composite CBR record (Peeters et al., 2004) (Fig. 2B). Time steps along both the stable isotope and sortable silt records vary between 0.2 and 1.5 kyr while those along the benthic foraminiferal Cd/Ca record increase to >4 kyr in some sections.

4. Results

4.1. Benthic foraminiferal oxygen and carbon isotopes

The benthic foraminiferal δ^{18}O profile displays orbital modulation with additional suborbital variability (Fig. 3A). The Holocene is not well developed in the record, due to core

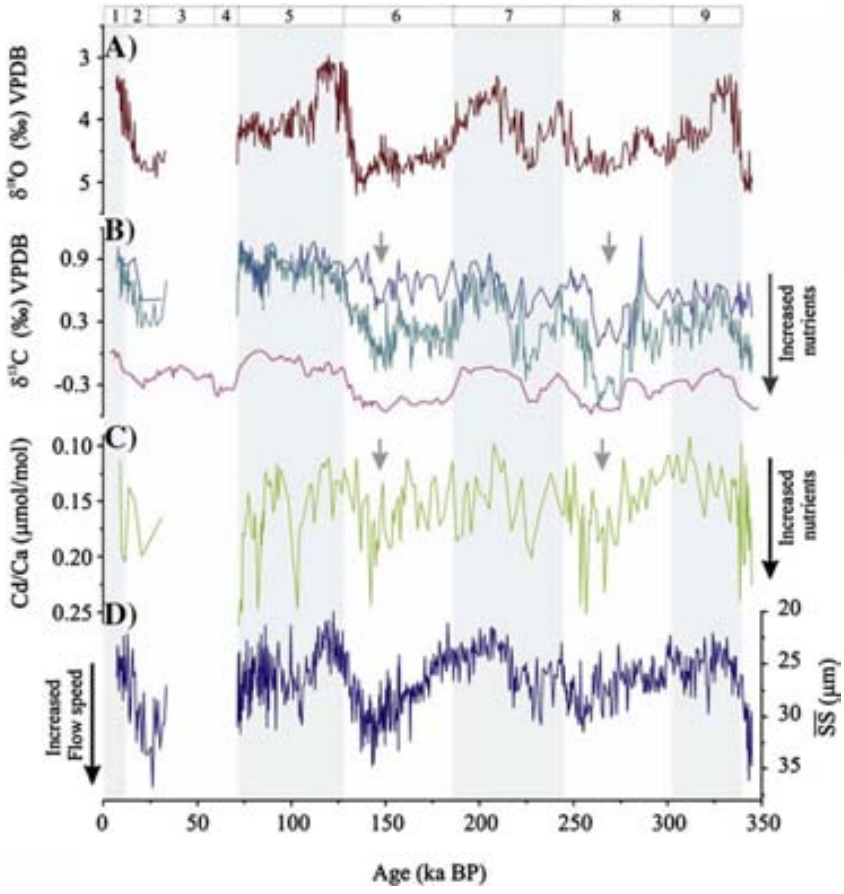

Fig. 3. Stable isotope and Cd/Ca records of *F. wuellerstorfi* and the record of sortable silt. A) Benthic $\delta^{18}O$ (‰ VPDB) on the *Uvigerina* scale. B) $\delta^{13}C$ record of *F. wuellerstorfi* (‰ VPDB; cyan). The overlain profile (blue line) is the benthic $\delta^{13}C$ after correction for changes in mean-ocean $\delta^{13}C$ that were derived from a stacked benthic $\delta^{13}C$ record (benthic $\delta^{13}C_{stack}$) that is shown as pink line below the benthic $\delta^{13}C$ profile. Details of the benthic $\delta^{13}C_{stack}$ record are provided in Supplementary materials S2. C) *F. wuellerstorfi* Cd/Ca (µmol/mol) (see Fig. S3 of Supplementary information S3 for the same record with individual data points indicated). D) Sortable silt mean grain size (µm). Top bar displays Marine Isotope Stages. Vertical shading highlights interglacials. Arrows mark culmination of glacial $\delta^{13}C$ depletion and coeval Cd/Ca increases. (For interpretation of the references to colour in this figure legend, the reader is referred to the web version of this article.)

disturbance, and thus, Termination I is not representative of the full-glacial/interglacial isotopic amplitude. Benthic foraminiferal $\delta^{18}O$ shifts for the previous glacial Terminations are 1.96‰ (TII), 1.08‰ (TIII) and 1.66‰ (TIV). These are well in excess of the mean-ocean change of 0.8–1.1‰ during these climatic transitions (Schrag et al., 2002; Waelbroeck et al., 2002). Excess isotopic change documents changes in deep-water temperature and $\delta^{18}O$ water at the core site.

Benthic foraminiferal $\delta^{13}C$ values along MD96-2080 are depleted during glacials (Fig. 3B) while amplitude modulation is reduced in interglacial intervals, a feature noted in the MD96-2080 benthic foraminiferal $\delta^{18}O$ and also seen in other southern records (Hall et al., 2001; Holbourn et al., 2005; McCave et al., 2005; Pahnke and Zahn, 2005). Since core-top sediments in MD96-2080 are not representative of modern water column $\delta^{13}C_{\Sigma CO_2}$ we compare core-top sediments of nearby core MD02-2594 (34°43′S, 17°20′E, 2440 m water depth) which are assumed to be modern in age to ambient bottom water $\delta^{13}C_{\Sigma CO_2}$ from GEOSECS Stations 93 (41°46′S, 18°27′E) and 103 (24°00′S, 8°30′E). MD02-2594 benthic foraminiferal $\delta^{13}C$ of +0.7‰ VPDB is similar to $\delta^{13}C_{\Sigma CO_2}$ of +0.6‰ VPDB measured at both GEOSECS stations at this water depth (Ostlund et al., 1987). This suggests that glacial benthic foraminiferal $\delta^{13}C$ was depleted by 0.3 to 0.4‰ VPDB at the Last Glacial Maximum (LGM) which is close to the coeval mean-ocean $\delta^{13}C$ shift (Duplessy et al., 1988). Benthic foraminiferal $\delta^{13}C$ shifts across TII and TIII were 0.2 to 0.4‰ VPDB, similar to the glacial–interglacial $\delta^{13}C$ amplitude displayed in a stacked benthic foraminiferal $\delta^{13}C$ record derived from sediment cores from the Atlantic, Indian and Pacific Oceans (Fig. 3B) (see Supplementary information S2 for explanatory notes on $\delta^{13}C_{stack}$ record development). Only late in glacials MIS 6 and 8 are depletions larger than coeval shifts in the $\delta^{13}C_{stack}$ record. Peak-negative $\delta^{13}C$ values reach levels 0.8‰ and 0.7‰ VPDB below benthic foraminiferal $\delta^{13}C$ of the subsequent interglacial periods and exceed the coeval $\delta^{13}C_{stack}$ amplitude by 0.5‰ and 0.3‰ VPDB (Fig. 3B). Prominent benthic foraminiferal $\delta^{13}C$ depletion is also recorded during MIS 7d, with values 0.4‰ VPDB lighter than coeval shifts in the $\delta^{13}C_{stack}$.

Benthic foraminiferal $\delta^{13}C$ displays a trend of values rising by some 0.4‰ VPDB during the past 345 kyr. A similar trend exists in other records (e.g. ODP 1123, Hall et al., 2001; MD01-2378, Holbourn et al., 2005) and is documented in the $\delta^{13}C_{stack}$

record (Fig. 3B; see Supplementary information S2). This trend likely reflects the long-term evolution of the marine carbon pool (e.g. Mix et al., 1995; Hoogakker et al., 2006; Rickaby et al., 2007) probably related to the 400 kyr eccentricity cycle.

4.2. Benthic foraminiferal Cd/Ca

Benthic foraminiferal Cd/Ca displays glacial trends towards maximum values that are reached in later stages of glacial periods, MIS 6 and 8 (Fig. 3C). During MIS 6 this trend contains recurrent excursions to minimum Cd/Ca ratios that approach interglacial levels. Applying a cadmium distribution coefficient (D_{Cd}) of 2.46 (Boyle, 1992), the down-core benthic foraminiferal Cd/Ca variation in MD96-2080 translates into equivalent seawater Cd concentrations (Cd_{sw}) of 0.37–0.81 nmol/kg (Fig. 4C) (excluding the short-lived maximum Cd/Ca excursions along the record). This range of values remains above Cd_{sw} in modern unaltered NADW (Boyle, 1992) and only marginally overlaps with glacial–interglacial Cd_{sw} ranges inferred at deep-water core sites in the North Atlantic (Cd_{sw}=0.17–0.45 nmol/kg, Boyle and Keigwin, 1985/86; Keigwin and Boyle, 1985). Interglacial Cd_{sw} values (0.37–0.67 nmol/kg) at MD96-2080 encompass Cd_{sw} levels inferred at South Atlantic sites at >3000 m water depth (e.g. Cd_{sw}=0.34–0.69 nmol/kg, Boyle, 1992; Oppo and Rosenthal, 1994; Lea, 1995; Rosenthal et al., 1997) while they are elevated over Holocene values at west South Atlantic sites located around 2000–2500 m water depth (e.g. Cd_{sw}=0.24–0.21 nmol/kg, Oppo and Horowitz, 2000). Elevated interglacial Cd_{sw} values suggest the presence at the MD96-2080 site of "aged" NADW possibly with contributions of Southern Component Water (SCW). Maximum Cd_{sw} values in excess of 1.0 nmol/kg are reached during brief excursions within MIS 5 and the later parts of MIS 6 and 8. These maxima are single-point excursions (see Fig. S3 in the Supplementary information) but we exclude possible contamination on the basis of Mn/Ca below 60 μmol/mol and Al/Ca values below 220 μmol/mol for all these samples. Similar elevated Cd/Ca values are known from other core sites in the northern and tropical Atlantic (see discussion below).

4.3. Sortable silt mean grain size

The $\overline{SS}$ paleocurrent record displays increased values in glacial sections (Fig. 3D). This reflects high near-bottom flow

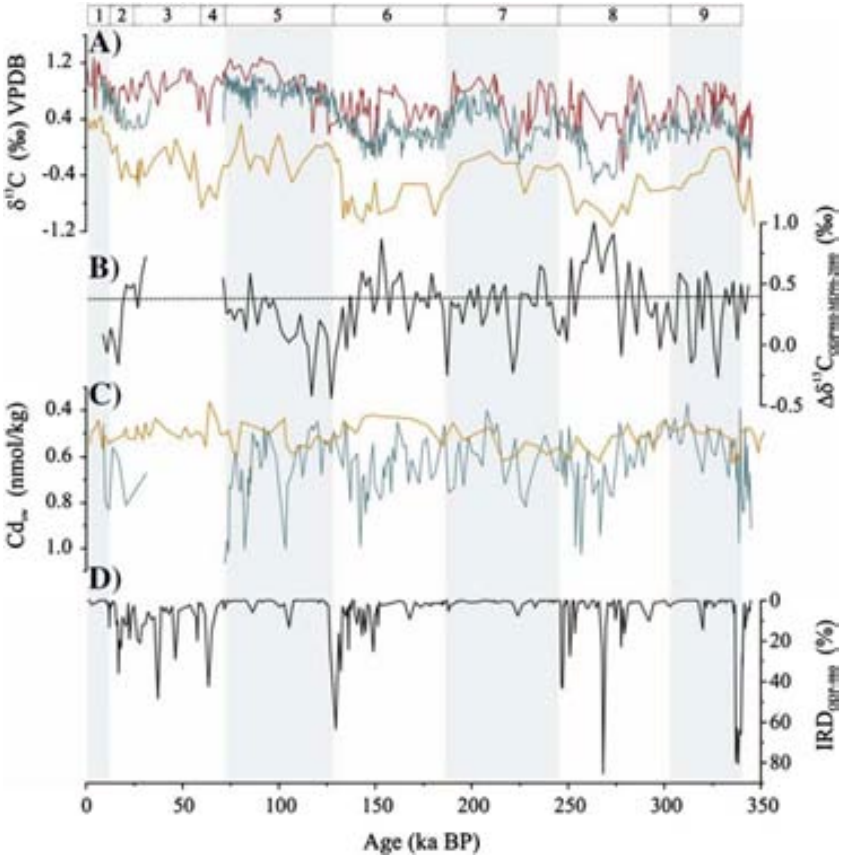

Fig. 4. Benthic carbon isotope records of MD96-2080 and reference cores in the North and South Atlantic, meridional carbon isotope gradient and seawater Cd compared with a North Atlantic IRD profile. A) Benthic $\delta^{13}C$ records (‰ VPDB) of MD96-2080 (cyan), North Atlantic ODP Site 980 (red, McManus et al., 1999) and Cape Basin core RC13-229 (orange, Oppo et al., 1990; Oppo and Rosenthal, 1994). Age models are synchronized with MD96-2080 (see Fig. S3 in the Supplementary information S3). B) $\delta^{13}C$ offset between MD96-2080 and Site 980. Horizontal dotted line denotes present $\delta^{13}C_{\Sigma CO_2}$ gradient between the core sites as computed from GEOSECS Stations 93 (41°46′S, 18°27′E, 2597 m, 0.6‰ VPDB) and 23 (60°25′N, 18°37′W, 2241 m, 1.04‰ VPDB). C) Cd_{sw} records of MD96-2080 (cyan) and RC13-229 (orange) (see Fig. S3 of Supplementary information S3 for the same records with individual data points indicated). Description of Cd_{sw} computation is provided in text. D) Ice-rafted debris (% IRD) record from ODP Site 980 (McManus et al., 1999). (For interpretation of the references to colour in this figure legend, the reader is referred to the web version of this article.)

speeds that fits with similar $\overline{SS}$ patterns reported from the Southwest Pacific (ODP Site 1123, 3290 m water depth; Hall et al., 2001) and the Agulhas Plateau (MD02-2589, 2660 m water depth; Molyneux et al., 2007) suggesting the pattern is representative of the circum-Antarctic region. In the lower section of the MD96-2080 record, before 250 ka, orbitally modulated amplitudes of $\overline{SS}$ change are reduced. The $\overline{SS}$ grain size range of 17 to 37 μm in core MD96-2080 is considerably larger than the range documented in the southwest Pacific (13–19 μm) by Hall et al. (2001) and at the southern Agulhas Plateau (19–24 μm) by Molyneux et al. (2007). McCave and Hall (2006) alluded to the particularly subtle way in which size distributions might be altered by sediment source-related signatures, through the fine tails of turbidity currents (see also Hall and McCave, 2000). While, in core MD96-2080, there is no visual evidence of major (i.e. turbidity current) down-slope deposition (Bertrand, 1997), an influence of down-slope deposition of fine material on the $\overline{SS}$ cannot entirely be disregarded. Rau et al. (2002) noted small but significant glacial increase in the lithogenic sand size fraction, suggesting either a likely source from the Antarctic ice sheet via iceberg transport, or from down-slope transfer of upper slope and shelf material. Either way an associated delivery of a substantial amount of unsorted terrigenous silt could cryptically affect the $\overline{SS}$ proxy record. In several sections of core MD96-2080 we observe a correspondence between inferred high flow-speed, elevated coarse fraction (>63 μm, not shown but consisting of foraminiferal sand) abundance and low sedimentation rates which is consistent with our interpretation of a dominant current sorted influence. Therefore we remain confident that the MD96-2080 $\overline{SS}$ signal predominantly provides an indication of climate induced changes of near-bottom current strength. The $\overline{SS}$ record suggests glacially increased near-bottom flow is a persistent feature at high southern latitude locations, opposite to North Atlantic flow-speed patterns (e.g. Hall and McCave, 2000).

5. Discussion

5.1. Northern versus Southern Component Waters

Palaeocirculation studies draw a consistent picture that deep-water convection in the last glacial North Atlantic was reduced to shallower depths (e.g. Boyle and Keigwin, 1985/86; Curry et al., 1988; Duplessy et al., 1988; Sarnthein et al., 1994) and lower rates (Rutberg et al., 2000; McManus et al., 2004; Piotrowski et al., 2005; Hall et al., 2006). Radiogenic isotopes (Yu et al., 1996) suggest southward advection of deep waters from the North Atlantic to the Southern Ocean at a rate similar to today while this contention has been challenged by numerical modeling (Marchal et al., 2000).

In the MD96-2080 benthic foraminiferal $\delta^{13}C$ record much of the depletion in early MIS 6 and 8 can be explained by mean-ocean changes suggesting little change in chemical ventilation (Fig. 3B). Cd_{sw} at the same time indicates a progressive increase in nutrient concentrations (Fig. 3C). During MIS 6 (and lesser MIS 8) the trend of increasing Cd_{sw} is superimposed by sub-orbital variability with values sporadically dropping to full-interglacial levels suggesting episodic incursions of a more nutrient-depleted water mass, presumably NCW. Only in the later sections of MIS 6 and 8 does benthic foraminiferal $\delta^{13}C$ drop to peak minimum values that coincide with maximum Cd_{sw} levels. This suggests that the progression towards full-glacial water mass ventilation at site MD96-2080 was gradual, with additional suborbital oscillation visible in MIS 6.

To assess benthic foraminiferal $\delta^{13}C$ and Cd_{sw} data patterns in MD96-2080 in the framework of the Atlantic MOC we compare our records with similar records from other Atlantic core sites (Table 1). ODP Site 980 (McManus et al., 1999) is positioned within newly formed deep water in the North Atlantic and serves as a reference for NCW formation and ventilation. First we enhanced graphical correlation between the benthic foraminiferal $\delta^{18}O$ record of ODP Site 980 and MD96-2080 for better synchrony between them (see Fig. S3 in the Supplementary information) and then sampled both benthic foraminiferal $\delta^{13}C$ records at 2 kyr time steps to determine the north–south gradient (Fig. 4A, B). The gradient maximizes in the later parts of MIS 6 and notably, in MIS 8 as $\delta^{13}C$ at ODP Site 980 remains positive while values at MD96-2080 drop to lower levels. Comparison of the north–south $\delta^{13}C$ gradient with Cd_{sw} at MD96-2080 (Fig. 4B, C) shows maximum gradients coincide with elevated Cd_{sw} that are indicative of enhanced nutrient concentrations in the south. Modulation of the $\delta^{13}C$ gradient from the south in conjunction with incursions of Cd_{sw} maxima at MD96-2080 either indicates reduced formation and southward advection of NCW, stronger northward advection of SCW, or some combination of both.

Table 1
Core locations

Sediment core	Water depth (m)	Core location	Reference
MD97-2120	1210	45°S, 175°E; Chatham Rise	Pahnke et al. (2003); Pahnke and Zahn (2005)
ODP 980	2170	55°N, 14°W; North Atlantic	McManus et al. (1999)
SO75-26KL	1099	38°N, 9.5°W; Iberian Margin	Willamowski and Zahn (2000)
M35003	1299	12.5°N, 61°W; Tobago Basin	Zahn and Stüber (2002)
KNR159-5-36	1268	27.5°S, 46.5°W; Brazil Margin	Came et al. (2003); Oppo and Horowitz (2000)
RC16-119	1567	28°S, 46.5°W; Brazilian Margin	Oppo and Horowitz (2000)
V24-253	2069	27°S, 45°W; Brazilian Margin	Oppo and Horowitz (2000)
MD96-2080	2488	36°S, 19°E; Agulhas Bank Slope	This study
RC13-228	3204	22°S, 11°E; Cape Basin	Boyle (1992); Rosenthal et al. (1997)
RC12-294	3308	37°S, 10°W; Central South Atlantic	Boyle (1992); Rosenthal et al. (1997)
CH82-24	3427	43°N, 33°W; Central North Atlantic	Boyle and Keigwin (1985/86)
RC13-229	4191	25.5°S, 11°E; Cape Basin	Oppo et al. (1990); Oppo and Rosenthal (1994)

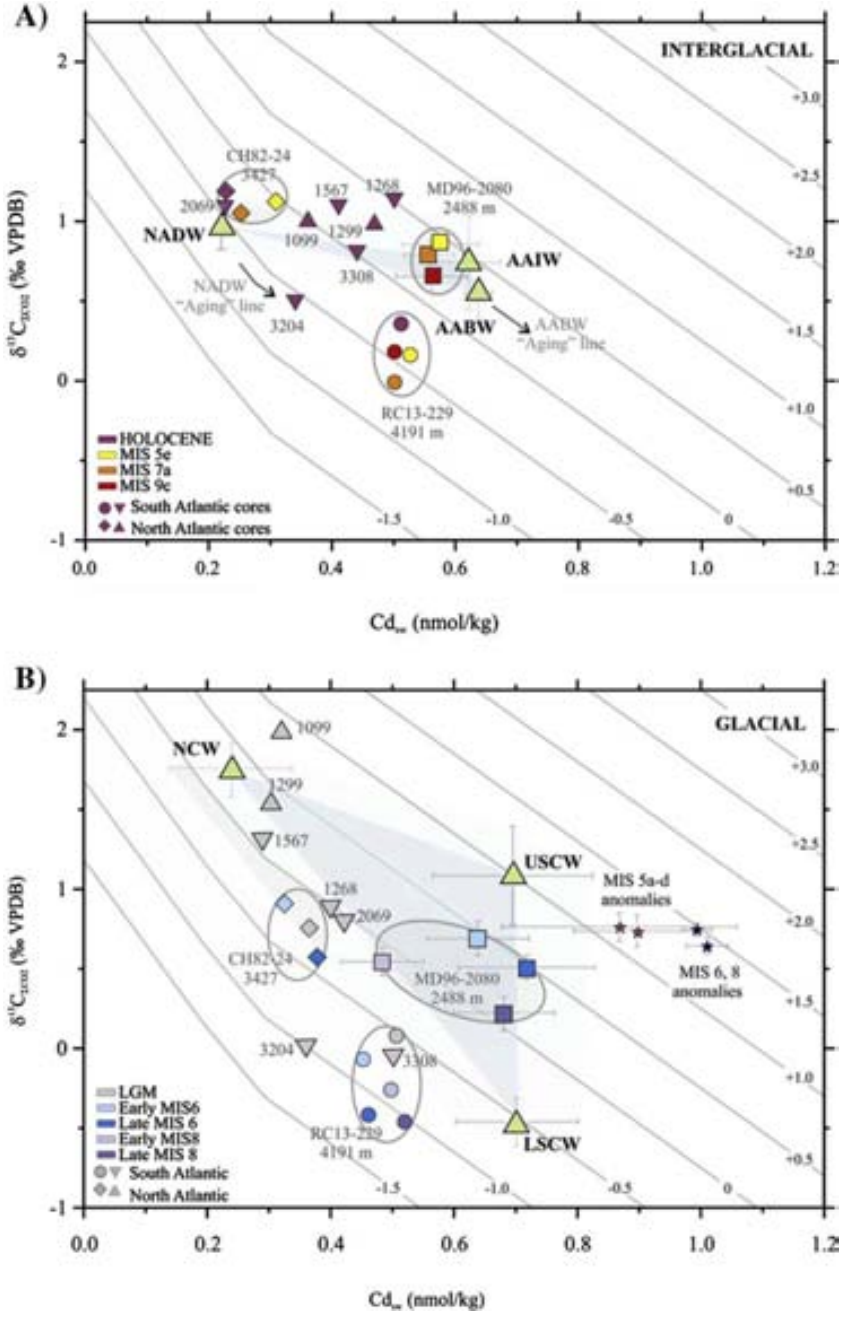

Fig. 5. Proxy–proxy diagrams displaying Cd_{sw} and $\delta^{13}C$ data from core MD96-2080 and reference cores. $\delta^{13}C_{as}$ isolines are computed using modern parameterization (Lynch-Stieglitz and Fairbanks, 1994; Lynch-Stieglitz et al., 1996) (see Supplementary information S4 for details). Glacial and interglacial sediment core $\delta^{13}C$ data are carbon-pool corrected to account for shifts in the marine carbon reservoir isotope signature. All data hence are normalized to Holocene level. Mixing fields between endmembers are highlighted with blue shading; faint shading indicates mixing field applying standard deviations (1σ) of endmember means (see Table 2). A) Interglacial Cd_{sw} versus $\delta^{13}C$ means from Atlantic sediment cores CH82-24 (diamonds, Boyle and Keigwin, 1985/86), SO75-26KL, M35003 (inverted triangles, Willamoski and Zahn, 2000; Zahn and Stüber, 2002), KNR159-5-36, RC16-119, V24-253, RC12-294, RC13-228 (triangles, Came et al., 2003; Oppo and Horowitz, 2000; Boyle, 1992; Rosenthal et al., 1997), RC13-229 (circles, Oppo et al., 1990; Oppo and Rosenthal, 1994) and MD96-2080 (squares). Water mass endmembers (green triangles) are North Atlantic Deep Water (NADW), Antarctic Intermediate Water (AAIW), and Antarctic Bottom Water (AABW) (see also Table 2). B) Same as in A but for glacials. Endmembers (green triangles) are Northern Component Water (NCW), Upper and Lower Southern Component Waters (USCW, LSCW) (see also Table 2). The cluster of elevated Cd_{sw} values >0.8 nmol/kg represents peak-maximum Cd_{sw} anomalies observed in MD96-2080 during MIS 5a–d (brown) and late MIS 6 and 8 (navy). Error bars for MD96-2080 data (1σ) combine analytical reproducibility and standard deviation of means. Uncertainty (standard deviation) associated with the Cd partition coefficient (D_{Cd}) between benthic Cd/Ca and Cd/Ca in seawater of 2.9±0.6 (Boyle, 1988) is not included. (For interpretation of the references to colour in this figure legend, the reader is referred to the web version of this article.)

Next we compare the MD96-2080 records with benthic $\delta^{13}C$ and Cd_{sw} records of core RC13-229 from the deep Cape Basin at 25°S (Figs. 1B and 4A, C) (Lea, 1995; Oppo and Fairbanks, 1987; Oppo et al., 1990; Oppo and Rosenthal, 1994). The Cd_{sw} record of RC13-229 was inferred from Cd/Ca applying a partition coefficient of 2.9 (Boyle, 1992). At 4191 m water depth

the RC13-229 core likely remained under a variable but persistent influence of SCW. Benthic $\delta^{13}C$ values along RC13-229 are consistently 0.7–1.0‰ VPDB more negative than in MD96-2080 reflecting better ventilation of the upper water column. Cd_{sw} on the other hand are nearly identical in both cores during interglacial periods mimicking modern $(PO_4)^{3-}$ patterns (Fig. 1B). Similar Cd_{sw} levels during early MIS 6 and 8 support our contention that deep ventilation was not substantially different at the initiation of glacial stages. Cd_{sw} values are increased at MD96-2080 over those at the deep core RC13-229 during late glacial times (Fig. 4A, C) suggesting elevated nutrient content in the upper water column. Cd_{sw} in RC13-229 shows little glacial–interglacial variation which contrasts with high-amplitude benthic $\delta^{13}C$ shifts in the core. Taken at face value, this suggests nutrient-enriched water masses with positive $\delta^{13}C$ that prevailed at MD96-2080 that did not reach the northerly and deeper site RC13-229.

An alternative explanation would be that benthic foraminiferal Cd/Ca at RC13-229 is underestimating glacial Cd_{sw} as a consequence of the invasion of bottom waters with lower carbonate ion concentration, either through dissolution of Cd bearing calcite (McCorkle et al., 1995) or through decreases of the D_{Cd} for cadmium uptake by the benthic foraminifera (e.g. Marchitto et al., 2000). While such influences cannot be ruled out, the Cd_{sw} and benthic foraminiferal $\delta^{13}C$ pattern suggests that MD96-2080 during late glacials was prominently influenced by nutrient-laden SCW maintaining a positive $\delta^{13}C$ signature, presumably through air–sea gas exchange (Zahn and Keir, 1992; Charles et al., 1993). Increased glacial flow speeds as indicated by the $\overline{SS}$ record (Fig. 3D) are likewise consistent with a stronger influence of SCW as has been inferred from other $\overline{SS}$ records from high southern latitudes (Hall et al., 2001; Molyneux et al., 2007). If the RC13-229 data adequately reflect bottom water biogeochemistry low nutrient concentrations at this site during glacials suggest enhanced nutrient transfer to the upper cell of the Southern Ocean overturning from depths, steepening nutrient gradients between RC13-229 and MD96-2080. Topographically steered upwelling of ACC flow provides a mechanism for such deep-to-shallow nutrient transfer (Garabato et al., 2007).

A series of recurrent peak Cd_{sw} maxima is observed along MD96-2080 reaching levels of ~1 nmol/kg, about threefold higher than Holocene levels and 1.5–2 times higher than LGM values in the area (Boyle, 1992; Rosenthal et al., 1997; Oppo and Horowitz, 2000). Cd_{sw} anomalies of similar magnitude have been reported for the last glacial from equatorial and North Atlantic cores (Willamowski and Zahn, 2000; Zahn and Stüber, 2002; Rickaby and Elderfield, 2005) and coincide with Heinrich events when NCW formation experienced slowdown. Comparison with the IRD record from ODP Site 980 (McManus et al., 1999) on a synchronized time scale shows the Cd_{sw} excursions in MD96-2080 overlap with periods of elevated IRD abundance in the North Atlantic (Fig. 4C, D). This correlation holds for Cd_{sw} maxima during MIS 5a–d that coincide with modest IRD maxima at ODP 980 (McManus et al., 1999) and in SU90-03 in the North Atlantic (Chapman et al., 2000). We consider the overlap between IRD events in the North and Cd_{sw} peak maxima at MD96-2080 indicates a slowed Atlantic MOC that enabled SCW to exert influence on South Atlantic mid-depth nutrient inventories.

5.2. $\delta^{13}C$–Cd_{sw} fingerprinting

Air–sea gas exchange in the Southern Ocean in conjunction with its thermodynamic imprint on carbon isotope fractionation decouples $\delta^{13}C$ regionally from global nutrient stoichiometry (Broecker and Maier-Reimer, 1992; Zahn and Keir, 1992). Benthic foraminiferal Cd/Ca is linked with biological nutrient cycling but is not influenced by air–sea exchanges and constitutes a more conservative nutrient proxy (Boyle, 1988). Paired benthic foraminiferal Cd/Ca and $\delta^{13}C$ therefore enables to derive the offset between measured benthic foraminiferal $\delta^{13}C$ and a $\delta^{13}C$ signal predicted from biological nutrient cycling ($\delta^{13}C_{bio}$) that can be estimated from Cd/Ca (or Cd_{sw}) using nutrient stoichiometry (Lynch-Stieglitz and Fairbanks, 1994; Lynch-Stieglitz et al., 1996; Marchitto and Broecker, 2006) (computational scheme is given in Supplementary materials S4).

We use proxy–proxy diagrams to plot sediment core $\delta^{13}C$/Cd_{sw} coordinates together with $\delta^{13}C_{as}$ fractionation isolines and water mass endmember $\delta^{13}C/Cd_{sw}$ from published data bases (Fig. 5; Tables 1, 3a, and 3b). Cd_{sw} has been derived from

Table 2
$\delta^{13}C_{\Sigma CO_2}$ and Cd_{sw} values of modern and glacial Atlantic water mass endmembers

Water mass	$\delta^{13}C_{\Sigma CO_2}\pm 1\sigma$, n (‰ PDB)	$Cd_{sw}\pm 1\sigma$, n (nmol/kg)	Data source	Reference
Modern		Derived from $(PO_4)^{3-}$	Atlantic GEOSECS Stations	
NADW	0.98±0.09, 36	0.22±0.01, 112	60–50°N; 19°E–43°W; 1.5–3 km	1
AAIW	0.73±0.29, 10	0.62±0.05, 33	33–55°S; 21–55°W; 0.75–1.1 km	1
AABW	0.55±0.16, 14	0.64±0.02, 82	45–60°S; 11°E–66°W; 6.5–4 km	1
Glacial[a]		Derived from benthic Cd/Ca	LGM benthic data	
NCW	1.75±0.2, 11	0.24±0.1, 12	20°–65°N; 1000–2000 m water depth	2–7
USCW	1.08±0.31, 4	0.69±0.13, 4	Off Tasmania, 800–1500 m water depth	8
LSCW	−0.48±0.15, 8	0.70±0.1	Southern Ocean, >3000 m water depth, and data extrapolation[b]	9,10

References used are (1) Ostlund et al. (1987); (2) Boyle (1992); (3) Bertram et al. (1995); (4) Willamowski and Zahn (2000); (5) Marchitto et al. (1998); (6) Rickaby et al. (2000); (7) Marchitto and Broecker (2006); (8) Lynch-Stieglitz et al. (1996); (9) Ninnemann and Charles (2002); (10) Marchitto and Broecker (2006).

[a] Glacial $\delta^{13}C_{\Sigma CO_2}$ data are corrected for carbon-pool changes by adding 0.32‰. No reservoir correction is applied to glacial Cd_{sw} (Boyle, 1988).

[b] $\delta^{13}C$ derived from benthic data; Cd_{sw} extrapolated using Atlantic $\delta^{13}C/Cd_{sw}$ relation from Fig. 6 in Marchitto and Broecker (2006).

Table 3a
Interglacial $\delta^{13}C_{\Sigma CO_2}$ and Cd_{sw} values from Atlantic sediment cores [a, b]

Sediment core	Holocene $\delta^{13}C \pm 1\sigma$, n (‰ VPDB)	Holocene $Cd_{sw} \pm 1\sigma$, n (nmol/kg)	MIS 5e $\delta^{13}C \pm 1\sigma$, n (‰ VPDB)	MIS 5e $Cd_{sw} \pm 1\sigma$, n (nmol/kg)	MIS 7a $\delta^{13}C \pm 1\sigma$, n (‰ VPDB)	MIS 7a $Cd_{sw} \pm 1\sigma$, n (nmol/kg)	MIS 9c $\delta^{13}C \pm 1\sigma$, n (‰ VPDB)	MIS 9c $Cd_{sw} \pm 1\sigma$, n (nmol/kg)
SO75-26KL	0.997±0.1; 8	0.15 ±0.05; 8	–	–	–	–	–	–
M35003	0.98±0.25; 3	0.47±0.1; 3	–	–	–	–	–	–
KNR159-5-36 [c]	1.14	0.5	–	–	–	–	–	–
RC16-119 [c]	1.1	0.41	–	–	–	–	–	–
V24-253 [c]	1.1	0.24	–	–	–	–	–	–
MD96-2080	–	–	0.86±0.015; 5	0.58±0.06; 5	0.79±0.1; 5	0.56±0.04; 4	0.66±0.1; 6	0.56±0.06; 6
RC13-228 [c]	0.5	0.34	–	–	–	–	–	–
RC12-294 [c]	0.81	0.44	–	–	–	–	–	–
CH82-24	1.19±0.12; 4	0.23±0.02; 4	1.13±0.17; 5	0.31±0.04; 5	1.05 ±0.1; 6	0.25 ±0.03; 7	–	–
RC13-229	0.36±0.07; 7	0.51 ±0.04; 7	0.16±0.1; 4	0.53±0.03; 2	−0.01±0.07; 3	0.50±0.04; 2	0.18±0.1; 4	0.50±0.03; 2

[a] All data are carbon-pool corrected.
[b] For data sources see references in Table 1.
[c] Data are compiled in Tables 1 and 3 in Marchitto and Broecker (2006) from published sources.

benthic foraminiferal Cd/Ca using Boyle's (1992) partition coefficients. $\delta^{13}C_{as}$ isolines are computed using Holocene parameterization and $\delta^{13}C$ core data are corrected for mean-ocean $\delta^{13}C$ shifts using the $\delta^{13}C_{stack}$ record (see above) i.e., glacial and interglacial data are carbon-pool corrected and normalized to Holocene levels. Water mass endmember values are given for Holocene and LGM (see Table 2 for references) but we note that these values may have been slightly different during previous glacials and interglacials (e.g. Raymo et al., 2004).

The Holocene $\delta^{13}C/Cd_{sw}$ coordinates of North Atlantic cores (CHN82-24, SO75-26KL) plot close to the northern endmember reflecting the influence of NADW at these sites (Fig. 5A) (Boyle and Keigwin, 1985/86; Willamowski and Zahn, 2000). NADW is also recorded at South Atlantic cores V24-253 (Oppo and Horowitz, 2000) and RC13-228 (Boyle, 1992; Rosenthal et al., 1997). $\delta^{13}C/Cd_{sw}$ of mid-depth core M35003 from the western tropical Atlantic mirrors the influence of AAIW at this location (Zahn and Stüber, 2002) which is also seen in cores KNR159-5-36 (Came et al., 2003; Oppo and Horowitz, 2000) and RC16-119 (Oppo and Horowitz, 2000) from the upper Brazil Margin.

The Holocene section of MD96-2080 is compromised by coring disturbance and is not used in this compilation. Instead we plot $\delta^{13}C/Cd_{sw}$ coordinates of interglacials MIS 5, 7 and 9. The modern *T-S* field at MD96-2080 indicates the presence of NADW and AABW that are mixing at a ratio of roughly 70:30. $\delta^{13}C/Cd_{sw}$ coordinates of MIS 5, 7, and 9 are shifted to Cd_{sw} values slightly higher than expected from mixing reflecting water mass chemical "aging". Interglacial $\delta^{13}C/Cd_{sw}$ coordinates of core RC13-229 from the deep Cape Basin likewise are shifted away from a conservative mixing line between AABW and NADW towards "aged" values.

$\delta^{13}C/Cd_{sw}$ coordinates of MIS 6 and 8 from MD96-2080 plot close to the $\delta^{13}C_{as}$ fractionation line of NCW in the north potentially indicating the presence of an aged NCW. This probably was the case during the early glacial stages when nutrient levels were only slightly increased. Late glacial $\delta^{13}C/Cd_{sw}$ are increased in nutrients and directly plot on the mixing line between Upper and Lower Southern Component Water (USCW and LSCW) (Fig. 5B). We consider this an indication of a prominent influence of SCW at the core location during advance glacial stages with the

Table 3b
Glacial $\delta^{13}C_{\Sigma CO_2}$ and Cd_{sw} values from Atlantic sediment cores [a, b]

Sediment core	LGM $\delta^{13}C \pm 1\sigma$, n (‰ VPDB)	LGM $Cd_{sw} \pm 1\sigma$, n (nmol/kg)	Late MIS 6 $\delta^{13}C \pm 1\sigma$, n (‰ VPDB)	Late MIS 6 $Cd_{sw} \pm 1\sigma$, n (nmol/kg)	Early MIS6 $\delta^{13}C \pm 1\sigma$, n (‰ VPDB)	Early MIS 6 $Cd_{sw} \pm 1\sigma$, n (nmol/kg)	Late MIS 8 $\delta^{13}C \pm 1\sigma$, n (‰ VPDB)	Late MIS 8 $Cd_{sw} \pm 1\sigma$, n (nmol/kg)	Early MIS 8 $\delta^{13}C \pm 1\sigma$, n (‰ VPDB)	Early MIS 8 $Cd_{sw} \pm 1\sigma$, n (nmol/kg)
SO75-26KL	1.99±0.03; 4	0.13±0.04; 4	–	–	–	–	–	–	–	–
M35003	1.55±0.1; 5	0.30±0.07; 6	–	–	–	–	–	–	–	–
KNR159-5-36 [c]	0.88	0.4	–	–	–	–	–	–	–	–
RC16-119 [c]	1.31	0.29	–	–	–	–	–	–	–	–
V24-253 [c]	0.8	0.42	–	–	–	–	–	–	–	–
MD96-2080	–	–	0.50±0.1; 6	0.72±0.1; 6	0.66±0.1; 7	0.64±0.1; 7	0.22±0.1; 10	0.68±0.1; 9	0.54±0.1; 7	0.481±0.07; 7
RC13-228 [c]	0.01	0.36	–	–	–	–	–	–	–	–
RC12-294 [c]	0.09	0.51	–	–	–	–	–	–	–	–
CH82-24	0.75±0.08; 4	0.36±0.03; 4	0.57±0.2; 9	0.37±0.04; 9	0.90±0.2; 8	0.32±0.03; 8	–	–	–	–
RC13-229	−0.075±0.2; 5	0.50±0.02; 5	−0.42±0.1; 9	0.46±0.3; 6	−0.1±0.04; 2	0.45±0.02; 2	−0.46±0.2; 5	0.52±0.05; 4	−0.26±0.05; 5	0.495±0.04; 4

[a] All data are carbon-pool corrected.
[b] For data sources see references in Table 1.
[c] Data are compiled in Tables 1 and 3 in Marchitto and Broecker (2006) from published sources.

$\delta^{13}C_{as}$ signature of MD96-2080 being a result of mixing between USCW and LSCW. This corroborates the meridional gradient in $\delta^{13}C$ across the Atlantic (see above) and supports our contention of a contribution of positive $\delta^{13}C$ to the core site from USCW. LGM data from the Brazilian Margin fit with this interpretation as they indicate NCW at approximately 1500 m and nutrient-enriched SCW above and below (Oppo and Horowitz, 2000). Deep (>3000 m) South Atlantic data cluster close to the LSCW endmember confirming the invasion at depth of the basin by LSCW with a negative $\delta^{13}C_{as}$ signature, and therefore, supporting the contrasting pattern in $\delta^{13}C$ and Cd_{sw} between RC13-229 and MD96-2080.

Recurrent peak-maximum Cd_{sw} anomalies along MD96-2080 plot substantially outside the $\delta^{13}C/Cd_{sw}$ field defined by glacial endmembers and sediment core data and are shifted to elevated $\delta^{13}C_{as}$ levels of +1–1.5‰. This mimics data patterns observed for Heinrich events in the North Atlantic (Willamowski and Zahn, 2000; Zahn and Stüber, 2002; Rickaby and Elderfield, 2005) confirming the suggestion that the Cd_{sw} anomalies at MD96-2080 are the South Atlantic equivalents of peak Cd_{sw} maxima associated with H-type IRD events in the North Atlantic and a substantially reduced Atlantic MOC.

6. Conclusions

High resolution benthic foraminiferal stable isotope, Cd/Ca and $\overline{SS}$ profiles from IMAGES core MD96-2080 record changes in past modes of ocean circulation in the South Atlantic. Benthic foraminiferal $\delta^{13}C$ and Cd/Ca display prominent orbital modulation with lower $\delta^{13}C$ and elevated Cd/Ca during glacial periods while the $\overline{SS}$ profile records elevated values suggesting higher near-bottom flow speeds at the same time when chemical ventilation was reduced. Transitions from interglacial to glacial modes of ventilation are gradual in the benthic $\delta^{13}C$ and Cd/Ca records with ventilation during the early phase of glacials MIS 6 and 8 similar to interglacial conditions. Substantial reduction in ventilation is then recorded during later stages of these glacial periods when southward advection of NCW was weakened as is indicated by maximum Cd_{sw} (inferred from benthic Cd/Ca) and minimum benthic foraminiferal $\delta^{13}C$. We conclude that the high-latitude South Atlantic increasingly came under the influence of SCW during late glacial periods likely in conjunction with northward expansion of the fast flowing ACC. Benthic foraminiferal $\delta^{13}C$ remains more positive than at core sites in the deep Cape Basin while Cd_{sw} indicates higher nutrient concentrations during late glacials at MD96-2080. From this we infer an influence of air–sea gas exchange on $\delta^{13}C$ pointing at a contribution of upper SCW similar to modern-day AAIW.

Recurrent Cd_{sw} peak maxima in MD96-2080 overlap in time with increased deposition of IRD in the North Atlantic and plot outside the $\delta^{13}C/Cd_{sw}$ field for water mass mixing in the South Atlantic. Overlap between IRD events in the North and Cd_{sw} maxima at MD96-2080 suggests the Atlantic MOC was substantially reduced at these times, similar to the 'collapsed' state of MOC during Heinrich events of the last glacial.

Acknowledgements

The sediment core for this study was provided by the International Marine Global Change Studies (IMAGES) project. We thank H. Medley, I. McMillan (Cardiff University) and J. Perona and T. Padró (Serveis Científic Tècnics, Universitat de Barcelona) for laboratory assistance with stable isotope and trace element analyses. T. Marchitto and three anonymous reviewers provided helpful comments on the manuscript. GMM and RZ acknowledge support from the Ministerio de Educación y Ciencia, Spain (grants BES2003-1530 and REN2002-01958), LDP and IC from the Comer Abrupt Climate Change Foundation (USA); IH acknowledges support by the Natural Environment Research Council (NERC). We are also grateful to the NERC Radiocarbon Laboratory in East Kilbride, UK, for the ^{14}C-AMS analyses.

Appendix A. Supplementary data

Supplementary data associated with this article can be found, in the online version, at doi:10.1016/j.epsl.2007.11.050.

References

Arhan, M., Mercier, H., Park, Y.-H., 2003. On the deep water circulation of the eastern South Atlantic Ocean. Deep-Sea Res., Part 1, Oceanogr. Res. Pap. 50, 889–916.

Bertram, C.J., Elderfield, H., Shackleton, N.J., MacDonald, J.A., 1995. Cadmium/calcium and carbon isotope reconstructions of the glacial northeast Atlantic Ocean. Paleoceanography 10, 563–578.

Bertrand, P., 1997. Les rapport de campagne à la mer à bord du Marion Dufresne - Campagne Nausicaa - IMAGES II - MD105 du 20/10/96 au 25/11/96. Shipboard Scientific Party, l'Institut Francais pour la Recherche et la technologie Polaires.

Bianchi, G.G., Hall, I.R., McCave, I.N., Joseph, L., 1999. Measurements of the sortable silt current speed proxy using the Sedigraph 5100 and Coulter Multisizer IIe: precision and accuracy. Sedimentology 46, 1001–1014.

Boyle, E.A., 1983. Manganese carbonate overgrowths on foraminifera tests. Geochim. Cosmochim. Acta 47 (10), 1815–1819.

Boyle, E.A., 1988. Cadmium: chemical tracer of deep-water paleoceanography. Paleoceanography 3, 431–489.

Boyle, E.A., 1992. Cadmium and $\delta^{13}C$ paleochemical ocean distributions during the stage 2 glacial maximum. Annu. Rev. Earth Planet. Sci. 20, 245–287.

Boyle, E.A., Keigwin, L.D., 1985/86. Comparison of Atlantic and Pacific paleochemical records for the last 215,000 years: changes in deep ocean circulation and chemical inventories. Earth Planet. Sci. Lett. 76 (1–2), 135–150.

Boyle, E.A., Rosenthal, Y., 1996. Chemical hydrography of the South Atlantic during the Last Glacial Maximum: Cd *vs* $\delta^{13}C$. In: Wefer, G., Berger, W.H., Siedler, G., Webb, D. (Eds.), The South Atlantic: Present, Past and Future. Springer-Verlag, Berlin, pp. 423–443.

Broecker, W.S., Maier-Reimer, E., 1992. The influence of air and sea exchange on the carbon isotope distribution in the sea. Glob. Biogeochem. Cycles 6 (3), 315–320.

Came, R.E., Oppo, D.W., Curry, W.B., 2003. Atlantic Ocean circulation during the Younger Dryas: insights from a new Cd/Ca record from the western subtropical South Atlantic. Paleoceanography 18 (4), 1086. doi:10.1029/2003PA000888.

Chapman, M.R., Shackleton, N.J., Duplessy, J.C., 2000. Sea surface temperature variability during the last glacial–interglacial cycle: assessing the magnitude and pattern of climate change in the North Atlantic. Palaeogeogr. Palaeoclimatol. Palaeoecol. 157 (1–2), 1–25.

Charles, C.D., Wright, J.D., Fairbanks, R.G., 1993. Thermodynamic influences on the marine carbon isotope record. Paleoceanography 8 (6), 691–698.

Charles, C.D., Lynch-Stieglitz, J., Ninnemann, U.S., Fairbank, R.G., 1996. Climate connections between the hemispheres revealed by deep sea sediment core/ice core correlations. Earth Planet. Sci. Lett. 142 (1–2), 19–27.

Curry, W.B., Duplessy, J.C., Labeyrie, L.D., Shackleton, N.J., 1988. Changes in the distribution of $\delta^{13}C$ of deep water $\sum CO_2$ between the last glaciation and the Holocene. Paleoceanography 3 (3), 317–341.

Diz, P., Hall, I.R., Zahn, R., Molyneux, E.G., 2007. Paleoceanography of the southern Agulhas Plateau during the last 150 ka: inferences from benthic foraminiferal assemblages and multispecies epifaunal carbon isotopes. Paleoceanography 22, PA4218. doi:10.1029/2007PA001511.

Duplessy, J.C., Shackleton, N.J., Matthews, R.K., Prell, W., Ruddiman, W.F., Caralp, M.H., Hendy, C.H., 1984. $\delta^{13}C$ record of benthic foraminifera in the last interglacial ocean: implications for the carbon cycle and the global deep water circulation. Quat. Res. 21, 225–243.

Duplessy, J.-C., Shackleton, N.J., Fairbanks, R.G., Labeyrie, L., Oppo, D.W., Kallel, N., 1988. Deepwater source variations during the last climatic cycle and their impact on the global deepwater circulation. Paleoceanography 3, 343–360.

Fairbanks, R.G., Mortlock, R.A., Chiu, T.-C., Cao, L., Kaplan, A., Guilderson, T.P., Fairbanks, T.W., Bloom, A.L., Grootes, P.M., Nadeau, M.-J., 2005. Radiocarbon calibration curve spanning 0 to 50,000 years BP based on paired $^{230}Th/^{234}U/^{238}U$ and ^{14}C dates on pristine corals. Quat. Sci. Rev. 24 (16–17), 1781–1796.

Garabato, A.C.N., Stevens, D.P., Watson, A.J., Roether, W., 2007. Short-circuiting of the overturning circulation in the Antarctic Circumpolar Current. Nature 447, 194–197.

Gordon, A., 1986. Inter-ocean exchange of thermocline water. J. Geophys. Res. 91 (C4), 5037–5046.

Gordon, A.L., Weiss, R.F., Smethie, J.W.M., Warner, M.J., 1992. Thermocline and intermediate water communication between the South Atlantic and Indian Oceans. J. Geophys. Res. 97, 7223–7240.

Hall, I.R., McCave, I.N., 2000. Palaeocurrent reconstruction, sediment and thorium focussing on the Iberian margin over the last 140 ka. Earth Planet. Sci. Lett. 178 (1–2), 151.

Hall, I.R., McCave, N., Shackleton, N.J., Weedon, G.P., Harris, S.E., 2001. Intensified deep Pacific inflow and ventilation in Pleistocene glacial times. Nature 412, 809–813.

Hall, I.R., Moran, S.B., Zahn, R., Knutz, P.C., Shen, C.-C., Edwards, R.L., 2006. Accelerated drawdown of meridional overturning in the late-glacial Atlantic triggered by transient pre-H event freshwater perturbation. Geophys. Res. Lett. 33, L16616. doi:10.1029/2006GL026239.

Holbourn, A., kuhnt, W., Kawamura, H., Jian, Z., Grrotes, P., Erlenkeuser, H., Xu, J., 2005. Orbitally paced paleoproductivity variations in the Timor Sea and Indonesian Throughflow variability during the last 460 ky. Paleoceanography 20, PA3002. doi:10.1029/2004PA001094.

Hoogakker, B.A.A., Rohling, E.J., Palmer, M.R., Tyrrell, T., Rothwell, R.G., 2006. Underlying causes for long-term global ocean [delta]13C fluctuations over the last 1.20 Myr. Earth Planet. Sci. Lett. 248 (1–2), 15.

Keigwin, L.D., Boyle, E.A., 1985. Carbon isotopes in deep-sea benthic foraminifera: precession and low latitude changes in biomass. In: Sundquist, E., Broecker, W.S. (Eds.), The Carbon Cycle and Atmospheric CO_2: Natural Variations Archean to Present. Tarpon Springs, FL, pp. 319–329.

Knorr, G., Lohmann, G., 2003. Southern Origin for the resumption of Atlantic thermohaline circulation during deglaciation. Nature 424, 532–536.

Lea, D.W., 1995. A trace metal perspective on the evolution of Antarctic Circumpolar Deep Water Chemistry. Paleoceanography 10 (4), 733–748.

Lynch-Stieglitz, J., Fairbanks, R.G., 1994. A conservative tracer for glacial ocean circulation from carbon isotope and paleonutrient measurements in benthic foraminifera. Nature 369, 308–310.

Lynch-Stieglitz, J., van Geen, A., Fairbanks, R.G., 1996. Interocean exchange of Glacial North Atlantic Intermediate Water: evidence from the subantarctic Cd/Ca and carbon isotope measurements. Paleoceanography 11 (2), 191–201.

Mackensen, A., Bickert, T., 1999. Stable carbon isotopes in benthic foraminifera: proxies for deep and bottom water circulation and new production. In: Fischer, G., Wefer, G. (Eds.), Use of Proxies in Paleoceanography: Examples from the South Atlantic. Springer, Verlag Berlin Heidelberg, pp. 229–254.

Mackensen, A., Hubberten, H.-W., Bickert, T., Fischer, G., Fütterer, D.K., 1993. The $\delta^{13}C$ in benthic foraminiferal tests on *Fontbotia wuellerstorfi* (Schwager) relative to the $\delta^{13}C$ of dissolved inorganic carbon in southern ocean deep water: implications for glacial ocean circulation models. Paleoceanography 8, 587–610.

Marchal, O., François, R., Stocker, T.F., Joos, F., 2000. Ocean thermohaline circulation and sedimentary $^{231}Pa/^{230}Th$ ratio. Paleoceanography 15 (6), 209–267.

Marchitto, T.M., Broecker, W.S., 2006. Deep water mass geometry in the glacial Atlantic Ocean: a review of constraints from the paleonutrient proxy Cd/Ca. Geochem., Geophys., Geosys. 7, Q12003. doi:10.1029/2006GC001323.

Marchitto, T.M., Curry, W.B., Oppo, D., 1998. Millennial-scale changes in North Atlantic circulation since the last glaciation. Nature 393, 557–561.

Marchitto, T.M., Curry, W.B., Oppo, D.W., 2000. Zn concentrations in benthic foraminifera reflect seawater chemistry. Paleoceanography 15 (3), 299–306.

McCave, I.N., Hall, I.R., 2006. Size sorting in marine muds: processes, pitfalls, and prospects for paleoflow-speed proxies. Geochem., Geophys., Geosys. 7, Q10N05. doi:10.1029/2006GC001284.

McCave, I.N., Manighett, B., Robinson, S.G., 1995. Sortable silt and fine sediment size/composition slicing: parameters for palaeocurrent speed and palaeoceanography. Paleoceanography 10, 593–610.

McCave, I.N., Kiefer, T., Thornalley, D.J.R., Elderfield, H., 2005. Deep flow in the Madagascar–Mascarene Basin over the last 150,000 years. Philos. Trans. R. Soc. Lond., A 363 (1826), 81–99.

McCorkle, D.C., Martin, P.A., Lea, D.W., Klinkhammer, G.P., 1995. Evidence of a dissolution effect on benthic foraminiferal shell chemistry: $\delta^{13}C$, Cd/Ca, Ba/Ca, and Sr/Ca results from the Ontong Java Plateau. Paleoceanography 10 (4), 699–714.

McManus, J.F., Oppo, D.W., Cullen, J.L., 1999. A 0.5-million-year record of millennial-scale climate variability in the North Atlantic. Science 283 (5404), 971–975.

McManus, J.F., Francois, R., Gherardi, J.-M., Keigwin, L.D., Brown-Leger, S., 2004. Collapse and rapid resumption of Atlantic meridional circulation linked to deglacial climate changes. Nature 428, 834–837.

Mix, A.C., Le, J., Shackleton, N.J., 1995. Benthic foraminiferal stable isotope stratigraphy of Site 846: 0–1.8 Ma. Proc. Ocean Drill. Program Sci. Results 138, 839–854.

Molyneux, E.G., Hall, I.R., Zahn, R., Diz, P., 2007. Deep water variability on the southern Agulhas Plateau: interhemispheric links over the past 170 ka. Paleoceanography 22, PA4209. doi:10.1029/2006PA001407.

Ninnemann, U.S., Charles, C.D., 2002. Changes in the mode of Southern Ocean circulation over the last glacial cycle revealed by foraminiferal stable isotopic variability. Earth Planet. Sci. Lett. 201 (2), 383.

Oppo, D.W., Fairbanks, R.G., 1987. Variability in the deep and intermediate water circulation of the Atlantic Ocean during the past 25,000 years: Northern Hemisphere modulation of the Southern Ocean. Earth Planet. Sci. Lett. 86, 1–15.

Oppo, D.W., Rosenthal, Y., 1994. Cd/Ca changes in a deep Cape Basin core over the past 730,000 years: response of circumpolar deepwater variability to northern hemisphere ice sheet melting? Paleoceanography 9 (5), 661–675.

Oppo, D.W., Horowitz, M., 2000. Glacial deep water geometry: South Atlantic benthic foraminiferal Cd/Ca and $\delta^{13}C$ evidence. Paleoceanography 15 (2), 147–160.

Oppo, D.W., Fairbanks, R.G., Gordon, A.L., Shackleton, N.J., 1990. Late Pleistocene Southern Ocean $\delta^{13}C$ variability: North Atlantic Deep Water modulation of atmospheric CO_2. Paleoceanography 5, 43–55.

Ostlund, H.G., Craig, H., Broecker, W.S., Spencer, D., 1987. Geosecs Atlantic, Pacific, and Indian Ocean expeditions. Shorebased Data and Graphics. National Science Foundation. 7.

Pahnke, K., Zahn, R., 2005. Southern Hemisphere water mass conversion linked with North Atlantic climate variability. Science 307 (5716), 1741–1746.

Pahnke, K., Zahn, R., Elderfield, H., Schulz, M., 2003. 340,000-year centennial-scale marine record of Southern Hemisphere climatic oscillation. Science 301, 948–952.

Paillard, D., Labeyrie, L., Yiou, P., 1996. Macintosh program performs time-series analysis. EOS, AGU 77, 379.

Peeters, F.J.C., Acheson, R., Brummer, G.-J.A., de Ruijter, W.P.M., Schneider, R., Ganssen, G., Ufkes, M.E., Kroon, D., 2004. Vigorous exchange between the Indian and Atlantic oceans at the end of the past five glacial periods. Nature 438 (7000), 661–665.

Pena, L., Calvo, E., Cacho, I., Eggins, S., Pelejero, C., 2005. Identification and removal of Mn–Mg-rich contaminant phases on framiniferal tests:

implications for Mg/Ca past temperature reconstructions. Geochem., Geophys., Geosys. 6, Q09P02. doi:10.1029/2005GC000930.

Piotrowski, A.M., Goldstein, S.L., Hemming, S.R., Fairbanks, R.G., 2005. Temporal relationships of carbon cycling and ocean circulation at glacial boundaries. Science 307 (5717), 1933–1938.

Rau, A.J., Rogers, J., Lutjeharms, J.R.E., Giraudeau, J., Lee-Thorp, J.A., Chen, M.-T., Waelbroeck, C., 2002. A 450-kyr record of hydrological conditions on the western Agulhas Bank Slope, south of Africa. Mar. Geol. 180 (1–4), 183–201.

Rau, A.J., Rogers, J., Chen, M.-T., 2006. Late Quaternary palaeoceanographic record in giant piston cores off South Africa, possibly including evidence of neotectonism. Quat. Int. 148 (1), 65–77.

Raymo, M.E., Oppo, D.W., Flower, B.P., Hodell, D.A., McManus, J.F., Venz, K.A., Kleiven, K.F., McIntyre, K., 2004. Stability of North Atlantic water masses in face of pronounced climate variability during the Pleistocene. Paleoceanography 19, PA2008. doi:10.1029/2003PA000921.

Rickaby, R.E.M., Elderfield, H., 2005. Evidence from the high-latitude North Atlantic for variations in Antarctic Intermediate water flow during the last deglaciation. Geochem., Geophys., Geosys. 6, Q05001. doi:10.1029/2004GC000858.

Rickaby, R.E.M., Greaves, M.J., Elderfield, H., 2000. Cd in planktonic and benthic foraminiferal shells determined by thermal ionisation mass spectrometry. Geochim. Cosmochim. Acta 64 (7), 1229.

Rickaby, R.E.M., Bard, E., Sonzogni, C., Rostek, F., Beaufort, L., Barker, S., Rees, G., Schrag, D.P., 2007. Coccolith chemistry reveals secular variations in the global ocean carbon cycle? Earth Planet. Sci. Lett. 253 (1–2), 83.

Rosenthal, Y., Boyle, E.A., Labeyrie, L., 1997. Last Glacial Maximum paleochemistry and deepwater circulation in the Southern Ocean: evidence from foraminiferal cadmium. Paleoceanography 12 (6), 787–796.

Rutberg, R.L., Hemming, S.R., Goldstein, S.L., 2000. Reduced North Atlantic deep water flux to the glacial Southern Ocean inferred from neodymium isotope ratios. Nature 405, 935–938.

Sarnthein, M., Winn, K., Jung, S.J.A., Duplessy, J.C., Labeyrie, L., Erlenkeuser, H., Ganssen, G., 1994. Changes in east Atlantic deep water circulation over the last 30,000 years: eight time slice reconstructions. Paleoceanography 9, 209–267.

Schrag, D.P., Adkins, J.F., McIntyre, K., Alexander, J.L., Hodell, D.A., Charles, C.D., McManus, J.F., 2002. The oxygen isotopic composition of seawater during the Last Glacial Maximum. Quat. Sci. Rev. 21 (1–3), 331–342.

Shackleton, N.J., 1974. Attainment of isotopic equilibrium between ocean water and the benthonic foraminifera genus *Uvigerina*: isotopic changes in the ocean during the last glacial. Colloques Internationaux du Centre National de la Recherche Scientifique 219, 203–209.

Southon, J., Kashgarian, M., Fontugne, M., Metivier, B., Yim, W.W.-S., 2002. Marine reservoir corrections for the Indian Ocean and Southeast Asia. Radiocarbon 44 (1), 167–180.

van Aken, H.M., Ridderinkhof, H., de Ruijter, W.P.M., 2004. North Atlantic Deep Water in the south-western Indian Ocean. Deep-Sea Res., Part 1, Oceanogr. Res. Pap. 51, 755–776.

Waelbroeck, C., Labeyrie, L., Michel, E., Duplessy, J.-C., McMAnus, J.F., Lambeck, K., Balbon, E., Labracherie, M., 2002. Sea-level deep water temperature changes derived from benthic foraminifera isotopic records. Quat. Sci. Rev. 21, 295–305.

Weijer, W., de Ruijter, W.P.M., Dijkstra, H.A., van Leeuwen, P.J., 1999. Impact of interbasin exchange on the Atlantic Overturning Circulation. J. Phys. Oceanogr. 29, 2266–2284.

Willamowski, C., Zahn, R., 2000. Upper ocean circulation in the glacial North Atlantic from benthic foraminiferal isotope and trace element fingerprinting. Paleoceanography 15, 515–527.

Yu, E.-F., Francois, R., Bacon, M.P., 1996. Similar rates of modern and last-glacial ocean thermohaline circulation inferred from radiochemical data. Nature 379 (6567), 689–694.

Zahn, R., Keir, R., 1992. Tracer–nutrient correlations in the upper ocean: observational and box model constrains on the use of benthic foraminiferal δ^{13}C and Cd/Ca as paleo-proxies for the intermediate-depth ocean. In: Zahn, R., Pedersen, T.F., Kaminski, M.A., Labeyrie, L. (Eds.), Carbon Cycling in the Glacial Ocean: Constrains on the Ocean's Role in Global Change. . NATO ASI Series. Springer, Berlin, pp. 195–221.

Zahn, R., Stüber, A., 2002. Suborbital intermediate water variability inferred from paired benthic foraminiferal Cd/Ca and δ^{13}C in the tropical West Atlantic and linking with North Atlantic climates. Earth Planet. Sci. Lett. 200, 191–205.

Zahn, R., Winn, K., Sarnthein, M., 1986. Benthic foraminiferal δ^{13}C and accumulation of organic carbon: *Uvigerina perigerina* and *Cibicidoides wuellerstorfi*. Paleoceanography 1 (1), 27–42.

Institut de Ciència i Tecnologia Ambientals
Universitat Autònoma de Barcelona
Edifici Cn - Campus UAB
E-08193 Bellaterra (Cerdanyola), Spain
Phone: +34 - 93 581 2974
Fax: +34 - 93 581 3331
doctorat.icta@uab.es